Design of Initiators for the Production of Bio-based Polymers

McKeown, Paul

Award date:
2017

Awarding institution:
University of Bath

Design of Initiators for the Production of Bio-based Polymers

Paul McKeown

A thesis submitted for the degree of Doctor of Philosophy

Department of Chemistry

University of Bath

February 2017

A. Contents

A. Contents i
B. Acknowledgements iv
C. Abstract v
D. Abbreviations vi
E. Publications vii

1. Introduction 1
1.1 The case for renewable polymers 2
1.2 Poly(lactic acid) 6
1.2.1 Lactide: preparation and properties 6
1.2.2 Poly(lactic acid): structure and properties 8
1.2.3 Polymerisation pathways 9
1.3 Polymer characterisation methods 16
1.3.1 NMR spectroscopy 16
1.3.2 GPC and MALDI-ToF 18
1.3.3 DSC 19
1.4 Stereoselective initiators for LA ROP 20
1.4.1 Group I initiators 21
1.4.2 Group II initiators 23
1.4.3 Zinc Initiators 32
1.4.4 Group III and lanthanide initiators 39
1.4.5 Group IV initiators 45
1.4.5 Group 13 initiators 54
1.5 Summary and project aims 67
1.6 References 67
Chapter 2: Synthesis of 2-(aminomethyl)piperidine based ligands 78
2.1 Introduction 78
2.2 Preliminary investigation 79
2.3 Monophenol ligand synthesis 87
2.4 Bisphenol ligand synthesis 92
2.5 Trisphenol ligand synthesis 98
2.6 Conclusions 100
2.7 References 101

Chapter 3: Complexation of 2-(aminomethyl)piperidine based ligands.... 104
3.1 Introduction.... 104
3.2 Monophenolate complexes.... 105
3.2.1 Imino-monophenolate complexes.... 105
3.2.2 Bicyclic monophenolates complexes.... 117
3.3 Aluminium bis/trisphenolates complexes.... 124
3.3.1 Aluminium bicyclic bisphenolate complexes.... 124
3.2.2 Aluminium salalen complexes.... 131
3.3.3 Aluminium salan complexes.... 137
3.3.4 Triaryl bis/trisphenolate complexes.... 147
3.4 Group IV complexes.... 152
3.4.1 Titanium complexes.... 152
3.4.2 Zirconium/Hafnium complexes.... 165
3.5 Conclusions.... 184
3.6 References.... 186
Chapter 4: 2-(Aminomethyl)piperidine based initiators for lactide polymerisation.... 190
4.1 Introduction.... 190
4.2 Polymerisations with monophenolate complexes.... 191
4.2.1 Aluminium monophenolate complexes.... 191
4.2.2 Magnesium/Zinc imino-monophenolate complexes.... 200
4.3 Polymerisations with aluminium bis/tris-phenolate complexes.... 204
4.3.1 Aluminium bicyclic bisphenolate complexes.... 204
4.3.2 Aluminium salalen complexes.... 207
4.3.3 Aluminium salan bisphenolate complexes.... 211
4.3.4 Aluminium triaryl complexes.... 230
4.4 Polymerisations with group IV complexes.... 231
4.4.1 Titanium complexes.... 231
4.4.2 Zirconium complexes.... 233
4.5 Conclusions.... 248
4.6 Future work.... 250
4.7 References.... 253
Chapter 5: Experimental.... 257
5.1 General experimental methods.... 257
5.2 General polymerisation methods.... 258
5.3 Ligand synthesis and characterisation (Chapter 2).... 259
5.3.1 Preliminary investigations.... 259

5.3.2 Monophenolate ligand synthesis 260
5.3.3 Bisphenolate ligand synthesis 267
5.3.4 Triaryl phenolate ligand synthesis 278
5.4 Complex synthesis and characterisation (Chapter 3) 279
5.4.1 Monophenolate complex synthesis 279
5.4.2 Bisphenolate aluminium complex synthesis 286
5.4.3 Group IV complexes 300
5.5 References 311
Chapter 6: Appendix 312
6.1 Ligand X-ray diffraction data (Chapter 2) 313
6.2 Complex X-ray diffraction data (Chapter 3) 317
6.3 Optimised DFT geometries and calculated Gibbs free energies 356
6.4 Selection of GPC traces (Chapter 4) 362

B. Acknowledgements

I would first like to thank Dr. Matthew Jones, without who this project would have not got anywhere. I am extremely grateful for his supervision and guidance during my PhD as well as his enthusiasm and encouragement. Dr. Matthew Jones is also acknowledged for the acquisition of crystallographic data. I would also like to thank Prof. Matthew Davidson for his support throughout my PhD. I would also like to thank the DTC in Sustainable Chemical Technologies for and the EPRSC for funding.

I also greatly appreciate the assistance and expertise provided by characterisation specialists at the University of Bath. In particular, I would like to thank Dr. John Lowe and Dr. Tim Woodman for their invaluable NMR support as well as Dr. Mary Mahon and Dr. Gabriele Kociok-Köhn for X-ray crystallography assistance. Dr. Anneke Lubben and Dr. Rémi Castaing are also thanked for their help with mass spectrometry and GPC respectively.

I am also grateful to the DTC in Sustainable Chemical Technologies for the opportunity to undertake a PhD at the University of Bath and for many training opportunities. I am also thankful for the cohort experience, and it's been a great pleasure to be a part of Cohort 12. I would like to give special mention to Chris Davey and Stephen Bradley for their positivity and constant readiness to venture to Parade.

I must also extend thanks to both the Jones and Davidson groups, past and present. Special mentions goes to Sarah Kirk, who has been my office buddy since before the PhD even started. I would also like acknowledge James Brown-Humes for his contribution to this thesis and being an excellent MChem student. I am also grateful to Helena Quilter, Mike Joyes, Heather Parker and James Beament for making the lab environment more fun and for useful discussions. We have also been privileged with exceptional visiting students, and it was a pleasure to work with Pascal Schafer, Fernando Peleias Junior and Simoní da Ros. I would also like to thank everyone else in the 5W SusChemLab, especially Dr. Antoine Buchard and Georgina Gregory for help with DFT.

C. Abstract

The current plastic production and use is unsustainable, relying on non-renewable sources. The pollution caused by petro-chemical based plastics is also becoming a problem due to non-biodegradation of these materials. The research into alternative bio-based plastics represents an important challenge in both academia and industry. At the forefront of such research is poly(lactic acid) (PLA), a biodegradeable polyester that also boasts biocompatibility. Chapter 1 discusses properties and synthesis routes for PLA as well initiators for the stereoselective polymerisation of *rac*-lactide.

In Chapter 2, the synthesis of ligands based on 2-(aminomethyl)piperidine (2-AMP) is discussed. In the first instance, a study exploring the ring-chain tautomerism of 2-AMP condensation products is discussed. This is followed by the realisation of a range a ligands including monophenols, bicyclic phenols, salalen and salan structures. These ligands were fully characterised by NMR spectroscopy and mass spectrometry.

In Chapter 3, the complexation of the 2-AMP based ligands is discussed. The choice of metals was dependent on the possible coordination modes of the ligand set. Mg(II) and Zn(II) complexes were realised for monophenolate based ligands, and Al(III) and group IV metals were applied to both monophenolate and bisphenolate motifs. Metal complexes were characterised in solution and in the solid-state by NMR spectroscopy and X-ray crystallography respectively. Due to the application of a racemic ligand, diastereomeric forms were commonly observed in solution for some complexes.

In Chapter 4, the catalytic activity of these complexes is assessed with respect to the ring opening polymerisation (ROP) of lactide. Both the solution and solvent-free ROP were trialled. Best results were achieved with Al(III) salan complexes which demonstrated high activity under both solution and solvent-free conditions. A strong degree of isotacticity was also realised within this series of initiators.

D. Abbreviations

2-AMP	2-(Aminomethyl)piperidine
2-AMP_y	2-(Aminomethyl)pyridine
CEM	Chain end mechanism
DSC	Differential scanning calorimetry
DOSY	Diffusion ordered spectroscopy
ESI	Electron spray ionisation
EXSY	Exchange spectroscopy
GPC	Gel permeation chromatography
k_{app}	Apparent rate constant
k_{prop}	Rate constant of propagation
LA	Lactide
LS	Light scattering
MALDI-ToF	Matrix assisted laser desorption ionisation
NMR	Nuclear magnetic resonance
nOe	nuclear Overhauser effect
P_r	Probability of heterotactic enchainment
P_m	Probability of isotactic enchainment
PBS	Poly(butylene succinate)
PEF	Poly(ethylene furanoate)
PET	Poly(ethylene terephthalate)
PHA	Poly(hydroxyl alkanoate)
PHB	Poly(hydroxyl butyrate)
PLA	Poly(lactic acid)
PP	Polypropylene
ppm	Parts per million
PS	Polystyrene
RI	Refractive index
rt	Room temperature
ROP	Ring opening polymerisation
SCM	Site controlled mechanism
ToF	Time of flight
VT	Variable temperature

E. Publications

Dalton Transactions

PAPER

Aminopiperidine based complexes for lactide polymerisation†

P. McKeown,[a,b] M. G. Davidson,[a,b] J. P. Lowe,[b] M. F. Mahon,*[c] L. H. Thomas,[b] T. J. Woodman[a] and M. D. Jones*[b]

Cite this: *Dalton Trans.*, 2016, **45**, 5374

Received 30th November 2015,
Accepted 18th February 2016

DOI: 10.1039/c5dt04695e

www.rsc.org/dalton

Herein we report the synthesis and characterisation of a series of salalen and salan ligands derived from 2-(aminomethyl)piperidine. Depending on the choice of starting salicylaldehyde, a bicyclic salan type ligand (**1–3**H$_2$) or imino salalen type ligand (**4–6**H, **7–9**H$_2$) were prepared. The ligands were successfully complexed to group 4 metals and aluminium; with hafnium and zirconium octahedral complexes, M(**1–3**)$_2$, were realised; whilst with aluminium tetrahedral and trigonal bipyramidal complexes, Al(**1–9**)Me$_x$ (x = 1,2), were isolated. The complexes have been characterised in solution *via* ^{1}H and ^{13}C{^{1}H} NMR spectroscopy and in the solid state by X-ray crystallography. The group 4 complexes were observed to have a *fac*–*fac* arrangement of ligands and there were two isomers present when **3**H$_2$ was ligated. The imino aluminium complexes Al(**7–9**)Me were isolated as a mixture of diastereoisomers. The resultant complexes were trialed in the ring opening polymerisation of *rac*-lactide with both heterotactic and isotactic PLA being demonstrated. Tacticity was found to be dependent on the nature of the ligand and metal used; the M(**1–3**)$_2$ complexes were generally found to have a heterotactic preference (P_r = 0.67–0.76) and the aluminium polymerisation outcome was dictated more by the steric influence of the ligand, particularly for Al(**4/6**)Me$_2$/Al(**7/9**)Me.

Introduction

Sustainable plastics are receiving increased interest due to dwindling petrochemical resources and a desire for more biodegradable materials. At the forefront of such research are polylactic acid (PLA) based materials, which can have similar properties to petrochemical derived polymers and a broad range of applications.[1] There are a range of polymer microstructures that can be accessed and this can be tuned by varying the stereochemistry of the monomer and judicious choice of initiator; in particular, there is great emphasis placed on controlling the chain stereoregularity in the polymerisation of *rac*-lactide (*rac*-LA) to achieve improved polymer properties.[2] For this, an initiator capable of polymerizing *rac*-LA with strong isoselectivity and fast kinetics is urgently being sought.[3] This is related to the desired properties (higher T_m) of the resulting polymer. There are a range of initiators in the literature with metals such as Sn(II),[4] Zn(II),[5] Al(III),[2g,6] In(III),[7] Group II,[5b,8] rare-earth[3,9] and Group IV[6a,10] being widely reported.

Common themes previously seen in successful ring opening initiators for lactide polymerisation include a cyclic backbone and a stereocentre, allowing for enantiomorphic control over the propagating chain.[2b,g,5a,e,6b,g,j,7a,e,10c,11] The metal centre employed can also have a profound effect on the polymerisation outcome.[6a,9b] Early work by Spassky and co-workers demonstrated this approach by using *R*-binapthyldiamine ligands with an Al(III) centre.[2g,6j] These salen complexes showed a distinct preference for the polymerisation of D-lactide leading to isotactic stereocomplexed PLA. Feijen *et al.* have utilized Jacobsen's ligand containing a *trans*-1,2-diaminocyclohexyl backbone for *rac*-LA polymerisation.[6g,11c] Once again, aluminium was used and isotactic PLA was realized on application of the racemic complex. A series of unsymmetrical Al(III) salalens based around this diaminocyclohexyl structure were prepared by Jones *et al.*[6b] Moderate stereocontrol was observed for all complexes with greatest heterotacticity being related to chloro-substituted phenyl moieties. More recently, work by Kol has demonstrated the use of chiral aminomethylpyrrolidine salalen ligands with aluminium giving heterotactic or gradient isotactic PLA depending on aryl substituents.[6c]

[a]*Doctoral Training Centre in Sustainable Chemical Technologies, University of Bath, Bath BA2 7AY, UK*

[b]*Department of Chemistry, University of Bath, Claverton Down, Bath BA2 7AY, UK. E-mail: mj205@bath.ac.uk; Fax: +44 (0)1225 386231; Tel: +44 (0)1225 384908*

[c]*Crystallography Centre, Department of Chemistry, University of Bath, Claverton Down, Bath BA2 7AY, UK. E-mail: m.f.mahon@bath.ac.uk*

†Electronic supplementary information (ESI) available: Full analysis of ^{1}H and ^{13}C{^{1}H} NMR spectra and data are provided as well as examples of polymer characterisation and the crystal data in the .cif format. CCDC 1432292–1432306. For ESI and crystallographic data in CIF or other electronic format see DOI: 10.1039/c5dt04695e

ChemComm

COMMUNICATION

View Article Online
View Journal | View Issue

Aluminium salalens *vs.* salans: "*Initiator Design*" for the isoselective polymerisation of *rac*-lactide†

Paul McKeown,[ab] Matthew G. Davidson,[b] Gabriele Kociok-Köhn[b] and Matthew D. Jones*[b]

Cite this: *Chem. Commun.*, 2016, 52, 10431

Received 14th July 2016,
Accepted 27th July 2016

DOI: 10.1039/c6cc05795k

www.rsc.org/chemcomm

We report the rationalised design of aluminium initiators and their application for ROP of *rac*-lactide (*rac*-LA). A very minor change to the ligand backbone (imine reduction) to give secondary amines was found to have a dramatic effect on activity and selectivity with isotactic PLA being realised.

There is a significant range of aluminium initiators reported for the ROP of *rac*-LA to afford polylactide (PLA). Aluminium is attractive as it is a highly abundant metal. Initiators based on aluminium are often reported to exert some degree of stereocontrol over the polymerisation of *rac*-LA with there being cases of both isotactic and heterotactic preference in the literature,[1] it is difficult to predict or rationalise the selectivity. While such polymerisations are well controlled in terms of polymer architecture and weight properties, they often suffer from slow rates with many hours to several days required in solution and even melt polymerisations. A challenge for the ROP of *rac*-LA is the preparation of isotactic stereoblock PLA under industrially relevant conditions and determining initiator structure activity relationships. Other metal centres that are active for the production of isotactic PLA include Zr(IV),[2] Hf(IV),[1l,2b,d] Y(III),[3] In(III),[4] Zn(II)[5] and lanthanides.[6]

One of the earliest examples of stereocontrolled PLA production was demonstrated by Spassky and co-workers.[1j] Using chiral binaphthyl Schiff base aluminium complexes, isotacticity resulted from the solution ROP (70 °C, toluene, [LA]:[Init] = 75:1) with evidence of stereocomplexation being observed. Reaction times from 5 hours (19% conversion) up to 281 hours (98% conversion) are reported for this system. An isotactic initiator was also prepared by Feijen *et al.*, also utilising an aluminium salen complex.[1k,n] In this case, the ligand backbone was *trans*-1,2-cyclohexyl and P_m values of 0.93 (solution, [LA]:[Init] = 62:1) and 0.88 (melt, [LA]:[Init] = 200:1) are reported with typical reaction times given in days. Examples of relatively fast and well controlled Al(III) salen mediated polymerisations are provided by Nomura *et al.*[1e,f] In one study, the identity of two key positions upon the ligand (substituents *ortho* to the phenoxy and the aliphatic backbone) are varied.[1f] The achiral salen complexes screened generally showed isotactic preference (P_m > 0.69) and solution reactions time varied from 0.4 to 72 hours depending on the nature of the substituents. In particular, excellent stereocontrol was realised with $^tBuMe_2Si$ *ortho* groups and this was largely maintained at high temperatures (130–180 °C, [LA]:[Init] = 300:1), however preparation of this particular initiator requires lengthy synthesis including protection and deprotection. Gibson *et al.* have prepared eight salan complexes based around a *N*,*N*′-disubstituted ethylenediamine backbone.[1c] Depending on substituent choice, strong heterotactic or moderate isotactic preference was observed with the solution polymerisation length typically being around 24 hours (70 °C, [LA]:[Init] = 100:1). More recently, Kol *et al.* have demonstrated enantiomerically pure salalens based upon an aminomethylpyrrolidine moiety.[1h] Application of these for ROP of *rac*-LA gave reasonable heterotacticity or gradient isotactic multiblock PLA (P_m = 0.82) in toluene (80 °C, [LA]:[Init] = 100:1).

In this work, a series of related salan complexes based on 2-aminopiperidine are reported. Reduction of the imine functionality of the salalen structure afforded a secondary amine salan and subsequent methylation at this position further yields a tertiary amine based salan (Scheme 1). Important for industrial applications, the salan ligands are colourless consequently affording colourless complexes and white polymer. Ligands **1–2H$_2$** are prepared *via* a simple three step synthesis which is achievable on a multigram scale within a day. All ligands have been characterised by ^1H and $^{13}C\{^1H\}$ NMR spectroscopy as well as ESI-MS. The initial complexation of **1–3H$_2$** with $AlMe_3$ (Scheme 2) afforded complexes each with 4 distinct species in solution. It is postulated that these species are a consequence of the inherent stereochemistry of the ligand and the new

[a] *Doctoral Training Centre in Sustainable Chemical Technologies, University of Bath, Bath BA2 7AY, UK*
[b] *Department of Chemistry, University of Bath, Claverton Down, Bath BA2 7AY, UK. E-mail: mj205@bath.ac.uk; Fax: +44 (0) 1225 386231; Tel: +44 (0) 1225 384908*

† Electronic supplementary information (ESI) available: Full experimental data and crystal data. CCDC 1491351–1491354. For ESI and crystallographic data in CIF or other electronic format see DOI: 10.1039/c6cc05795k

Chapter 1

Introduction

1. Introduction

1.1 The case for renewable polymers

Currently, the majority of plastics (~95%) are derived from petrochemical resources, which are a non-renewable feedstock and will eventually run out.[1] Despite conflicting reports as to fossil fuel depletion,[2] the environmental impact of their usage is universally agreed.[3, 4] The use of petrochemicals has been shown to contribute greatly to Global Warming, and the associated issues, for example CO_2 levels are now as high as 400 ppm.[5, 6] As a consequence, the reliance on fossil fuels is under scrutiny with efforts being made to reduce usage and related emissions.[7] This desire to utilise less fossil carbon is in stark contrast to the global demand for plastics which has been increasing annually, and this is predicted to continue (Figure 1.1).[8] An increase in current plastic production would add further reliance to fossil carbon use as well as increased emissions and pollution (Figure 1.2).

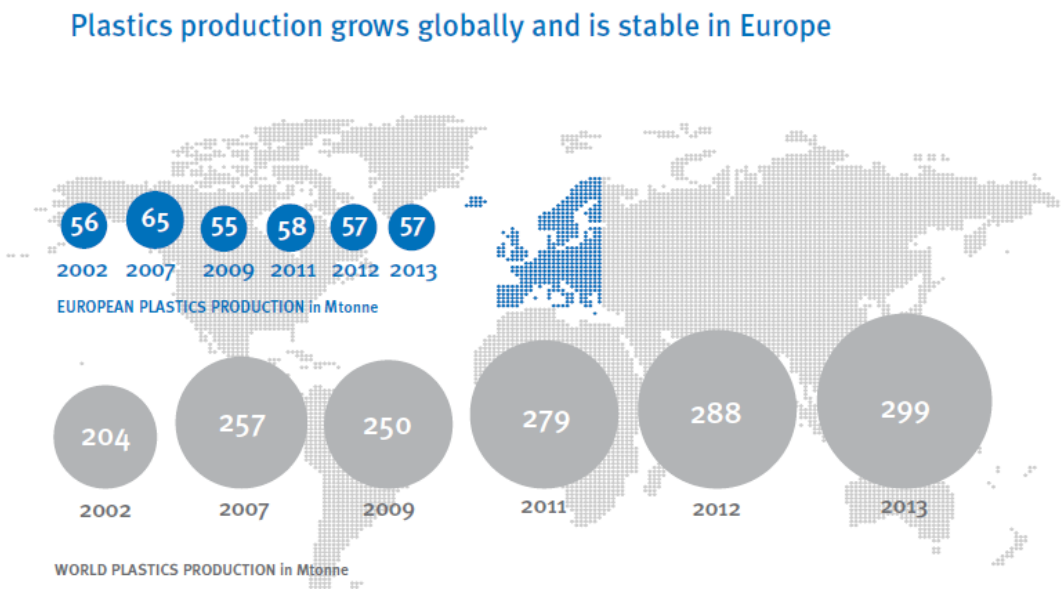

Figure 1.1: Growth in global plastic production and trend in European plastic production.[8]

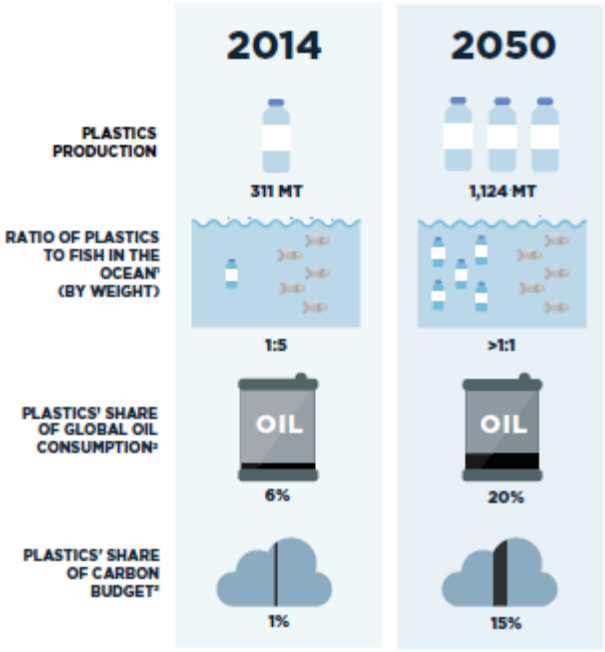

Figure 1.2: Impact of increased global plastic production.[9]

One of the current hurdles facing renewable plastics expansion is the economics of the process. Plastics derived from petrochemicals are manufactured and processed by a long established and optimised industry meaning production is relatively cheap though subject to fluctuations in the price of oil. In contrast, the production of renewable plastics follows different routes as necessitated by alternative feedstocks and while some commercial bioplastics have been achieved manufacturing costs can be high. As a consequence, renewable plastics are more of a high end product, subject to a price premium.[10, 11]

As well as current economic viability, the oil based plastics have many ideal properties which has lead them being so widely used in many different forms and applications. For example, both polystyrene (PS) and polyethylene terephthalate (PET) have good thermal properties with relatively high glass temperatures and melt temperatures.[12] PET also has high tensile strength and gas permeability properties, which permits the long term storage of carbonated drinks. While highly desirable during lifetime use, these material properties can later become a severe disadvantage. Plastic pollution is becoming a critical problem and challenge of the 21st century, having a wide range impact. The persistence of plastic materials means that a significant quantities are ending up in landfill sites or free in the environment, such as in the sea. In 2012, 8 MT

or 31% of plastic waste in the EU ended its life in landfill sites.[8] In 2010, it was estimated that 4.8 – 12.7 MT leaked into the oceans.[13] The current technologies being based on petrochemical resources also mean that the production of conventional plastics can often be associated with relatively high carbon footprint and emissions (Figure 1.3). [9]

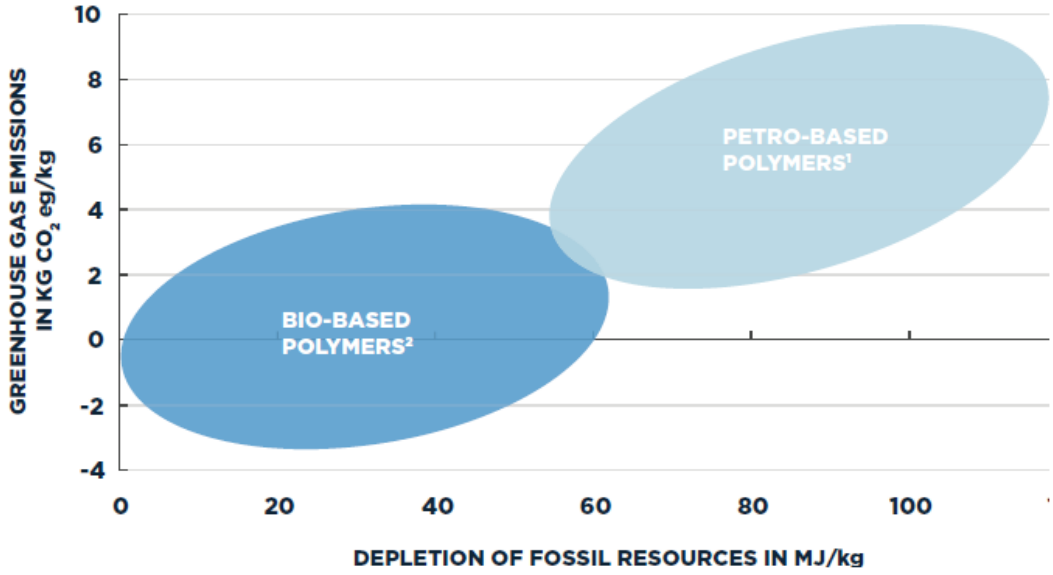

Figure 1.3: Greenhouse emission and fossil fuel use for the preparation of petro- and bio-based polymers. [9]

In the meantime, there are drives to make current plastics "greener". An excellent example to illustrate this is provided by current methods for the preparation of PET bottles. Conventional sourcing of materials is completely oil based, deriving the two monomers ethylene glycol and terephthalic acid for polycondensation reaction to produce PET. However, ethylene glycol can also be derived from sugar and sugar waste. Incorporation of this bio-ethylene glycol into bottles furnishes so called "bio-bottles," which have a 30% renewable component. These bottles have been commercialised by Coca-Cola® and are widely available.[14] Coca-Cola® have also recently demonstrated a fully biomass derived bottle.[15]

With current issues associated with conventional plastics, there is a growing need to develop new materials to meet the growing demand. Importantly, these materials must be able to mimic oil based plastic properties, which would require a portfolio of

different polymer systems. For these new systems, which must be renewable, there is an opportunity to tailor in other desirable properties such as biodegradability, and biocompatibility. One report has estimated the technical substitution of petrochemical based plastics by bio-based plastics to be 90%, demonstrating the applicability of such materials.[11] Examples of highly promising renewable polymers are PEF {poly(ethylene furanoate)}, PHAs (polyhydroxyalkanoates), PBS (polybutylene succinate) and PLA (polylactic acid).

PEF represents an alternative to PET based on ethylene glycol and 2,5-furandicarboxylic acid (FDCA), two renewable monomers. Compared to PET, PEF has superior gas sorption properties, as well as improved mechanical and thermal properties, specifically having a high modulus and high glass transition temperature (T_g).[16, 17] FDCA is also amenable to be employed in current PET production infrastructure and production has been shown to generate less greenhouse gas emissions.[18] PHAs represent a class of biodegradable bioplastics produced naturally by fermentation, an example of which is poly-3-hydroxybutyrate. There is great diversity in the structures of PHAs, with a range of aliphatic sidechains. For some PHAs, properties can be comparable to that of polypropylene (PP).[19] These bioplastics have been commercialised for a range of applications with biodegradation being a main driver to their development and use.[20] PBS has recently received more attention due to successful attempts to prepare bio-based succinic acid. One commercial example, BioPBS, from PTTMCC/Mitsubishi Chemical, highlight the ease of degradation as well as biocompatibility making it highly attractive for single use food packaging.[21]

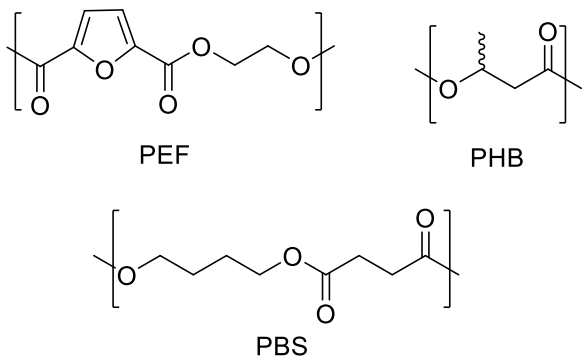

Figure 1.4 Structure of bio-based plastics PEF, PHB and PBS.

1.2 Poly(lactic acid)

Poly(lactic acid) meets the criteria of a renewable polymer. The monomer is lactic acid, or lactic acid based, which is an annually renewable feedstock derived from food crops as well as inedible food waste. It is crucial that the production of lactic acid does not consume edible feedstocks which would affect food resources and prices which would be highly undesirable. PLA has properties that make it amenable for a wide range of applications, having overlapping material properties with PS, PET and PP.[22-24] However, a relatively low T_g and low impact strength is a noted limitation.[25] PLA is also biocompatible and biodegradable as well as being amenable to recycling and industrial composting. Currently, PLA is a commercial bioplastic, being prepared on a 140,000 T scale by Natureworks.[26] Corbion Purac have also disclosed their intention to construct a PLA plant with the ability to produce 75,000 T per year.[27, 28] The production of this bioplastic is boasted to have a relatively low CO_2 footprint and this is anticipated to decrease leading to a carbon neutral material.[26, 29, 30] Despite these facts, there are still important challenges to be overcome in controlling the properties of PLA which will be detailed in the next sections.

1.2.1 Lactide: preparation and properties

PLA can be prepared directly through a polycondensation route, in which lactic acid molecules are condensed with the loss of a water molecule. This route is an equilibrium which is severely limited by the need to remove water. As a consequence, low molecular weights often result from this process, and this can be remedied by introducing chain coupling agents, increasing the cost of the process. Within this reaction mechanism, there is also no chiral control, if racemic lactic acid is used, and hence no control over resultant polymer microstructure.

Instead, it is more common to first prepare the lactic acid dimer, lactide. While this is not ideal, representing an additional step, hence financial and environmental cost, in the process to form plastics, better control and high molecular weight can be achieved by polymerising lactide. The preparation of lactide utilises oligomers from the condensation route which are depolymerised to form the new monomer at high temperature (150 - 250 °C) under reduced pressure in the presence of a catalyst (Figure

1.5). These conditions also produce epimerised products as well as oligomeric waste. Recently, an interesting development has been made to reduce the economic impact of this step.[31] The use of size selective catalysts in the form of zeolites provides the means to convert lactic acid directly into lactide under more facile conditions with less waste. Zeolite H-Beta gave the best results with 79% selectivity for the lactide dimer in the absence of epimerisation (Figure 1.5). Based on this pathway, a process scheme was suggested with the ability to recycle oligomers and solvent with reuse of the zeolite also shown to be viable.

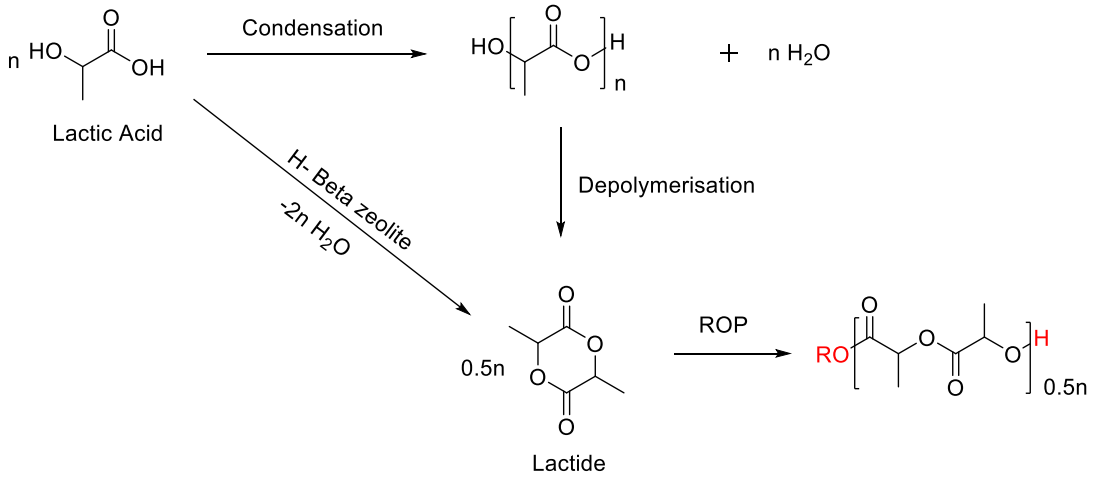

Figure 1.5: Routes towards lactide and PLA.

Lactic acid possesses chirality, leading to new stereoisomeric relationships on formation of the dimer. As a consequence, lactide has three stereoisomeric forms: *L*-, *D*- and *meso* (Figure 1.6). The enantiomers, *L*- and *D*- LA have a melting point of 97 °C. Combining these two forms causes an increase in melt temperature and a decrease on solubility due to co-crystallisation, giving a *rac*-LA blend with a melt temperature of approximately 130°C.[32] These structures provide a means to prepare polymers with different microstructures.

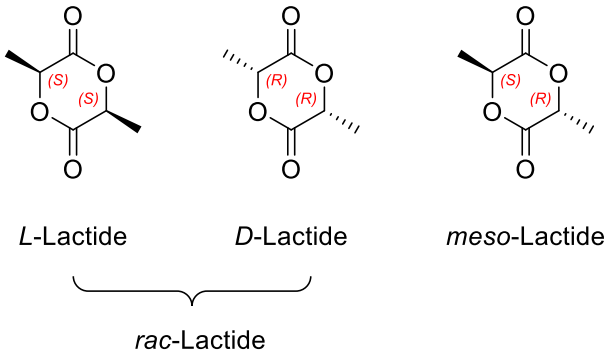

Figure 1.6: Stereoisomers of lactide.

1.2.2 Poly(lactic acid): structure and properties

The structure of PLA is made up of repeating lactic acid units regardless of the monomer used. The linkages are ester based, providing the handle for future polymer degradation. The relative orientation of the methyl groups adds another dimension to the structure of the polymer (Figure 1.7). The polymerisation of the chiral monomers, *L*-LA or *D*-LA, furnishes a homo-polymer, in which all methyl groups are pointing in the same direction (-*RR*- or -*SS*-) as dictated by the stereochemistry of the monomer. This is commonly referred to as isotactic PLA, PLLA or PDLA. The resulting thermal properties of isotactic PLA are enhanced relative to the other tacticities, being crystalline and having an increased melt temperature (T_m = 180 °C). The polymerisation of *meso* lactide can furnish atactic, heterotactic (-*RRSS*-) or syndiotactic (-*RS*-) PLA; highly syndiotactic PLA has been shown to be semi-crystalline (T_m = 152 °C).[33] The microstructures derived from the polymerisation of *rac*-LA are equally numerous and also rely on a form of stereocontrol being exerted over the reaction. Heterotactic PLA results when alternating units of *L*- and *D*- are incorporated into the polymer chain leading to a -*RRSS*- linkages. Atactic PLA describes the random distribution of *L*- and *D*- monomers giving a polymer with no chiral control. The latter tacticities are observed to be amorphous having a glass transition of 45 °C. Isotactic PLA can also be prepared from *rac*-LA as a block copolymer {$(SS)_n$-$(RR)_n$} or separate homopolymers. When highly isotactic PLLA and PDLA, as two homopolymers or block co-polymers, are mixed under the right conditions, a stereocomplex can form. This stereocomplexation is the result of a strong

interactions between the two different chiralities and improves mechanical and thermal properties of the resultant polymer ($T_m \leq 230$ °C).[34]

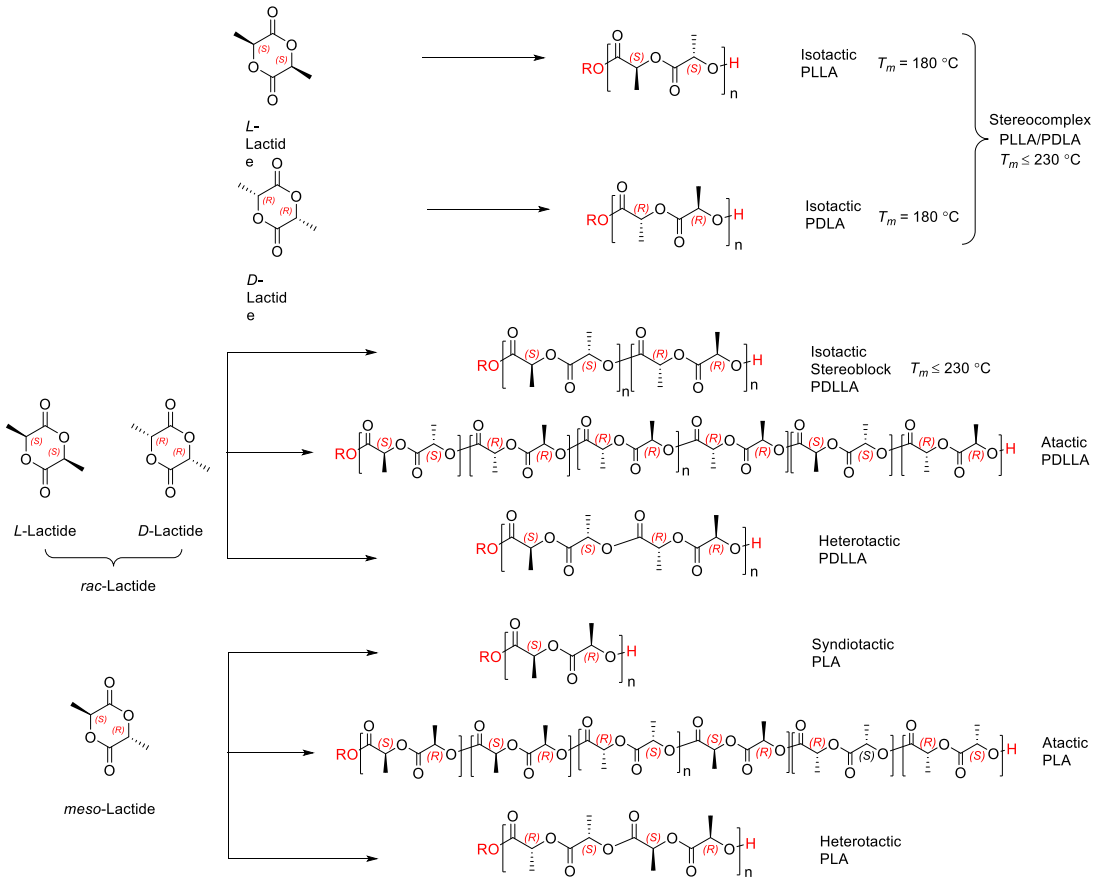

Figure 1.7: Possible microstructures on polymerisation of *L*-, *D*-, *rac*- and *meso*-LA (Adapted from Coates *et al.*[35]).

1.2.3 Polymerisation pathways

There are a range of methods to achieve the ring opening polymerisation (ROP) of the lactide monomer. The exact mechanism is dependent upon the nature of the reagents used. The general subdivisions are cationic, anionic, organocatalytic, activated monomer and coordination insertion.

The anionic polymerisation of LA was part of early investigations into lactide polymerisation. This mechanism involves the attack of a nucleophile at the lactide carbonyl group, causing acyl-oxygen bond cleavage. The polymeryl anion that is

generated can then propagate the polymerisation (Figure 1.8). Due to the nature of the anionic nucleophiles, to achieve a controlled polymerisation, lower temperatures are sometimes required to reduce the extent of epimerisation.[36-38]

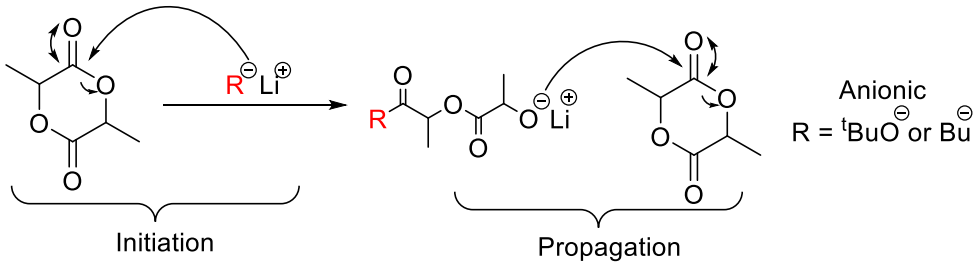

Figure 1.8: General mechanism for anionic ROP.[36-38]

Cationic polymerisation involves the activation of the lactide unit with a proton (or alkyl group) which makes the monomer more susceptible to attack of an acid counterion (Figure 1.9). Attack in this mechanism occurs at an sp^3 carbon centre leading to alkyl-oxygen bond cleavage. Propagation occurs when the ring opened monomer proceeds to open another protonated monomer. The optimum temperature for this reaction was found to be 50°C, and both trifluoromethanesulfonic acid and methyl triflate were found to be efficient for this mechanism.[39, 40]

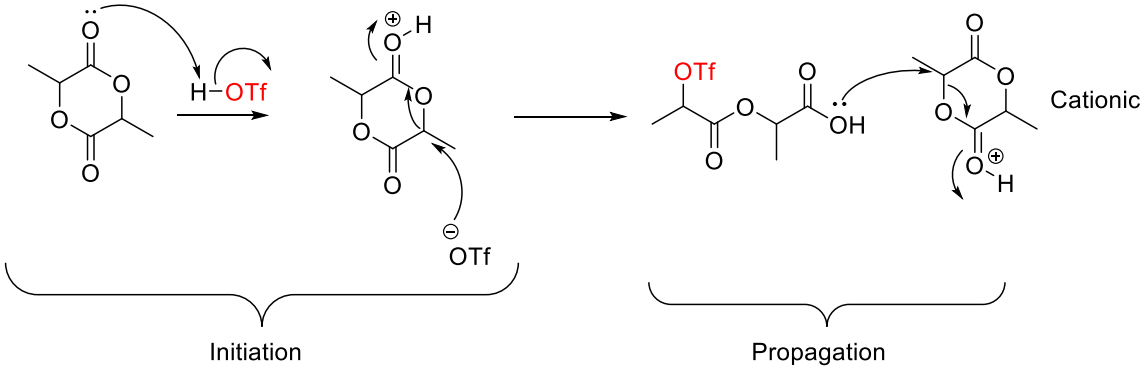

Figure 1.9: General mechanism for cationic ROP.[36, 39, 40]

Organocatalytic polymerisation generally involves the initial ring opening step to be achieved by a neutral organic molecule. Once opened, the nucleophile group can be readily displaced by a co-initiator, typically an alcohol (Figure 1.10). In some cases, the organocatalyst may be incorporated into the polymer as the chain end. Organocatalysis is a popular route for polymerisation as it yields metal-free polymer

with high activity in solution at room temperature. Recent examples of organocatalytic polymerisation highlight the use of carbenes, guandines (TBD), amidines (DBU) and thioureas.[41-45]

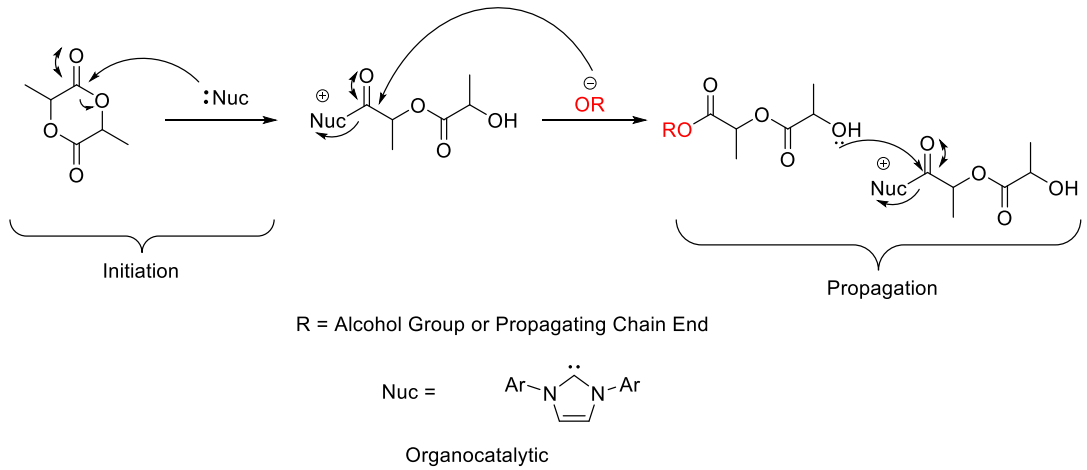

Figure 1.10: General mechanism for organocatalytic ROP. [32, 41-45]

The most widely reported ROP mechanism is the so-called coordination-insertion process.[36] This requires a Lewis acid site that acts to activate the carbonyl group to attack *via* coordination of the latter. The ring opening event is achieved by the insertion of a labile group upon the metal centre into the carbonyl bond of the lactide. A four membered transition state is expected for the insertion step (Figure 1.11). The inserting group is typically an alkoxide. Following this initiation step, the ring opened product remains bound to the metal centre and is able to insert into an incoming monomer to propagate the polymerisation. Due to the fact that the polymer remains attached to the metal, good weight and stereocontrol can often be achieved by this mechanism.

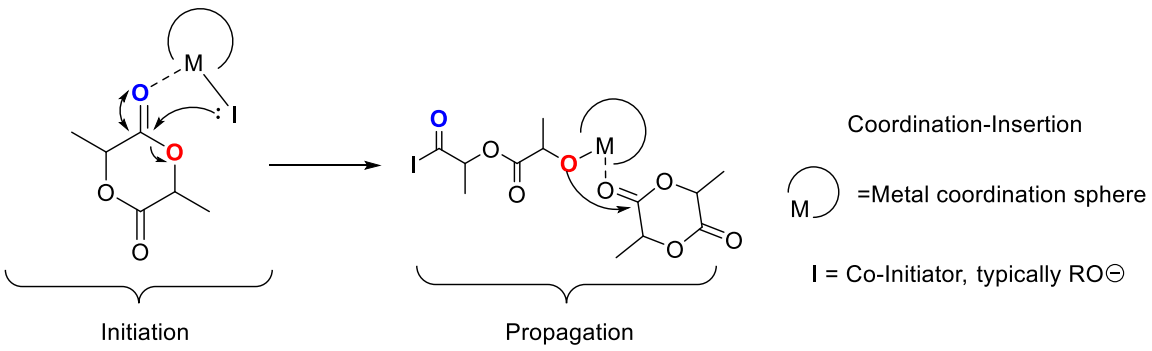

Figure 1.11: General mechanism for coordination-insertion ROP.

Within the coordination-insertion mechanism there are two different pathways to achieving stereocontrol. A chain end mechanism (CEM) is often cited as the pathway of stereocontrol for an achiral initiator.[46-48] In this mechanism, the last inserted lactide in the polymer chain dictates the next monomer insertion. For an isoselective initiator, this would imply there is a preference for enchainment of the same monomer chirality each time. A mis-insertion of the "wrong" monomer, in this case, would change the preference of the initiator and enchainment of the new monomer would follow. In this way, stereoblocks of *L*- and *D*- would result (Figure 1.12). Typically, CEM can be deduced from the relative rate constants for the polymerisation of *L*- or *D*-LA. For an ideal system, the enchainment of both lactide enantiomers would be equal, leading to equal rates of polymerisation. For a heterotactic PLA, the CEM would operate with preferential insertion of the opposing monomer chirality, leading to a -*RRSS*- repeat unit. As a consequence of this enchainment preference, the polymerisation rate for *rac*-LA is expected to be faster than that of *L*- or *D*-LA.

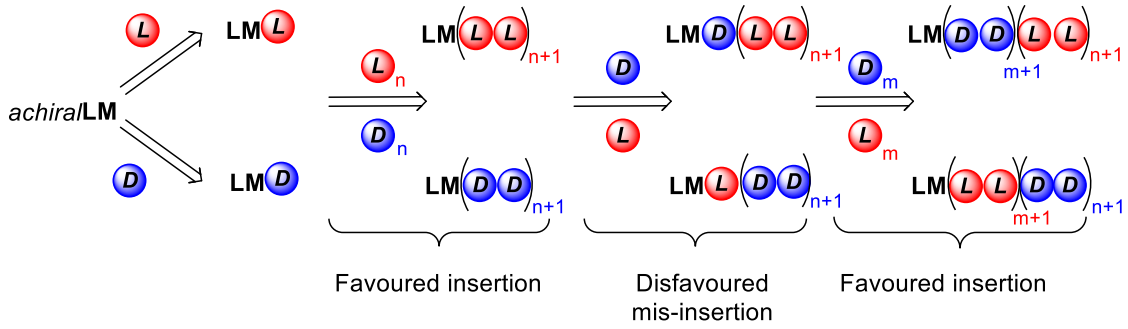

Figure 1.12: Propagation of an isoselective polymerisation controlled by CEM. Each sphere represents a lactide unit (Adapted from Nomura *et al.*[47]).

In contrast, chiral initiators can also propagate *via* an enantiomorphic site control mechanism (SCM). In this situation, the initiator has an initial chiral preference for the incoming monomer unit and this is fixed throughout the polymerisation. Physically, this manifests as a faster polymerisation rate of either *L*- or *D*-LA, leading to preferential consumption of one monomer over the other, assuming an enantiopure initiator (Figure 1.13). This can also cause conversions to be limited to 50% depending on the extent of the rate mismatch. A mis-insertion for this mechanism can hinder the polymerisation rate and cause microstructural defects that are observable by NMR spectroscopy. On the application of a racemic initiator, higher conversions are

achievable due to the preferential consumption of each monomer by the corresponding initiator enantiomer (Figure 1.14). On the event of a mis-insertion, a correction can be realised *via* the exchange of polymers between initiators of opposite chirality.[49, 50] This also produces stereoblock PLA. However, the use of *rac*-initiators can reduce the overall stereocontrol due to polymer exchange mechanism reducing the length of isotactic blocks.

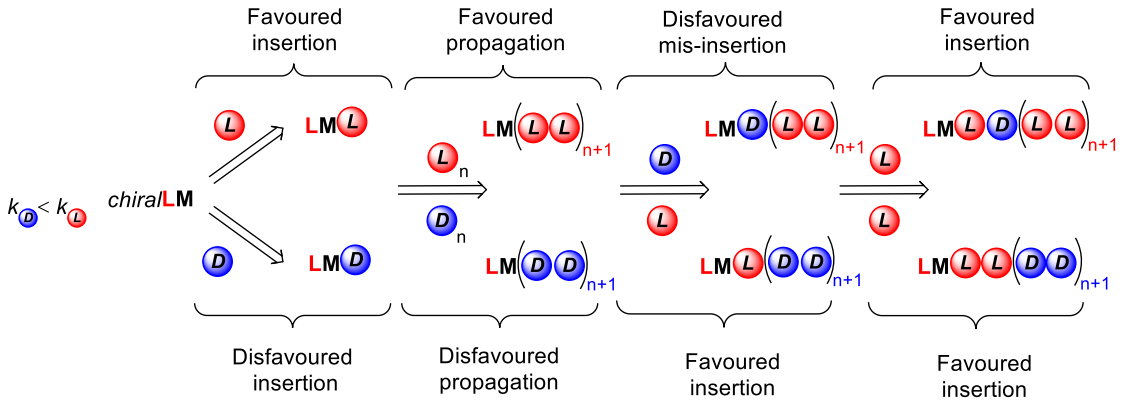

Figure 1.13: Propagation of a polymerisation controlled by SCM for an enantiopure initiator (Adapted from Nomura *et al.*[47]).

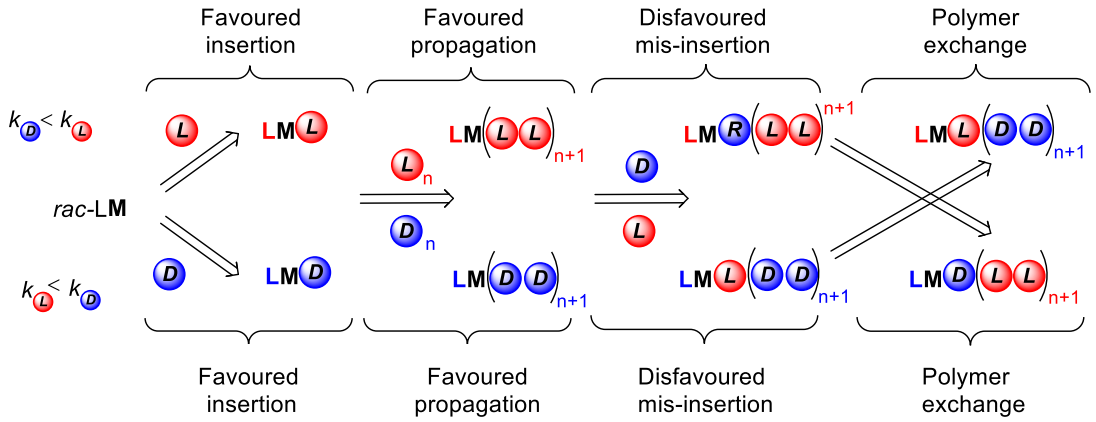

Figure 1.14: Propagation of a polymerisation controlled by SCM for a racemic initiator (Adapted from Nomura *et al.*[47]).

A variation to the coordination insertion mechanism is an activated monomer mechanism. This pathway involves the same activation of the carbonyl oxygen *via* a coordinative interaction to a metal centre but the distinction comes on the attack of the co-initiator. Instead of being within the metal coordination sphere, the ring opening

attack occurs with no involvement of the metal other than the activation (Figure 1.15). In cases without a co-initiator, the ring opening step can be achieved by the insertion of a ligand group ultimately yielding a cyclic structure (Figure 1.16). This structure can be opened by protonolysis. The activated monomer mechanism often applies for coordinatively saturated complexes with no labile groups for insertion[51, 52] or inert groups.[53]

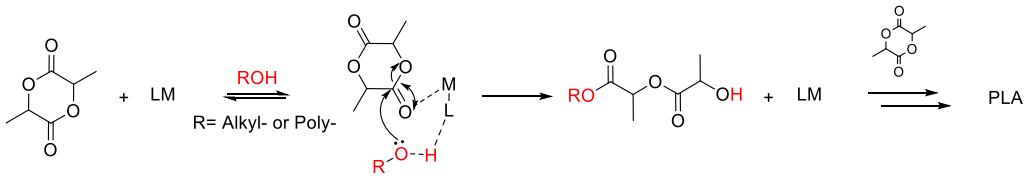

Figure 1.15 Activated monomer mechanism in the presence of co-initiator.[51]

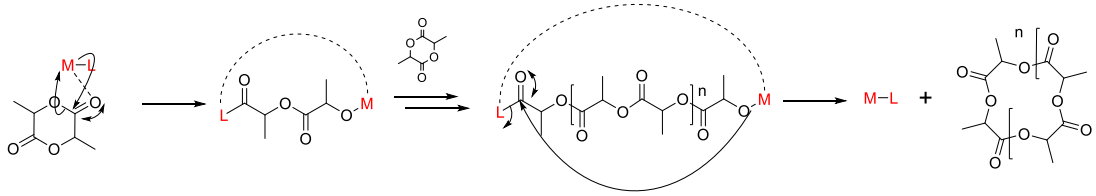

Figure 1.16: Activated monomer mechanism in the absence of co-initiator.[52]

Polymerisations may be described as “living” if certain criteria are met. A living polymerisation describes the linear growth of polymer chains/weight yielding a narrow distribution of sizes. This is achievable when the rate of initiation is much faster than that of propagation. In this pathway, the resultant molecular weight of the polymer is predictable by the ratio of monomer to initiator (Figure 1.17). The addition of extra monomer to a living polymerisation will facilitate further polymerisation. In this scenario, polymerisation is only terminated by the addition of chain terminator such as an alcohol. This mechanism is in contrast to “immortal” polymerisation. An immortal polymerisation describes an initiator’s ability to maintain activity despite the addition of excess alcohol and is therefore related to robustness. The alcohol acts as an efficient chain transfer through rapid alkoxide exchange at the metal centre and increases the amount of polymer chains (Figure 1.17). When the exchange at the metal centre is sufficiently fast, a narrow distribution of chains is still anticipated and the

ratio of monomer-to-alcohol becomes the decisive factor in predicting molecular weight.

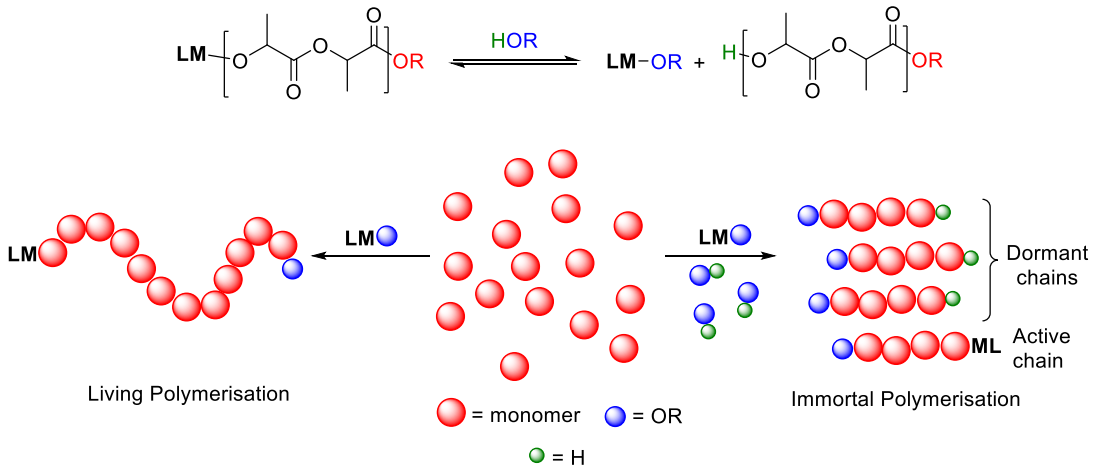

Figure 1.17: Alkoxide exchange at metal centre (top) and living and immortal polymerisation schemes (bottom).

The ROP of LA is also subject to side reactions which can typically occur regardless of the propagation pathway. The extent of these reactions depends on many factors including the nature of the catalysis and also the temperature of the polymerisation. Higher temperatures favour transesterification reactions, which can scramble polymer stereochemistry as well as increase chain moleculer weight distribution. It is a challenge, therefore, to design initiator systems that are capable of carrying out ROP at high temperatures with a low susceptibility to these detrimental reactions. There are two main types of transesterification for a coordination-insertion mechanism, for which the metal centre is involved. Intermolecular transesterification involves the insertion of a growing polymer chain (Figure 1.18, Blue) into the carbonyl group of a second chain (Figure 1.19, Red). This produces a lengthened polymer chain as well as a shortened polymer fragment. Both of which can continue propagation after this transesterifcation event. A second mechanism is transesterifcation *via* intramolecular attack. In this side reaction, the active polymer chain end inserts or “back bites” into the same chain leading to a cyclic product as well as a shorter polymer fragment. The number of active centres is unchanged by either route.

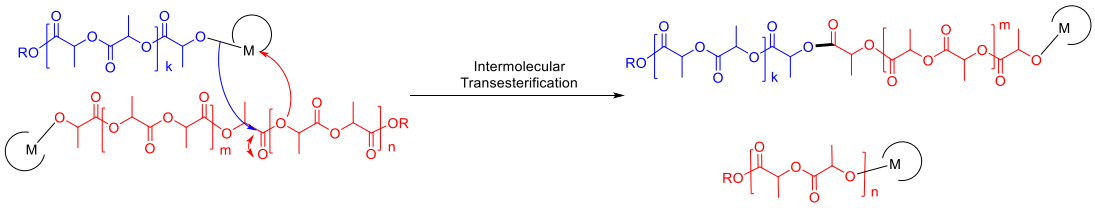

Figure 1.18: Mechanism for intermolecular transesterification.[54]

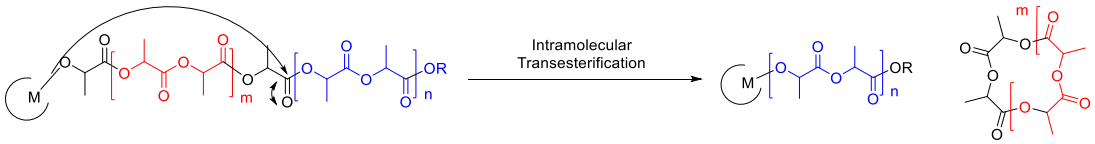

Figure 1.19: Mechanism for Intramolecular Transesterification.[54]

1.3 Polymer characterisation methods

1.3.1 NMR spectroscopy

The conversion of monomer to polymer is assessed by ^{1}H NMR spectroscopy, usually by comparison of the methine region (~5 ppm) of the polymer and unreacted monomer. In some cases, it is also possible to use ^{1}H NMR spectroscopy to assign end groups and estimate chain length based on the ratio of polymer to end group signals. The determination of polymer microstructure is also achieved by ^{1}H NMR *via* homonuclear decoupling. Removal of the coupling between the methine and methyl region simplifies the former region to a series of singlets rather than quartets (Figure 1.20). The singlets are related to the different combinations of stereochemical connections in the polymer chain, and describe a series of four lactyl units or tetrads (Figure 1.21). The relative stereochemistry of two adjacent units is labelled *i* or *s* for isotactic and syndiotactic relationships respectively. For the polymerisation of *rac*-LA, without epimerisation or transesterification events, five tetrads are possible {*iii*, *isi*, *sis*, *sii* and *iis*}. The polymerisation of *meso*-LA afford different relationships {*sss*, *ssi* and *iss*}. Tetrad assignment, for both ^{1}H and ^{13}C{^{1}H} NMR spectroscopy, has been elucidated by the using 2D heteronuclear NMR experiments.[55] The relative integration of these tetrads is related to polymer microstructure *via* Bernouillian

statistics (Table 1.1).[56] This analysis affords P_r, the probability of heterotactic enchainment, and P_m, the probability of isotactic enchainment (Table 1.2); the sum of these probabilities is equal to 1. Further information on polymerisation mechanism, relating to the operation of SCM or CEM, may also be derived from closer examination of the relative intensities of each tetrad.

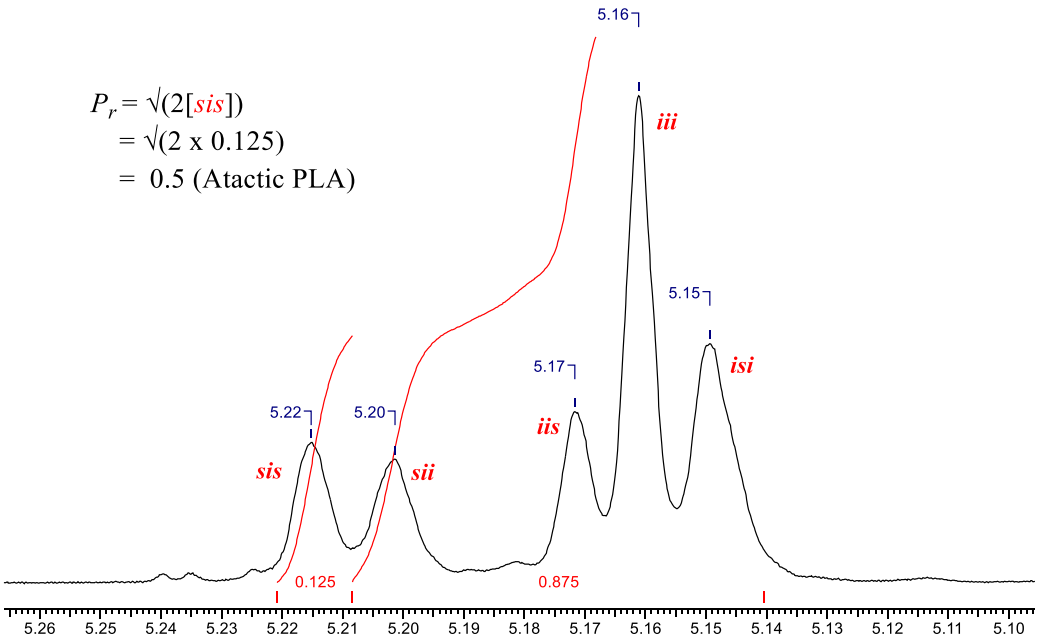

Figure 1.20: Homonuclear decoupled ^{1}H NMR spectrum of atactic PLA derived from *rac*-LA.

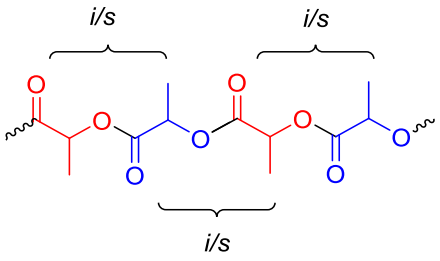

Figure 1.21: Tetrad of PLA with possible stereochemical relationships.

Table 1.1: Relation of tetrads to P_r/P_m for polymeriation of *rac*-LA.

Tetrad	Probability
[*iii*]	$P_m^2 + P_rP_m/2$
[*iis*]	$P_rP_m/2$
[*sii*]	$P_rP_m/2$
[*sis*]	$P_r^2/2$
[*isi*]	$(P_r^2 + P_rP_m)/2$

Table 1.2: Assignment of polymer microstructure based on P_r and P_m for polymeriation of *rac*-LA.

P_r	P_m	Microstructure
$0.5 < P_r \leq 1$	$0 \leq P_m < 0.5$	Heterotactic
$0 \leq P_r < 0.5$	$0.5 < P_m \leq 1$	Isotactic
$P_r = 0.5$	$P_m = 0.5$	Atactic

1.3.2 GPC and MALDI-ToF

The molecular weight of polymers is typically acquired from gel permeation chromatography (GPC). This characterisation technique separates polymer chains based on size and is known a size exclusion chromatography (SEC). Separation is achieved through passing a polymer sample through a column containing porous microbeads. The smaller molecules are able to diffuse into the beads which leads them on a more circuitous, lengthened path which causes a slower elution. In contrast, larger molecules cannot pass through these beads affording faster elution. There are a range of detection methods available for analysing the GPC eluent, the most common being refractive index (RI). RI detection is based on changes in refractive index relative to a cell of pure solvent. Responses in this parameter are calibrated to a range of narrowly distributed samples, typically polystyrene (PS). When detecting polymers different to PS it is important to note that the acquired molecular weight is not absolute as solvent effects mean polymers can have different sizes in solution. A correction factor of 0.58 is often applied to molecular weights of PLA acquired against PS standards.[57] Other detectors are available to allow for the evaluation of absolute molecular weight. Light scattering (LS) relies on the scattering radiation by a polymer chain with a change in intensity. Measurement of the intensity of scattered radiation can be related to molecular weight and it is not necessary to use external calibrants. The angle of

measurement is important and multi angle measurements are often used to achieve more accurate results. Viscometry also allows for the evaluation of accurate molecular weights *via* the plotting of a universal calibration curve. The molecule size measured by standard GPC elution is converted to molecular weight by measuring the intrinsic viscosity (IV) of a sample.[58] Further to this, a Mark-Houwink plot {log(IV) vs log(M_w)} can give structural information. The use of triple detection uses all of these responses to more precisely determine the molecular weight and is particulary suited to the characterisation of new materials.

A complementary technique for analysing molecular properties of a polymer is matrix-assisted laser desorption/ionisation time of flight (MALDI-ToF) mass spectrometry. This involves the mixing of a polymer sample with a suitable matrix and ion source which assist with the ionisation and charging respectively. The mass of the ions is determined by the time taken to reach the detector. From this method, the mass and the distribution of the chain lengths can be determined. The resolution of MALDI-ToF is such that individual chain masses can be quantified accurately. From the distribution the monomer repeat unit is readily assessed. The chain ends can also be assessed which can give important information on the polymerisation mechanism and the extent of side reactions. A limitation of this method is the need to ionise the polymer chains and for these to also be susceptible to an electric field. As a consequence of this, the observed spectrum is not necessarily representative of the polymer sample and there is a maximum molecular weight that can be analysed.

1.3.3 DSC

Differential scanning calorimetry allows for the calculation of the thermal properties of polymer samples. The experimental set up involves the heating of a reference and sample and comparing the difference of heat flow required to attain the same temperatures. These differences relate to phase changes of the sample allowing for the evaluation of glass and melting transitions, T_g and T_m as well as the crystallisation temperature, T_c.

1.4 Stereoselective initiators for LA ROP

For many years, there has been strong interest in the application of tin octanoate {$Sn(Oct)_2$} to the ROP of *L*-LA. There have been several studies into the activity and mechanism of this system,[59-65] highlighting good activity and furnishing high molecular weight under industrial conditions (180 – 210 °C, [$Sn(Oct)_2$] = 100-1000 ppm).[10, 32] The mechanism has been shown to be coordination-insertion, generally carried out in the presence of a co-initiator (Figure 1.22).[59] As $Sn(Oct)_2$ is amenable to immortal polymerisation conditions, is commercially available, robust and cheap, it is currently the industrially preferred initiator. However, there are disadvantages to the use of tin octanoate. Despite $Sn(Oct)_2$ being approved as a food additive by the US FDA, there are concerns surrounding the toxicity of related Sn(IV) compounds, particularly for biocompatible PLA applications.[36, 66] Further to this, $Sn(Oct)_2$ does not afford any stereocontrol towards the polymerisation of *rac*-LA hence not being able to access different microstructures to afford enhanced polymer properties.

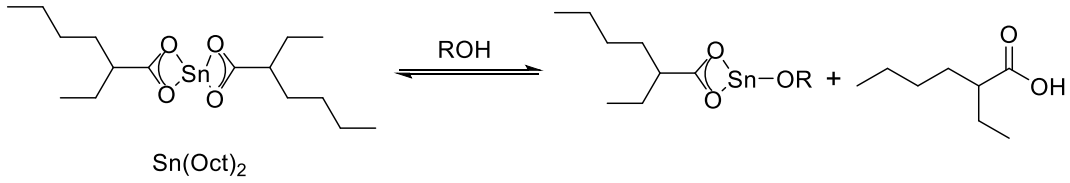

$Sn(Oct)_2$

Figure 1.22: $Sn(Oct)_2$ structure and alkoxide exchange equilibria to generate active species.

Indeed, there is a lack of stereoselective Sn(II) initiators in the literature, despite reports of heteroleptic complexes applied to the polymerisation of *rac*-LA.[67, 68] A series of a heteroselective Sn(II) initiators has however been realised by Dove *et al* (Figure 1.23).[69, 70] The ligand set, **1**H, featured a range of *β*-diketiminate (BDI) structures with variation in the aryl substituents. Polymerisation of *rac*-LA was carried at 60 °C in toluene with reaction times being on the order of hours (1.5 – 8 hours). An induction period was observed for each initiator studied which is related to the Sn(II) lone pair. This lone pair is suggested to hinder lactide coordination by posing geometric constraints and causing electron repulsion. An enhancement of rate was generally observed for electron withdrawing halo substituents and for all initiators, similar heteroselectivity was afforded (P_r = 0.62 – 0.67).

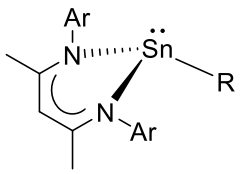

Sn(**1**)R

R = O^{i}Pr or NMe_2

Ar = 2,6-$^{i}Pr_2C_6H_3$
2,6-$Me_2C_6H_3$
2,6-ClC_6H_3
2,6-$Br_2C_6H_3$
2,4,6-ClC_6H_3
2,4,6-$Br_2C_6H_3$
C_6H_5

Figure 1.23: Sn(II) complexes based on a series of BDI ligands. [62, 63]

1.4.1 Group I initiators

Group I metals, especially Na(I) and K(I), are attractive for PLA production as they are biocompatible and abundant. While often cited as highly active,[71-77] stereocontrol is less common and often achieved under undesirable conditions, e.g. low temperatures. The nature of Group 1 metal initiators are often multinuclear, with bulky ligands required to furnish mononuclear forms. [51, 71-73, 76, 78-80] In the simplest of cases, Kasperczyk has demonstrated the application of LiO^{t}Bu to yield heterotactic PLA.[38] This was achieved at 20 °C with a 60 minute reaction time. A degree of heterotacticity was realised with BuLi as the initiator.[37]

Wu *et al* have reported a series of alkali monophenolate systems for the stereocontrolled polymerisation of *rac*-LA.[81-85] The use of 2,6 – dixanthenylphenol (**2**H) is sufficient to prepare mononuclear sodium and potassium complexes in conjugation with a crown ether (Figure 1.24). For this system, the active metal centre is said to be sandwiched between two planes imposed by the ether and ligand system which increases the catalytic interaction.[82] At room temperature ([LA]:[M]:[BnOH] = 100:1:1), high conversion is observed for both metals with a reaction time of 10 minutes. There is an isotactic bias observed for all conditions/initiators tested (P_m > 0.62) and this was shown to be enhanced by polymerisation at 0 °C (K(**2**){18-crown-6}, P_m = 0.82, T_m = 166 °C).

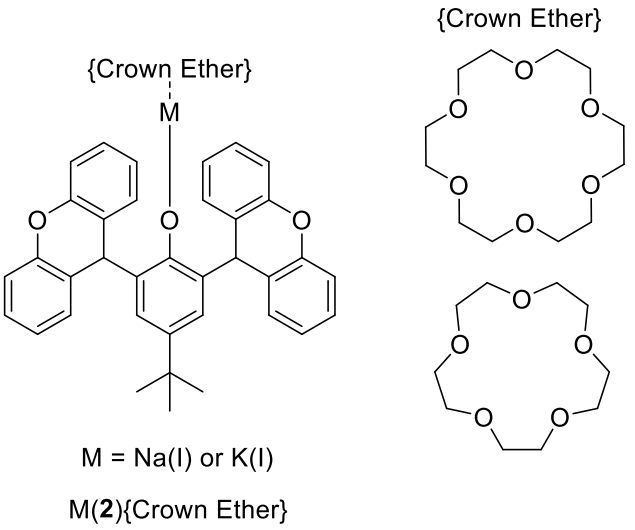

Figure 1.24: Na(I) and K(I) monophenolates initiators employed by Wu *et al*.[82]

In a subsequent investigation, a bulkier xanthenyl group was employed in one *ortho* position with the remaining *ortho* and *para* positions being occupied by ^{t}Bu groups (Figure 1.25).[83] Mono-ligated species, M(**3**) were also isolated and tested for their activity in the ROP of *rac*-LA. Both M(**3**) and M(**3**){Crown Ether} were shown to be active for polymerisation, achieving high conversion within 10 minutes at -60 °C. Stereocontrol exerted by both types of initiators was found to be isotactic (P_m = 0.63-0.86, T_m = 182 °C). Interestingly, a slower reaction was observed at room temperature.

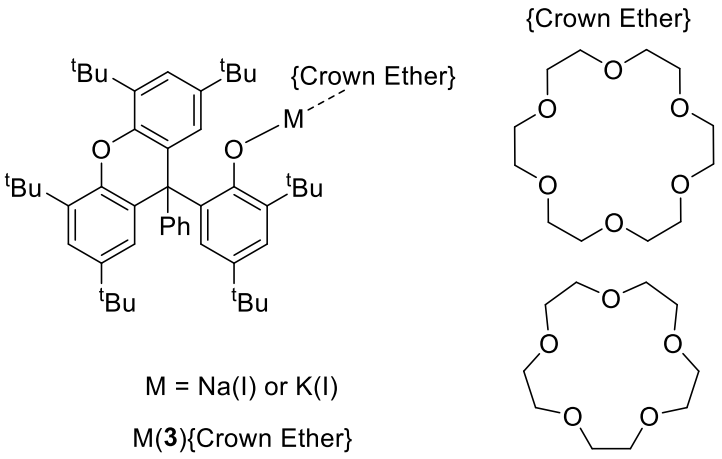

Figure 1.25: Na(I) and K(I) monophenolates initiators employed by Wu *et al.* [83]

More recently, Wu *et al* have utilised an *ortho* trityl group to furnish initiators M(**4**){crown ether} (Figure 1.26) .[84] The remaining *ortho* position was either unsubstituted or featured a ^{t}Bu and the *para* position was also varied. Once more, an

isotactic tendency is revealed at room temperature (P_m = 0.62 - 0.77) and further enhancement was achieved *via* reaction at -60 °C (P_m = 0.89, T_m = 187.8 °C). Replacing the trityl group with an anthryl, while maintaining the other substituents, also furnished an initiator capable of the isoselective polymerisation of *rac*-LA.[85] In this study, the highest isoselectivity for an alkali-metal initiator was achieved at -70°C (P_m = 0.94, T_m = 192.5 °C). While these results reflect an excellent degree of control, the conditions employed (solution, < 0 °C) are energetically impractical for industrial use.

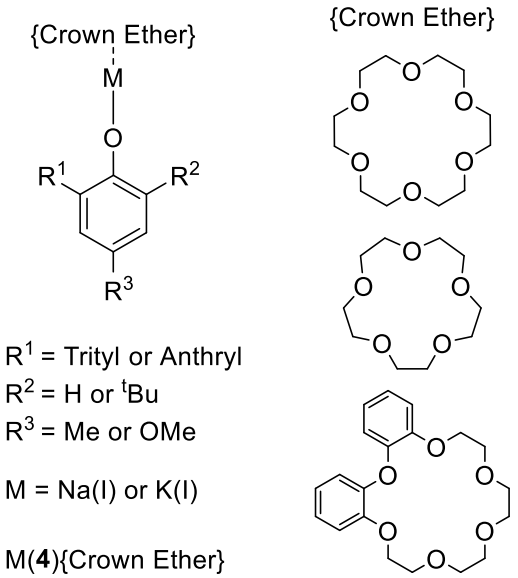

Figure 1.26: Na(I) and K(I) monophenolates initiators employed by Wu *et al.* [84,85]

1.4.2 Group II initiators

Group II metal based initiators are often characterised by their high activity towards the ROP of LA which is typically related to their high Lewis acidity. The majority of reports concern the application Mg(II) with Ca(II) initiators being less common. Due to a similar charge and valency, Zn(II) is often reported and contrasted with Group II metals. The stereochemical preference of Group II initiators is typically heteroselective, but there are exceptions to this and the choice of solvent can often be a determining factor.[86, 87] There are many examples of Mg(II),[52, 74, 88-91] Ca(II),[88-90, 92-94] and even Sr(II)[93-95] initiators that furnish atactic PLA or are applied to the ROP of *L*-LA only.

β-diketiminate ligands have been applied to Mg(II) on several occasions with extensions towards Ca(II).[35, 96-101] Initial investigation carried out by Coates *et al* compared Zn(II) and Mg(II) systems, with ^{i}Pr groups at the 2-6 position of the aryl rings (Figure 1.27).[35] Initially, the monomeric silylamido complex, Mg(**5**)N(SiMe$_3$)$_2$, was prepared and upgraded to an alkoxide bridged dimer [Mg(**5**)O^{i}Pr]$_2$. Despite being highly active for the ROP of *rac*-LA (CH_2Cl_2, 20 °C, 1 - 5 minutes), no stereocontrol was exerted by this initiator. In a follow up study, Chisholm *et al* prepared a monomeric alkoxide version, Mg(**5**)O^{t}Bu, using the bulkier ^{t}BuO to achieve this.[97] Similar polymerisation results are reported for this initiator compared with [Mg(**5**)O^{i}Pr]$_2$. Intriguingly, changing the solvent to THF afforded highly heterotactic PLA (P_r = 0.90) with a slightly extended reaction time of 5 minutes. The difference in result is attributed to the coordination of a THF molecule to the Mg(II) centre leading to more sterically hindered active site. This system has recently been probed more thoroughly *via* NMR and simulation studies. The associative and dissociative behaviour of THF was explored as well as the rotations of the aryl groups.[102] A comparison has been made between the related complexes Mg(**5**)N(SiMe$_3$)$_2$ and Ca(**5**)N(SiMe$_3$)$_2$, both of which are observed to be monomeric in the solid state.[100] The magnesium complex demonstrates similar reactivity to the previously discussed *t*-butoxide species, requiring 5 minutes to reach high conversion and furnish heterotactic PLA in THF. The calcium analogue only provides atactic PLA under the same conditions, with a 2 hour polymerisation time. The difference is attributed to the less defined Ca(II) species that result during ROP due to the larger metal radius.

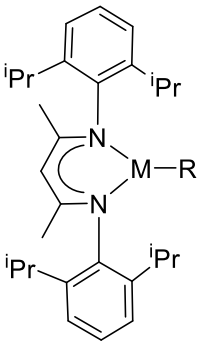

R = N(SiMe$_3$)$_2$ or O^{t}Bu
M = Mg(II) or Ca(II)

M(**5**)R

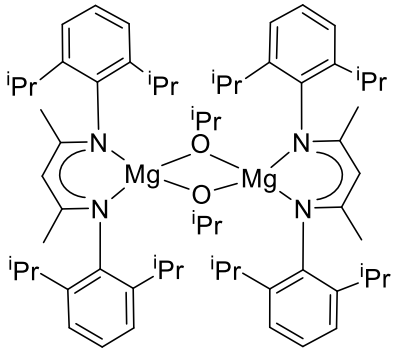

[Mg(**5**)O^{i}Pr]$_2$

Figure 1.27: Group (II) BDI initiators.[35, 96-100]

A further study was carried out, investigating the effect of aryl ether groups on the complex structure and ROP.[96] A five coordinate complex is realised on preparation of the silyl amido species, yielding Mg(**6**)N(SiMe$_3$)$_2$ (Figure 1.28). However, bis-ligated ([Mg(**6**)$_2$]) and bridged *t*-butoxide ([Mg(**6**)O^{t}Bu]$_2$) forms were also realised in this study. On the application of the alkoxide to the ROP of *rac*-LA, atactic PLA was afforded through reaction in CH_2Cl_2. However, carrying out the polymerisation in THF improved the stereocontrol, instead furnishing heterotactic PLA (P_r = 0.85). Once again, coordination of a THF molecule is anticipated to make the Mg(II) centre more congested, allowing for increased control. There is also competition for coordination due to the potential to association and dissociation the methoxy groups. This ligand modification reduces the activity of the initiator, with 90 minutes being required to attain high conversion.

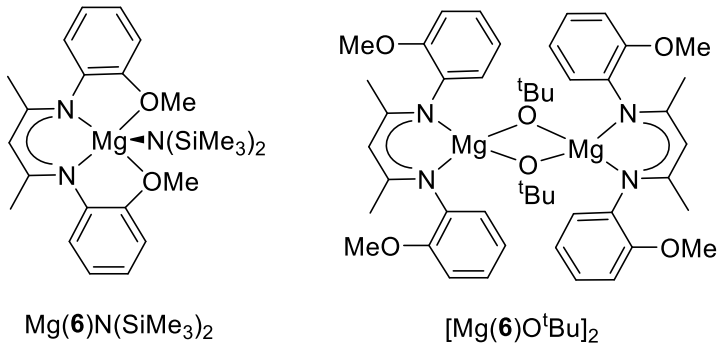

Mg(**6**)N(SiMe$_3$)$_2$ [Mg(**6**)O^{t}Bu]$_2$

Figure 1.28: Further Mg(II) BDI initiators employed by Chisholm *et al.*[96]

As a comparison to the *β*-diketiminate system, Chisholm *et al* have prepared a pyrromethane based ligand **7**H (Figure 1.29).[103] The resultant complex was deemed to be more sterically hindered compared to Mg(**5**)R and less susceptible to the Schlenk equilibrium. On the application of Mg(**7**)^{n}Bu{THF} to the ROP of *rac*-LA, high activity was realised, with strong heterotactic bias in THF (1.5 minutes, P_r = 0.94). Notably, the pyrromethane based complex maintains a degree of heteroselectivity in CH_2Cl_2 (P_r = 0.79). These results are competitive with the corresponding Zn(II) complex.[104] The demonstration of stereoselectivity in CH_2Cl_2 contrasts to the Mg(II) *β*-diketiminate complex, Mg(**5**)R, which can only facilitate the preparation of atactic PLA (P_r = 0.56) in the same solvent. This difference is said to implicate THF in the transition state of Mg(**5**)R.

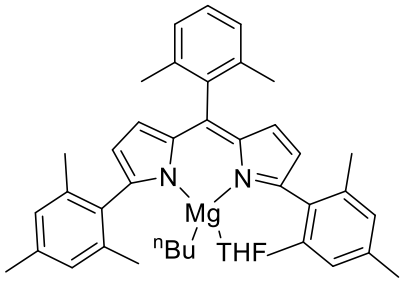

Mg(**7**)^{n}Bu{THF}

Figure 1.29: Pyrromethane based Mg(II) initiator employed by Chisholm *et al.* [103]

Examples of stereocontrol being induced by Ca(II) initiators have been demonstrated by Chisholm *et al*.[99, 100] The ligands used in this study were based on bulky tris-pyrazolyl borates, yielding single site calcium initiators Ca(**8**-**9**)R (Figure 1.29). Typically, high conversion of *rac*-LA was achieved within 5 minutes at room temperature (THF, 200:1). Best results were achieved with the ^{t}Bu substituted pyrazolyls which afforded highly heterotactic PLA after 1 minute (P_r = 0.90).

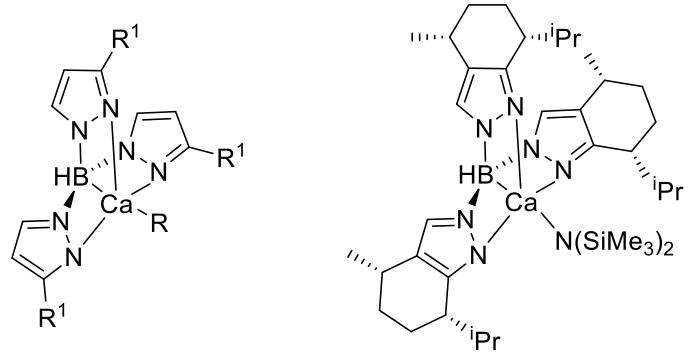

R = $N(SiMe_3)_2$ or O-2,6-$iPr_2C_6H_3$
R^1 = ^{t}Bu or ^{i}Pr

Ca(**8**)R

Ca(**9**)$N(SiMe_3)_2$

Figure 1.29: Tris-pyrazolyl Ca(II) initiators employed by Chisholm *et al.*[99, 100]

Ma *et al* have applied chiral aminophenols to Mg(II), preparing diastereomeric mixtures, Mg(**10**)$N(SiMe_3)_2$ (Figure 1.30).[105, 106] The preparation of complexes containing an *ortho* trityl (R^2 = trityl) substituents yielded a 7:1 ratio of diastereomers regardless of pyrrolidine nitrogen substituents (R^3). Both ligand chiralities were employed when this group was butyl (R^3 = ^{n}Bu), furnishing two complexes with an enantiomeric relationship. As initiators for the ROP of *rac*-LA, these complexes had

identical activities and stereocontrol, furnishing heterotactic PLA after 25 minutes (toluene, $P_r = 0.78$).[105] Unlike previous examples, switching to a coordinating solvent only acted to decrease the stereocontrol. Increasing the chain length of the N-substituent ($R^3 = {}^n$Octyl) afforded similar stereocontrol but increased the reaction time to 40 minutes. An unusual example of isoselectivity is also exhibited by this family of complexes. Reduction of the steric bulk of the aryl substituents ($R^1 = R^2 =$ Me) allowed for an almost equal ratio of diastereoisomers to be isolated.[106] The ROP of *rac*-LA was shown to be readily facilitated by this complex, requiring minutes to attain high conversion, even at low initiator loading ([LA]:[Mg] = 1000:1). Moderate isoselectivity results from the polymerisation in toluene at room temperature (P_m = 0.67).

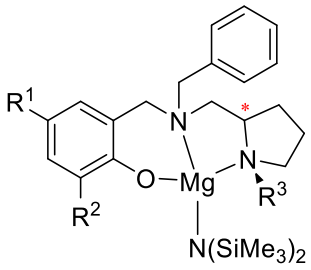

R^1 = Me, R^2 = Trityl, $R^3 = {}^n$Bu (*S* or *R*)
$R^1 = R^2$ = Me, $R^3 = {}^n$Bu (*S*)
R^1 = Me, R^2 = Trityl, $R^3 = {}^n$Octyl (*S*)

Mg(**10**)N(SiMe$_3$)$_2$

Figure 1.30: Chiral aminophenolate Mg(II) complexes employed by Ma *et al.*[102, 103]

Yi and Ma have also prepared Group 2 achiral iminophenolates for the ROP of *rac*-LA (Figure 1.31).[107, 108] Each of these ligands has a pendant aryl donor group which is observed to coordinate to the metal under certain circumstances. A stronger preference for coordination was observed for a methoxy donor group, which allowed the preparation of four coordinate metal centres in each case. The coordination of the dimethyl amine group was found to be less favourable with bulky substituents requiring a THF molecule to stabilise an otherwise three coordinate Mg(II) centre. Relatively small, electron withdrawing groups favoured the formation of a dinuclear phenoxy bridged complex, [Mg(**12**)N(SiMe$_3$)$_2$]$_2$ (Figure 1.31). An example of a monomeric Ca(II) complex was also realised with the MeO donor group and bulky

cumyl groups. A reduction of aryl bulk, even to ^{t}Bu, afforded the homoleptic complex Ca(**11**)$_2$. ROP of *rac*-LA in THF at room temperature generally furnished heterotactic PLA (P_r = 0.60-0.75). Increasing the steric bulk at the *ortho* position increased the activity of the initiator. The THF solvent is thought to be non-innocent in the polymerisation, changing the coordination sphere at the metal by displacing the donor group. Tacticity was maximised by carrying out the polymerisation at -38 °C for the *ortho* trityl/OMe donor complex (2 days, P_r = 0.81). Reaction at 70 °C in toluene was enough to destroy any heterotactic bias and in some cases causes a marginal shift to isotacticity (P_m = 0.60). In toluene, the active species is initially anticipated to still have the donor group coordinated. While similar activity was realised, Ca(**11**)N(SiMe$_3$)$_2$ afforded atactic PLA. Similar results were achieved by employing a modified ligand of **11**H. Changing the biphenyl group to binapthyl, while maintaining an NMe$_2$ donor, furnished identical metal coordination. The resulting complexes demonstrated similar activities and heteroselectivities.[109]

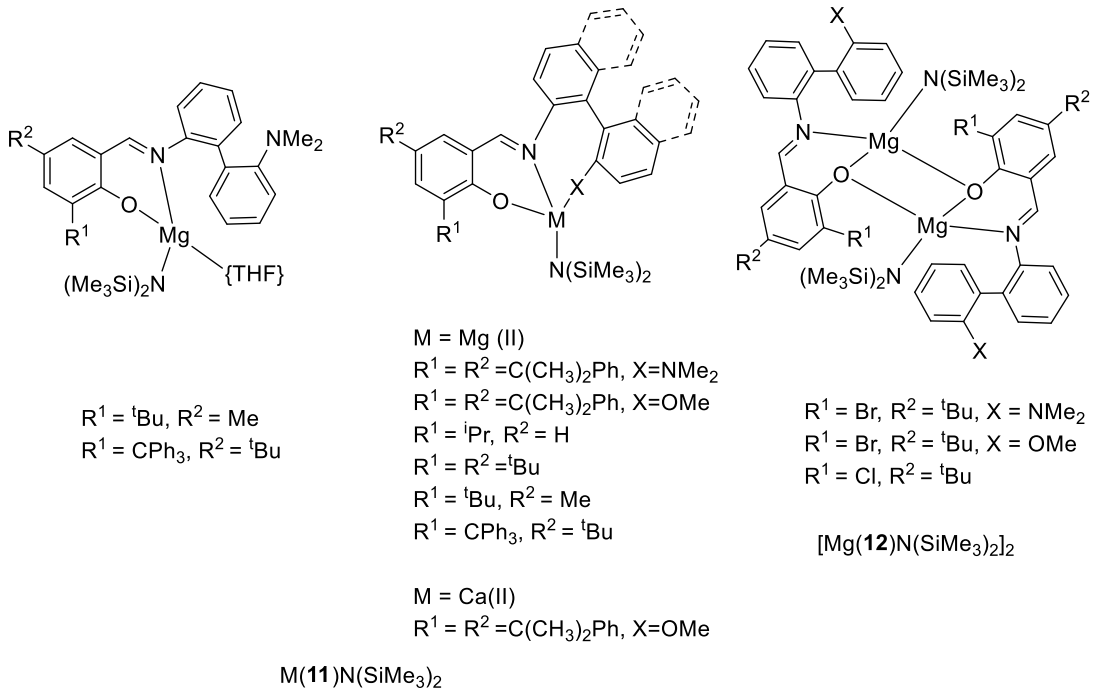

Figure 1.31: Iminophenolate Group (II) complexes employed by Ma *et al.*[107-109]

A series of Mg(II) heteroscorpionate complexes, based upon a pyrazol motif, have been prepared by Otero *et al* (Figure 1.32).[110-112] In the first instance, a mononuclear species, Mg(**13**)R, was synthesised as a single site initiator for ROP. [53.]When the N-substituents were inequivalent ($R^1 \neq R^2$), structural isomerism was observed due to

coordination of either amine group and these structures were successfully separated. These initiators demonstrated high activity for both LA and ε-caprolactone, with reaction times being quoted in minutes for the room temperature ROP. Excellent control over the resultant polymer molecular weights is achieved with predictable weights recorded as well as narrow chain length distributions. The reaction with *rac*-LA furnished heterotactic PLA which was enhanced by low temperature reaction without a loss of activity (P_r = 0.70 - 0.79). A reduction of pyrazol substituent bulk, from ^{t}Bu to Me, while offering similar control over polymer weight properties, severely reduces activity and furnishes atactic PLA.[112] This difference is attributed to the operation of Schlenk type mechanisms to give heteroleptic complexes. Reaction of these mononuclear complexes with a further equivalence of Mg(II) afforded a multinuclear species with a apical C-Mg bond.[111] In THF, a dinuclear species, Mg_2(**13**)R_2{THF}, is formed and in the presence of dioxane, a tetranuclear complex, [Mg_2(**13**)R_2]$_2${Dioxane}, results. On the application of these initiators to the ROP of *L*-LA and ε-CL, high activity is realised, being comparable to that of Mg(**13**)R. Unusually, the polymerisation of *rac*-LA was observed to be slower than the former monomers, requiring several hours to reach moderate conversions even at a higher temperature. The selectivity exerted by these structures was heterotactic (P_r = 0.68 – 0.78) and there is evidence that the bias is increased with increasing initiator nuclearity.

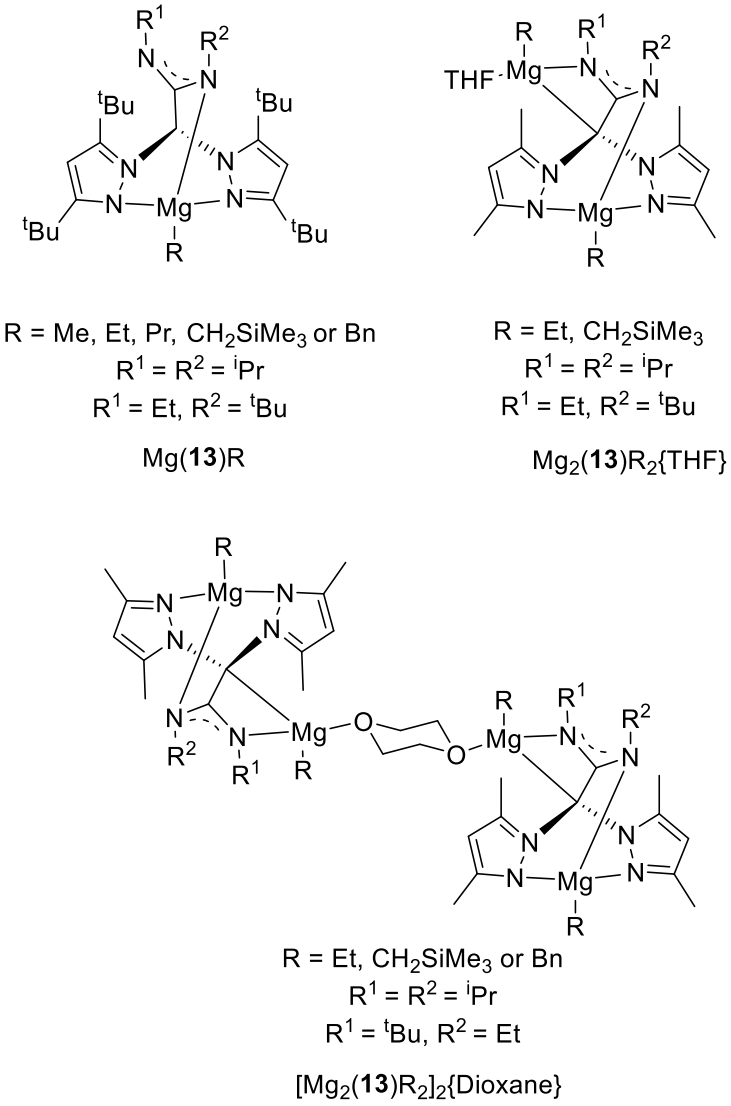

Figure 1.32: Heteroscorpionate Mg(II) complexes employed by Otero *et al.*[110-112]

The Mg(II) calixarene, Mg(**14**)^{n}Bu, has been prepared by Redshaw *et al* (Figure 1.33).[87] An investigation into alcohol co-initiator addition revealed BnOH to facilitate the fastest reaction as well as immortal polymerisation characteristics. The polymerisation in THF afforded heterotactic PLA ([LA]:[Mg]:[BnOH] = 100:1:1, 3 minutes, P_r = 0.85). In contrast, reaction in toluene afforded an isotactic bias (5 minutes, P_m = 0.70). In this case, higher activity and stereocontrol is observed compared to analogous complexes with Zn(II).[113]

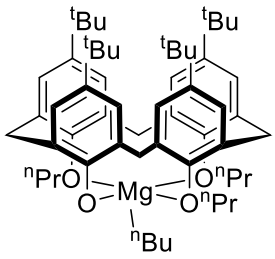

Mg(**14**)^{n}Bu

Figure 1.33: Calixarene Mg(II) complex employed by Redshaw *et al.*[87]

The highest heteroselective Mg(II) initiator to date has been realised by Cui *et al.*[114] Three different families of ligands were prepared [Mg(**15**-**17**)Bu{THF}], all based upon a phosphinimino-amine framework (Figure 1.34). On application to the polymerisation of *rac*-LA, all initiators prepared exhibited a heterotactic preference in THF. Interestingly, there was no reaction in CH_2Cl_2 and stereocontrol was lost for polymerisations performed in toluene. In general, reaction times were short (10 minutes) and strong heterotacticity was demonstrated at 25 °C (P_r = 0.62-0.93). This could be enhanced by the ROP of *rac*-LA at 0 °C (P_r = 0.98, 30 minutes).

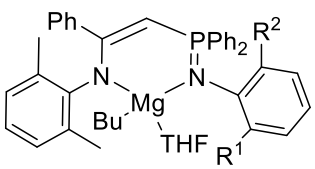

$R^1 = R^2$ = H, Me, Et or ^{i}Pr
R^1 = Cl, R^2 = H
Mg(**15**)Bu{THF}

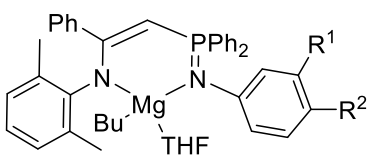

$R^1 = CF_3$, R^2 = H
R^1 = H, R^2 = OMe
Mg(**16**)Bu{THF}

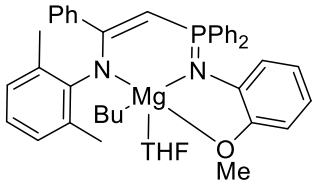

Mg(**17**)Bu{THF}

Figure 1.34: Phosphinimino-amine Mg(II) complexes employed by Cui *et al.*[114]

While not being stereoselective, a recent system described by Kol *et al* demonstrates elegant use of a Mg(II) initiator (Figure 1.35).[53] Mg(*R*,*R*-**18**)Cl was found to be highly active towards the ROP of lactide furnishing high molecular weight (266,000 gmol^{-1}) and good control in 6 minutes. The polymerisations were revealed to have immortal and living characteristics and an activated monomer mechanism was suggested. Due to these polymerisation properties, this initiator was applied to the one-pot formation of *L*-/*D*- stereoblocks. Notably, the formation of stereoblocks was associated with no tapering or stereoerrors due to complete conversion of the previous monomer. This approach was extended to the preparation of up to an "octa-block" structure which was

achievable in 1 hour, albeit with slightly less control. Stereocomplexation was achievable and demonstrated for 6 blocks. Best results were achieved for the initial di-block (T_m = 215 °C) with the subsequent tri and tetra blocks also having enhanced melting points (T_m = 206-208 °C) compared to homopolymer.

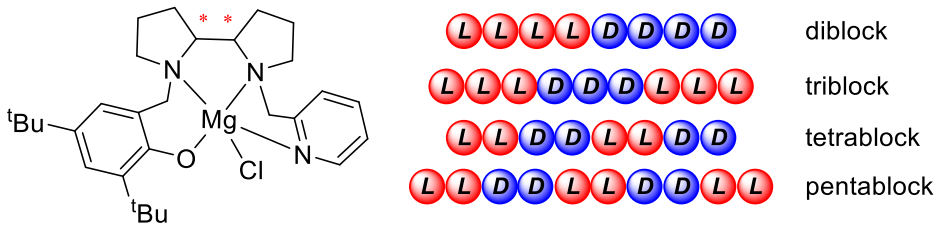

Mg(*R,R*-**18**)Cl

Figure 1.35: Bipyrrolidine Mg(II) initiator employed by Kol *et al* for the preparation of stereoblocks.[53]

1.4.3 Zinc Initiators

An attraction of zinc initiators is the high activity that is often displayed.[115, 116] An early example by Tolman *et al* who utilised an diamino monophenol ligand, **19**H (Figure 1.36).[116] The Zn(II) ethyl species was initially formed and upgraded to the ethoxide complex which was revealed to be dimeric in the solid state. On application to the polymerisation of *rac*-LA, very fast reaction is observed, with high molecular weight being achievable in less than 20 minutes at room temperature. Despite reports of high activity, the realisation of highly stereoselective Zn(II) initiators remains an important research goal.

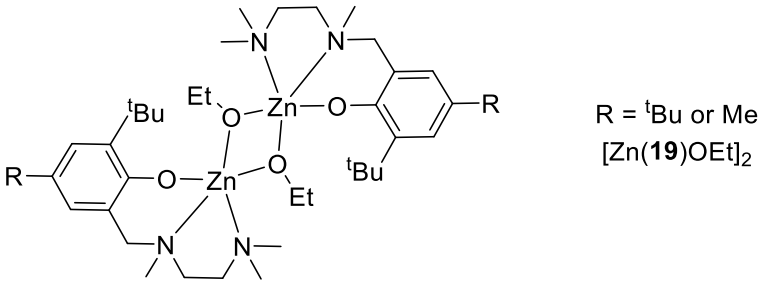

Figure 1.36: Aminophenolate Zn(II) complex employed by Tolman *et al.*[116]

Modifications on the initiators presented by Tolman provides an interesting structural and catalytic comparison. Darensbourg and Karroonnirun have prepared half salen structures, **20**H, with chirality in the backbone, and successfully coordinated these to Zn(II) (Figure 1.37).[117] The resultant complexes were mononuclear, being isolated as the trimethylsilyl amide form, Zn(**20**)N(SiMe$_3$)$_2$. For the ROP of *rac*-LA, there is a heterotactic preference however, this is achieved with a loss in activity relative to [Zn(**19**)OEt]$_2$ (P_r = 0.89 - 0.83, -30 to 23 °C). Despite the chiral nature of these initiators, the control is thought to arise from a chain end mechanism.

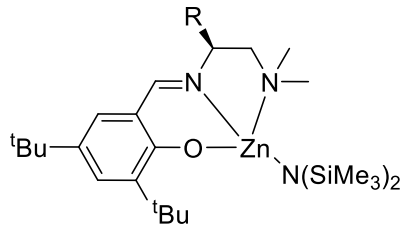

R = Bn, ^{i}Bu,2-(MeS)Et or H

Zn(**20**)N(SiMe$_3$)$_2$

Figure 1.37: Iminophenolate Zn(II) complexes employed by Darensbourg and Karroonnirun.[117]

Coates *et al* have also demonstrated a strongly heteroselective zinc initiator based on a β-diketiminate ligand, **5**H (Figure 1.38).[35, 56] The solid state structure revealed a dimeric species, similar to that of the related Mg(II) complex, [Mg(**5**)O^{i}Pr]$_2$. Unlike the Mg(II) analogue, on application of [Zn(**5**)O^{i}Pr]$_2$ to the ROP of *rac*-LA, a high degree of heterotactic bias is realised (P_r = 0.90 {20 °C, 20 minutes}, 0.94 {0 °C, 2 hours}). In an extension to this system, Schaper *et al* have exchanged the aryl groups with benzylic groups offering the potential for chirality ([Zn(**21**)O^{i}Pr]$_2$, Figure 1.38).[118] The dimeric nature of the alkoxide is still evident in the solid-state structure for this complex. While being active for the ROP of *rac*-LA, the modification affords both reduced activity and less heterotactic bias than the original system (1.5 - 3 hours, P_r < 0.87). A further variation by Schaper employs a bulkier anthracene group, also yielding a dimeric solid-state structure with tetrahedral Zn(II) centres. A similar reduced activity is observed, but a stronger heterotactic bias is realised (P_r = 0.93).

While the distribution of chain lengths is relatively low, (Đ < 1.16), the resultant molecular weight was higher than expected.

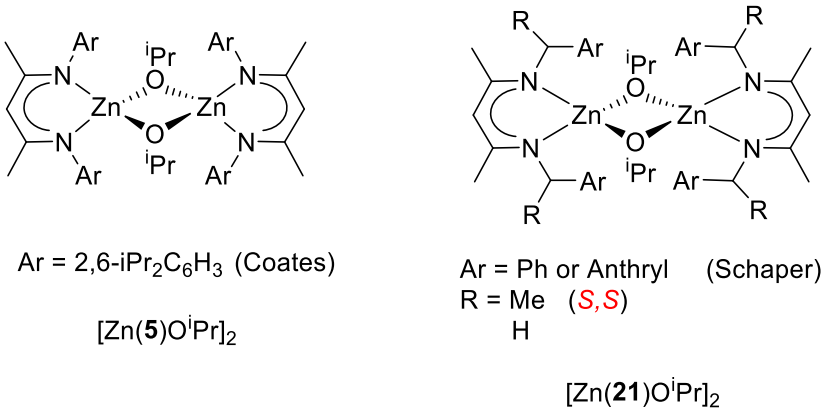

Figure 1.38**:** BDI Zn(II) complexes employed by Coates *et al.*[35] and Schaper *et al.*[101, 118]

Ma *et al* have produced a series of zinc aminophenolates, exploring the effects of chirality and pendant groups upon the polymerisation outcome (Figure 1.39).[115, 119-122] Initially, enantiopure ligand, **22**H, was prepared affording diastereomers on complexation due to increased coordination at a nitrogen centre.[115] The ratio of diastereomers was found to be dependent on both the aryl and nitrogen substituents. With bulkier substituents in each position, the isolation of an enantiopure complex was realised (R^2 = trityl, R^3 = ^{n}Bu). Indeed, best results were achieved with the enantiopure Zn(II) initiator, with high isotactic preference being realised in toluene (P_m = 0.80 - 0.84, T_m = 166 °C). Polymerisation time was measured in minutes to hours depending on the bulk of substituents. The mechanism is described to involve both enantiomorphic site control, with *D*-LA polymerising at a faster rate, and also chain end control leading to polymers with a stereoblock sequence. Varying degrees of isoselectivity are also realised for the diastereo-mixtures (P_m = 0.59 - 0.77) and in one instance there is a heterotactic preference (P_r = 0.61, R^1 = R^2 = Cl). A follow up study expanded upon the range of substituents, exploring the tuneability of the system towards the preparation of enantiopure complexes. It is suggested that the activity of this system may be independent of the ratio of diastereomers in solution but rather more sensitive to the nature of the ligand substituents.[119] In an extension to this series of ligands, tetradentate based structures, **23-25**H, have also been prepared (Figure 1.39).[120] Two distinct classes were prepared, with an aliphatic or pyrrolidine

backbone. Despite having potential for tetradentate binding, only tridentate coordination was realised on reaction to Zn(II), with alkyl or aryl amine binding. It is observed that the pendant alkyl moiety has a stronger tendency to coordinate to zinc {Zn(**23**)N(SiMe$_3$)$_2$} but this bias could be reduced by increasing the alkyl amine bulk {R^3 = ^{i}Pr, Zn(**24**)N(SiMe$_3$)$_2$}. This series of initiators was tested in both toluene and THF with the former giving the best results. The polymerisation of *rac*-LA achieved high conversion in less than 2 hours in each case. Coordination of the aryl amine furnished a slight heterotactic bias (P_r = 0.60) whereas alkyl amine coordination afforded isotactic PLA (P_m = 0.70 - 0.81). With respect to metal concentration, a non-integer rate order was observed suggesting cooperation of metal centres during polymerisation.

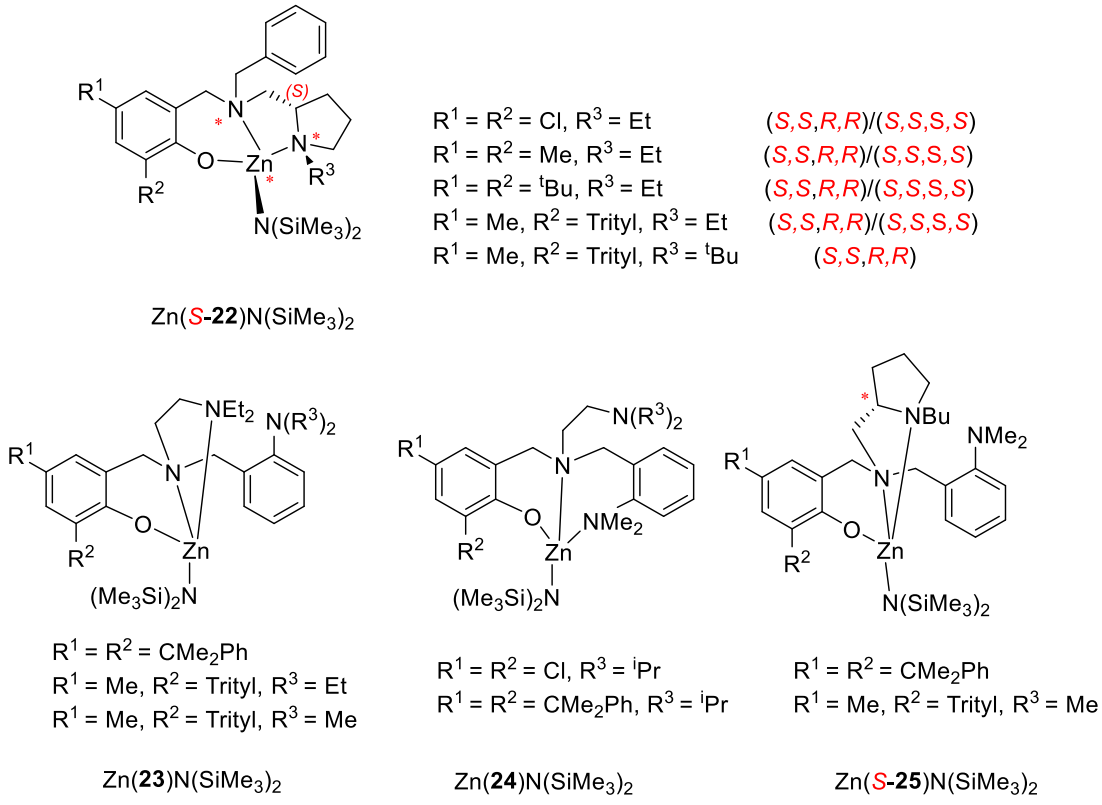

Figure 1.39: Aminophenolate based Zn(II) initiators employed by Ma *et al.*[115, 119, 120]

Otero *et al* have explored the use of a series of scorpionate ligands for the Zn(II) mediated ROP of LA.[123-125] All ligands described are based upon a bis(pyrazol-1-yl)ethyl structure, with substitutions and chirality at the ethyl position (Figure 1.39). Reaction of **26**H with 1 equivalent of Zn(II) provided a mononuclear species or a dimeric dinuclear species depending on the nature of the zinc source.[124] Of the two

forms, the most active and selective species was observed to be the dinuclear structure, [Zn(**26**)R]$_2$, with which heterotactic PLA was realised at 50 – 65 °C (P_r = 0.64 – 0.77) within 1-3 hours.

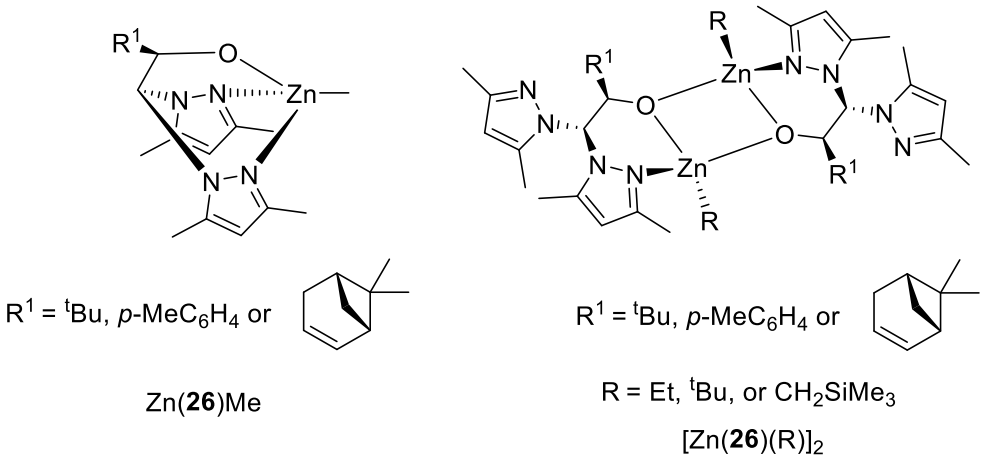

Figure 1.40: Heteroscorpionate Zn(II) complexes employed by Otero *et al.*[123, 124]

Reaction of enantiopure scorpionate ligand, **26**H, with two equivalences of zinc afforded a range of binuclear complexes with different labile groups (Figure 1.41).[125] Both Zn_2(**26**)$(CH_2SiMe_3)_3$ and Zn_2(**26**)(OAr)$(CH_2SiMe_3)_2$ were shown to be active for the ROP of *rac*-LA. Polymerisation were carried out at 20 – 50 °C and generally achieved less than 50% conversion irrespective of reaction time. The stereocontrol exerted by these initiators is isotactic, being more pronounced for Zn_2(**26**)(OAr)$(CH_2SiMe_3)_2$ (P_m = 0.74, T_m = 166 °C). The polymerisation of *L*-LA was found to possess a higher rate constant compared to that for *rac*-LA. Further analysis of the polymer microstructure and the previous observations indicated an enantiomorphic site control. Compared to other zinc species, the activity of this series is lower requiring 1-4 hours to achieve these conversions. Exchanging the alcohol with a cyclopentadiene group afforded a mononuclear zinc alkyl species which was also capable of inducing isoselective polymerisation (P_m = 0.77).[123]

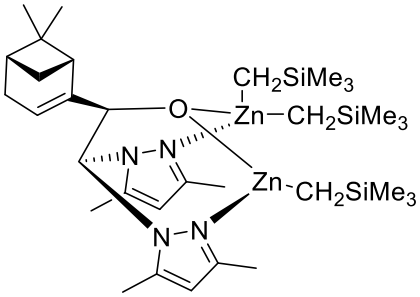

Zn(**26**)$(CH_2SiMe_3)_2$

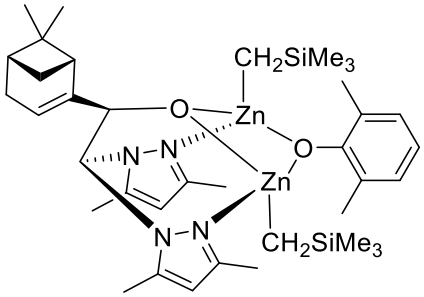

Zn(**26**)(O-2,6-$C_6H_3Me_2$)$(CH_2SiMe_3)_2$

Figure 1.41: Heteroscorpionate Zn(II) complexes employed by Otero *et al.* [125]

Related to these structures is an achiral iminophosphine heteroscorpionate, **27**H. Coordination to Zn(II) afforded a zwitterionic structure, yielding a four coordinate tetrahedral metal centre (Figure 1.44).[126] A range of labile groups were prepared and the resultant complexes assessed for their ROP activity. Initial reactions were carried out in THF, with results high dependent on the labile group. Long reactions (10-36 hours) were observed for Cl or alkyl R groups, despite a high reaction temperature (70°C). A very slight heterotacticity was exerted by these initiators (P_r = 0.64). Amido groups were amenable to reaction at 30 °C albeit, with a long reaction time. Isoselectivity is realised for such initiators under these condition (P_m = 0.74). Best results were achieved with the benzyl alkoxide group which inserted efficiently, with high conversion being achieved after 3 hours. In general, there is a close match between measured molecular weights with the theoretical weights. However, the distribution of polymer weights is broad (Đ = 1.27 – 2.01). For the amido group, $N(SiHMe_2)_2$, increased activity was realised in non-coordinating solvents such as benzene and toluene. There was also an enhancement of stereocontrol in these solvents (P_m = 0.85, T_m = 167.4 °C). The origin of the stereochemical bias was attributed to a chain end mechanism based on identical polymerisation rates of *L* and *D*-LA and optical activities during reaction.

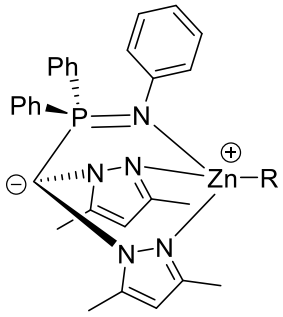

R = Cl, Et, OBn, $N(SiHMe_2)_2$, $N(SiMe_3)_2$ or CH_2SiMe_3

Zn(**27**)R

Figure 1.42: Zwitterionic iminophosphine Zn(II) complexes employed by Cui *et al.*[126]

To date, the most isoselective Zn(II) initiator system has been described by Abbina and Du.[127] This was achieved using chiral amido-oxazolinates, **28**H, which allowed the preparation of a three coordinate metal centre (Figure 1.43). For all substituents, an isotactic preference was demonstrated with high conversion being achieved after 30 minutes at 50 °C (P_m = 0.67 - 0.86). Lower temperatures furnished enhanced control, albeit with an increase in polymerisation time (23 °C, P_m = 0.91, T_m = 212 °C, 44 hrs). The origin of the stereocontrol is postulated to be from a combination of SCM and CEM as there is small difference between the rate constants of *rac*- and *L*-LA but microstructural analysis indicates a polymer of a "blocky" nature. Encouragingly, a melt polymerisation was also attempted with a substantial degree of isotacticity being maintained (P_m = 0.77, 8 minutes).

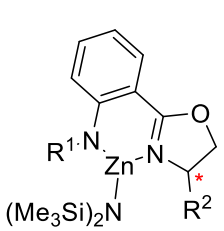

Zn(**28**)$N(SiMe_3)_2$

R^1 = 2,6-$Me_2C_6H_3$ R^2 = (*S*)-^{i}Pr
R^2 = (*R*)-Ph
R^2 = (*S*)-^{s}Bu

R^1 = 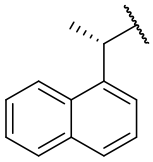 R^2 = (*S*)-^{i}Pr

R^1 = 2,6-$^i Pr_2C_6H_3$ R^2 = (*S*)-^{i}Pr

R^1 = 3,5-$(CF_3)_2C_6H_3$ R^2 = (*R*)-Ph

R^1 = 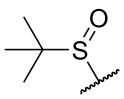 R^2 = (*S*)-^{i}Bu

Figure 1.43: Chiral amido-oxazolinate Zn(II) complexes employed by Abbina and Du.[127]

Recently, Kol *et al* have applied bipyrrolidine, (*R*,*R*)-**18**H, to Zn(II), providing an analogue to their work with Mg(II) (Figure 1.44).[53, 128] In the same study, a more flexible, achiral ethylenediamino ligand, **29**H, is also coordinated to zinc. Both structures are observed to be monomeric, yielding five coordinate Zn(II) ethyl complexes. Subsequent polymerisation demonstrates these systems to be highly active for the ROP of *rac*-LA. The bipyrrolidine system, Zn(**18**)Et, achieved high conversion within 15 minutes (CH_2Cl_2, room temperature) and imparted a slight isotactic preference (P_m = 0.71). The more flexible initiator system, Zn(**29**)Et was shown to have an induction period prior to polymerisation, being attributed to the formation of the active benzyl alkoxide complex. After this period, polymerisation was also revealed to be rapid and a stronger isoselectivity was achieved on application of the bulkier ligand (P_m = 0.81, R = Bn).

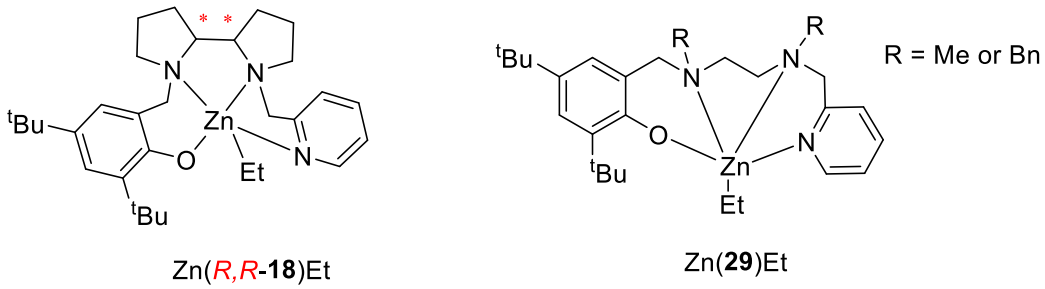

Zn(*R*,*R*-**18**)Et Zn(**29**)Et

Figure 1.44: Bipyrrolidine Zn(II) initiator employed by Kol *et al* [128]

1.4.4 Group III and lanthanide initiators

The majority of catalysis carried out with Group III metals, including the lanthanide series, is focussed on yttrium[129-141] but other metals have be used including Sc(III),[142, 143] La(III), Nd(III),[144, 145] Sm(III),[146] Lu(III)[147] and Yb(II/III).[148, 149] Having a +3 oxidation state, there is also interesting comparisons and overlap with Al(III) based initiators. Such complexes are characteristically highly active with stereocontrol also being observable.

Ligand **27**H, which has previously shown to produce isotactic PLA for Zn(II) complexes (Figure 1.42), has also been applied to the lanthanides.[147] Due to the higher coordination, such complexes are revealed to have two labile groups, maintaining the zwitterionic structure (Figure 1.45). In the first instance, two equivalent alkyl groups

are bound to the metal centres, furnishing M(**27**)$(CH_2SiMe_3)_2${THF}. For the ROP of *rac*-LA, these initiators produced heterotactic PLA (P_r = 0.84) within 15 minutes at room temperature in THF. At low initiator-to-monomer ratios, resultant molecular weights are consistent with propagation of polymer from one site suggesting aggregation of the active species. In contrast, decreasing the amount of initiator yielded molecular weights more consistent with two chains per metal centre. Y(III) was observed to have a faster rate than Lu(III) for these complexes. Investigations into mono-halo complexes, Y(**28**)RX{THF} provided an interesting contrast. The halo groups, X, are considered inert to insertion during polymerisation, making this series single site initiators. As a consequence of this, activity is reduced with 1 hour now required to reach high conversion. Regardless of the labile group, R, enhanced heteroselectivity is realised (P_r = 0.97-0.98).

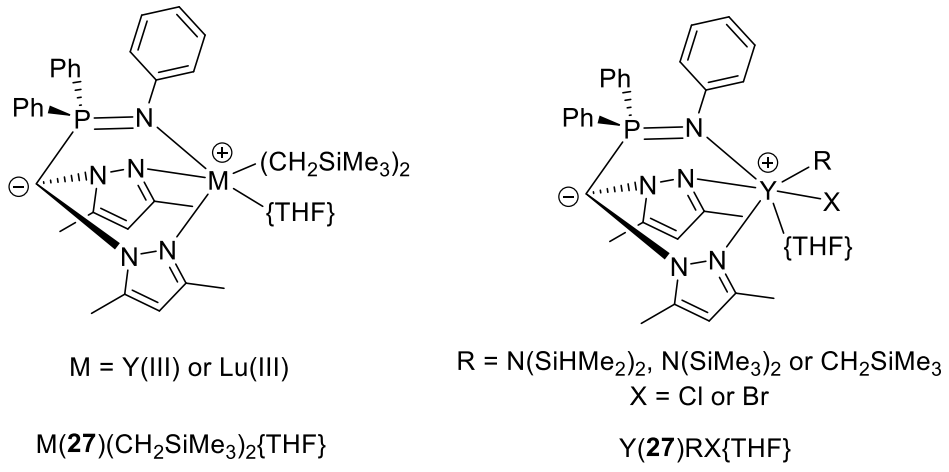

Figure 1.45: Zwitterionic iminophosphine rare earth complexes employed by Cui *et al* [147]

Williams *et al* have applied a series of phosphasalen ligands to rare earth metals affording well defined complexes.[132-135, 150] Initial investigations involved the variation of aryl substituents presenting a series of yttrium complexes, Y(**30**-**31**)OR (Figure 1.46).[135] A lack of aryl substituents favours the formation of dinuclear species, $[Y(\mathbf{30})OR]_2$, with the identity of the alkoxide dictating the bridging groups. When substituents are present on the aryl ring, the mononuclear structure, Y(**31**)O^{t}Bu, can be isolated. Room temperature polymerisation afforded good conversion and heterotacticity (P_r > 0.78) within one hour. Best results were realised with Y(**31**)O^{t}Bu

($R^1 = R^2 = {}^t$Bu), which achieved the highest tacticity (P_r = 0.90), even at low initiator loading ([LA]:[Y]:[HO^{i}Pr] = 1000:1:1). These results were achieved after just 70 seconds. The isopropoxide group, added as a co-initiator to the polymerisation, was suggested to be a more efficient initiating group compared to *tert*-butoxide, dominating the subsequent polymerisation. Exchange of the *para* position for a OMe group afforded a faster reaction with identical stereocontrol.[133] Variation of the backbone tended to decrease the extent of stereocontrol and activity while increasing the polymer molecular weight control.[132]

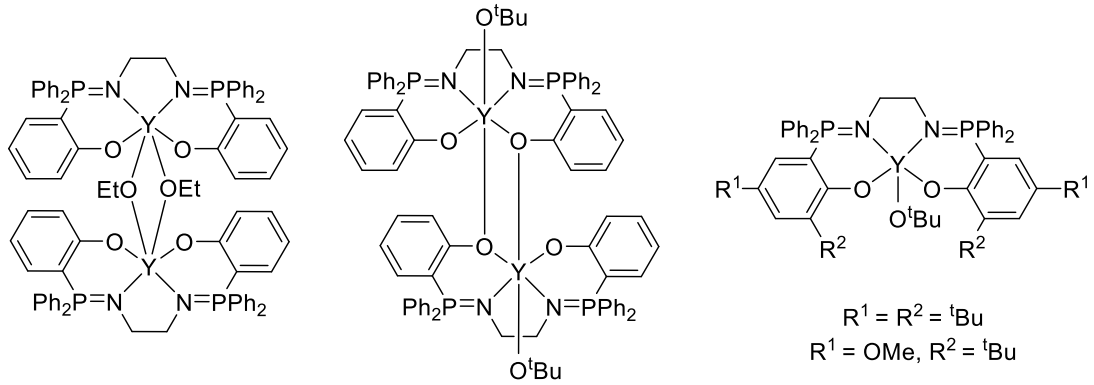

[Y(**30**)OR]$_2$ Y(**31**)O^{t}Bu

Figure 1.46: Phosphasalen Y(III) complexes employed by Williams *et al*.[133, 135]

Expanding the backbone to include an amine group initially yielded the yttrium complexes, Y(**32**)OR (Figure 1.47).[132, 134, 150] *tert*-Butoxide, methoxide and ethoxide forms were prepared in the presence of bulky aryl substituents. Each of these initiators furnished isotactic PLA (P_m > 0.72) albeit at different rates. The fastest room temperature polymerisation was achieved by the Y(**32**)OMe, which required 30 minutes to reach high conversion ([LA]:[Y] = 500:1). For Y(**32**)O^{t}Bu, the stereocontrol was enhanced by carrying out the reaction at -15 °C (P_m = 0.84). In contrast, the analogous Sc(III) initiator was observed to ring open one lactide unit to form a stable species that did not propagate. Further to this, the Sc(**32**)OMe complex unsuccessfully polymerised *rac*-*β*-butyrolactone while showing only moderate activity towards *ε*-caprolactone.[134] The smaller scandium radius is anticipated to account for some of these observations. The influence of metal size is further explored by preparing the lutetium and lanthanum analogues.[150] Once again, the butoxide initiator is observed to yield a less controlled polymerisation which was remedied by

preparing the ethoxide complex {Lu(**32**)O^{t}Bu vs. Lu(**32**)OEt}. Comparable isoselectivity (P_m = 0.75 - 0.89, T_m = 178 °C) is achieved albeit at a slower rate compared to Y(**32**)OEt. Interestingly, the larger La(III) complex afforded the highest activity in this series but gave a complete reversal in stereocontrol. A moderate degree of heterotacticity results (P_r = 0.72) and this switch is related to the increased fluxionality of La(**32**)O^{t}Bu.

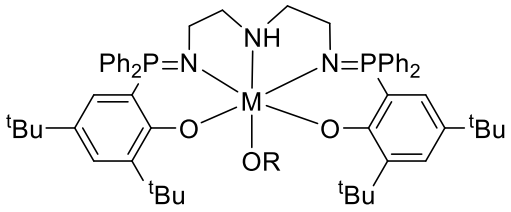

M = Sc(III), Y(III), La(III) or La(III)
R = ^{t}Bu, Et or Me

M(**32**)OR

Figure 1.47: Phosphasalen rare earth complexes employed by Williams *et al*.[132, 134, 150]

While uncommon, there are further examples of an isotactic bias being demonstrated by lanthanide complexes.[151, 152] In work carried out by Arnold *et al*, a bidentate ligand based on phosphine oxide and hydroxyl functionalities was prepared (Figure 1.50).[152] On the application to a series of lanthanides, octahedral complexes were realised with diastereomeric structures also observable *via* NMR spectroscopy for Y(III). The metal centres also possess a C_3 symmetric structure. Y(**33**)$_3$ was applied to the ROP of *rac*-LA at -18 °C demonstrating a high activity at this temperature (10 minutes, [LA]:[Y] = 200:1). The polymerisation was observed to be initiated by a ligand, which was incorporated into the polymer, and affords a reasonable degree of isotacticity in CH_2Cl_2 (P_m = 0.83).

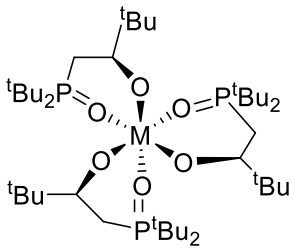

M = Y(III), Eu(III) or Er(III)

M(**33**)$_3$

Figure 1.48: Phosphine oxide based rare earth complexes employed by Arnold *et al.*[152]

Carpentier *et al* have successfully complexed a range of rare earth metals to a bisphenol ligand with a pendant donor group (Figure 1.49).[129-131, 153, 154] Initially, a methoxy donor ligand was applied to Y(III) and La(III) with both aryl substituents (R^1/R^2) being ^{t}Bu.[153] These initiators facilitated the ROP of *rac*-LA, demonstrating high activity at room temperature (THF, [500]:[1], <1 hr). However, a difference is observed in the stereocontrol, with Y(**34**)N(SiHMe$_2$)$_2${THF} exerting a higher heterotactic bias compared to La(**34**)N(SiHMe$_2$)$_2${THF} {Y(III), P_r = 0.80, La(III), P_r = 0.64). Shen *et al* have also applied Yb(III) to this ligand system, producing Yb(**34**)OAr{THF}.[148] This complex was observed to have a greater heterotactic preference (P_r = 0.98) than the corresponding Y(III) complex. Expansion of the ligand set towards Nd(III) caused the stereocontrol to be completely lost, yielding atactic PLA.[131] The difference between metals, in each case, is attributed to the size of the metal radii. The degree of stereocontrol exerted by the yttrium complex could be enhanced by making the *ortho* ^{t}Bu groups bulkier.[129, 131] Adamantyl groups were insufficient to increase the stereocontrol, however, the use of a CMe$_2$Ph aryl substituents afforded highly heterotactic PLA (P_r = 0.90) albeit at a reduced rate. For this particular ligand system, the corresponding Sc(III) complex was shown to be less active requiring elevated temperatures to achieve similar results achieved with Y(**34**)R{THF}.[154] It was also noted that THF as polymerisation medium tended to hinder the reaction of Sc(**34**)R by preventing coordination of the monomer. A heterotactic bias is still maintained albeit slightly reduced compared to the analogous Y(III) complexes (P_r = 0.83).

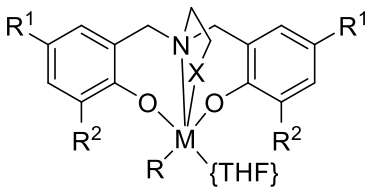

M(**34**)R{THF}

Carpentier *et al*
X = OMe or NMe_2
R = $N(SiHMe_2)_2$, $N(SiMe_3)_2$ or O^iPr
$R^1 = R^2 = {}^tBu$, CMe_2Ph or Me
R^1 = Me or ^tBu R^2 = Ad
M = Sc(III), Y(III), La(III) or Nd(III)

Wang *et al*
X = NMe_2
R = OCH_2CF_3, OBn or O^iPr
$R^1 = R^2 = {}^tBu$
M = Y(III), Yb(III), Er(III) or Sm(III)

Figure 1.49: Pendant bisphenolates lanthanide complexes employed by Carpentier *et al*[127, 151-153] and Wang *et al.*[147]

For the amine pendant donor, X = NMe_2, and ^{t}Bu aryl substituents, Carpentier *et al* produced an silylamido complex, Y(**34**)$N(SiHMe_2)_3$. While demonstrating good activity, the stereocontrol achieved was reduced compared to the methoxy analogue (P_r = 0.60). Wang *et al* have revisited this ligand set, exclusively preparing alkoxides species utilising other metals {Yb(III), Er(III) and Sm(III)}.[149] For the ROP of *rac*-LA, all initiators were able to control the polymerisation, giving narrow molecular weight distributions. The activities of the Y(III) initiators are slightly poorer compared to that of the previously reported silylamido system. However, the stereocontrol exerted by the alkoxide species are profoundly higher. For Y(**34**)(OCH_2CF_3){THF} the P_r value is found to be >0.97. A comparison of the different metals shows the larger radii to yield faster rates, with Sm(III) being the most active. For stereocontrol, the opposite trend is observed with Yb(III) yielding almost perfectly heterotactic PLA (P_r = 0.99). *rac*-β-butyrolactone is also amenable to ROP by this series of initiators with good activity and syndiotacticity (P_r ~ 0.82) being demonstrated.

Carpentier *et al* have also reported a pyridine-bis(phenolate) based yttrium complexes, Y(**35**)$\{N(SiHMe_2)\}_2$ (Figure 1.50).[155] The amido complex was observed to be highly active towards the ROP of *rac*-LA. Typical polymerisation times are reported in minutes and stereocontrol is enhanced by carrying out the reaction in THF relative to toluene at room temperature (P_r = 0.96). Despite the high stereocontrol, the molecular weights observed were higher than predicted with a broad chain length distribution.

The same initiator was active in the production of syndiotactic poly(β-butyrolactone) (P_r = 0.86). The equivalent Al(III) complex, Al(**35**){lactate}, was revealed to be much less active requiring 17 hours at 80 °C, affording atactic PLA.

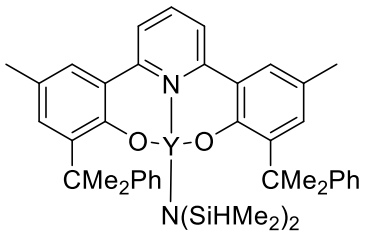

Y(**35**)N(SiHMe$_2$)$_2$

Figure: 1.50: Pyridine bisphenolate Y(III) complex employed by Carpentier *et al*. [155]

1.4.5 Group IV initiators

Group IV initiators are also a popular choice for the ROP of LA due to the oxophilicity of the metal centres. The complexes are generally based upon the 4+ oxidation state and these metal centres {Ti(IV) - Hf(IV)} are reported to show activity the ROP of LA. The extent of group IV initiators established in the literature for the ROP of lactide monomers is worthy of a review article.[156] Due to the similarity of metals, the preparation and application of a combination of group IV metal initiators are typically reported together.

In general, the use of titanium initiators, while showing high activity, yields PLA with modest or no stereocontrol. When stereocontrol is observed, the tendency is towards heterotactic PLA. Application of a series of $TiCl_x(O^iPr)_{4-x}$ species demonstrated a heterotactic bias (albeit unquantified) which was more pronounced for the single site initiator $TiCl_3O^iPr$.[157] Recent examples of titanium complexes that exert a degree of stereoselectivity have been reported by Gao *et al* (Figure 1.51).[158, 159] Phenanthrene derivatives, **36**H$_2$, afforded tetrahedral titanium structures on complexation. The solution and bulk polymerisation of *rac*-LA was assessed with slight heterotacticity (P_r = 0.63) being realised at 50 °C.[158] The achiral salen, **37**H$_2$, was also coordinated with Ti(IV) yielding an octahedral β-*cis* complex. In solution (toluene, 100 °C, [LA]:[Ti] = 100:1), a moderate heterotactic bias (P_r = 0.67) is observed, after a reaction time of 48 hours.[159] This bias is lost after extended reaction time under melt

conditions. The same ligand when used in conjugation with Al(III) is found to be isoselective.[47]

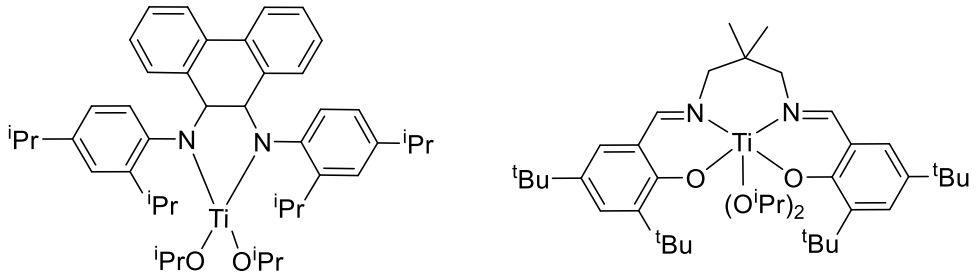

Ti(**36**)$(O^iPr)_2$ Ti(**37**)$(O^iPr)_2$

Figure 1.51: Examples of stereoselective Ti(IV) complexes employed by Gao *et al.* [158, 159]

A series of chiral monophenols, **38**H, have been described by Davidson *et al.* (Figure 1.52).[160] These Schiff bases were coordinated to both Ti(IV) and Zr(IV) yielding bis-ligated *pseudo α-cis* octahedral complexes for which the diastereomeric nature was investigated in solution. For the zirconium complexes, solution ROP of *rac*-LA demonstrated the heterotactic preference (P_r < 0.78) for this initiator system. This preference was maintained under melt conditions. Encouragingly, this system was found to be robust, as the deliberate inclusion of water did not massively impact the polymerisation outcome. The related Ti(IV) complexes were deemed inactive towards the polymerisation in solution and afforded atactic PLA in the solvent free ROP of *rac*-LA.

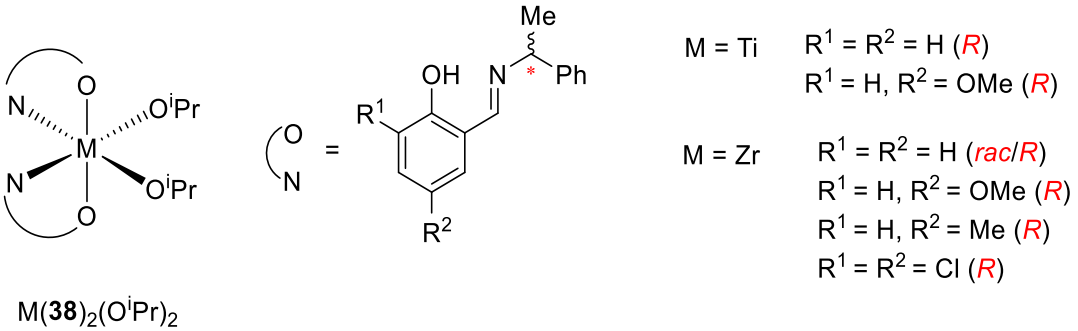

M(**38**)$_2(O^iPr)_2$

Figure 1.52: Monophenolate Ti(IV)/Zr(IV) complexes employed by Davidson *et al.*[160]

Group IV salalens have been demonstrated by Jones *et al.*[161] A series of ligands, **39**H_2, featuring an ethylene backbone with Me or Ph substitution of the salan nitrogen fragment were coordinated to Ti(IV), Zr(IV) and Hf(IV) (Figure 1.53). Each complex was observed to form an octahedral species with a *fac-mer* geometry. For these initiators, there was a difference in stereochemical preference between Zr(IV) and Hf(IV) with the same ligand set; Zr(**39**)(O^iPr)$_2$ exhibited a mild heterotactic preference (P_r = 0.57) while Hf(**39**)(O^iPr)$_2$ yielded isotactic PLA (P_m < 0.75). Both metal centres were observed to be active under solution and melt conditions, however, the Hf(IV) initiators were much slower, especially under melt conditions. The application of Ti(**39**)(O^iPr)$_2$ demonstrated high activity, in solution and melt but yielded atactic PLA.

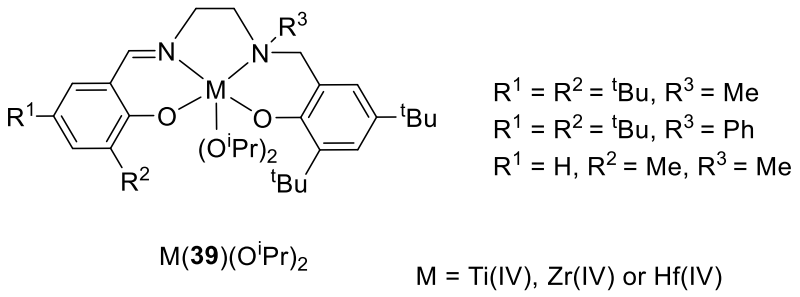

Figure 1.53: Salalen group IV complexes employed by Jones *et al.*[161]

A series of ONSO salalens have been reported by Kol *et al.* (Figure 1.54).[162, 163] Initially, the coordination of a salalen with a flexible ethylene diamine afforded a *fac-mer* octahedral geometry for Zr(**40**)(O^tBu)$_2$.[162] Fluxionality was observed for all complexes prepared and the barrier to interconversion was readily related to the steric bulk of the ligands. ROP of *rac*-LA was carried out under both melt and solution conditions with this series of initiators. For solvent free reactions (140°C), reasonable conversion is generally achieved within 10 minutes, however only chloro bearing initiators yield any meaningful tacticity (P_r = 0.58 - 0.63). In solution (70 °C, 20 hours), this stereocontrol is accentuated (P_r = 0.65 - 0.72). For the adamantyl based initiators, an interesting selectivity is observed depending on the distribution of aryl substituents. Under solution conditions, a slight isotacticity is demonstrated for the two aryl adamantyl based initiator (P_m = 0.67). This tacticity is mirrored by the Cl/Ad salan/salen fragments, which has slightly reduced stereocontrol (P_m = 0.63). Reversal of this structure, Ad/Cl salan/salen fragments, causes a reversal in the observed

tacticity (P_r = 0.63). In contrast to the ethylene backbone, a phenylene backbone offers a more rigid structure. Zr(**41**)(O^tBu)$_2$ adopts a *fac-fac* arrangement in the solid state for all aryl substituents (Figure 1.54). Interconversion was also observed between the enantiomers in solution, and in some instances the formation of a homoleptic complex, Zr(**41**)$_2$, was also observable. Polymerisations were initially carried out in toluene with a reaction time of 4 - 24 hours at 70 °C. When tacticity was observable, a heterotactic preference was observed. Best results in terms of tacticity were achieved when all aryl substituents were halogens (a combination of Cl and Br), yielding heterotactic PLA (P_r = 0.78) A stronger heterotactic bias was demonstrated at 50 °C. (P_r = 0.87). The origin of tacticity for these initiators is suggested to be dependent on the nature of the aryl substituents rather than complex fluxionality.

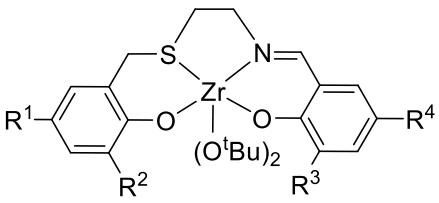

$R^1 = R^2 = R^3 = R^4 = Cl$
$R^1 = R^2 = R^3 = R^4 = {}^t\text{Bu}$
$R^1 = R^2 = {}^t\text{Bu}$, $R^3 = R^4 = Cl$
$R^1 = R^2 = Cl$, $R^3 = Ad$, $R^4 = Me$
$R^1 = Me$, $R^2 = Ad$, $R^3 = R^4 = Cl$
$R^1 = Me$, $R^2 = Ad$, $R^3 = Ad$, $R^4 = Me$

Zr(**40**)O^tBu_2

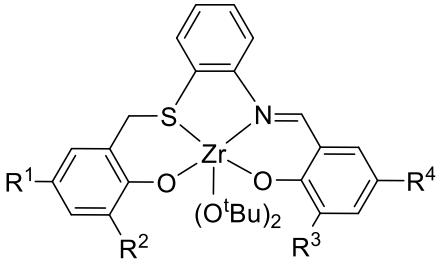

$R^1 = R^2 = R^3 = R^4 = Cl$
$R^1 = R^2 = R^3 = R^4 = Br$
$R^1 = R^2 = Cl$, $R^3 = R^4 = Br$
$R^1 = R^2 = Br$, $R^3 = R^4 = Cl$
$R^1 = R^2 = Cl$, $R^3 = R^4 = {}^t\text{Bu}$
$R^1 = R^2 = {}^t\text{Bu}$, $R^3 = R^4 = Cl$
$R^1 = R^2 = Cl$, $R^3 = Ad$, $R^4 = Me$
$R^1 = Me$, $R^2 = Ad$, $R^3 = R^4 = Cl$

Zr(**41**)O^tBu_2

Figure 1.54: ONSO salalen Zr(IV) complexes employed by Kol *et al.*[162, 163]

Comparisons to these ONSO structures have been demonstrated by dithiodolate ligands **42**H_2 and **43**H_2, based on a OSSO motif (Figure 1.55).[164] Without the constraint of an imino group, both ligands are observed to adopt a *fac-fac* geometry with group IV metals. The complexes were also observed to be fluxional in solution. For each initiator, high activities were generally observed in both solution and melt. For the solvent free reaction, hafnium based initiator were observed to be more active than the corresponding zirconium species {Hf(**43**)(O^tBu)$_2$, [LA]:[Hf] = 300:1, 1

minute}. Titanium initiators yielded atactic PLA. Whereas heterotacticity was afforded in the melt ($P_r \sim 0.70$) and solution {70 °C, Zr(**43**)(O^tBu)$_2$, $P_r = 0.89$} by Zr(IV) and Hf(IV).

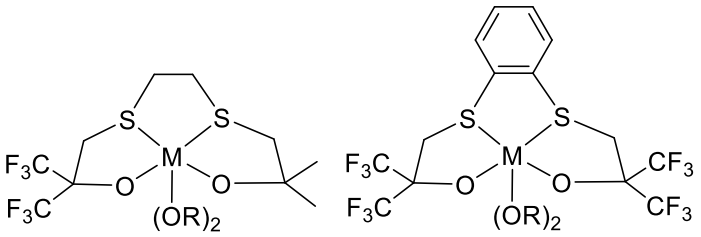

M = Ti(IV), R = ^{i}Pr
M = Zr(IV), R = ^{t}Bu
M = Hf(IV), R = ^{t}Bu

M(**42**)(OR)$_2$

M = Ti(IV), R = ^{i}Pr
M = Zr(IV), R = ^{t}Bu
M = Hf(IV), R = ^{t}Bu

M(**43**)(OR)$_2$

Figure 1.55: OSSO group IV complexes employed by Kol *et al*.[164]

There a range of examples of ethylene bridged salans with various aryl and N-substituents different group IV metals.[165-167] The most selective system has been demonstrated by Davidson *et al*, alongside a distinctly different pyridine based bisphenol (Figure 1.56).[168] The complex types, M(**44**)(O^iPr)$_2$ and M(**45**)(O^iPr)$_2$, both offer tetradentate binding towards a metal centre and form discrete group IV octahedral complexes. All metals employed {Ti, Zr and Hf} were shown to be highly active under melt conditions requiring 2 hours to reach reasonable molecular weight and conversion. However, when the aryl groups were ^{t}Bu, there was a dramatic change in activity with 24 hours instead being required under the same conditions. The ethylene diamine backbone motif with methyl aryl groups was shown to have the strongest isotactic enchainment ($P_m < 0.75$) with zirconium and hafnium.

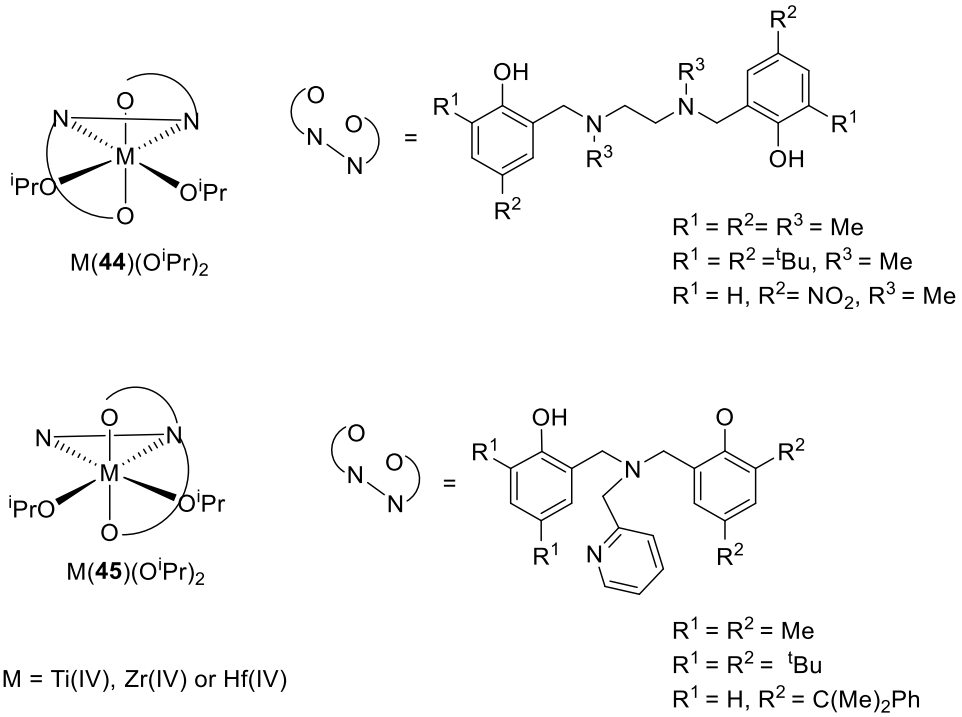

Figure 1.56: Bisphenolate group IV complexes employed by Davidson *et al*.[168]

An example of a phenylenediamine with a more rigid backbone has been realised with group IV metal centres (Figure 1.57).[169] Initial complexation of ligand, **46**H_2, with a phenylenediamine backbone yielded an interesting dinuclear species with bridging isopropoxide groups. The mononuclear forms was achievable through use of bulkier metal sources bearing O^{t}Bu groups. The subsequent polymerisation of *rac*-LA was carried out with complexes M(**46**)(O^{t}Bu)$_2$ where M = Ti(IV), Zr(IV) and Hf(IV). Unprecedented activity is observed with titanium, with a reaction time of less than a minute being achieved under solvent free conditions ([LA]:[I] = 300:1). A degree of heteroselectivity {P_r = 0.68 (solution), 0.62 (melt)} is also realised for Ti(**46**)(O^{t}Bu)$_2$. Enhanced stereocontrol is also achieved through application of Zr(**46**)(O^{t}Bu)$_2$ {P_r = 0.87 (solution), 0.72 (melt)}.

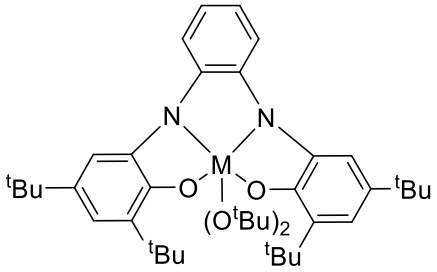

M = Ti(IV), Zr(IV) or Hf(IV)

M(**46**)(O^tBu)$_2$

Figure 1.57: Bisphenolate group IV complexes employed by Kol *et al*.[169]

In a recent development, Jones *et al* have utilised the bipyrrolidine salan ligands, **47**H_2, for the group IV initiated ROP of *rac*-LA (Figure 1.58).[170, 171] The application of the chiral ligands yielded single enantiomers (*Λ- SS / Δ -RR*) with a predetermination caused by the ligands.[172] The application of the *meso* ligand gave a *fac-mer* arrangement with both enantiomers being observed in the crystal structure (*Λ- SR / Δ -RS*) as well as the potential for exchange of *Λ-Δ* forms in solution. These initiators provide an example of group IV initiators furnishing isotactic PLA. Under melt conditions, a moderate degree of isoselectivity is exerted (P_m < 0.70) with a higher activity being achieved for the *meso* complex. The control is further enhanced in solution with best selectivity achieved at 20 °C in $CDCl_3$ (P_m < 0.86, T_m = 176 °C). It is suggested that an enantiomorphic site control is in operation which accounts for the reduced activity of the chiral initiators which have a preference for incoming monomer chirality. The improved rate observed for the *meso* initiator is accounted for by the fluxional process which allows for the complexes' chirality to be switched on mis-insertion also providing stereoblock PLA.

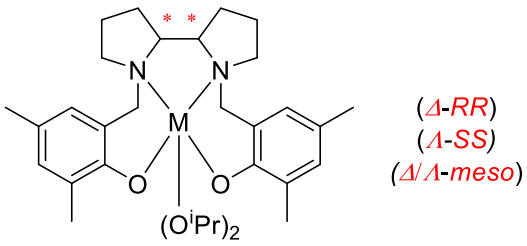

Figure 1.58: Bipyrrolidine group IV complexes employed by Jones *et al.*[170, 171]

A modification of Zr/Hf(**45**)(O^iPr)$_2$, as well as reduced steric bulk of one of the aryl rings allows the formation of unsymmetrical dinuclear complexes (Figure 1.59).[173] On coordination to a metal centre {Zr(IV) or Hf(IV}, the nitrogen atoms gain chirality, yielding homochiral complex, [M(**48**)Cl](μ-OH)[M(**48**)Cl_2]. As a consequence of this chirality, the resultant metal complexes of **48**H_2, exist as enantiomers and each isomer was isolated and characterised by X-ray crystallography. On application of these initiators to the ROP of *rac*-LA, a moderate isoselectivity (P_m = 0.72) is achieved as well as a controlled polymerisation (toluene, 130 °C). An example of 8-coordinate Zr(IV) was also reported however, this was found to be inactive for LA polymerisation.

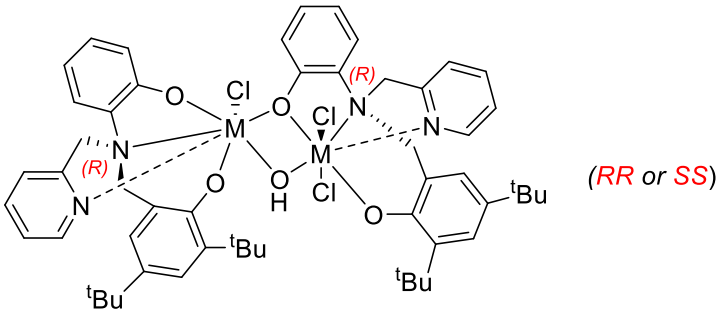

Figure 1.59: Dinuclear bisphenolate group IV complexes employed by Sun *et al.*[173]

The preparation of single site group IV initiators has been investigated for the ROP of LA. The C_3 symmetric trisphenol, **49**H_3, was complexed to Ti(IV), Zr(IV) and Hf(IV) (Figure 1.60) yielding 5 coordinate metal centres in each case.[174] Each initiator was observed to be active in the melt enabling fast polymerisation (t < 30 minutes). For the Zr(**49**)O^{i}Pr and Hf(**49**)O^{i}Pr, there was a strong preference for heterotactic enchainment which was most pronounced for Zr(IV) (P_r = 0.96). Carrying out the polymerisation at room temperature in solution enhanced this selectivity further (P_r = 0.98, 48 hours) yielding a near perfect heterotactic microstructure. Accordingly, kinetic analysis revealed the polymerisation of *L*-LA to be seven times slower compared to *rac*-LA. The Ti(IV) analogue was shown exert no stereocontrol over the reaction. The initiators Ti(**49**)O^{i}Pr and Zr(**49**)O^{t}Bu have also shown to be less active towards *L*-LA under melt conditions.[167]

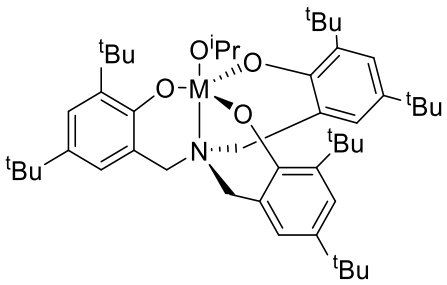

M=Ti(IV), Zr(IV) or Hf(IV)

M(**49**)O^{i}Pr

Figure 1.60: Trisphenolate group IV complexes employed by Davidson *et al.*[174]

An example of highly heteroselective polymerisation has also been demonstrated with a Zr(IV) *N*-heterocyclic carbene.[175] The complexation of **50**H_2 is realised with the coordination of Cl and THF to afford a distorted octahedral metal centre (Figure 1.61). Application of this initiator towards the ROP of *rac*-LA affords highly heterotactic PLA (P_r > 0.95) in solution at room temperature after 15-20 hours (CH_2Cl_2, [LA]:[I] = 100:1-300:1). The degree of control is reduced for the solvent free polymerisation (P_r = 0.82, 3 minutes, [LA]:[Zr] = 100:1). The immortal nature of the polymerisation was also demonstrated for this initiator ([LA]:[BnOH]:[Zr] = 1000:10:1).

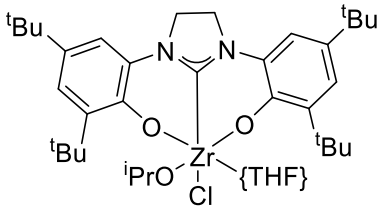

Zr(**50**)(O^{i}Pr)(Cl){THF}

Figure 1.61: Bisphenolate carbene Zr(IV) complexes employed by Dagorne *et al.* [175]

1.4.5 Group 13 initiators

Aluminium is a popular choice for the ROP of LA, having a good history of demonstrating stereocontrol. The inherent ability of aluminium to act as an initiator for ROP is apparent with Al(O^{i}Pr)$_3$ being reported in the literature.[176, 177] To achieve control of tacticity, however, it is necessary to employ ligands with greater coordination and steric bulk. A recent review highlights the importance and range of aluminium based initiators for the polymerisation of LA.[178]

An early example of a stereocontrolled polymerisation with an Al(III) initiator was demonstrated by Spassky *et al* (Figure 1.62).[179] Using a single enantiomer of an aluminium binaphthyl salen, Al(**51**)OMe, a preference was observed for the insertion of *D*-LA especially at low conversion. At higher conversion, and more incorporation of *L*-LA, there was evidence of stereocomplexation with an increase in melting temperature (T_m = 185 – 187 °C). The stereocontrol for this system is based on an enantiomorphic site control mechanism. Further work with this system by other groups has realised the preparation of syndiotactic PLA from *meso*-LA[33] and an improvement in polymer melt temperature due to use of racemic initiator.[49, 180, 181]

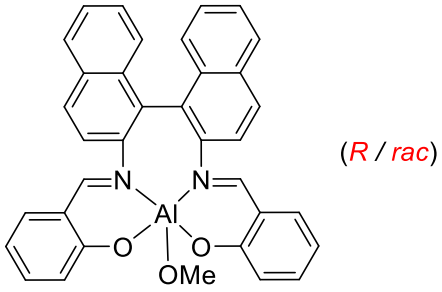

Al(**51**)OMe

Figure 1.62: Salen Al(III) complex employed by Spassky *et al*.[179]

Another pivotal salen aluminium initiator is revealed by Feijen and co-workers who utilised Jacobsen's ligand (Figure 1.63).[182, 183] Similar to Spassky's system, Al(**52**)O^{i}Pr shows enantiomorphic site control during the polymerisation of *rac*-LA with each enantiomer of the initiator having a preference for the insertion of one lactide monomer over the other leading to isotactic enrichment. Application of the racemic initiator results in an increased melt temperature (T_m ~ 185 °C). Both solution (70 °C, toluene, [LA]:[I] = 62:1, 12 days, P_m = 0.93) and melt (130° C, [LA]:[I] = 200:1, 2 days, P_m = 0.88) polymerisations were described, with relatively slow polymerisation rates. Recently, Carpentier *et al* have shown a further example of a chiral salen, Al(**53**)O^{i}Pr (Figure 1.65).[184] The backbone is instead made up of two phenyl groups and there is enough flexibility in this system to allow for the formation a binuclear species Al_2(**53**)Me_4. The mononuclear forms of this initiator show a reasonable degree of isotacticity (P_m ~ 0.80-0.90) with reaction carried out in solution only. The origin of this stereocontrol is thought to be *via* a chain end control mechanism. The dinuclear complexes, while active, did not exert stereocontrol on the growing polymer.

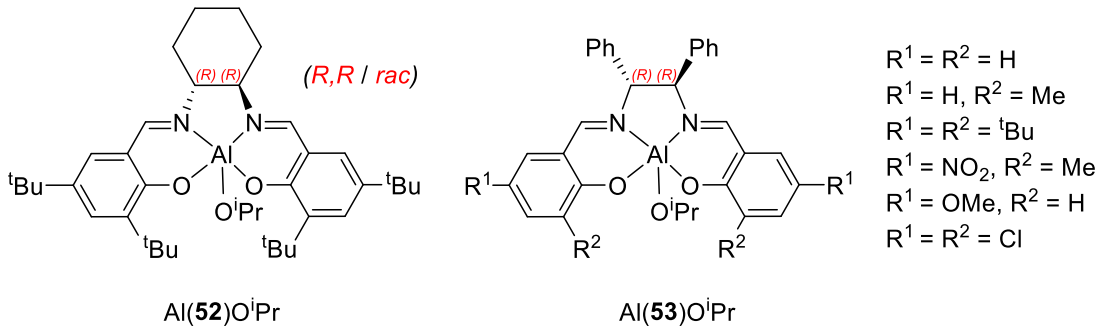

Al(**52**)O^{i}Pr Al(**53**)O^{i}Pr

Figure 1.63: Chiral salen Al(III) complexes employed by Feijen *et al*[182, 183] and Carpentier *et al*.[184]

It is noted that there is often an overlap between Al(III) and group (IV) pro-ligands. However, there is also a divergence in structural features and activity This is demonstrated by the use of Jacobsen's ligand, **52**H_2, which furnishes binuclear complexes [Zr_2(**52**)(O^{i}Pr)$_6$] and [Hf_2(5**2**)(O^{t}Bu)$_6$].[185] While the observed activities were a vast improvement compared to the aluminium analogue the selectivity suffered with atactic PLA being realised with this group IV system.

Achiral salen structures are also known with aluminium, with a general ligand form shown in Figure 1.64 The simplest salen was trialled by Spassky *et al* (Figure 1.64a).[186] Spassky's variant on of Al(**54**)OMe involves two unsubstituted aryl groups simply connected by an ethylene bridge. For this initiator system, there is an isotactic preference *via* a chain end controlled polymerisation. In an extensive follow up study, Nomura varied both the aryl substituents and the aliphatic backbone to screen a range of groups of different steric bulk and electronic properties with the general structure denoted by Al(**54**)Et (Figure 1.64b).[46, 47] It was observed that the steric bulk of the *ortho* aryl position was most readily related to the resultant stereocontrol and the nature of the aliphatic backbone; increasing the length of the backbone was found to generally enhance the rate. In all cases, there was a tendency to form isotactic PLA (P_m > 0.69). Best results were achieved with a neopentyl linker and ^{t}BuMe$_2$Si in the *ortho* aryl positions. This combination yielded a very high degree of isotacticity in toluene at 70 °C ([LA]:[I] =100:1, 14 hours, P_m = 0.98, T_m = 209 °C) which was reasonably maintained in the melt at high temperatures (130°C, [LA]:[I] =300:1, 30 minutes, P_m = 0.92, T_m = 189 °C; 180 °C, [LA]:[I] =300:1, 20 minutes, P_m = 0.84, T_m = 176 °C). An addition to this series has been recently been shown by Shaver *et al* (Figure 1.64c).[187] A variation on Al(**54**)Et with an ethylene backbone (Y) and

adamantyl ortho substituent (R^1) was also shown to have a strong isotactic preference (P_m = 0.88) even under immortal polymerisation conditions ([LA]:[Al]:[BnOH] = 1000:1:10).

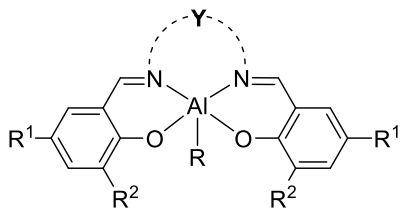

Al(**54**)R

a. Y = CH_2CH_2 $R^1 = R^2$ = H (Spassky *et al*)

b. Y = CH_2CH_2 R^1 = H, R^2 = Ph (Nomura *et al*)
Y = $CH_2CH_2CH_2$ $R^1 = R^2 = {}^tBu$
Y = $CH_2CMe_2CH_2$ R^1 = H, $R^2 = {}^tBuMe_2Si$

c. Y = CH_2CH_2 R^1 = Me R^2 = Ad (Shaver *et al*)

d. Y = $CH_2CMe_2CH_2$ $R^1 = R^2$ = Cumyl
Y = $CH_2CH_2CH(CH_2CH_3)$
Y = 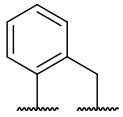 (Lin *et al*)

Figure 1.64: Achiral salen Al(III) complexes employed by a.) Spassky *et al*,[186] b.) Nomura *et al*,[46, 47] c.) Shaver *et al*,[187] and d.) Lin *et al*.[188]

A selection of achiral salens has also been reported by Hormnirun *et al*.[48] This work is distinct to that of Nomura due to the inclusion of aromatic moieties in the backbone instigating a greater degree of inflexibility for Al(**55**)Me (Figure 1.65). In the majority of cases, the best stereocontrol was achieved with the bulkier ^{t}Bu group in the *ortho* position, identical to the conclusion drawn by Nomura. PLA of reasonable isotacticity was achieved (P_m < 0.88). Further to the Nomura and Hormnirun systems, Lin *et al* employed a Me_2PhC aryl substituent to great effect increasing the stereocontrol compared to the analogous ^{t}Bu initiators (Figure 1.64d).[188] With this aryl substituent, isoselectivity remains high under solution conditions (70 °C, P_m = 0.94 - 0.97, 12 - 24 hours, T_m = 203 - 205 °C).

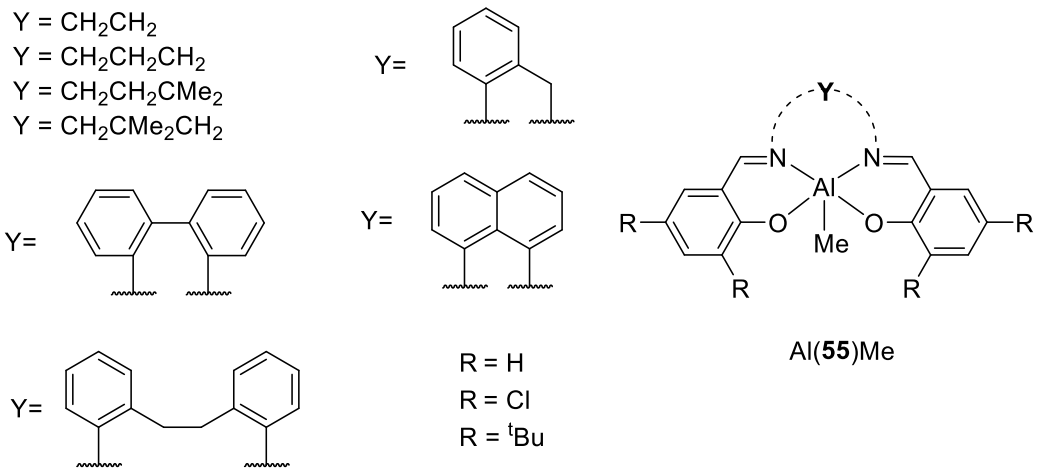

Figure 1.65: Achiral salen Al(III) complexes employed by Hormnirun *et al.*[48]

Another important ligand class used with aluminium are salalens. Such initiators provide a new position to derivatise, i.e. the amine nitrogen, allowing for greater structural diversity. An early example of Al(III) salalen complexes applied to *rac*-LA is demonstrated by Jones *et al* who utilised a simple C_2 backbone reminiscent of Spassky's salen, yielding Al(**56**)Me (Figure 1.66).[189] Both heterotacticity (P_r < 0.75) and isotacticity (P_r > 0.39) was shown within this initiator series with the decisive factor found to be the nature of the amine substituent, R^3, rather than the aryl substituents. When R^3 was Me, heterotactic bias was generally observed and for Ph groups there was a slight isotactic preference. Reaction times for these complexes was between 24 – 72 hours at 80 - 100 °C ([LA]:[BnOH]:[Al] = 100:1:1). Lanthanide metals {Y(III), Nd(III) and Sm(III)} have also been employed with this ligand.[190] In contrast to the equivalent Al(III) initiator, M(**56**)N$(SiMe_3)_2${THF} demonstrates higher activity requiring 1 hour to polymerise 2000 equivalents of LA at room temperature. Depending on the metal, enhanced or reduced stereocontrol was observed {Y(III), P_r = 0.85, Sm(III), P_r = 0.72 and Nd(III), P_r = 0.69}.

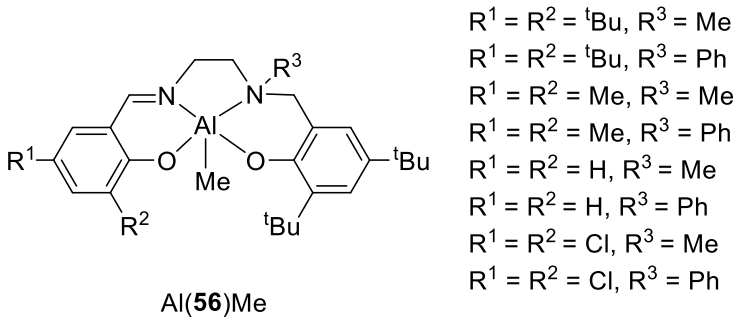

Figure 1.66: Salalen Al(III) complexes employed by Jones *et al.*[189]

A modification of the Feijen system gave another series of salalens.[191] Selective methylation of the amine functionality gave rise to the asymmetric salalen, **57**H_2, with variation of aryl substituents (Figure 1.67). Similar to Feijen's salen system, polymerisation times are quoted in days. Unlike the corresponding salen, the best stereocontrol was exerted by Cl containing initiators with both heterotacticity (P_r < 0.73) and isotacticity (P_r > 0.31) being realised.

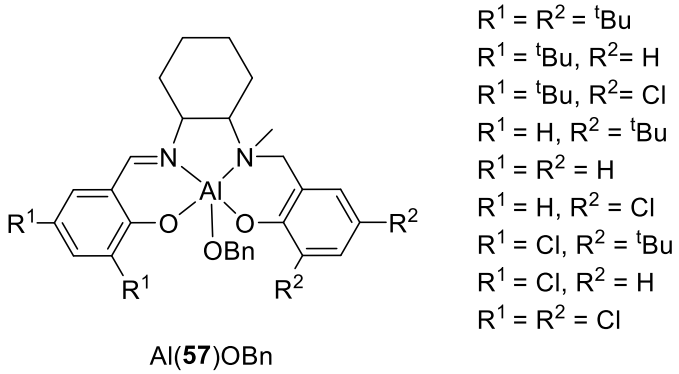

Figure 1.67: Salalen Al(III) complexes employed by Jones *et al.*[191]

A more recent example of an aluminium salalen has been shown by Kol *et al.*[192] Within this system is chirality from the pyrrolidine ring with enantiomerically pure initiators, Al(**58**)O^{i}Pr being synthesised (Figure 1.68). A trend was seen between the aryl substituents and stereocontrol; when the substituents of the imino aryl ring were chloro and the amino aryl substituents bulky, heterotacticity was observed (P_r = 0.76) and for the opposite configuration, isotacticity results (P_m < 0.82). With operation of both CEM and SCM, it is postulated that a novel gradient isotactic multiblock polymer results from application of the isoselective initiators.

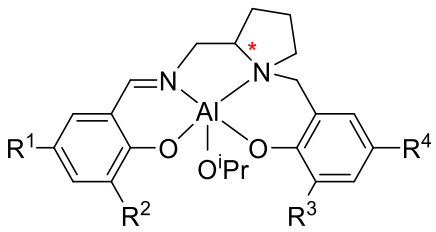

Al(**58**)O^{i}Pr

$R^1 = R^2 = Cl, R^3 = Ad, R^4 = Me$ (*S*)
$R^1 = Me, R^2 = Ad, R^3 = R^4 = Cl$ (*S*)
$R^1 = R^2 = {}^{t}Bu, R^3 = R^4 = Cl$ (*S*), (*R*)
$R^1 = R^2 = {}^{t}Bu, R^3 = R^4 = I$ (*R*)

Figure 1.68: Salalens Al(III) complexes employed by Kol *et al*.[192]

Total reduction of the nitrogen functionality generates the salan structure, which often have the advantage of being white solids. An early example of Al(III) salan initiators, Al(**59**)Me, for *rac*-LA polymerisation was shown by Gibson *et al*.[193] In this case, the ethylene backbone is fully saturated and the two amines bear methyl or benzyl substituents (Figure 1.69). Stereochemical bias was generally maintained regardless of the nature of the amine group R^2. Strong heterotactic preference (P_r = 0.80 - 0.96) was shown when the aryl substituents were chloro or methyl groups with reasonable isoselectivity (P_m = 0.79) for the unsubstituted aryl rings.

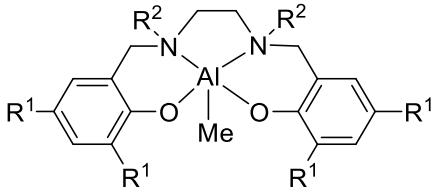

Al(**59**)Me

R^1= H, R^2 = Me
$R^1 = R^2$ = Me,
$R^1 = {}^{t}Bu, R^2$ = Me
R^1= Cl, R^2 = Me
R^1= Bn, R^2 = H
R^1= Me, R^2 = Bn
$R^1 = {}^{t}Bu, R^2$ = Bn
R^1= Cl, R^2 = Bn

Figure 1.69: Salan Al(III) complexes employed by Gibson *et al.*[193]

In a similar fashion, complete reduction of the Feijen's original system led to the corresponding chiral salan with the both nitrogen centres being methylated {Al(**60**)OBn} (Figure 1.70).[194] These initiators were applied as diastereomers to the ROP of *rac*- and *meso*-LA. Isotacticity (P_m = 0.66, R = H), heterotacticity (P_r < 0.73) and for *meso*-LA syndiotacticity (P_r < 0.70) were observed. The manifestation of tacticity was ascribed to be due to both the SCM and CEM and an enhancement on application of a racemic initiator was postulated to be due to polymer exchange.

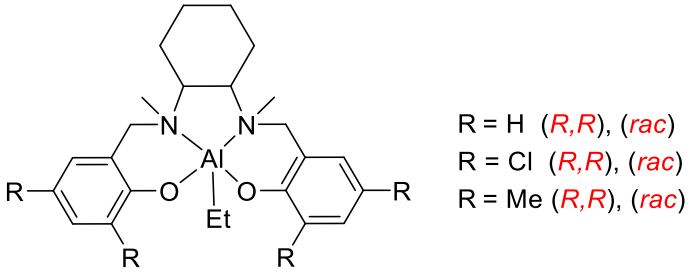

Al(**60**)OBn

Figure 1.70: Salan Al(III) complexes employed by Feijen *et al*.[194]

A more recent example of an aluminium chiral salan, Al(**47**)O^{i}Pr has been shown by Jones *et al* (Figure 1.71).[170] Under both melt and solution conditions, reaction was observed to be relatively slow, requiring 24 hours and 5 days respectively. Of the initiators tested, the *meso* form with methyl aryl substituents was found to be the most selective furnishing heterotactic PLA ($P_r < 0.87$) in solution. Neither the *S,S/R,R* forms or the ^{t}Bu *meso* form exerted any stereocontrol over the polymerisation. Interestingly, the tacticity bias of Al(*meso*-**47**)O^{i}Pr is the opposite of the corresponding group IV complexes {Zr/Hf(**47**)(O^{i}Pr)$_2$}.

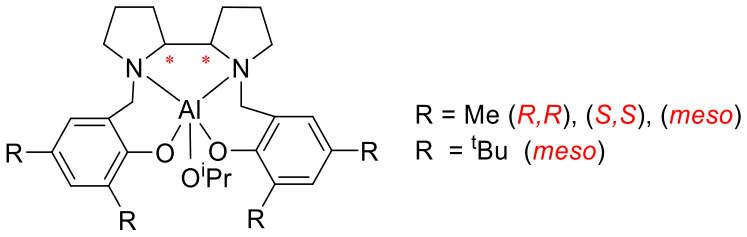

Al(**47**)O^{i}Pr

Figure 1.71: Chiral salan Al(III) complexes employed by Jones *et al*.[170]

A common issue with aluminium based initiators is low activity which undermines the high stereoselectivity that is achievable. More recently, greater attention has been directed towards the next two metals in group 13, Ga(III) and In(III).

The first example of Ga(III) activity in ROP of cyclic esters has been reported by Horeglad *et al*.[195] Reaction with (*S*)-methyl lactate affords a binuclear species in which both metal centres have two alkyl groups (Figure 1.74). The gallium centres adopt a trigonal bipyramidal structure due to a lactate bridging alkoxide as well as lactate

carbonyl coordination. Reaction times are given in days for the ROP of *rac*-LA at various temperatures. The reaction in CH_2Cl_2 afforded no control stereocontrol for the resultant PLA. However, when the reaction is carried out in THF, a heterotactic bias is observed (P_r = 0.68). Further to this, the addition of picoline to polymerisations in CH_2Cl_2 was observed to facilitate a stereoselective reaction (P_r = 0.78). The origin of this selectivity, therefore, is attributed to the tuning of the electronic properties of the Ga(III) centre by Lewis bases. The donation of electron density to the Ga(III) centre was further explored by introducing a carbene donor, **61**. This allowed for the preparation of well-defined structures as well as increasing steric protection of the metal centre.[196] The formation of the carbene complex caused a dramatic increase in activity relative to the original lactate complex, with polymerisations being carried out at -20 °C in CH_2Cl_2. For the carbene-lactate complex, Ga(**61**)Me_2{Lactate}, high conversion was achieved after 4 hours ([LA]:[Ga] = 90:1) or 16 hours ([LA]:[Ga] = 320:1). At this temperature, moderate isoselectivity is observed (P_m = 0.78). At room temperature, the degree of stereocontrol is noted to be reduced (P_m = 0.65). While being observed to be more active and furnishing equal stereocontrol, reaction with Ga(**63**)Me_2(OMe) exhibited poorer molecular weight control as shown by a broad distribution of chain lengths (Đ > 1.94). Further studies have expanded the scope of applied carbenes, polymerisation conditions, chiralities and metal choice.[197-199]

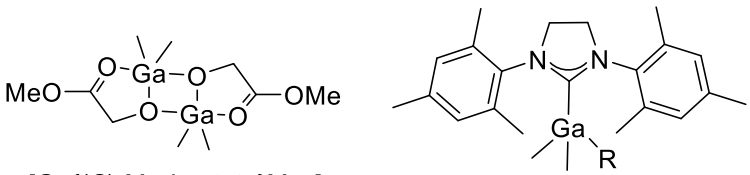

Figure 1.72: Lactate and carbene Ga(III) complexes employed by Horeglad *et al.*[195, 196]

Isoselective Ga(III) initiators have also been realised by Williams *et al.*[200] A range of structures were obtained through the reaction of 8-quinolinlato with either $GaCl_3$ or $GaMe_3$, including mono- and bis-ligated complexes (Figure 1.73). The polymerisation of *rac*-LA with Ga(**62**)$_2O^tBu$ was suggested to proceed *via* an activated monomer mechanism. Best results were achieved with the bis-ligated complex, Ga(**62**)$_2O^tBu$

which demonstrated isotacticity (P_m = 0.70). The stereocontrol imparted is identical to that obtained with the analogous aluminium complex, Al(**62**)$_2$Et, under the same conditions.[201] However, the gallium initiator benefits from a three-fold increase in rate.

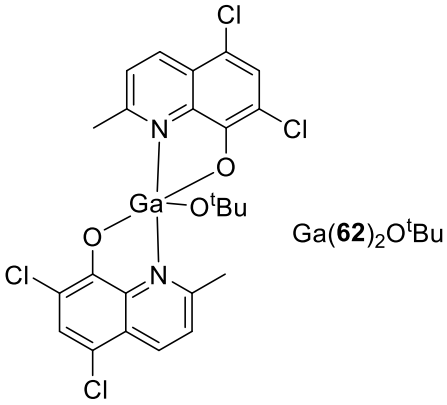

Figure 1.73: Quinolinato Ga(III) complex employed by Williams *et al.* [200]

A series of Ga(III) and In(III) initiators were prepared by Chakraborty *et al.*[202] The complexes, M(**63**)^{t}Bu$_2$, are characterised as tetrahedral centres, despite the potential for tridentate coordination of the ligand (Figure 1.74). Subsequent polymerisations with *rac*-LA are carried out at 140 °C without the addition of co-initiator. Good activity and control is demonstrated by this system, with reaction time, at 200:1 [LA]:[I] ratio, within an hour. The Ga(III) species are observed to be more active than the corresponding In(III) complexes and there is good molecular weight control exerted by both complexes. MALDI-ToF analysis of oligomeric material reveals the α end group to be the ligand, *via* the phenoxide group. Despite the high reaction temperature, a reasonable degree of isotacticity (P_m < 0.84) is maintained by the initiators, being slightly enhanced for the Ga(III) complexes.

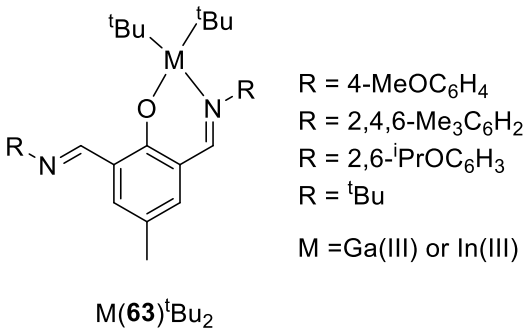

Figure 1.74: Di-imino monophenolate Ga(III)/In(III) complexes employed by Chakraborty *et al.*[202]

For In(III), great success was realised through application of the trichloride species.[203, 204] In the first instance, the catalytic system comprises of $InCl_3$, BnOH and NEt_3, each of which are required for successful polymerisation of LA. Both $AlCl_3$ and $GaCl_3$ were found to be inactive in this system. $InCl_3$ demonstrates good activity for the polymerisation of *rac*-LA, achieving high conversion at room temperature after 5 hours. Remarkably, there is a strong heterotactic bias (P_r = 0.94-0.97, 25 – 0 °C) provided by this system despite the absence sterically cumbersome ligands. Unusually, there is no stereocontrol exerted over the polymerisation of *meso*-LA. In a follow up study, a dinuclear species is postulated as the active species (Figure 1.75), with NEt_3 acting to solubilise the $InCl_3$ and as well as being present as a counterion, Et_3NH^+.[205] The bridging alkoxide, being either benzyl or growing polymer, is able to attack the incoming LA monomer in a coordination insertion mechanism.

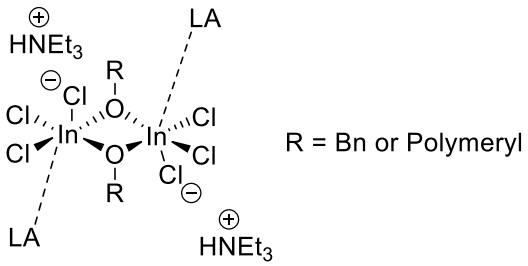

Figure 1.75: Predicted active species for polymerisation with $InCl_3$.[155, 156]

A range of In(III) complexes have been realised using pro-ligands previously employed with Al(III). As indium has a larger metal radius, there is invariably a deviation in structure. Complexation of a binaptyl salen (**51**H_2, Figure 1.62) with

methyl/^{t}Bu aryl groups has been reported with In(III).[206] Unlike the Al(III) complex, the indium species exists as an ethoxy-bridged dinuclear complex surrounded by two ligands [In(**51**)OEt]$_2$. Two structural isomers were observed and on the application of these to *rac*-LA, very low activity was observed as well as a slight heterotactic bias (P_r = 0.60). In a similar vein, Jacobsen's ligand (**52**H$_2$, Figure 1.63) has also been employed with In(III).[207, 208] Once again, a dinuclear species, [In(**52**)OEt]$_2$, is isolated from the complexation mixture. Both *rac*- and *R,R*- versions of the complex are prepared and application to ROP of *rac*-LA demonstrates a higher activity compared to the mononuclear Al(III) complex. At 25°C, 200 equivalences of LA could be polymerised in 30 minutes. Stereocontrol is also exerted under these conditions, with an isotactic preference realised (P_m = 0.74-0.77, T_m = 140 °C) but these values are greatly reduced compared to that achievable with Al(**52**)Me. Further In(III) salen complexes have been reported using **53**H$_2$ (Figure 1.63) as ligand.[209] Unlike previous examples, the mononuclear species are realised for In(III), providing a more closer comparison with Al(III). In all cases, In(**53**)CH$_2$SiMe$_3$ provide a substantial reduction in stereocontrol, with slight isotacticity resultant (P_m < 0.60). Unusually, the In(III) species are observed to be inert to alcohols implying ROP proceeds *via* an activated monomer mechanism.

A range of In(III) monophenolate species have been prepared (Figure 1.76).[203, 204, 210] In each case, the formation of bridged dimer, [In(**64**)Cl$_2$](μ-Cl)(μ-OEt) occurs on attempts to form an alkoxide. Despite there being four chiral centres in the structure, only one species is observable *via* NMR indicating the isolation of the homochiral complexes. These species tend to have high activity but only a modest contribution to polymer stereochemistry (P_m > 0.62). Nevertheless, good control over molecular weight is achieved and these In(III) complexes can efficiently polymerise *rac*-LA at low loadings ([LA]:[In] = 880:1). Further investigations expanded the scope of the initiator structure as well as elucidated the mechanism.[204] It was deduced that these dinuclear species are maintained during polymerisation. This indium monophenolate system has also been shown to be highly active for the polymerisation of β-butyrolactone.[211]

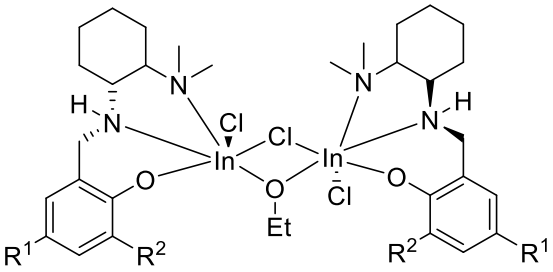

$R^1 = R^2 = {}^t$Bu (*rac*)
R^1 = Me, $R^2 = {}^t$Bu (*RR*)
R^1 = Me, $R^2 = SiPh_3$ (*rac / RR*)
$R^1 = {}^t$Bu, R^2 = Ad (*rac / RR*)
$R^1 = R^2 = C(CH_3)_2Ph$ (*rac / RR*)

[In(**64**)Cl]$_2$ (μ-Cl)(μ-OEt)

Figure 1.76: Dinuclear monophenolate In(III) complexes employed by Mehrkhodavandi *et al.* [203, 204, 210]

More recently, dinuclear mono-ligated monophenolate In(III) complexes have been demonstrated (Figure 1.77). The motivation behind preparing these dinucleating motifs was to prevent dissociative reactions potentially involved in previously mentioned dinuclear systems.[212] [In$_2$(**65-66**)Cl$_4$](μ-OEt) are prepared as well defined complexes, with two six coordinate metal centres. Both initiators likely consist of a pair of enantiomers due to ligand and octahedral chirality. As a consequence of the dinucleating motif, the activity of these initiators is much reduced with days being required at room temperature to attain high conversion ([LA]:[In] = 200:1). However, a strong degree of heterotactic bias is realised under these conditions for both initiators (P_r = 0.87 - 0.89).

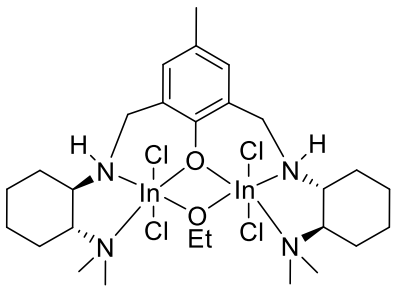

[In$_2$(*R,R*/*R,R*-**65**)Cl$_4$](μ-OEt)

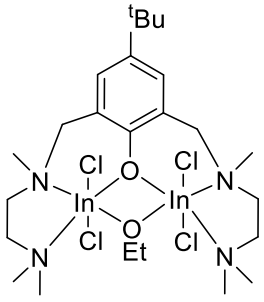

[In$_2$(**66**)Cl$_4$](μ-OEt)

Figure 1.77:Dinucleating monophenolate In(III) complexes employed by Mehrkhodavandi *et al.*[212]

1.5 Summary and project aims

The majority of plastics are derived from petrochemical sources which represent a volatile resource and contribute greatly to global pollution. The production of renewable polymers offers a further opportunity to prepare benign, biodegradable materials as well as being more reliable in the long term. Poly(lactic acid) is an example of a renewable and biodegradable material which has properties in common with conventional petrochemical plastics.

A range of initiators have been reported in the literature for the ROP of *rac*-LA, the scope of which is broad. Many metal centres and even more ligands have been applied to this reaction with the goal of ring opening lactide with high activity and control. The area of PLA remains a highly active of research, with important challenges yet to be overcome. A main goal is the preparation of highly isotactic PLA from *rac*-LA affording enhanced material and temperature properties. A suitable initiator for this must be robust and highly active, especially under industrial conditions.

The aim of this research, therefore, is to prepare a series of well-defined initiators for the application of ROP of *rac*-LA. 2-(Aminomethyl)piperidine is employed as a common core in the preparation of a diverse range of ligand structures. Coordination of these ligands is achieved with a range of metals and the subsequent initiators are employed for the ROP of *rac*-LA.

1.6 References

1. S. Shafiee and E. Topal, *Energy Policy*, 2009, **37**, 181-189.
2. The Telegraph, (2015), *The Earth is not running out of oil and gas, BP says* [Online] Available at: http://www.telegraph.co.uk/finance/newsbysector/energy/oilandgas/11971280/The-Earth-is-not-running-out-of-oil-and-gas-BP-says.html. [Date accessed: 24/10/2016]
3. N. Oreskes, *Science*, 2004, **306**, 1686.
4. C. John, N. Dana, A. G. Sarah, R. Mark, W. Bärbel, P. Rob, W. Robert, J. Peter and S. Andrew, *Environ. Res. Lett*, 2013, **8**, 024024.
5. IPCC, 2013: *Climate Change 2013: The Physical Science Basis. Contribution of Working Group I to the Fifth Assessment Report of the Intergovernmental Panel on Climate Change* [Stocker, T.F., D. Qin, G.-K. Plattner, M. Tignor, S.K. Allen, J. Boschung, A. Nauels, Y. Xia, V. Bex and P.M. Midgley (eds.)].

Cambridge University Press, Cambridge, United Kingdom and New York, NY, USA, 1535 pp, doi:10.1017/CBO9781107415324.
6. The Guardian, (2016), *'New era of climate change reality' as emissions hit symbolic threshold* [Online] Available at: https://www.theguardian.com/environment/2016/oct/24/new-era-of-climate-change-reality-as-emissions-hit-symbolic-threshold (Date accessed: 24/10/2016).
7. B. K. Sovacool, *Energy Research & Social Science*, 2016, **13**, 202-215.
8. PlasticsEurope, (2014) *Plastics -the Facts 2014 / 2015*. Available at: http://www.plasticseurope.org/Document/plastics-the-facts-2014.aspx. Date accessed: 11/10/2016.
9. World Economic Forum, Ellen MacArthur Foundation and McKinsey & Company, *The New Plastics Economy* (2016). Available at: http://www.ellenmacarthurfoundation.org/publication. [Date accessed: 11/10/16]
10. R. E. Drumright, P. R. Gruber and D. E. Henton, *Adv. Mater.*, 2000, **12**, 1841-1846.
11. L. Shen, E. Worrell and M. Patel, *Biofuels, Bioprod. Biorefin.*, 2010, **4**, 25-40.
12. M. Jamshidian, E. A. Tehrany, M. Imran, M. Jacquot and S. Desobry, *Compr. Rev. Food Sci. Food Saf.*, 2010, **9**, 552-571.
13. J. R. Jambeck, R. Geyer, C. Wilcox, T. R. Siegler, M. Perryman, A. Andrady, R. Narayan and K. L. Law, *Science*, 2015, **347**, 768-771.
14. Coca-Cola, (2016), *PlantBottle* [Online] Available at: http://www.coca-colacompany.com/PlantBottle. [Date accessed: 17/10/2016)
15. Coca-Cola, (2016) *PlantBottle 2.0* [Online] Available at: http://www.coca-colacompany.com/stories/plantbottle-20-coca-cola-unveils-worlds-first-pet-plastic-bottle-made-entirely-from-plants. [Date accessed: 17/10/2016]
16. S. K. Burgess, R. M. Kriegel and W. J. Koros, *Macromolecules*, 2015, **48**, 2184-2193.
17. Corbion Purac, (2015), *FDCA for PEF* [Online] Availble at: http://www.corbion.com/bioplastics/products/fdca-for-pef. [Date accessed: 25/10/2016]
18. A. J. J. E. Eerhart, A. P. C. Faaij and M. K. Patel, *Energy Environ. Sci.*, 2012, **5**, 6407-6422.
19. R. A. Gross and B. Kalra, *Science*, 2002, **297**, 803-807.
20. Metabolix, (2016), *Metabolix Performance PHA Biopolymers*, [Online] Available at: http://www.metabolix.com/products/biopolymers. [Date accessed: 25/10/2016]
21. pttMCC Biochem, (2014) *Introducing BioPBS* [Online] Available at: http://www.pttmcc.com/new/content.php?mid=W040. [Date accessed: 25/10/2016]
22. R. Auras, B. Harte and S. Selke, *Macromol. Biosci.*, 2004, **4**, 835-864.
23. R. Auras, S. Singh and J. Singh, *J. Test. Eval.*, 2006, **34**, 1-7.
24. R. A. Auras, S. P. Singh and J. J. Singh, *Packag. Technol. Sci.*, 2005, **18**, 207-216.
25. C. K. Williams and M. A. Hillmyer, *Polym. Rev.*, 2008, **48**, 1-10.
26. E. T. H. Vink, D. A. Glassner, J. J. Kolstad, R. J. Wooley and R. P. O'Connor, *Ind. Biotechnol.*, 2007, **3**, 58-81.

27. Corbion Purac, (2014), *Corbion Purac intends to construct a 75kTpa PLA production plant*, [Online] Available at: http://www.corbion.com/media/press-releases?newsId=1867550. [Date accessed: 25/10/2016]
28. Corbion Purac, (2016), *Corbion launches PLA portfolio of neat bioplastic resins for the North American market*, [Online] Available at: http://www.corbion.com/media/press-releases?newsId=2013684. [Date accessed: 25/10/2016]
29. Corbion Purac, (2016), *PLA Bioplastics* [Online] Available at: http://www.corbion.com/media/75646/corbion_bioplastics_brochure.pdf. [Date accessed: 11/10/2016]
30. X. Pang, X. Zhuang, Z. Tang and X. Chen, *Biotechnol. J.*, 2010, **5**, 1125-1136.
31. M. Dusselier, P. Van Wouwe, A. Dewaele, P. A. Jacobs and B. F. Sels, *Science*, 2015, **349**, 78-80.
32. K. Masutani and Y. Kimura, in *Poly(lactic acid) Science and Technology: Processing, Properties, Additives and Applications*, The Royal Society of Chemistry, Editon edn., 2015, pp. 1-36.
33. T. M. Ovitt and G. W. Coates, *J. Am. Chem. Soc.*, 1999, **121**, 4072-4073.
34. H. Tsuji, *Macromol. Biosci.*, 2005, **5**, 569-597.
35. B. M. Chamberlain, M. Cheng, D. R. Moore, T. M. Ovitt, E. B. Lobkovsky and G. W. Coates, *J. Am. Chem. Soc.*, 2001, **123**, 3229-3238.
36. O. Dechy-Cabaret, B. Martin-Vaca and D. Bourissou, *Chem. Rev.*, 2004, **104**, 6147-6176.
37. J. Kasperczyk and M. Bero, *Polymer*, 2000, **41**, 391-395.
38. J. E. Kasperczyk, *Macromolecules*, 1995, **28**, 3937-3939.
39. H. R. Kricheldorf and R. Dunsing, *Die Makromolekulare Chemie*, 1986, **187**, 1611-1625.
40. H. R. Kricheldorf and I. Kreiser, *Die Makromolekulare Chemie*, 1987, **188**, 1861-1873.
41. Y. Wang, L. Zhang, X. Guo, R. Zhang and J. Li, *J. Polym. Res.*, 2013, **20**, 87.
42. A. P. Dove, R. C. Pratt, B. G. G. Lohmeijer, R. M. Waymouth and J. L. Hedrick, *J. Am. Chem. Soc.*, 2005, **127**, 13798-13799.
43. G. Nogueira, A. Favrelle, M. Bria, J. P. Prates Ramalho, P. J. Mendes, A. Valente and P. Zinck, *React. Chem. Eng.*, 2016, **1**, 508-520.
44. B. G. G. Lohmeijer, R. C. Pratt, F. Leibfarth, J. W. Logan, D. A. Long, A. P. Dove, F. Nederberg, J. Choi, C. Wade, R. M. Waymouth and J. L. Hedrick, *Macromolecules*, 2006, **39**, 8574-8583.
45. R. C. Pratt, B. G. G. Lohmeijer, D. A. Long, R. M. Waymouth and J. L. Hedrick, *J. Am. Chem. Soc.*, 2006, **128**, 4556-4557.
46. N. Nomura, R. Ishii, M. Akakura and K. Aoi, *J. Am. Chem. Soc.*, 2002, **124**, 5938-5939.
47. N. Nomura, R. Ishii, Y. Yamamoto and T. Kondo, *Chem. Eur. J.*, 2007, **13**, 4433-4451.
48. P. Hormnirun, E. L. Marshall, V. C. Gibson, R. I. Pugh and A. J. P. White, *Proc. Natl. Acad. Sci. U. S. A.*, 2006, **103**, 15343-15348.
49. T. M. Ovitt and G. W. Coates, *J. Polym. Sci., Part A: Polym. Chem.*, 2000, **38**, 4686-4692.
50. T. M. Ovitt and G. W. Coates, *J. Am. Chem. Soc.*, 2002, **124**, 1316-1326.
51. S.-C. Rosca, D.-A. Rosca, V. Dorcet, C. M. Kozak, F. M. Kerton, J.-F. Carpentier and Y. Sarazin, *Dalton Trans.*, 2013, **42**, 9361-9375.

52. K. Devaine-Pressing, J. H. Lehr, M. E. Pratt, L. N. Dawe, A. A. Sarjeant and C. M. Kozak, *Dalton Trans.*, 2015, **44**, 12365-12375.
53. T. Rosen, I. Goldberg, V. Venditto and M. Kol, *J. Am. Chem. Soc.*, 2016, **138**, 12041-12044.
54. R. H. Platel, L. M. Hodgson and C. K. Williams, *Polym. Rev.*, 2008, **48**, 11-63.
55. M. T. Zell, B. E. Padden, A. J. Paterick, K. A. M. Thakur, R. T. Kean, M. A. Hillmyer and E. J. Munson, *Macromolecules*, 2002, **35**, 7700-7707.
56. M. Cheng, A. B. Attygalle, E. B. Lobkovsky and G. W. Coates, *J. Am. Chem. Soc.*, 1999, **121**, 11583-11584.
57. J. Baran, A. Duda, A. Kowalski, R. Szymanski and S. Penczek, *Macromol. Rapid Commun.*, 1997, **18**, 325-333.
58. Z. Grubisic, P. Rempp and H. Benoit, *J. Polym. Sci., Part B: Polym. Lett.*, 1967, **5**, 753-759.
59. A. Kowalski, A. Duda and S. Penczek, *Macromolecules*, 2000, **33**, 7359-7370.
60. A. Kowalski, J. Libiszowski, T. Biela, M. Cypryk, A. Duda and S. Penczek, *Macromolecules*, 2005, **38**, 8170-8176.
61. H. R. Kricheldorf, I. Kreiser-Saunders and A. Stricker, *Macromolecules*, 2000, **33**, 702-709.
62. S. Y. Lee, P. Valtchev and F. Dehghani, *Green Chemistry*, 2012, **14**, 1357-1366.
63. G. Schwach, J. Coudane, R. Engel and M. Vert, *J. Polym. Sci., Part A: Polym. Chem.*, 1997, **35**, 3431-3440.
64. S. Penczek, A. Duda, A. Kowalski, J. Libiszowski, K. Majerska and T. Biela, *Macromol. Symp.*, 2000, **157**, 61-70.
65. S. Sosnowski and P. Lewinski, *Polym. Chem.*, 2015, **6**, 6292-6296.
66. J. Guo, P. Haquette, J. Martin, K. Salim and C. M. Thomas, *Angew. Chem. Int. Ed.*, 2013, **52**, 13584-13587.
67. K. B. Aubrecht, M. A. Hillmyer and W. B. Tolman, *Macromolecules*, 2002, **35**, 644-650.
68. N. Nimitsiriwat, E. L. Marshall, V. C. Gibson, M. R. J. Elsegood and S. H. Dale, *J. Am. Chem. Soc.*, 2004, **126**, 13598-13599.
69. A. P. Dove, V. C. Gibson, E. L. Marshall, H. S. Rzepa, A. J. P. White and D. J. Williams, *J. Am. Chem. Soc.*, 2006, **128**, 9834-9843.
70. A. P. Dove, V. C. Gibson, E. L. Marshall, A. J. P. White and D. J. Williams, *Chem. Commun.*, 2001, 283-284.
71. B. Calvo, M. G. Davidson and D. García-Vivó, *Inorg. Chem.*, 2011, **50**, 3589-3595.
72. H.-Y. Chen, J. Zhang, C.-C. Lin, J. H. Reibenspies and S. A. Miller, *Green Chemistry*, 2007, **9**, 1038-1040.
73. Y. Huang, Y.-H. Tsai, W.-C. Hung, C.-S. Lin, W. Wang, J.-H. Huang, S. Dutta and C.-C. Lin, *Inorg. Chem.*, 2010, **49**, 9416-9425.
74. Y. Huang, W. Wang, C.-C. Lin, M. P. Blake, L. Clark, A. D. Schwarz and P. Mountford, *Dalton Trans.*, 2013, **42**, 9313-9324.
75. W.-Y. Lu, M.-W. Hsiao, S. C. N. Hsu, W.-T. Peng, Y.-J. Chang, Y.-C. Tsou, T.-Y. Wu, Y.-C. Lai, Y. Chen and H.-Y. Chen, *Dalton Trans.*, 2012, **41**, 3659-3667.
76. H.-W. Ou, K.-H. Lo, W.-T. Du, W.-Y. Lu, W.-J. Chuang, B.-H. Huang, H.-Y. Chen and C.-C. Lin, *Inorg. Chem.*, 2016, **55**, 1423-1432.

77. J. Zhang, C. Jian, Y. Gao, L. Wang, N. Tang and J. Wu, *Inorg. Chem.*, 2012, **51**, 13380-13389.
78. D. Alhashmialameer, N. Ikpo, J. Collins, L. N. Dawe, K. Hattenhauer and F. M. Kerton, *Dalton Trans.*, 2015, **44**, 20216-20231.
79. R. K. Dean, A. M. Reckling, H. Chen, L. N. Dawe, C. M. Schneider and C. M. Kozak, *Dalton Trans.*, 2013, **42**, 3504-3520.
80. C.-A. Huang and C.-T. Chen, *Dalton Trans.*, 2007, 5561-5566.
81. J. Xiong, J. Zhang, Y. Sun, Z. Dai, X. Pan and J. Wu, *Inorg. Chem.*, 2015, **54**, 1737-1743.
82. Z. Dai, Y. Sun, J. Xiong, X. Pan and J. Wu, *ACS Macro Lett.*, 2015, 556-560.
83. J. Zhang, J. Xiong, Y. Sun, N. Tang and J. Wu, *Macromolecules*, 2014, **47**, 7789-7796.
84. Z. Dai, Y. Sun, J. Xiong, X. Pan, N. Tang and J. Wu, *Catal. Sci. Technol.*, 2016, **6**, 515-520.
85. Y. Sun, J. Xiong, Z. Dai, X. Pan, N. Tang and J. Wu, *Inorg. Chem.*, 2016, **55**, 136-143.
86. S. Song, H. Ma and Y. Yang, *Dalton Trans.*, 2013, **42**, 14200-14211.
87. M. J. Walton, S. J. Lancaster and C. Redshaw, *ChemCatChem*, 2014, **6**, 1892-1898.
88. C. A. Wheaton, P. G. Hayes and B. J. Ireland, *Dalton Trans.*, 2009, 4832-4846.
89. V. Poirier, T. Roisnel, J.-F. Carpentier and Y. Sarazin, *Dalton Trans.*, 2009, 9820-9827.
90. X. Xu, Y. Chen, G. Zou, Z. Ma and G. Li, *J. Organomet. Chem.*, 2010, **695**, 1155-1162.
91. L. Wang and H. Ma, *Macromolecules*, 2010, **43**, 6535-6537.
92. H.-Y. Chen, H.-Y. Tang and C.-C. Lin, *Polymer*, 2007, **48**, 2257-2262.
93. L. Clark, G. B. Deacon, C. M. Forsyth, P. C. Junk, P. Mountford, J. P. Townley and J. Wang, *Dalton Trans.*, 2013, **42**, 9294-9312.
94. M. Kuzdrowska, L. Annunziata, S. Marks, M. Schmid, C. G. Jaffredo, P. W. Roesky, S. M. Guillaume and L. Maron, *Dalton Trans.*, 2013, **42**, 9352-9360.
95. Z. Tang, X. Chen, Q. Liang, X. Bian, L. Yang, L. Piao and X. Jing, *J. Polym. Sci., Part A: Polym. Chem.*, 2003, **41**, 1934-1941.
96. M. H. Chisholm, J. C. Gallucci and K. Phomphrai, *Inorg. Chem.*, 2005, **44**, 8004-8010.
97. M. H. Chisholm, J. Gallucci and K. Phomphrai, *Inorg. Chem.*, 2002, **41**, 2785-2794.
98. M. H. Chisholm, J. C. Huffman and K. Phomphrai, *J. Chem. Soc., Dalton Trans.*, 2001, 222-224.
99. M. H. Chisholm, J. Gallucci and K. Phomphrai, *Chem. Commun.*, 2003, 48-49.
100. M. H. Chisholm, J. C. Gallucci and K. Phomphrai, *Inorg. Chem.*, 2004, **43**, 6717-6725.
101. T. J. J. Whitehorne, B. Vabre and F. Schaper, *Dalton Trans.*, 2014, **43**, 6339-6352.
102. M. H. Chisholm, K. Choojun, A. S. Chow, G. Fraenkel and J. C. Gallucci, *Inorg. Chem.*, 2013, **52**, 11302-11310.
103. M. H. Chisholm, K. Choojun, J. C. Gallucci and P. M. Wambua, *Chem. Sci.*, 2012, **3**, 3445-3457.
104. V. Balasanthiran, M. H. Chisholm, K. Choojun, C. B. Durr and P. M. Wambua, *J. Organomet. Chem.*, 2016, **812**, 56-65.

105. H. Wang, Y. Yang and H. Ma, *Macromolecules*, 2014, **47**, 7750-7764.
106. H. Wang, J. Guo, Y. Yang and H. Ma, *Dalton Trans.*, 2016, **45**, 10942-10953.
107. W. Yi and H. Ma, *Inorg. Chem.*, 2013, **52**, 11821-11835.
108. W. Yi and H. Ma, *Dalton Trans.*, 2014, **43**, 5200-5210.
109. M. Huang, C. Pan and H. Ma, *Dalton Trans.*, 2015, **44**, 12420-12431.
110. L. F. Sánchez-Barba, A. Garcés, J. Fernández-Baeza, A. Otero, C. Alonso-Moreno, A. Lara-Sánchez and A. M. Rodríguez, *Organometallics*, 2011, **30**, 2775-2789.
111. A. Garcés, L. F. Sánchez-Barba, J. Fernández-Baeza, A. Otero, M. Honrado, A. Lara-Sánchez and A. M. Rodríguez, *Inorg. Chem.*, 2013, **52**, 12691-12701.
112. L. F. Sánchez-Barba, A. Garcés, M. Fajardo, C. Alonso-Moreno, J. Fernández-Baeza, A. Otero, A. Antiñolo, J. Tejeda, A. Lara-Sánchez and M. I. López-Solera, *Organometallics*, 2007, **26**, 6403-6411.
113. M. J. Walton, S. J. Lancaster, J. A. Wright, M. R. J. Elsegood and C. Redshaw, *Dalton Trans.*, 2014, **43**, 18001-18009.
114. H. Xie, Z. Mou, B. Liu, P. Li, W. Rong, S. Li and D. Cui, *Organometallics*, 2014, **33**, 722-730.
115. H. Wang and H. Ma, *Chem. Commun.*, 2013, **49**, 8686-8688.
116. C. K. Williams, L. E. Breyfogle, S. K. Choi, W. Nam, V. G. Young, M. A. Hillmyer and W. B. Tolman, *J. Am. Chem. Soc.*, 2003, **125**, 11350-11359.
117. D. J. Darensbourg and O. Karroonnirun, *Inorg. Chem.*, 2010, **49**, 2360-2371.
118. F. Drouin, P. O. Oguadinma, T. J. J. Whitehorne, R. E. Prud'homme and F. Schaper, *Organometallics*, 2010, **29**, 2139-2147.
119. H. Wang, Y. Yang and H. Ma, *Inorg. Chem.*, 2016, **55**, 7356-7372.
120. Y. Yang, H. Wang and H. Ma, *Inorg. Chem.*, 2015, **54**, 5839-5854.
121. S. Song, X. Zhang, H. Ma and Y. Yang, *Dalton Trans.*, 2012, **41**, 3266-3277.
122. L. Wang and H. Ma, *Dalton Trans.*, 2010, **39**, 7897-7910.
123. M. Honrado, A. Otero, J. Fernández-Baeza, L. F. Sánchez-Barba, A. n. Lara-Sánchez, J. Tejeda, M. a. P. Carrión, J. Martínez-Ferrer, A. Garcés and A. M. Rodríguez, *Organometallics*, 2013, **32**, 3437-3440.
124. A. Otero, J. Fernández-Baeza, L. F. Sánchez-Barba, J. Tejeda, M. Honrado, A. Garcés, A. Lara-Sánchez and A. M. Rodríguez, *Organometallics*, 2012, **31**, 4191-4202.
125. M. Honrado, A. Otero, J. Fernández-Baeza, L. F. Sánchez-Barba, A. Garcés, A. Lara-Sánchez and A. M. Rodríguez, *Organometallics*, 2014, **33**, 1859-1866.
126. Z. Mou, B. Liu, M. Wang, H. Xie, P. Li, L. Li, S. Li and D. Cui, *Chem. Commun.*, 2014, **50**, 11411-11414.
127. S. Abbina and G. Du, *ACS Macro Lett.*, 2014, **3**, 689-692.
128. T. Rosen, Y. Popowski, I. Goldberg and M. Kol, *Chem. Eur. J.*, 2016, **22**, 11533-11536.
129. A. Amgoune, C. M. Thomas and J.-F. Carpentier, *Macromol. Rapid Commun.*, 2007, **28**, 693-697.
130. A. Amgoune, C. M. Thomas, S. Ilinca, T. Roisnel and J.-F. Carpentier, *Angew. Chem. Int. Ed.*, 2006, **45**, 2782-2784.
131. A. Amgoune, C. M. Thomas, T. Roisnel and J.-F. Carpentier, *Chem. Eur. J.*, 2006, **12**, 169-179.
132. C. Bakewell, T.-P.-A. Cao, X. F. Le Goff, N. J. Long, A. Auffrant and C. K. Williams, *Organometallics*, 2013, **32**, 1475-1483.

133. C. Bakewell, T.-P.-A. Cao, N. Long, X. F. Le Goff, A. Auffrant and C. K. Williams, *J. Am. Chem. Soc.*, 2012, **134**, 20577-20580.
134. C. Bakewell, A. J. P. White, N. J. Long and C. K. Williams, *Inorg. Chem.*, 2015, **54**, 2204-2212.
135. T.-P.-A. Cao, A. Buchard, X. F. Le Goff, A. Auffrant and C. K. Williams, *Inorg. Chem.*, 2012, **51**, 2157-2169.
136. B. M. Chamberlain, Y. Sun, J. R. Hagadorn, E. W. Hemmesch, V. G. Young, M. Pink, M. A. Hillmyer and W. B. Tolman, *Macromolecules*, 1999, **32**, 2400-2402.
137. W. Gu, P. Xu, Y. Wang, Y. Yao, D. Yuan and Q. Shen, *Organometallics*, 2015, **34**, 2907-2916.
138. L. M. Hodgson, A. J. P. White and C. K. Williams, *J. Polym. Sci., Part A: Polym. Chem.*, 2006, **44**, 6646-6651.
139. R. H. Platel, A. J. P. White and C. K. Williams, *Chem. Commun.*, 2009, 4115-4117.
140. R. H. Platel, A. J. P. White and C. K. Williams, *Inorg. Chem.*, 2011, **50**, 7718-7728.
141. L. Clark, M. G. Cushion, H. E. Dyer, A. D. Schwarz, R. Duchateau and P. Mountford, *Chem. Commun.*, 2010, **46**, 273-275.
142. J.-C. Buffet, A. Kapelski and J. Okuda, *Macromolecules*, 2010, **43**, 10201-10203.
143. J.-C. Buffet and J. Okuda, *Dalton Trans.*, 2011, **40**, 7748-7754.
144. A. Otero, J. Fernández-Baeza, A. Lara-Sánchez, C. Alonso-Moreno, I. Márquez-Segovia, L. F. Sánchez-Barba and A. M. Rodríguez, *Angew. Chem. Int. Ed.*, 2009, **48**, 2176-2179.
145. A. Buchard, R. H. Platel, A. Auffrant, X. F. Le Goff, P. Le Floch and C. K. Williams, *Organometallics*, 2010, **29**, 2892-2900.
146. H. E. Dyer, S. Huijser, N. Susperregui, F. Bonnet, A. D. Schwarz, R. Duchateau, L. Maron and P. Mountford, *Organometallics*, 2010, **29**, 3602-3621.
147. Z. Mou, B. Liu, X. Liu, H. Xie, W. Rong, L. Li, S. Li and D. Cui, *Macromolecules*, 2014, **47**, 2233-2241.
148. S. Yang, K. Nie, Y. Zhang, M. Xue, Y. Yao and Q. Shen, *Inorg. Chem.*, 2014, **53**, 105-115.
149. K. Nie, L. Fang, Y. Yao, Y. Zhang, Q. Shen and Y. Wang, *Inorg. Chem.*, 2012, **51**, 11133-11143.
150. C. Bakewell, A. J. P. White, N. J. Long and C. K. Williams, *Angew. Chem. Int. Ed.*, 2014, **53**, 9226-9230.
151. R. Heck, E. Schulz, J. Collin and J.-F. Carpentier, *J. Mol. Catal. A: Chem.*, 2007, **268**, 163-168.
152. P. L. Arnold, J.-C. Buffet, R. P. Blaudeck, S. Sujecki, A. J. Blake and C. Wilson, *Angew. Chem. Int. Ed.*, 2008, **47**, 6033-6036.
153. C.-X. Cai, A. Amgoune, C. W. Lehmann and J.-F. Carpentier, *Chem. Commun.*, 2004, 330-331.
154. Y. Chapurina, J. Klitzke, O. d. L. Casagrande Jr, M. Awada, V. Dorcet, E. Kirillov and J.-F. Carpentier, *Dalton Trans.*, 2014, **43**, 14322-14333.
155. J. S. Klitzke, T. Roisnel, E. Kirillov, O. d. L. Casagrande and J.-F. Carpentier, *Organometallics*, 2013, **33**, 309-321.
156. A. Sauer, A. Kapelski, C. Fliedel, S. Dagorne, M. Kol and J. Okuda, *Dalton Trans.*, 2013, **42**, 9007-9023.

157. Y. Kim, G. K. Jnaneshwara and J. G. Verkade, *Inorg. Chem.*, 2003, **42**, 1437-1447.
158. B. Gao, Q. Duan, Y. Li, D. Li, L. Zhang, Y. Cui, N. Hu and X. Pang, *RSC Adv.*, 2015, **5**, 13437-13442.
159. B. Gao, X. Li, R. Duan and X. Pang, *New J. Chem.*, 2015, **39**, 2404-2408.
160. A. J. Chmura, D. M. Cousins, M. G. Davidson, M. D. Jones, M. D. Lunn and M. F. Mahon, *Dalton Trans.*, 2008, 1437-1443.
161. E. L. Whitelaw, M. D. Jones and M. F. Mahon, *Inorg. Chem.*, 2010, **49**, 7176-7181.
162. A. Stopper, J. Okuda and M. Kol, *Macromolecules*, 2012, **45**, 698-704.
163. A. Stopper, K. Press, J. Okuda, I. Goldberg and M. Kol, *Inorg. Chem.*, 2014, **53**, 9140-9150.
164. E. Sergeeva, J. Kopilov, I. Goldberg and M. Kol, *Inorg. Chem.*, 2010, **49**, 3977-3979.
165. S. H. Kim, J. Lee, D. J. Kim, J. H. Moon, S. Yoon, H. J. Oh, Y. Do, Y. S. Ko, J.-H. Yim and Y. Kim, *J. Organomet. Chem.*, 2009, **694**, 3409-3417.
166. M. D. Jones, M. G. Davidson and G. Kociok-Kohn, *Polyhedron*, 2010, **29**, 697-700.
167. S. Gendler, S. Segal, I. Goldberg, Z. Goldschmidt and M. Kol, *Inorg. Chem.*, 2006, **45**, 4783-4790.
168. A. J. Chmura, M. G. Davidson, M. D. Jones, M. D. Lunn, M. F. Mahon, A. F. Johnson, P. Khunkamchoo, S. L. Roberts and S. S. F. Wong, *Macromolecules*, 2006, **39**, 7250-7257.
169. A. L. Zelikoff, J. Kopilov, I. Goldberg, G. W. Coates and M. Kol, *Chem. Commun.*, 2009, 6804-6806.
170. M. D. Jones, L. Brady, P. McKeown, A. Buchard, P. M. Schafer, L. H. Thomas, M. F. Mahon, T. J. Woodman and J. P. Lowe, *Chem. Sci.*, 2015, **6**, 5034-5039.
171. M. D. Jones, S. L. Hancock, P. McKeown, P. M. Schafer, A. Buchard, L. H. Thomas, M. F. Mahon and J. P. Lowe, *Chem. Commun.*, 2014, **50**, 15967-15970.
172. E. Sergeeva, J. Kopilov, I. Goldberg and M. Kol, *Chem. Commun.*, 2009, 3053-3055.
173. M. Hu, M. Wang, H. Zhu, L. Zhang, H. Zhang and L. Sun, *Dalton Trans.*, 2010, **39**, 4440-4446.
174. A. J. Chmura, M. G. Davidson, C. J. Frankis, M. D. Jones and M. D. Lunn, *Chem. Commun.*, 2008, 1293-1295.
175. C. Romain, B. Heinrich, S. B. Laponnaz and S. Dagorne, *Chem. Commun.*, 2012, **48**, 2213-2215.
176. P. Dubois, C. Jacobs, R. Jerome and P. Teyssie, *Macromolecules*, 1991, **24**, 2266-2270.
177. A. Kowalski, A. Duda and S. Penczek, *Macromolecules*, 1998, **31**, 2114-2122.
178. A. Routaray, N. Nath, T. Maharana and A. K. Sutar, *Catal. Sci. Technol.*, 2015.
179. N. Spassky, M. Wisniewski, C. Pluta and A. LeBorgne, *Macromol. Chem. Phys.*, 1996, **197**, 2627-2637.
180. K. Majerska and A. Duda, *J. Am. Chem. Soc.*, 2004, **126**, 1026-1027.
181. C. P. Radano, G. L. Baker and M. R. Smith, *J. Am. Chem. Soc.*, 2000, **122**, 1552-1553.
182. Z. Zhong, P. J. Dijkstra and J. Feijen, *J. Am. Chem. Soc.*, 2003, **125**, 11291-11298.

183. Z. Y. Zhong, P. J. Dijkstra and J. Feijen, *Angew. Chem. Int. Ed.*, 2002, **41**, 4510-4513.
184. N. Maudoux, T. Roisnel, V. Dorcet, J.-F. Carpentier and Y. Sarazin, *Chem. Eur. J.*, 2014, **20**, 6131-6147.
185. T. K. Saha, V. Ramkumar and D. Chakraborty, *Inorg. Chem.*, 2011, **50**, 2720-2722.
186. M. Wisniewski, A. LeBorgne and N. Spassky, *Macromol. Chem. Phys.*, 1997, **198**, 1227-1238.
187. E. D. Cross, L. E. N. Allan, A. Decken and M. P. Shaver, *J. Polym. Sci., Part A: Polym. Chem.*, 2013, **51**, 1137-1146.
188. H.-L. Chen, S. Dutta, P.-Y. Huang and C.-C. Lin, *Organometallics*, 2012, **31**, 2016-2025.
189. E. L. Whitelaw, G. Loraine, M. F. Mahon and M. D. Jones, *Dalton Trans.*, 2011, **40**, 11469-11473.
190. K. Nie, W. Gu, Y. Yao, Y. Zhang and Q. Shen, *Organometallics*, 2013, **32**, 2608-2617.
191. S. L. Hancock, M. F. Mahon and M. D. Jones, *Dalton Trans.*, 2013, **42**, 9279-9285.
192. A. Pilone, K. Press, I. Goldberg, M. Kol, M. Mazzeo and M. Lamberti, *J. Am. Chem. Soc.*, 2014, **136**, 2940-2943.
193. P. Hormnirun, E. L. Marshall, V. C. Gibson, A. J. P. White and D. J. Williams, *J. Am. Chem. Soc.*, 2004, **126**, 2688-2689.
194. H. Du, A. H. Velders, P. J. Dijkstra, J. Sun, Z. Zhong, X. Chen and J. Feijen, *Chem. Eur. J.*, 2009, **15**, 9836-9845.
195. P. Horeglad, P. Kruk and J. Pécaut, *Organometallics*, 2010, **29**, 3729-3734.
196. P. Horeglad, G. Szczepaniak, M. Dranka and J. Zachara, *Chem. Commun.*, 2012, **48**, 1171-1173.
197. M. Cybularczyk, M. Dranka, J. Zachara and P. Horeglad, *Organometallics*, 2016, **35**, 3311-3322.
198. P. Horeglad, M. Cybularczyk, A. Litwinska, A. M. Dabrowska, M. Dranka, G. Z. Zukowska, M. Urbanczyk and M. Michalak, *Polym. Chem.*, 2016, **7**, 2022-2036.
199. P. Horeglad, M. Cybularczyk, B. Trzaskowski, G. Z. Żukowska, M. Dranka and J. Zachara, *Organometallics*, 2015, **34**, 3480-3496.
200. C. Bakewell, A. J. P. White, N. J. Long and C. K. Williams, *Inorg. Chem.*, 2013, **52**, 12561-12567.
201. C. Bakewell, R. H. Platel, S. K. Cary, S. M. Hubbard, J. M. Roaf, A. C. Levine, A. J. P. White, N. J. Long, M. Haaf and C. K. Williams, *Organometallics*, 2012, **31**, 4729-4736.
202. S. Ghosh, R. R. Gowda, R. Jagan and D. Chakraborty, *Dalton Trans.*, 2015, **44**, 10410-10422.
203. K. M. Osten, D. C. Aluthge and P. Mehrkhodavandi, *Dalton Trans.*, 2015, **44**, 6126-6139.
204. I. Yu, A. Acosta-Ramírez and P. Mehrkhodavandi, *J. Am. Chem. Soc.*, 2012, **134**, 12758-12773.
205. A. Pietrangelo, S. C. Knight, A. K. Gupta, L. J. Yao, M. A. Hillmyer and W. B. Tolman, *J. Am. Chem. Soc.*, 2010, **132**, 11649-11657.
206. D. C. Aluthge, E. X. Yan, J. M. Ahn and P. Mehrkhodavandi, *Inorg. Chem.*, 2014, **53**, 6628-6836.

207. D. C. Aluthge, B. O. Patrick and P. Mehrkhodavandi, *Chem. Commun.*, 2013, **49**, 4295-4297.
208. D. C. Aluthge, J. M. Ahn and P. Mehrkhodavandi, *Chem. Sci.*, 2015, **6**, 5284-5292.
209. N. Maudoux, T. Roisnel, V. Dorcet, J.-F. Carpentier and Y. Sarazin, *Chem. Eur. J.*, 2014, **20**, 6131-6147.
210. A. F. Douglas, B. O. Patrick and P. Mehrkhodavandi, *Angew. Chem. Int. Ed.*, 2008, **120**, 2322-2325.
211. C. Xu, I. Yu and P. Mehrkhodavandi, *Chem. Commun.*, 2012, **48**, 6806-6808.
212. A. B. Kremer, K. M. Osten, I. Yu, T. Ebrahimi, D. C. Aluthge and P. Mehrkhodavandi, *Inorg. Chem.*, 2016, **55**, 5365-5374.

Chapter 2

Synthesis of 2-(aminomethyl)piperidine based ligands

Chapter 2: Synthesis of 2-(aminomethyl)piperidine based ligands

2.1 Introduction

A range of initiators for the ROP of LA have been described in Chapter 1. A variety of structural motifs have been shown to influence the ROP of cyclic esters with a judicious choice of metal. A common theme for a successful initiator system is the incorporation of either a cyclic moiety and/or chirality into the backbone, both of which can contribute to activity and stereocontrol.[1, 2-8] A wide range of ligand structures are based upon salen,[6, 7, 9-16] salan[3, 4, 8, 17, 18] and salalen[5, 19-22] motifs due to their ease of preparation and functionalisation. The nature of aryl substituents also plays an important role in defining performance during ROP.[10, 12, 18]The use of 2-(aminomethyl)piperidine (2-AMP) allows for the preparation of salalen and salan motifs, possessing both chirality and a cyclic backbone.

A study carried out by Beim and Day explored the condensation reaction of 2-AMP with a range of aldehydes demonstrating the interesting ring-chain tautomerism that occurs in this system.[23] Instead of the expected imino form **A**H, analysis of products by NMR spectroscopy revealed the presence of a bicyclic system **B**H, classified as octahydroimidazo[1,5-*a*]pyridines. For benzaldehyde and *tert*-butanal, there was also evidence of **A**H as a minor product. Simple aldehydes were employed for the condensation leading to the preparation of unfunctionalised heterocycles (Figure 2.1).

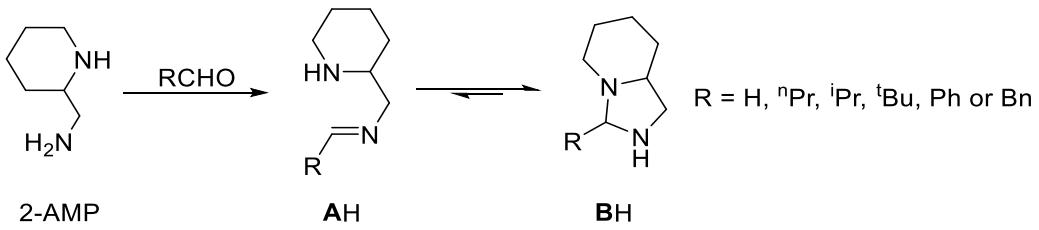

Figure 2.1: Ring-chain tautomerism of 2-AMP/aldehyde adducts.[23]

There are few reports concerning the incorporation of the 2-AMP moiety into a structure useful for catalysis. The only relevant example of a 2-AMP ligand suitable for complexation has been shown by Gowda and Chen.[24] The bisphenol, **C**H_2, was prepared by a standard two step procedure used for salalen structures. There was, however, no variation in the aryl groups and no discussion of the manifestation of the tautomerism. Ligation to zirconium afforded a complex active for the polymerisation of butyrolactones.[24]

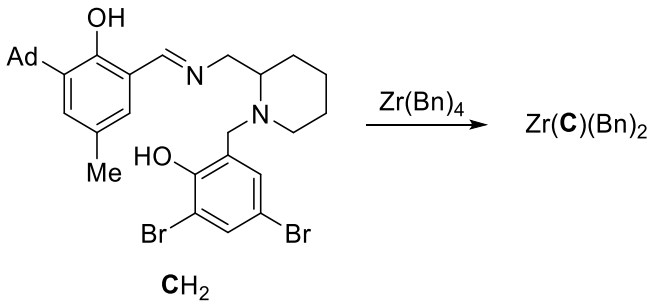

Figure 2.2: Literature example of 2-AMP ligand suitable for complexation and catalysis.[24]

In this chapter, a detailed investigation is carried out on the effect of aryl substituents upon the tautomerism observed for 2-AMP condensations followed by the realisation of ligands suitable for complexation.

2.2 Preliminary investigation

The initial reaction involved the condensation of 2-(aminomethyl)piperidine with substituted salicylaldehydes. The substituents ranged from electron donating alkyl substituents (^{t}Bu, Me, Ad) to more electron withdrawing halo substituents (Cl, Br, I). The formation of the imino adduct is uniquely set up to allow for cyclisation to afford an interesting bicyclic structure with a new 5 membered ring being formed (Figure 2.3). This phenomenon was noted in the 1960/1970s by a range of studies.[23, 25, 26] In the report by Beim and Day, unsubstituted benzaldehyde, among other substrates, was reacted with the amine.[23] The cyclisation process was noted to be dynamic with interconversion, between **A**H and **B**H, occurring in solution.

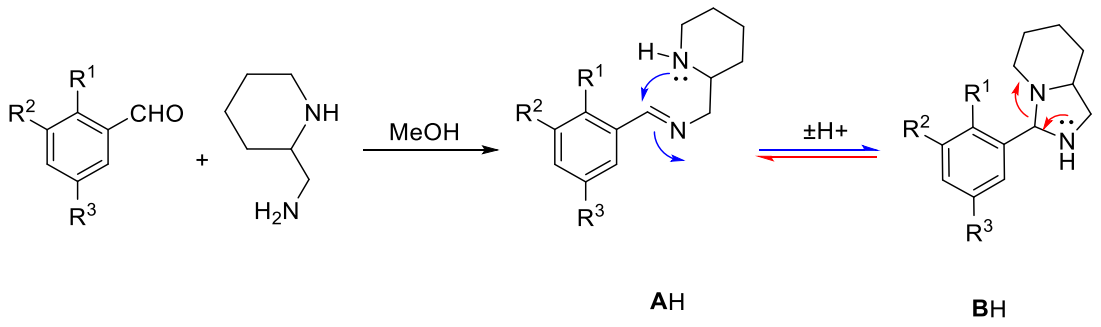

Figure 2.3: Imine condensation of substituted salicylaldehydes with 2-AMP (MeOH, rt).

In extension to previous work,[23] the introduction of groups onto the aryl ring was investigated. Depending on the nature of the substituents, the equilibrium could be tuned to favour either the imino form, **A**H, or the cyclic form, **B**H. As previously indicated by Beim and Day, an unsubstituted ring preferentially forms **B**H with **A**H as the minor product.[23, 25, 26] In this current investigation, the ratio of ratio of **A**H:**B**H was found to be ~1:4 *via* ^{1}H NMR spectroscopy ($CDCl_3$, 25°C). The introduction of the hydroxy moiety *ortho* to the aldehyde affords a dramatic change in the distribution of products with the **A**H now dominating (**A**H:**B**H ~ 3:1). This may be related to the donation of the oxygen lone pair into the imino system making the benzylic carbon relatively more electron rich hence deactivating this position towards the intramolecular cyclisation (Figure 2.4).

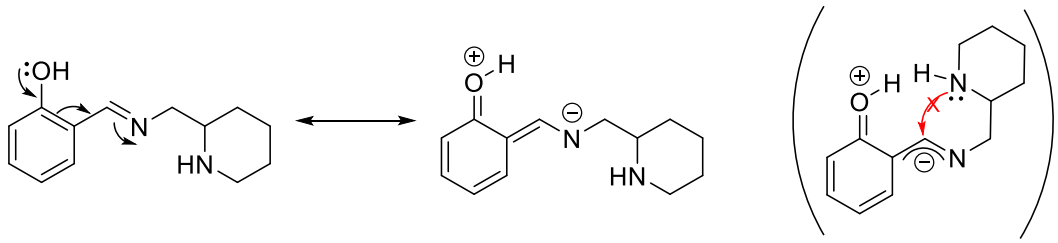

Figure 2.4: Resonance structures depicting interaction of hydroxyl group with the imine.

In tandem with the hydroxyl group's interaction with the imine, there are also resonance structures showing the distribution of electron density around the aryl ring. These different forms (Figure 2.5) rationalise the observation of the different product distributions related to the R substituents on the aryl group. When electron

withdrawing substituents are present in a *meta* position to the benzylic carbon, the bicyclic structure is observed to be the major product. This is due to the reduction of the electron density within the ring by these substituents ultimately making the benzylic carbon less electron rich and hence more susceptible to attack. Conversely, electron donating groups in these positions were observed to increase the likelihood of the imino product. For this system, the donation of electrons into the aryl ring by the OH is disfavoured by such groups, directing electron density increasingly to the benzylic position.

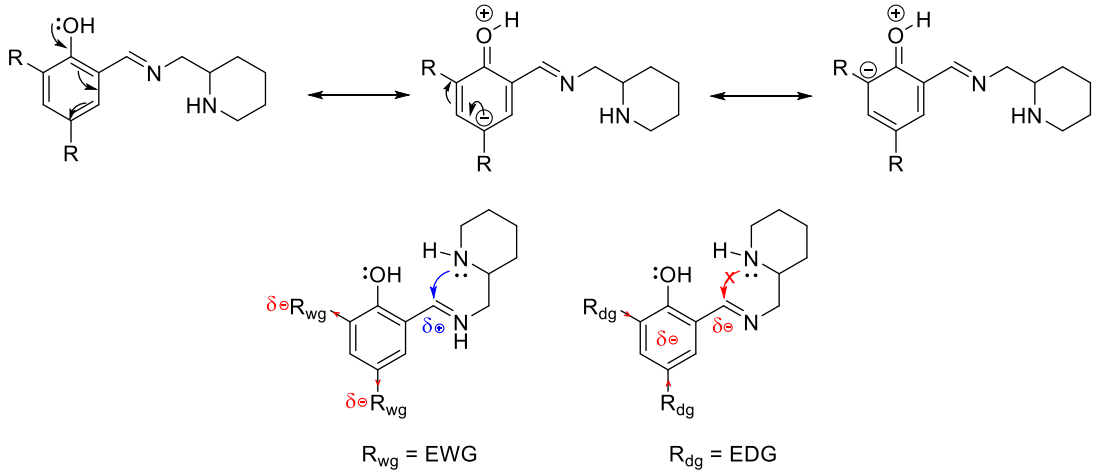

Figure 2.5: Resonance structures depicting interaction of hydroxyl group with aryl ring substituents.

The imino and bicyclic forms were distinguished primarily through ^{1}H NMR spectroscopy, specifically by identifying the benzylic resonance which represents one proton for each form. The most diagnostic resonances are due to the imine group around 8 ppm for **A**H and a singlet due to the isolated benzylic CH around 4 ppm for **B**H (Figures 2.6-2.7). Further characterisation included ^{13}C{^{1}H} NMR spectroscopy in which the diagnostic resonances were due to the imine (**A**H, ~170 ppm) and the relatively electron rich CH (**B**H, ~90 ppm) (Figure 2.8). Analysis by ESI-MS further highlights this isomerism with only one product peak being observed. The dynamic equilibrium between the different forms was also shown *via* variable temperature (VT)-NMR and exchange spectroscopy (EXSY). A summary of the various substituents and the tautomeric preference is shown in Table 2.1

Table 2.1: Influence of Aryl substituents on the formation of imine or cyclic form (298K, $CDCl_3$, 400MHz, [Aldehyde] ~0.41 M).

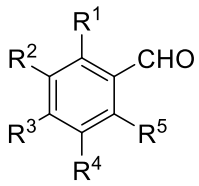

Substituents	Imine	Cyclic
R^1= N*	4	96
R^3= NO_2	7	93
R^1= Cl	7	93
R^1=R^2=R^3= R^4= R^5 = H	18	82
R^2=R^3= Napthyl	21	79
R^1= $P(Ph)_2$	23	77
R^3= ^{i}Pr	25	75
R^1=OH, R^2= R^4= X**	35	65
R^2= OMe	37	63
R^2= R^3= OMe	40	60
R^1=OH, R^4= NO_2	41	59
R^1=OH, R^4= Br	52	48
R^1=OH, R^2=OMe	66	34
R^1=OH, R^2=Trityl, R^4= Me	69	31
R^1=OH	74	26
R^1=OH, R^2= R^4= Me	77	23
R^1=OH, R^2=Me	79	21
R^1=R^2= OH	82	18
R^1=OH, R^2=Ad, R^4= Me	88	12
R^1=OH, R^2= R^4= ^{t}Bu	89	11
R^1=OH, R^3=OH	100	0

Omitted substituents = H
* 2-Pyridinecarboxaldehyde
** X = F, Cl, Br or I

The cyclic form, **B**H was strongly favoured by deactivated aryl systems, featuring pyridine, NO_2 and Cl substituents which were found to also strongly favour cyclisation *via* resonance withdrawl and induction respectively. The introduction of a hydroxyl group in an *ortho* position has a pronounced effect on the preference for the imino structure and this can be augmented by electron releasing akyl groups (^{t}Bu, Me, Ad) or reduced by electron withdrawing substituents (Halo, NO_2).

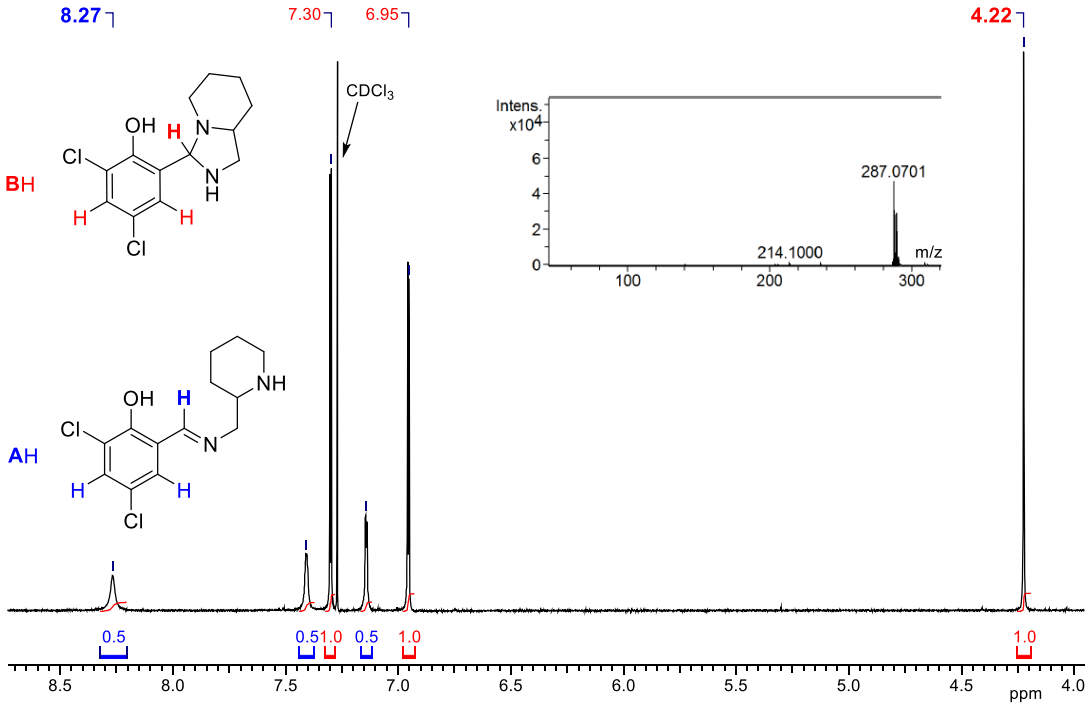

Figure 2.6: ^{1}H NMR ($CDCl_3$ 400MHz) spectrum of aromatic/benzylic regions for **B**H as dominant product. Inset: ESI-TOF spectrum.

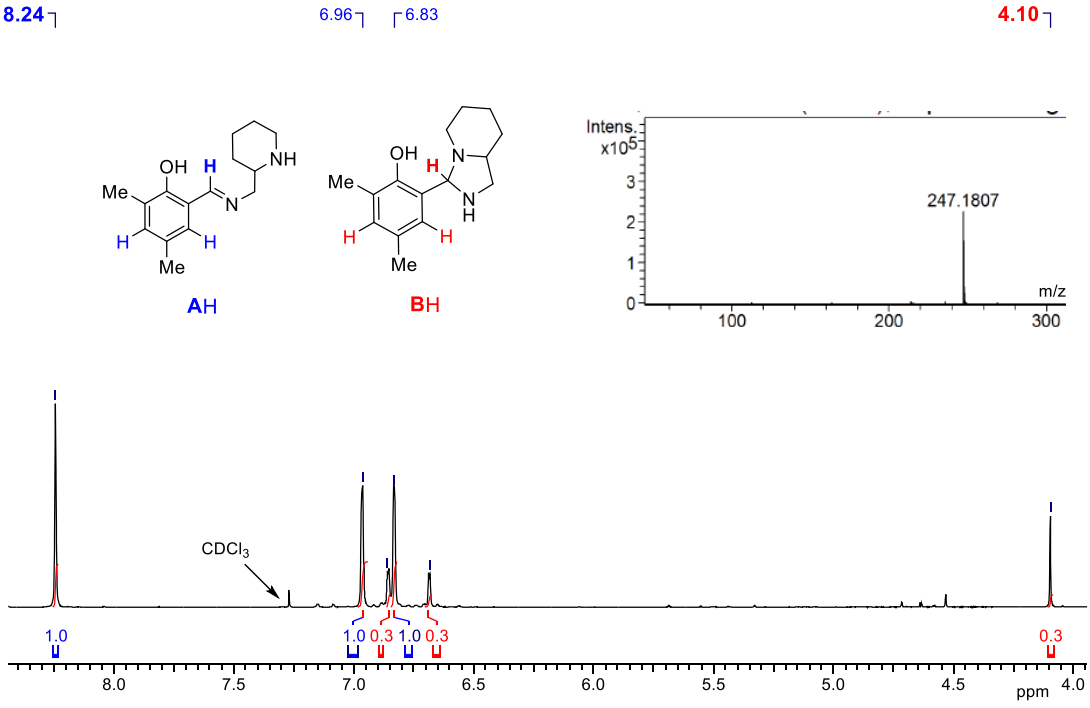

Figure 2.7: ^{1}H NMR ($CDCl_3$ 400MHz) spectrum of aromatic/benzylic region for **A**H as dominant product. Inset: ESI-TOF spectrum.

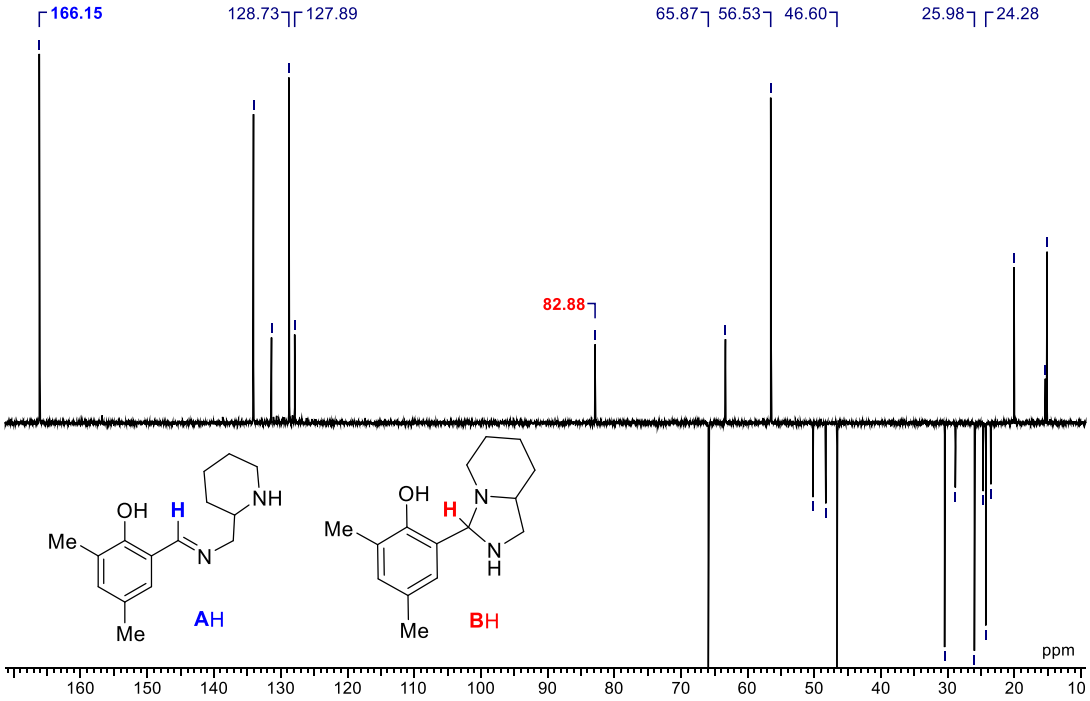

Figure 2.8: $^{13}C\{^{1}H\}$ DEPT NMR ($CDCl_3$ 100MHz) spectrum for **A**H as dominant product (**4**H).

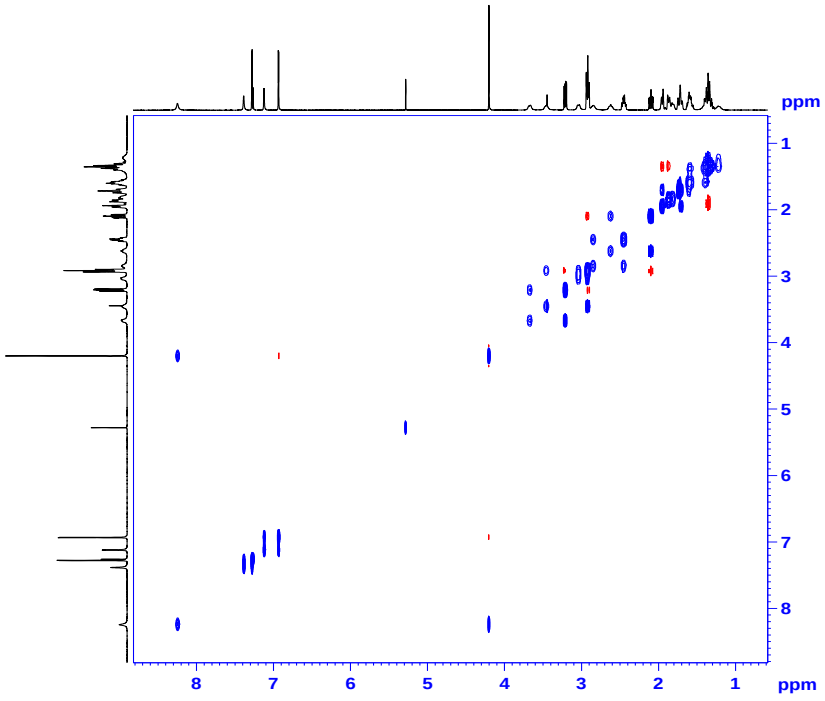

Figure 2.9: ^{1}H - ^{1}H EXSY NMR ($CDCl_3$, 500 MHz, mixing time 0.6 s) spectrum of **B**H with blue cross peaks showing chemical exchange and red cross peaks showing nOe.

The thermodynamic values for the process of interconversion between imino and cyclic form, **A**H and **B**H (defined in Figure 2.10), were determined *via* variable temperature (VT) NMR spectroscopy (d_8-toluene, 298-363K, [**A**H + **B**H] ~ 0.2 M). At each temperature, the equilibrium constant was evaluated through integration of the benzylic resonances of each form. This was carried out for H, ^{t}Bu and Cl aryl substituents with a van't Hoff plot for each system. The van't Hoff plot was constructed with lnK_{eq} on the y axis and 1/T on the x axis (Figure 2.11). From the graph, the gradient is related to the change in enthalpy, ΔH, and the intercept to the change of entropy, ΔS (Equation 2.1). The Gibbs free energy change, ΔG, for this system was also calculated at 298K at a concentration of 0.2 M. The calculated thermodynamic values are summarised in Table 2.2.

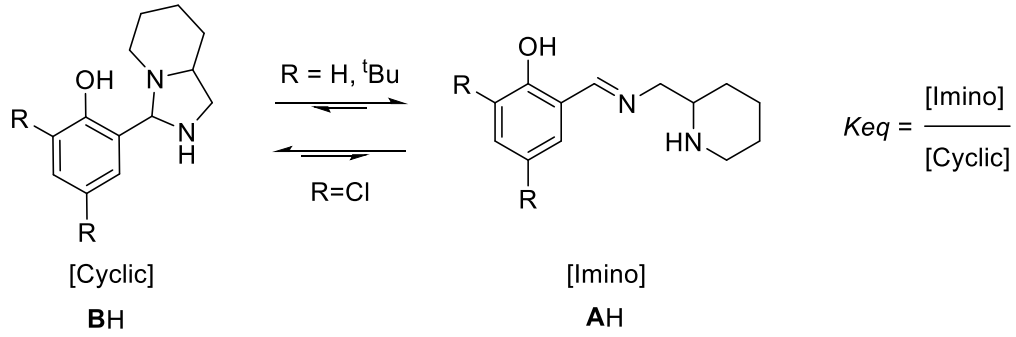

Figure 2.10: Dynamic process investigated by van't Hoff plot.

$$lnK_{eq} = -\frac{\Delta H}{RT} + \frac{\Delta S}{R}$$

Equation 2.1: van't Hoff equation.

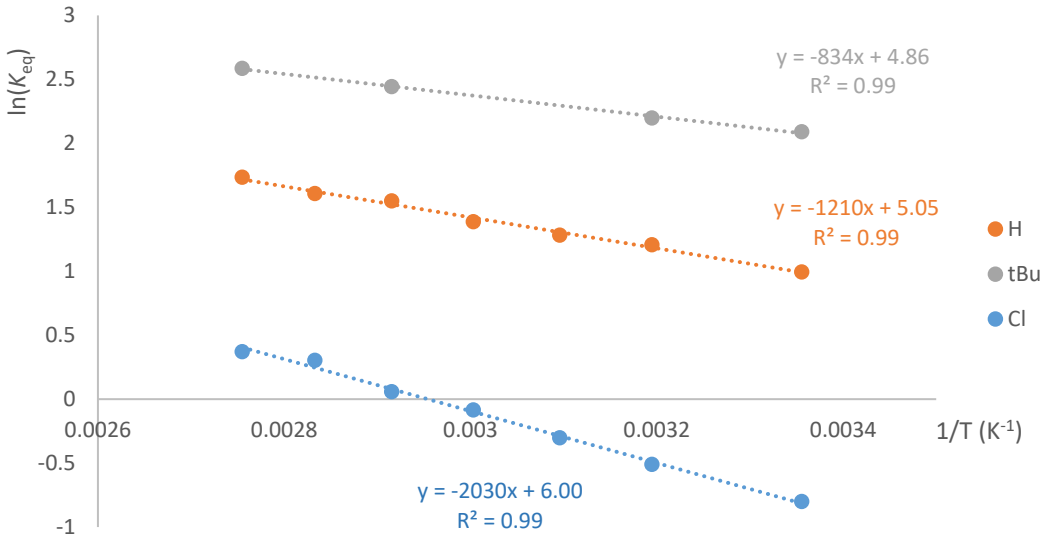

Figure 2.11: van't Hoff plot for interconversion of **B**H to **A**H for different aryl substituents.

Table 2.2: Thermodynamic values for interconversion between imino and cyclic forms (d_8-toluene, 298 – 363 K).

	R = H	**R = ^{t}Bu**	**R = Cl**
ΔH / kJ mol^{-1}	10.1 ± 0.4	6.9 ± 0.3	16.6 ± 0.6
ΔS / J mol^{-1} K^{-1}	42.0 ± 1.3	40.1 ± 0.8	49.0 ± 1.9
$\Delta G_{(298\ K)}$ / kJ mol^{-1}	-2.5 ± 0.8	-5.1 ± 0.5	2.0 ± 0.1

In all cases, the formation of the imino form, from the cyclic form, is observed to be an endothermic process ($\Delta H > 0$ kJ mol^{-1}). This is in contrast to the initial condensation which is exothermic. The degree of endothermicity correlates with the preference for the imino form with the ^{t}Bu system being less {ΔH = (6.9 ± 0.3) kJ mol^{-1}} and the Cl system being more {ΔH = (16.6 ± 0.6) kJ mol^{-1}} endothermic. For H substituents, an intermediate value for enthalpy is observed {ΔH = (10.1 ± 0.4) kJ mol^{-1}}. The formation of the imino form is accompanied by an increase in entropy for the system ($\Delta S > 40$ J mol^{-1} K^{-1}). This may be related to the increase in flexibility of the molecule, due to the release of the piperidine ring, which is now free to rotate and also change

ring conformation. The Gibbs free energy for this process was also evaluated for these three systems at 298K. Accordingly, conversion to the imino form with the ^{t}Bu substituted ring was found to be most thermodynamically viable, with the most negative value {$\Delta G = (-2.5 \pm 0.8)$ kJ mol^{-1}}. Conversely, chloro groups disfavoured the imino form with a positive Gibbs free energy value {$\Delta G = (+2.0 \pm 0.1)$ kJ mol^{-1}}.

2.3 Monophenol ligand synthesis

Due to this equilibrium, the imino and cyclic form could not be separated. For the aryl substituents which pushed the equilibrium in favour of the imine functionality, the ligand mixture was generally amenable to purification *via* complexation. Hence, a range of imine based monophenols were realised as suitable ligands in complexation (Figure 2.12). These ligands were characterised by ^{1}H, ^{13}C{^{1}H} NMR spectroscopy and ESI mass spectrometry (for **4**H, Figure 2.7-2.8).

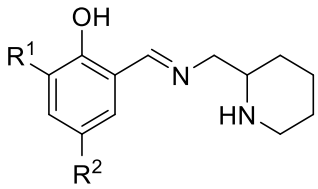

1H, $R^1=R^2=^{t}$Bu,
2H, R^1=Ad, R^2=Me
3H,R^1=Trityl, R^2=Me
4H,$R^1=R^2$=Me
5H,R^1=OMe, R^2=H
6H, R^1=H, R^2=Br

Figure 2.12: Imine monophenols, **1**-**6**H, amenable to complexation.

A further reaction was carried out to cap the amine functionality and prevent the exchange between the two forms. This involved a simple S_N2 reaction with benzyl bromide to afford the diaryl monophenols **7**-**10**H (Figure 2.13). The preparation of **7**H/**10**H was contributed to by James Brown Humes (MChem student, 2015/16). The form that dominated in the tautomerism was expected to be isolable product and this was true for ^{t}Bu and Cl substituted rings. However, for methyl substituted and unsubstituted salicylaldehyde, the cyclic forms were isolated through recrystallisation. Attempts to vary steric bulk at this position by methylation with iodomethane were unsuccessful leading to a mixture of products. Beim and Day also noted a similar phenomenon for the unfunctionalised system, attributing this to cleavage reactions.[23]

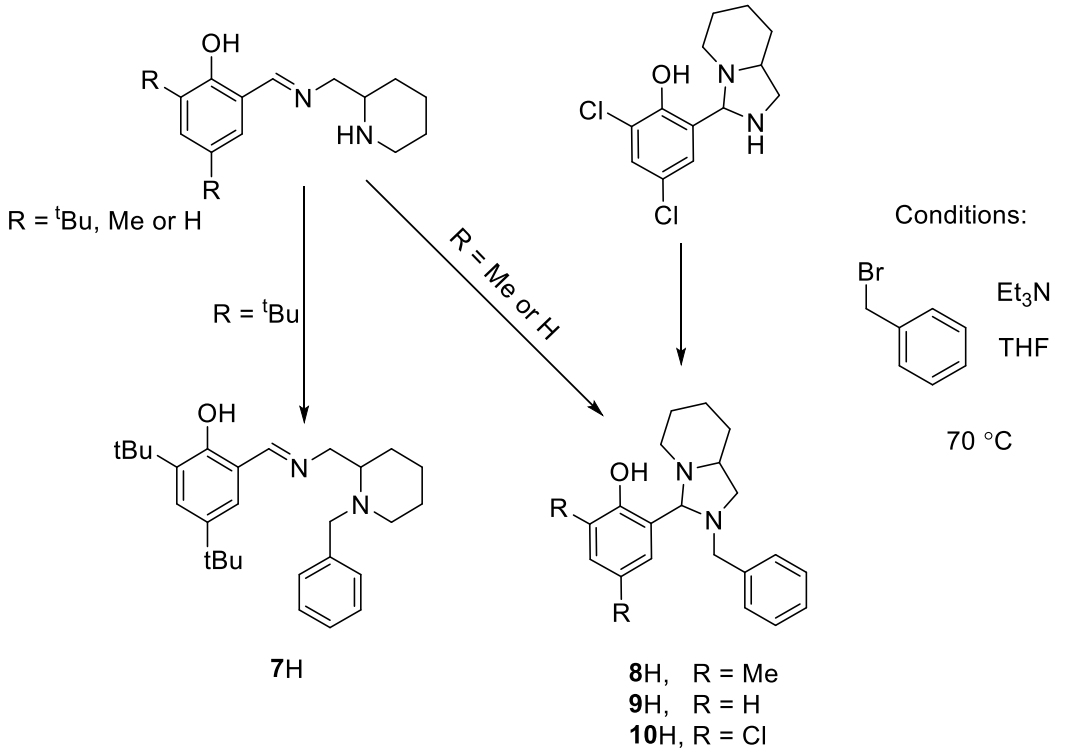

Figure 2.13: Synthesis of biaryl monophenols, **7**-**10**H.

The successful preparation of the benzyl capped species was demonstrated by mass spectrometry, in which there was only one species. The isolation of a single form was shown by ^{1}H and $^{13}C\{^{1}H\}$ NMR spectroscopy (for **7**H, Figure 2.14 / for **8**H, Figure 2.15). Regardless of the form, a new series of doublets resulted from the introduction of new benzyl protons (Figure 2.14-2.15, highlighted) as well as five new aromatic resonances. Similarly, these new environments are accounted for by $^{13}C\{^{1}H\}$ NMR with four new aromatic resonances and a new CH_2 resonance. The bicyclic form of **10**H was further demonstrated by a solid-state structure (Figure 2.16), revealing a hydrogen bond between the phenol group and N(1).

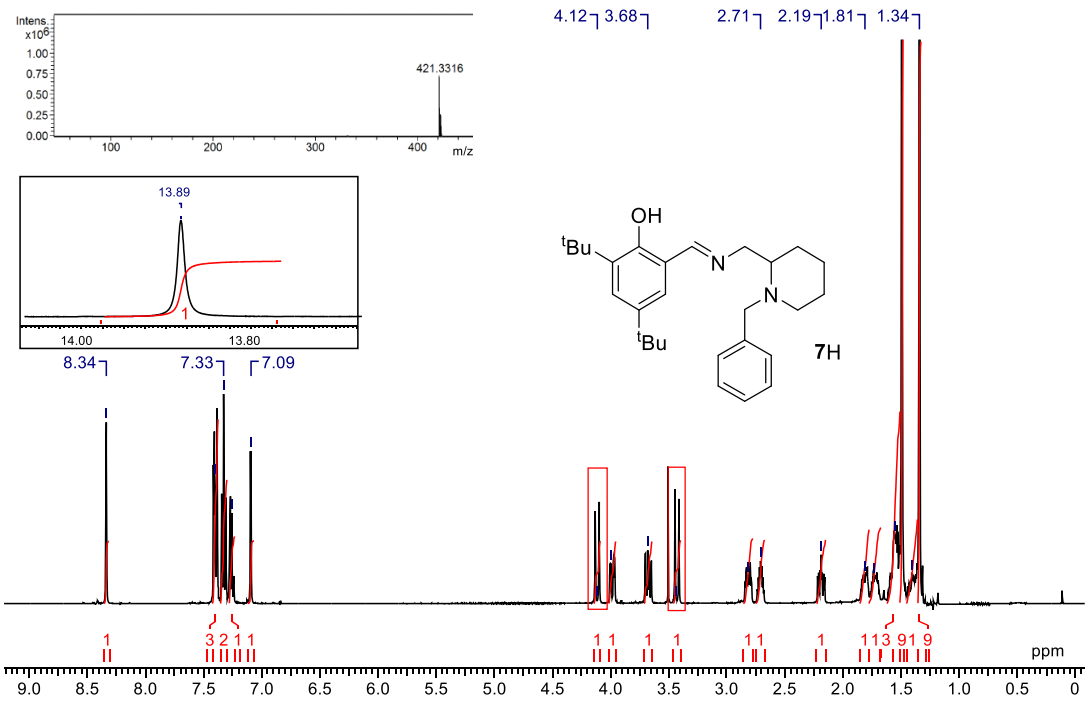

Figure 2.14: ^{1}H NMR ($CDCl_3$, 400MHz) spectrum of **7**H. Inset: ArOH resonance and ESI-ToF spectrum.

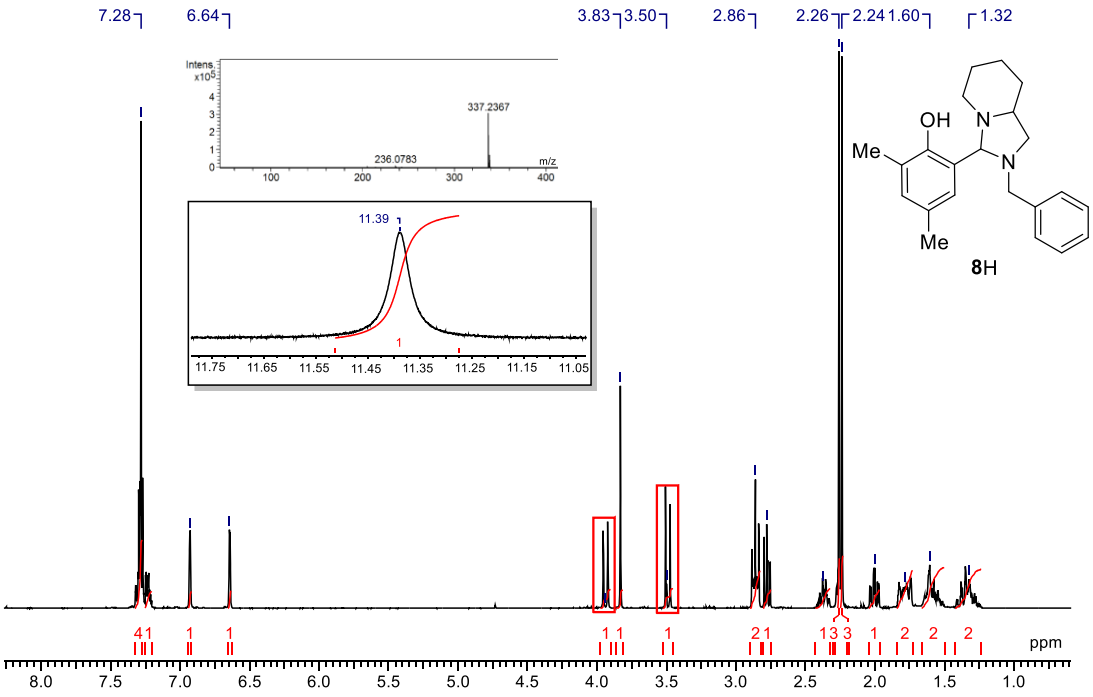

Figure 2.15: ^{1}H NMR ($CDCl_3$, 400MHz) spectrum of **8**H. Inset: ArOH resonance and ESI-ToF spectrum.

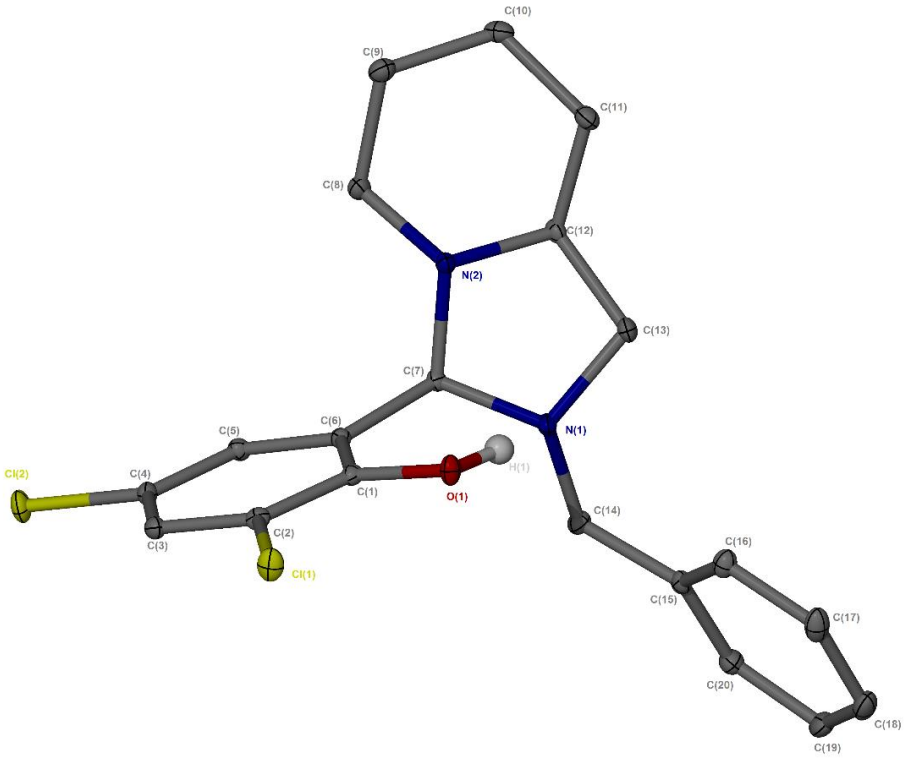

Figure 2.16: Solid state structure of **10**H. Ellipsoids are shown at the 30% probability level and all hydrogen atoms, except those involved in H-bonding, have been removed for clarity.

Reduction of the imine functionality generates a diamine, **D**H (Figure 2.17). Due to the close proximity of the two nitrogens, this system is perfectly set up for a range of intramolecular cyclisations. This general reaction has been demonstrated in the literature with simple ethylene diamine salan,[27] for preparation of pyridine based ligands,[28, 29] as a carbonyl protection method,[30] and a precursor for carbene synthesis.[31] Favourable results for this system were achieved *via* thermal cyclisation (hexane, 70°C), without additives, though it is noted the process is not optimised. In some cases, an impurity is observed in the synthesis and it is speculated that this species is an iminium resulting from an incomplete cyclisation. It is noted that the diamine is unsymmetrical and rigid with the 2-aminopiperdine backbone and this may restrict cyclisation depending on where the iminium ion forms.

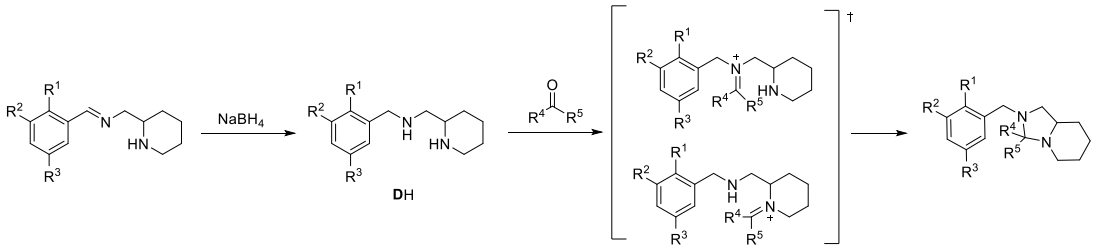

Figure 2.17: Synthesis of diamine, **D**H, and intramolecular cyclisation.

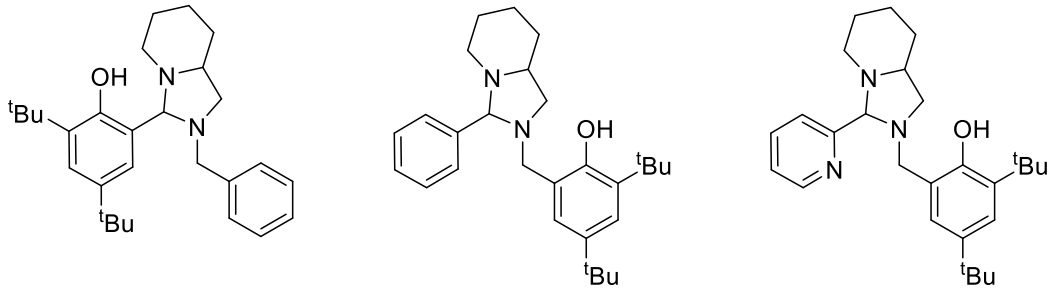

Figure 2.18 Further bicyclic monophenol ligands, **11**H-**13**H.

This route expands the scope for monophenol bicyclic structures, potentially allowing for a library of structures to be prepared. Due to the equilibrium, the reduction reaction is applicable regardless of the dominant isomer ultimately providing the aliphatic benzyl position. In the simplest of cases, reaction with formaldehyde presents an unsubstituted 5 membered fused ring. A range of aldehydes were shown to be active in this reaction, furnishing the general structure shown in Figure 2.17. This approach was also successfully applied to ketones such as acetone and cyclohexanone. The bicyclic analogue of **7**H was realised by this method through the reaction of unsubstituted **D**H with 3,5-di-*tert*-butylsalicylaldehyde (**11**H, Figure 2.18). This could only be isolated in extremely low yields by the S_N2 reaction shown in Figure 2.12. A further structural isomer, **12**H, can be prepared using the 3,5-di-*tert*-butylsalicylaldehyde based **D**H in cyclisation with benzaldehyde. Reaction with 2-pyridinecarboxaldehyde afforded a tridentate ligand, **13**H.

Ligands **11**H-**13**H were characterised by ^{1}H / $^{13}C\{^{1}H\}$ NMR spectroscopy and ESI mass spectrometry. Similar observations were made relative to **8-10**H, with new CH and CH_2 resonances being observable *via* NMR spectroscopy.

2.4 Bisphenol ligand synthesis

The corresponding bisphenols were prepared using the same protocol as to cap the monophenols in the previous section; an S_N2 reaction with 3,5-di-*tert*-butyl-2-hydroxybenzylbromide was employed in THF with Et_3N at reflux to afford the dominant equilibrium structure after recrystallisation (Figure 2.19). The bicyclic bisphenol ligands were characterised by a combination of $^{1}H/^{13}C\{^{1}H\}$ NMR spectroscopy as well as ESI mass spectrometry.

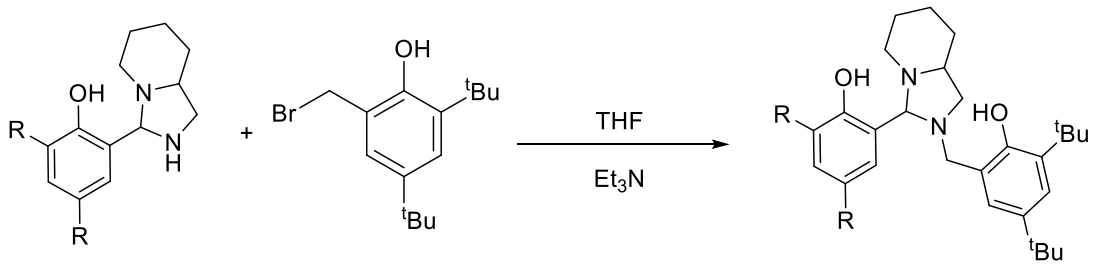

14H_2, R = Cl
15H_2, R = Br
16H_2, R = I

Figure 2.19: Synthesis of bicyclic bisphenol ligands, **14-16**H_2.

Three bicyclic bisphenols were prepared by this method, yielding slightly yellow powders. The bicyclic structure was confirmed *via* ^{1}H NMR spectroscopy. Only four doublet resonances are observable in the aromatic/imine region demonstrating the absence of the salalen product. The benzyl protons are present at around 4 ppm, occurring as a singlet and two doublets subject to roofing. The remaining spectrum conforms to the structure, with splitting patterns resolvable in this instance (Figure 2.22). The benzylic carbon that is bonded to two nitrogen centres is also readily assigned in the $^{13}C\{^{1}H\}$ NMR spectrum, with the resonance shifted downfield at 88 ppm. The bicyclic form was further characterised through X-ray crystallography which revealed hydrogen bonding between each phenol proton and a nitrogen (**14**H_2,

Figure 2.20). In this structure, the chiral centre on the piperidine ring is displayed to be in an *S* configuration, with the *P-1* space-group also implying the *R* form in the solid-state. The two enantiomers are anticipated to be present in solution. This structure offers tridentate coordination *via* an [ONO] manner.

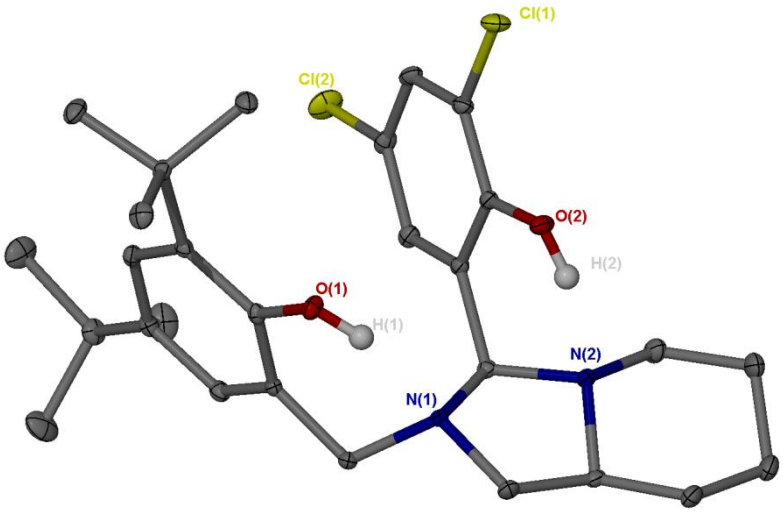

Figure 2.20: Solid state structure of **14**H_2. Ellipsoids are shown at the 30% probability level and all hydrogen atoms have been removed for clarity.

Using the reduced diamine, **D**H, the substituents that preferentially yield the imino bisphenol can be obtained in the bicyclic motif. Reaction of **D**H with a salicylaldehyde connects the phenol directly to the 5 membered ring hence representing the synthesis of the bicyclic from the opposite side of the molecule (Figure 2.21). The benefit of this approach is the ease in varying aryl substituents by use of commercially available salicylaldehydes. The purity of the ligands *via* this route is also improved as white solids are isolated compared with the yellow discolouration of the bicyclic forms through the S_N2 reaction, which is likely a consequence of a low concentration imine form contamination. These structures conform to the previous characterisation of this series (Figure 2.22).

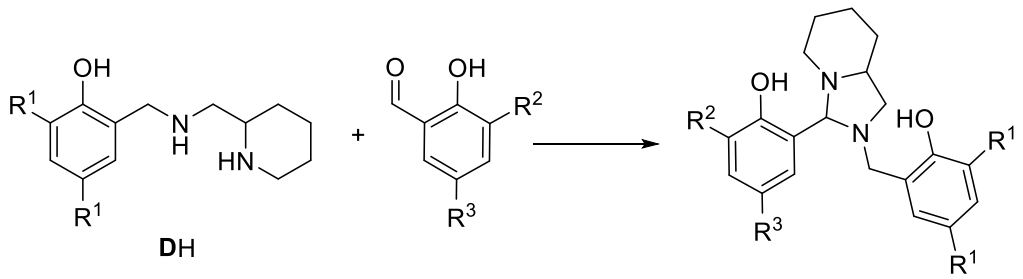

17H_2, R^1 = ^{t}Bu, R^2 = H, R^3 = Br
18H_2, R^1 = ^{t}Bu, R^2 = H, R^3 = NO_2
19H_2, R^1 = ^{t}Bu, R^2 = R^3 = H
20H_2, R^1 = ^{t}Bu, R^2 = R^3 = Me
21H_2, R^1 = ^{t}Bu, R^2= Ad, R^3 = Me
22H_2, R^1 = R^2 = R^3 = ^{t}Bu
23H_2, R^1 = R^2 = R^3 = H
24H_2, R^1 = R^2 = R^3 = Cl
25H_2, R^1 = Cl, R^2 = R^3 = ^{t}Bu

Figure 2.21: Further bicyclic ligands derived from the reduced diamine, **D**H.

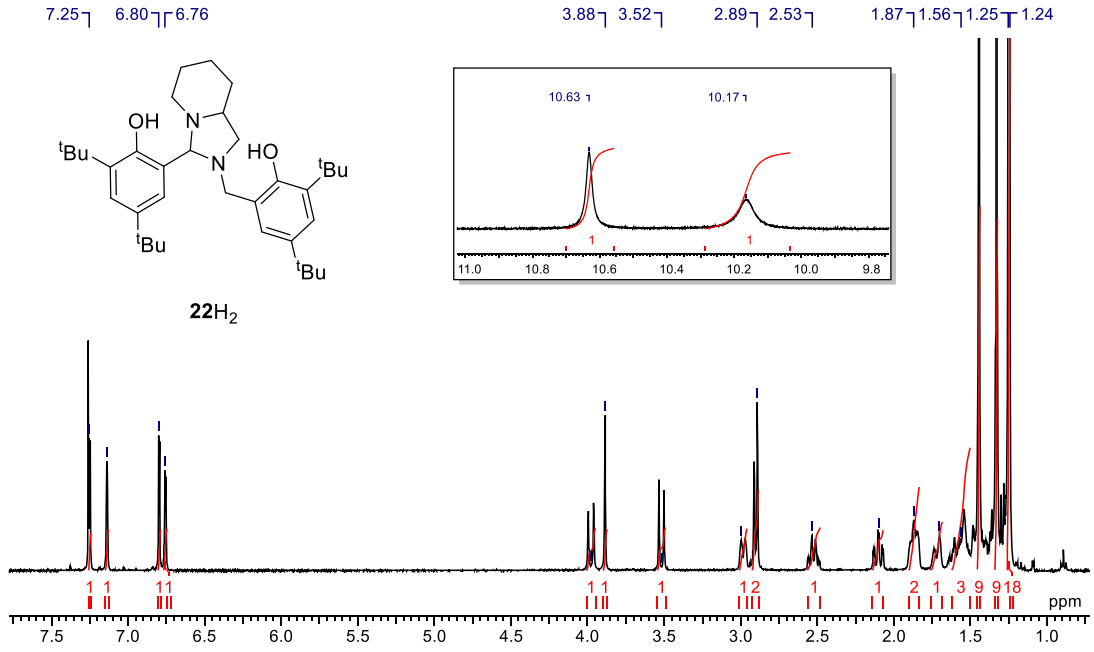

Figure 2.22: ^{1}H NMR ($CDCl_3$, 400MHz) spectrum of **22**H_2. Inset: ArOH resonances.

For the salalen ligands, **26**-**30**H_2 yellow powders were isolated *via* recrystallisation (Figure 2.23). The salen fragment is limited to alkyl aryl substituents whereas greater variation was achieved for the salan fragment. Characterisation *via* ^{1}H NMR (Figure

2.24) demonstrates the imino form over the cyclic form through the observation of an imine resonance at ~8.3 ppm. The remaining spectrum is broad, with no resolvable splitting patterns. The origin of this broadness is likely due to interconversion of chair forms of the piperidine ring. One of the OH resonances also suffers from broadening, which could also imply the presence of a hydrogen bond which is associating and dissociating on the NMR timescale. A small amount (<5%) of bicyclic impuritity is also observable (compared with Figure 2.22). These salalen structures offer tetradentate, [ONNO], coordination.

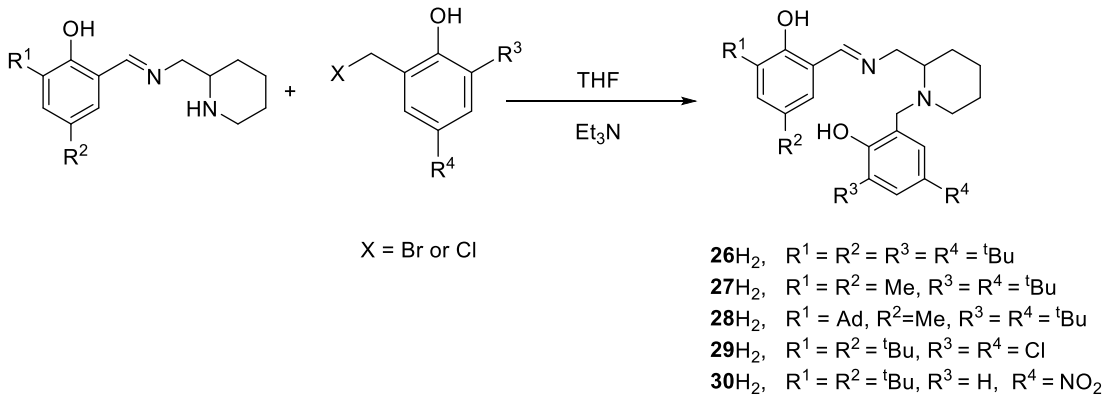

Figure 2.23: Synthesis of salalen ligands, **26**-**30**H_2.

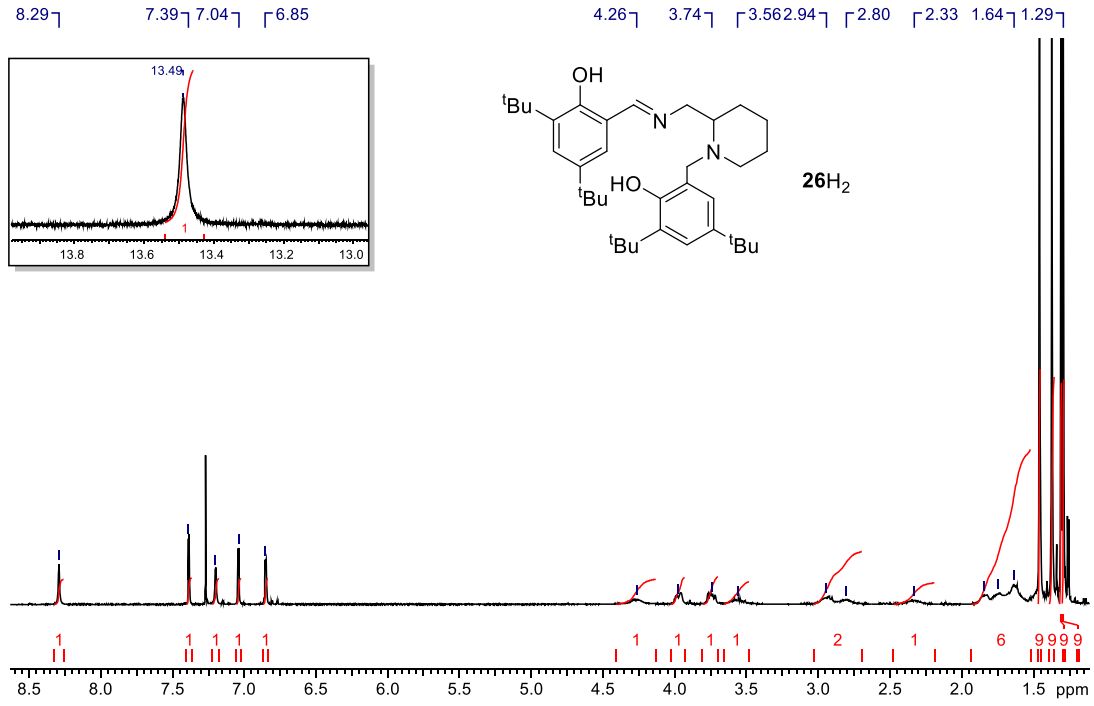

Figure 2.24: ^{1}H NMR ($CDCl_3$, 400MHz) spectrum of **26**H_2. Inset: ArOH resonance.

A series of salan ligands based on the parent imino ligands, **31**-**34**H_2, were also realised (Figure 2.25). Reduction of the imine functionality provided the amine which allows greater flexibility in the backbone giving an interesting comparison for the subsequent coordination chemistry. The secondary amine also creates opportunity for further ligand design, which was utilised to furnish the methylated product, **35**H_2.

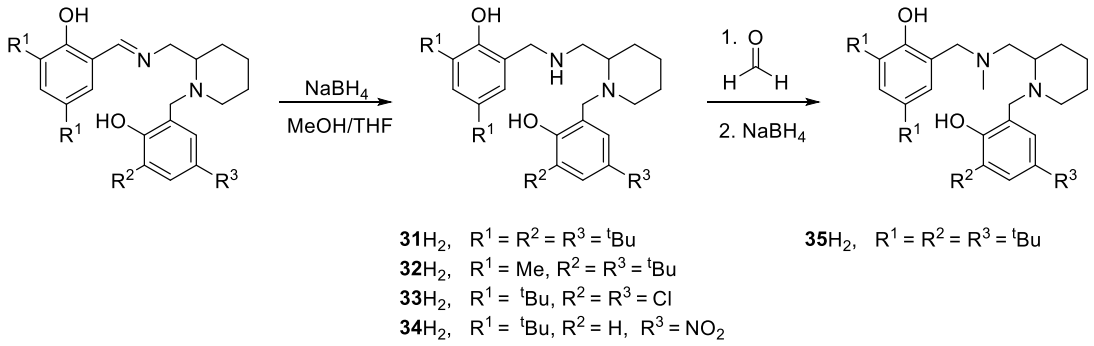

Figure 2.25: Synthesis of salan ligands, **31**-**34**H_2 and **35**H_2.

The successful preparation of these ligands was shown by $^{1}H/^{13}C\{^{1}H\}$ NMR spectroscopy and ESI mass spectrometry. Generally, the ^{1}H NMR spectra revealed the required number of aromatic resonances, with no evidence of a signal due to an imine. The remaining spectra has a similar broadness to that of the parent imino ligand, however, benzylic doublets are typically observable. Mass spectrometry confirms the reduction of the imine for **31**-**34**H_2 and the methylation for **35**H_2.

In an extension to these ligands, an example of a triaryl bisphenol was also prepared by James Brown-Humes (MChem student, 2015/2016). A similar reduction method is used on the capped ligand, **7**H, followed by S_N2 reaction to install the second phenol (Figure 2.26). The ligand, **36**H_2, was isolated as a white powder. Characterisation *via* ^{1}H NMR spectroscopy revealed the two phenols to be magnetically equivalent, causing two sharp aromatic resonances that integrate to 2 protons each (Figure 2.27). In total, there are two pairs of benzylic resonances at a ratio of 2:1, manifesting as doublets, indicating the diastereotopic nature of these positions. Similar to the related salan and salalen spectra, the remaining spectra is broad and the corresponding $^{13}C\{^{1}H\}$ NMR spectrum only reveals one resonance attributed to a CH_2 group.

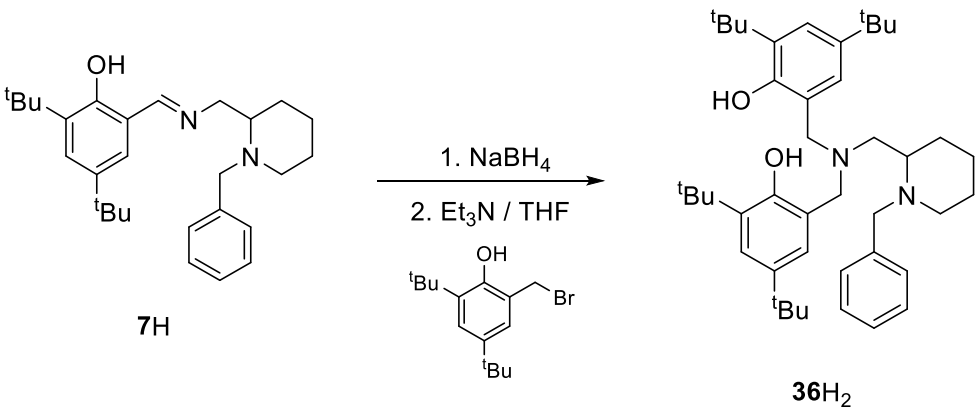

Figure 2.26: Synthesis of triaryl bisphenol ligand, **36**H_2.

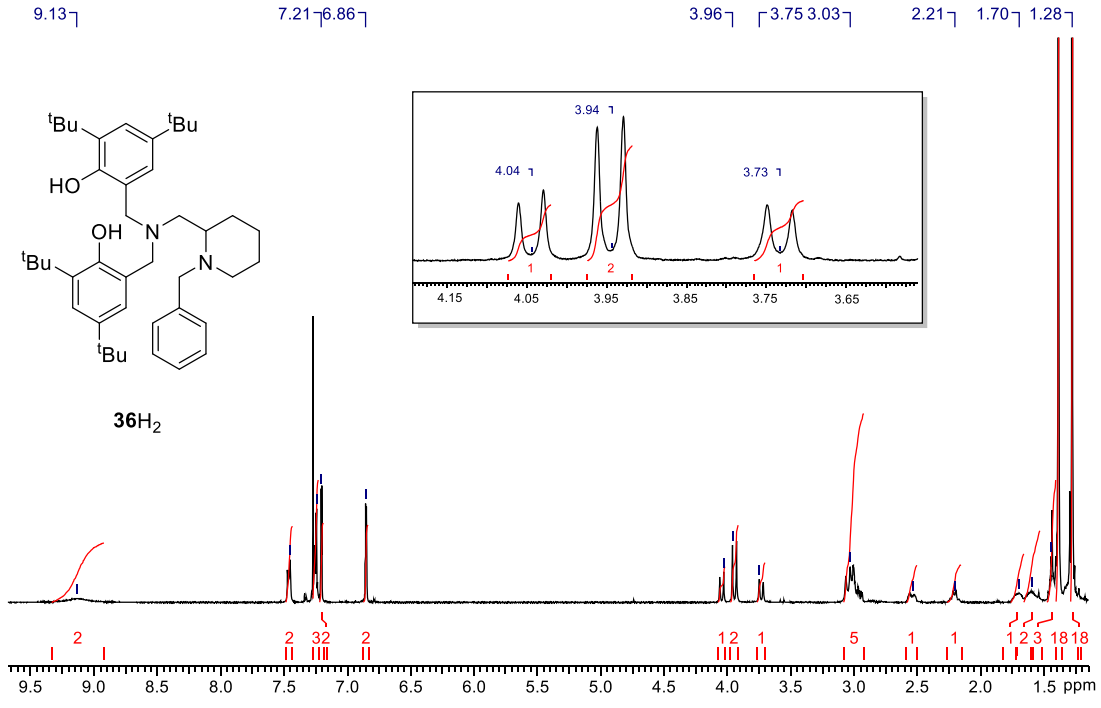

Figure 2.27: ^{1}H NMR ($CDCl_3$, 400MHz) spectrum of **36**H_2. Inset: Two equivalent and one inequivalent benzylic resonances.

2.5 Trisphenol ligand synthesis

In extension to the bisphenol systems, trisphenols were also investigated. During the synthesis of the bisphenols using 3,5-di-*tert*-butyl-2-hydroxybenzylbromide a trace amount of trisphenol was observed *via* mass spectrometry, with the mass being independent of the starting salicylaldehyde. Evidently, this molecule formed from unreacted 2-(aminomethyl)piperidine and the substituted benzyl bromide. Attempts to target the trisphenol directly by this method were complicated, with a mixture of mono- and bis-phenols resulting. Instead, the trisphenol was accessed through the preparation of the the salan, **31**H_2, followed by a more controlled S_N2 reaction, yielding **37**H_3 as a white powder (Figure 2.28). In this way, side products were reduced and there is potential to vary aryl substituents at each point.

This structure was fully characterised in solution *via* $^1H/^{13}C\{^1H\}$ NMR spectroscopy; the two groups attached to the exocyclic nitrogen are chemically equivalent contributing to the same aromatic, benzylic and *tert*-butyl resonances (Figure 2.29). Within the ^1H NMR aromatic region, there are two pairs of resonances at a ratio of 2:1 relating the equivalent bisphenols and the third inequivalent phenol. Similar observations are made for the benzylic protons which are observed as two pairs of doublets in an identical ratio; the benzylic resonances associated with the inequivalent aryl ring are noted to be broadened. This broadness persists for the remaining piperidine ring protons and both instance are attributed to ring conformational changes.

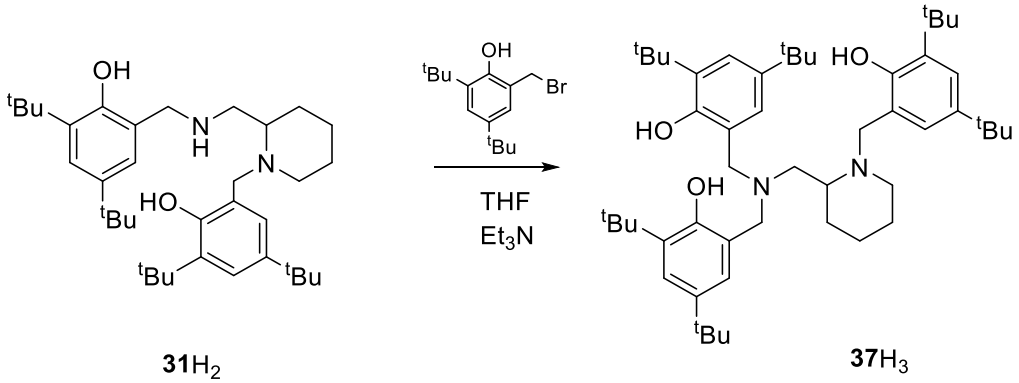

31H_2 **37**H_3

Figure 2.28: Synthesis of trisphenol ligand, **37**H_3, from **31**H_2

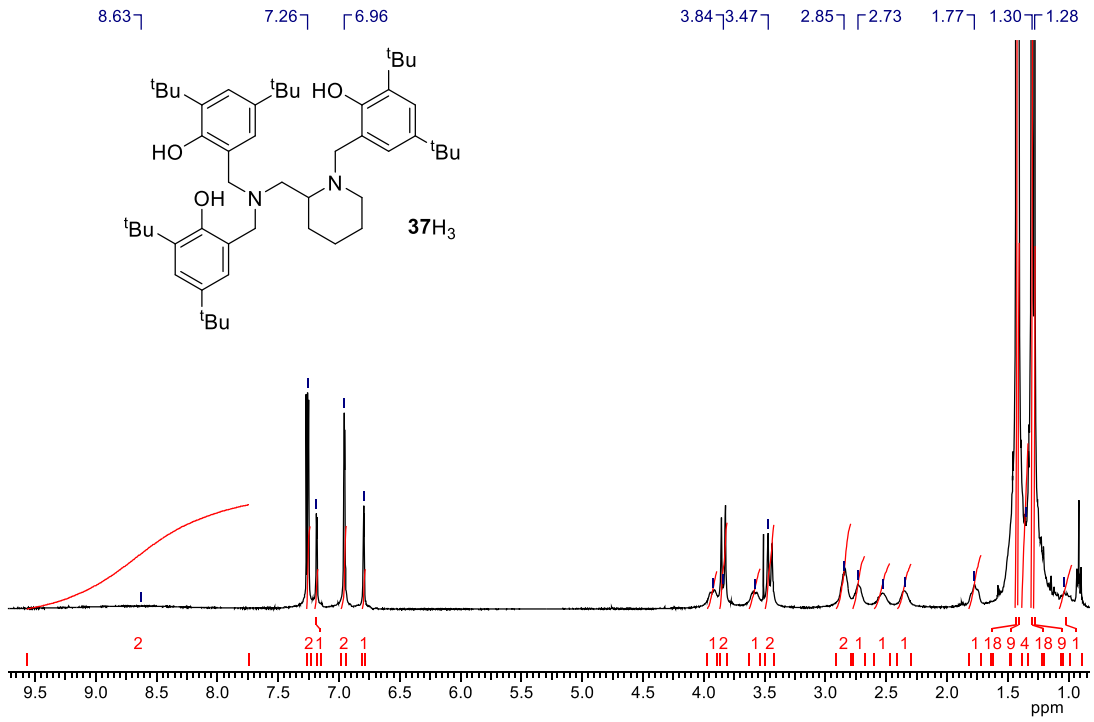

Figure 2.29: ^{1}H NMR ($CDCl_3$ 400MHz) spectrum of **37**H_3.

The structure of the trisphenol was demonstrated in the solid-state through X-ray crystallography (Figure 2.30). In this structure, the piperidine chiral centre is displayed as an *R* configuration, with the *S* enantiomer implied by the *P-1* space group. Hydrogen bonding is present between the proton on O(1) and N(1) and also between the hydrogen on O(3) and N(2).

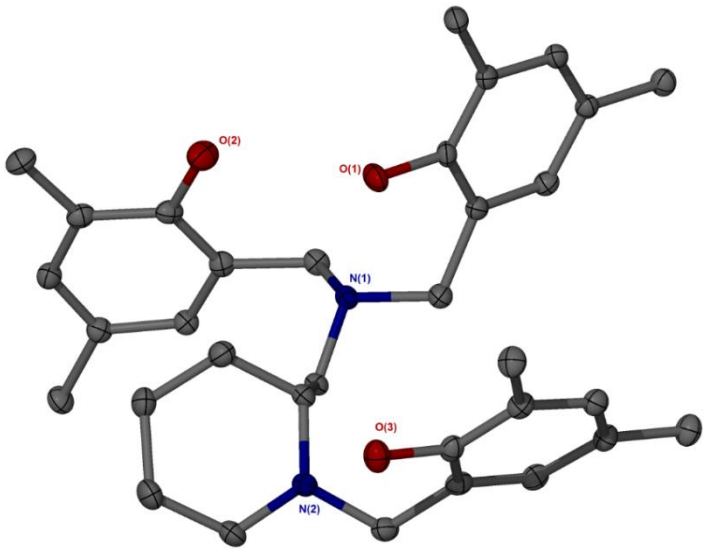

Figure 2.30: Solid state structure of **37**H_3. Ellipsoids are shown at the 30% probability level and all hydrogen atoms and ^{t}Bu methyl groups have been removed for clarity.

2.6 Conclusions

The initial imine condensation between 2-(aminomethyl)piperidine and substituted salicylaldehydes has been investigated. Two forms, **A**H and **B**H, resulted from this reaction, the latter being a cyclisation product of the imino species. These two forms were found to exist in a dynamic equilibrium which is influenced by aryl substituents, solvent and temperature. A range of salicylaldehydes were trialled for this condensation and the preference for cyclic or imino form rationalised by the electron donating/withdrawing abilities of these groups. Representative thermodynamic data was obtained for three substitutions (H, ^{t}Bu and Cl). These results demonstrated the conversion from cyclic to imino form to be endothermic ($\Delta H > 0$ kJ mol^{-1}) and associated with an increase in entropy (ΔS = 40-49 J mol^{-1} K^{-1}).

Various classes of ligands were prepared based on the 2-AMP motif. **1**-**6**H represent imino monophenols, being the dominant product of the condensation with alkyl based salicylaldehydes. Biaryl and "capped" monophenols were also isolated as one main species by further reactions affording **7**-**13**H. Greater structural diversity could be introduced through preparation and reaction of the diamine **D**H, which is amenable to cyclisation with carbonyl groups.

Using the diamine or electron withdrawing aryl groups afforded a range of bisphenols based upon the bicyclic motif. **14**-**25**H_2 represent a range of substitutions on the aryl ring, including electron withdrawing and donating groups. A tridentate bonding mode is anticipated for this ligand class. In contrast, preparation of the salalens, **26**-**30**H_2, bearing an alkyl aryl salen fragment, offers tetradentate coordination. Reduction of these ligands, afforded salan type ligands, **31**-**34**H_2, and methylation yielded **35**H_2.

Triaryl ligands were also prepared. An example of a triaryl bisphenol, **36**H_2, was realised by reduction and further reaction of **7**H. For this ligand, the two phenol groups are connected to the same nitrogen centre and, hence, are equivalent. In extension to this, a trisphenol system, **37**H_3, was also prepared by further reaction of **31**H_2. Similar observations are made as to the equivalence of the two adjacent phenol groups.

These ligands will be coordinated to various metal centres and the resultant complexes assessed in their ability to polymerise *rac*-lactide, these being discussed in Chapter 3 and Chapter 4 respectively.

2.7 References

1. A. Stopper, K. Press, J. Okuda, I. Goldberg and M. Kol, *Inorg. Chem.*, 2014, **53**, 9140-9150.
2. S. Abbina and G. Du, *ACS Macro Lett.*, 2014, **3**, 689-692.
3. M. D. Jones, L. Brady, P. McKeown, A. Buchard, P. M. Schafer, L. H. Thomas, M. F. Mahon, T. J. Woodman and J. P. Lowe, *Chem. Sci.*, 2015, **6**, 5034-5039.
4. M. D. Jones, S. L. Hancock, P. McKeown, P. M. Schafer, A. Buchard, L. H. Thomas, M. F. Mahon and J. P. Lowe, *Chem. Commun.*, 2014, **50**, 15967-15970.
5. A. Pilone, K. Press, I. Goldberg, M. Kol, M. Mazzeo and M. Lamberti, *J. Am. Chem. Soc.*, 2014, **136**, 2940-2943.
6. Z. Zhong, P. J. Dijkstra and J. Feijen, *J. Am. Chem. Soc.*, 2003, **125**, 11291-11298.
7. Z. Y. Zhong, P. J. Dijkstra and J. Feijen, *Angew. Chem. Int. Ed.*, 2002, **41**, 4510-4513.
8. H. Du, A. H. Velders, P. J. Dijkstra, J. Sun, Z. Zhong, X. Chen and J. Feijen, *Chem. Eur. J.*, 2009, **15**, 9836-9845.
9. H. Du, X. Pang, H. Yu, X. Zhuang, X. Chen, D. Cui, X. Wang and X. Jing, *Macromolecules*, 2007, **40**, 1904-1913.
10. P. Hormnirun, E. L. Marshall, V. C. Gibson, R. I. Pugh and A. J. P. White, *Proc. Natl. Acad. Sci. U. S. A.*, 2006, **103**, 15343-15348.
11. N. Nomura, R. Ishii, M. Akakura and K. Aoi, *J. Am. Chem. Soc.*, 2002, **124**, 5938-5939.
12. N. Nomura, R. Ishii, Y. Yamamoto and T. Kondo, *Chem. Eur. J.*, 2007, **13**, 4433-4451.
13. N. Spassky, M. Wisniewski, C. Pluta and A. LeBorgne, *Macromol. Chem. Phys.*, 1996, **197**, 2627-2637.
14. N. Maudoux, T. Roisnel, V. Dorcet, J.-F. Carpentier and Y. Sarazin, *Chem. Eur. J.*, 2014, **20**, 6131-6147.
15. S. L. Hancock, M. F. Mahon and M. D. Jones, *New J. Chem.*, 2013, **37**, 1996-2001.
16. H.-L. Chen, S. Dutta, P.-Y. Huang and C.-C. Lin, *Organometallics*, 2012, **31**, 2016-2025.
17. E. D. Cross, L. E. N. Allan, A. Decken and M. P. Shaver, *J. Polym. Sci., Part A: Polym. Chem.*, 2013, **51**, 1137-1146.
18. P. Hormnirun, E. L. Marshall, V. C. Gibson, A. J. P. White and D. J. Williams, *J. Am. Chem. Soc.*, 2004, **126**, 2688-2689.
19. E. L. Whitelaw, G. Loraine, M. F. Mahon and M. D. Jones, *Dalton Trans.*, 2011, **40**, 11469-11473.
20. A. Yeori, S. Gendler, S. Groysman, I. Goldberg and M. Kol, *Inorg. Chem. Commun.*, 2004, **7**, 280-282.
21. E. L. Whitelaw, M. D. Jones and M. F. Mahon, *Inorg. Chem.*, 2010, **49**, 7176-7181.
22. S. L. Hancock, M. F. Mahon and M. D. Jones, *Dalton Trans.*, 2013, **42**, 9279-9285.
23. H. J. Beim and A. R. Day, *J. Heterocycl. Chem.*, 1970, **7**, 355-360.
24. R. R. Gowda and E. Y. X. Chen, *Dalton Trans.*, 2013, **42**, 9263-9273.

25. T. A. Crabb, P. J. Chivers and R. F. Newton, *Org. Magn. Reson.*, 1973, **5**, 397-399.
26. M. E. Freed and A. R. Day, *J. Org. Chem.*, 1960, **25**, 2108-2113.
27. A. Rivera, R. Quevedo, M. A. Navarro and M. Maldonado, *Synth. Commun.*, 2004, **34**, 2479-2485.
28. A. Gonzalez-de-Castro, C. M. Robertson and J. Xiao, *J. Am. Chem. Soc.*, 2014, **136**, 8350-8360.
29. T. Zaman, R. Frauenlob, R. McCarthy, C. M. Walsh and E. Bergin, *J. Organomet. Chem.*, 2012, **716**, 159-166.
30. A. J. Carpenter and D. J. Chadwick, *Tetrahedron*, 1985, **41**, 3803-3812.
31. G. W. Nyce, S. Csihony, R. M. Waymouth and J. L. Hedrick, *Chem. Eur. J.*, 2004, **10**, 4073-4079.

Chapter 3

Complexation of 2-(aminomethyl)piperidine based ligands

Chapter 3: Complexation of 2-(aminomethyl)piperidine based ligands

3.1 Introduction

In Chapter 2, the synthesis and solution properties of a range of ligands based upon 2-AMP were discussed. These are classified as either monophenol, bisphenol or trisphenols. As demonstrated in Chapter 1, a range of metal complexes have shown activity for the polymerisation of LA and other cyclic esters. Indeed, the choice of metal is often decisive in relation to the overall stereocontrol of the ligand-metal system. There are a few examples of the same ligand set giving the opposite stereochemical outcome with a different metal centre.[1-3]

The ligands prepared herein provide different coordination possibilities covering tridentate and tetradentate binding as well as mono- and bis-anionic combinations. In this chapter, the coordination of a selection of ligands is realised; metal centres employed are Mg(II), Zn(II), Al(III), Ti(IV), Zr(IV) and Hf(IV) as these have shown promise in the field.[3-10] These cover a range of possible geometries and will facilitate a variety of structural and solution motifs. Where possible, the structure of these complexes are compared with similar examples shown in the literature; such complexes are labelled alphabetically to distinguish from the prepared complexes which are labelled numerically. In particular, there are many reports involving 2-(aminomethyl)pyridine (2-AMPy) which represents the unsaturated analogue of 2-AMP (Figure 3.1).[11-14]

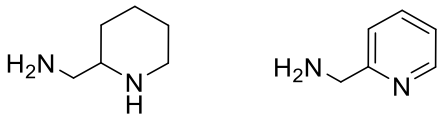

2-AMP 2-AMP$_y$

Figure 3.1: Comparison of 2-AMP and 2-AMP$_y$

3.2 Monophenolate complexes

3.2.1 Imino-monophenolate complexes

Initial complexation studies involving the monophenols explored the use of the dynamic mixture of the two forms, a mixture of imino and bicyclic structures, as shown previously in Chapter 2 (Figure 2.3). In the first instance, Al(III) was employed in a 1:1 metal source to ligand ratio. When the imino form was more prevalent than the related bicyclic form, as in **1**-**5**H, the aluminium complex was successfully formed and isolated (Figure 3.2). Even a 50:50 mixture of the two forms, as seen for **6**H, yielded the aluminium imino complex but with a reduction in yield. However, when the bicyclic form dominated the equilibrium, successful purification of a pure compound was not realised, perhaps due to the difference in solubility of the two forms upon complexation. This was also the case when other metals {Mg(II) and Zn(II)} were trialled (Figure 3.2).

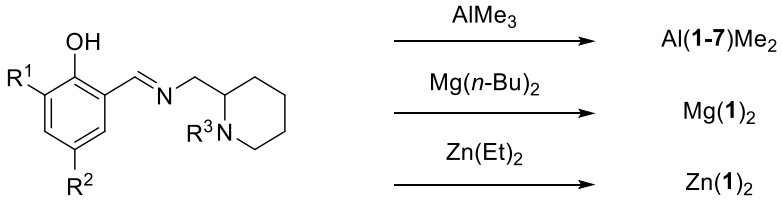

1H, $R^1 = R^2 = {}^tBu$, R^3 = H
2H, R^1 = Ad, R^2 = Me, R^3 = H
3H, R^1 =Trityl, R^2 = Me, R^3 = H
4H, $R^1 = R^2$ = Me, R^3 = H
5H, R^1 = OMe, $R^2 = R^3$ = H
6H, R^2 = Br, $R^1 = R^3$ = H
7H, $R^1 = R^2 = {}^tBu$, R^3 = Bn

Figure 3.2: Complexation of imino monophenols to Al(III), Mg(II) and Zn(II).

The complexation of the uncapped imino functionality, where R^3 = H, yielded the monoligated complexes, Al(**1**-**6**)Me_2. Typically, purification was achieved *via* recrystallisation from the reaction solvent, toluene, yielding yellow/orange crystals. A solid-state structure was obtained in most cases (Table 3.1, Figure 3.3 - 4). For each of these aluminium monophenolate solid-state structures, a monoclinic crystal system was observed with either a *P2₁/c* {Al(**1**/**2**)Me_2} or a *P2₁/n* Al(**4**/**5**)Me_2 space group observed. An exception to this was Al(**3**)Me_2 which was found to be triclinic with a *P-1* space group. A *pseudo* trigonal bipyramidal aluminium centre was revealed in

each case with both imine and amine nitrogen atoms participating in bonding {for Al(**1**)Me_2, N(1)-Al-N(2) = 76.53(6)°}. The *ortho* position on the aryl ring is parallel to the equatorial position plane of the metal coordination sphere and in the case of Al(**5**)Me_2, the methoxy group is orientated away from the aluminium centre (Figure 3.4). The imine-metal bond length was found to be shorter than that of amine-metal, for example in Al(**1**)Me_2, Al(1)-N(1) = 2.0010(15) Å compared to Al(1)-N_p(2) = 2.2613 (17) Å. The piperidine nitrogen and phenolate group occupy the axial position of the trigonal bipyramidal geometry with a deviation from the ideal 180° angle {O(1)-Al(1)-N_p(2) = 161.8(2)° - 165.71(10)°}, within the equatorial sites are the aluminium methyl groups and the imine and there is both a negative and positive deviation from ideality for these three angles {for Al(**1**)Me_2, C(1)-Al(1)-C(2) = 123.47(8)° and N(1)-Al(1)-C(2) = 112.10(7)°}. The amine hydrogen, R^3, is present and accounted for in all of the refined structures precluding the formation of an amido complex.

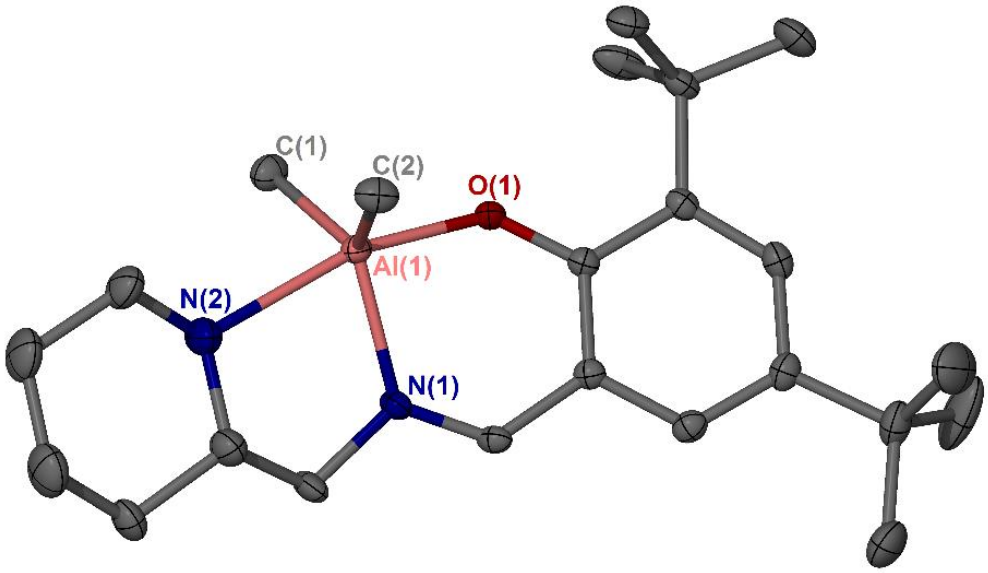

Figure 3.3: Solid-state structures of Al(**1**)Me_2. Ellipsoids are shown at the 30% probability level and all hydrogen atoms have been removed for clarity.

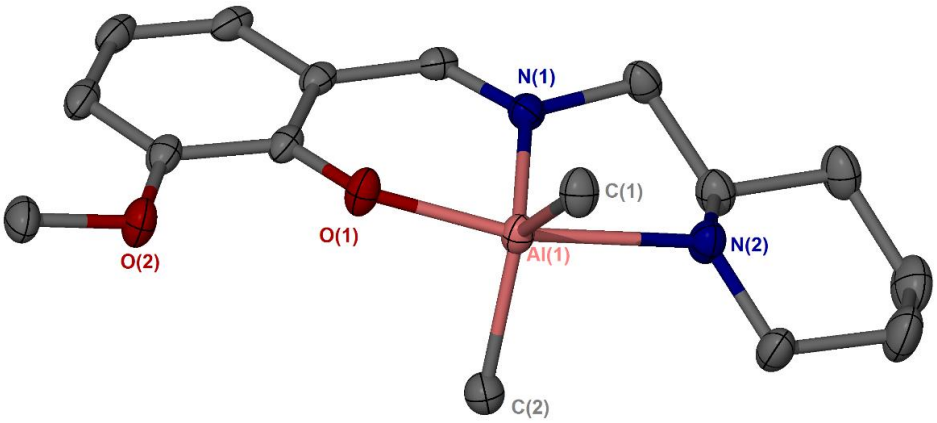

Figure 3.4: Solid-state structures of Al(**5**)Me_2 . Ellipsoids are shown at the 30% probability level and all hydrogen atoms have been removed for clarity.

This series of complexes were shown to have a similar tendency towards the trigonal bipyramidal structure. The preference of a five coordinate complex towards a square based pyramidal or trigonal bipyramidal structure is commonly quantified by the τ value.[15] This structural factor is calculated from the difference between the two largest bond angles, α/β, and their relative difference in the idealised geometries (60°). The τ value for this series of complexes was in a range of 0.64 - 0.67 indicating a slight preference towards the trigonal bipyramidal structure (Table 3.1). A comparison of a solid-state structure with a similar system from the literature is shown in (Figure 3.5, Table 3.1). The related complexes based upon 2-(aminomethyl)pyridine {Al(**A/B**)Me_2} were shown to have the same coordination geometry with similar bond lengths, angles and τ values.[11,14]

Table 3.1: Selected bond distances (Å) and bond angles (°) for Al(**1-5**)Me_2 and literature complexes, Al(**A**/**B**)Me_2, for comparison.[11,14]

	Al(**A**)Me_2	Al(**B**)Me_2	Al(**1**)Me_2	Al(**2**)Me_2	Al(**3**)Me_2	Al(**4**)Me_2	Al(**5**)Me_2
Al-O(1)	1.854(2)	1.861(2)	1.8530(13)	1.851(4)	1.8553(10)	1.857 (3)	1.865(2)
Al-C(1)	1.975(2)	1.979(3)	1.9883(19)	1.967(6)	1.9717(16)	1.985(6)	1.971(3)
Al-C(2)	1.952(3)	1.973(3)	1.9836(19)	1.991(5)	1.9753(15)	1.985(5)	1.994(3)
Al-N_p(2)*	2.254(2)	2.184(3)	2.2613(17)	2.211(6)	2.2462(18)	2.204(5)	2.256(2)
Al-N (1)	1.999(2)	2.027(3)	2.0010(15)	2.027(4)	2.0210(12)	2.022(4)	2.000(2)
O(1)-Al-C(1)	98.97(10)	95.8(1)	96.58(7)	93.6(2)	99.00(6)	94.65(19)	96.11(12)
O(1)-Al-N(1)	88.11(7)	87.27(10)	87.88(6)	86.92(17)	95.91(6)	94.65(19)	89.07(9)
O(1)-Al-N_p(2)	162.52(8)	161.89(11)	163.28(6)	161.8(2)	163.12(6)	164.16(18)	165.71(10)
N_p(2)-Al-C(1)	89.78(10)	89.67(13)	86.87(8)	89.2(3)	93.29(8)	87.8(2)	93.28(12)
C(1)-Al-C(2)	123.69(12)	121.84(15)	123.47(8)	121.9(2)	126.11(8)	125.5(2)	125.59(15)
N(1)-Al-C(1)	118.18(10)	124.53(13)	122.23(7)	123.5(2)	120.05(6)	120.4(2)	115.07(12)
N(1)-Al-C(2)	115.47(10)	112.11(13)	112.10(7)	113.4(2)	111.98(6)	112.7(2)	117.66(13)
τ	0.65	0.62	0.66	0.64	0.62	0.65	0.67

*N_P refers to the piperidine ring nitrogen and for literature examples pyridine ring nitrogen

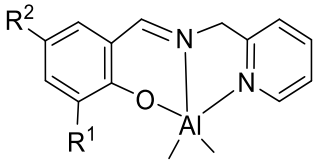

Al(**A**)Me_2 R^1 = R^2 = ^{t}Bu
Al(**B**)Me_2 R^1 = $SiPh_3$, R^2 = Me

Figure 3.5: Literature aluminium complexes based upon 2-(aminomethyl)pyridine.[11,14]

Analysis by solution state ^{1}H NMR spectroscopy (d_8-toluene, 298K) indicated the solid-state structure to be maintained in solution with two aluminium methyl and two aromatic resonances consistent with a monomeric complex (Figure 3.6). Complexation had a profound effect on the NMR spectrum with the piperidine protons being more readily assigned due to "locking" of the ring conformation giving discrete resonances; further to this the NH resonance was now present and elucidated *via* 2D-HSQC NMR spectroscopy.

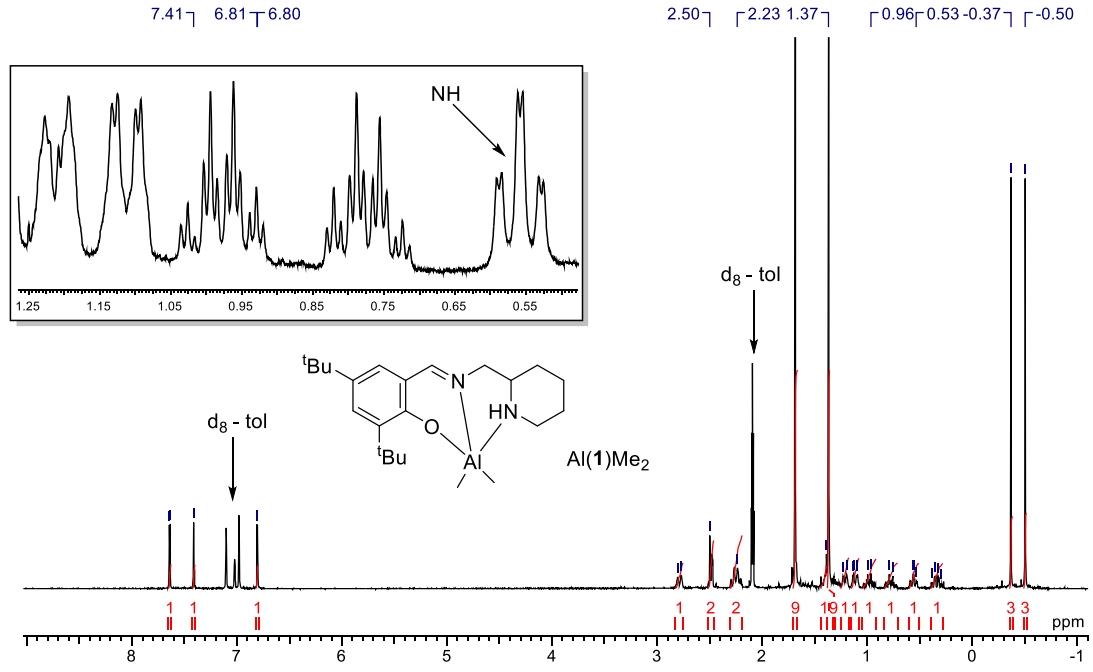

Figure 3.6: ^{1}H NMR (d_8-Toluene, 298 K) spectrum of Al(**1**)Me_2. Inset: "locked" CH_2 resonances and NH resonance.

The amine functionalised monophenol **7**H, where R^3 = Bn, was also complexed to Al(III) however, no suitable crystals were grown for analysis by X-ray crystallography. The complex, Al(**7**)Me_2, was initially prepared by James Brown-Humes (MChem student, 2015-2016). The crude complex is analytically pure showing one main species *via* NMR spectroscopy. The ^{1}H NMR spectrum contains one aluminium methyl resonance, two *t*-butyl resonances as well as a characteristic pair of diastereotopic benzylic doublets (Figure 3.7). The $^{13}C\{^1H\}$ NMR spectrum is unambiguous. It is unclear whether the Al(III) centre is four or five coordinate in this instance. DFT prediction of the structure of Al(**7**)Me_2 suggests a tetrahedral aluminium centre due to coordination with the imine and phenoxy moiety only (Figure 3.8). For these calculations, the *t*-butyl groups were removed to reduce the time required and the level of theory chosen has been previously demonstrated for Al(III) complexes in the literature {rωb97xD/6-311$^+$G(d) in toluene}(See experimental section for more details).[2] In particular, this functional has previously provided a good comparison of calculated geometry against solid-state structure and successfully predicted the most stable stereoisomer present in solution.[2] There is also evidence of π stacking of the aromatic rings with these groups position in a parallel albeit staggered configuration with a centroid separation of 3.84 Å. For similar series of imino [ONO] and [ONN] Al(III) complexes, a tetrahedral metal centre has been demonstrated in the solid-state, further supporting such a geometry for Al(**7**)Me_2.[16]

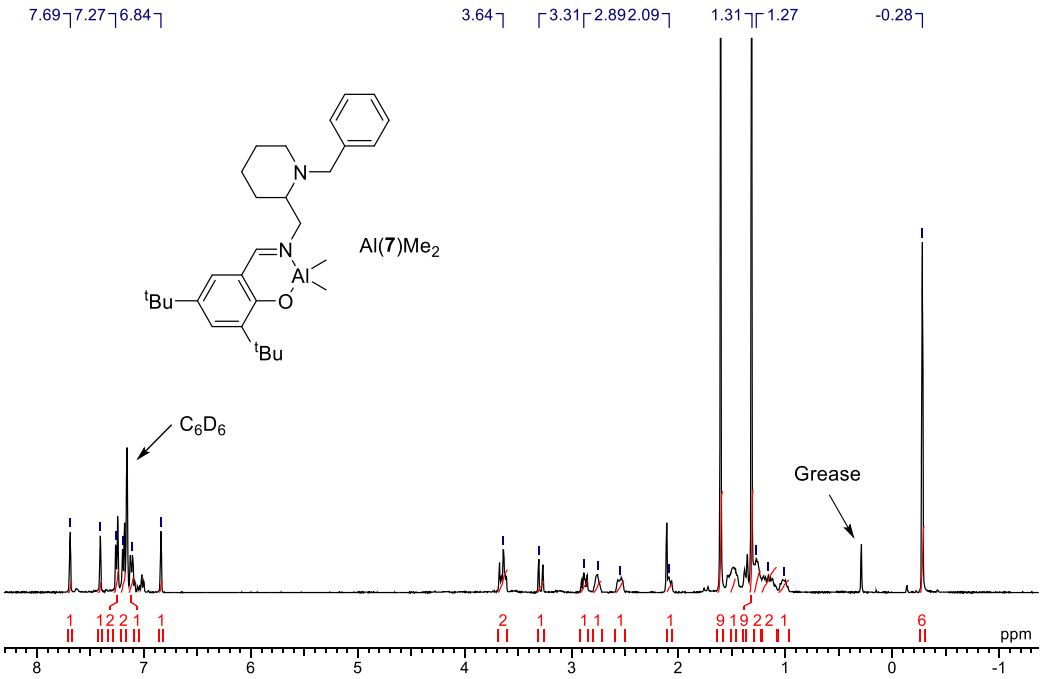

Figure 3.7: ^{1}H NMR (C_6D_6, 298 K) spectrum of Al(**7**)Me_2.

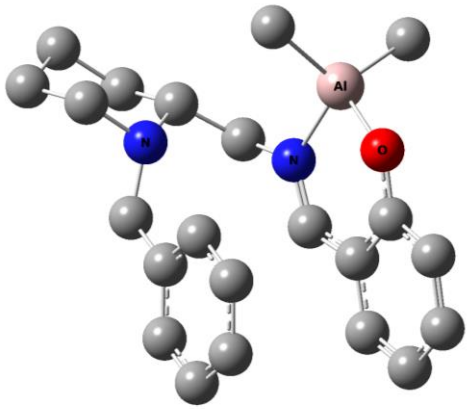

Figure 3.8: Predicted structure of Al(**7**)Me_2 based on DFT calculations {rωb97xD/6-311$^+$G(d) in toluene, 298 K}.

Complexation of **1**H to Mg(II) and Zn(II) afforded coordinatively saturated bis-ligated complexes, facilitated by the larger metal radii (Figure 3.9). There was no evidence of a metal alkyl complex *via* ^{1}H NMR spectroscopy for the isolated samples, even when the complexation was carried out on a 1:1 basis. It is possible that a Schlenk type equilibrium is in operation with the M(**L**)$_2$ form being isolated from this equilibrium mixture by virtue of its solubility. The Mg(**1**)$_2$ complex and crystals were prepared by James Brown-Humes (MChem student, 2015-2016).

The solid-state structures of Mg/Zn(**1**)$_2$ were determined by X-ray crystallography, both containing 6 coordinate metal centres displaying with a *mer-mer* coordination of the ligands; disorder was also suggested around the amine and 2- position of the piperidine ring. For Mg(**1**)$_2$, there are two positions, at a ratio of 50:50, for every atom within one piperidine ring and the connected imino-methyl arm, represented by N(3A)/N_p(4A) (Table 3.2). Identical disorder, in a ratio of 60:40, is seen for Zn(**1**)$_2$, affecting both piperidine rings but not extending to the imino nitrogen giving one disordered metal to ligand bond based on N_p(4A). These secondary positions clearly show an exchange in groups at the chiral centre with the ring "flipped" to maintain the imino methyl group in the equatorial position (Figure 3.10). As a consequence, there are diastereomeric relationships in the form of (*RR/RS)* and (*SS*/*SR*), for both Mg(**1**)$_2$ and Zn(**1**)$_2$.

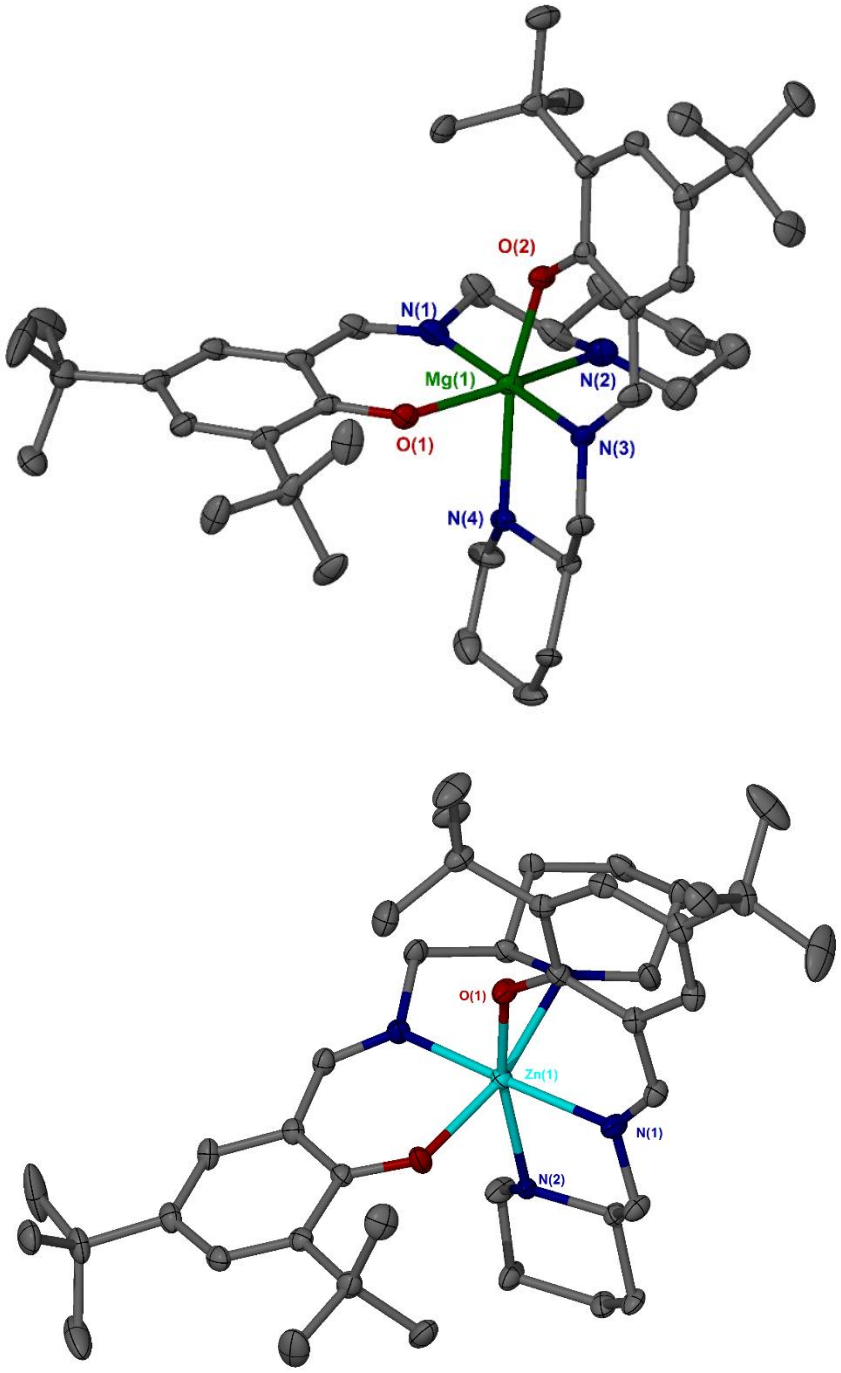

Figure 3.9: Solid-state structures of Mg(**1**)$_2$ (top) and Zn(**1**)$_2$ (bottom). Ellipsoids are shown at the 30% probability level and all hydrogen atoms have been removed for clarity.

The magnesium complex crystallised in a monoclinic form with a $P2_1/n$ spacegroup and the zinc in a tetragonal system with a $I\text{-}4_2d$ space group. Crystallographically, the two ligands in Zn(**1**)$_2$ are equivalent hence there is only half a complex contained in the unit cell. Both structures show deviations from idealised octahedral geometry. The three *trans* groups show deviation between the anticipated 180° bond angle with the more rigid *trans* imino groups being closer to ideality {O(1/2)-Mg-N$_p$(2/4) = 158.95(7)°/ 163.2(2)°, N(1)-Zn-N(3) = 178.62(18)° / O(1)-Zn-N$_p$(2) = 165.48(16)°, N(1)-Zn-N(3) = 171.56(8)°}. There are also fluctuations around the expected 90° angle for *cis* related groups {L(*cis*)-Mg-L(*cis*) = 74.8(3) ° - 106.45(7) ° /L(*cis*)-Zn-L(*cis*) = 78.77(15)° - 100.4(2)°}.

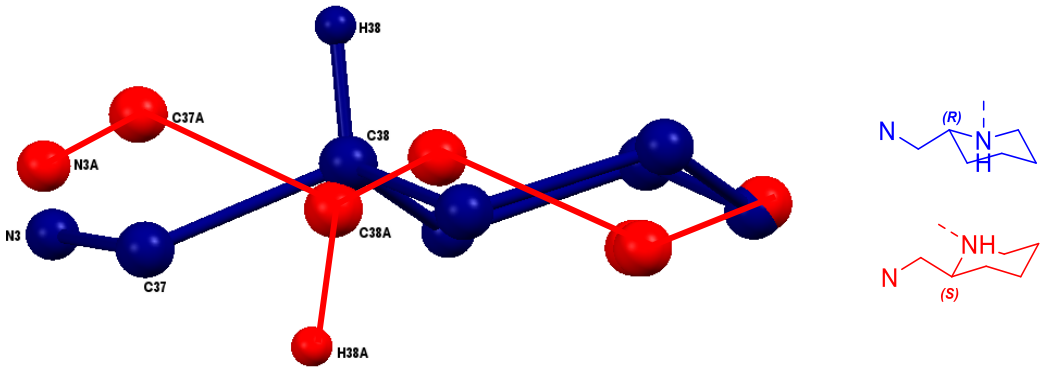

Figure 3.10: Disordered positions of piperidine ring in Mg(**1**)$_2$.

A zinc analogue with 2-(aminomethyl)pyridine, Zn(**A**)$_2$, is known with a solid-state structure reported.[12] Interestingly, in this crystal system, the pyridine nitrogen of one of the ligands does not bind to the metal generating a square pyramidal zinc centre (τ = 0.03). As a consequence of the non-bonding pyridine nitrogen, the metal to ligand bond lengths for Zn(**A**)$_2$ are all shorter relative to the Zn(**1**)$_2$ indicating stronger coordination. In the same report, it is suggested, *via* NMR spectroscopy, and computationally that an octahedral *mer-mer* geometry, with the pyridine nitrogen coordinated, is however present in solution. The possibility of an alkyl zinc complex is also realised for this ligand, **A**H, in which a dimer forms with bridging phenoxy groups when excess ZnEt$_2$ is used (Figure 3.11).[12]

Table 3.2: Selected bond distances (Å), diameters (Å) and bond angles (°) for Zn/Mg(**1**)$_2$ and literature complex, Zn(**A**)$_2$, for comparison.[12]

	Mg(**1**)$_2$	Zn(**1**)$_2$	Zn(**A**)$_2$
M-O(1)	1.9963(16)	2.0139(12)	1.9760(20)
M-O(2)	1.9751(15)	2.0139(12)*	1.9785(19)
M-N(1)	2.1359(18)	2.1182(4)	2.086(2)
M-N(3)	2.105(9)	2.1182(4)	2.033(2)
M-N(3A)	2.205(9)	-	
M-N$_p$(2)	2.326(2)	2.2560(6)	2.152(3)
M-N$_p$(4)	2.257(7)	2.2560(6)	**
M-N$_p$(4A)	2.304(8)	2.309(11)	-
d$_{\{N(1)-N(3)\}}$	4.2409	4.2364	-
d$_{\{N(1)-N(3A)\}}$	4.3409	-	-
d$_{\{O(1)-Np(2)\}}$	4.3223	4.2699	-
d$_{\{O(2)-Np(4)\}}$	4.2321	4.2699	-
d$_{\{O(2)-Np(4A)\}}$	4.2791	4.3229	-
O(1)-M-O(2)	106.45(7)	99.33(8)	95.66(8)
O(1)-M-N$_p$(2)	158.95(7)	165.48(16)	155.09(9)
O(1)-M-N(1)	85.11(7)	86.76(5)	103.39(9)
O(1)-M-N(3)	93.55(7)	81.98(11)	153.42(9)
O(2)-M-N$_p$(4)	163.2(2)	165.48(16)	**
N$_p$(2)-M-N$_p$(4)	95.78(17)	100.4(2)	**
N(1)-M-N(3)	178.62	171.56(8)	113.17(9)

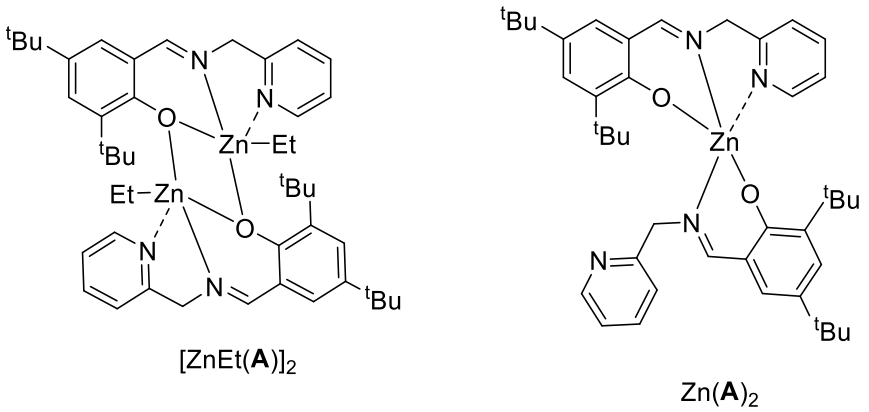

Figure 3.11: Literature zinc complexes based upon 2-(aminomethyl)pyridine.[12]

The presence of diastereomers for Mg/Zn(**1**)$_2$ is supported by ^{1}H NMR spectroscopy, in which there is no evidence of free ligand or contributions from bicyclic species (Figure 3.12). The region ~7-8 ppm (Figure 3.12, inset) consists of three narrow multiplets with the most deshielded series being assigned to the imine. The characteristic singlet resonance of the imine functionality is now represented by four distinct signals which agrees with a bis-ligated system of a pair diastereomers in which each ligand is chemically inequivalent. Similarly, there are multiple resonance which correspond to the *tert*-butyl resonances, together accounting for 18 protons. The remaining spectra consists of overlapping multiplets which integrate to the correct number of CH_2/CH protons. Further insight is provided by the diffusional properties of these complexes.

Diffusional ordered spectroscopy (DOSY) NMR analysis was carried out for both complexes (C_6D_6, 298 K). For both Mg(**1**)$_2$ and Zn(**1**)$_2$, there were two distinct sets of diffusion coefficients with a small difference in each case. For Mg(**1**)$_2$, these values are measured to be 4.67×10^{-10} m^2s^{-1} and 4.78×10^{-10} m^2s^{-1}. Larger values are found for Zn(**1**)$_2$, equal to 5.47×10^{-10} m^2s^{-1} and 5.56×10^{-10} m^2s^{-1}. The close agreement of these values for each complex series is further evidence that the samples are made up exclusively of bis-ligated species and the difference is due to isomerism. For comparison, the diffusion coefficient of the free ligand is also given; uncoordinated **1**H diffuses at a faster rate relative to the complexes {$D_{\mathbf{1}H} = 6.87 \times 10^{-10}$ m^2s^{-1}).

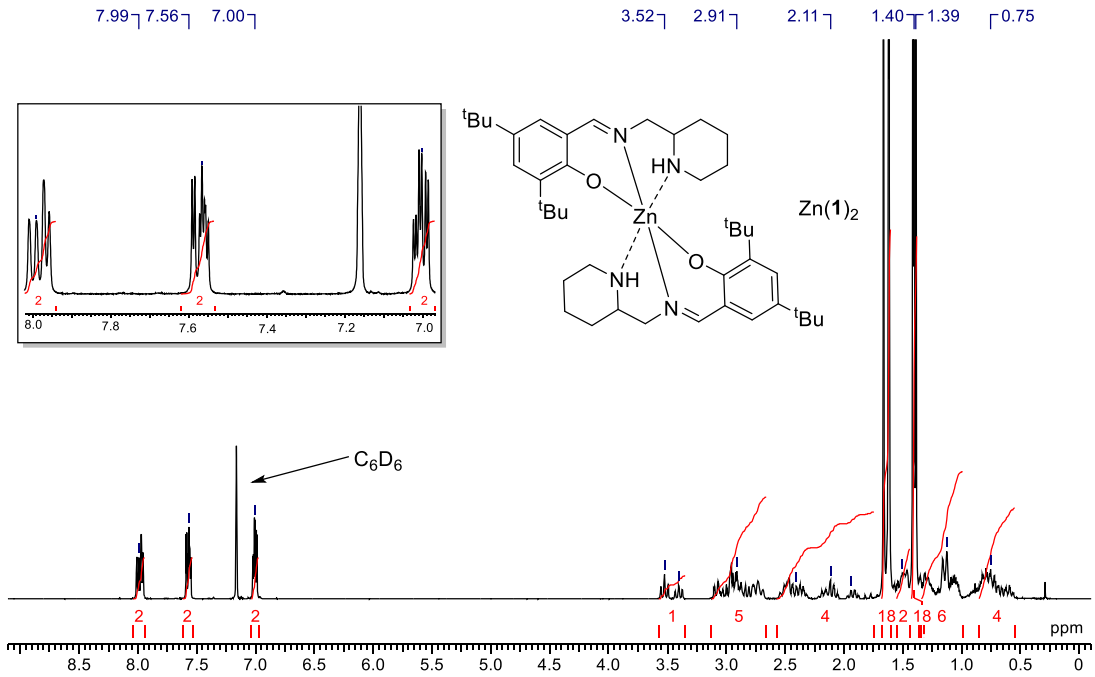

Figure 3.12: ^{1}H NMR (C_6D_6, 298 K) spectrum of Zn(**1**)$_2$. Inset: Aromatic/imine region.

The diffusion coefficients also correlate well with the solid-state structures. In this case, the diameter is calculated as a sum of the immediate bond lengths around the metal centre, with the assumption that these lengths are proportional to the true diameter of the complex, allowing for relative comparison. While the Mg-O bonds are shorter relative to the zinc analogue, there is more variation in the Mg-N bonds. This leads to generally larger diameters for this complex (for Mg(**1**)$_2$, $d_{\{N(1)\,-\,N(3)\}}$ = 4.2409 Å, $d_{\{O(1)\,-\,Np(2)\}}$ = 4.3223 Å / for Zn(**1**)$_2$, $d_{\{N(1)\,-\,N(3)\}}$ = 2.2364 Å, $d_{\{O(1)\,-\,Np(2)\}}$ = 4.2699 Å). Hence, Zn(**1**)$_2$ is observed to diffuse faster than Mg(**1**)$_2$. As mentioned previously, there is disorder in the crystal structure giving rise to multiple positions for some atoms leading to a potential for different bond lengths. For Zn(**1**)$_2$, this disorder is mainly around the piperidine nitrogen N_p(2) and causes a 1.2% increase in the immediate diameter; accordingly, the second diffusing species is approximately 1.6% times slower. A similar treatment can be carried out for Mg(**1**)$_2$ for which diffusion rate is reduced by approximately 2.4% and there are two points of disorder causing a total diameter increase of 1.5%.

Table 3.3: Diffusion coefficients ($x10^{-10}$ m^2s^{-1}) of Mg(**1**)$_2$, Zn(**1**)$_2$, and **1**H (C_6D_6, 298 K).

Mg(**1**)$_2$	Zn(**1**)$_2$	**1**H
4.78	5.56	6.87
4.67	5.47	

For comparison of catalytic activity, the 2-AMP$_y$ analogue, Mg(**A**)$_2$ was prepared from the reaction of **A**H with Mg(^{n}Bu)$_2$. Based on a lack of alkyl resonances in the ^{1}H NMR spectrum, the successful preparation of the corresponding bis-ligated species is deduced. The ^{1}H and ^{13}C{^{1}H} show a single series of resonances assignable to one ligand unit indicating both ligating species are equivalent. Hence, an octahedral complex is likely present in solution in an analogous fashion to Mg(**1**)$_2$. Unlike the free ligand, the CH_2 groups connected to the pyridine moiety are now split into a pair of doublets, indicating their inequivalence once coordinated

3.2.2 Bicyclic monophenolates complexes

Attempts were made to coordinate monophenol bicyclic ligands, **8**-**12**H, to Al(III) (Figure 3.13). The complexes Al(**8**-**12**)Me$_2$ were found to be extremely soluble in common organic solvents and no purification was realised.

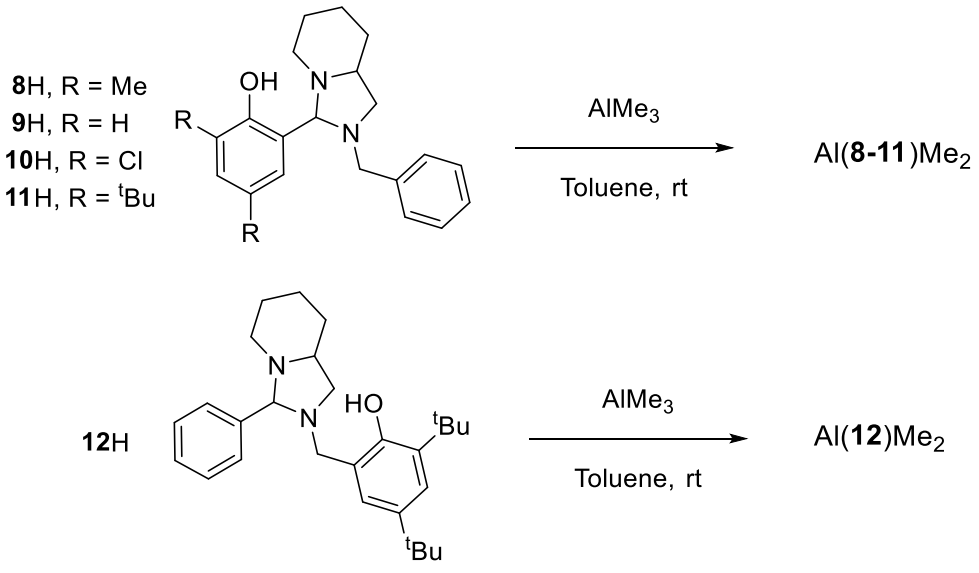

Figure 3.13: Complexation of biaryl monophenols, **8**-**12**H, to Al(III)

For Al(**8-10**)Me_2, a number of species were observed in solution *via* ^{1}H NMR spectroscopy. While the expected product was present, there were extra resonances, particularly in the aluminium methyl region, < 0 ppm. It is unclear at this point if these species are due to a free aluminium species or correspond to unexpected complexes. A brief investigation was carried out to explore possible structures *via* DFT analysis of these systems comparing the possibility of binding to each nitrogen within the bicyclic ring. Based on the solid-state structure of **10**H, with both chlorines removed to reduce computational time, the two different binding motifs were set up. An energy minimisation {rωb97xD/6-311$_+$G(d) in toluene, 25°C} of the structures showed a preference between the two motifs. A preliminary investigation explored the conformation of pendant benzyl group and a preference was found for this group to be directed away from the rest of the molecule. Analysis of the Al(III) binding position generated reasonable structures for each nitrogen participation in bonding. However, there was a slight preference (~3 kcal/mol) for aluminium coordination to the nitrogen centre within the five membered ring rather than the bridging nitrogen atom (Figure 3.14). The low coordination of the aluminium centre may also allow for the formation of dinuclear and/or bis-ligated species and such structures may also contribute to the extra resonances observed *via* ^{1}H NMR spectroscopy (Figure 3.15).[17]

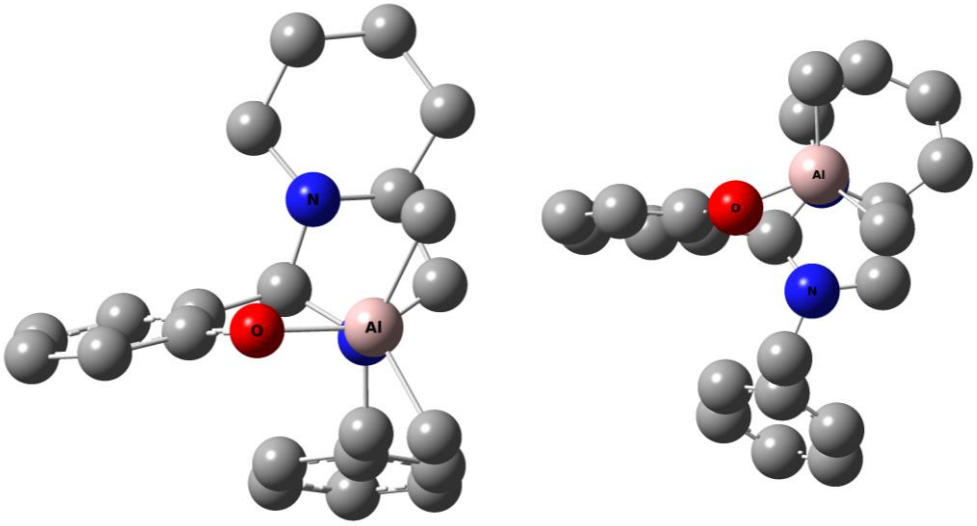

Figure 3.14 Predicted structures of Al(**9**)Me_2 from DFT calculations {rωb97xD/6-311$^+$G(d) in toluene, 298 K}.

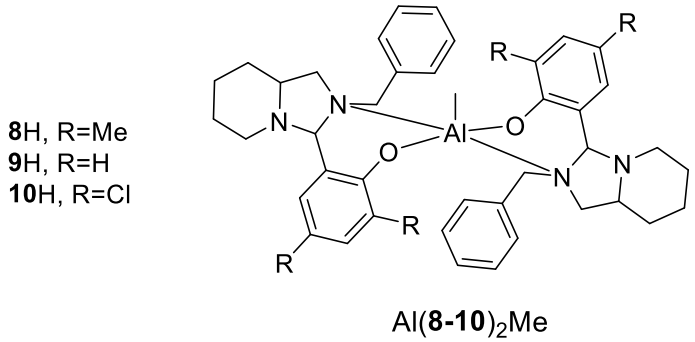

Figure 3.15: A further possible structure contributing to impurities for Al(**8**-**10**)Me_2.

When the bulk of the aryl substituents was increased, as in the case of **11**H, the isolated complex was seen to be purer *via* ^{1}H NMR spectroscopy. However, there were still impurities in the baseline of the spectra, which were particularly noticeable in the aluminium methyl region. Al(**11**)Me_2 still remains purer than the previous complexes, Al(**8**-**10**)Me_2, and it is suggested that the increased steric bulk is a factor, reducing the extent of side products and dimerisation. The major species conforms to the anticipated structure with sharp resonances from the phenoxy ring, bicyclic CH singlet, *t*-butyl and aluminium methyl groups. The benzylic CH_2 resonances are inequivalent in this system giving rise to a pair of doublets subject to roofing (Figure 3.16). Without crystallographic structural evidence, this complex is predicted to have a 4 coordinate tetrahedral aluminium centre.

The coordination of Al(III) with the structural isomer, **12**H, afforded similar results. Without purification, Al(**12**)Me_2 was isolated with impurities, albeit to a lesser extent than Al(**11**)Me_2. The ^{1}H NMR spectrum is consistent with the monomeric form, with two sharp Al-Me resonances and seven aromatic protons (Figure 3.17). There are differences between the spectra of Al(**11**)Me_2 and Al(**12**)Me_2, indicating distinct structural motifs. Most significant is the relative shifts of the benzylic CH, which is shifted approximately 1 ppm downfield for Al(**12**)Me_2 relative to Al(**11**)Me_2. This could indicate proximity to the Al(III) centre in case of Al(**12**)Me_2. The aluminium methyl resonances are in a similar region in both spectra, indicating a similar coordination interaction.

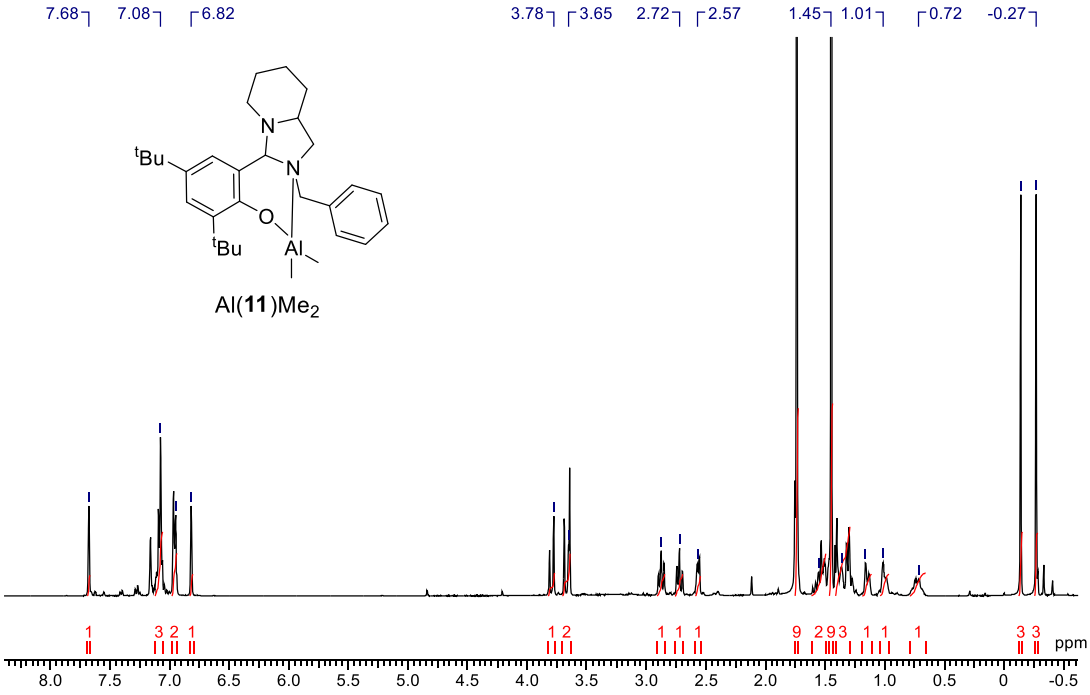

Figure 3.16: ^{1}H NMR (C_6D_6, 298 K) spectrum of Al(**11**)Me_2.

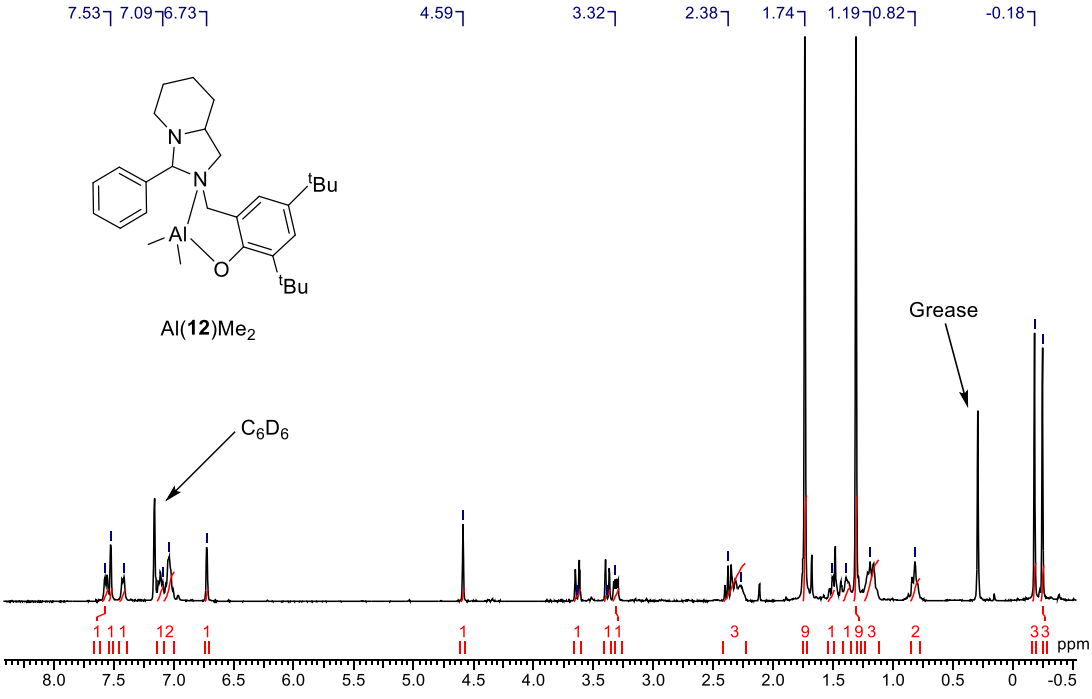

Figure 3.17: ^{1}H NMR (C_6D_6, 298 K) spectrum of Al(**12**)Me_2.

Coordination of monophenol heterocycle, **13**H, with the bicyclic backbone was found to be more amenable to purification *via* recrystallisation (Figure 3.18). As with the iminophenolates, Al(**1**-**6**)Me_2, this structure is shown to be trigonal bipyramidal *via* X-ray crystallography (Figure 3.19, Table 3.4). Al(**13**)Me_2 was found in a monoclinic crystal system with a spacegroup of $P2_1$ with *RRS* and *SSR* enantiomers making up the unit cell. Chirality in this system refers to the 2-position of the piperidine ring, the benzylic position connected to the pyridine ring and the nitrogen atom coordinating to the metal centre. The bond lengths for Al(**13**)Me_2 are comparable to the Al(**1**-**6**)Me_2 series and the bond angles are also similar to those of the imino monophenolate system, specifically the *t*-butyl analogues Al(**A**/**1**)Me_2. However, the geometry is slightly less ideal with a lower τ value (τ = 0.61). The axial axis contains the phenoxy group and the pyridine ring {O(1)-Al-N(1) = 161.10(12)°} which are generally at less than 90° to the equatorial groups { L(*trans*)-Al-L(*cis*) = 75.81(11)° - 92.23(12)°}. The relative equatorial positions also show the deviation from ideality with angles above and below 120° {C(1)-Al-C(2) = 124.21(18)° / N(2)-Al-C(2) = 115.89(14)°}.

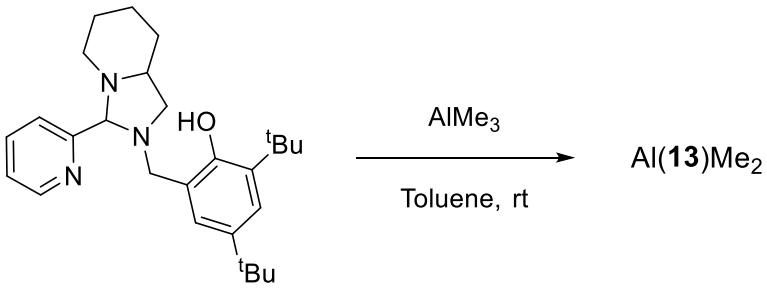

Figure 3.18: Complexation of pyridine based monophenol, **13**H, to Al(III).

Characterisation of Al(**13**)Me_2 in solution *via* ^{1}H NMR spectroscopy revealed a broadening relative to Al(**12**)Me_2 but assignment was unambiguous (Figure 3.20). This affected one of the benzylic CH_2 resonances, both CH and an Al-Me resonance and could be a due to a fluxional process around the aluminium centre. These resonances were also absent in the $^{13}C\{^1H\}$ NMR spectrum and deduced by 2D-HSQC.

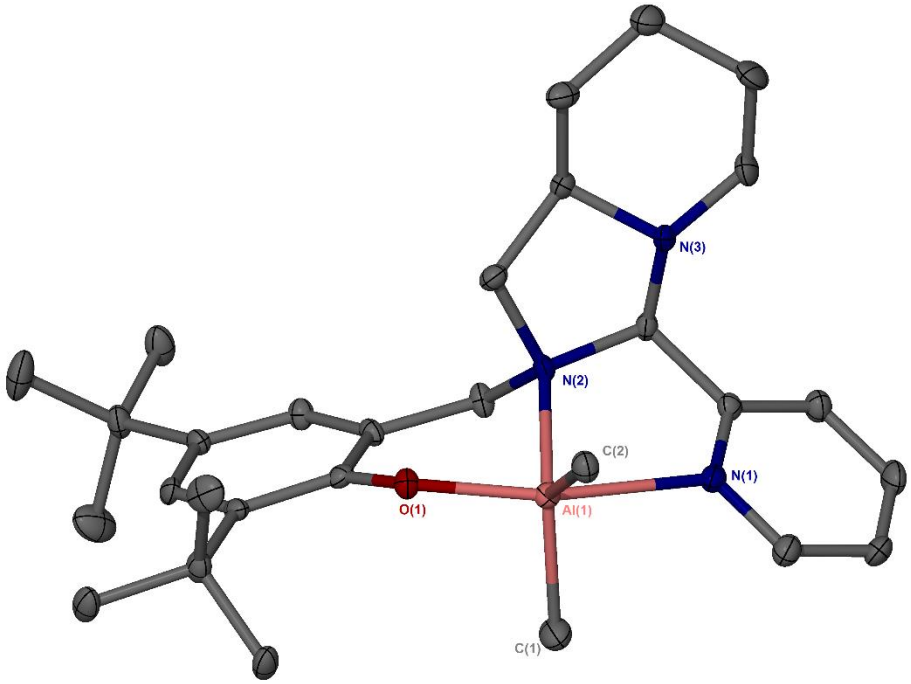

Figure 3.19: Solid-state structure of Al(**13**)Me_2, displaying *RRS* enantiomer. Ellipsoids are shown at the 30% probability level and all hydrogen atoms have been removed for clarity.

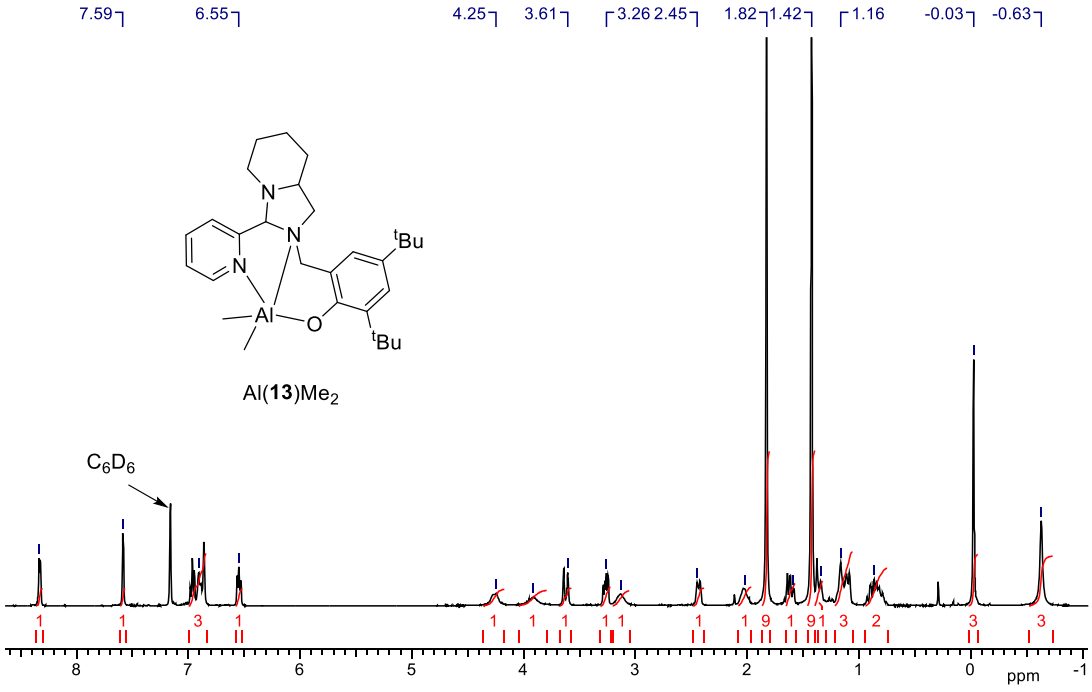

Figure 3.20: ^{1}H NMR (C_6D_6, 298 K) spectrum of Al(**13**)Me_2.

Table 3.4: Selected bond distances (Å) and bond angles (°) for Al(**13**)Me_2

	Al(**13**)Me_2
Al-O(1)	1.825(2)
Al-C(1)	1.982(4)
Al-C(2)	1.970(3)
Al-N (2)	2.083(3)
Al-N (1)	2.264(3)
O(1)-Al-C(1)	98.19(3)
O(1)-Al-N(1)	161.10(12)
O(1)-Al-N (2)	86.38(11)
N(2)-Al-C(1)	117.08(15)
N(2)-Al-C(2)	115.89(14)
C(1)-Al-C(2)	124.21(18)
N(1)-Al-C(1)	84.65(13)
N(1)-Al-C(2)	92.23(12)
τ	0.61

3.3 Aluminium bis/trisphenolates complexes

3.3.1 Aluminium bicyclic bisphenolate complexes

The complexation of the bisphenols with the bicyclic motif in the backbone was initially carried out at room temperature. In some cases {Al(**14**-**20**)Me}, the reaction mixture was amenable to purification through recrystallisation from hexane or a hexane/toluene mixture yielding pale yellow or colourless crystals. However, the ability to crystallise or yield a precipitate was reduced by increasing the number of alkyl groups on the aryl rings {Al(**20**-**22**)Me}. In such cases, the complex was highly soluble and solvent was removed to furnish a pure material in good yield (Figure 3.21). Attempts to complex **23**-**25**H_2 were less successful. For **23**H_2, in which both aryl rings are unsubstituted, a small crop of crystals were isolated. Despite low solubility in d_8-toluene, ^{1}H NMR spectroscopy suggests the formation of a [Al(**23**)Me]$_2$ species, likely a consequence of the reduced steric bulk of the ligand. Treatment of **24**/**25**H_2 ($R^1 = R^2 = {}^t$Bu, $R^3 = R^4 = Cl$ and $R^1 = R^2 = R^3 = R^4 = Cl$ respectively) with $AlMe_3$ afforded the desired species however, there were also considerable impurities contained within these samples.

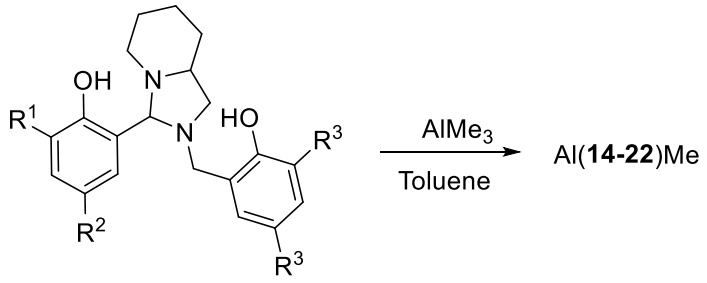

14H_2, $R^1 = R^2 = Cl$, $R^3 = {}^t$Bu
15H_2, $R^1 = R^2 = Br$, $R^3 = {}^t$Bu
16H_2, $R^1 = R^2 = I$, $R^3 = {}^t$Bu
17H_2, $R^1 = H$, $R^2 = Br$, $R^3 = {}^t$Bu
18H_2, $R^1 = H$, $R^2 = NO_2$, $R^3 = {}^t$Bu
19H_2, $R^1 = R^2 = H$, $R^3 = {}^t$Bu
20H_2, $R^1 = R^2 = Me$, $R^3 = {}^t$Bu
21H_2, $R^1 = Ad$, $R^2 = Me$, $R^3 = {}^t$Bu
22H_2, $R^1 = R^2 = R^3 = {}^t$Bu

Figure 3.21: Complexation of bicyclic bisphenols, **14**-**22**H_2, to Al(III).

Al(**14-15**/**19**)Me were structurally characterised by X-ray crystallography (Table 3.5, Figure 3.22). Al(**14**)Me was found in a triclinic crystal system with a *P-1* space group whereas Al(**15/19**)Me were both observed in a monoclinic system with $P2_1/n$ and *Ia* space groups respectively. The solid-state structure of these complexes conclusively shows the presences of a tetrahedral metal centre with the aluminium coordinating to the two phenoxy groups and only one nitrogen centre. Both phenoxy groups occupy the same plane of the tetrahedron and of the structures analysed, it is found that the both oxygens have a similar bond length to the metal {for Al(**14**)Me, Al-O(1) = Al-O(2) = 1.7440(10) Å and for Al(**19**)Me, Al-O(1) = 1.7445(13) Å / Al-O(2) = 1.7492(13) Å }. The ligand to metal bond angles are found to be in a range around the ideal tetrahedral angle with the phenoxy separation closer to ideality {for Al(**14**)Me, O(1)-Al-O(2) = 109.47(5)°/ C(1)-Al-N(1) = 117.97(6)° and for Al(**19**)Me, O(1)-Al-O(2) = 111.66(7)°/ C(1)-Al-N(1) = 116.72(8)°}.

Three chiral centres are present, all within the five membered ring and are displayed as *RRS* with the *S* referring to the aluminium coordinating nitrogen, N(1) (Figure 3.22). These complexes exist as enantiomers, with the *SSR* form also being present as seen previously for Al(**13**)Me_2. The aluminium is also a stereocentre, bearing an *S* configuration in this instance. The preference for a tetrahedral or square planar structure can be quantified using the four coordinate tau value, τ'_4.[18] This value is calculated using the two largest bonding angles relative to the ideal tetrahedral angle. This analysis reveals these complexes to be close to the ideal tetrahedral structure (τ'_4 = 0.86 - 0.9). A comparison of these structures may be made with a literature tridentate ONO complex, Al(**C**)Me (Figure 3.23).[19] The bond lengths to the Al(III) centre are reasonably similar with greatest deviation seen for the Al-N(1) bond which are shorter in the bicyclic complexes {for Al(**14**)Me, Al-N(1) = 1.9894(12) Å compared to Al(**C**)Me Al-N(1) = 2.022(2) Å}. This difference is likely due to the rigidity of the bicyclic backbone. In comparison, the bond angles are also of a similar magnitude with the largest difference being ~6/7° for the C(1)-Al-N(1) angle; as a consequence of this increased angle, Al(**C**)Me is found to be less ideal with respect to tetrahedral geometry.

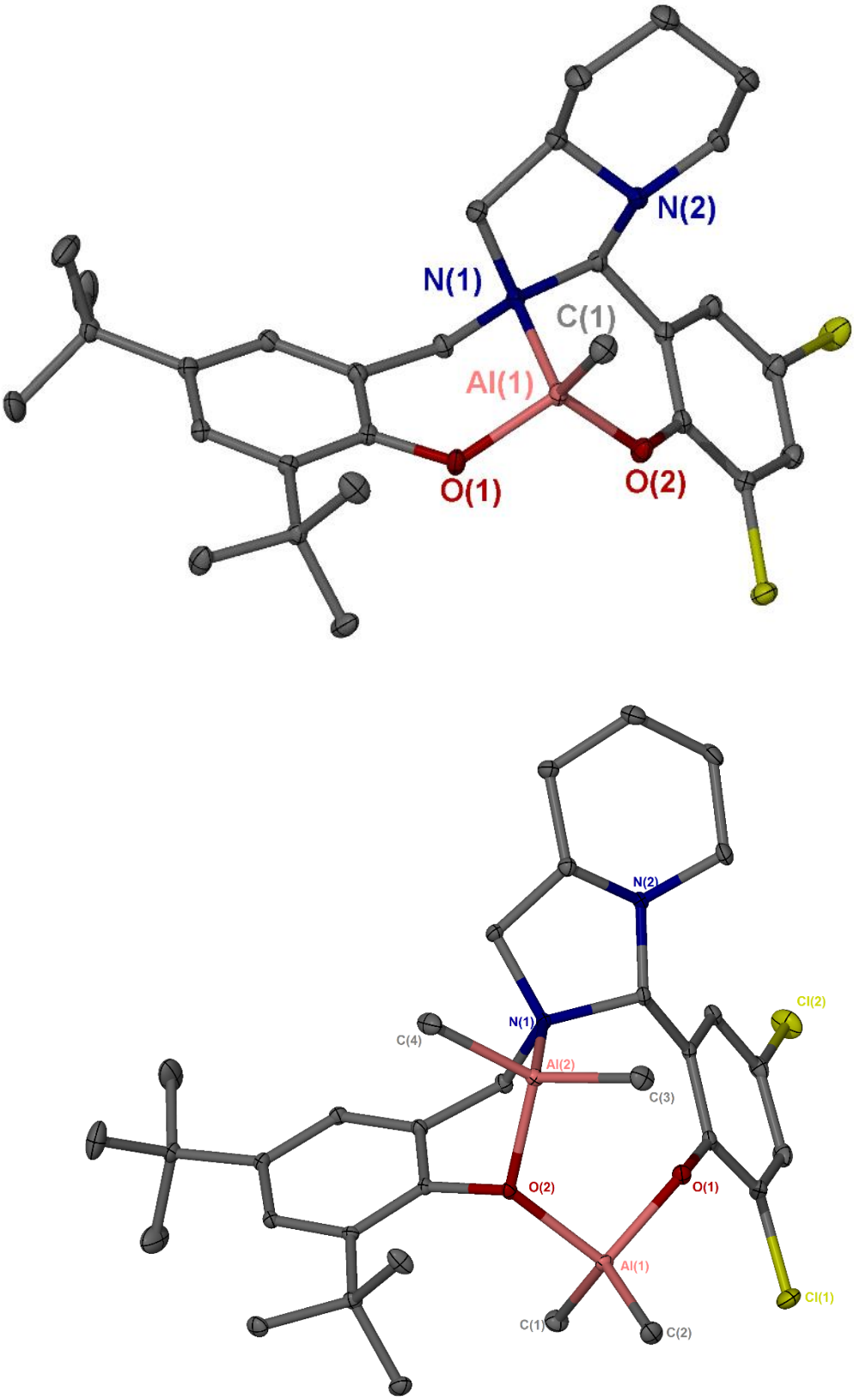

Figure 3.22: Solid-state structures of Al(**14**)Me (top) and Al_2(**14**)Me_4 (bottom). Ellipsoids are shown at the 30% probability level and all hydrogen atoms have been removed for clarity.

Table 3.5: Selected bond distances (Å) and bond angles (°) for Al(**14-15/19**)Me and literature comparison, Al(**C**)Me.[19]

	Al(**C**)Me	Al(**14**)Me	Al(**15**)Me	Al(**19**)Me
Al-O(1)	1.739(5)	1.7440(10)	1.7493(17)	1.7492(13)
Al-O(2)	1.734(5)	1.7440(10)	1.7470(16)	1.7445(13)
Al-N(1)	2.022(2)	1.9894(12)	1.9937(19)	1.9889(16)
Al-C(1)	1.934(7)	1.9429(16)	1.937(2)	1.943(2)
O(1)-Al-O(2)	112.07(10)	109.47(5)	112.50(8)	111.66(7)
O(1)-Al-C(1)	109.06(13)	115.00(6)	114.29(10)	113.57(7)
O(1)-Al-N(1)	98.71(10)	98.61(5)	96.35(8)	97.54(6)
O(2)-Al-N(1)	98.27(9)	98.03(5)	99.41(8)	99.83(6)
O(2)-Al-C(1)	113.88(13)	115.40(6)	111.49(1)	115.47(8)
C(1)-Al-N(1)	123.69(11)	117.97(6)	121.30(10)	116.72(8)
τ'[4]	0.84	0.90	0.86	0.91

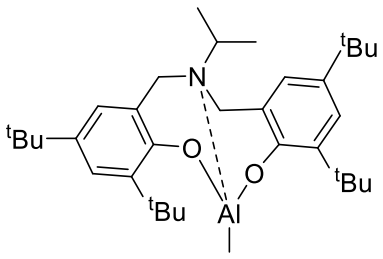

Al(**C**)Me

Figure 3.23: Literature comparison of ONO type Al(III) complex.[19]

Solution state ^{1}H NMR spectroscopy demonstrates the solid-state structure to be maintained in solution with four discrete doublets in the aromatic region to one aluminium methyl resonance for each complex (Figure 3.24). The benzylic protons are shown to be inequivalent with a relatively large shift to one another (~1ppm); this shift is due to the orientation of this position in the complex which directs a proton into the vicinity of the metal centre.

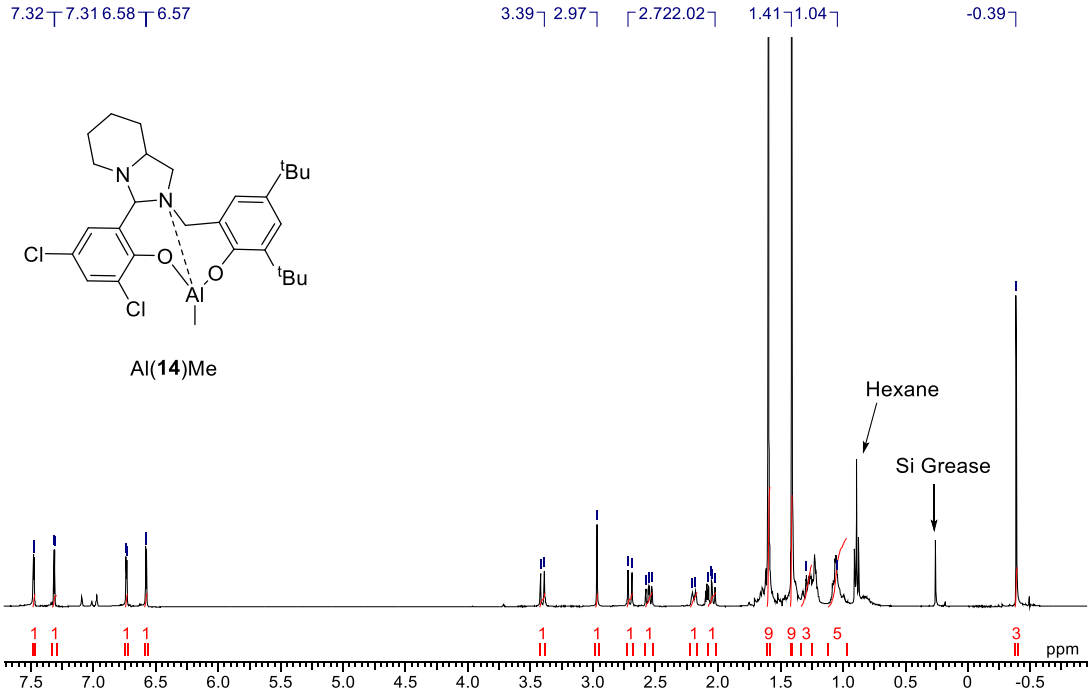

Figure 3.24: ^{1}H NMR (d_8-Toluene 298 K) spectrum of Al(**14**)Me.

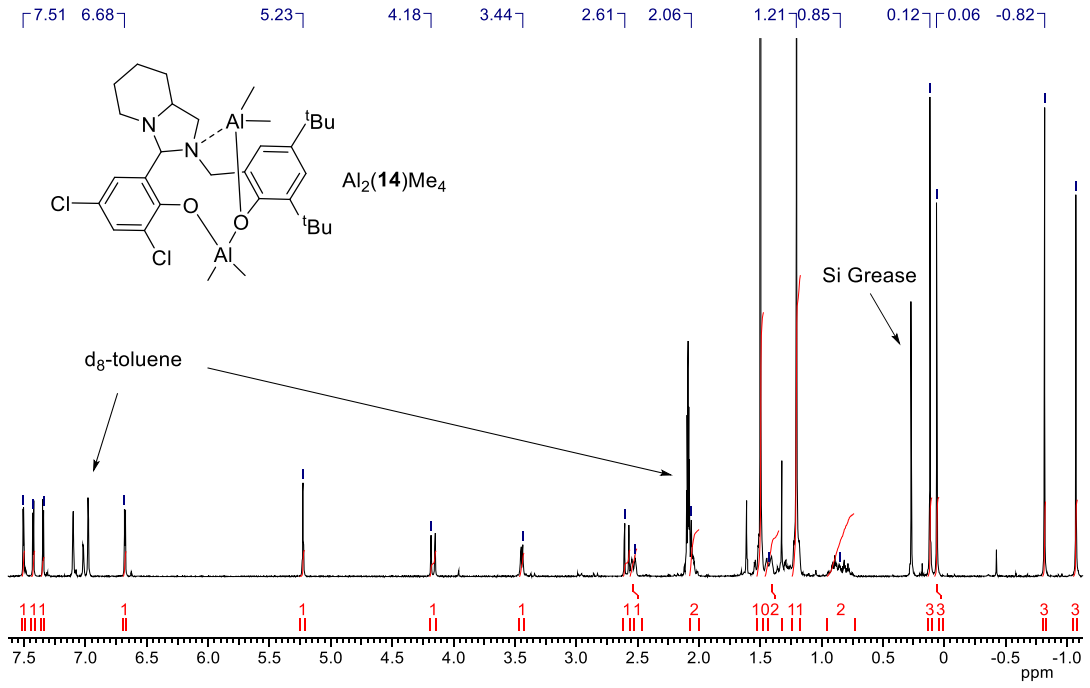

Figure 3.25: ^{1}H NMR (d_8-Toluene, 298 K) spectrum of Al_2(**14**)Me_4.

Carrying out this complexation on a 1:1 ratio at room temperature was observed to form a secondary product for **14**-**16**H_2. This side reaction was identified to be the formation of a binuclear structure of the form [Al_2(**L**)Me_4] through NMR spectroscopy and X-ray crystallography (Figure 3.22/3.25, Table 3.6). This product could be supressed by increasing the complexation temperature (50°C for addition of $AlMe_3$, followed by 80°C) with slower addition of $AlMe_3$; equally, this product could be favoured by increasing the ratio of $AlMe_3$ with a relatively fast introduction of the metal at room temperature. This structure was targeted, isolated and characterised fully for **14**H_2 and **16**H_2. Identical crystal systems (triclinic) and space groups (*P-1*) were found for these two complexes. The binuclear compound has two tetrahedral aluminium centres; these four coordinate systems are achieved due to a bridging phenoxy group, O(2) which shares Al(2) with N(1) and Al(1) with O(1) (Figure 3.22). Once again, N(2), the amine bridging the 5- and 6-memebered ring plays no part in the coordination to the metal centres. The conformation of the ligand is essentially unchanged relative to the Al(**L**)Me form. Compared to mononuclear form, the Al(1)-O bonds are unevenly elongated with stronger bonding between Al(1)-O(1) {for Al_2(**14**)Me_2, Al(1)-O(1) = 1.7887(12) Å / Al(1)-O(2) = 1.9096(11) Å}; the bridging oxygen, O(2), as expected, also shares a relatively long bond with Al(2) {for Al_2(**14**)Me_2, Al(1)-O(1) = 1.8569(11) Å} and these observations are due to the redistribution of charge density to accommodate the two metal centres. The bond angle for the two phenoxy groups, which was ideal for the mononuclear form, is much reduced {for Al(**14**/**16**)Me, O(1)-Al-O(2) = 97.71(5)°} The tetrahedral centres are found to be slightly less ideal for Al_2(**L**)Me_4 relative to Al(**L**)Me. The chirality of the coordinating nitrogen is observed to be switched due to the second aluminium being positioned on the opposite face of the complex leading to an *RRR* configuration.

The binuclear motif is maintained in solution as evidenced *via* ^{1}H NMR spectroscopy (Figure 3.24). The same resonances are present but there are some key shifts that distinguishes the binuclear spectrum form that of the mononuclear. An aromatic resonances is shifted to higher frequency and this is likely induced by the second aluminium centre; this centre is also responsible for a similar shift for the benzylic CH within the 5 membered ring which is *cis* to the metal. There are also two new resonances with a slightly positive ppm due to the new Al-Me groups.

Table 3.6: Selected bond distances (Å), and bond angles (°) for Al(**14**/**16**)Me_2.

	Al_2(**14**)Me_4	Al_2(**16**)Me_4
Al(1)-O(1)	1.7887(12)	1.799(4)
Al(1)-O(2)	1.9096(11)	1.919(4)
Al(1)-C(1)	1.9635(17)	1.962(6)
Al(1)-C(2)	1.9504(17)	1.952(6)
Al(2)-O(2)	1.8569(11)	1.862(4)
Al(2)-N(1)	2.0466(14)	2.053(4)
Al(2)-C(3)	1.9559(18)	1.935(6)
Al(2)-C(4)	1.9571(18)	1.965(6)
O(1)-Al(1)-O(2)	97.71(5)	97.71(5)
O(1)-Al(1)-C(1)	113.49(7)	113.1(2)
C(1)-Al(1)-C(2)	121.05(8)	123.0(3)
O(2)-Al(1)-C(2)	107.64(7)	108.3(2)
O(2)-Al(2)-N(1)	93.39(5)	92.94(16)
O(2)-Al(2)-C(3)	111.49(7)	111.3(2)
C(3)-Al(2)-C(4)	113.90(8)	114.9(3)
C(3)-Al(2)-N(1)	117.95(7)	117.2(2)
τ'^4 Al(1)	0.86	0.85
τ'^4 Al(2)	0.89	0.90

3.2.2 Aluminium salalen complexes

Coordination of the salalen ligands, **26**-**30**H_2, with $AlMe_3$ was carried out in toluene at elevated temperatures (50 - 80 °C) (Figure 3.26). The isolation of these complexes was generally achieved *via* recrystallisation from hexane or a hexane/toluene mixture ultimately yielding yellow/orange microcrystalline powders. Suitable crystals for X-ray analysis were obtained for Al(**26**/**27**)Me allowing for the evaluation of the solid-state structure. For further comparison, the benzyl alkoxide form, Al(**26**)OBn, was also generated and characterised.

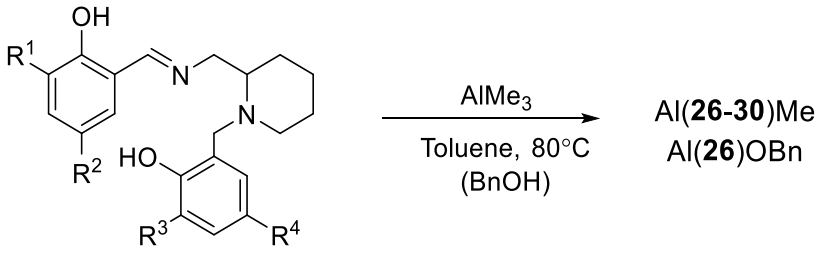

26H_2, $R^1 = R^2 = R^3 = R^4 = {}^t$Bu
27H_2, $R^1 = R^2 = Me$, $R^3 = R^4 = {}^t$Bu
28H_2, $R^1 = Ad$, $R^2 = Me$, $R^3 = R^4 = {}^t$Bu
29H_2, $R^1 = R^2 = {}^t$Bu, $R^3 = R^4 = Cl$
30H_2, $R^1 = R^2 = {}^t$Bu, $R^3 = H$, $R^4 = NO_2$

Figure 3.26: Complexation of salalens, **26**-**30**H_2, to Al(III).

In each case, the anticipated 5 coordinate Al(III) centre was found to have a *pseudo* trigonal bipyramidal geometry (Table 3.7, Figure 3.28). The imino nitrogen, N(2), in an equatorial position, is observed to have a shorter bond relative to the piperidine nitrogen, $N_p(1)$, in an axial site {for Al(**25**)Me, Al-N(2) = 1.974(4) Å / Al-$N_p(1)$ = 2.239(4) Å}. Also occupying an axial position is the imino phenoxy group and for this axis both Al(**26**-**27**)Me have similar bond angles {for Al(**26**)Me, O(2)-Al-$N_p(1)$ = 164.7(2)°/ for Al(**27**)Me, O(2)-Al-$N_p(1)$ = 165.78(14)°}. In contrast, this same axis for the alkoxide complex is slightly more ideal {for Al(**26**)OBn, O(2)-Al-$N_p(1)$ = 168.02(5)°}. This tendency towards a more linear axial bond causes an increase in the equatorial angle between the salan phenoxy and the alkoxy groups whereas for the aluminium methyl complexes, these are closer to 120° {for Al(**26**)OBn, O(1)-Al-OBn = 124.59(5)° compared with Al(**26**)Me, O(1)-Al-C(1) = 121.8(2)°}. The difference is

likely related to the accommodation of the bulkier benzylic group into the metal coordination sphere but on the whole, these complexes have the same τ value (τ = 0.72) and are therefore conform to the same ideality with regards to trigonal bipyramidal structure. A recent literature report described the use of a similar system, Al(**D**)Et, with a five membered pyrrolidine ring being the main structural difference (Figure 3.27).[20] The distribution of groups within the trigonal bipyramidal positions is identical albeit represented as the relative mirror image/different chirality. Between the two sets of complexes, there is reasonable agreement between bond lengths. There is, however, a greater degree of variation in bond angles, either as a consequence of the stereochemistry or the incorporation of a small ring into the backbone. Al(**D**)Et is revealed to have no marked preference for neither the trigonal bipyramidal or square pyramidal geometries (τ = 0.54).

In solution, the solid-state geometry is maintained as evidenced *via* ^{1}H NMR spectroscopy (Figure 3.29). However, there are two distinct species in solution for Al(**26-30**)Me while Al(**26**)OBn is isolated as a single compound. For the aluminium methyl complexes, the two series contain the same characteristic imine and aluminium methyl resonances in the correct ratio and overall both series integrate to the same chemical formula indicating both the species are isomers. In contrast to the ligand, the CH_2 groups are unambiguously assignable in the $^{13}C\{^{1}H\}$ NMR spectrum, indicating the inability of the piperidine ring to "flip" on coordination. VT-NMR (d_8-tol, 298 K-353 K) demonstrated that there was no interchange between the two species. DOSY NMR for Al(**26**)Me shows both of the species in solution diffuse at the same rate (d_8-Toluene, 298 K, D = 5.69×10^{-10} m^2s^{-1}) (Figure 3.30). Elemental analysis of these samples also conforms to expected formula for the monomeric complex.

Table 3.7: Selected bond distances (Å) and bond angles (°) for Al(**26**-**27**)Me, Al(**26**)OBn and literature comparison, Al(**D**)Et.[20]

	Al(**D**)Et	Al(**26**)Me	Al(**26**)OBn	Al(**27**)Me
Al-O(1)	1.794(2)	1.758(4)	1.7585(10)	1.779(3)
Al-O(2)	1.816(2)	1.842(4)	1.8262(10)	1.831(3)
Al-N_p(1)	2.326(2)	2.239(4)	2.1386(12)	2.180(3)
Al-N(2)	1.984(3)	1.974(4)	1.9670(12)	2.004(3)
Al-R	1.974(3)	1.985(7)	1.7356(10)	1.969(4)
O(1)-Al-O(2)	93.6 (1)	91.10(18)	95.3(5)	93.4(1)
O(1)-Al-N(2)	128.0(1)	120.6(2)	95.30(5)	93.41(13)
O(2)-Al-N_p(1)	160.1(1)	164.7(2)	117.42(5)	113.79(15)
O(1)-Al-R	112.4(1)	121.8(2)	168.02(5)	165.78(14)
O(2)-Al-R	102.8(1)	99.1(2)	124.59(5)	121.09(19)
N_p(1)-Al-R	95.7(1)	93.7(2)	97.48(5)	94.88(17)
N(2)-Al-R	117.7(1)	116.9(2)	117.4(1)	124.7(2)
τ	0.54	0.72	0.72	0.69

For Al(**26**-**27**)Me, R = C(1) and for Al(**26**)OBn, R = O(3).

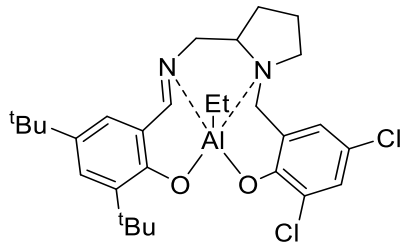

Al(**D**)Et

Figure 3.27: Literature comparison with a related structure Al(**D**)Et.[20]

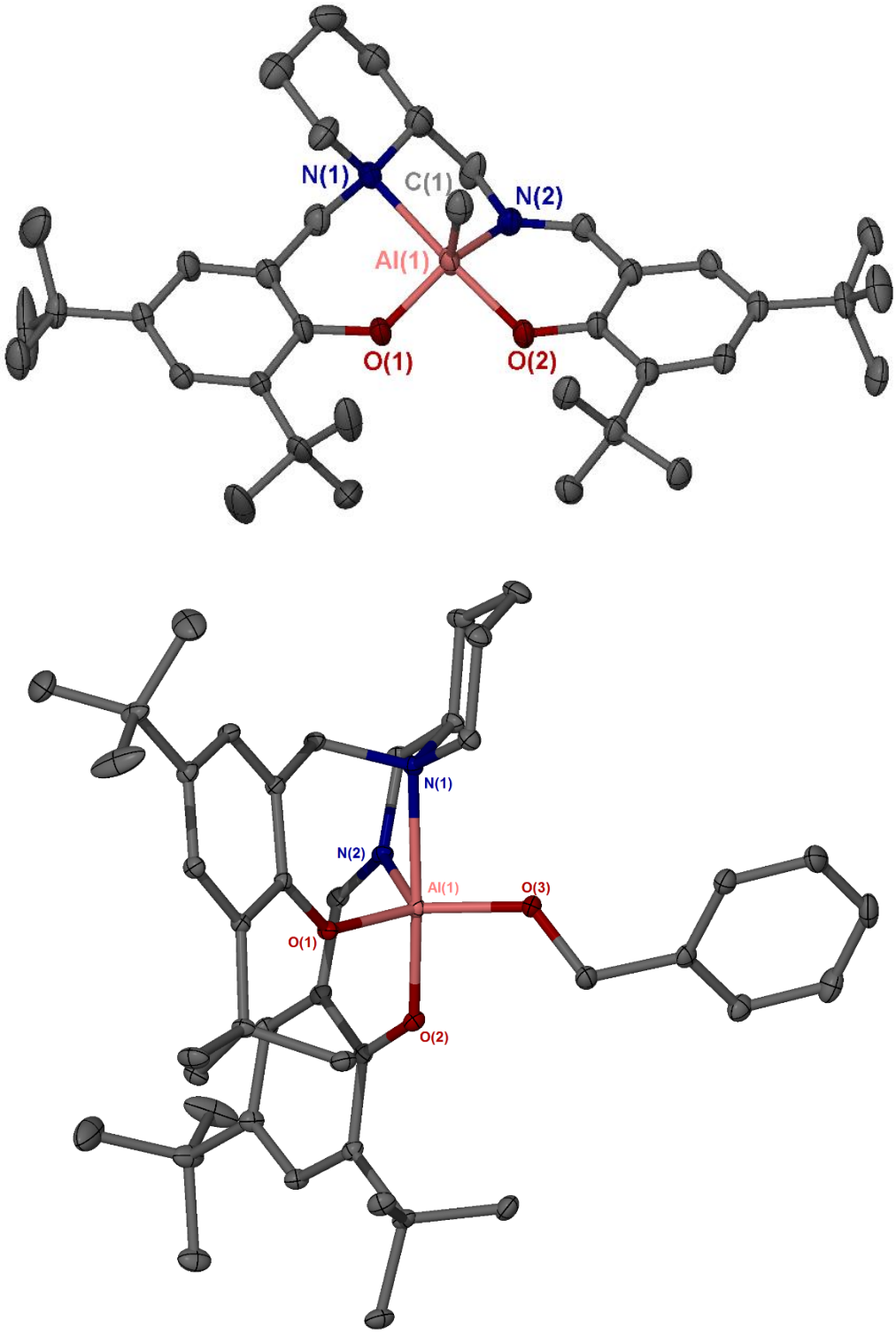

Figure 3.28: Solid-state structures of Al(**26**)Me (Top) and Al(**26**)OBn (Bottom). Ellipsoids are shown at the 30% probability level and all hydrogen atoms have been removed for clarity.

It is suggested therefore that these different species are in fact diastereomeric forms. There is inherent stereochemistry at the two position of the aminopiperidine ring and a new chiral centre is possible on coordination of the tertiary amine. The observed stereochemistry for the solid-state structures is *RR/SS*, hence *RS/SR* isomers are anticipated with the latter forms having a diastereomeric relationship with the former (Figure 3.31). For the literature example, Al(**D**)Et, the form found through X-ray crystallography was the *RS* form illustrating the possibility of such a configuration in a comparable system. Diastereomeric Al(III) complexes due to prochiral nitrogen centres have previously been reported in the literature.[21]

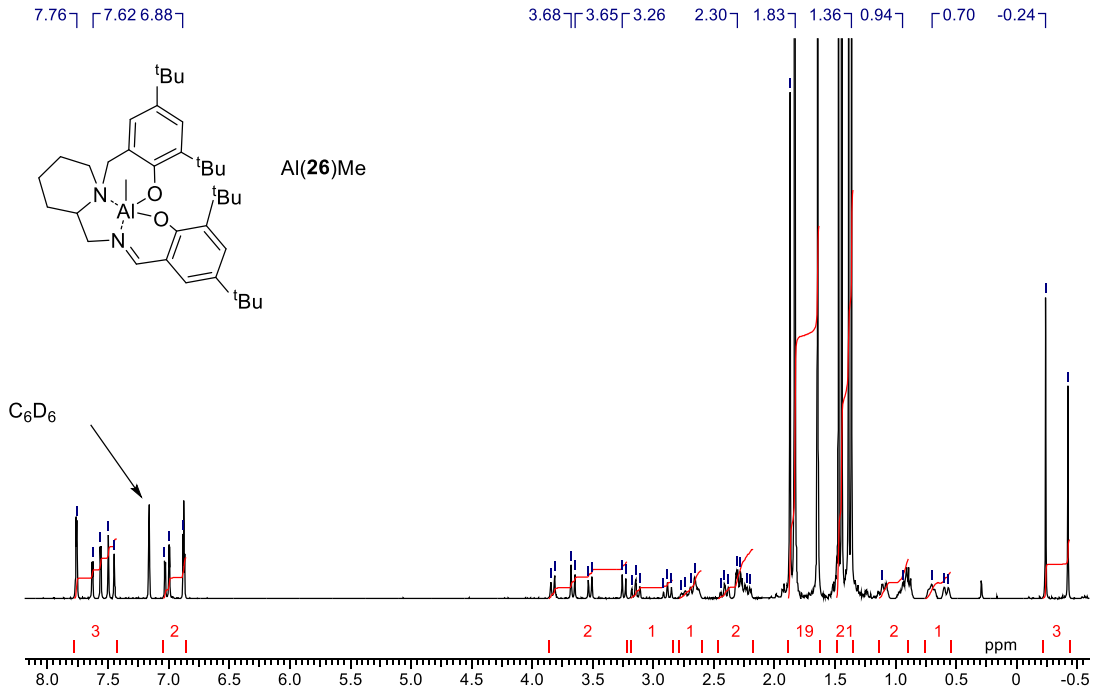

Figure 3.29: ^{1}H NMR (C_6D_6, 298 K) spectrum of Al(**26**)Me.

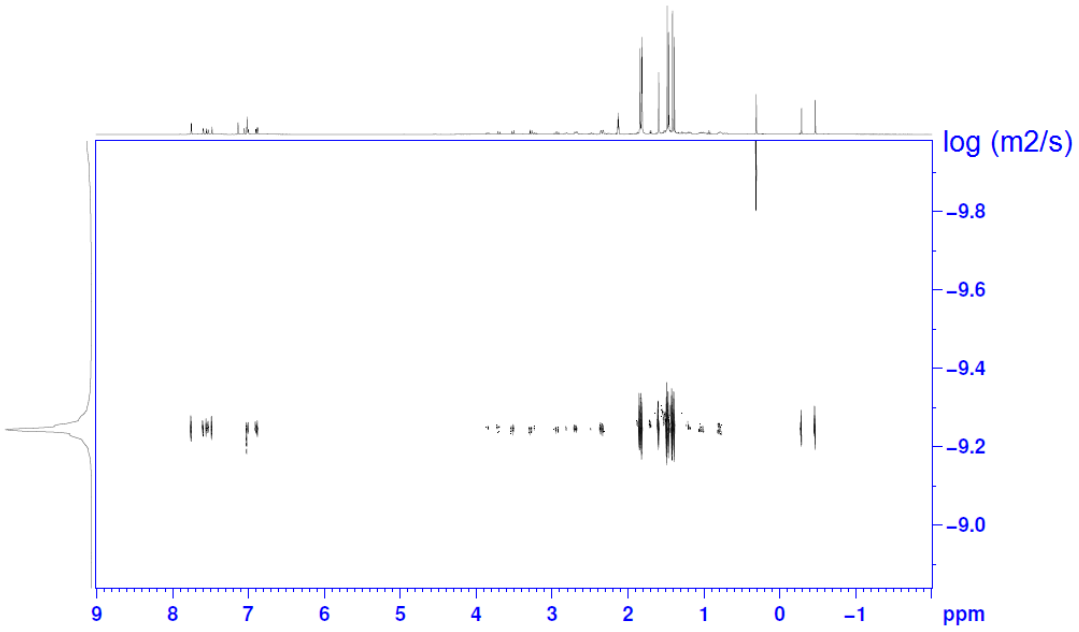

Figure 3.30: DOSY spectrum (d_8-Toluene, 298K) of Al(**26**)Me.

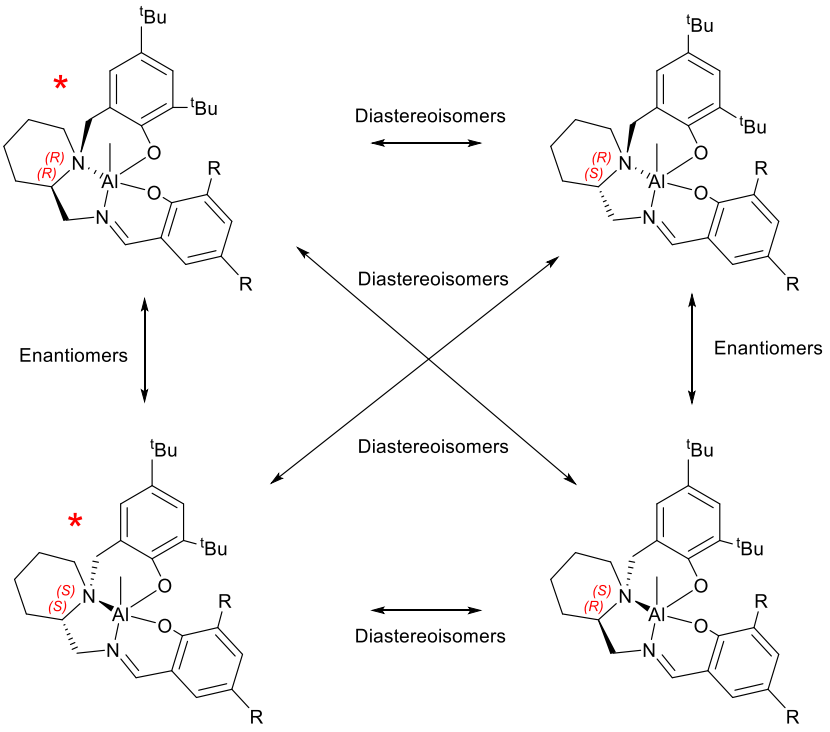

Figure 3.31: Possible stereoisomers for Al(**26-30**)Me and their relationships.

* denotes configurations found in solid-state structure.

3.3.3 Aluminium salan complexes

The reduced salan forms, **31**-**33**H_2 and **35**H_2 were successfully coordinated with Al(III), typically yielding white powders (Figure 3.32). However, attempts to complex **34**H_2 afforded a brown insoluble mixture which was not amenable to full characterisation. However, elemental analysis for this compound is in agreement with the expected structure.

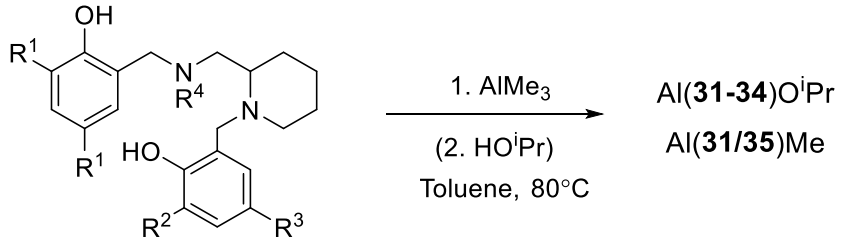

31H_2, $R^1 = R^2 = R^3 = {}^t$Bu, R^4 = H
32H_2, R^1 = Me, $R^2 = R^3 = {}^t$Bu, R^4 = H
33H_2, $R^1 = {}^t$Bu, $R^2 = R^3$ = Cl, R^4 = H
33H_2, $R^1 = {}^t$Bu, R^2 = H, $R^3 = NO_2$, R^4 = H
35H_2, $R^1 = R^2 = R^3 = {}^t$Bu, R^4 = Me

Figure 3.32: Complexation of salans, **31**-**34**H_2 and **35**H_2, to Al(III).

Initially, the aluminium methyl form, Al(**31**)Me, was isolated but suitable crystals were not successfully grown for X-ray crystallography. ^{1}H NMR analysis reveals a complicated spectrum with four different species, as clearly indicated by the aluminium methyl region (Figure 3.33). Integration of the aromatic and the aluminium methyl regions reveals a ratio of 4:3 which fits with the proposed monomeric structure, Al(**31**)Me. The remaining spectrum was analysed on this basis, which integrated to the correct number of protons. These extra resonances are attributed to the generation of further diastereomeric forms. Due to coordination, a new stereocentre is formed at the secondary amine position which increases the points of chirality to three. Analysis *via* DOSY NMR supports this, showing all species to be diffusing at a similar rate (C_6D_6, 298K, $D = 5.50 \times 10^{-10}$ m^2s^{-1}). The observed diffusion coefficient for Al(**31**)Me ($D = 5.69 \times 10^{-10}$ m^2s^{-1}) is slower than that of Al(**26**)Me. This may well be within the experimental error or in fact related to the increased bond length as a consequence of new amino functionality relative to the previous imino functionality.

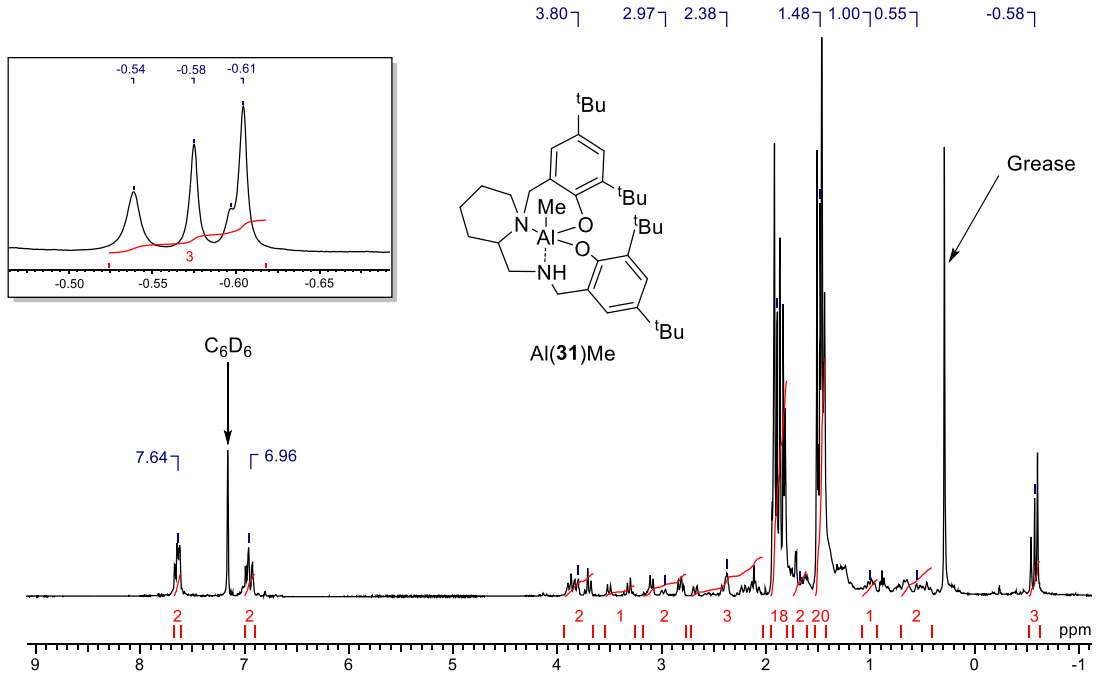

Figure 3.33: ^{1}H NMR (C_6D_6, 298 K) spectrum of Al(**31**)Me. Inset: AlMe region showing 4 resonances.

The generation of an alkoxide species was achieved by adding excess alcohol during complexation. For **31**-**33**H_2, best results were achieved with ^{i}PrOH which enabled the growth of suitable crystals of the form Al(**31**-**33**)O^{i}Pr as well as allowing for the isolation of a single diastereomer.

Interestingly, while these complexes are shown to be in a *psuedo* trigonal bipyramidal geometry, there is a rearrangement of the ligand around the metal centre relative to the salalen complexes Al(**26**-**27**/**D**)R (Figures 3.34-3.35). The piperidine ring now coordinates in an equatorial position, *via* N_p, with the aliphatic amine in the axial site. This change is thought to be motivated by a weak hydrogen bonding interaction; placing the secondary amine in the axial position causes the N-H bond to be parallel to the Al-O^{i}Pr bond and while these moieties are not at the ideal orientation for a full hydrogen bond they are in close proximity (for Al(**31**)O^{i}Pr, N-H…O = 2.227 Å). Both Al(**31**/**32**)O^{i}Pr were found in a monoclinic crystal system with *I2/a* and *P2$_1$/c* space groups respectively. Al(**33**)O^{i}Pr was observed to be triclinic with a *P-1* space-group (Table 3.8). The stereochemistry in the obtained solid-state structure is *SRS* with the *S* chirality on the nitrogen centres. For this series of initiators, bond lengths are generally consistent between structures; both nitrogen centres have a similar bond length to the

metal centre albeit in each case the piperidine nitrogen is slightly shorter likely by virtue of the equatorial position {for Al(**31**)O^{i}Pr, Al-N_p(1) = 2.0672(10) Å / Al-N(2) = 2.1072(10) Å}. A slight variation is observed for Al(**33**)O^{i}Pr for which the bond between aluminium and the chloro substituted phenoxy is reatively longer {for Al(**33**)O^{i}Pr, Al-O(1) = 1.8237(10) Å compared with Al(**31**)O^{i}Pr, Al-O(1) = 1.7991(8) Å }. This lengthening of the bond is attributed to the electron withdrawal by the chloro substituents giving the phenoxy group less electron density to donate to the metal centre. The axial bond angle shows a slight deviation from the ideal linearity {in the extreme case, Al(**32**)O^{i}Pr, O(1)-Al-N(2) = 169.19(4)°} similarly the equatorial angles show deviations from 120 ° {in the extreme case Al(**33**)O^{i}Pr, N_p(1)-Al-R = 111.95(5)° / O(2)-Al-N_p = 117.91(5) / O(2)-Al-R = 128.52(5)°}. The alkyl substituted rings generally give a more idealised trigonal bipyramidal structiure (τ = 0.77-0.78) whereas the structure containing chloro groups is seen to be less ideal (τ = 0.71). For symmetrical Al(III) salans reported in the literature, there is a general agreement of ligand arrangement around the metal centre.[21, 22] The bond lengths and angle of Al(**E**)R are compared against Al(**31**-**33**)O^{i}Pr and Al(**35**)R (Figure 3.36, Table 3.8). Despite the different ligand backbone and symmetry, there is a reasonable agreement with this literature complex.

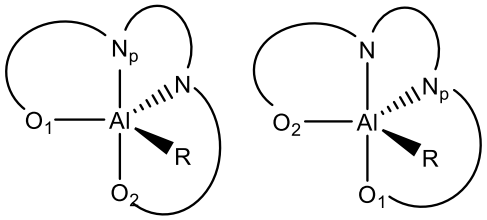

Al(**26-27**)Me
Al(**26**)OBn
Al(**35**)Me
Al(**35**)O^{i}Pr
Al(**D**)Et

Al(**31-33**)O^{i}Pr

Figure 3.34: Observed structural isomerism for salalen and salan Al(III) complexes.

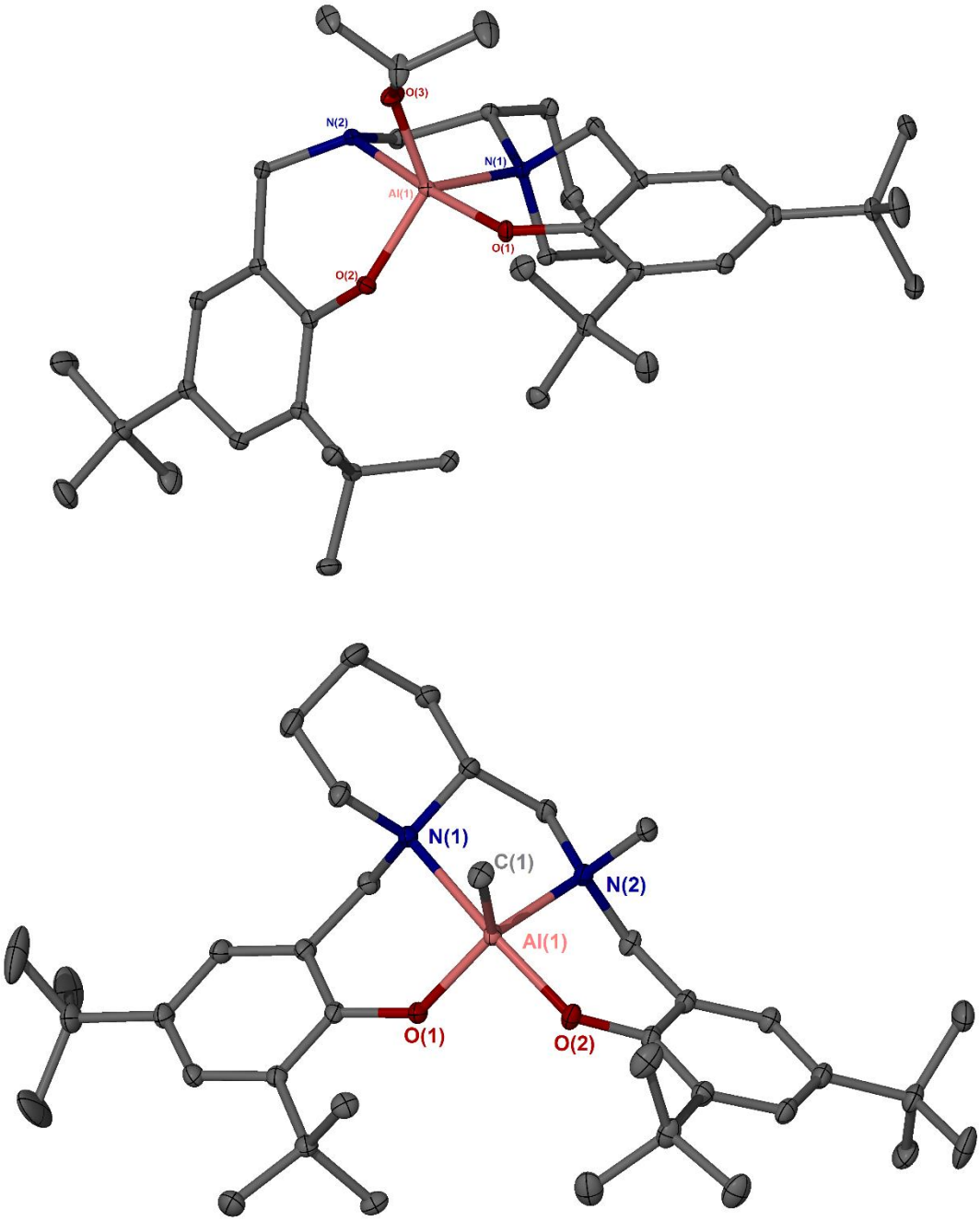

Figure 3.35: Solid-state structures of Al(**31**)O^{i}Pr (Top) and Al(**35**)Me (Bottom). Ellipsoids are shown at the 30% probability level and all hydrogen atoms have been removed for clarity.

Table 3.8: Selected bond distances (Å) and bond angles (°) for Al(**31-33**)O^{i}Pr, Al(**35**)Me, Al(**35**)O^{i}Pr and literature comparison, Al(**E**)R.[2]

	Al(**E**)O^{i}Pr	Al(**31**)O^{i}Pr	Al(**32**)O^{i}Pr	Al(**33**)O^{i}Pr	Al(**E**)Me	Al(**35**)Me	Al(**35**)O^{i}Pr
Al-O(1)	1.8063(16)	1.7991(8)	1.7955(9)	1.8237(10)	1.7669(18)	1.7633 (10)	1.7671(16)
Al-O(2)	1.7579(16)	1.7730(8)	1.7644(9)	1.7609(10)	1.8276(19)	1.8024 (10)	1.8018(16)
Al-N$_p$(1)*	2.0220(20)	2.0672(10)	2.0622(1)	2.0571(12)	2.3070(20)	2.2834 (12)	2.1270(18)
Al-N(2)	2.1241(19)	2.1072 (10)	2.1122(10)	2.0829(12)	2.0540(20)	2.0786 (12)	2.0953(18)
Al-R	1.7414(17)	1.7400(9)	1.7418(9)	1.7373(10)	1.9730(30)	1.9765 (15)	1.7373(16)
O(1)-Al-O(2)	93.20(8)	94.55(4)	96.12(4)	92.18(5)	97.96(9)	91.39 (5)	90.83(7)
O(1)-Al-N(2)	170.26(8)	170.31(4)	169.19(4)	171.41(5)	110.51(9)	125.09(5)	127.72(7)
O(2)-Al-N$_p$(1)	109.68(8)	117.49 (4)	113.74(4)	117.91(5)	168.66(9)	163.28 (5)	163.75(7)
O(1)-Al-R	99.70(8)	102.45 (4)	101.55(4)	99.98(5)	122.10(1)	122.02 (6)	123.66(8)
O(2)-Al-R	128.36(8)	124.16 (4)	120.53(4)	128.52(5)	94.80(1)	102.08 (6)	104.28(7)
N$_p$(1)-Al-R	120.33(8)	115.37 (4)	122.62(4)	111.95(5)	90.3(1)	93.19 (6)	89.09(7)
N(2)-Al-R	85.43(7)	82.35 (4)	82.13(4)	84.75(5)	125.60(1)	115.56 (6)	107.47(8)
N-H…O	-	2.227	2.275	2.269	-	-	-
O(1)-Al/ N(1)-H(2)**	-	20.187	27.985	10.810	-	-	-
τ	0.70	0.77	0.78	0.71	0.72	0.64	0.60

* N$_p$ refers to piperidine nitrogen for Al(**31-33**)O^{i}Pr and Al(**35**)R. For Al(**E**)O^{i}Pr, this is the equatorial nitrogen and for Al(**E**)Me, the axial nitrogen.
**Torsion angle between N-H and Al-O planes

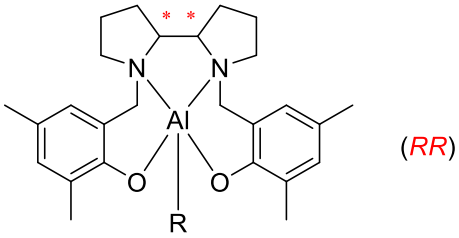

R = O^{i}Pr or Me

Al(**E**)R

Figure 3.36: Literature comparison of a related structure Al(**E**)R.[2]

Solution state ^{1}H NMR spectroscopy conforms to the expected structure, with four aromatic resonances, two of which are almost equivalent occurring close to the residual chloroform signal (Figure 3.37). There are also four doublets related to the inequivalent benzylic positions as well as a septet resonance and doublets for the isopropoxide moiety.

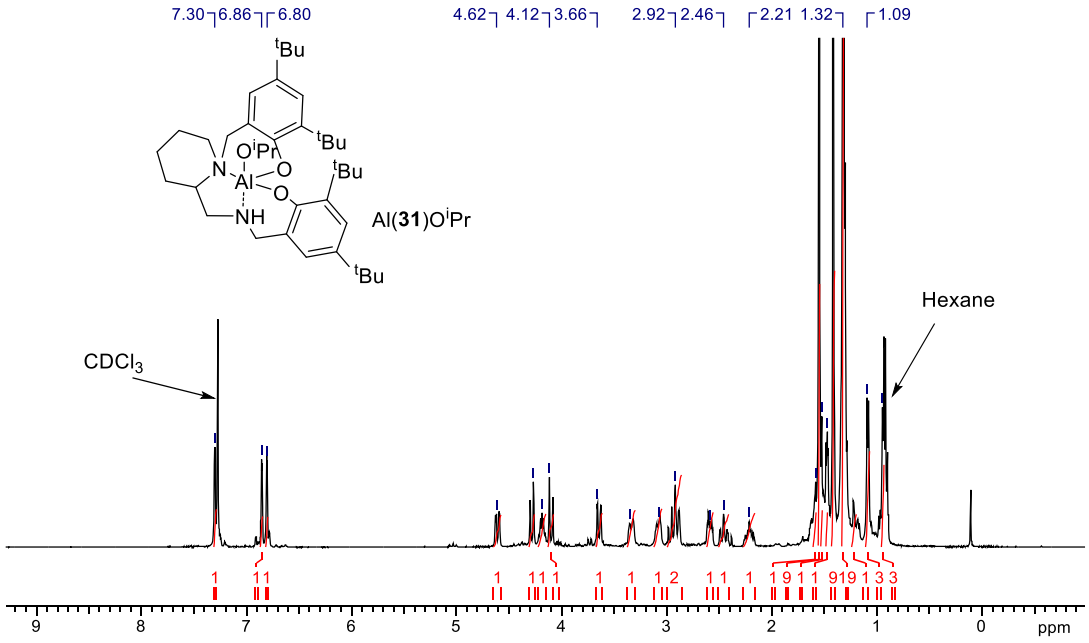

Figure 3.37: ^{1}H NMR ($CDCl_3$ 298 K) spectrum of Al(**31**)O^{i}Pr.

The methylated ligand, **35**H_2, was also successfully complexed to Al(III) (Figure 3.32). Similar observations are made regarding the presence of multiple species in solution for the complex Al(**35**)Me with diastereomers again the likely explanation. Unlike the previous family of complexes, Al(**35**)Me was amenable to recrystallisation and a solid-state structure was obtained (Table 3.8). The coordination of the ligand around the metal centre is analogous to the aluminium salalen complexes, Al(**26-27**)Me, with the piperidine ring occupying the axial position rather than the equatorial site (Figure 3.34-3.35). The stereocentres in the solid-state structure are observed to be *RRS* with the *S* chiral centre on the aliphatic nitrogen, this also parallels the structures of Al(**26-27**)Me. The reversion to this particular arrangement of ligand could also be an indication of the hydrogen bonding interaction dictating the structure for the previous complexes. The crystal system of Al(**35**)Me was measured to be monoclinic with a $P2_1/c$ space-group (Table 3.8). Bond lengths and angles are shifted with respect to Al(**26-27**)O^{i}Pr to reflect this change in bonding; the piperidine nitrogen to metal bond is extended due to an axial placement while the equatorial methylated nitrogen is slightly shortened {Al-N_p(1) = 2.2834(12) Å / Al-N(2) = 2.0786(12) Å}. Equally, the relative magnitude of the oxygen-to-metal bond lengths are reversed to reflect the exchange of axial and equatorial positions {Al-O(1) = 1.7633(10) Å / Al-O(2) = 1.8024(10) Å}. The main axis involving the piperidine and phenoxy bonds to the metal is observed to be less than ideal {O(2)-Al- N_p(1)= 163.28(5)°} and there is a 5° fluctuation around the idealised equatorial angle. The solid-state structure of Al(**35**)Me is deemed to be the least ideal trigonal bipyramid of both the salalen and salan series of complexes ($\tau = 0.64$). The ^{1}H NMR spectrum was treated as one species with the aromatic region integrated to four protons relative to the Al-Me region of three. Resonances due to the *tert*-butyl groups and *N*-methyl were also identifiable.

Attempts were made to isolate the alkoxide complex, Al(**35**)O^{i}Pr, generating crystals suitable for solid-state analysis. This crystal structure revealed an identical arrangement for the ligand around the metal centre relative to Al(**35**)Me (Figure 3.34). However, the stereochemical centres were found to be in a *SSS* configuration which is a diastereomer in relation to the structure of Al(**35**)Me (*RRS*). The unit cell was found to be triclinic with a *P-1* space-group (Table 3.8). The bond lengths and angles are broadly similar to that of Al(**35**)Me; the main deviations are centred around the chiral centres N_p(1) and N(2) and the structure is slightly less ideal with regards to trigonal

bipyramidal bond angles ($\tau = 0.60$). Subsequent ^{1}H NMR analysis revealed multiple species in solution indicating no discrimination of the different diastereomers on recrystallisation.

Further investigations were undertaken to determine the robustness of the Al(III) salan structure. Exposure of a $CDCl_3$ solution to air over several days resulted in the growth of new crystals. X-ray crystallography analysis revealed a di-μ-hydroxy bridged dimer, [Al(**31-32**)(μ-OH)]$_2$ with moisture from the air contributing to the formation (Figure 3.38). Both structures are found to be triclinic in a *P-1* space-group. The solid-state structure depicts two hydrogen bonding interactions between the two ligands originating from the secondary amine towards a phenoxy oxygen {for [Al(**31**)OH]$_2$, N-H…O = 2.52(3) Å}. The two ligands involved in the dimer are crystallographically equivalent with opposing stereochemistry, being *RSR* and *SRS* respectively. These stereochemical configurations correlate with that observed for the monomeric form and confirms these exist as enantiomeric pairs. Both aluminium centres are observed to be *pseudo* octahedral with the previous distribution of groups maintained; the axial position remains occupied by the secondary amine and a phenoxy group with a similar angle to the monomeric form{for [Al(**31**)OH]$_2$, O(1)-Al-N(2) = 171.88(10)°}. The piperidine ring nitrogen remains in an equatorial position and now represents the longest nitrogen-to-metal bond {for [Al(**31**)OH]$_2$, Al-N(1) = 2.126(2) Å/ Al-N(2) = 2.075(3) Å} presumably due to increased congestion in the equatorial plane. The bonding of the bridging hydroxyl groups are inequivalent with one oxygen binding more strongly to the aluminium centres{for [Al(**31**)OH]$_2$, Al-O(3) = 1.861(2)° / Al-O(3)# = 1.960(2)°} where the longer bond is found to be *cis* to an amine group and *trans* to a phenoxy group. The ^{1}H NMR spectra of [Al(**31-32**)OH]$_2$ conforms to this structure with the OH resonance being present at around 5.2 ppm. The dimeric structure is further confirmed in solution as for [Al(**31**)OH]$_2$, there are four aromatic and four *tert*-butyl resonances and no evidence of isopropoxide groups. There is also a minor series that has the same characteristic ArH, OH and ^{t}Bu resonances suggesting an isomer or perhaps the monomeric form, Al(**31**)OH. Such dimeric motifs have previously been reported in the literature.[23-26] There is good general agreement between bond angles and bond lengths compared with a symmetrical ^{t}Bu salan, [Al(**E**)OH]$_2$ despite the differences in ligand structure (Table 3.9, Figure 3.39).[26]

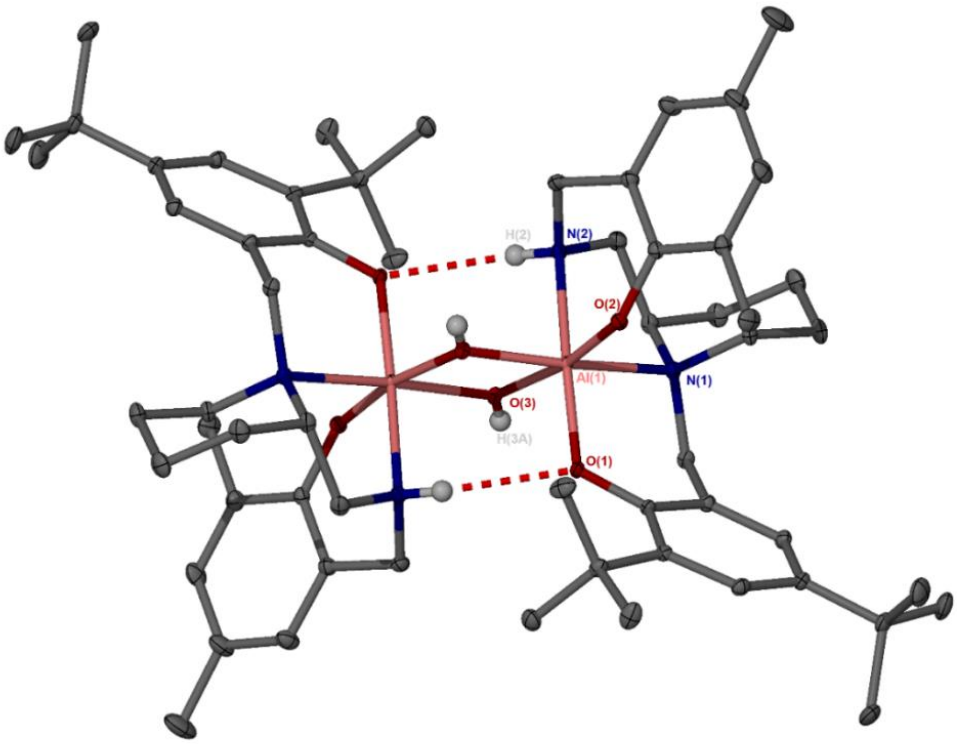

Figure 3.38: Solid-state structures of [Al(**32**)(OH)]$_2$. Ellipsoids are shown at the 30% probability level and all hydrogen atoms, except those bonded to N and O, have been removed for clarity.

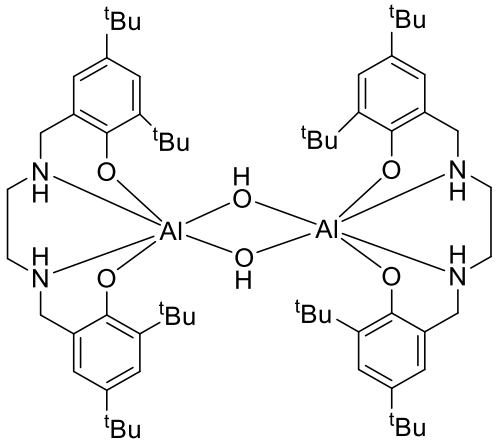

[Al(**F**)OH]$_2$

Figure 3.39: Literature comparison of hydroxy bridged salan, [Al(**F**)OH]$_2$.[26]

Table 3.9: Selected bond distances (Å) and bond angles (°) for [Al(**31-32)**OH]$_2$ and literature comparison, [Al(**F)**OH]$_2$.[26]

	[Al(**F**)OH]$_2$	[Al(**31**)OH]$_2$	[Al(**32**)OH]$_2$
Al-O(1)	1.829(7)	1.825(2)	1.8315(12)
Al-O(2)	1.834(7)	1.842(2)	1.8072(12)
Al-O(3)	1.852(6)	1.861(2)	1.8721(12)
Al-O(3)#	1.965(6)	1.960(2)	1.9108(13)
Al-N(1)	2.112(7)	2.126(2)	2.1670(14)
Al-N(2)	2.064(7)	2.075(3)	2.0678(14)
O(1)-Al-O(2)	96.3(3)	94.04(9)	95.08(5)
O(1)-Al-O(3)	95.5(3)	96.53(9)	95.00(5)
O(1)-Al-O(3)#	91.7(3)	95.78(9)	90.83(5)
O(1)-Al-N(1)	91.2(3)	90.50(9)	92.43(5)
O(1)-Al-N(2)	170.5(3)	171.88(10)	170.51(6)
O(2)-Al-O(3)	99.4(3)	94.76(9)	95.09(6)
O(2)-Al-O(3)#	171.7(3)	166.20(9)	169.44(6)
O(2)-Al-N(1)	91.0(3)	99.88(9)	95.03(5)
O(2)-Al-N(2)	88.7(3)	88.44(10)	91.89(6)
O(3)-Al-O(3)#	77.3(3)	74.52(9)	75.64(6)
N(1)-Al-N(2)	80.7(3)	81.45(9)	80.53(6)
N(1)-Al-O(3)	167.0(3)	163.27(9)	166.86(5)
N(1)-Al-O(3)#	91.4(3)	89.72(9)	93.45(5)
N(2)-Al-O(3)	91.5(3)	90.96(10)	90.77(6)
N(2)-Al-O(3)#	83.7(3)	83.17(10)	83.30(6)
N-H…O	-	2.52(3)	2.258

3.3.4 Triaryl bis/trisphenolate complexes

The triaryl bisphenol, **36**H_2, was also coordinated to Al(III) (Figure 3.40). Initially, the aluminium methyl form was targeted but greater success was achieved in the preparing the isopropoxide version, Al(**36**)O^{i}Pr, for which a crystal structure was obtained within a monoclinic system with a *P2₁/n* space group. Both Al(**36**)O^{i}Pr complex and crystals were prepared by James Brown-Humes (MChem student, 2015-2016). Interestingly in the solid-state structure the Al(III) centre has a trigonal bipyramidal geometry with both phenoxy groups as well as both amines contributing to the coordination (Figure 3.41, Table 3.10).

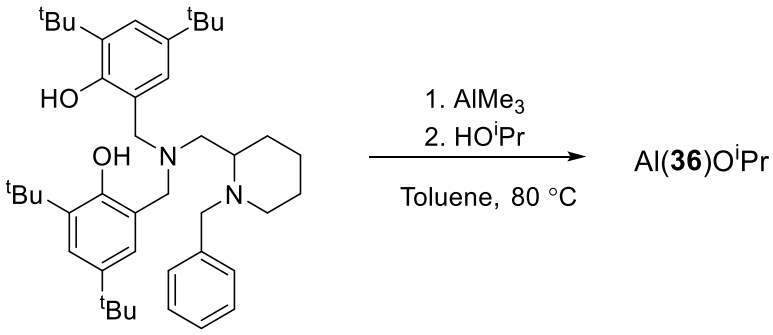

Figure 3.40: Complexation of triaryl bisphenol, **36**H_2, to Al(III).

On coordination of the piperidine nitrogen to the Al(III) centre, an *RS* configuration is observed, with the *R* chirality in the two position of the piperidine ring. The aluminium sits directly above the nitrogen atom that links the two phenoxy rings with the isopropoxide in the opposite axial position {R-Al-N(1) = 162.78(9)°}. Despite being in the equatorial position, the piperidine nitrogen has the longest of metal-to-nitrogen bonds {Al-N(1) = 2.140(2) Å/ Al-N_p(2) = 2.160(2) Å}. The distribution of the equatorial group hints at the different environments of the phenoxy groups with O(2) being closer than O(1) to N(2) {O(1)-Al-N(2) = 130.21 (10)° / O(2)-Al-N(2) = 112.08 (10)°} and this is undoubtedly due to the phenyl group which is impinging on the equatorial plane on the side of O(1). Due to this, the τ value for this structure reflects only a very slight preference for the trigonal bipyramidal motif (τ = 0.54); a distorted square pyramidal structure can equally be imagined with O(2) occupying the apical position. The analogue with a pyridine ring rather than a piperidine ring has previously been reported (Figure 3.42).[27] Accordingly, Al(**G**)Me was found to have a similar

arrangement of ligands around the metal centre. The crucial difference is in the equatorial plane in which bond angles are closer to 120° indicating a more ideal trigonal bipyramidal structure ($\tau = 0.81$).

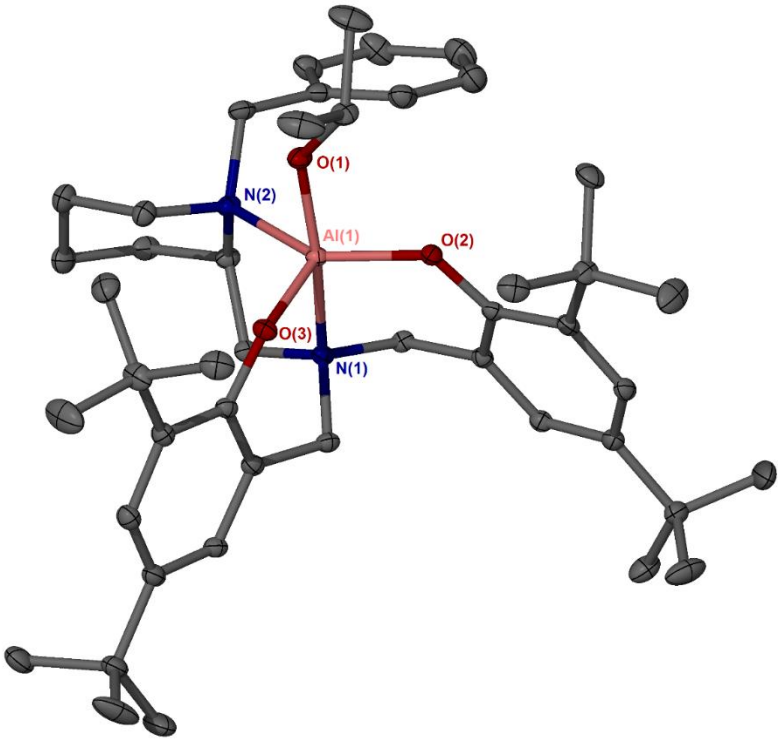

Figure 3.41: Solid-state structures of Al(**36**)O^{i}Pr. Ellipsoids are shown at the 30% probability level and all hydrogen atoms have been removed for clarity.

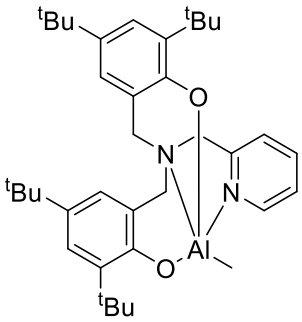

Al(**G**)Me

Figure 3.42: Literature comparison of triaryl bisphenolate, Al(**G**)Me.[27]

Table 3.10: Selected bond distances (Å) and bond angles (°) for Al(**36**)O^{i}Pr and literature comparison Al(**G**)Me.[27]

	Al(**G**)Me	Al(**36**)O^{i}Pr
Al-R	1.981(2)	1.747(2)
Al-O(1)	1.7516(15)	1.778(2)
Al-O(2)	1.7573(14)	1.770(2)
Al-N(1)	2.2150(16)	2.140(2)
Al-N$_p$(2)	2.0570(18)	2.160(2)
R-Al-O(1)	97.43(9)	97.06(9)
R-Al-O(2)	96.55(8)	101.88(10)
O(1)-Al-O(2)	124.22(8)	116.08(10)
R-Al-N$_p$(2)	97.64(9)	84.62(9)
O(1)-Al-N$_p$(2)	116.53(7)	130.21(10)
O(2)-Al-N$_p$(2)	114.58(8)	112.08(10)
R-Al-N(1)	172.99(9)	162.78(9)
O(2)-Al-N(1)	85.81(6)	89.25(9)
N(1)-Al-N$_p$(2)	75.40(7)	79.11(8)
τ	0.81	0.54

R = C for Al(**G**)Me and O for Al(**26**)O^{i}Pr

Analysis, in solution, by ^{1}H NMR spectroscopy conforms to the solid-state structure (Figure 3.43). Each ring is observed to be magnetically inequivalent based on the observation of four aromatics resonances for the ^{t}Bu substituted aryls and five doublets due to diastereotopic benzylic protons. This is in comparison, the free ligand, **36**H$_2$, for which two of the aryl rings were equivalent. The isopropoxide group is confirmed with a septet at 4.66 ppm and two doublets which overlap with the ^{t}Bu resonances.

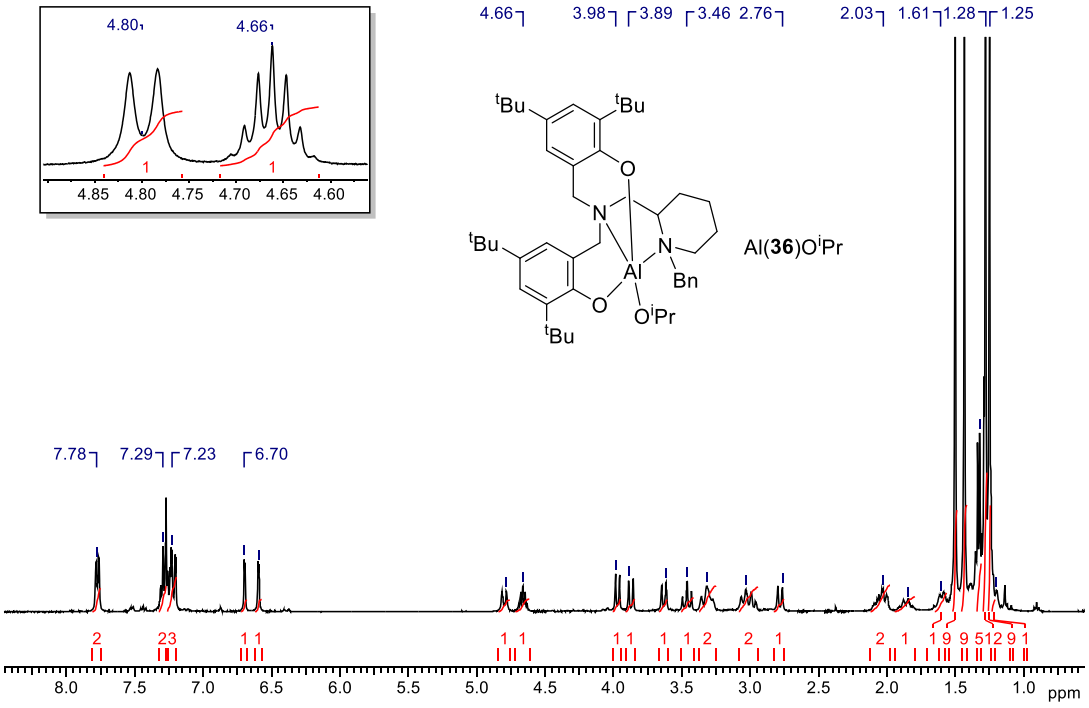

Figure 3.43: ^{1}H NMR ($CDCl_3$, 298 K) spectrum of Al(**36**)O^{i}Pr. Inset: Benzylic resonance and isopropoxide methine resonance.

The trisphenol, **37**H_2 was also successfully coordinated to Al(III), isolated as a pale yellow powder from hexane. ^{1}H NMR analysis (C_6D_6) indicated the isolation of one major species in solution. A trace amount of an aluminium methyl species is present (<3%) with no further species in the region. This impurity is likely to be Al(**37**)Me, as there are also small resonances within the baseline of the aromatic region, at a ratio of 1:3 with the AlMe resonance. This integration is consistent with an uncoordinated aryl group. The absence of other metal-alkyl resonances suggests the coordination of all three phenoxy groups yielding Al(**37**) (Figure 3.44).

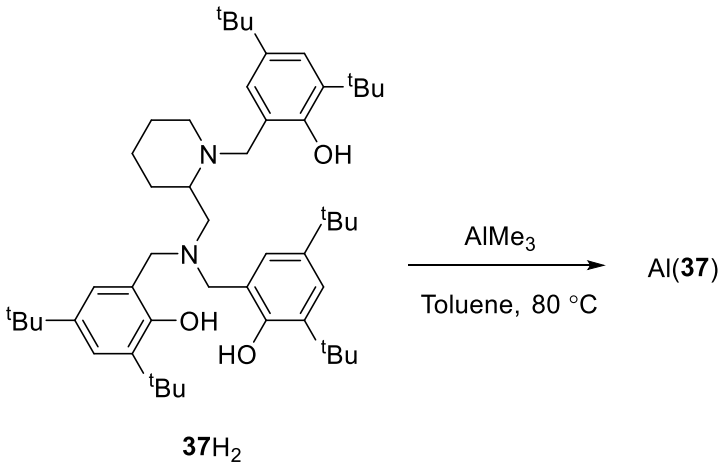

Figure 3.44: Complexation of trisphenol, **37**H_2, to Al(III).

As a consequence of the complexation, each phenoxy ring is now inequivalent giving rise to six aromatic and six *tert*-butyl resonances (Figure 3.45). There are also several doublets related to the six diastereotopic benzylic protons. The geometry of this structure is predicted to be similar to that of Al(**36**)O^{i}Pr, with a five coordinate *pseudo* trigonal bipyramidal aluminium centre (Figure 3.41). The third phenoxy group is expected to coordinate in a similar place to that of the O^{i}Pr. In comparison to the NMR spectrum of the ligand, Al(**37**) is less broad giving rise to discrete resonances.

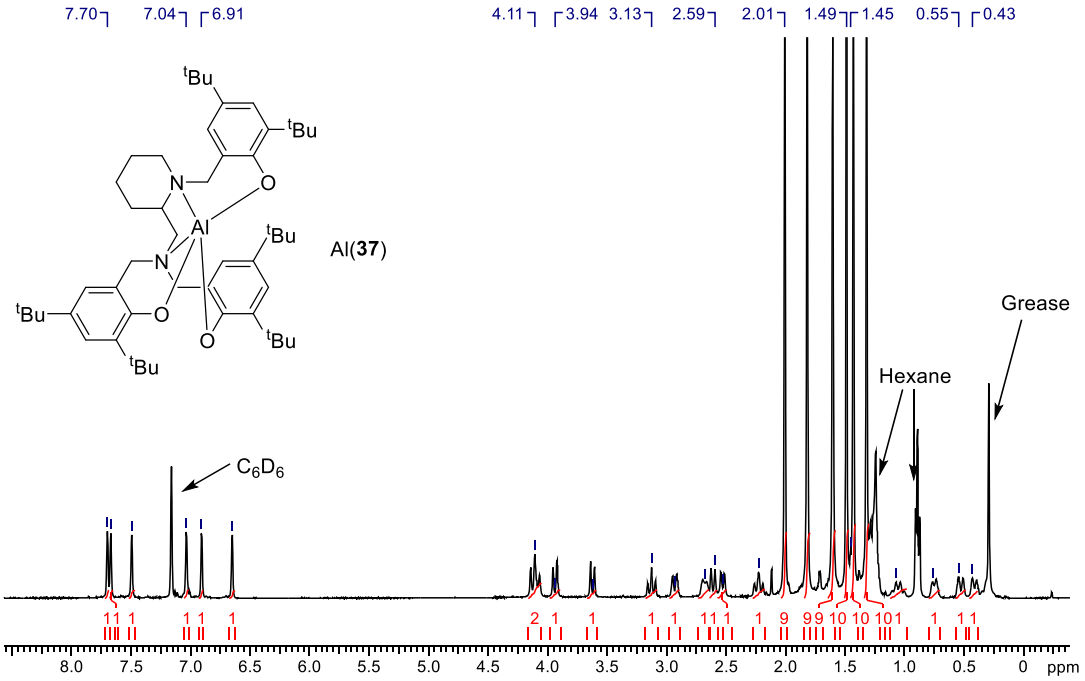

Figure 3.45: ^{1}H NMR (C_6D_6, 298 K) spectrum of Al(**37**).

3.4 Group IV complexes

3.4.1 Titanium complexes

The coordination of the 2-aminopiperidine based ligands with group 4 metals presented a range of interesting structures based on the different possible bonding modes and metal size. Ligands **1**H, **14**/**22**H_2, **26**H_2 and **31**H_2, representing half salen, bicyclic, salalen and salan structures respectively, were successfully complexed to Ti(IV) (Figure 3.46).

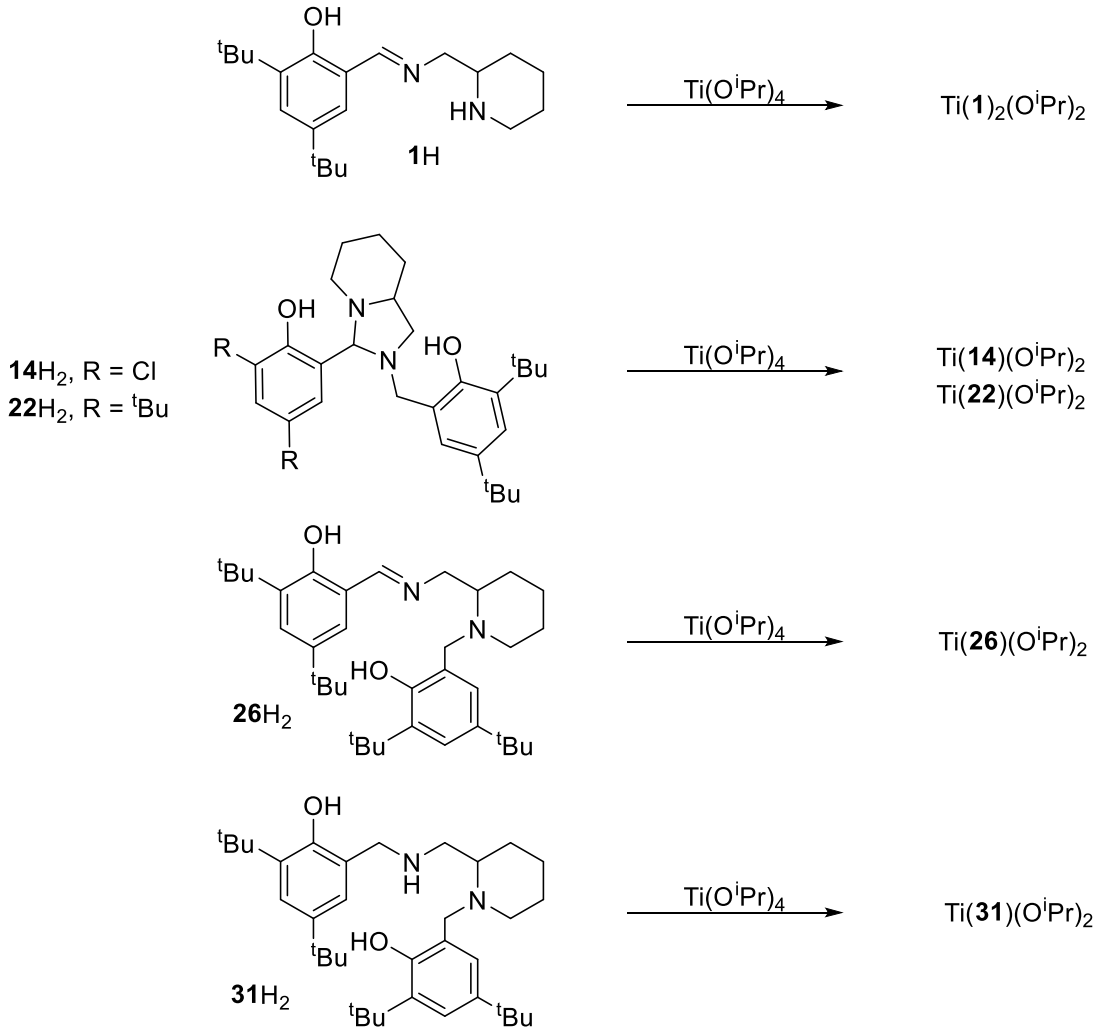

Figure 3.46: Complexation of **1**H, **14**H_2, **22**H_2, **26**H_2 and **31**H_2 to Ti(IV)

The coordination of the monophenol, **1**H, afforded the biligated titanium species, Ti(**1**)$_2$(O^{i}Pr)$_2$. The solid state structure revealed a *pseudo* octahedral metal centre, in an α-*cis* conformation with *trans* phenoxy groups {O(3)-Ti-O(4) = 167.12(5)°} and *cis* isopropoxide groups {O(1)-Ti-O(2) = 104.60(6)°} (Figure 3.47, Table 3.11). This structure was observed to be in a triclinic crystal system with a *P-1* space group. The stereochemistry was observed to be *Δ-SS* for the Ti(IV) and ligands respectively with the *Λ-RR* enantiomer implied by the centrosymmetric space group. The isopropoxide groups have both a *cis* and *trans* relationship to the imino groups {O(1)-Ti-N(1) = 87.99(5)°/ O(1)-Ti-N(3) = 162.39(5)°}. The isopropoxide to metal bond represents the shortest bond length {Ti(1)-O(1) = 1.8037(12) Å }. In contrast, the phenoxy bonds to the metal centre are lengthened {Ti-O(3) = 1.9473(10) Å }.

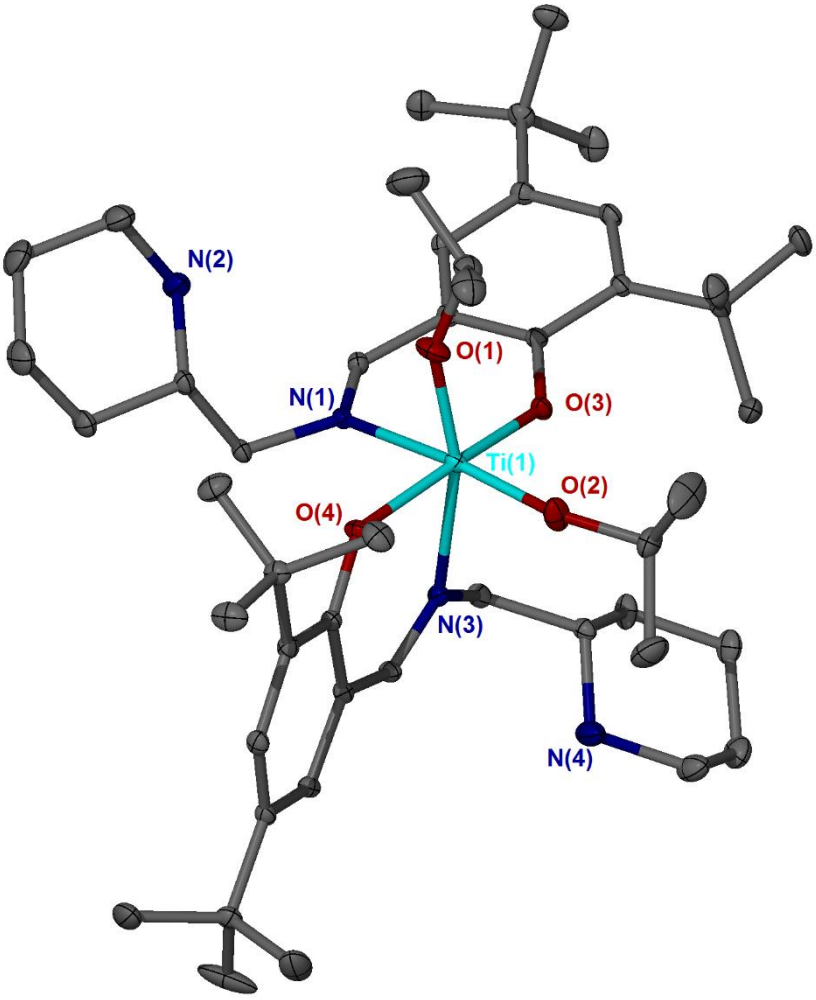

Figure 3.47: Solid-state structures of Ti(**1**)$_2$(O^{i}Pr)$_2$. Ellipsoids are shown at the 30% probability level and all hydrogen atoms have been removed for clarity.

Table 3.11: Selected bond distances (Å) and bond angles (°) for Ti(**1**)$_2$(O^{i}Pr)$_2$ and literature comparison, Ti(**H**)$_2$(O^{i}Pr)$_2$.[28]

	Ti(**H**)$_2$(O^{i}Pr)$_2$	Ti(**1**)$_2$(O^{i}Pr)$_2$
Ti-O(1)	1.8200(14)	1.8037(12)
Ti-O(2)	1.8200(14)	1.7852(12)
Ti-O(3)	1.8991(14)	1.9473(10)
Ti-O(4)	1.8991(14)	1.9316(10)
Ti-N(1)	2.3253(17)	2.2628(13)
Ti-N(3)	2.3253(17)	2.2825(12)
O(1)-Ti-O(2)	101.86(9)	104.60(6)
O(1)-Ti-O(3)	94.53(6)	96.09(5)
O(1)-Ti-O(4)	94.53(6)	92.75(5)
O(1)-Ti-N(1)	85.83(6)	87.99(5)
O(1)-Ti-N(3)	172.30(6)	162.39(5)
O(2)-Ti-N(1)	172.30(6)	166.05(6)
O(2)-Ti-O(4)	94.53(6)	95.83(5)
O(3)-Ti-O(4)	162.16(8)	167.12(5)
O(3)-Ti-N(3)	82.23(5)	88.19(4)
N(1)-Ti-N(3)	86.48(8)	75.71(4)

Ti(**H**)$_2$(O^{i}Pr)$_2$ provides a structural comparison to Ti(**1**)$_2$(O^{i}Pr)$_2$, being an imino monophenolate complex which has ligand chirality (Figure 3.48, Table 3.11).[28] As for Ti(**1**)$_2$(O^{i}Pr)$_2$, Ti(**H**)$_2$(O^{i}Pr)$_2$ adopts an α-*cis* geometry. The length of the titanium oxygen bonds are slightly different between each structure, with Ti(**H**)O^{i}Pr$_2$ having shorter ligand-to-metal bonds and longer isopropoxide bonds. This may be a consequence of the bulkier ^{t}Bu groups of **1**H. The imino bonding to the metal also gives rise to shorter bonds for Ti(**1**)$_2$(O^{i}Pr)$_2$. The bond angles also show deviations which can be as great as 10° in some instances.

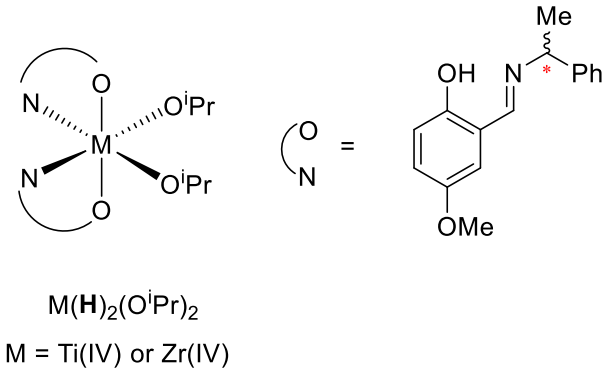

$M(\mathbf{H})_2(O^iPr)_2$

M = Ti(IV) or Zr(IV)

Figure 3.48: Literature comparison of a monophenolate group IV complexes, $M(\mathbf{H})_2(O^iPr)_2$.[28]

Analysis of the ^1H NMR spectrum revealed multiple species in solution (Figure 3.49). This is to be expected due to the potential for diastereomeric relationships, with three points of chirality in the structure. Due to the use of racemic ligand, (*Δ-RS* / *Λ-SR*) and (*Λ-RS* / *Δ-SR*) forms are predicted as well as the diastereomer of the crystal structure configuration, *Λ–SS*. It is assumed that the major isomer is that observed for the crystal structure and the remaining species are due to the remaining diastereomers. Similar observations were made for $M(\mathbf{H})_2(O^iPr)_2$ {M = Ti(IV) or Zr(IV)} The $^{13}C\{^1H\}$ provides further evidence for the species to be related diastereomers, having four distinct resonances for the imino functionality matching up with the number of inequivalent species (Figure 3.49). Further analysis *via* DOSY NMR spectroscopy suggested the species in solution were diffusing at a similar rate ($CDCl_3$, 298K, D = 5.47×10^{-10} m^2s^{-1}).

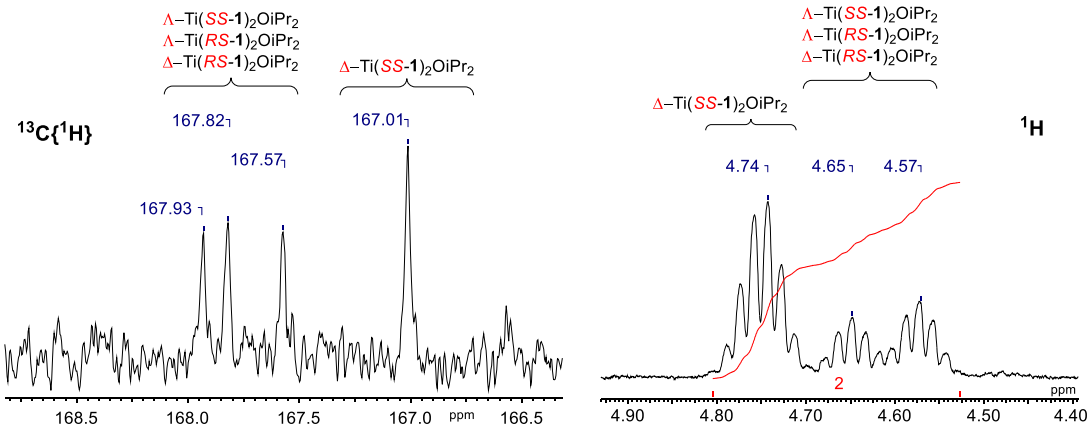

Figure 3.49: $^{13}C\{^1H\}$ NMR spectrum showing imino region and ^1H NMR spectrum showing methine region of $Ti(\mathbf{1})_2(O^iPr)_2$. Diastereomers have only been indicated but are present as enantiomeric pairs.

Ti(**14**)(O^iPr)$_2$ was characterised as a five coordinate complex in a trigonal bipyramidal geometry in the solid-state (Figure 3.50, Table 3.12). The crystal system is triclinic with a *P-1* space-group. The isopropoxide groups are observed to be in both an axial and equatorial position and the ligand has a *RRR* configuration in the obtained crystal structure. The axial position also contain the nitrogen atom N(1) with an overall angle close to ideality {O(2)-Ti-N(1) = 177.24(11)°}. The equatorial groups are separated by angles close to 120° {O(3)-Ti-O(4) = 120.52(10)° / O(2)-Ti-O(4) = 116.07(11)°}. These angles demonstrate a strong conformation to the trigonal bipyramidal geometry as indicated by a high τ value (τ = 0.95).

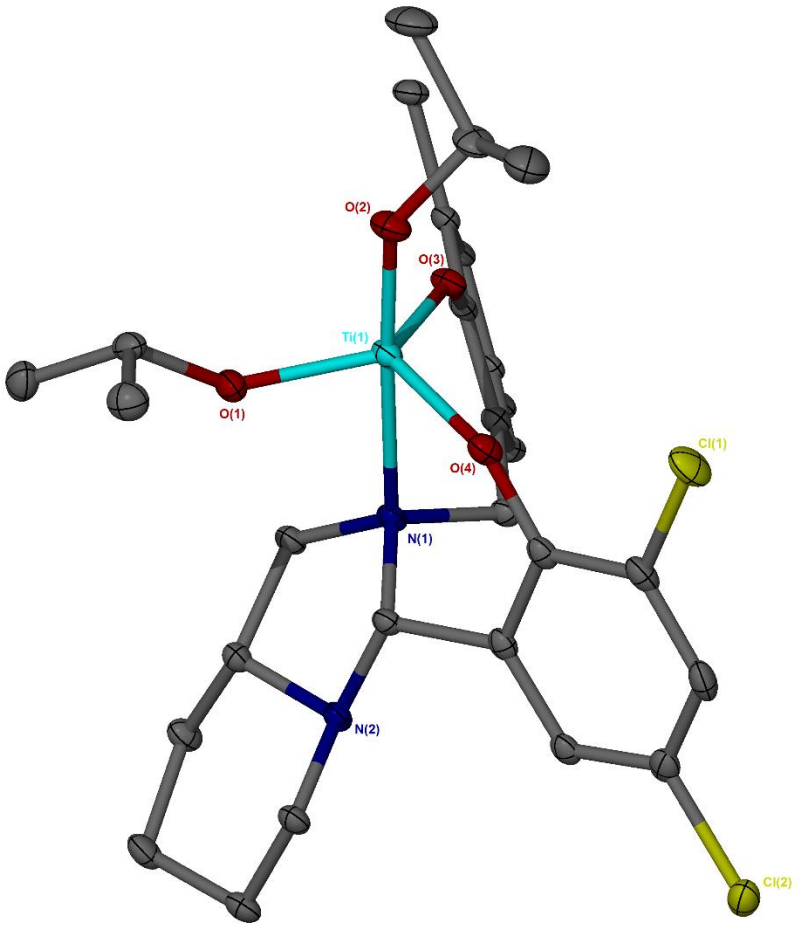

Figure 3.50: Solid-state structures of Ti(**14**)O^iPr_2. Ellipsoids are shown at the 30% probability level and all hydrogen atoms and ^{t}Bu methyl groups have been removed for clarity.

Table 3.12: Selected bond distances (Å)and bond angles (°) for Ti(**14**)(O^iPr)$_2$ and literature comparison Ti(**I**)(O^iPr)$_2$.[29]

	Ti(**I**)(O^iPr)$_2$	Ti(**14**)(O^iPr)$_2$
Ti-O(1)	1.800(1)	1.803(2)
Ti-O(2)	1.781(1)	1.783(2)
Ti-O(3)	1.850(1)	1.864(2)
Ti-O(4)	1.860(1)	1.912(2)
Ti-N(1)	2.330(1)	2.308(3)
O(1)-Ti-O(2)	99.70(6)	99.94(11)
O(1)-Ti-O(3)	121.42(7)	118.26(11)
O(1)-Ti-O(4)	113.87(7)	116.07(11)
O(1)-Ti-N(1)	83.76(5)	82.81(1)
O(2)-Ti-N(1)	178.20(6)	177.24(11)
O(2)-Ti-O(4)	96.94(5)	95.92(11)
O(3)-Ti-O(4)	118.66(6)	120.52(10)
τ	0.95	0.95

It is not unusual for tridentate ligands to form bis-ligated species with Ti(IV).[29-31] However, it is found that a systems with two *ortho* ^{t}Bu groups, or bulkier, preferentially form the mono-ligated species[29, 30, 32] and it is evident that having one ^{t}Bu substituted aryl ring is sufficient to prevent the formation of Ti(**L**)$_2$ in this case. Compared to a similar literature complex, Ti(**I**)(O^iPr)$_2$ (Figure 3.51), Ti(**14**)(O^iPr)$_2$ is found to have an identical distribution of groups in the trigonal bipyramidal sites.[29] Bond lengths and angles are also consistent with this report with variation in aryl substituents and the rigidity of the nitrogen environment causing the slight differences. Carrying out a complexation with the unsubstituted analogue, **23**H$_2$, afforded a range of species in solution. Full characterisation was not undertaken but analysis by ^{1}H NMR spectroscopy strongly indicated the formation of Ti(**23**)$_2$, with no evidence of

resonances due to an alkoxide. The extra species in solution are assumed to be structural isomers {c.f. Zr/Hf(**16**)$_2$}. The predicted structure for Ti(**23**)$_2$ is shown in Figure 3.51.

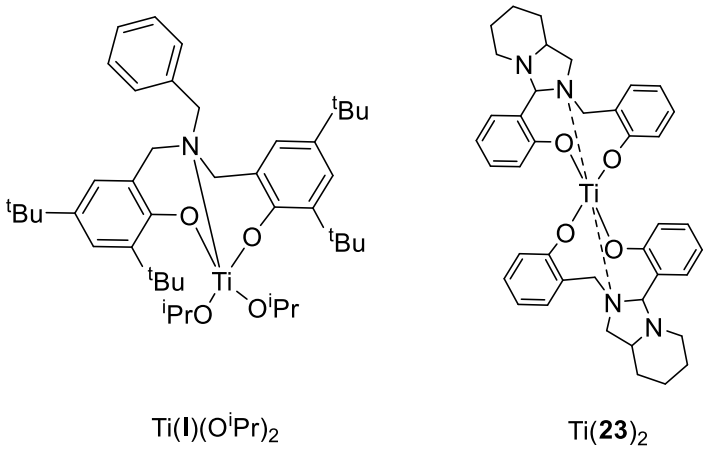

Ti(**I**)(O^{i}Pr)$_2$ Ti(**23**)$_2$

Figure 3.51: Literature comparison of a ONO Ti(IV) complex, Ti(**I**)(O^{i}Pr)$_2$ and predicted structure of **23**H$_2$ complexation with Ti(IV).[29]

The solid-state structure for Ti(**14**)(O^{i}Pr)$_2$ is shown to be maintained in solution *via* ^{1}H NMR spectroscopy (Figure 3.52). The monomeric form is highlighted by the observation of isopropoxide septets around 5 ppm; further to this, their inequivalence is demonstrated by the resonances asymmetrical appearance (Figure 3.52: inset). Four aromatic resonances are also observed as well as two signals for the diastereotopic benzylic position. The ^{1}H NMR spectrum for Ti(**22**)(O^{i}Pr)$_2$ is broadly comparable, suggesting the same structure is adopted for this complex. Due to the aryl rings having the same ^{t}Bu substituents, there are only three resonances in the aromatic region in a ratio of 1:2:1. There are also two new ^{t}Bu resonances which overlap with the isopropoxide methyl groups.

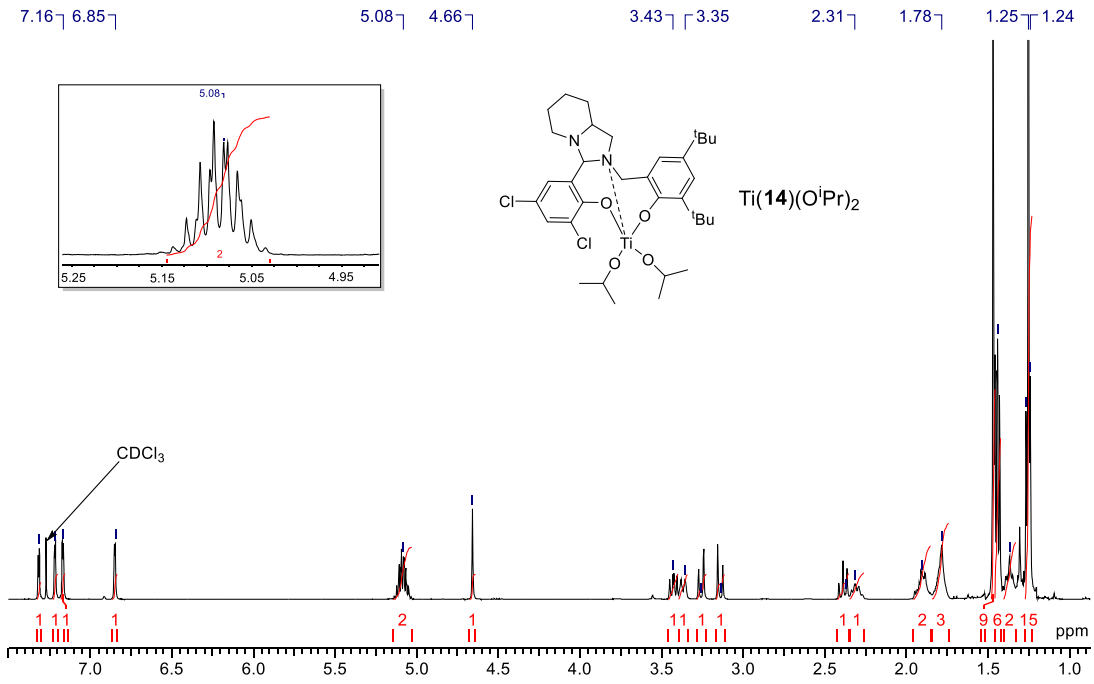

Figure 3.52: ^{1}H NMR ($CDCl_3$, 298 K) spectrum of Ti(**14**)(O^iPr)$_2$. Inset: Methine region.

This is contrasted with the salalen, Ti(**26**)(O^iPr)$_2$, which is six coordinate leading to a *pseudo* octahedral structure in the solid-state (Figure 3.53). Ti(**26**)(O^iPr)$_2$ was found in a monoclinic *I2/a* space group with an *RS* configuration on the carbon and nitrogen respectively. The wrapping of the ligand around the titanium centre is in a *fac-mer* fashion giving a β-*cis* structure with *Λ* chirality. Accordingly, the isopropoxide groups are mutually *cis* occupying a *pseudo* equatorial and axial site {O(1)-Ti-O(2) = 92.57(5)°}. The axial axis was found to also contain the salan phenoxy {O(2)-Ti-O(4) = 169.64(5)°}. Of the two nitrogen environments, the imine was observed to have a shorter bond length to metal relative to the amine {Ti-N(1) = 2.2038(13) / Ti-N(2) = 2.3101(13) Å}. Comparison of Ti(**26**)(O^iPr)$_2$ with a literature titanium salalens is favourable with identical wrapping of ligand around the metal being observed and good agreement of bond lengths and angles.[33-35] For comparison, the solid-state data for Ti(**J**)(O^iPr)$_2$ is displayed in Table 3.13 (Figure 3.54).

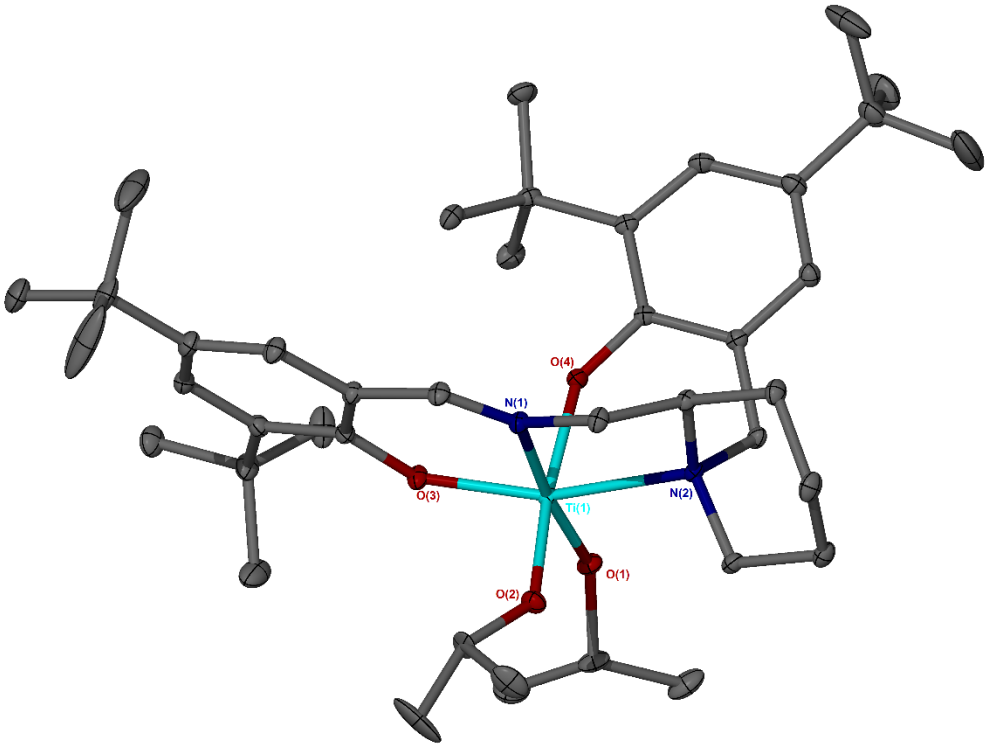

Figure 3.53: Solid-state structures of Ti(**26**)(O^iPr)$_2$. Ellipsoids are shown at the 30% probability level and all hydrogen atoms have been removed for clarity.

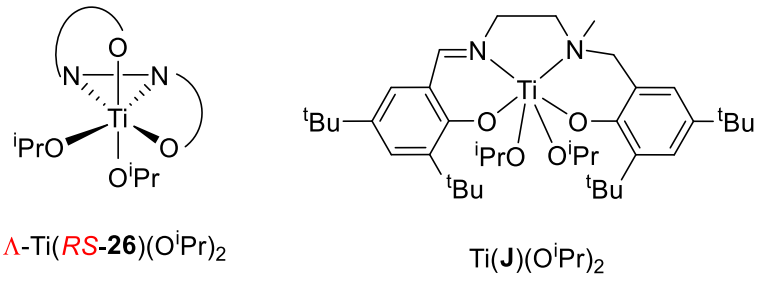

Λ-Ti(*RS*-**26**)(O^iPr)$_2$ Ti(**J**)(O^iPr)$_2$

Figure 3.54: Solid-state geometry of Ti(**26**)(O^iPr)$_2$ and literature comparisons of Ti(IV) salalen, Ti(**J**)(O^iPr)$_2$.[29]

Table 3.13: Selected bond distances (Å) and bond angles (°) for Ti(**26**)(O^iPr)$_2$ and literature comparison Ti(**J**)(O^iPr)$_2$.[29]

	Ti(**J**)(O^iPr)$_2$	Ti(**26**)(O^iPr)$_2$
Ti-O(1)	1.841(1)	1.8351(11)
Ti-O(2)	1.827(2)	1.8537(12)
Ti-O(3)	1.903(1)	1.8890(12)
Ti-O(4)	1.941(1)	1.9257(11)
Ti-N(1)	2.197(2)	2.2038(13)
Ti-N(2)	2.305(1)	2.3101(13)
O(1)-Ti-O(2)	92.71(6)	92.57(5)
O(1)-Ti-O(3)	108.65(1)	106.21(5)
O(1)-Ti-O(4)	91.97(6)	92.42(5)
O(1)-Ti-N(1)	171.2(1)	169.83(5)
O(1)-Ti-N(2)	96.5(1)	95.47(5)
O(2)-Ti-N(1)	85.0(1)	82.94(5)
O(2)-Ti-O(4)	168.43(6)	169.64(5)
O(3)-Ti-O(4)	90.30(6)	91.79(5)
O(3)-Ti-N(2)	156.64(6)	157.54(5)
N(1)-Ti-N(2)	74.86(6)	75.41(5)

Analysis by ^{1}H NMR spectroscopy reveals two species in solution at a ratio of 5:1 (Figure 3.55). Both series have identical resonances namely four aromatic signals plus one imine as well as two isopropoxide septets and the associated methyl doublets. The presence of two isopropoxide resonances in each series suggests the solid-state structure is maintained in solution, indicating these groups are in inequivalent environments i.e. *trans* to different groups. It is proposed that the second series is due presence of diastereomers in solution. The observed stereochemical configuration in the solid-state structure is *Λ-RS* and as a racemic ligand is employed, an *S* configuration is also expected for the carbon centre. Application of achiral salalens

typically lead to single diastereomers in solution despite the chirality at both metal and nitrogen centres.[33, 34, 36] It is therefore tentatively suggested that the extra resonances are due to a *Λ-SS* species, with the metal and nitrogen chirality remaining unchanged. The *Λ-RS* form is anticipated to be the major product. Due to the imine rigidity and the inflexibility of the piperidine ring, it is also unlikely the remaining isomers of *trans* and *α-cis* can be adopted by this ligand.

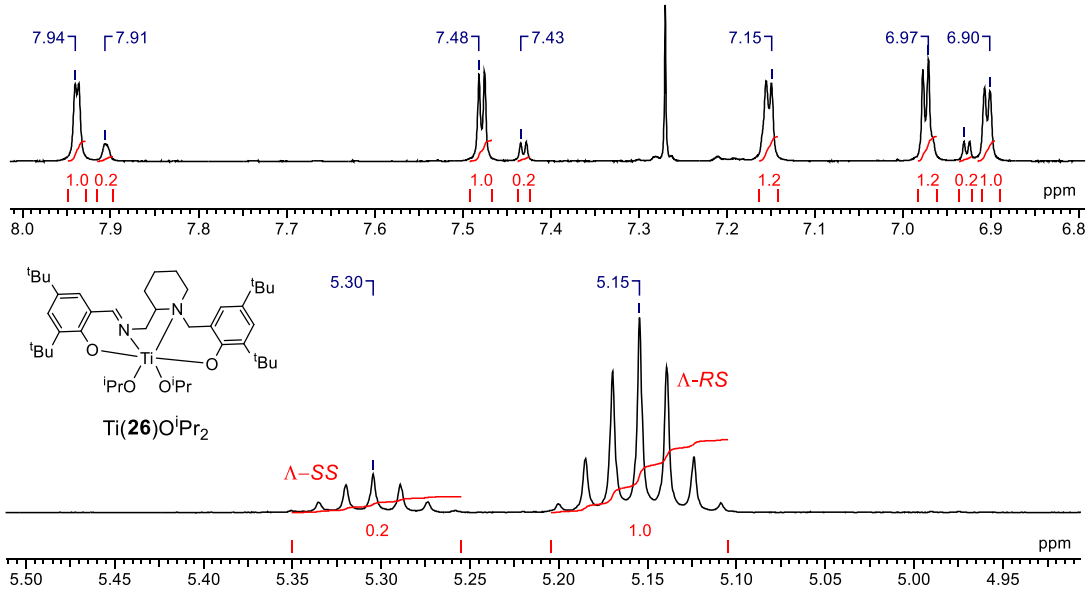

Figure 3.55: ^{1}H NMR ($CDCl_3$, 298 K) spectra of Ti(**26**)(O^iPr)$_2$ showing imino-aromatic region and methine region with *Λ-RS* and *Λ-SS* assignment.

The reduced salan ligand, **31**H_2, afforded Ti(**31**)(O^iPr)$_2$ on complexation, with characterisation by X-ray crystallography (Figure 3.56, Table 3.14). The solid state structure conforms to that of a typical salan-Ti(IV) complex, having a *trans* arrangement of phenoxy groups {O(3)-Ti-O(4) = 161.33(5)°} due to the increased flexibility at N(2), overall adopting an α-*cis* geometry.[37-39] The two isopropoxide groups are observed to be mutually *cis* {O(1)-Ti-O(2) = 105.58(6)°} and *Δ* octahedral chirality is observed. The nitrogen centre within the piperidine ring has a lengthened bond relative to that of the secondary amine {Ti-N_p(1) = 2.3876(13) Å / Ti-N(2) = 2.2797(13) Å}. Both phenoxy-to-metal bond lengths are almost identical {Ti-O(3) = 1.9138(11) Å / Ti-O(4) = 1.9121(11) Å}. The structure of Ti(**31**)(O^iPr)$_2$ was compared to a literature salan, Ti(**K**)(O^iPr)$_2$, which features equivalent aryl groups (Figure 3.57).[40] Due to a more symmetrical backbone, the titanium-to-nitrogen bond lengths

for Ti(**K**)(O^iPr)$_2$ are observed to be intermediate than that of Ti(**31**)(O^iPr)$_2$. Bond angles are also in good agreement despite the difference in the ligand backbone.

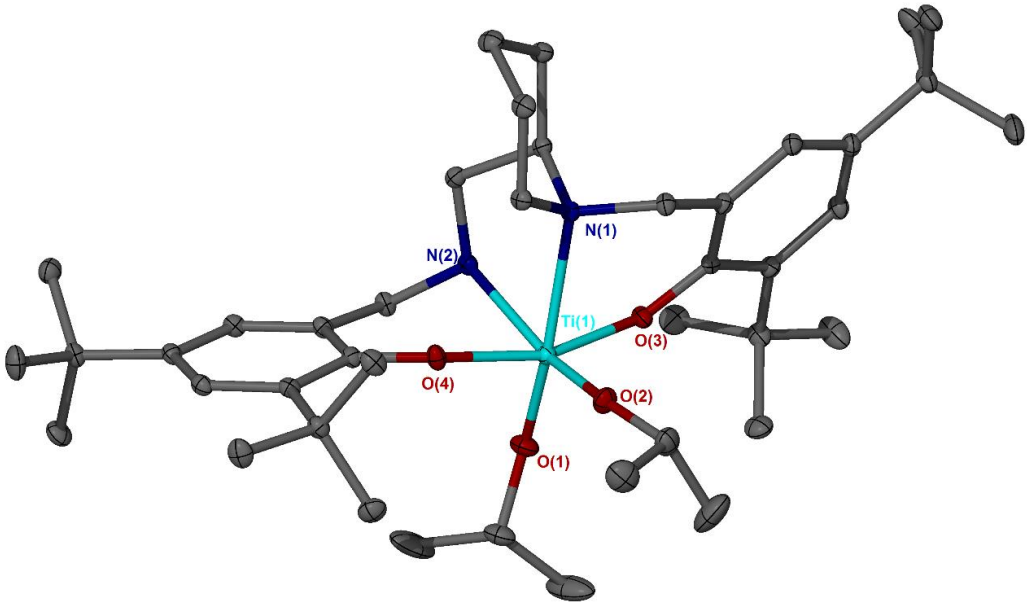

Figure 3.56: Solid-state structures of Ti(**31**)(O^iPr)$_2$. Ellipsoids are shown at the 30% probability level and all hydrogen atoms have been removed for clarity.

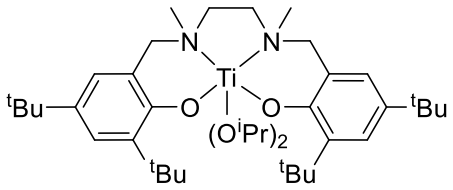

Ti(**K**)(O^iPr)$_2$

Figure 3.57: Literature comparison of a Ti(IV) salan, Ti(**K**)(O^iPr)$_2$.[40]

Table 3.14: Selected bond distances (Å) and bond angles (°) for Ti(**31**)(O^iPr)$_2$ and literature comparison Ti(**K**)(O^iPr)$_2$.[40]

	Ti(**K**)(O^iPr)$_2$	Ti(**31**)(O^iPr)$_2$
Ti-O(1)	1.819(2)	1.8079(12)
Ti-O(2)	1.780(2)	1.7906(12)
Ti-O(3)	1.905(2)	1.9138(11)
Ti-O(4)	1.914(2)	1.9121(11)
Ti-N(1)	2.336(2)	2.3876(13)
Ti-N(2)	2.353(2)	2.2797(13)
O(1)-Ti-O(2)	103.65(10)	105.58(6)
O(1)-Ti-O(3)	93.41(9)	91.88(5)
O(1)-Ti-O(4)	95.14(9)	95.80(6)
O(1)-Ti-N(1)	165.94(10)	163.11(5)
O(1)-Ti-N(2)	91.22(9)	90.52(5)
O(2)-Ti-N(1)	89.09(10)	90.06(5)
O(2)-Ti-O(4)	93.41(9)	94.26(5)
O(3)-Ti-O(4)	161.67(9)	161.33(5)
O(3)-Ti-N(2)	81.35(8)	83.70(5)
N(1)-Ti-N(2)	76.32(9)	75.54(5)

Investigation by ^{1}H NMR spectroscopy revealed a minor series which made up ~10% of the sample. Nevertheless, the resonances of the major product correlate to the solid-state structure of Ti(**31**)(O^iPr)$_2$. Observable in the ^{1}H NMR spectrum are four doublets, relating to the diastereotopic benzylic positions, four doublets, relating to the isopropoxide methyl groups, as well as three ^{t}Bu singlets with an integral sum of 36. The possibility of the impurity being the related bicyclic complex, Ti(**22**)(O^iPr)$_2$, was ruled out by comparison of the ^{1}H NMR spectra. While likely diastereotopic in nature, the exact assignment of the extra resonances are increasingly difficult due to four points of chirality for Ti(**31**)(O^iPr)$_2$. Previous reports concerning the coordination of

chiral ligands to Ti(IV) have demonstrated a change in chirality at the metal centre is common for these systems.[38, 40, 41] A switch to *Λ* chirality at the metal could be the origin of the diastereomers for this system, with the *Δ* chirality being preferred during synthesis or recrystallisation (Figure 3.58).

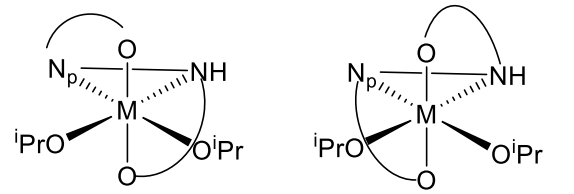

Δ–Ti(*SRS*-**31**)$_2$(O^{i}Pr)$_2$ Λ–Ti(*SRS*-**31**)$_2$(O^{i}Pr)$_2$

Figure 3.58: Potential diastereomers for Ti(**31**)(O^{i}Pr)$_2$.

3.4.2 Zirconium/Hafnium complexes

The imino-monophenol, **1**H, was successfully complexed to Zr(IV), with a solid-state structure being obtained with a *P-1* space-group and triclinic crystal system (Figures 3.59-3.60). An identical arrangement of ligands around the *psuedo* octahedral metal centre is observed compared to Ti(**1**)$_2$(O^{i}Pr)$_2$ and literature complex, Zr(**H**)$_2$(O^{i}Pr)$_2$. An α-*cis* geometry was realised and the bonding of ligand-to-metal is similar for each ligand set. For Zr(**1**)$_2$(O^{i}Pr)$_2$, the isopropoxide groups are in a *cis* relationship {O(1)-Zr-O(2) = 101.64(6)°} each with a *trans* relationship to the imino group {for example, O(1)-Zr-N(3) = 161.42(6)°}. The stereochemistry in the solid-state structure is observed to be *RR* at the ligands with *Λ* chirality at the metal centre. Bond lengths and angles are reasonably similar to that of Zr(**H**)$_2$(O^{i}Pr)$_2$ (Table 3.15, Figure 3.48).

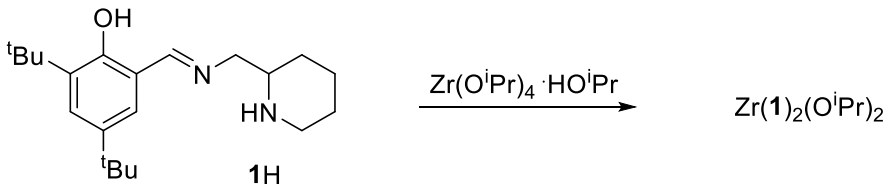

Figure 3.59: Complexation of **1**H to Zr(IV).

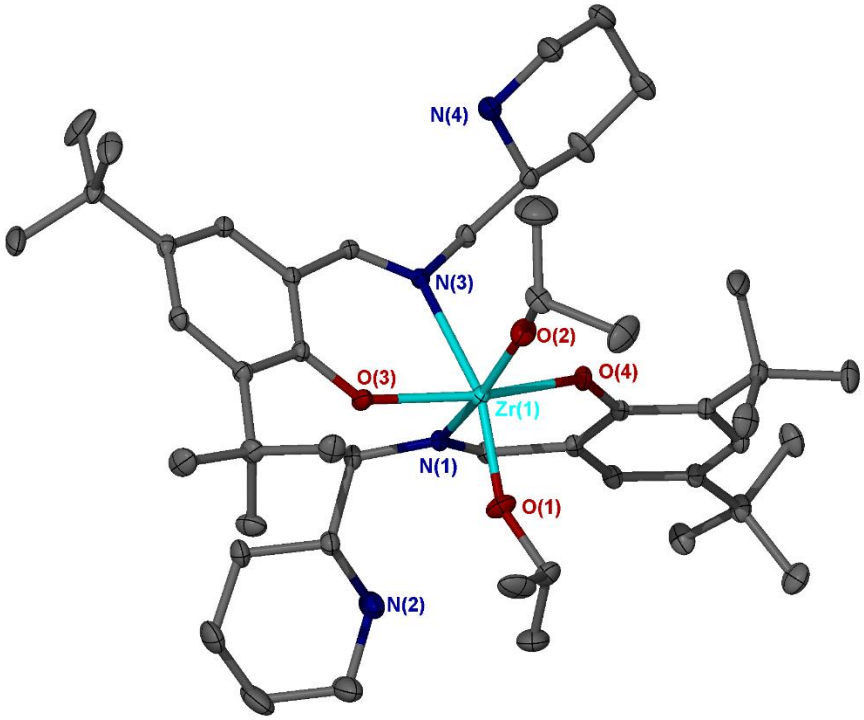

Figure 3.60: Solid-state structures of Zr(**1**)$_2$(O^{i}Pr)$_2$. Ellipsoids are shown at the 30% probability level and all hydrogen atoms have been removed for clarity.

Analysis of Zr(**1**)$_2$(O^{i}Pr)$_2$ *via* ^{1}H NMR spectroscopy revealed multiple species are present in solution in a similar manner to Ti(**1**)$_2$(O^{i}Pr)$_2$. These species are closely related, occurring within a narrow ppm window. In the imino to aromatic region, there are three main series related to the imino group and the two aromatic protons. Within the methine region, a series of septets is observed, with a dominating resonance and two smaller signals. Analysis of the diffusional properties of the Zr(**1**)$_2$(O^{i}Pr)$_2$ demonstrated a single broad peak ($CDCl_3$, 298K, $D = 4.35 \times 10^{-10}\ m^2s^{-1}$). This rate of diffusion is slower than that of Ti(**1**)$_2$(O^{i}Pr)$_2$ ($CDCl_3$, 298K, $D = 5.47 \times 10^{-10}\ m^2s^{-1}$) and this is undoubtedly related to the larger metal radius of Zr(IV). The species in solution for Zr(**1**)$_2$(O^{i}Pr)$_2$ are also suggested to be diastereomers, with the solid-state configuration of *Λ-RR*, as observed in the solid-state structure, predicted to be the major species in solution.

Table 3.15: Selected bond distances (Å) and bond angles (°) for Zr(**1**)$_2$(O^{i}Pr)$_2$, literature complex Zr(**H**)$_2$(O^{i}Pr)$_2$ and Ti(**1**)$_2$(O^{i}Pr)$_2$ for comparison.[28]

	Zr(**H**)$_2$(O^{i}Pr)$_2$	Ti(**1**)$_2$(O^{i}Pr)$_2$	Zr(**1**)$_2$(O^{i}Pr)$_2$
M-O(1)	1.9355(16)	1.8037(12)	1.9245(13)
M-O(2)	1.9355(16)	1.7852(12)	1.9289(13)
M-O(3)	2.0425(14)	1.9473(10)	2.0587(11)
M-O(4)	2.0425(14)	1.9316(10)	2.0596(12)
M-N(1)	2.4350(19)	2.2628(13)	2.3979(14)
M-N(3)	2.4350(19)	2.2825(12)	2.3954(13)
O(1)-M-O(2)	99.63(10)	104.60(6)	104.64(6)
O(1)-M-O(3)	98.98(7)	96.09(5)	92.94(6)
O(1)-M-O(4)	98.98(7)	92.75(5)	97.70(6)
O(1)-M-N(1)	86.97(6)	87.99(5)	89.59(5)
O(1)-M-N(3)	171.41(7)	162.39(5)	161.42(6)
O(2)-M-N(1)	171.41(7)	166.05(6)	163.43(5)
O(2)-M-O(4)	96.11(6)	95.83(5)	92.78(5)
O(3)-M-O(4)	156.51(8)	167.12(5)	163.02(5)
O(3)-M-N(3)	77.32(6)	88.19(4)	76.47(4)
N(1)-M-N(3)	87.03(8)	75.71(4)	75.45(5)

The bicyclic bisphenol ligands, **14**-**16**H$_2$, were coordinated to zirconium and hafnium. Rather than the mono-ligated species, there was a pronounced preference for the homoleptic complex, M(**L**)$_2$ (Figure 3.61). Various conditions were trialled to control the product of the reaction, including the use of coordinating solvents and different metal to ligand ratios but, due to solubility, the isopropoxide species was never isolated as a pure compound and often contaminated with unreacted M(O^{i}Pr)$_4$·HO^{i}Pr. The conditions used to furnish the bis-ligated complex involved heating in hexane for 16 hours, after which the product was isolated by filtration directly from the reaction mixture.

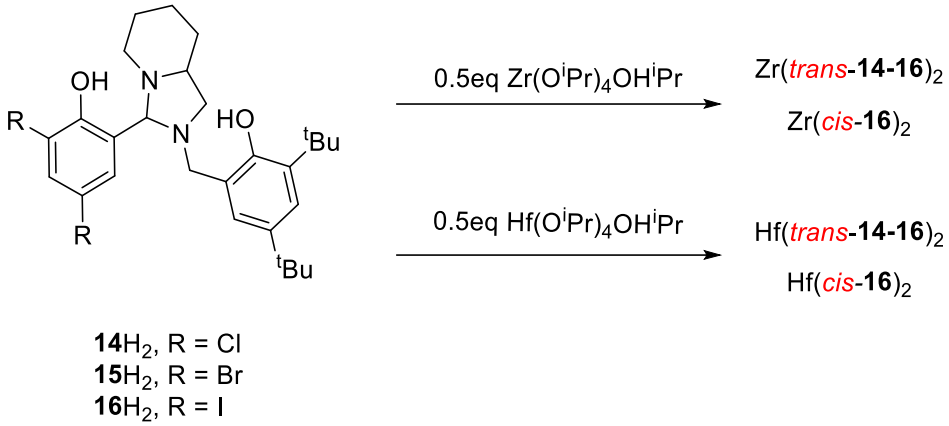

Figure 3.61: Synthesis of bis-ligated Zr(IV) and Hf(IV) complexes.

Solid-state structures were acquired exhibiting octahedral metal complexes. In all cases, the ligands are arranged in a *fac-fac* manner (Figure 3.62, Table 3.16). For chloro- and bromo- bearing phenoxy groups of M(**14**/**15**)$_2$, a mutual *trans* relationship was observed in the solid-state *via* X-ray crystallography (Figure 3.63). Each structure, with zirconium and hafnium, are found in a triclinic system with a *P-1* space-group. Both ligands have identical stereochemistry, *SSR* with the *R* chirality referring to the nitrogen. Between Zr(**14**)$_2$ and Zr(**15**)$_2$ there is very little difference in bond length and angles. The adopted structure is more symmetrical with each ligand set having the same *trans* relationships also leading to similar bond lengths and angles within the same complex. The ^{t}Bu phenoxy groups have the shortest ligand to metal bonds due to the electron releasing alkyl groups and a *trans* relationship to nitrogen {for Zr(**14**)$_2$, Zr-O(1) = 1.976(4) Å / Zr-O(1) = 2.026(3) Å}. The halo substituted phenoxys are observed to have a relatively lengthened bond due to their electron withdrawing nature. The bonding of the nitrogen centres to the metal are observed to be relatively long but comparable with a related literature example {for Zr(**14**)$_2$, Zr-N(1) = 2.467(4) Å, for Zr(**J**)$_2$, Zr-N(1) = 2.406(1) Å}. The phenoxy groups with in the same ligand are observed to be *cis* {for Zr(**14**)$_2$, O(1)-Zr-O(2) = 100.37(14)°}. The bond angle between the halo substituted phenoxy groups is approaching a *trans* relationship albeit deviating greatly from ideality {for Zr(**14**)$_2$, O(2)-Zr-O(4) = 137.54(14)°}. Comparatively, the angles involving the ^{t}Bu phenoxy groups are found to be closer to that of an ideal octahedral structure {for Zr(**14**)$_2$, O(1)-Zr-O(3) = 91.62(13)° / O(1)-Zr-N(3) =168.88 (14)°}. There are also indications there may be π-π stacking between the aromatic rings of the same ligand which are parallel orientated with a centroid

distance around the upper limit for this interaction {for Zr(**1**)$_2$, Ar-Ar = 4.08 Å}. There is a reasonable agreement between the bond lengths and angles of the Zr(IV) and Hf(IV) complexes.

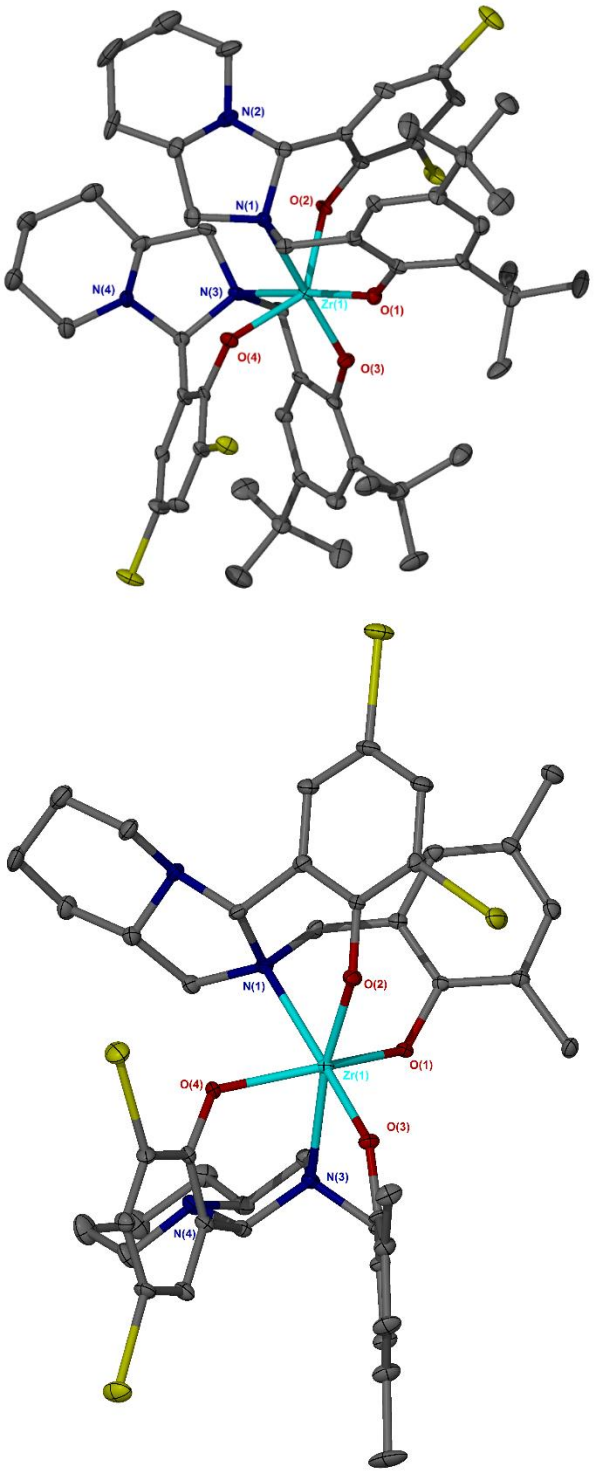

Figure 3.62: Solid-state structures of Zr(*trans*-**14**)$_2$ (Top) and Zr(*cis*-**16**)$_2$ (Bottom).Ellipsoids are shown at the 30% probability level and all hydrogen atoms and ^{t}Bu methyl groups have been removed for clarity.

Table 3.16: Selected bond distances (Å) and bond angles (°) for M(**14**-**16**)$_2$ and literature comparison M(**O**)$_2$.[29]

	Zr(**O**)$_2$	Zr(**14**)$_2$	Zr(**15**)$_2$	Zr(***cis*-16**)$_2$	Hf(**O**)$_2$	Hf(**14**)$_2$	Hf(**15**)$_2$	Hf(***cis*-16**)$_2$
M-O(1)	2.0022(16)	1.976(4)	1.972(3)	2.010(4)	1.9974(15)	1.989(2)	1.981(3)	1.956(3)
M-O(2)	2.0158(16)	2.026(3)	2.026(3)	2.026(4)	2.0093(16)	2.013(2)	2.001(3)	2.037(3)
M-O(3)	2.0022(16)	1.980(3)	1.977(4)	1.960(4)	1.9981(18)	1.989(2)	1.982(3)	2.010(3)
M-O(4)	2.0158(16)	2.025(4)	2.029(3)	2.056(4)	2.0109(17)	2.024(2)	2.012(3)	2.009(3)
M-N(1)	2.4061(19)	2.467(4)	2.471(4)	2.438(4)	2.3514(19)	2.455(2)	2.453(4)	2.390(3)
M-N(3)	2.4061(19)	2.459(4)	2.469(4)	2.445(4)	2.3690(20)	2.424(2)	2.435(4)	2.435(3)
Ar_R -Ar_{tBu}	-	4.08/4.06	4.08	4.07/3.81	-	4.23 /3.99	4.27/4.00	4.00/3.83
O(1)-M-O(3)	92.09(10)	91.62(13)	92.78(14)	104.25(16)	90.72(7)	89.47(7)	89.35(12)	103.94(11)
O(2)-M-O(4)	91.28(10)	137.54(14)	137.51(14)	107.46(15)	90.53(8)	137.84(8)	138.02(13)	104.19(10)
O(1) -M-O(4)	91.59(7)	108.76(14)	108.54(14)	144.93(16)	90.24(7)	108.52(8)	108.26(13)	147.98(11)
O(3)-M-O(2)	91.59(7)	109.25(14)	108.72(14)	94.50(15)	94.05(8)	107.69(8)	107.69(1)	96.35(11)
O(4)-M-N(1)	96.27(6)	77.05(14)	77.19(14)	78.77(15)	103.14(7)	77.55(7)	76.92(12)	77.58(10)
O(2)-M-N(3)	81.20(6)	77.18(14)	76.99(14)	171.43(15)	93.43(7)	76.73(7)	76.50(13)	175.12(10)
O(1)-M-N(3)	79.34(6)	168.88(14)	169.87(15)	79.30(15)	104.92(7)	166.81(8)	166.52(12)	80.00(10)
O(3)-M-N(1)	103.20(6)	168.60(14)	170.00(14)	173.33(15)	94.31(7)	168.39(7)	167.92(13)	173.17(10)

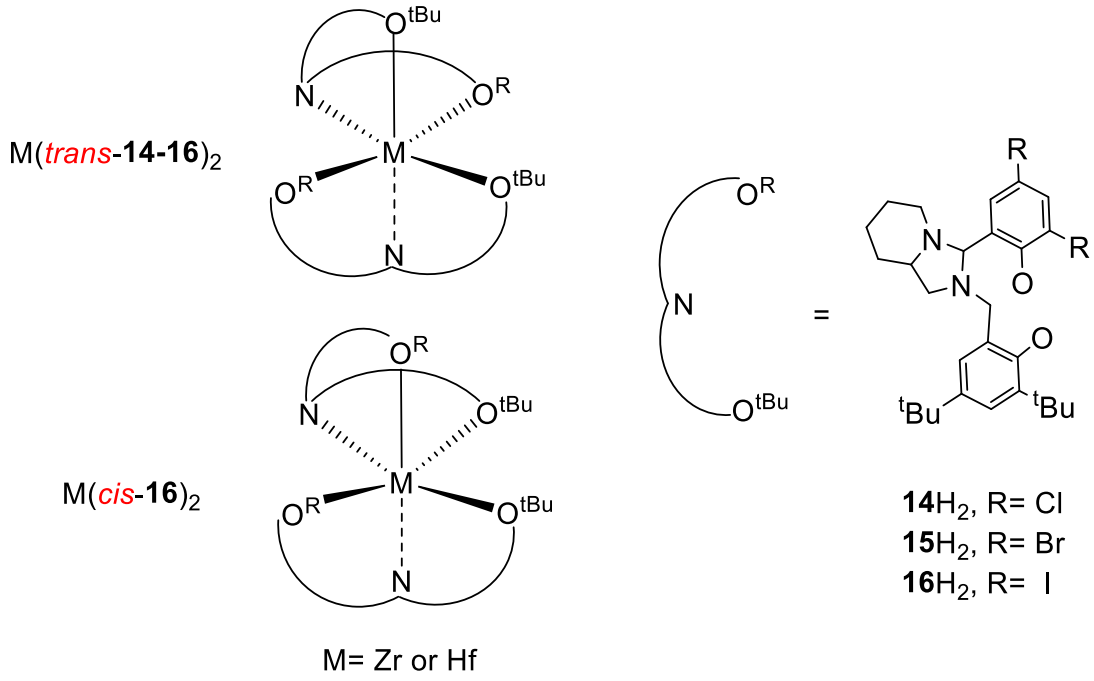

Figure 3.63: Observed geometries of M(**14**-**16**)$_2$ in the solid state.

However, for the ligand **16**H$_2$, the iodo phenoxy groups were observed to be mutually *cis* in the solid-state for both metals (Figure 3.62-3.63, Table 3.16). This form was found to be favoured when the complexation was carried out in CH_2Cl_2 and exclusive to **16**H$_2$. The *trans* form was observed as the major product in solution from hexane but suitable crystals for solid-state analysis were not acquired. Zr(*cis*-**16**)$_2$ was found to be monoclinic in a *P2$_1$/c* space-group while Hf(*cis*-**16**)$_2$ was orthorhombic with a *Fdd2* space-group. Due to the reversal of one ligand relative to the other, both sets have different chirality at the nitrogen centre giving *SSR* and *SSS* configurations. Bond lengths of this complex are comparable to that of the *trans* complexes with subtle differences. Due to a *trans* tendency between iodo and ^{t}Bu phenoxy, there is a lengthening of bonds to the metal, which is more pronounced for the alkyl bearing ring {for Zr(*cis*-**16**)$_2$, Zr-O(1) = 2.010(4) Å}. The coordinating nitrogen centres are inequivalent due to a *trans* relationship to different aryl groups. As a consequence, one metal-to-nitrogen bond is relatively longer being *trans* to an iodo aryl ring {for Hf(*cis*-**16**)$_2$, Hf-N(3) = 2.435(3) Å}. Due to the rearrangement of ligands, more profound changes are observed for bond angles. While maintaining a *cis* relationship, the two alkyl phenoxy groups are separated by an increased angle relative to the previous

configuration {for Zr(*cis*-**16**)$_2$, O(1)-Zr-O(3) = 104.25(16)°}. Accordingly, the iodo phenoxy groups tend towards a *cis* geometry with a bond angle of a similar magnitude for the alkyl phenoxy groups {O(2) -Zr-O(4) = 107.46(15)°}. As a consequence of this geometry, the iodo-to-alkyl phenoxy bond angles are now inequivalent leading to two difference tendencies {for Zr(*cis*-**16**)$_2$, O(1)-Zr-O(4) = 144.93(16)° / O(3)-Zr-O(2) = 94.50(15)°}. Both nitrogen groups are involved in the other linear axis albeit opposite different phenoxy rings {for Zr(*cis*-**16**)$_2$, O(2)-Zr-N(3)= 171.43(15)° / O(3)-Zr-N(1) = 173.33(15)°}. A further difference due to the geometry is the reduction of aryl centroid distance. For both Zr(*cis*-**16**)$_2$ and Hf(*cis*-**16**)$_2$, the distance is below 4 Å indicating stronger potential for π-π stacking.

Literature examples of Zr/Hf(**L**)$_2$ are relatively uncommon and this may be due to design, in which complexes with labile groups are targeted. One relevant example is provided by an iminobisphenolate system, Zr(**N**)$_2$, were **N**H$_2$ is an ONO type ligand (Figure 3.64).[32] Interestingly, the bis-ligated form is observed despite the use of bulky *ortho* substituents which are sufficient to ensure monomeric titanium under the same conditions. The ligands are arranged in a *mer-mer* geometry due to the rigidity of the imino group. A switch to the monoligated form was successfully instigated in this instance by the use THF as a coordinating solvent. A further demonstration of the inability of larger *ortho* substituents to prevent bisligation has also been shown for M(**O**)$_2$, which also assumes a *mer-mer* geometry (Figure 3.64).[33] These structures provide a useful analogue for the comparison of M(**14**-**16**)$_2$, having the same number of carbon atoms separating the two aryl rings. A difference in noted between the arrangement of ligands, with M(**O**)$_2$ having both nitrogen centres *trans*, in an *pseudo* axial position giving rise to a more symmetrical structure. In contrast, M(**14**-**16**)$_2$ have both nitrogen centres *cis*. Despite the difference in octahedral geometry, the bond lengths for both the Zr(IV) and Hf(IV) complexes are comparable (Table 3.16). The main difference between bond lengths is observed for the metal-to-nitrogen bonds which are relatively longer for M(**14**-**16**)$_2$. This is likely related to the rigidity of the bicyclic backbone as well as the effect of different *trans* groups.

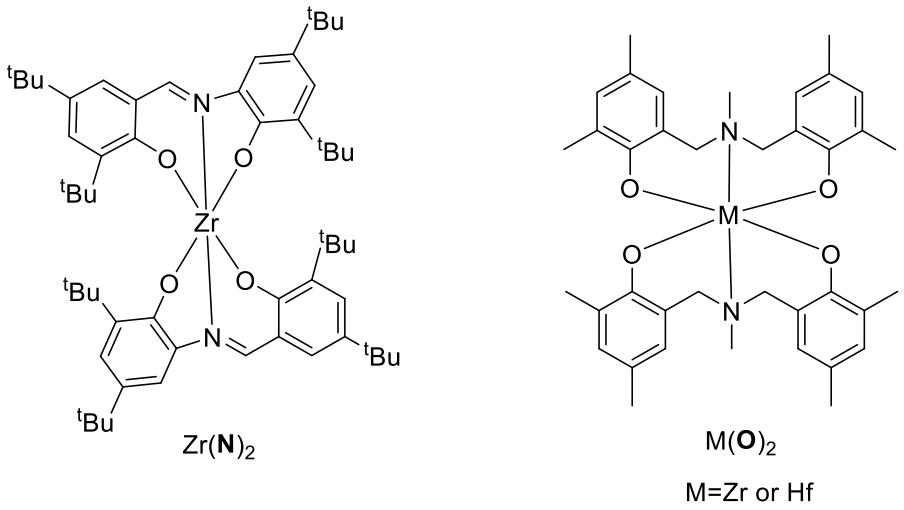

Figure 3.64: Literature comparisons of zirconium/hafnium bis-ligated complexes, $Zr(\mathbf{N})_2$ and $M(\mathbf{O})_2$.

For M(*trans*-**14-16**)$_2$, the symmetrical arrangement of ligands was further corroborated in solution *via* ^{1}H NMR spectroscopy (Figure 3.65). There are four resonances in the aromatic region due each group having the same *trans* relationships. One resonance is relatively deshielded compared to the other occurring at approximately 6 ppm; this is attributed to the proximity of an aryl ring causing a slight magnetic anisotropy effect. A benzylic proton resonance is also observed to be relatively deshielded occurring at ~5.3 ppm, examination of the crystal structure indicates this to be caused by both the halogen group and metal which are found to be adjacent to this position. The bis-ligated nature of the complex is demonstrated by the absence of resonances assignable to an isopropoxide group.

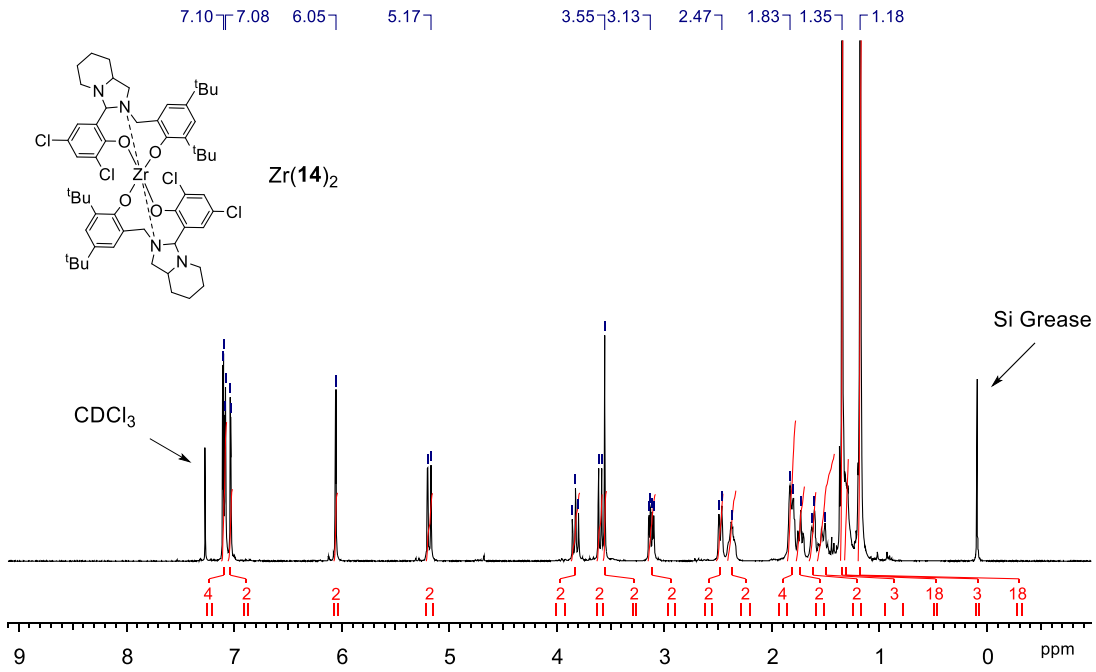

Figure 3.65: ^{1}H NMR ($CDCl_3$, 298 K) spectrum of Zr(**14**)$_2$.

For the iodo-complexes, M(**16**)$_2$, both the *cis* and *trans* form were observable and distinguishable in solution and there was no evidence of an isopropoxide species. When prepared in hexane, the isomer present was deduced to be the *trans* form due to the symmetry implied by the number of resonances and good correlation with that of M(**14**/**15**)$_2$ (Figure 3.66). A small amount of this *cis* form is also present. Similar observations are made regarding shifts in benzylic and aromatic resonances. For M(*cis*-**16**)$_2$, prepared from CH_2Cl_2, ^{1}H NMR spectroscopy analysis shows the solution structure to be in line with the solid-state structure (Figure 3.67). There are eight resonances assigned to aromatic groups and four for the *t*-butyl groups demonstrating the different environments of the two ligands. The previously observed shifts due to magnetic anisotropy remain observable with a CH singlet of the 5 membered ring now also being deshielded by the neighbouring metal/halogen as implied to by solid-state structure.

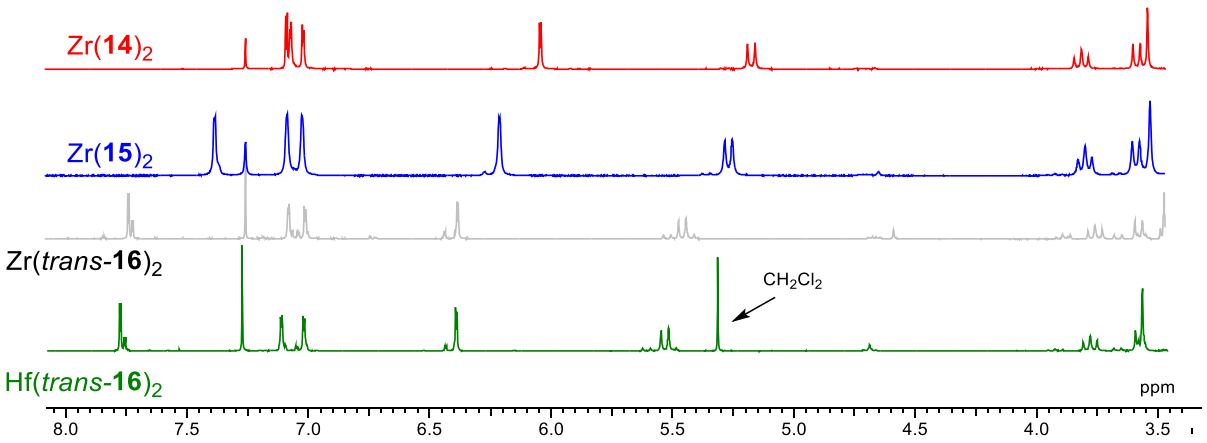

Figure 3.66: ^{1}H NMR ($CDCl_3$, 298 K) spectra of M(*trans*-**14**-**16**)$_2$.

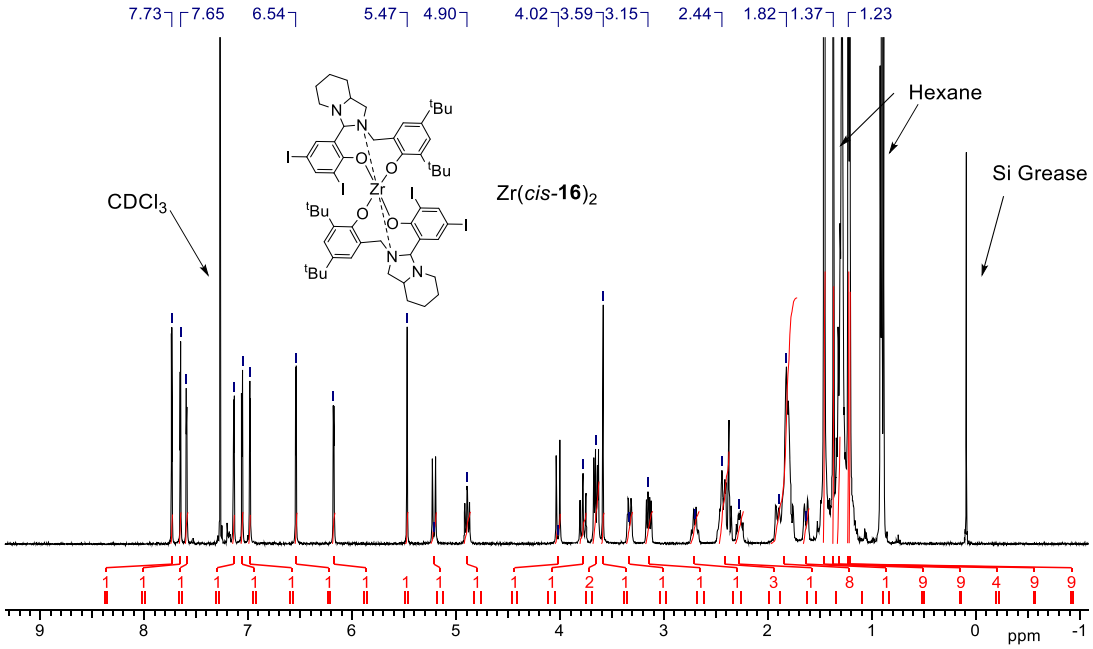

Figure 3.67: ^{1}H NMR ($CDCl_3$, 298 K) spectrum of Zr(*cis*-**16**)$_2$.

Different metal sources were explored in an attempt to isolate the mono-ligated complexes of **14**H_2. The use of $Zr(NMe_2)_4$ had a similar outcome to that of zirconium isopropoxide, with a strong preference for Zr(**14**)$_2$. Employment of a bulkier labile group in the form of $Zr(O^tBu)_4$ did favour the alkoxide form, however, there remained some impurity of the bis-ligated species, Zr(**14**)$_2$ (Figure 3.68). The added benefit of using this reagent was the ability to isolate the products from the metal precursor as Zr(**14**)$(O^tBu)_2$ was amenable to recrystallisation.

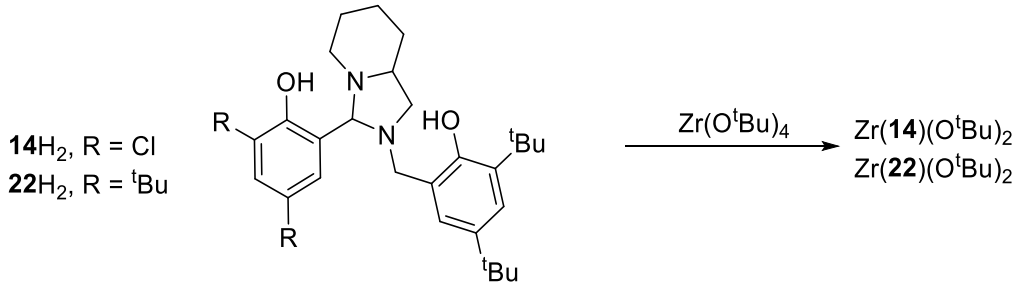

Figure 3.68: Synthesis of mono-ligated bicyclic-Zr(IV) complexes.

The solid-state structure revealed the presence of two *tert*-butoxide groups as well as a coordinating ^{t}BuOH with a relatively long oxygen-to-metal bond length {Zr-O(5) = 2.3265(12) Å} The structure was found in a monoclinic crystal system with a $P2_1/c$ spacegroup. This extra coordination caused the zirconium centre to be *pseudo* octahedral with the ligand and *tert*-butoxide groups occupying *fac* positions (Figure 3.69, Table 3.17). The metal-to-nitrogen bond is also observed to be lengthened to accommodate the ^{t}BuOH group {Zr-N(1) = 2.5149(12) Å}. The stereochemical configuration for the ligand in this solid state structure was observed to be *SRS*, with the *R* chirality upon the coordinating nitrogen centre. The alcohol was revealed to have a hydrogen bonding interaction with the non-coordinating nitrogen within the bicyclic ring {O-H--N = 2.50 Å}. Purification by washing the complex with hexane rather than recrystallisation afforded the complex without the coordinative alcohol as evidenced by ^{1}H NMR spectroscopy.

Complexation of the **22**H_2, which has bulkier ^{t}Bu on both aryl rings, afforded the desired complex with no evidence of the bis-ligated species. Suitable crystals were grown for X-ray crystallography, demonstrating a trigonal bipyramidal geometry in the solid-state (Figure 3.69, Table 3.17). The crystal system of Zr(**22**)(O^{i}Bu)$_2$ is triclinic with a *P-1* spacegroup. The solid-state structure is comparable to that of a bicyclic Ti(IV) complex {Ti(**14**)(O^{i}Pr)$_2$, Figure 3.49}. Accordingly, identical chirality is observed for Zr(**22**)(O^{i}Bu)$_2$ (*SSS*) relative to Ti(**14**)(O^{i}Pr) (*RRR*). Occupying the *pseudo* axial positions are the ligand nitrogen centre and a *tert*-butoxide group {O(1)-Zr-N(1) = 168.83(7)°}. The deviation of the axial angle from ideality reduces the τ value relative to that of Ti(**14**)(O^{i}Pr)$_2$ {for Zr(**22**)(O^{t}Bu)$_2$, τ = 0.78, Ti(**14**)(O^{i}Pr)$_2$, τ = 0.95}. The ligand phenoxy groups are separated by an angle that is close to ideality

for a trigonal bipyramidal structure {O(1)-Zr-N(1) = 122.23(8)°}. The remaining angles between Zr(**22**)(O^tBu)$_2$ and Ti(**14**)(O^iPr)$_2$ are comparable.

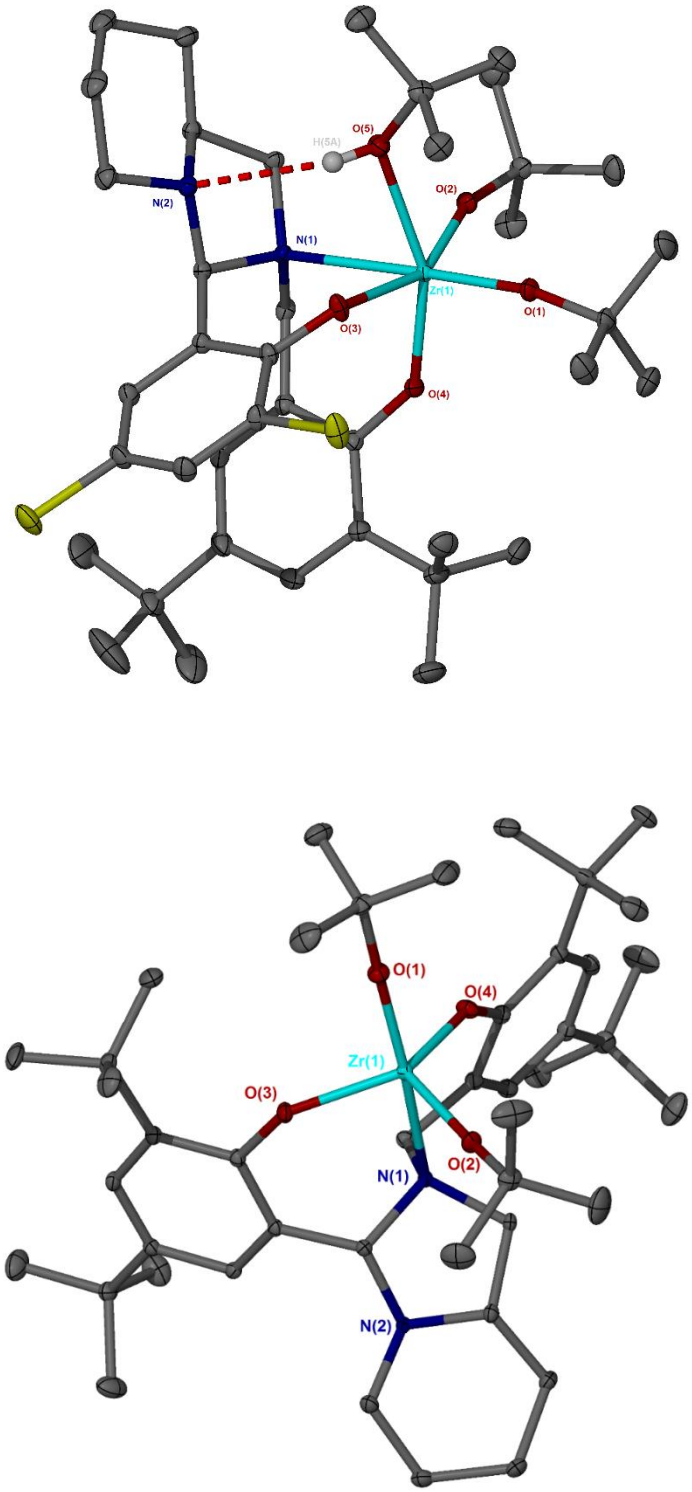

Figure 3.69: Solid-state structures of Zr(1**4**)(O^tBu)$_2$·HO^tBu (Top) and Zr(**22**)(O^tBu)$_2$ (Bottom). Ellipsoids are shown at the 30% probability level and all hydrogen atoms, except those involved in hydrogen bonding, have been removed for clarity.

Table 3.17: Selected bond distances (Å) and bond angles (°) for Zr(**14**/**22**)(O^tBu)$_2$ and Ti(**14**)(O^iPr)$_2$ for comparison.

	Ti(**14**)(O^iPr)$_2$	Zr(**14**)(O^tBu)$_2$·HO^tBu	Zr(**22**)(O^tBu)$_2$
M-O(1)	1.803(2)	1.9235(11)	1.9229(18)
M-O(2)	1.783(2)	1.9494(10)	1.9300(17)
M-O(3)	1.912(2)	2.0883(11)	2.0181(18)
M-O(4)	1.864(2)	2.0110(11)	1.9890(18)
M-O(5)	-	2.2365(12)	-
M-N(1)	2.308(3)	2.5149(12)	2.420(2)
O(1)-M-O(2)	99.94(11)	99.98(5)	104.28(8)
O(1)-M-O(3)	95.92(11)	98.06(5)	97.63(8)
O(1)-M-O(4)	96.96(10)	99.87(5)	96.16(8)
O(1)-M-N(1)	177.24(11)	176.59(4)	168.83(7)
O(2)-M-N(1)	82.81(1)	83.40(4)	86.77(7)
O(2)-M-O(3)	116.07(11)	155.66(5)	113.98(8)
O(2)-M-O(4)	118.26(11)	100.42(5)	116.18(8)
O(3)-M-O(4)	120.52(10)	92.40(5)	122.23(8)
O(1)-M-O(5)		176.59(4)	-
N(1)-M-O(5)	-	80.26(4)	-
O(3)-M-O(5)	-	78.57(4)	-
τ	0.95	-	0.78

Analysis of Zr(**22**)(O^tBu)$_2$ by ^{1}H NMR spectroscopy shows the solid-state structure to be maintained in solution (Figure 3.70). The expected resonances for the complex are found within the spectra including four aromatic resonances, a sharp, deshielded singlet due to the benzylic methine group and six *tert*-butyl resonances. For the ^{1}H NMR of Zr(**14**)(O^tBu)$_2$, similar resonances are observed to confirm the presence of the alkoxide species. However, there is also ~10% of the bis-ligated form, Zr(**14**)$_2$.

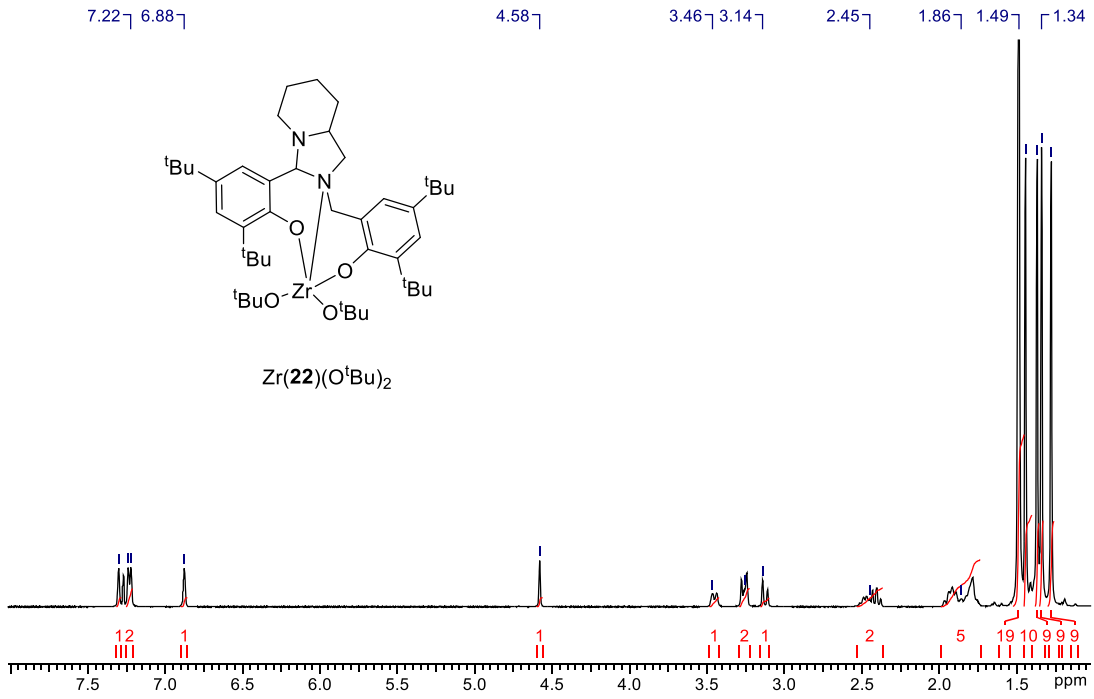

Figure 3.70: ^{1}H NMR ($CDCl_3$, 298 K) spectrum of Zr(**22**)(O^tBu)$_2$.

The salalen ligand, **26**H_2, was also coordinated to Zr(IV). Complexation attempts using Zr(O^iPr)$_4$·(HO^iPr) yielded one major species *via* ^{1}H NMR but successful purification was not realised. More success was realised by employing Zr(O^tBu)$_4$ as metal source, which allowed for the crystallisation of Zr(**26**)(O^tBu)$_2$ (Figures 3.71-3.72, Table 3.18).

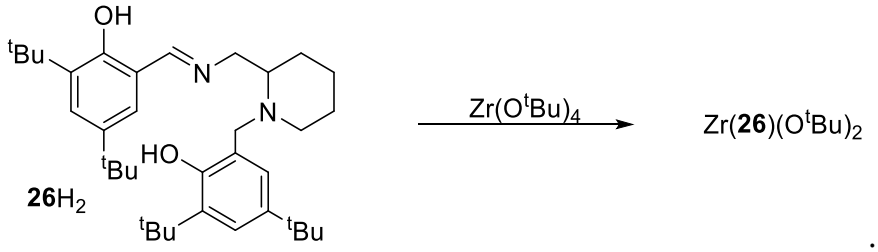

Figure 3.71: Synthesis of salalen Zr(IV) complex, Zr(**26**)(O^tBu)$_2$.

The solid-state structure was found in a monoclinic crystal system with a *C2/c* space-group. The structure revealed a *pseudo* octahedral geometry with a β-*cis* or *fac-mer* arrangement of ligand around the metal centre (Figure 3.72). Such a structure is consistent with previous group IV salalen complexes.[33-36] Conforming to this geometry, the *tert*-butoxide groups have a *cis* relationship {O(1)-Zr-O(2) =

96.75(4)°}. The phenoxy groups are also mutually *cis* for Zr(**26**)(O^tBu)$_2$ {O(3)-Zr-O(4) = 91.45(5)°}. The imino bond-to-metal is observed to be shorter relative to the amino bond {Zr-N(1) = 2.3417(16) Å / Zr-N(2) = 2.3417(16) Å}. The stereochemical configuration of the structure is represented by *SR* chirality on the ligand, referring to the carbon and nitrogen centres respectively. The chirality at the metal centre was found to be *Δ*. There is close agreement of the bond angles with Ti(IV) analogue, Ti(**26**)(O^iPr)$_2$, and good agreement of bond lengths and angles with literature complex, Zr(**J**)(O^iPr)$_2$ (Figure 3.54).[36]

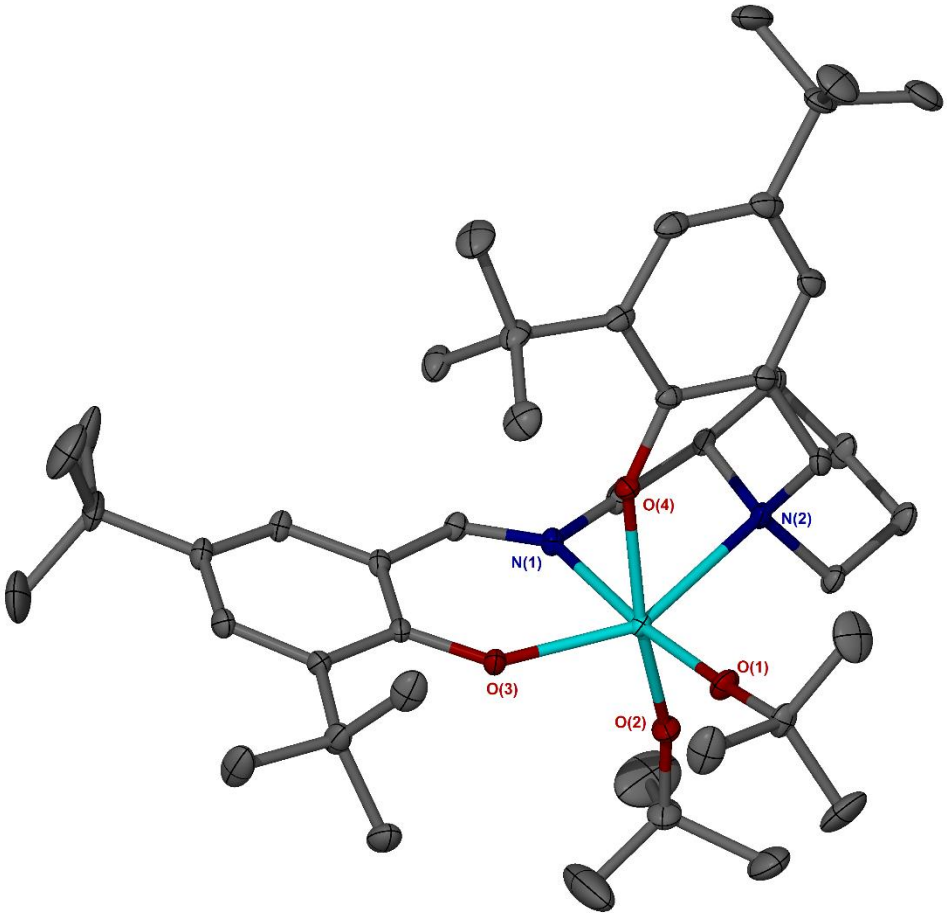

Figure 3.72: Solid-state structures of Zr(**26**)(O^tBu)$_2$. Ellipsoids are shown at the 30% probability level and all hydrogen atoms have been removed for clarity.

Table 3.18: Selected bond distances (Å) and bond angles (°) for Zr(**26**)$_2$(O^{t}Bu)$_2$, literature complex, Zr(**J**)$_2$(O^{i}Pr)$_2$,[36] and Ti(**26**)$_2$(O^{i}Pr)$_2$ for comparison.

	Zr(**J**)(O^{i}Pr)$_2$	Ti(**26**)(O^{i}Pr)$_2$	Zr(**26**)(O^{t}Bu)$_2$
M-O(1)	1.9788(12)	1.8351(11)	1.9398(14
M-O(2)	1.9567(12)	1.8537(12)	1.9535(14)
M-O(3)	2.0268(11)	1.8890(12)	2.0209(12)
M-O(4)	2.0534(11)	1.9257(11)	2.0731(13)
M-N(1)	2.3385(14)	2.2038(13)	2.3417(16)
M-N(2)	2.4335(14)	2.3101(13)	2.4371(15)
O(1)-MO(2)	93.15(5)	92.57(5)	96.75(4)
O(1)-M-O(3)	112.96(5)	106.21(5)	106.83(6)
O(1)-M-O(4)	93.05(5)	92.42(5)	92.88(6)
O(1)-Mi-N(1)	168.59(5)	169.83(5)	174.48(6)
O(1)-Ti-N(2)	97.06(5)	95.47(5)	102.31(6)
O(2)-M-N(1)	83.85(5)	82.94(5)	84.73(6)
O(2)-M-O(4)	166.41(5)	169.64(5)	163.88(6)
O(3)-M-O(4)	91.51(5)	91.79(5)	91.45(5)
O(3)-M-N(2)	148.79(5)	157.54(5)	149.11(5)
N(1)-M-N(2)	71.94(5)	75.41(5)	72.37(5)

Analysis of Zr(**26**)(O^{t}Bu)$_2$ *via* ^{1}H NMR spectroscopy revealed two species in solution. These species were observed at a 5:1 ratio paralleling the distribution of products for the related Ti(IV) complex, Ti(**26**)(O^{i}Pr)$_2$. For both series, an imino resonance, four aromatic resonances as well as six *tert*-butyl resonances were identifiable suggesting the maintaining of the solid-state structure in solution. As for Ti(**26**)(O^{i}Pr)$_2$, the second species observed *via* NMR spectroscopy is speculated to be a diastereomeric form.

In one instance, the coordination of **14**H_2 with zirconium isopropoxide yielded an unexpected product which was revealed by X-ray crystallography (Figure 3.73). Evidently, the ligand still contained traces of the imino form which was observed to form an μ-oxo zirconium complex with terminal isopropoxide groups, [Zr(**14***)(O^iPr)]$_2$O. The bridge is assumed to be formed *via* oxygen activation from the air. Both zirconium centres are observed to be octahedral with a *fac-mer* ligand orientation characteristic of group IV salalens, and similar to that of Zr(**26**)(O^tBu)$_2$. The stereochemistry of both ligands is identical, being *RS* for carbon and nitrogen respectively. The two chlorinated phenoxy rings are parallel and in close proximity suggesting a π-π stacking interaction (Ar-Ar = 3.46 Å).

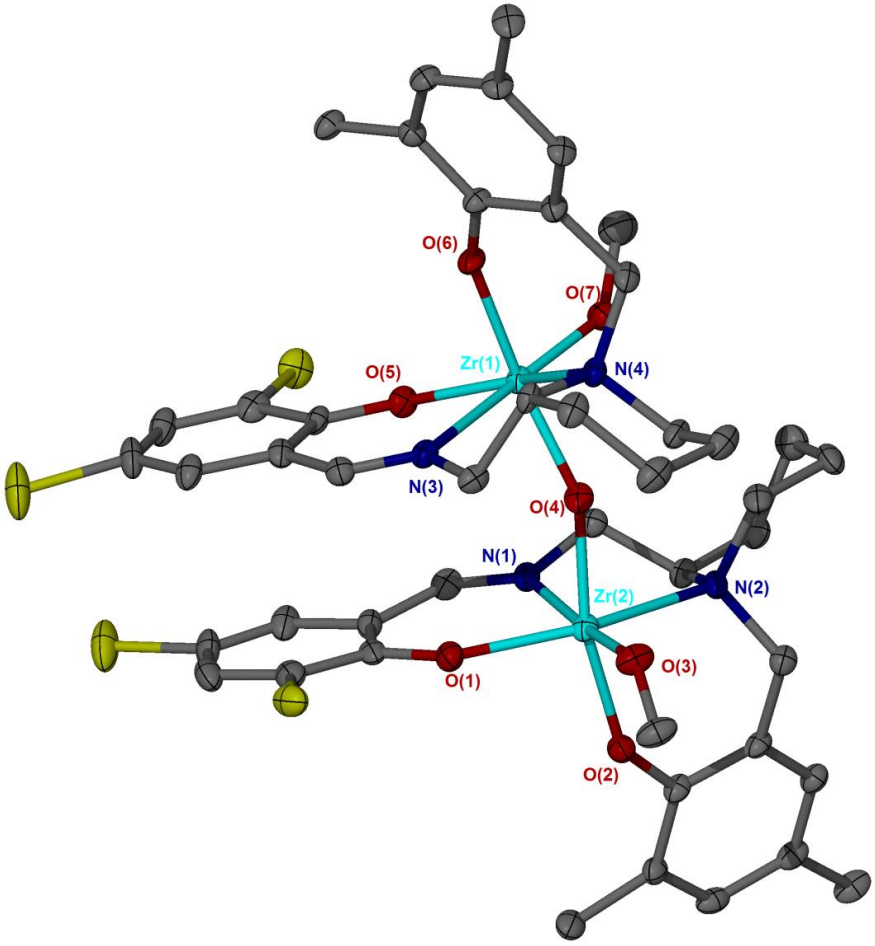

Figure 3.73: Solid-state structures of [Zr(**14***)(O^iPr)]$_2$O. Ellipsoids are shown at the 30% probability level and all hydrogen atoms and O^iPr methyl groups have been removed for clarity.

Coordination of salan, **31**H_2, to Zr(IV) was also achieved using the *tert*-butoxide metal source (Figure 3.74). Suitable crystals for X-ray crystallography were not realised but sufficient analysis was provided by NMR spectroscopy and elemental analysis.

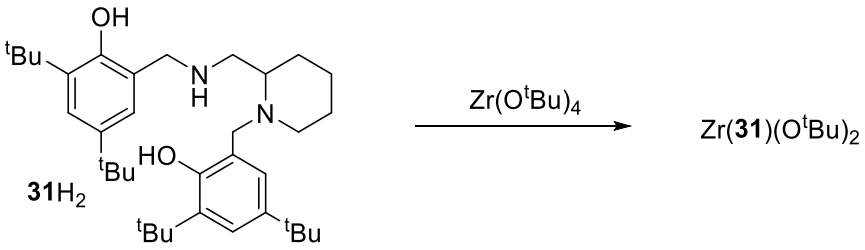

Figure 3.74: Synthesis of salan Zr(IV) complex, Zr(**31**)(O^{t}Bu)$_2$.

The ^{1}H NMR spectrum for Zr(**31**)(O^{t}Bu)$_2$ revealed the presence of a pure complex in solution (Figure 3.75). Two extra ^{t}Bu resonances are identifiable suggesting the successful preparation of the alkoxide complex. Four aromatic and four benzylic resonances are also observable, the latter indicating the diastereotopic nature of that position. The NH resonance is also present in the spectra, occurring at 2.29 ppm, being deduced *via* 2D-HSQC. Group IV salans, including Ti(**31**)(O^{i}Pr)$_2$, are typically observed to adopt an α-*cis* configuration.[37, 38, 40, 41] Such a geometry is also anticipated for Zr(**31**)(O^{t}Bu)$_2$.

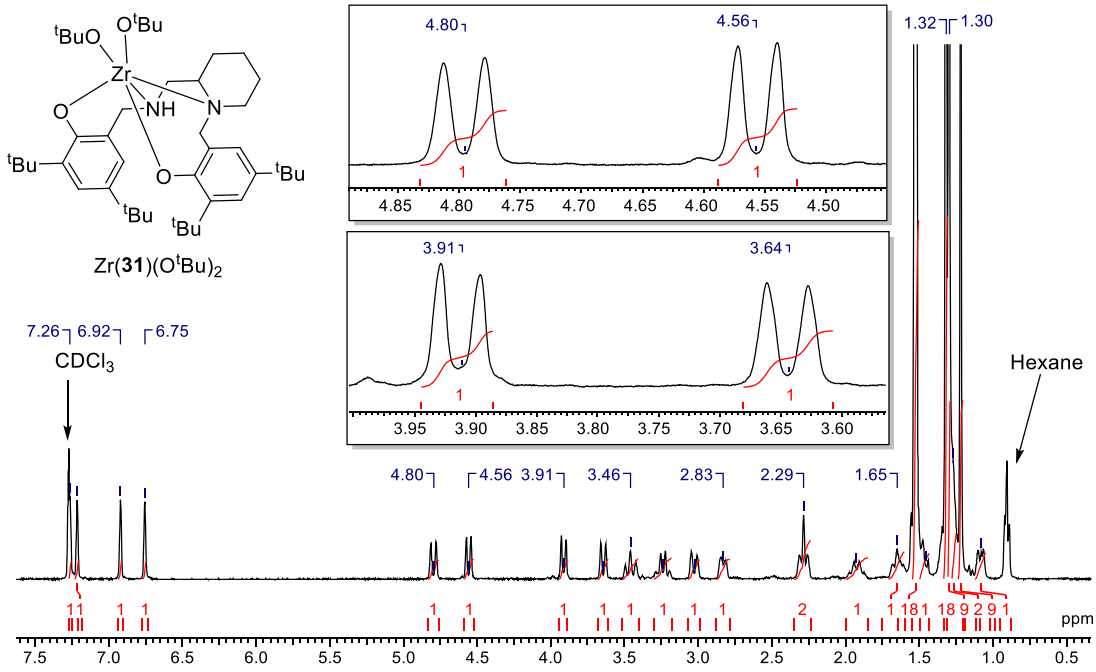

Figure 3.75: ^{1}H NMR ($CDCl_3$, 298 K) spectrum of Zr(**31**)(O^{t}Bu)$_2$.

3.5 Conclusions

A range of complexes based around a 2-(aminomethyl)piperidine motif have been prepared and characterised. For simple monophenols, resulting from the direct condensation between a salicylaldehyde and the amine, the imino form was found to be amenable for complexation and successful separation from the bicyclic form. A series of such complexes was realised with aluminium, in which the *ortho* and *para* positions were varied. Al(**1**-**6**)Me_2 were observed to contain a trigonal bipyramidal metal centre in the solid-state. The capability of this ligand forming complexes with other metals was demonstrated for the *tert*-butyl substituted phenoxy ring generating both Mg(**1**)$_2$ and Zn(**1**)$_2$. The magnesium and zinc complexes were comparable, with octahedral metal centres being found in the solid-state as well as diastereomeric forms in solution. An example of a benzyl capped imino form was also of complexed to aluminium giving Al(**7**)Me_2. This structure is predicted to have a tetrahedral Al(III) centre by DFT calculations. Functionalised bicyclic monophenols were also coordinated to aluminium yielding Al(**11**-**12**)Me_2 where the position of the phenoxy group is explored. Without X-ray crystallographic evidence, these bicyclic monophenolate structures are also predicted to be four coordinate. An extension to these structures is realised, with exchange of a benzene for a pyridine ring yielding Al(**13**)Me_2. Solid-state analysis revealed this structure to be five coordinate by virtue of the heterocyclic coordination.

The coordination of bisphenol groups to aluminium is split up into bicyclic, salalen and salan classes. Coordination of the bicyclic form yielded Al(**14**-**22**)Me, with a tetrahedral aluminium centre being depicted in the solid-state structure. It was also possible to form the binuclear species Al_2(**14**/**16**)Me_4 which was isolated when excess $AlMe_3$ was used. The solid-state structure of this dinuclear species contained two tetrahedral metal centres. Coordination of the salalens, **26**-**30**H_2, afforded a five coordinate metal centre in the solid-state. In solution, there was evidence of diastereomeric forms being present due to the pro-chirality of the amine group. The aluminium complexes of the salans, Al(**31**-**33**)O^{i}Pr, were observed to have a different arrangement of ligands around the metal centre compared to the salalens. A single species was isolated as the isopropoxide form of the complex despite the observation of disastereomers for the aluminium methyl form. The methylated salan, Al(**35**)Me

reverts back to the salalen coordination structure and is isolated as a mixture of stereoisomers.

The triaryl bisphenol, **36**H_2, was shown to have a trigonal bipyramidal solid-state structure when coordinated to aluminium as an isopropoxide species. The coordination of the trisphenol ligand, **37**H_2, was shown to be successful *via* NMR spectroscopy. Based on the absence of any major Al-Me resonances, it is assumed all phenolate groups take part in the metal coordination, yielding Al(**37**).

The monophenol ligand, **1**H, was also successfully coordinated to Ti(IV) and Zr(IV), yielding M(**1**)$_2$(O^iPr)$_2$. An octahedral geometry was found in the solid state structure for both metal centres with diastereomeric forms being observed in solution. The bicyclic ligands, **14**H_2 and **22**H_2, were successfully coordinated to Ti(IV) and Zr(IV), yielding mono-ligated species. For Zr(IV), this was achieved by using a more hindered Zr(IV) source. Ti(**14**)(O^iPr)$_2$ and Zr(**22**)(O^tBu)$_2$ were characterised as trigonal bipyramidal structures in the solid-state. Use of M(O^iPr)$_4$·HO^iPr yielded the bicyclic complexes, M(**14**-**16**)$_2$ for both Zr(IV) and Hf(IV). An octahedral metal centre was observed in the solid-state with the iodo complexes, M(**16**)$_2$ being found to adopt different structural isomers. Salalen group IV complexes were also realised. Both Ti(**26**)(O^iPr)$_2$ and Zr(**26**)(O^tBu)$_2$ were found to have an octahedral geometry in the solid-state, with a *fac-mer* ligand arrangement. Two species were observed *via* solution-state NMR spectroscopy and this was attributed to formation of *Λ*/*Δ* octahedral isomers. A μ-oxo bridged dimer was also observed for the salalen form of **14**H_2. Salan complexes were also realised for Ti(IV) and Zr(IV), with a solid-state structure acquired for Ti(**31**)(O^iPr)$_2$. The Ti-salan was observed to have an α-*cis* octahedral structure in the solid-state and a second species revealed *via* NMR spectroscopy. In contrast, Zr(**31**)(O^tBu)$_2$ was isolated as a single diastereomer and assumed to have an identical geometry to the Ti(IV) analogue.

The majority of these prepared complexes are suitable for catalysis, in particular ROP of lactide and other cyclic esters. This suitability arises from the presence of Lewis acidic metals, which are amenable to the coordination-insertion polymerisation, and, in most cases, labile groups that are able to initiate this mechanism. Within families of complexes, there is also potential evaluate contributions of different substituents and structure to activity relationships.

3.6 References

1. H. Wang, Y. Yang and H. Ma, *Macromolecules*, 2014, **47**, 7750-7764.
2. M. D. Jones, L. Brady, P. McKeown, A. Buchard, P. M. Schafer, L. H. Thomas, M. F. Mahon, T. J. Woodman and J. P. Lowe, *Chem. Sci.*, 2015, **6**, 5034-5039.
3. M. D. Jones, S. L. Hancock, P. McKeown, P. M. Schafer, A. Buchard, L. H. Thomas, M. F. Mahon and J. P. Lowe, *Chem. Commun.*, 2014, **50**, 15967-15970.
4. B. M. Chamberlain, M. Cheng, D. R. Moore, T. M. Ovitt, E. B. Lobkovsky and G. W. Coates, *J. Am. Chem. Soc.*, 2001, **123**, 3229-3238.
5. Y. Yang, H. Wang and H. Ma, *Inorg. Chem.*, 2015, **54**, 5839-5854.
6. K. Devaine-Pressing, J. H. Lehr, M. E. Pratt, L. N. Dawe, A. A. Sarjeant and C. M. Kozak, *Dalton Trans.*, 2015, **44**, 12365-12375.
7. A. J. Chmura, M. G. Davidson, C. J. Frankis, M. D. Jones and M. D. Lunn, *Chem. Commun.*, 2008, 1293-1295.
8. B. Gao, X. Li, R. Duan and X. Pang, *New J. Chem.*, 2015, **39**, 2404-2408.
9. N. Nomura, R. Ishii, Y. Yamamoto and T. Kondo, *Chem. Eur. J.*, 2007, **13**, 4433-4451.
10. Z. Zhong, P. J. Dijkstra and J. Feijen, *J. Am. Chem. Soc.*, 2003, **125**, 11291-11298.
11. P. A. Cameron, V. C. Gibson, C. Redshaw, J. A. Segal, A. J. P. White and D. J. Williams, *J. Chem. Soc., Dalton Trans.*, 2002, 415-422.
12. L. Cuesta-Aluja, A. Campos-Carrasco, J. Castilla, M. Reguero, A. M. Masdeu-Bultó and A. Aghmiz, *J. CO_2 Util.*, 2016, **14**, 10-22.
13. J. B. L. Gallaway, J. R. K. McRae, A. Decken and M. P. Shaver, *Can. J. Chem.*, 2012, **90**, 419-426.
14. M. Normand, V. Dorcet, E. Kirillov and J.-F. Carpentier, *Organometallics*, 2013, **32**, 1694-1709.
15. A. W. Addison, T. N. Rao, J. Reedijk, J. van Rijn and G. C. Verschoor, *J. Chem. Soc., Dalton Trans.*, 1984, 1349-1356.
16. M. Bouyhayi, Y. Sarazin, O. L. Casagrande and J.-F. Carpentier, *Appl. Organomet. Chem.*, 2012, **26**, 681-688.
17. N. Ikpo, S. M. Barbon, M. W. Drover, L. N. Dawe and F. M. Kerton, *Organometallics*, 2012, **31**, 8145-8158.
18. A. Okuniewski, D. Rosiak, J. Chojnacki and B. Becker, *Polyhedron*, 2015, **90**, 47-57.
19. L.-C. Liang, S.-T. Lin and C.-C. Chien, *J. Chin. Chem. Soc.*, 2013, **60**, 710-718.
20. A. Pilone, K. Press, I. Goldberg, M. Kol, M. Mazzeo and M. Lamberti, *J. Am. Chem. Soc.*, 2014, **136**, 2940-2943.
21. H. Du, A. H. Velders, P. J. Dijkstra, J. Sun, Z. Zhong, X. Chen and J. Feijen, *Chem. Eur. J.*, 2009, **15**, 9836-9845.
22. P. Hormnirun, E. L. Marshall, V. C. Gibson, A. J. P. White and D. J. Williams, *J. Am. Chem. Soc.*, 2004, **126**, 2688-2689.
23. M. Bouyahyi, E. Grunova, N. Marquet, E. Kirillov, C. M. Thomas, T. Roisnel and J.-F. Carpentier, *Organometallics*, 2008, **27**, 5815-5825.
24. T. D. Nixon, S. Dalgarno, C. V. Ward, M. Jiang, M. A. Halcrow, C. Kilner, M. Thornton-Pett and T. P. Kee, *Comptes Rendus Chimie*, 2004, **7**, 809-821.

25. X. Li, H. Song, L. Duan, C. Cui and H. W. Roesky, *Inorg. Chem.*, 2006, **45**, 1912-1914.
26. P. Wei and D. A. Atwood, *Polyhedron*, 1999, **18**, 641-646.
27. C.-T. Chen, C.-A. Huang and B.-H. Huang, *Dalton Trans.*, 2003, 3799-3803.
28. A. J. Chmura, D. M. Cousins, M. G. Davidson, M. D. Jones, M. D. Lunn and M. F. Mahon, *Dalton Trans.*, 2008, 1437-1443.
29. A. J. Chmura, M. G. Davidson, M. D. Jones, M. D. Lunn and M. F. Mahon, *Dalton Trans.*, 2006, 887-889.
30. E. Y. Tshuva, I. Goldberg, M. Kol and Z. Goldschmidt, *Inorg. Chem.*, 2001, **40**, 4263-4270.
31. E. Y. Tshuva, M. Versano, I. Goldberg, M. Kol, H. Weitman and Z. Goldschmidt, *Inorg. Chem. Commun.*, 1999, **2**, 371-373.
32. T. Xu, J. Liu, G.-P. Wu and X.-B. Lu, *Inorg. Chem.*, 2011, **50**, 10884-10892.
33. K. Press, A. Cohen, I. Goldberg, V. Venditto, M. Mazzeo and M. Kol, *Angew. Chem. Int. Ed.*, 2011, **50**, 3529-3532.
34. A. Yeori, S. Gendler, S. Groysman, I. Goldberg and M. Kol, *Inorg. Chem. Commun.*, 2004, **7**, 280-282.
35. K. Huang, S. Zhou, D. Zhang, X. Gao, Q. Wang and Y. Lin, *J. Organomet. Chem.*, 2013, **741–742**, 83-90.
36. E. L. Whitelaw, M. D. Jones and M. F. Mahon, *Inorg. Chem.*, 2010, **49**, 7176-7181.
37. A. J. Chmura, M. G. Davidson, M. D. Jones, M. D. Lunn, M. F. Mahon, A. F. Johnson, P. Khunkamchoo, S. L. Roberts and S. S. F. Wong, *Macromolecules*, 2006, **39**, 7250-7257.
38. E. Sergeeva, J. Kopilov, I. Goldberg and M. Kol, *Chem. Commun.*, 2009, 3053-3055.
39. H. Glasner and E. Y. Tshuva, *Inorg. Chem.*, 2014, **53**, 3170-3176.
40. J. Balsells, P. J. Carroll and P. J. Walsh, *Inorg. Chem.*, 2001, **40**, 5568-5574.
41. A. Yeori, S. Groysman, I. Goldberg and M. Kol, *Inorg. Chem.*, 2005, **44**, 4466-4468.
42. H.-Y. Chen, H.-Y. Tang and C.-C. Lin, *Polymer*, 2007, **48**, 2257-2262.
43. M. H. Chisholm, J. Gallucci and K. Phomphrai, *Chem. Commun.*, 2003, 48-49.
44. M. H. Chisholm, J. C. Gallucci and K. Phomphrai, *Inorg. Chem.*, 2004, **43**, 6717-6725.
45. M.-W. Hsiao, G.-S. Wu, B.-H. Huang and C.-C. Lin, *Inorg. Chem. Commun.*, 2013, **36**, 90-95.
46. V. Poirier, T. Roisnel, J.-F. Carpentier and Y. Sarazin, *Dalton Trans.*, 2009, 9820-9827.
47. D. C. Aluthge, B. O. Patrick and P. Mehrkhodavandi, *Chem. Commun.*, 2013, **49**, 4295-4297.
48. D. C. Aluthge, E. X. Yan, J. M. Ahn and P. Mehrkhodavandi, *Inorg. Chem.*, 2014, **53**, 6628-6836.
49. A. F. Douglas, B. O. Patrick and P. Mehrkhodavandi, *Angew. Chem. Int. Ed.*, 2008, **120**, 2322-2325.
50. S. Ghosh, R. R. Gowda, R. Jagan and D. Chakraborty, *Dalton Trans.*, 2015, **44**, 10410-10422.
51. N. Maudoux, T. Roisnel, J.-F. Carpentier and Y. Sarazin, *Organometallics*, 2014, **33**, 5740-5748.

52. N. Maudoux, T. Roisnel, V. Dorcet, J.-F. Carpentier and Y. Sarazin, *Chem. Eur. J.*, 2014, **20**, 6131-6147.
53. K. M. Osten, D. C. Aluthge and P. Mehrkhodavandi, *Dalton Trans.*, 2015, **44**, 6126-6139.
54. A. Pietrangelo, M. A. Hillmyer and W. B. Tolman, *Chem. Commun.*, 2009, 2736-2737.
55. I. Yu, A. Acosta-Ramírez and P. Mehrkhodavandi, *J. Am. Chem. Soc.*, 2012, **134**, 12758-12773.
56. A. Kapelski and J. Okuda, *J. Polym. Sci., Part A: Polym. Chem.*, 2013, **51**, 4983-4991.
57. C. Bakewell, A. J. P. White, N. J. Long and C. K. Williams, *Inorg. Chem.*, 2013, **52**, 12561-12567.
58. P. Horeglad, P. Kruk and J. Pécaut, *Organometallics*, 2010, **29**, 3729-3734.
59. S. Gendler, S. Segal, I. Goldberg, Z. Goldschmidt and M. Kol, *Inorg. Chem.*, 2006, **45**, 4783-4790.

Chapter 4

2-(Aminomethyl)piperidine based initiators for lactide polymerisation

Chapter 4: 2-(Aminomethyl)piperidine based initiators for lactide polymerisation

4.1 Introduction

The complexes described in Chapter 3 were trialled for their activity in the ring opening polymerisation of lactide. Lactide was chosen as a model to demonstrate activity towards ROP and allow for stereocontrol to also be assessed. Generally, polymerisations were attempted using *rac*-lactide to demonstrate any stereocontrol initiators impart on the polymer, however, *L*-lactide was also used on occasion to highlight and rationalise kinetics and the resultant stereochemistry. Unless otherwise stated, the lactide used was singly recrystallised to align with industrial processes. Common practice for investigations in academia is to sublime the monomer prior to use to remove trace impurities, typically lactic acid and water, to reduce side reactions and protect moisture sensitive initiators. However, this is an energy intensive process, being carried out at high vacuum and temperature (for *rac*-lactide,~110 °C), making it impractical on a large scale.

A range of conditions were employed and these were related to the nature of the metal complex and the desired outcome of the polymerisation. Typical solution polymerisations were carried out in dry toluene at 80 °C at a concentration of [LA] = 0.69 M. Where possible, more industrially relevant melt conditions were applied without solvent at 130 °C. Lower temperature polymerisations, for the purpose of maximising stereocontrol, were carried out in CH_2Cl_2.Various monomer:initiator ratios were applied to yield polymer of different chain lengths and to test the effect of initiator loading.

The term initiator is used to describe the active metal species involved in a living polymerisation and this usage is widely supported by the literature. However, it is noted that initiator does not fully cover the role of the active species, which also facilitates propagation of the polymer chain. For immortal polymerisations, the term pre-catalyst is used to recognise the reduction of active species concentration.

4.2 Polymerisations with monophenolate complexes

4.2.1 Aluminium monophenolate complexes

The polymerisation of the aluminium monophenolate complexes, Al(**1**-**6**)Me_2, were carried out in toluene at 80 °C at a [LA]:[I]:[BnOH] ratio of 100:1:1 (Table 4.1). The addition of co-initiator was necessary to generate the active initiator *in-situ*, with an alkoxide being more efficient at insertion into the carbonyl bond and this is common practice in the literature.[1-5] The literature complex Al(**A**)Me_2 based upon 2-(aminomethyl)pyridine was also trialled for the ROP of LA (Chapter 3, Figure 3.5); a cationic version of this initiator has previously been tested for ethylene polymerisation activity.[6] Polymerisation data for Al(**B**)Me_2 have previously been reported by Carpentier *et al* and this result is shown in Table 4.1 for comparison.[7] For the majority of entries, it can be seen that reasonable conversion is achieved within 24 hours.

Conversion is observed to decrease with increasing steric bulk (relative to ^{t}Bu) in the *ortho* position as shown by Al(**2**/**3**)Me_2 which are the adamantyl and trityl substitutions respectively. In comparison to Al(**1**)Me_2 (77%, 16 hrs), Al(**2**)Me_2 (72%, 24 hrs) and Al(**3**)Me_2 (40%, 48 hrs) attain a lower conversion despite longer reaction times. In comparison, the literature based initiators, Al(**A**-**B**)Me_2, achieve reasonable conversion after 16 hours, which matches the bulk of their *ortho* substituents (R^1 = ^{t}Bu or $SiPh_3$ respectively). It is noted that the ROP with Al(**B**)Me_2 is carried out at 100 °C which accounts for the relatively high conversion despite a relatively bulky *ortho* substituent.[7] In a direct comparison between Al(**1**)Me_2 and Al(**A**)Me_2, it can be observed that the pyridine based initiator is relatively slower (52%, 16 hrs).

Groups smaller than ^{t}Bu in the *ortho* position {Al(**4**-**6**)Me_2, R^1 = Me, OMe or H} are found to require a quarter of the time to reach similar conversions (for example, R^1 = Me, 77%, 4 hrs). There is not a significant difference between having a Me or H *ortho* substituent (R^1 = H, 80%, 4 hrs). On comparing the activity of different *ortho* substituent, it is clear that this position has a profound effect on the polymerisation for these imino monophenolate Al(III) initiators. This effect can be rationalised by examination of the crystal structures which show this position to be parallel to the Al(III) centre.

Table 4.1: Polymerisation data for *rac*-LA with Aluminum monophenolates, Al(**1**-**13**)Me_2 and Al(**A**)Me_2. Al(**B**)Me_2 data from literature.[7]

Initiator	t /h	Conv. /%[a]	P_r[b]	$M_{n,theo}$[c]	M_n[d]	Đ[d]
Al(**A**)Me_2	16	52	0.33	7600	6650	1.11
Al(**B**)Me_2*	16	78	0.50	11200	7300	1.24
Al(**1**)Me_2	16	77	0.73	11200	6400	1.06
Al(**2**)Me_2	24	72	0.39	10500	8450	1.05
Al(**3**)Me_2	48	40	0.60	5850	2800	1.18
Al(**4**)Me_2	4	77	0.72	11200	5800	1.18
Al(**5**)Me_2	4	65	0.65	9450	5700	1.20
Al(**6**)Me_2	4	80	0.65	11600	7400	1.29
Al(**7**)Me_2	16	50	0.31	7300	5100	1.11
Al(**11**)Me_2	8	42	0.58	6150	3850	1.11
Al(**12**)Me_2	2	73	0.28	10600	5700	1.19
Al(**13**)Me_2	24	84	0.48	12200	7850	1.21

Conditions: [LA]:[I]:[BnOH]=100:1:1, 80 °C, toluene. [a.] Determined *via* ^{1}H NMR spectroscopy. [b] P_r is the probability of heterotactic enchainment, determined *via* homonuclear decoupled ^{1}H NMR spectroscopy, [c.] Theoretical molecular weight calculated from conversion {100 × (Conv. × 144.13) + 108.14} (rounded to the nearest 50), [d] Determined from GPC (in THF) referenced against polystyrene standards with a correction factor of 0.58 applied.*100°C with HO^{i}Pr co-initiator.[7]

The benzyl capped initiator, Al(**7**)Me_2 (R^3 = Bn), was also assessed for activity in the ROP of *rac*-LA. The results are similar to that of Al(**A**/**1**)Me_2, which have identical aryl substituents of ^{t}Bu (50%, 16 hrs). The corresponding bicyclic form of this initiator, Al(**11**)Me_2 was observed to be more active for the ROP of *rac*-LA despite the presence of bulky groups (42%, 8 hrs). This initiator is anticipated to contain a tetrahedral centre which may account for the increased activity. A further increase in activity is realised for the structural isomer, Al(**12**)Me_2 (73%, 2 hrs). This initiator, also assumed to be based on a tetrahedral Al(III) centre, which is further away from the bicyclic ring which may decrease the steric crowding around the active site. In comparison, the pyridine based initiator, Al(**13**)Me_2, demonstrates an activity more

comparable to Al(**A**/**1**-**2**)Me_2 (84%, 24 hrs). This initiator was shown to be five coordinate in the solid-state similar to that of the imino-monophenolate complexes. The coordination of the pyridine ring evidently has a great effect on catalytic activity.

Each of the imino-monophenolate Al(III) initiators display modest stereocontrol over the polymerisation of *rac*-LA with both isotactic {Al(**A/2**)Me_2} and heterotactic {Al(**1,3-6**)Me_2} PLA being formed. For the piperidine based initiators, the general preference is heterotacticity {P_r < 0.69, for Al(**4**)Me_2, Figure 4.1} with only the adamantyl *ortho* substituent {Al(**2**)Me_2} causing a switch to slight isoselectivity (P_r < 0.39). Interestingly, employment of the *t*-butyl substituted aryl ring with a pyridine based pendant arm {Al(**A**)Me_2} yielded the opposite stereocontrol compared to the piperidine arm {Al(**1**)Me_2} as well as being less active over the 24 hour period. As discussed in Chapter 3, both Al(**A**/**1**)Me_2 have very similar solid state structures with comparable metric data. The origin of the polymerisation difference may be due to electronics; the different donation capabilities of the piperidine and pyridine nitrogen atoms towards the aluminium centre. One might also expect the pyridine structure to be less flexible, making it less efficient at accommodating the incoming monomer.

The capped imino-monophenolate initiator, Al(**7**)Me_2, has an isotactic preference similar to that of Al(**A**)Me_2 (P_r = 0.31). The switch in stereocontrol relative to that of Al(**1**)Me_2 could be an indication of a different coordination of the ligand-to-metal, with a four coordinate centre possible for Al(**7**)Me_2. The stereocontrol of the bicyclic monophenolates is observed to be either isotactic {Al(**12**)Me_2} or atactic {Al(**13**)Me_2}. A moderate degree of control is exerted by Al(**12**)Me_2 (P_r = 0.28), with the *iii* tetrad dominating the spectrum, indicating isoselectivity (Figure 4.2). The stereocontrol is lost due to coordination of pyridine ring for Al(**13**)Me_2 (P_r = 0.48).

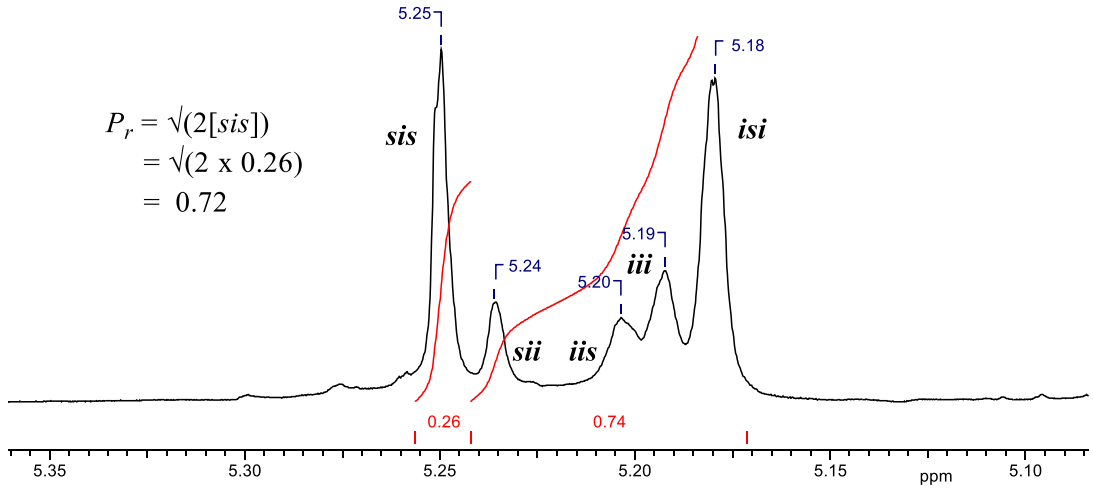

Figure 4.1: ^{1}H NMR ($CDCl_3$, 400MHz) homonuclear decoupled spectrum of heterotactic PLA synthesised from solution polymerisation with Al(**4**)Me_2 (Toluene, 80 °C).

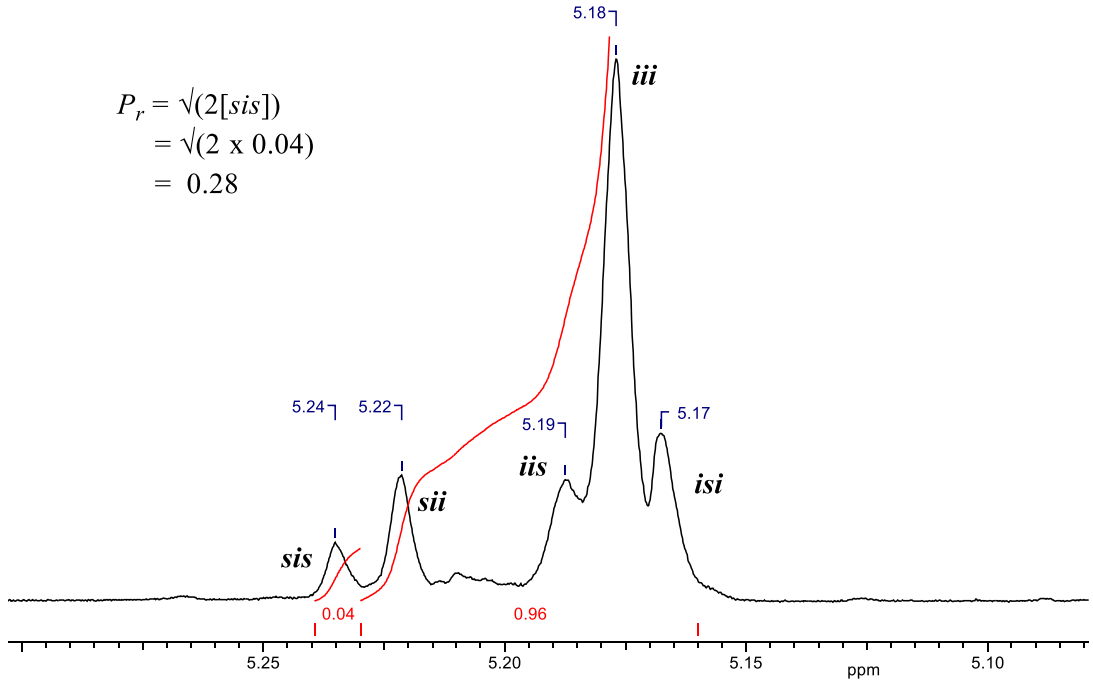

Figure 4.2: ^{1}H NMR ($CDCl_3$, 400MHz) homonuclear decoupled spectrum of isotactic PLA synthesised from solution polymerisation with Al(**12**)Me_2 (Toluene, 80 °C).

Kinetic experiments were carried out on the majority of aluminium imino-monophenolate initiators on a lab scale (1 g) with each time point representing a batch experiment. Only four points have been collected for each initiator but the results are unambiguous and self-consistent, however it is noted that greater confidence would be gained through carrying out more experiments. The polymerisation of lactide commonly proceeds with a first order dependence on the consumption of [LA]. This dependence is tested by plotting the natural logarithm of concentration against time, as indicated by the derivation of the integrated first order rate law (Equation 1). It is assumed that the concentration and order of the initiator are constant throughout the polymerisation. Therefore a linear plot of $\ln([LA]_0/[LA]_t)$ against time demonstrates a first order reaction with respect to [LA] and yields the apparent rate constant, k_{app}, from the gradient.

$$\frac{d[LA]}{dt} = -k_p[LA][Al]$$

$$\frac{d[LA]}{dt} = -k_{app}[LA], \qquad k_{app} = k_p[Al]$$

$$\frac{1}{[LA]}d[LA] = -k_{app}\,dt$$

$$\ln\left(\frac{[LA]_0}{[LA]_t}\right) = k_{app}t$$

Equation 1: Derivation of the integrated first order rate law for consumption of [LA].

The results of these studies are shown in Figures 4.3-4.4 and Table 4.2. All plots show a linear relationship, as expected for a *pseudo* first order dependence on lactide concentration. It can be seen that Al(**1**)Me_2 is ever so slightly faster than Al(**A**)Me_2 in solution at 80 °C though there is an overlap in the error intervals {k_{app} = (96.0 ± 5.46) × 10^{-3} hr^{-1} and (79.7 ± 11.46) × 10^{-3} hr^{-1} respectively}. A difference in rate between these two systems might be expected based upon their different stereocontrol preference; having a heterotactic bias means polymerisation might be anticipated to be faster with *rac*-LA. The results also indicate an induction period for polymerisation with Al(**A**)Me_2, and this may suggest the formation of the active alkoxide species is slower.

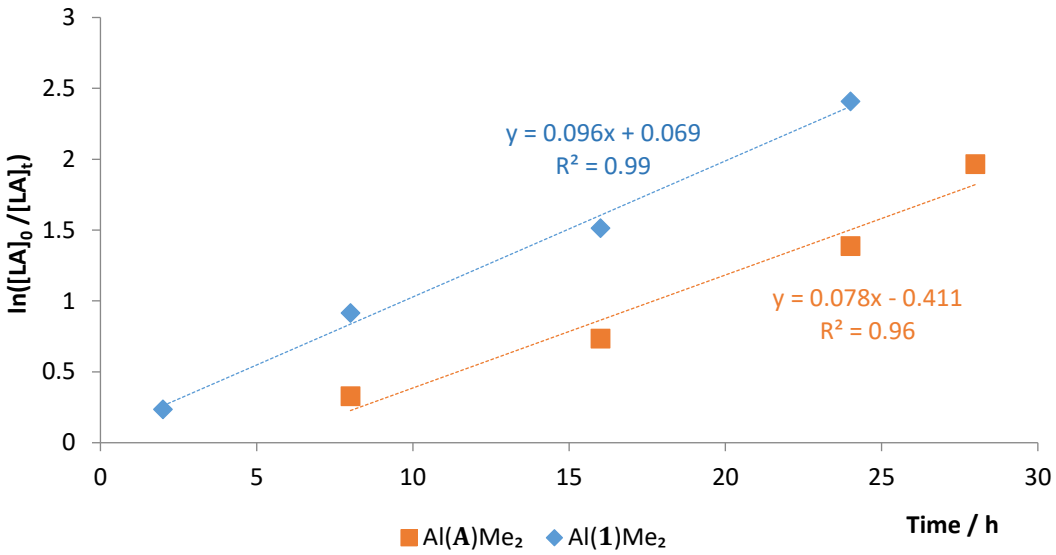

Figure 4.3: Semi-logarithmic plot for the solution polymerisation of Al(**A**/**1**)Me_2. Conditions: Toluene, 80°C, [LA]:[Al(**A**/**1**)Me_2]:[BnOH] = 100:1:1.

The rate constants for Al(**4**-**6**)Me_2 quantifies the effect of reducing steric bulk at the *ortho* position. Relative to Al(**1**)Me_2, the initiators are observed to be ca. 3-5 times faster. When the *ortho* groups are Me or H, as for Al(**4**)Me_2 and Al(**6**)Me_2 respectively, the fastest rates are observed, with these initiators having very similar activities {k_{app} = (344 ± 11.6) × 10^{-3} hr^{-1} and (340 ± 18.9) × 10^{-3} hr^{-1} respectively}. When R^1 is an OMe group {Al(**5**)Me_2}, the rate is reduced {(228± 14.2) × 10^{-3} hr^{-1}}. This could be due to an electronic effect whereby the methoxy group donates electron density into the aryl ring, ultimately decreasing the Lewis acidity of the aluminium centre.

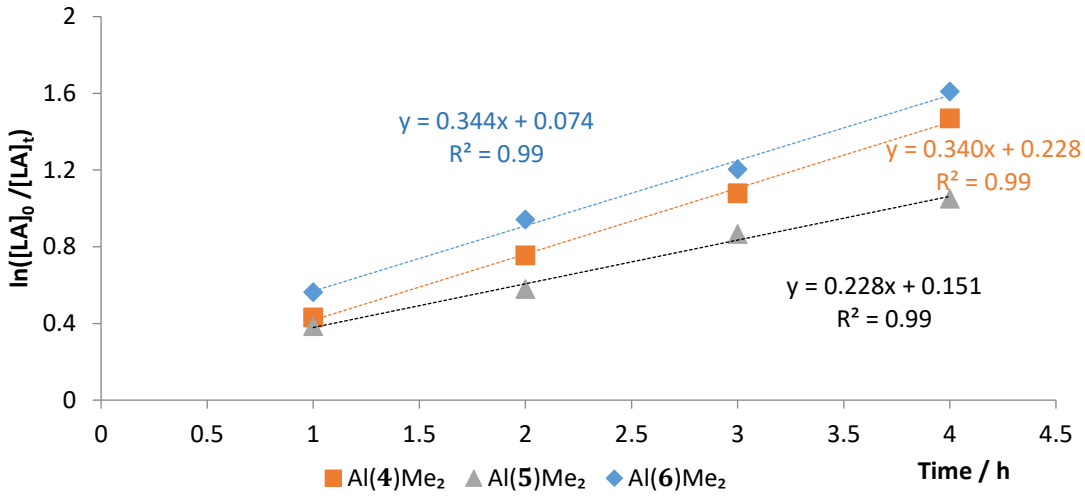

Figure 4.4: Semi-logarithmic plot for the solution polymerisation of Al(**4-6**)Me_2. Conditions: Toluene, 80°C, [LA]:[Al(**4-6**)Me_2]:[BnOH] = 100:1:1.

Table 4.2: Rate constants, k_{app}, for solution ROP of Al(**A/1/4-6**)Me_2.

Initiator	k_{app} ($\times 10^{-3}$ hr^{-1})
Al(A)Me_2	79.7 ± 11.4
Al(1)Me_2	96.0 ± 5.46
Al(4)Me_2	344 ± 11.6
Al(5)Me_2	228 ± 14.2
Al(6)Me_2	340 ± 18.9

Conditions: [LA]:[Al]:[BnOH] = 100:1:1, 80 °C, Toluene.

$$M_{n,theo} = \frac{[LA]}{[I]}\{Conversion, \% \times M_n(LA)\} + M_n(End\ groups)$$

Equation 2: Calculation of theoretical molecular weight based on conversion.

The molecular weight of polymers are consistently reduced with respect to the theoretical molecular weight, calculated based on BnO- and H- end groups (Equation 2). This could be due to impurities in the monomer initiating an increased number of chains or the presence of side reactions. It is also possible that two chains are being initiated per metal centre. The distribution of molecular weights are relatively narrow

(Đ < 1.29) with a broadening being observed on reduction of the *ortho* steric bulk as shown for Al(**4-6**)Me_2. A plot of molecular weight against conversion for Al(**1**)Me_2 further shows the controlled nature of these polymerisations with a positive linear correlation between these two parameters (Figure 4.5). There is also very little change to the polymer polydispersity as the reaction progresses. Similar plots were acquired for each set of kinetic experiments and the R^2 values are generally high (> 0.95).

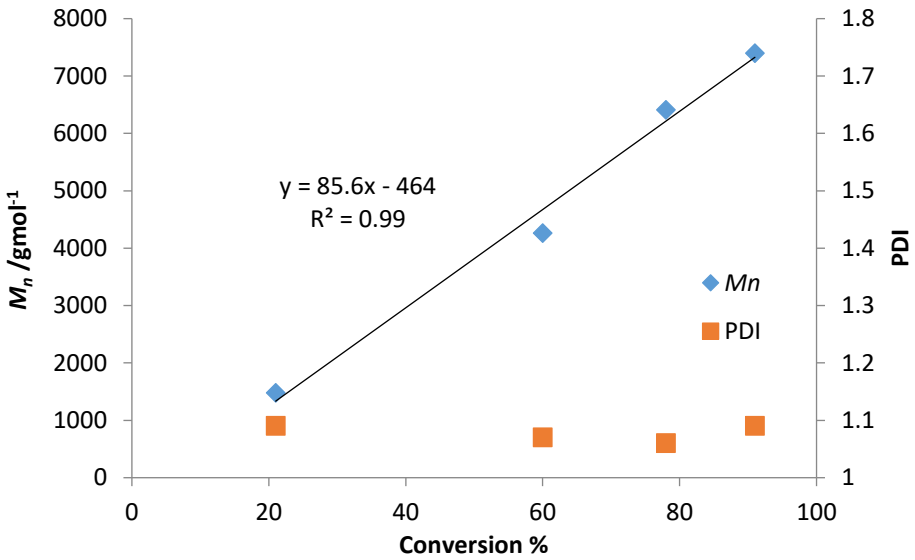

Figure 4.5: M_n and M_w/M_n against conversion for solution polymerisation of Al(**1**)Me_2.

The molecular weight properties of these polymers was further investigated *via* MALDI-ToF (Matrix Assisted Laser Desorption Ionisation-Time of Flight). For the polymer samples analysed, BnO- and H- were observed to be the end groups as expected. In all cases, this technique revealed two polymeric series indicating the presence of undesirable transesterification reactions {Figure 4.6, Al(**A**)Me_2}. The results of MALDI-ToF analysis are summarised in Table 4.3. In some instances Al(**4-5/13**)Me_2, there is also evidence of cyclic oligomers, as deduced by a lack of end group. The spectrum of Al(**13**)Me_2 is not symmetrical, with a tail towards low molecular weight indicating the presence of oligomers.

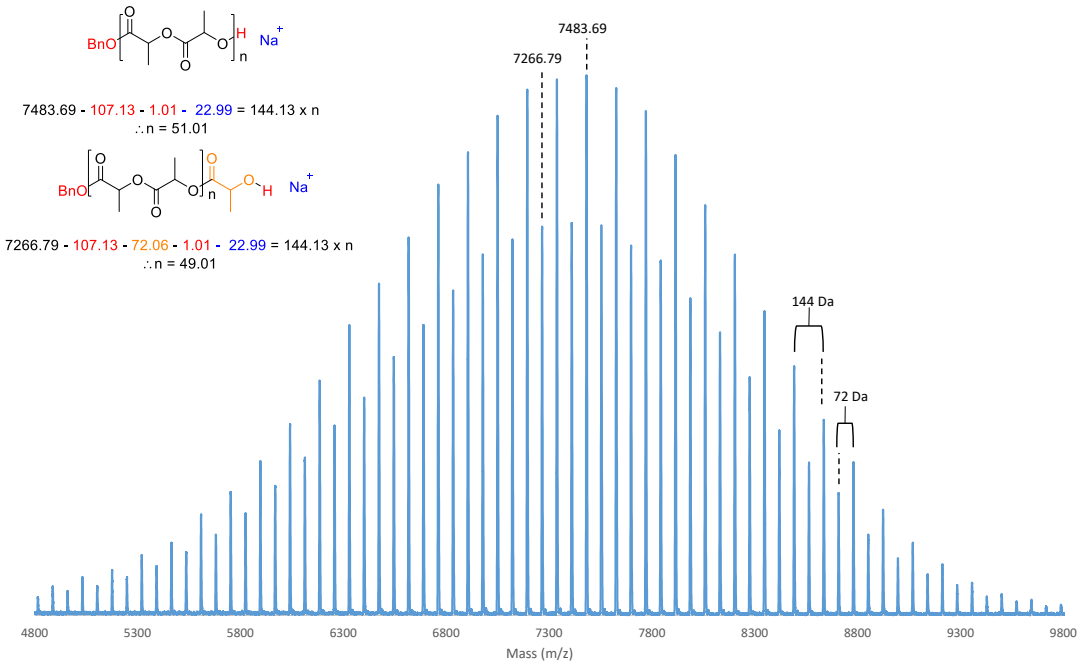

Figure 4.6: MALDI-ToF of PLA from solution polymerisation with Al(**A**)Me$_2$.

Table 4.3: Summary of MALDI-ToF analysis of Al(III) monophenolates.

Initiator	Series	M_p /Da	End groups	n
Al(A)Me$_2$	1$_{Main}$	7483.69	BnO-, H-, Na$^+$	51
	2$_{Trans}$	7266.76	BnO-, H-, Na$^+$	49.5
Al(1)Me$_2$	1$_{Main}$	8633.68	BnO-, H-, Na$^+$	59
	2$_{Trans}$	8705.75	BnO-, H-, Na$^+$	59.5
Al(4)Me$_2$	1$_{Main}$	7483.84	BnO-, H-, Na$^+$	51
	2$_{Trans}$	7411.79	BnO-, H-, Na$^+$	50.5
	3$_{Cyclic}$	4347.60	Na$^+$	30
Al(5)Me$_2$	1$_{Main}$	7769.68	BnO-, H-, Na$^+$	53
	2$_{Trans}$	7698.71	BnO-, H-, Na$^+$	52.5
	3$_{Cyclic}$	5357.41	Na$^+$	37
Al(7)Me$_2$	1$_{Main}$	6042.13	BnO-, H-, Na$^+$	41
	2$_{Trans}$	5970.65	BnO-, H-, Na$^+$	40.5
Al(13)Me$_2$	1$_{Main}$	8924.14	BnO-, H-, Na$^+$	61
	2$_{Trans}$	8852.01	BnO-, H-, Na$^+$	60.5
	3$_{Cyclic}$	3630.72	Na$^+$	25

Conditions: [LA]:[Al]:[BnOH] = 100:1:1, 80°C, Toluene

4.2.2 Magnesium/Zinc imino-monophenolate complexes

Initial polymerisations of Mg(**A/1**)$_2$ and Zn(**1**)$_2$ were carried out in solution at 80 °C. In the first instance, an equivalence of benzyl alcohol was added to initiate the polymerisation (Table 4.4). For all initiators, high conversion was achievable within one hour, with the Zn(II) initiator displaying greater activity. These activities are improved compared to Al(**A**/**1**)Me$_2$, despite the absence of an active site. The PLA afforded by these initiators was essentially atactic. There was very little difference between the activity and stereocontrol exerted by Mg(**A**)$_2$ and Mg(**1**)$_2$. For the Mg(II) initiators, it was found that the addition of excess alcohol facilitated the rapid depolymerisation and as a consequence these polymerisations were not quenchable hinting at immortal characteristics. It is also noted that the Mg(**A**)$_2$ initiator initially afforded pale yellow polymer which became red on prolonged exposure to air. This has previously been observed and attributed to a ligand oxidation process.[8]

The resultant molecular weight of polymerisations carried out in solution in the presence of benzyl alcohol demonstrates a reasonable correlation with the predicted value. In each case, the distribution of molecular weights is also narrow illustrating a controlled polymerisation (Đ < 1.10). Further analysis *via* MALDI-ToF gives comparable values of molecular weight. This technique also shows the presence of polymer chains with a BnO- end group in each case. For both Mg(II) complexes, there is a minor series due to undersirable transesterification side reactions {for Mg(**1**)$_2$, Figure 4.7}. For Mg(**A**)$_2$, there is also evidence of intramolecular transesterification with low molecular weight cyclic oligomers being observed. The data collected for Zn(**1**)$_2$ is of low quality but demonstrates an one series separated by 144 g mol^{-1} suggesting the absence of transesterification.

The literature example, Zn(**A**)$_2$, was shown to be active in the absence of co-initiator under solution conditions.[9] Under similar conditions, the activity of the initiators is observed to be much reduced within the same time frame, with Zn(**1**)$_2$ remaining the most active. Despite the low conversion, relatively high molecular weights are afforded with the distribution of polymer chain remaining narrow. It is unclear if initiation is due to a ligand phenoxy group or monomer impurities.

Table 4.4: Polymerisation data for *rac*-LA with magnesium/zinc monophenolates, Mg/Zn(**1**)$_2$. Zn(**A**)$_2$ data from the literature.[9]

Initiator	Time /h	Conv. %[e]	P_r[f]	$M_{n,theo}$[g]	M_n[h]	Đ[h]
Mg(**A**)$_2$[a]	1	81	0.53	11800	10000	1.10
Mg(**1**)$_2$[a]	1	72	0.51	10500	8300	1.10
Zn(**1**)$_2$[a]	0.5	97	0.55	14100	11150	1.11
Mg(**A**)$_2$[b]	1	25	0.52	3700	48450	1.19
Mg(**1**)$_2$[b]	1	17	0.53	2600	28800	1.14
Zn(**A**)$_2$[*]	4	94	-	13900	20500	1.39
Zn(**1**)$_2$[b]	0.5	41	0.58	6000	82300	1.28
Mg(**A**)$_2$[c]	0.15	64	0.66	27750	19500	1.57
Mg(**1**)$_2$[c]	0.5	61	0.61	26450	23250	1.81
Mg(**1**)$_2$[d]	0.5	74	0.60	32050	17400	1.49
Zn(**1**)$_2$[c]	0.15	49	0.59	21250	42300	1.37
Zn(**1**)$_2$[d]	0.1	69	0.57	29900	32250	1.18

Conditions: [a][LA]:[I]:[BnOH] = 100:1:1, 80 °C, toluene [b][LA]:[I] = 100:1, 80 °C, toluene, [c][LA]:[I] = 300:1, 130 °C, [d][LA]:[I]:[BnOH] = 300:1:1, 130 °C, [e] Determined *via* ^{1}H NMR spectroscopy. [f] P_r is the probability of heterotactic enchainment, determined *via* homonuclear decoupled ^{1}H NMR spectroscopy. [g] Theoretical molecular weight calculated from conversion {[LA]/[BnOH] × (Conv. × 144.13) + 108.14} (rounded to the nearest 50), [h] Determined from GPC (in THF) referenced against polystyrene standards with a correction factor of 0.58 applied.[*] 70 °C, 3ml toluene.[9]

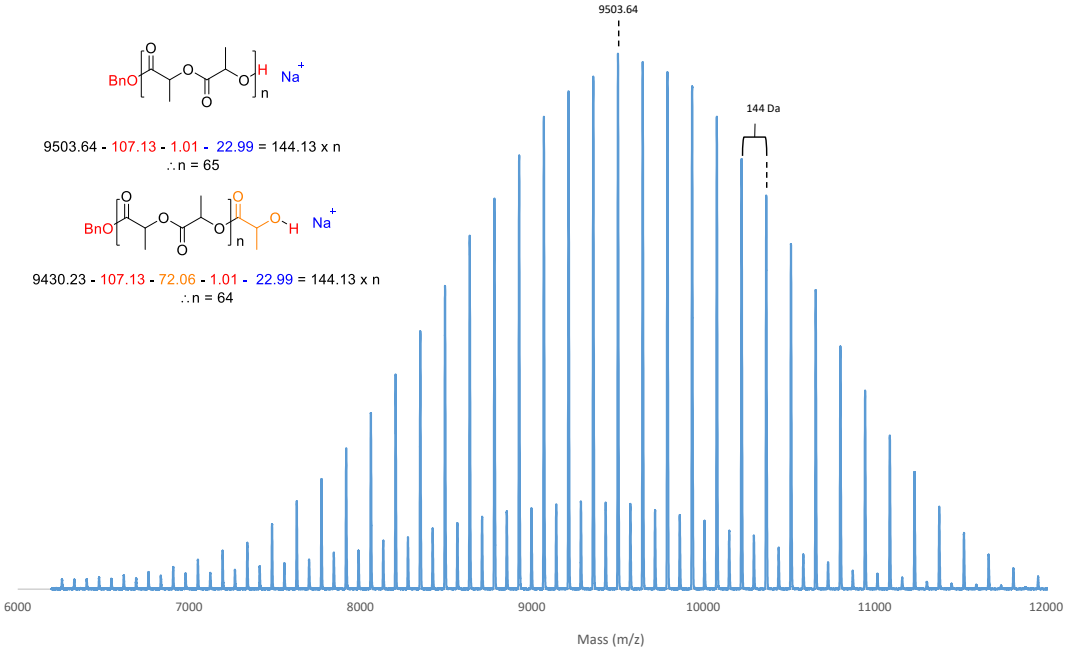

Figure 4.7: MALDI-ToF of PLA from solution polymerisation with Mg(**1**)$_2$.

Table 4.5: Summary of MALDI-ToF analysis of PLA from Mg(**A/1**)$_2$ and Zn(**1**)$_2$.

Initiator	Series	M_p /Da	End groups	n
Mg(A)$_2$	1_{Main}	11521.78	BnO-, H-, Na^+	79
	2_{Trans}	11017.88	BnO-, H-, Na^+	75.5
	3_{Cyclic}	3901.15	-	27
Mg(1)$_2$	1_{Main}	9503.64	BnO-, H-, Na^+	65
	2_{Trans}	9430.23	BnO-, H-, Na^+	64.5
Zn(1)$_2$	1_{Main}	11517.0	BnO-, H-, Na^+	79

Conditions: [LA]:[I]:[BnOH] = 100:1:1, 80°C, toluene.

The activity of these initiators was also tested under solvent free conditions (130 °C, [LA]:[I] = 300:1). The polymerisations with Mg(**A/1**)$_2$ were hampered by the insolubility of these complexes in the molten LA. As a consequence, the reaction time is lengthened. The molecular weight control afforded by these initiators is poor, with lower than theoretical values being realised, even in the absence of BnOH. However, slight heterotacticity is demonstrated by these Mg(II) systems (P_r = 0.60 - 0.66). Better results are achieved by employing Zn(**1**)$_2$, which is observed to be fully soluble in the LA melt. At this higher temperature, the reaction in the absence of benzyl alcohol

achieves higher conversion, indicating the initiation step may have a thermal barrier, perhaps due to insertion of a ligand phenoxy group. Under these conditions, a higher molecular weight is afforded than predicted, indicating less chains are initiated relative to the amount of metal centres. The addition of BnOH yields PLA with a good agreement of molecular weight with that predicted.

Due to the absence of co-initiator groups or vacant active sites on the metal centres, the mechanism for these polymerisations is anticipated to be an activated monomer mechanism (Figure 4.8). In the presence of benzyl alcohol, this co-initiator is expected to initiate polymerisation by attack of the LA carbonyl group. In the absence of co-initiator, and assuming no impurities are present, a ligand phenoxide is suggested to ring open the monomer.

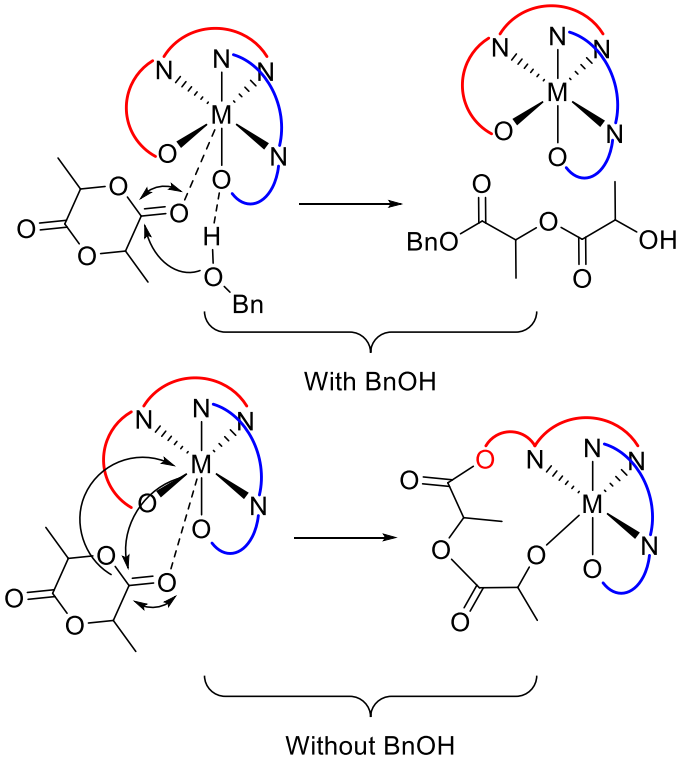

Figure 4.8: Initiation mechanisms for M(**A**/**1**)$_2$, where M = Mg(II) or Zn(II).

4.3 Polymerisations with aluminium bis/tris-phenolate complexes

4.3.1 Aluminium bicyclic bisphenolate complexes

The bicyclic motif offers tridentate coordination affording four coordinate tetrahedral aluminium complexes. Polymerisation data for with this structural motif is shown in Table 4.6. Reasonable conversion is obtained after 24 hours at 80°C in toluene at a 100:1:1 monomer to initiator to benzyl alcohol. For this series, there is no clear trend between activity and aryl substituents but the degree of stereocontrol is broadly the same, with a very slight heterotactic preference in most cases. The molecular weight of these polymers is reasonable for the respective conversions and good weight control is demonstrated by a narrow molecular weight distribution.

The similarity in conversion and stereocontrol between different initiators is likely a reflection on the sterically unhindered metal centre. For the obtained solid-state structures, a tetrahedral centre Al(III) was demonstrated. The greatest contribution to steric hindrance is likely to be from the bicyclic ring and the *ortho* position, R^3, of the second aryl ring, which is ^{t}Bu in the majority of initiators. The first aryl ring bearing *ortho* position, R^1, is tilted slightly directing this group away from the aluminium methyl bond. Hence, similar contributions towards the steric hindrance are anticipated for each initiator.

MALDI-ToF analysis was carried out on PLA from a range of Al(III) bicyclic bisphenolate {for Al(**14**)Me, Figure 4.9, Table 4.7). In all cases, a series relating to BnO- and H- capped PLA is observable, expected from the operation a coordination insertion mechanism. It was revealed that low steric bulk on one of the aryl rings afforded one major distribution with a peak spacing of 144 g mol^{-1} with minimal evidence of transesterifcation {Al(**14**/**15**/**17**/**19**}Me}. Of these initiators, Al(**15**)Me (R^1 = R^2 = Br) demonstrated an increased degree of transesterification, the complex representing a relative increase in steric bulk. A further increase in steric bulk, as observed for Al(**21**-**22**)Me_2 (R^1 = ^{t}Bu or Ad respectively) also increases the amount of transesterification. For Al(**21**)Me, the MALDI-ToF spectrum contains one symmetrical main series separated by 72 g mol^{-1}. However, for Al(**22**)Me, identical spacing is observed as well as a severe tail to low molecular weight and evidence of

cyclic species. From these results, it is suggested that an increased initiator steric bulk reduces the control of molecular weight during ROP.

Table 4.6: Polymerisation data for *rac*-LA with aluminum bicyclic bisphenolates, Al(**14**-**22**)Me.

Initiator	**Conv. %**[a]	P_r[b]	$M_{n,theo}$[c]	M_n[d]	Đ[d]
Al(**14**)Me	72	0.51	10500	9200	1.04
Al(**15**)Me	72	0.54	10500	10250	1.04
Al(**16**)Me	85	0.56	12350	12650	1.05
Al(**17**)Me	62	0.58	9000	7300	1.06
Al(**18**)Me	62	0.60	9000	7100	1.04
Al(**19**)Me	63	0.55	9200	7200	1.09
Al(**20**)Me	73	0.47	10600	7250	1.10
Al(**21**)Me	90	0.50	13100	9650	1.21
Al(**22**)Me	71	0.53	10350	7400	1.07

Conditions: [LA]:[I]:[BnOH]=100:1:1, 80 °C, toluene, 24 hours. [a.] Determined *via* ^{1}H NMR spectroscopy. [b] P_r is the probability of heterotactic enchainment, determined *via* homonuclear decoupled ^{1}H NMR spectroscopy, [c.] Theoretical molecular weight calculated from conversion {100 × (Conv. × 144.13) + 108.14} (rounded to the nearest 50), [d] Determined from GPC (in THF) referenced against polystyrene standards with a correction factor of 0.58 applied.

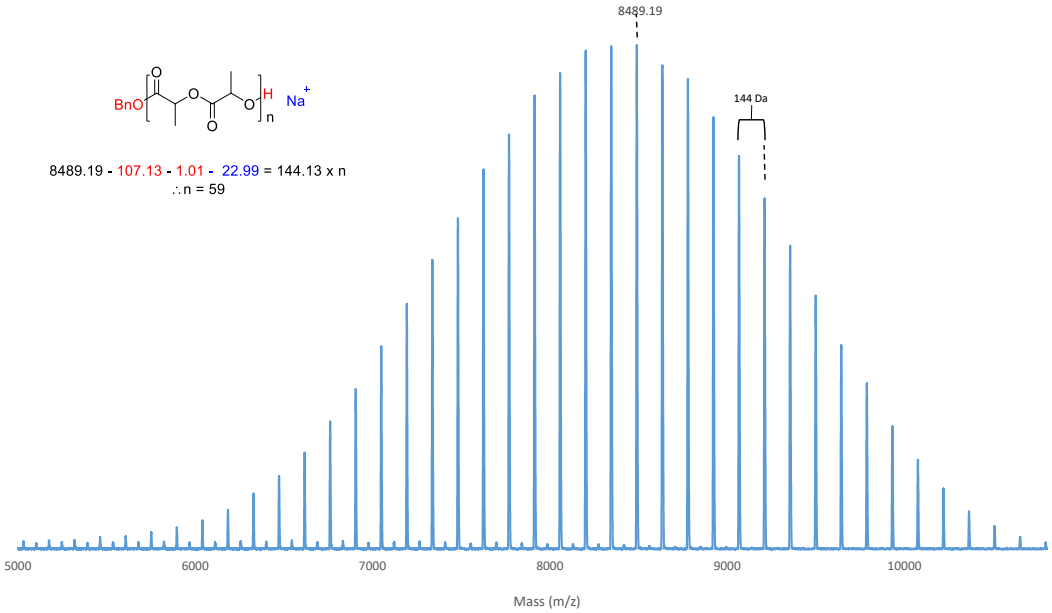

Figure 4.9: MALDI-ToF of PLA from solution polymerisation with Al(**14**)Me.

Table 4.7: Summary of MALDI-ToF analysis of PLA from bisphenolate bicyclic Al(III) complexes.

Initiator	Series	M_p /Da	End groups	n
Al(14)Me	1_{Main}	8489.19	BnO-, H-, Na^+	59
Al(15)Me	1_{Main}	9644.62	BnO-, H-, Na^+	66
	2_{Trans}	9715.45	BnO-, H-, Na^+	66.5
Al(17)Me	1_{Main}	8486.20	BnO-, H-, Na^+	58
Al(19)Me	1_{Main}	8492.41	BnO-, H-, Na^+	58
Al(21)Me	1_{Main}	8205.32	BnO-, H-, Na^+	56
	2_{Trans}	8275.56	BnO-, H-, Na^+	56.5
Al(22)Me	1_{Main}	9785.43	BnO-, H-, Na^+	67
	2_{Trans}	9893.00	BnO-, H-, Na^+	67.5
	2_{Cyclic}	3770.78	Na^+	26

Conditions: [LA]:[Al]:[BnOH] = 100:1:1, 80°C, toluene.

4.3.2 Aluminium salalen complexes

For the related salalen complexes Al(**26**-**30**)Me, the solution polymerisation was found to be relatively slow at 80°C. Several days were required to achieve reasonable conversion in each case (Table 4.8). These complexes feature a trigonal bipyramidal aluminium centre and relatively bulky groups which undoubtedly contributes to the low activity of these initiators, hindering coordination of the monomer. For Al(**26**-**28**)Me (R^1 = ^{t}Bu, Me and Ad respectively), 10 days were required to reach a reasonable conversion (88-89%). Relieving the steric congestion by reducing the size of the *ortho* substituent was shown to increase activity for this system. For Al(**29**-**30**)Me, this is achieved by introducing Cl- and H- moieties respectively, both on the salan side of the ligand. For these initiators, the ROP activity is increased with 2 days being sufficient to reach moderate to high conversion (69-79%). The increased activity may also be related to the presence of electron withdrawing groups which can increase the Lewis acidity of the Al(III) centre.

The stereochemical preference of this system is found to vary with the aryl substituents. For Al(**26**)Me, where the both aryl rings contain ^{t}Bu groups, a slight tendency towards isotactic PLA was demonstrated (P_r = 0.37) whereas Al(**28**)Me, with an adamantyl *ortho* groups, has a heterotacticity bias (P_r = 0.69). These tendencies are opposite to that observed for the related half salens, Al(**1**/**2**)Me_2.When the groups on the salen ring are methyl, there is only a weak heterotactic bias (P_r = 0.56-62). Accordingly, the homonuclear ^{1}H NMR spectrum for polymer derived from Al(**26**)Me shows the dominance of the *iii* tetrad (Figure 4.10). Conversely, the heterotactic bias of Al(**28**)Me is shown by the relative magnitude of the *isi* and *sis* tetrads (Figure 4.11). Incorporation of electron withdrawing aryl groups into the initiators {Al(**29**-**30**)Me}leads to a reduction in stereocontrol, generally affording atactic PLA.

Table 4.8: Polymerisation data for *rac*-LA with aluminum salalen complexes, Al(**26-30**)Me_2. Al(**D**)O^{i}Pr data from the literature.[10]

Initiator	Time /h	Conv. %[a]	P_r[b]	$M_{n,theo}$[c]	M_n[d]	Đ[d]
Al(**26**)Me	240	88	0.37	12800	13150	1.06
Al(**26**)Me	24	16	-	-	-	-
Al(**27**)Me	240	88	0.56	12800	11900	1.08
Al(**27**)Me	120	42	0.62	6150	4650	1.07
Al(**28**)Me	240	89	0.68	12900	11200	1.05
Al(**29**)Me	48	69	0.57	10050	7150	1.06
Al(**30**)Me	48	79	0.58	11500	7550	1.10
Al(**D**)O^{i}Pr*	24	78	0.18	11500	11200	1.07

Conditions: [LA]:[I]:[BnOH]=100:1:1, 80 °C, toluene. [a.] Determined *via* ^{1}H NMR spectroscopy. [b] P_r is the probability of heterotactic enchainment, determined *via* homonuclear decoupled ^{1}H NMR spectroscopy, [c.] Theoretical molecular weight calculated from conversion {100 × (Conv. × 144.13) + 108.14} (rounded to the nearest 50), [d] Determined from GPC (in THF) referenced against polystyrene standards with a correction factor of 0.58 applied.* [LA]:[I]=100:1.[10]

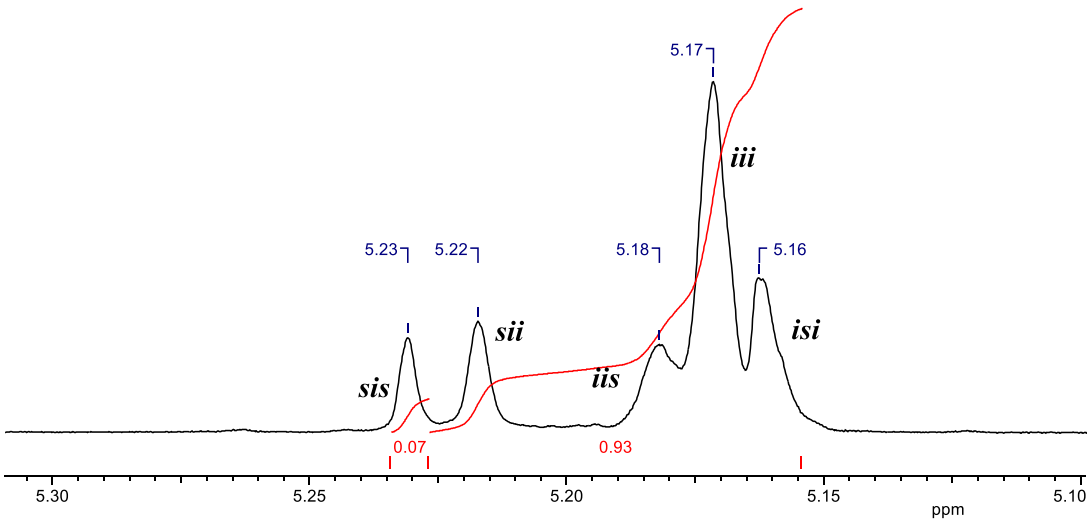

Figure 4.10: ^{1}H NMR ($CDCl_3$, 400MHz) homonuclear decoupled spectrum of PLA synthesised from solution polymerisation with Al(**26**)Me.

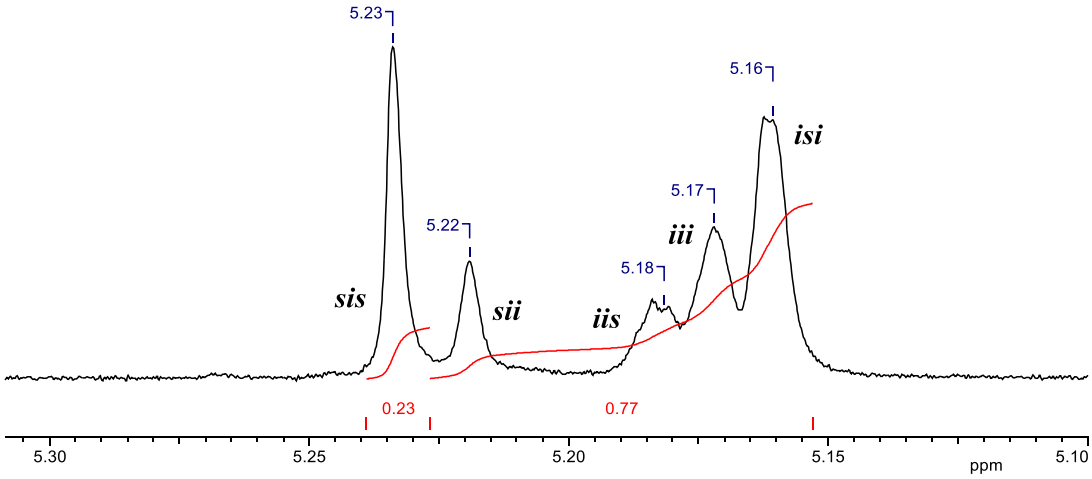

Figure 4.11: ^{1}H NMR ($CDCl_3$, 400MHz) homonuclear decoupled spectrum of heterotactic PLA synthesised from solution polymerisation with Al(**28**)Me.

The molecular weight values recorded show reasonable agreement with conversion and a narrow molecular weight distribution is observed in all cases. A slight broadening is observed for Al(**30**)Me, for which one *ortho* position is a H moiety (Đ = 1.10). The polymer end groups were confirmed by MALDI-ToF analysis for Al(**26-30**)Me, with the expected BnO- and H- groups being observable. There is, however, a degree of transesterification for all samples, as demonstrated by a minor series with a spacing of ~72 g mol^{-1}. This is likely due to the extended reaction time necessary to achieve these conversions. In support of this, the observed degree of transesterification is reduced for Al(**29**-**30**)Me, which are also the more active Al(III) salalen initiators {for Al(**29**)Me, Figure 4.12}.

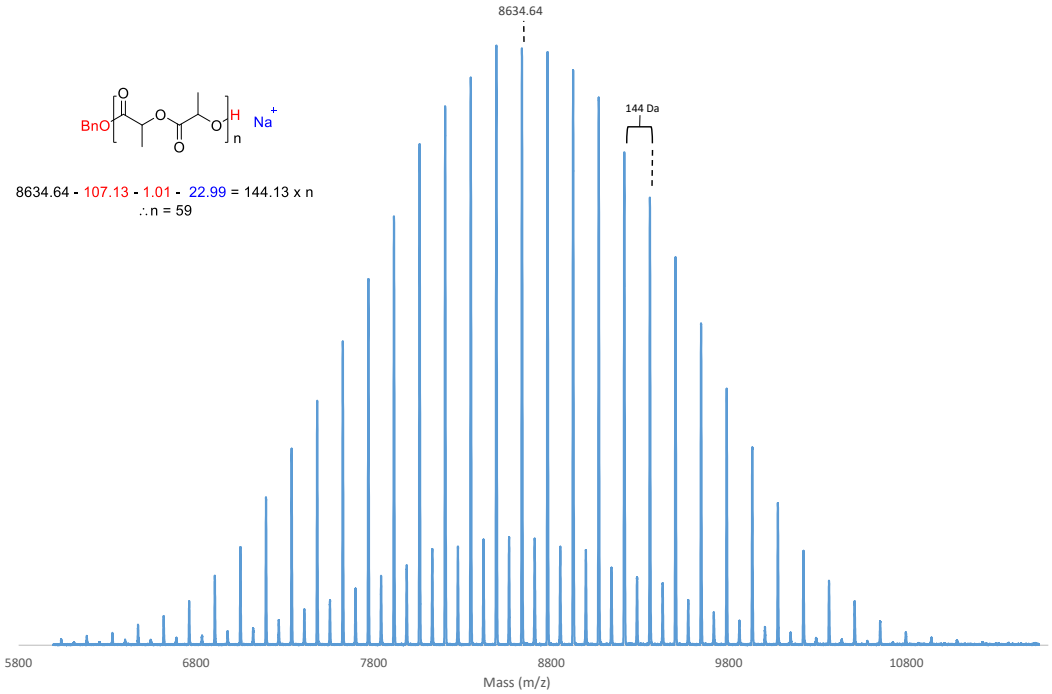

Figure 4.12: MALDI-ToF of PLA from solution polymerisation with Al(**29**)Me.

Table 4.8: Summary of MALDI-ToF analysis of PLA from salalen Al(III) complexes.

Initiator	Series	M_p /Da	End groups	n
Al(26)Me	1_{Main}	10939.12	BnO-, H-, Na^+	75
	2_{Trans}	11011.21	BnO-, H-, Na	75.5
Al(27)Me	1_{Main}	10653.37	BnO-, H-, Na^+	73
	2_{Trans}	10438.51	BnO-, H-, Na^+	71.5
Al(28)Me	1_{Main}	10654.1	BnO-, H-, Na^+	73
	2_{Trans}	10727.05	BnO-, H-, Na^+	73.5
Al(29)Me	1_{Main}	8634.64	BnO-, H-, Na^+	59
	2_{Trans}	8707.18	BnO-, H-, Na^+	59.5
Al(30)Me	1_{Main}	9068.59	BnO-, H-, Na^+	62
	2_{Trans}	9139.25	BnO-, H-, Na^+	62.5

Conditions: [LA]:[Al]:[BnOH] = 100:1:1, 80°C, toluene.

Comparison of a related chiral aluminium salalen system (Chapter 3, Figure 3.27) reveals Al(**26-30**)Me to be much slower initiators for *rac*-LA polymerisation.[10] The 2-(aminomethyl)pyrrolidine based initiators, Al(**D**)O^{i}Pr, achieved reasonable conversion within 24 hours. It is worth noting that these initiators described in the previous investigation generally have bulky aryl groups in conjunction with electron withdrawing, smaller groups.[10] The stereocontrol for Al(**D**)O^{i}Pr is also improved relative to the 2-(aminomethyl)piperidine based initiators. Both isotactic tendencies (P_m = 0.82) and heterotactic tendencies (P_r = 0.77) are reported. In a direct comparison, the same aryl substituents of ^{t}Bu on the salen fragment and Cl salan aryl {Al(**29**)Me} substituents were found to require 48 hours to achieve moderate conversion and yielded a very slight heterotactic bias (P_r = 0.57). This would suggest the change in nitrogen based heterocycle size is a crucial factor in determining the polymerisation outcome for this system. As the two systems have an identical wrapping of ligand around the metal, the ring size is the only difference and the extra carbon atom evidently has a profound impact on both polymerisation rate and stereocontrol.

4.3.3 Aluminium salan bisphenolate complexes

The salan complexes, Al(**31-33**)O^{i}Pr, were observed to have a different ligand arrangement to that of the salalens, Al(**26-30**)Me, while maintaining a five coordinate metal centre (Figure 4.13). The application of these to the polymerisation of *rac*-lactide demonstrated a dramatic change in activity and selectivity for such a small ligand modification (Table 4.9). These alkoxide complexes required no co-initiator and yielded white polymer. For comparison, Al(**31**)Me was also trialled for ROP activity and for contrast, the methylated salan, Al(**35**)Me, is also included in this series. The latter initiators are used with a benzyl alcohol co-initiator.

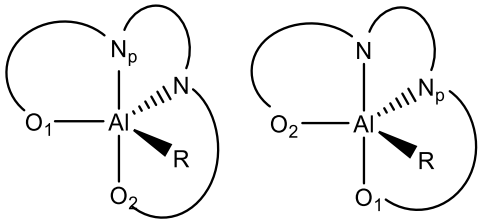

Al(**26-27**)Me
Al(**35**)Me
Al(**D**)Et

Al(**31-33**)O^{i}Pr

Figure 4.13: Observed structural isomerism for salalen and salan Al(III) complexes.

Table 4.9: Polymerisation data for LA with Aluminum salan complexes, Al(**31**-**33**)O^{i}Pr, Al(**31**/**35**)Me. Al(**E**)O^{i}Pr data from the literature.[11]

Initiator	Time /h	Conv. %[e]	P_m[f]	$M_{n,theo}$[g]	M_n[h]	Đ[h]
Al(**31**)Me[a]	3	65	0.75	9450	8600	1.06
Al(**31**)O^{i}Pr[b]	3	66	0.79	9550	9700	1.04
Al(**31**)O^{i}Pr[b,c]	3	82	-	11850	14800	1.04
Al(**31**)O^{i}Pr[b,d]	120	60	0.83	8700	9150	1.04
Al(**32**)O^{i}Pr[b]	0.5	76	0.59	11000	10400	1.03
Al(**33**)O^{i}Pr[b]	0.3	78	0.35	11300	11150	1.06
Al(**35**)Me[a]	120	49	0.64	7150	10900	1.13
Al(**E**)O^{i}Pr[*]	120	72	0.18	10450	9450	1.07

Conditions: Toluene, 80 °C. [a] [LA]:[I]:[BnOH]=100:1:1, [b] [LA]:[I]:=100:1, [c] *L*-LA, [d] CH_2Cl_2, 25°C, [e] Determined *via* ^{1}H NMR spectroscopy. [f] P_m is the probability of isotactic enchainment, determined *via* homonuclear decoupled ^{1}H NMR spectroscopy with deconvolution and averaging of the five equations, [g] Theoretical molecular weight calculated from conversion {100 × (Conv. × 144.13) + $M_{n(ROH)}$} (rounded to the nearest 50), [h] Determined from GPC (in THF) referenced against polystyrene standards with a correction factor of 0.58 applied.[*] Toluene, 80 °C. [LA]:[I]=100:1.[11]

Encouragingly, both the alkoxide and aluminium methyl species (with BnOH co-initiator) yielded similar results, further suggesting Al(**31**)Me contains related isomeric forms in solution rather than impurities, dimeric species or binuclear species. For the series Al(**31**-**33**)O^{i}Pr, reasonable conversion is achieved in the space of hours rather than days and it is now possible to distinguish between initiators in terms of activity. Al(**31**)O^{i}Pr is observed to have an 80 fold increase in activity compared the related salalen, Al(**26**)Me, yet is found to be the least active in this series presumably due to steric bulk of two *ortho* ^{t}Bu groups. Al(**32**)O^{i}Pr is almost 500 times more active than the related salalen, Al(**27**)Me, also being faster than Al(**31**)O^{i}Pr due to reduced steric bulk offered by the *ortho* methyl group. When the a pair of *tert*-butyl groups are exchanged for chloro groups {Al(**33**)O^{i}Pr}, there is a further observed improvement in rate which is attributed to the electron withdrawing nature of these groups making the aluminium centre more Lewis acidic, i.e. more susceptible towards lactide coordination. The origin of the activity enhancement for the aluminium salans is unproven. It is postulated that it may be directly related to the change in the complex structure, indicating a switch to an initiator that can more readily accommodate incoming monomer units despite the presence of bulky groups. The position of the amine hydrogen could also imply a role in the polymerisation, possessing the ability to hydrogen bond to monomer and perhaps stabilise intermediate states in the coordination insertion mechanism. When this hydrogen is replaced with a methyl group, affording Al(**35**)Me, the geometry reverts back to that of the aluminium salalens and the extent of polymerisation is similarly reduced. This implies that the change to the salan functionality is not solely responsible for the improvement in catalysis. Compared to literature Al(III) salans, Al(**31**-**33**)O^{i}Pr are found to be relatively more active.[2, 11, 12] For comparison, Al(**E**)O^{i}Pr requires 5 days to achieve comparable conversion under the same conditions (Table 4.9) which is more similar to the activity of Al(**35**)Me.

The stereocontrol of the secondary amine salans are also enhanced relative to the related salalens. The highest control of tacticity is achieved by Al(**31**)O^{i}Pr, which displays strong isotactic bias in toluene at 80°C (P_m = 0.79). This can be slightly improved upon by reaction at room temperature in CH_2Cl_2 affording PLA with a melt temperature comparable to that of PLLA homopolymer after five days (P_m = 0.83, T_m = 177°C, Figures 4.14 - 4.16). For this sample, the ^{1}H homonuclear decoupled

spectrum highlights the isotactic tendency, with a small contribution form the *sis* resonance and dominance of the *iii* resonance (Figure 4.14). Closer inspection of the remaining tetrads suggest a 1:1:1 ratio of *sii*, *iis*, and *isi* which implies the formation of alternating stereoblocks of PLLA and PDLA.[13] The ligands in these systems are chiral, therefore an enantiomorphic site control mechanism (SCM) is anticipated. In this polymerisation pathway, each enantiomer of the initiator has a preference towards incoming monomer chirality and incorporation of the "incorrect" monomer can lead to a polymer exchange event. While being a correction method for incorrect insertions, polymer exchange can also reduced overall tacticity depending on the frequency of their occurrence. The $^{13}C\{^{1}H\}$ NMR spectrum also illustrates the high degree of isotacticity, with a small resonance due to *isi* tetrad (Figure 4.15).

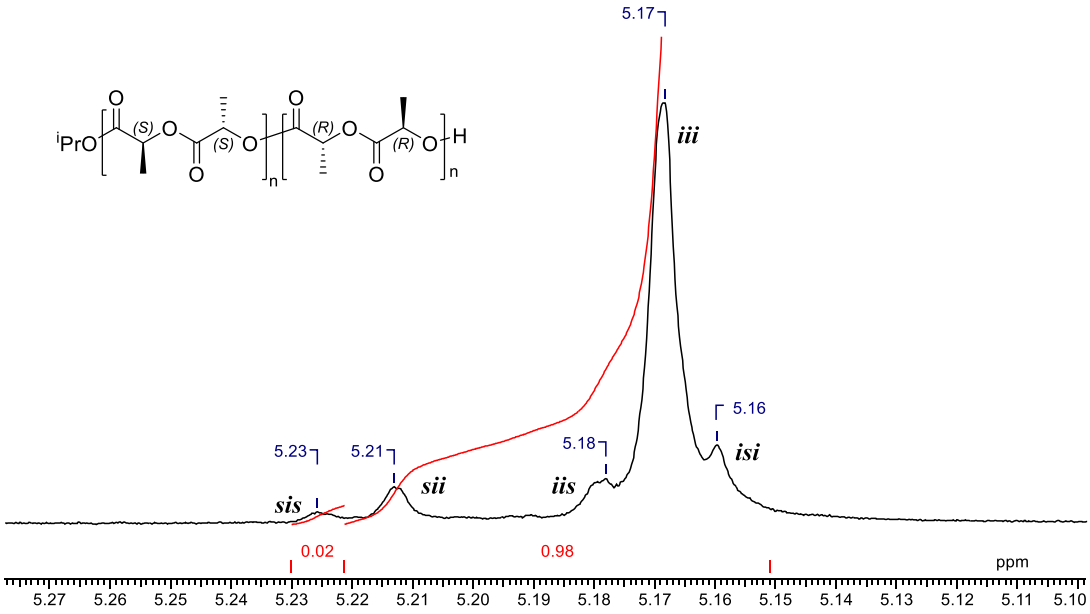

Figure 4.14: ^{1}H NMR ($CDCl_3$, 400MHz) homonuclear decoupled spectrum of isotactic PLA synthesised from solution polymerisation with Al(**31**)O^{i}Pr (CH_2Cl_2, 25°C).

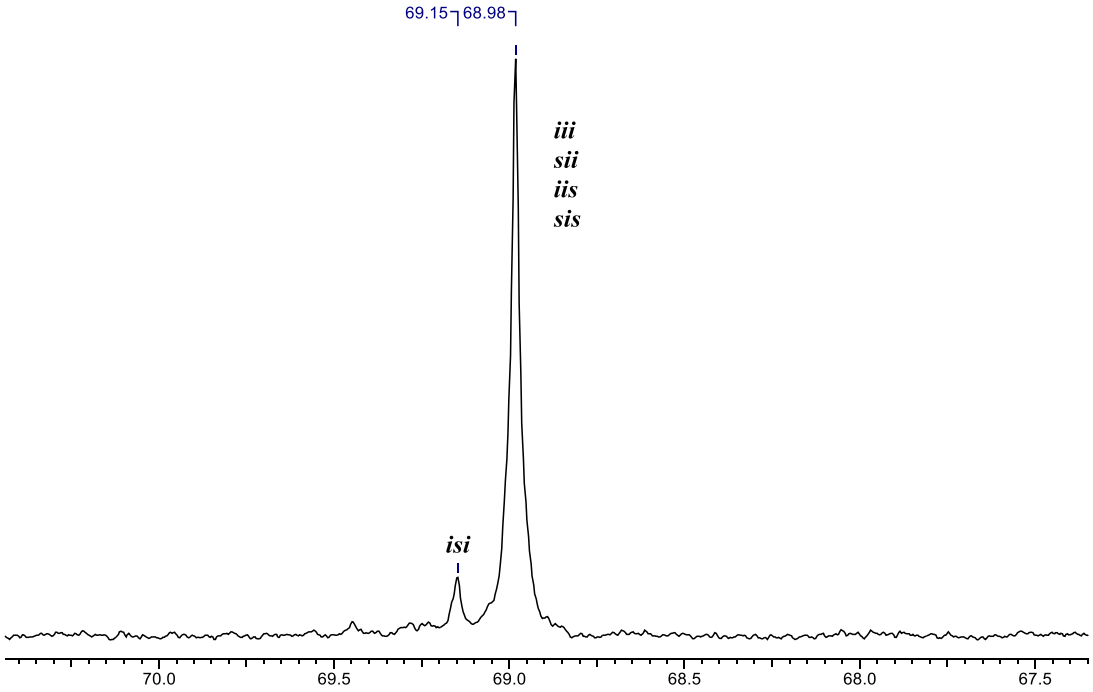

Figure 4.15: $^{13}C\{^{1}H\}$ NMR ($CDCl_3$, 100MHz) spectra of methine region for PLA from Al(**31**)O^{i}Pr (CH_2Cl_2, 25°C).

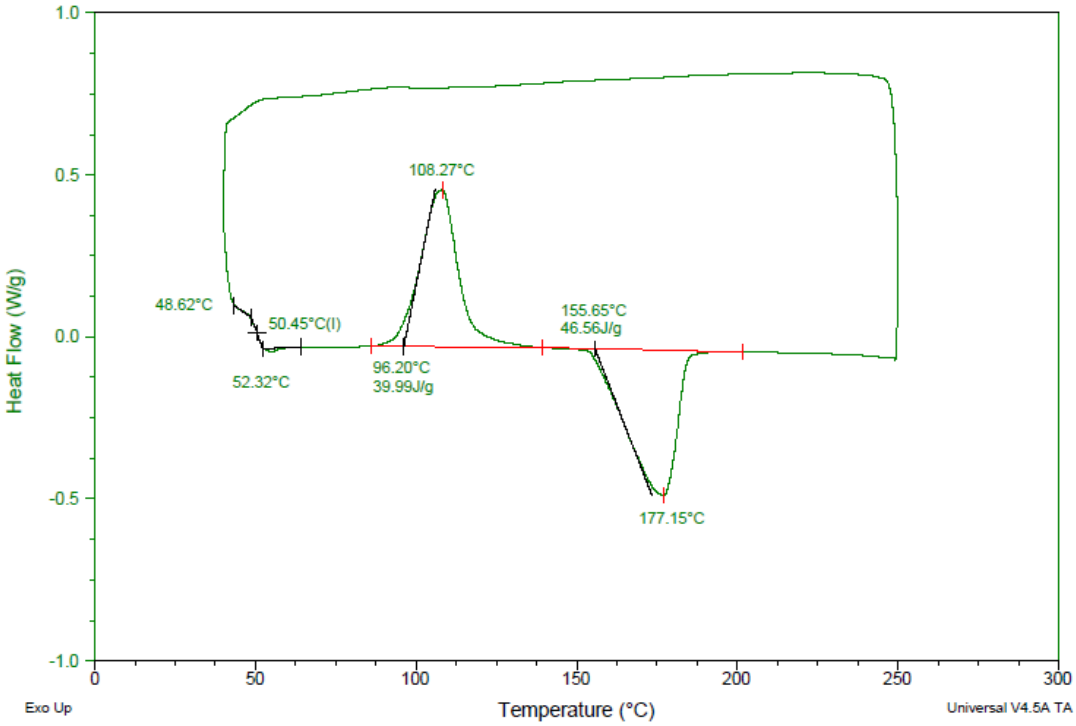

Figure 4.16: DSC scan of PLA from Al(**31**)O^{i}Pr (CH_2Cl_2, 25°C).

The stereochemical preference for Al(**32**)O^{i}Pr is observed to be slightly isotactic contrasting to the related salalen, Al(**27**)Me, which had a slight heterotactic preference. For the chloro containing complex, Al(**33**)O^{i}Pr, a switch in stereocontrol is observed with a slight heterotactic bias being observed (P_r = 0.65).

Kinetic analysis was carried out on Al(**31**-**33**)Me. A plot of the semi-logarithmic concentration:time graph demonstrates a first order dependence on [LA] in all cases (Figures 4.17 - 4.18). The apparent rate constants, $k_{app,}$ increases as the steric bulk is reduced such that ^{t}Bu < Me < Cl. For the ^{t}Bu aryl substituents, k_{app} = (0.37 ± 0.01) hr^{-1} and for the ^{t}Bu/Cl aryl groups, there is a 15 fold increase in rate with k_{app} = (5.52 ± 0.47) hr^{-1} (Table 4.10). The apparent rate constant of propagation is comparable between the solution ROP with Al(**31**)O^{i}Pr and solvent free polymerisation with Al(**33**)O^{i}Pr.

The polymerisation of Al(**31**)O^{i}Pr with *L*-lactide was also assessed (Figure 4.17). With the enantiopure monomer, the apparent rate constant was observed to increase {k_{app} = (0.58 ± 0.06) hr^{-1}} which is a typical observation for an isotactic initiator following a SCM. The relative ratio of rate constants between *rac* and *L*-LA can be used to deduce the P_m value from a kinetic perspective assuming the initiator order is the same for both systems.[4] This calculation yields a P_m value of 0.78 which is in good agreement with the tacticity measured by homonuclear decoupled ^{1}H NMR spectroscopy. For the *L*-LA polymerisations, there is also no evidence of epimerisation of the chiral centres.

$$P_m = \frac{k_L}{2k_{rac}}$$

Equation 3: Kinetic evaluation of P_m based on relative rate constants for *rac*- and *L*-LA.[4]

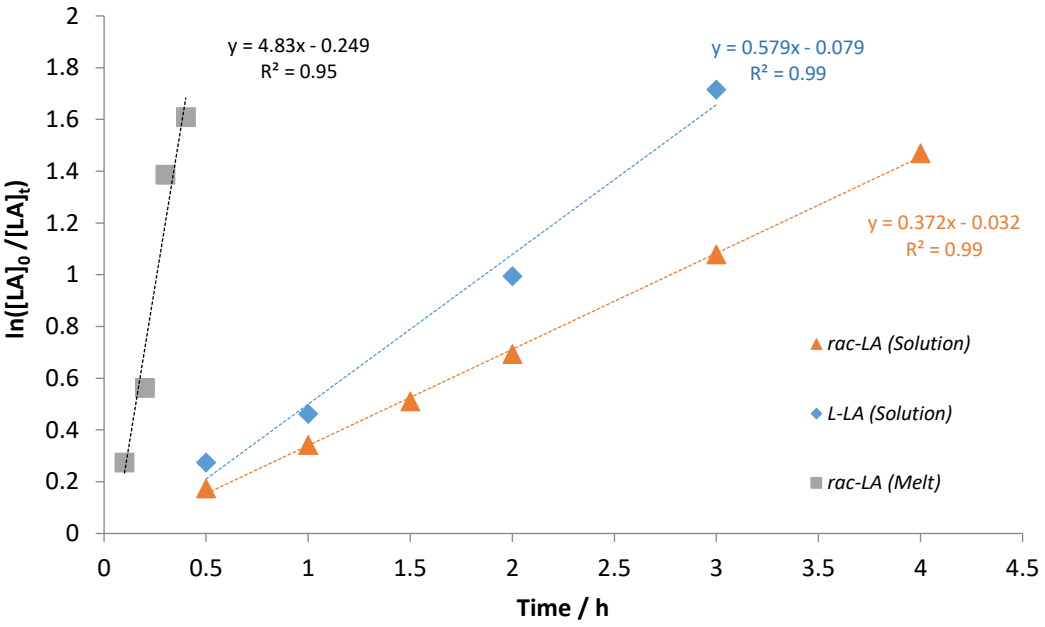

Figure 4.17: Semi-logarithmic plot for the solution polymerisation of Al(**31**)O^{i}Pr. Conditions: Toluene, 80°C, [LA]:[Al(**31**)O^{i}Pr]: = 100:1 / Solvent-free, 130 °C, [LA]:[Al(**31**)O^{i}Pr]: = 300:1.

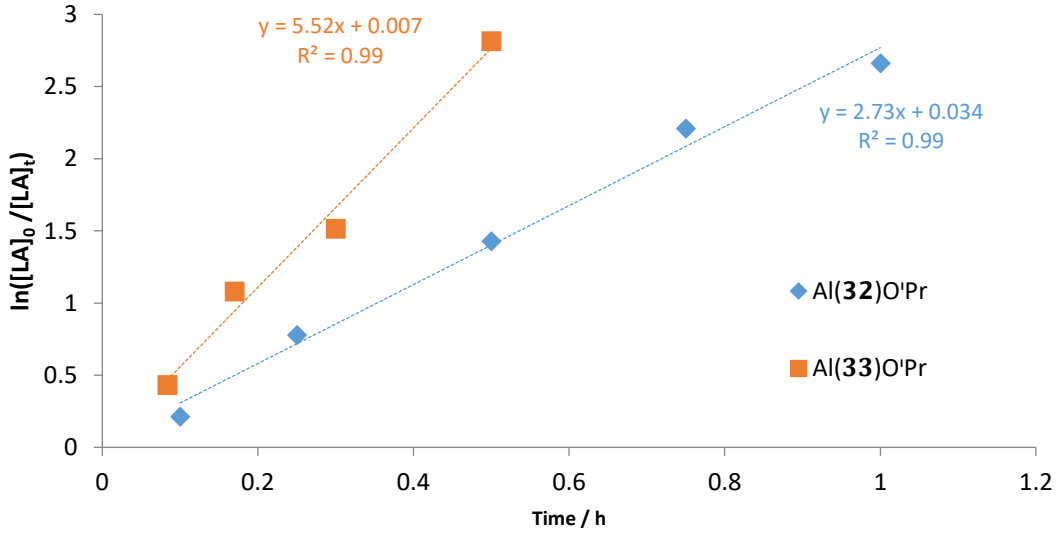

Figure 4.18: Semi-logarithmic plot for the solution polymerisation of Al(**32-33**)O^{i}Pr. Conditions: Toluene, 80°C, [LA]:[Al(**32-33**)O^{i}Pr]: = 100:1.

Table 4.10: Rate constants for polymerisation of LA with initiators Al(**31-33**)O^{i}Pr

Initiator	k_{app} (hr^{-1})
Al(**31**)O^{i}Pr[a]	0.37 ± 0.01
Al(**31**)O^{i}Pr[b]	0.58 ± 0.05
Al(**32**)O^{i}Pr[a]	2.73 ± 0.16
Al(**33**)O^{i}Pr[a]	5.52 ± 0.47
Al(**31**)O^{i}Pr [c]	4.83 ± 0.81

Conditions: [a][LA]:[I]:=100:1, 80 °C, toluene, *rac*-LA
[b][LA]:[I]:=100:1, 80 °C, toluene, *L*-LA
[c][LA]:[I]:=300:1, 130 °C, solvent free, *rac*-LA

For all solution polymerisations carried out with the initiators Al(**31-33**)O^{i}Pr, good molecular weight control is observed with good correlation between experimental and theoretical values. The distribution of polymer weights is also found to be narrow (Đ ≤ 1.05). Molecular weight is also shown to have a linear relationship with conversion (Figures 4.19 - 4.20), further demonstrating a controlled polymerisation. Comparatively, the polymerisation with the methylated salan, Al(**35**)Me, yielded a broadened distribution (Đ = 1.13) indicating a slightly less controlled process.

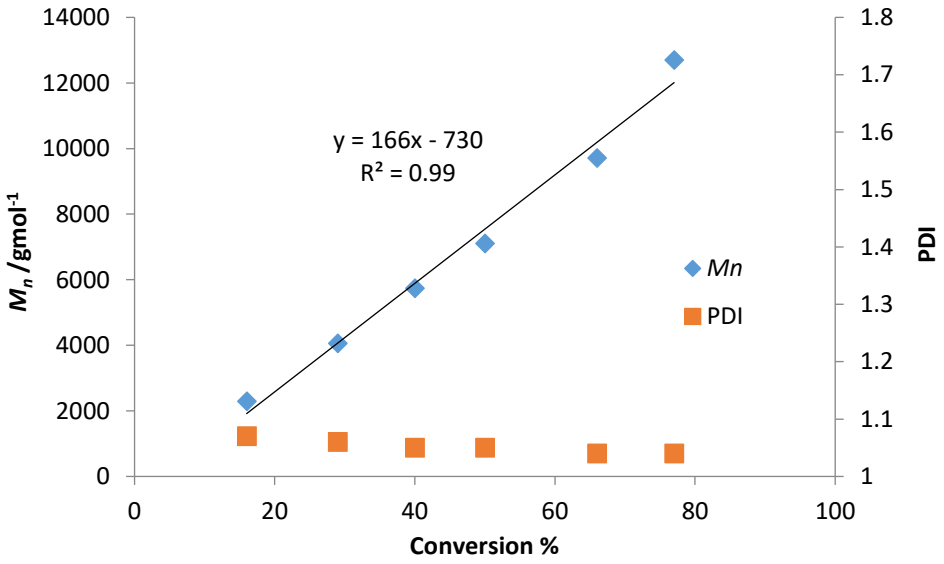

Figure 4.19: M_n and M_w/M_n against conversion for solution polymerisation of Al(**31**)O^{i}Pr.

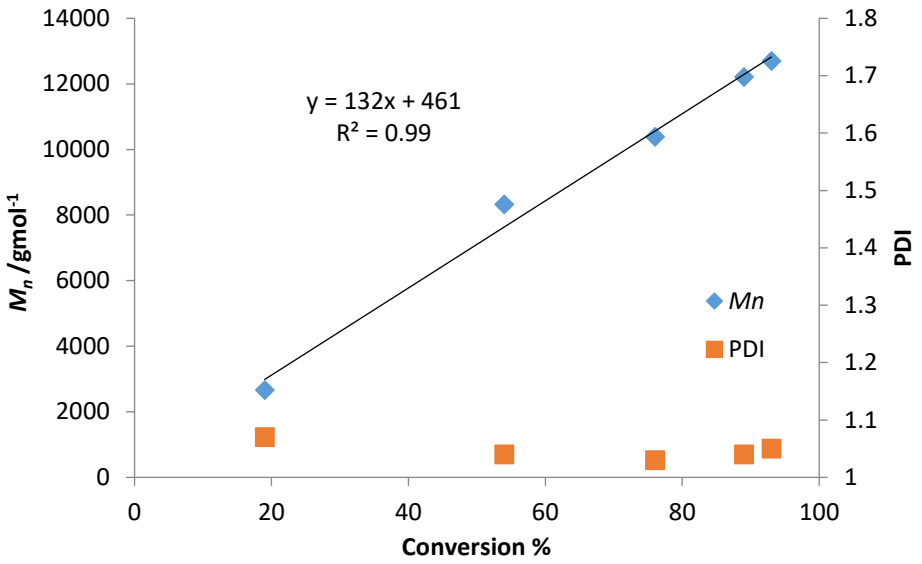

Figure 4.20: M_n and M_w/M_n against conversion for solution polymerisation of Al(**32**)O^{i}Pr.

Analysis of polymer samples by MALDI-ToF further highlights the ability of these initiators to control ROP (Figures 4.21-4.22). For Al(**31**-**33**)O^{i}Pr, a symmetrical distribution was observed with peak spacing equal to one monomer unit, indicating the absence of undesirable transesterification reactions. Further to this, the residual mass fits with the expected end groups of ^{i}PrO- and H-, demonstrating the operation of the coordination insertion mechanism. The measured molecular weights are also in good agreement with conversion for each sample. Data from MALDI-ToF analysis is summarised in Table 4.11.

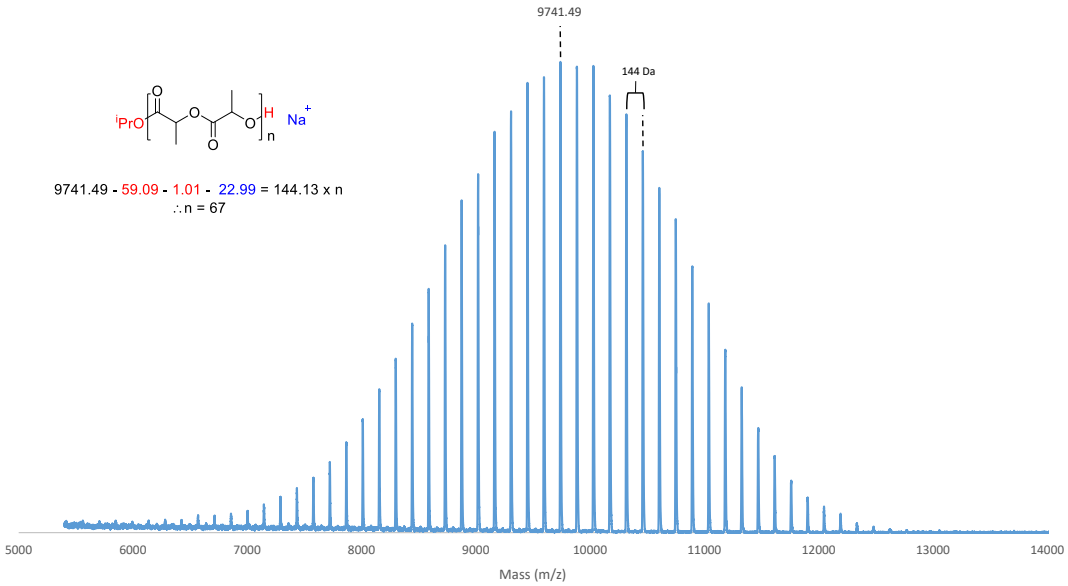

Figure 4.21: MALDI-ToF of PLA from solution polymerisation with Al(**31**)O^{i}Pr.

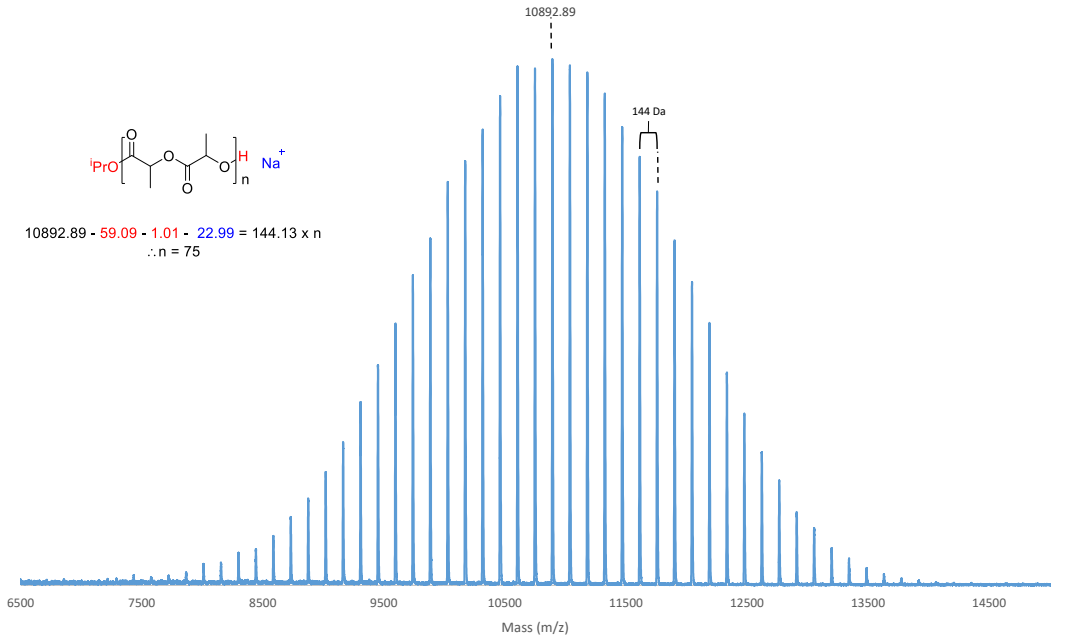

Figure 4.22: MALDI-ToF of PLA from solution polymerisation with Al(**33**)O^{i}Pr..

Table 4.11: Summary of MALDI-ToF analysis of PLA from salan Al(III) complexes.

Initiator	Series	M_p /Da	End groups	n
Al(31)O^{i}Pr	1_{Main}	9741.49	^{i}PrO-, H-, Na^+	67
Al(32)O^{i}Pr	1_{Main}	10892.89	^{i}PrO -, H-, Na^+	73
Al(33)O^{i}Pr	1_{Main}	10889.38	^{i}PrO -, H-, Na^+	75

Further experiments were carried out with Al(**31**)O^{i}Pr to determine the order with respect to the metal for the solution polymerisation with *rac*-LA. A plot of k_{app} against [Al] {[Al] = (4.63 - 6.94) × 10^{-3} mol.dm^{-3}} yielded a strong linear relationship (Figure 4.23). The order with respect to metal can then be evaluated by taking natural logarithms of both k_{app} and [Al] (Equation 4) and analysing the gradient of the resulting plot. This approach yields an order of 1.56 ± 0.04 for the initiator (Figure 4.24). A fractional order towards the initiator has precedent in the literature, particularly where aggregation and multinuclear species are possible.[14-17] The value found for Al(**31**)O^{i}Pr is intermediate to that of a first order and a second order rate dependence. This may be an indication of a cooperative effect between aluminium centres. It is noted that a dinuclear μ-hydroxy species, [Al(**31**/**32**)OH]$_2$ was observed for this ligand/metal system, and a similar aggregation could account for the observed order.

$$k_{app} = k_p[Al]^x$$

$$\therefore \ ln(k_{app}) = xln[Al] + lnk_p$$

Equations 4: Relation of k_{app} and aluminium concentration, [Al].

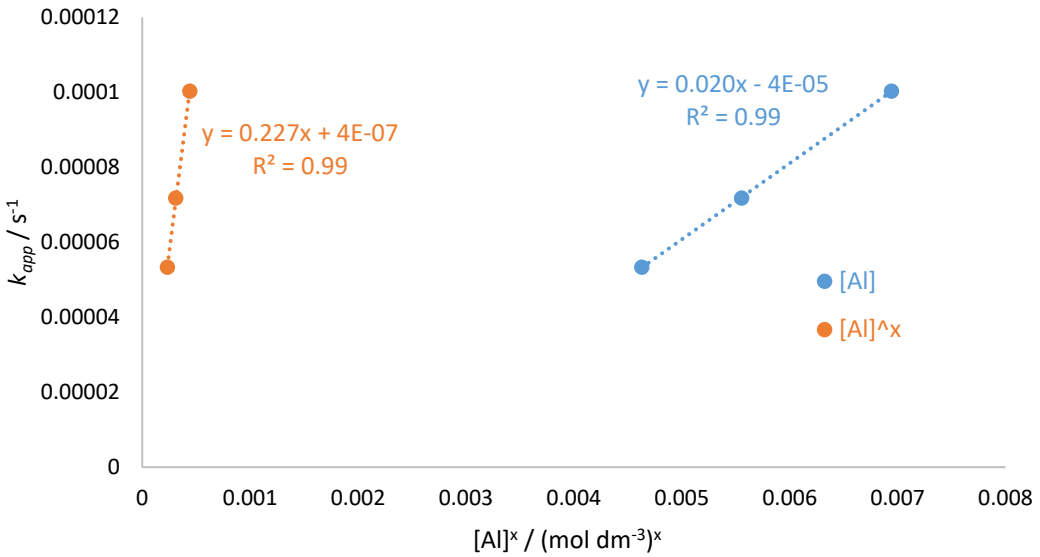

Figure 4.23: k_{app} *vs*. [Al] and k_{app} *vs*. [Al]^x for solution polymerisation of *rac*-LA with Al(**31**)O^{i}Pr.

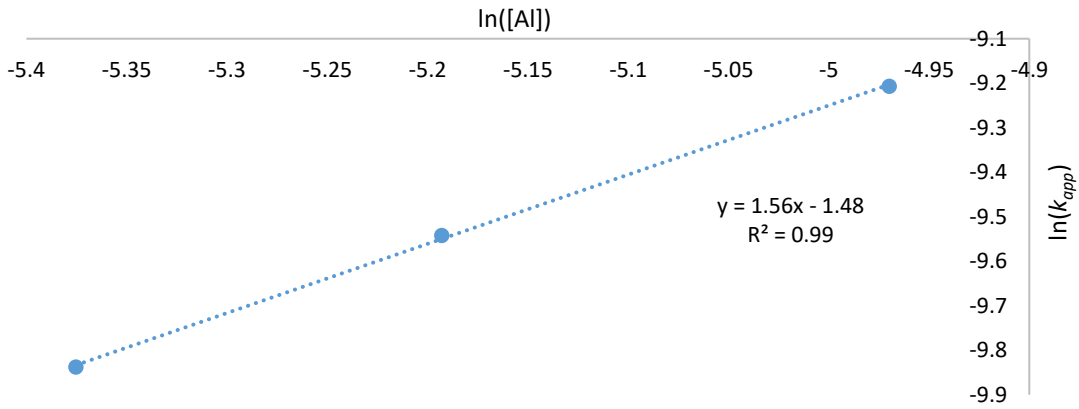

Figure 4.24: Evaluation of order with respect to [Al].

A further plot of k_{app} versus [Al]$^{1.56}$ allows for the evaluation of the rate constant for polymerisation propagation, k_p, derived from the gradient (Equation 4, Figure 4.20). This value is found observed to be (0.227 ± 0.005) $M^{-1.56}$ s^{-1}. The intercept should be 0 for a perfect system, reflecting the absence of polymerisation without initiator present. A small positive intercept is not uncommon in the literature and has been related to initiator aggregation or impurities capable of polymerising LA.[18-20]

Therefore, the overall order of reaction for the polymerisation of *rac*-LA by Al(**31**)O^{i}Pr is rate = k_p [Al]$^{1.56}$[LA].

Further kinetic analysis for the polymerisation of *rac*-LA with Al(**31**)O^{i}Pr was also carried out. In the first instance, the apparent rate constant, k_{app}, was evaluated at different temperatures (T = 323 – 353 K) on an NMR scale. Comparison of the batch kinetics at 353 K (Figure 4.25, Table 4.10) to the continuous NMR kinetics is favourable yielding similar rate constants. On reduction of the temperature, the rate constant was observed to also reduce. It is assumed that at each temperature, the order with respect to initiator is unchanged. On this basis, k_p was evaluated at each temperature allowing for the plotting of the Eyring equation (Equation 5, Table 4.12, Figure 4.26).

$$ln\frac{k}{T} = \frac{-\Delta H}{R}\frac{1}{T} + ln\frac{k_B}{h} + \frac{\Delta S}{R}$$

Equation 5: Eyring Equation

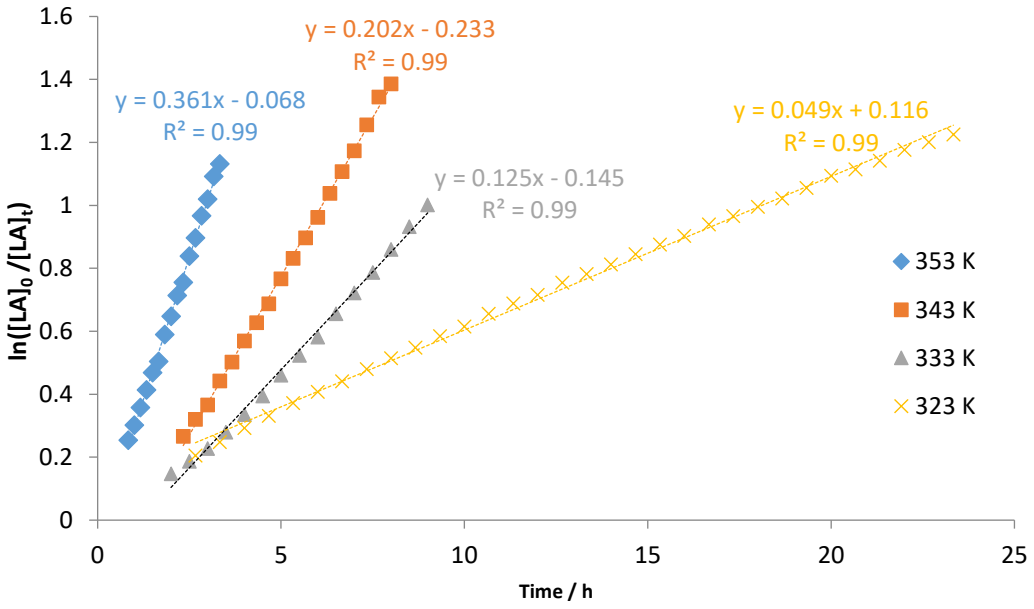

Figure 4.25: NMR scale kinetics for ROP of *rac*-LA with Al(**31**)O^{i}Pr at 323 – 353 K.

Table 4.12: Data used for Eyring plot.

T / K	k_{app} / hr^{-1}	k_{app} / s^{-1}	k_p / $M^{-1.56}$ s^{-1}	1/T (K^{-1})	ln(k_p/T)
353	0.361	1.00×10^{-4}	0.234	0.0028	-7.32
343	0.202	5.60×10^{-5}	0.130	0.0029	-7.88
333	0.125	3.46×10^{-5}	0.081	0.0030	-8.33
323	0.049	1.36×10^{-5}	0.032	0.0031	-9.23

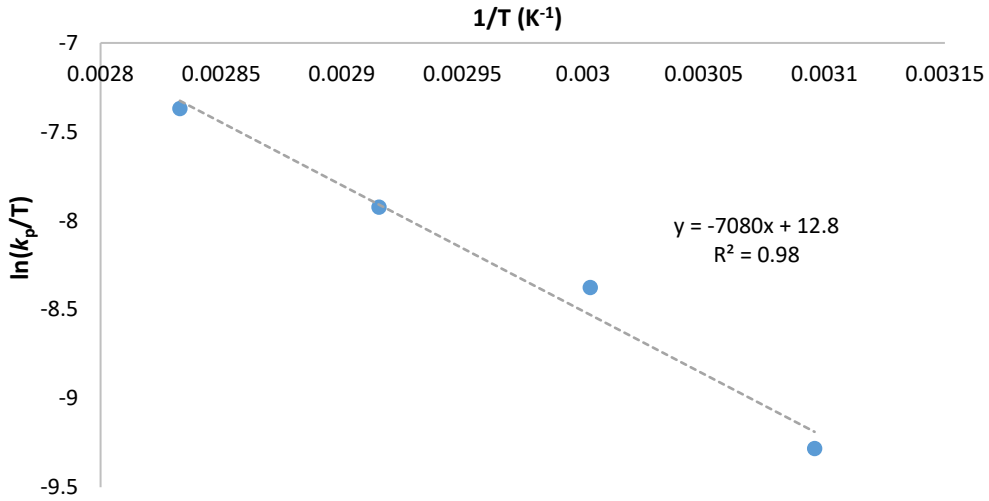

Figure 4.26: Eyring plot for ROP of *rac*-LA with Al(**31**)O^{i}Pr.

From the Eyring plot, the values of activation enthalpy and entropy, $\Delta H^{\ddagger}$ and $\Delta S^{\ddagger}$, can be calculated from the gradient and intercept respectively (Table 4.13). From these values, the Gibbs free energy, $\Delta G^{\ddagger}$, can then be found. This analysis yields values of $\Delta H^{\ddagger}$ = (58.9 ± 5.6) kJ mol^{-1}, $\Delta S^{\ddagger}$ = (-91.7 ± 16.6) J mol^{-1} K^{-1} and $\Delta G^{\ddagger}_{(353K)}$ = (91.2 ± 11.5) kJ mol^{-1}. These values are comparable to that found in the literature for the polymerisation of LA.[18, 20-22] For example, Okuda *et al* reported values of $\Delta H^{\ddagger}$ = (62 ± 3) kJ mol^{-1} and $\Delta S^{\ddagger}$ = (-89 ± 1) J mol^{-1} K^{-1} for an In(III) OSSO initiator.[22] The decrease in entropy indicates an increase in order for the transition state which supports the organised coordination-insertion mechanism.

Table 4.13: Kinetic parameters for ROP of *rac*-LA with Al(**31**)O^{i}Pr

$\Delta H^{\ddagger}$	(58.9 ± 5.6) kJ mol^{-1}
$\Delta S^{\ddagger}$	(-91.3 ± 16.6) J mol^{-1} K^{-1}
$\Delta G^{\ddagger}_{(353\ K)}$	(91.2 ± 11.5) kJ mol^{-1}

As these initiators are highly active in solution, they were also tested for activity under melt conditions. The three isopropoxide initiators were initially tested at 130°C with a 300:1 monomer to Al loading. As before, there is an increase in activity related to the reduction of steric bulk with reaction time going from 18 minutes, for Al(**31**)O^{i}Pr, to 1 minute for Al(**33**)O^{i}Pr. Melt kinetics were measured for Al(**31**)O^{i}Pr yielding an apparent rate constant of (4.83 ± 0.81) hr^{-1}. Interestingly, the level of stereocontrol is increased relative to the polymerisations in toluene for Al(**31**/**32**)O^{i}Pr (P_m = 0.81/0.73)(Figure 4.27, Table 4.14). In contrast, the chloro containing initiator, Al(**33**)O^{i}Pr yields atactic PLA under these conditions. The Al(III) salan bearing an NO_2 moiety {Al(**34**)O^{i}Pr} was also tested for ROP activity under these conditions despite full structural characterisation. This complex afforded reasonable conversion after 3 minutes despite initially being poorly soluble in the LA melt.

Table 4.14: Solvent-free polymerisation data for LA with Aluminum salan complexes, Al(**31**-**34**)O^{i}Pr (300:1).

Initiator	Time /h	Conv. %[c]	P_m[d]	$M_{n,theo}$[e]	M_n[f]	Đ[f]
Al(**31**)O^{i}Pr[a]	0.3	75	0.81	32450	30300	1.04
Al(**32**)O^{i}Pr[a]	0.1	85	0.73	36800	32350	1.13
Al(**33**)O^{i}Pr[a]	0.016	85	0.48	36800	42100	1.31
Al(**34**)O^{i}Pr[a]	0.05	76	0.51	32900	39750	1.18
Al(**31**)O^{i}Pr[b]	0.1	79	0.73	34200	27600	1.26
Al(**32**)O^{i}Pr[b]	0.05	89	0.72	38500	31150	1.25

Conditions: [a] [LA]:[I]:=300:1, 130 °C, [b] [LA]:[I]:=300:1, 180 °C, [c] Determined *via* ^{1}H NMR spectroscopy. [d] P_m is the probability of isotactic enchainment, determined *via* homonuclear decoupled ^{1}H NMR spectroscopy with deconvolution and averaging of the five equations. [e] Theoretical molecular weight calculated from conversion {300 × (Conv. × 144.13) + 60.1} (rounded to the nearest 50), [f] Determined from GPC (in THF) referenced against polystyrene standards with a correction factor of 0.58 applied.

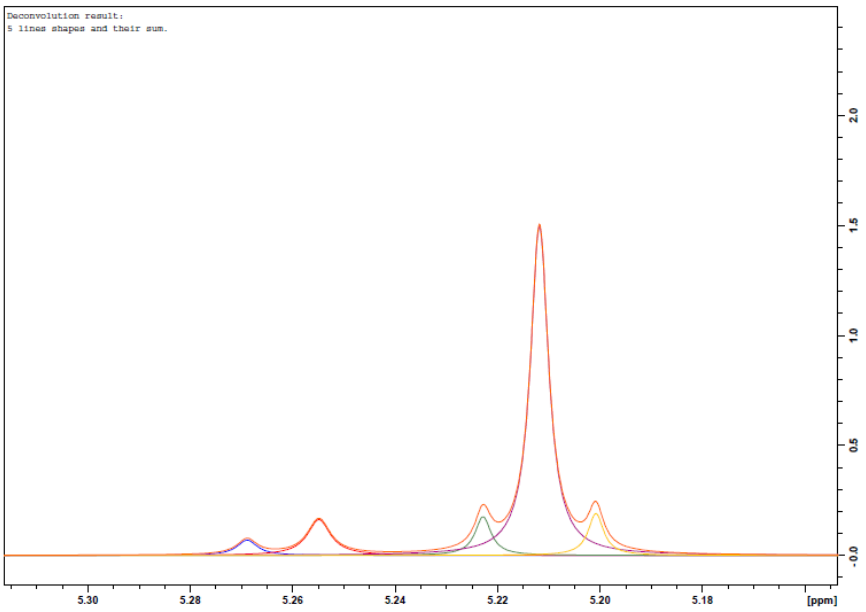

Figure 4.27: ^{1}H NMR ($CDCl_3$, 400MHz) homonuclear decoupled spectrum, with deconvolution, of isotactic PLA synthesised from solvent free polymerisation with Al(**31**)O^{i}Pr (130°C).

A reasonable molecular weight is reached for each initiator however, there is a broadening of Đ as the steric bulk is reduced (Đ = 1.04 – 1.31). This is attributed to increased side reactions at this elevated temperature which are favoured by a less sterically protected metal. A linear increase of molecular weight vs. conversion is observed for Al(**31**)O^{i}Pr under these conditions (Figure 4.28). For Al(**33**)O^{i}Pr, the increased molecular weight relative to the theoretical value is likely related to the speed of the polymerisation, with the system not attaining homogeneity before solidifying due to an increased viscosity. In a similar fashion, the lower than expected molecular weight value for polymerisation with Al(**34**)O^{i}Pr is likely related to the initial insolubility of the initiator, assuming the complex is pure.

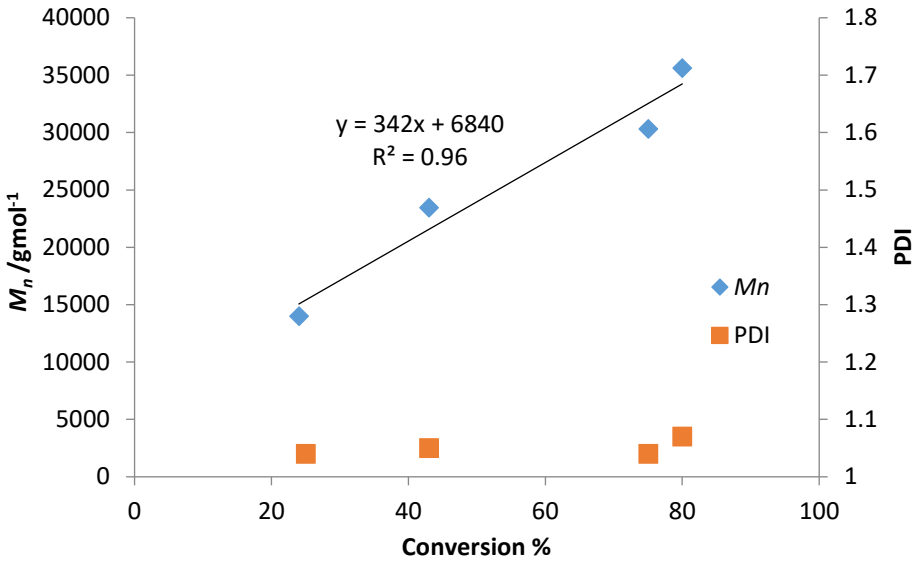

Figure 4.28: M_n and M_w/M_n against conversion for solution polymerisation of Al(**31**)O^{i}Pr.

The tolerance of this system to lower initiator loadings was also tested at this temperature (Table 4.15). The ROP with Al(**31-33**)O^{i}Pr was shown to be feasible at a 900:1 monomer-to-initiator ratio, furnishing higher molecular weight polymer (M_n = 66200 – 83650 g mol^{-1}). The time taken to achieve this reaction is tripled for each initiator, with the most active initiator still Al(**33**)O^{i}Pr (t = 3 min). A reasonable degree of stereocontrol is maintained for the isoselective initiators Al(**31/32**)O^{i}Pr. Different trends are observed for the polymer distributions relative to the initial bulk loading of 300:1. For the slowest initiator, Al(**31**)O^{i}Pr, there is an appreciable broadening of the molecular weight distribution (Đ = 1.31) and this is related to the extended time required at higher temperature to reach reasonable conversion. In contrast, the initiators with methyl and chloro aryl substituents are subject to a decrease in Đ and this is likely related to the reduction of reaction time and metal concentration which limits potential side reaction.

The monomer loading of 900:1 was also demonstrated at 150 °C for Al(**31/32**)O^{i}Pr. Similar results are achieved in a shorter time frame with only a slight reduction in selectivity for Al(**31**)O^{i}Pr. Temperature was further increased to 180°C to mimic more industrial relevant conditions. At this temperature, loadings of 300:1 and 900:1 were employed for ROP with Al(**31/32**)O^{i}Pr. Under these conditions, the stereocontrol

imparted by the two systems is comparable, with a pronounced bias for isotactic PLA still being observed (P_m = 0.73/0.72 at 300:1 and P_m = 0.70 at 900:1). For the 300:1 polymerisation at 180 °C, the molecular weight is still controlled with recorded M_n values being reasonable based on LA conversion. The polymer distribution is broadened as a consequence of the higher temperature (Đ = 1.26). The polymer samples produced at a 900:1 monomer-to-initiator ratio at 180 °C had a similar polymer distribution but the measured molecular weights are slightly lower than anticipated based on conversion.

Table 4.15: Solvent-free polymerisation data for LA with Aluminum salan complexes, Al(**31**-**33**)O^{i}Pr (900:1).

Initiator	Time /h	Conv. %[d]	P_m[e]	$M_{n,theo}$[f]	M_n[g]	Đ[g]
Al(**31**)O^{i}Pr[a]	1	55	0.78	71350	66200	1.18
Al(**32**)O^{i}Pr[a]	0.3	50	0.73	64850	66850	1.09
Al(**33**)O^{i}Pr[a]	0.05	67	0.50	86900	83650	1.20
Al(**31**)OPr[b]	0.5	47	0.75	60950	55200	1.13
Al(**32**)O^{i}Pr[b]	0.3	54	0.74	70050	52850	1.17
Al(**31**)O^{i}Pr[c]	0.2	45	0.70	58400	31600	1.24
Al(**32**)O^{i}Pr[c]	0.2	68	0.70	88200	38350	1.29

Conditions: [a] [LA]:[I]:=900:1, 130 °C, [b] [LA]:[I]:=900:1, 150 °C, [c] [LA]:[I]:=900:1, 180 °C, [d] Determined *via* ^{1}H NMR spectroscopy. [e] P_m is the probability of isotactic enchainment, determined *via* homonuclear decoupled ^{1}H NMR spectroscopy with deconvolution and averaging of the five equations. [f] Theoretical molecular weight calculated from conversion {900 × (Conv. 144.13) + 60.1} (rounded to the nearest 50), [g] Determined from GPC (in THF) referenced against polystyrene standards with a correction factor of 0.58 applied.

The ability to reduce metal loading further is also an industrially important target, affording purer polymer. This was achieved by adding a chain transfer agent/co-initiator to moderate the molecular weight of the polymer. Polymerisations using an addition co-initiator were carried out at a 3000:1:10 ratio of [LA]:[Al]:[BnOH] on a 2 g *rac*-lactide basis (Table 4.16). Initial studies at 150°C demonstrated good control over the polymerisation for both Al(**31/32**)O^{i}Pr. Despite an extended reaction time, an isotactic bias is maintained for both initiators (P_m = 0.70) and the measured molecular

weight correlates well with conversion for a nominal 300:1 metal loading. The polydispersity for these samples is also relatively low being comparable to polymerisation at 130°C. This is likely due to the further reduction of metal centres consequently facilitating less transesterification reactions. Employing this loading at 180°C required extended reaction times for Al(**31**)O^{i}Pr, which greatly impacted the control of this initiator over the polymerisation. While a reasonable conversion is achieved, there is poor correlation with the measured molecular weight and a broad distribution of polymer chain lengths (Đ = 1.55). The isotactic preference of this initiator is also much reduced under these conditions (P_m = 0.59). Evidently, the activity of this initiator is too low to furnish polymer in a reasonable time frame being instead more susceptible to side reactions. For Al(**32**)O^{i}Pr, a more controlled polymerisation is realised under these conditions albeit at a moderate conversion. The degree of stereocontrol is reduced to a moderate isotacticity (P_m = 0.65) and the measured molecular weight is reasonable based on conversion and loading. Application of Al(**33**)O^{i}Pr under these industrial relevant conditions gives the best results, affording a well-controlled polymerisation despite the challenging conditions.

Table 4.16: Solvent-free, immortal polymerisation data for LA with Aluminum salan complexes, Al(**31**-**34**)O^{i}Pr.

Initiator	**Time /h**	**Conv. %**[c]	P_m[d]	$M_{n,theo}$[e]	M_n[f]	**Đ**[f]
Al(**31**)O^{i}Pr[a]	6.25	53	0.70	23000	21600	1.15
Al(**32**)O^{i}Pr[a]	1	70	0.70	30350	29750	1.12
Al(**31**)O^{i}Pr[b]	5	60	0.59	26000	14800	1.55
Al(**32**)O^{i}Pr[b]	1	36	0.65	15650	13350	1.21
Al(**33**)O^{i}Pr[b]	0.17	79	0.49	34250	30150	1.22

Conditions: [a] [LA]:[I]:[BnOH]=3000:1:10, 150 °C, [b] [LA]:[I]:[BnOH]=3000:1:10, 180 °C. [c] Determined *via* ^{1}H NMR spectroscopy. [d] P_m is the probability of isotactic enchainment, determined *via* homonuclear decoupled ^{1}H NMR spectroscopy with deconvolution and averaging of the five equations. [e] Theoretical molecular weight calculated from conversion {300 × (Conv. × 144.13) + 108.1} (rounded to the nearest 50), [f] Determined from GPC (in THF) referenced against polystyrene standards with a correction factor of 0.58 applied.

It was noted that di-μ-hydroxy bridged dimers, [Al(**31/32)**OH]$_2$, are formed on exposure of the alkoxide complexes to air and moisture. It is therefore of interest to assess the ROP ability of these species as they are likely side or decomposition products of the initiators. Attempts to initiate polymerisation with [Al(**31)**OH]$_2$ wereunsuccessful in the temperature range of 130-180 °C suggesting these dimeric species would play no role in the ROP of LA.

4.3.4 Aluminium triaryl complexes

The ROP activity of Al(**36**)O^{i}Pr was assessed both in solution and under melt conditions (Table 4.17). In toluene at 80 °C, good conversion is achievable after a 24 hour reaction time. The molecular weight of the resultant polymer is comparable to the theoretical value and the distribution of polymer chains is narrow (Đ = 1.13). Under solvent free conditions, high molecular weight is achieved in 4 hours (53 % conversion). As for the solution state polymerisation, there is good control of molecular weight and only a slight broadening of molecular weight distribution is observed (Đ = 1.16). The PLA afforded by the melt polymerisation is also atactic.

A literature comparison with an analogous compound, Al(**G**)O^{i}Pr, is provided in solution.[23] While this complex is active, direct comparison is not possible due to different conditions (70°C, 50:1, 16 hours). There are, however, similarities between the two systems. For both sets of initiators, there is a good correlation between measured and calculated molecular weight values. However, Al(**G**)O^{i}Pr has a relatively broadened polymer distribution (Đ = 1.28) and this may be a reflection of the reduced steric bulk associated with this literature initiator. Atactic PLA is also afforded by Al(**G**)O^{i}Pr.[23]

Table 4.17: Solutions polymerisation data for LA with Aluminum triaryl complexes, Al(**36**)O^{i}Pr and Al(**37**). Al(**G**)O^{i}Pr data from the literature.[23]

Initiator	Time /h	Conv. %[d]	P_r[e]	$M_{n,theo}$[f]	M_n[g]	Đ[g]
Al(**36**) O^{i}Pr[a]	24	84	0.55	12150	12800	1.13
Al(**36**)O^{i}Pr[b]	4	53	0.45	22950	22400	1.16
Al(**37**)[c]	120	17	-	-	-	-
Al(**G**)O^{i}Pr[*]	16	92	-	6700	6900	1.28

Conditions: [a][LA]:[I] = 100:1, 80 °C toluene, [b][LA]:[I]=300:1, 130°C, solvent free [c][LA]:[I]:[BnOH]=100:1:1, 80 °C, toluene. [d] Determined *via* ^{1}H NMR spectroscopy. [e] P_r is the probability of heterotactic enchainment, determined *via* homonuclear decoupled ^{1}H NMR spectroscopy, [f.] Theoretical molecular weight calculated from conversion {[LA]/[I] × (Conv. × 144.13) + 108.14} (rounded to the nearest 50), [g] Determined from GPC (in THF) referenced against polystyrene standards with a correction factor of 0.58 applied [*][LA]:[I] = 50:1, 70 °C toluene.[23]

Al(**37**) was shown to have limited to no activity under solution and melt conditions. This is undoubtedly related to the steric bulk of the ligand and the absence of an active site on the metal centre. An activated monomer mechanism would be anticipated for this initiator, and due to the presence of three *ortho tert*-butyl groups the initial monomer coordination is likely disfavoured.

4.4 Polymerisations with group IV complexes

4.4.1 Titanium complexes

The titanium based initiators were all tested under melt conditions (130°C, 300:1), having isopropoxide groups to initiate polymerisation directly (Table 4.18). The bicyclic motif of **14**H$_2$ afforded the fastest polymerisation for this series, reaching reasonable conversion after 30 minutes. The initiator, Ti(**14**)(O^{i}Pr)$_2$, was characterised as a five coordinate complex and it is suggested it is the lower coordination and reduced aryl bulk that causes the relatively fast polymerisation. In contrast, Ti(**22**)(O^{i}Pr)$_2$ demonstrates low activity requiring 24 hours, to achieve reasonable conversion. The presence of four ^{t}Bu groups could make it harder for the monomer to approach to the Ti(IV) centre despite the lower metal coordination.

The salalen complex, Ti(**26**)(O^iPr), was observed to only reach 17% conversion after 24 hours under these conditions. In this instance, the ease of monomer coordination may be expected to be even less likely due to the higher metal coordination. The titanium salan complex, Ti(**31**)(O^iPr)$_2$ was observed to be more active than the other ^{t}Bu substituted initiators being able to reach a high conversion within 3 hours. Geometrically, the structures are different with the salalen adopting a *fac-mer* geometry and the salan, a *fac-fac* arrangement. This increased activity on going from salalen to salan also correlates with the observations made for the respective aluminium complexes {Al(**26**)Me/Al(**31**)Me}.

The bis-ligated complex, Ti(**1**)$_2$(O^iPr)$_2$, was also found to be a poor initiator for the ROP of *rac*-LA achieving 58 % under melt conditions after 24 hours. In no instance is stereocontrol exerted by this series of initiators which is analogous to the majority of Ti(IV) initiators in the literature.[24-29]

Table 4.18: Solvent-free polymerisation data for *rac*-LA with Ti(IV) complexes, Ti(**1**)$_2$(O^iPr)$_2$, Ti(**14/22/26/31**)(O^iPr)$_2$. Ti(**H**)$_2$(O^iPr)$_2$ and Ti(**J**)(O^iPr)$_2$ data from the literature.[24, 28]

Initiator	Time /h	Conv. %[a]	P_r[b]	$M_{n,theo}$[c]	M_n[d]	Đ[e]
Ti(**1**)$_2$(O^iPr)$_2$	24	58	0.49	12550	2850	1.36
Ti(**14**)(O^iPr)$_2$	0.5	67	0.50	14200	12050	1.04
Ti(**22**)(O^iPr)$_2$	24	76	0.51	16450	10600	1.34
Ti(**26**)(O^iPr)$_2$	24	17	-		-	-
Ti(**31**)(O^iPr)$_2$	3	75	0.52	16250	13900	1.04
Ti(**H**)$_2$(O^iPr)$_2$*	0.5	90	0.50	19500	14800	1.20
Ti(**J**)(O^iPr)$_2$*	0.25	89	0.50	19250	22050	1.44
Ti(**K**)(O^iPr)$_2$*	2	74	0.50	16050	19140	1.64

Conditions: [LA]:[I]=300:1, 130 °C, solvent free. [a]Determined *via* ^{1}H NMR spectroscopy. [b] P_r is the probability of heterotactic enchainment, determined *via* homonuclear decoupled ^{1}H NMR spectroscopy, [d] Theoretical molecular weight calculated from conversion {300 × (Conv. × 144.13) + 60.1}/2 (rounded to the nearest 50), [e] Determined from GPC (in THF) referenced against polystyrene standards with a correction factor of 0.58 applied. *[LA]:[I]=300:1, 130°C, solvent free, twice sublimed LA.[24, 28]

When recorded, the molecular weight of the polymers is generally half than expected for a 300:1 monomer to metal loading. It is suggested that both isopropoxide groups are able to initiate the growth of PLA chains in this system, leading to two polymers per metal centre. The distribution of chain length is narrow for Ti(**14**/**31**)(O^iPr)$_2$ (Đ = 1.04) indicating a controlled polymerisation. Relative broadening of this distribution is observed for Ti(**22**)(O^iPr)$_2$ and this is likely due to the extended time at high temperature. For Ti(**1**)$_2$(O^iPr)$_2$, the observed molecular weight is much lower than anticipated suggesting the formation of oligomers rather than polymer chains.

It is noted that a literature Ti(IV) salalen complex, Ti(**J**)(O^iPr)$_2$, with identical aryl groups to Ti(**26**)(O^iPr)$_2$, achieves high conversion with 15 minutes under melt conditions.[28] This implies that the identity of the initiator backbone could also contribute to the poor performance of Ti(**26**)(O^iPr)$_2$. The salan complex Ti(**31**)(O^iPr)$_2$ was found to have a comparable activity to literature initiator, Ti(**K**)(O^iPr)$_2$. This initiator features a *N*,*N'*-Dimethylethylenediamine backbone and identical aryl groups and reaches high conversion after 2 hours under melt conditions.[30] However, Ti(**31**)(O^iPr)$_2$ demonstrates better molecular weight control compared to Ti(**K**)(O^iPr)$_2$, having a narrower distribution of molecular weight. For the bis-ligated initiator, Ti(**1**)$_2$(O^iPr)$_2$, there is also structural similarity with a literature initiator, Ti(**H**)$_2$(O^iPr)$_2$ (Chapter 3, Figure 3.48). The activity of Ti(**H**)$_2$(O^iPr)$_2$ is reported to be superior to Ti(**1**)$_2O^iPr$ (300:1, 0.5 hr, 90 - 95 %).[24] These literature initiators generally have sterically undemanding aryl groups (OMe or H) which likely contributes to the success of the polymerisation, as well as the use of purer lactide.

4.4.2 Zirconium complexes

Polymerisation with the homoleptic bisphenolate zirconium and hafnium, M(**14**-**16**)$_2$ initiators was carried out with addition of benzyl alcohol co-initiator due to an absence of a labile group on the metal centres (Table 4.19). For the zirconium initiators, Zr(**14**-**16**)$_2$, good conversion is achieved in toluene at 80°C within 24 hours. There is a marked heterotactic bias (P_r = 0.76) for Zr(**14**/**15**)$_2$ under these conditions as shown by the dominance of the *isi* and *sis* tetrads in the ^{1}H homonuclear decoupled NMR spectrum (Figure 4.29). Comparatively, the stereocontrol is reduced for Zr(*cis*-**15**)$_2$ (P_r = 0.66) and this may be a consequence of the larger iodo radius or the change in

coordination for this initiator. These initiators furnish PLA with comparable molecular weights which are slightly lower than expected based on conversion. The distribution of polymer weights is also narrow (Đ = 1.04 - 1.11) highlighting the controlled nature of the polymerisation.

Table 4.19: Polymerisation data for lactide with Group 4 initiators, M(**14-16**)$_2$.

Initiator	Time /h	Conv. %[r]	P_r[f]	$M_{n,theo}$[g]	M_n[h]	Đ[h]
Zr(**14**)$_2$[a]	24	93	0.76	13500	9300	1.05
Zr(**14**)$_2$[b]	3	96	0.42	41550	17350	1.06
Zr(**14**)$_2$[a,c]	8	29	-	-	-	-
Zr(**14**)$_2$[a,d]	24	94	0.76	13650	8350	1.07
Zr(**15**)$_2$[a]	24	81	0.76	11650	8650	1.04
Zr(*cis*-**16**)$_2$[a]	24	95	0.66	13800	8950	1.11
Hf(**14**)$_2$[a]	24	55	0.76	8050	7750	1.04
Hf(**14**)$_2$[a,d]	24	72	0.74	10500	6800	1.04
Hf(**15**)$_2$[a]	24	35	0.74	5150	3750	1.04
Hf(*trans*-**16**)$_2$ [a]	24	31	0.69	4550	3950	1.05
Hf(*cis*-**16**)$_2$ [a]	24	28	0.67	4150	4100	1.04

Conditions: [a] [LA]:[I]:[BnOH]=100:1:1, 80 °C, toluene, [b] [LA]:[I]:[BnOH]=300:1:1, 130 °C, solvent free, [c] *L*-LA [d] Sublimed *rac*-LA, [e] Determined *via* ^{1}H NMR spectroscopy. [f] P_r is the probability of heterotactic enchainment, determined *via* homonuclear decoupled ^{1}H NMR spectroscopy, [g] Theoretical molecular weight calculated from conversion {100 × (Conv. × 144.13) + 108.1} (rounded to the nearest 50), [h] Determined from GPC (in THF) referenced against polystyrene standards with a correction factor of 0.58 applied.

Further investigation was carried out for Zr(**14**)$_2$. An increase of benzyl alcohol concentration by two is observed to effectively half the molecular weight of the resultant polymer. This indicates BnOH is involved initiation of polymer chains as well as chain transfer reactions. Increasing the amount of benzyl alcohol causes a further reduction in polymer molecular weight (Figure 4.30). It is noted that increasing

the amount of co-initiator allows higher conversion to be achieved more rapidly, indicating [BnOH] is likely present in the rate equation.

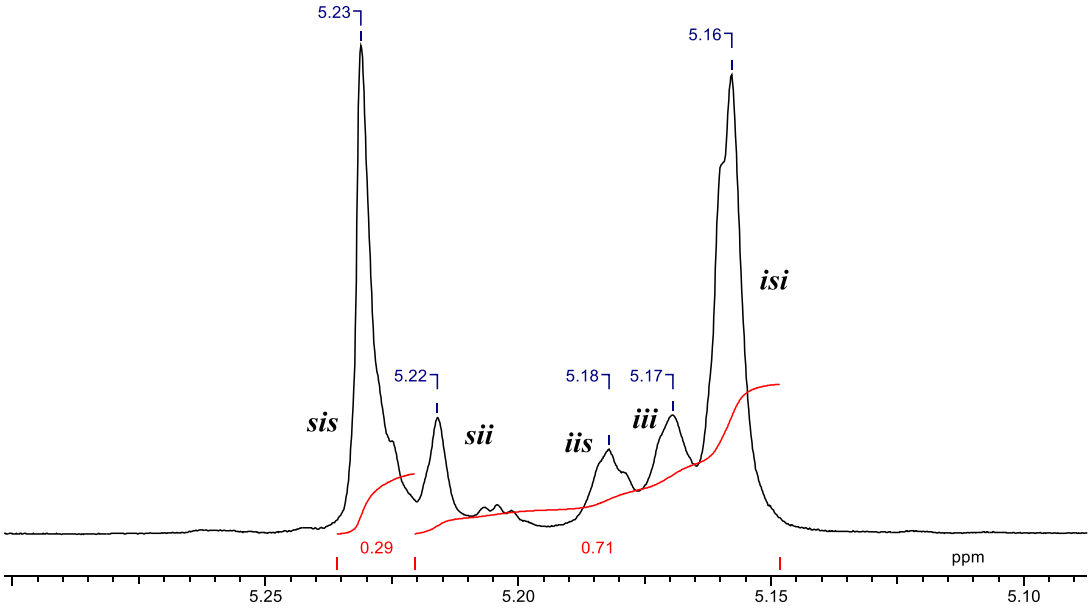

Figure 4.29: ^{1}H NMR ($CDCl_3$, 400MHz) homonuclear decoupled spectrum of heterotactic PLA synthesised from solution polymerisation with Zr(**14**)$_2$ (toluene, 80 °C).

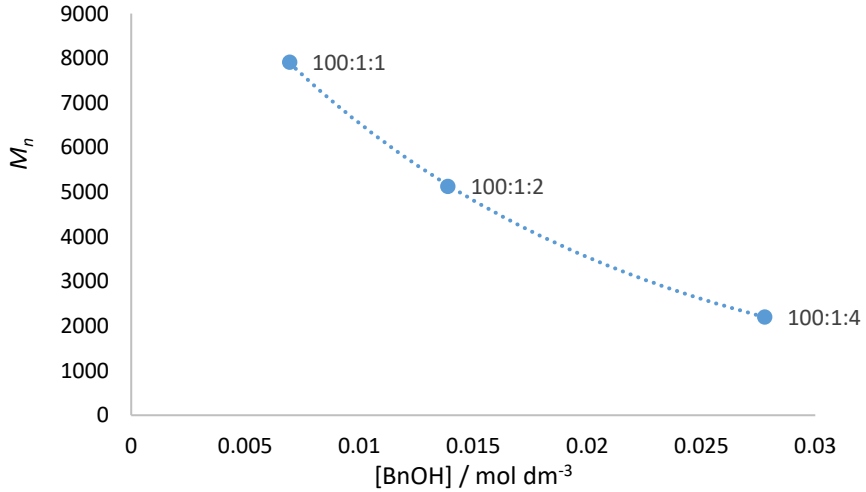

Figure 4.30: Effect of concentration of BnOH on molecular weight for ROP with Zr(**14**)$_2$. Note: data points represent a similar conversion of LA (84-89%).

The polymerisation was also trialled under solvent free conditions (130°C, 300:1:1 [LA]:[Zr]:[BnOH]). With Zr(**14**)$_2$, high conversion was realised after 3 hours with a slight isotactic tendency (P_r = 0.42). The molecular weight, while being narrowly distributed (Đ = 1.06), is lower than anticipated for this (co-)initiator loading.

Batch kinetics were carried out for Zr(**14**/**15**)$_2$ revealing polymerisation by the chloro containing initiator to be almost twice as fast as the bromo initiator {Zr(**14**)$_2$, k_{app} = 0.115 hr^{-1}, Zr(**15**)$_2$, k_{app} = 0.069 hr^{-1}} (Table 4.20, Figure 4.31). This may be due to the slight difference in size between the substituents of **14**H$_2$ and **15**H$_2$, with the latter being slightly larger making it more sterically difficult for monomer to coordinate to the metal centre. There is a reasonable linear correlation between molecular weight and conversion for these initiators demonstrating a controlled polymerisation (R^2 = 0.99) (Figure 4.32).

The polymerisation of *L*-LA by Zr(**14**)$_2$ was observed to give a lower conversion relative to *rac*-LA (*L*-LA, 8 hrs, 29% / *rac*-LA, 8 hrs, 67%). This observation is expected for a heterotactic initiator which has a preference to insert the opposite enantiomer with a slower insertion rate for the same enantiomer.

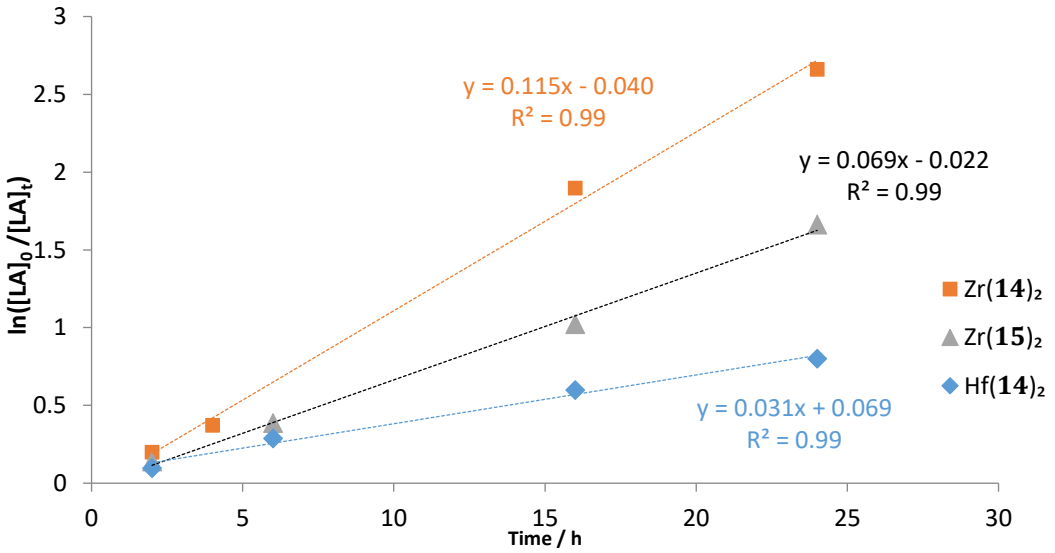

Figure 4.31: Semi-logarithmic plot for the solution polymerisation of Zr(**14**/**15**)$_2$ and Hf(**14**)$_2$. Conditions: Toluene, 80°C, [LA]:[I]:[BnOH] = 100:1:1.

Table 4.20: Rate constants, k_{app}, for solution ROP of M(**14-15**)$_2$.

Initiator	k_{app} (hr^{-1})
Zr(**14**)$_2$	0.115 ± 0.005
Zr(**15**)$_2$	0.069 ± 0.003
Hf(**14**)$_2$	0.031 ± 0.002

Conditions: [LA]:[I]:[BnOH] = 100:1:1, 80 °C, toluene, *rac*-LA.

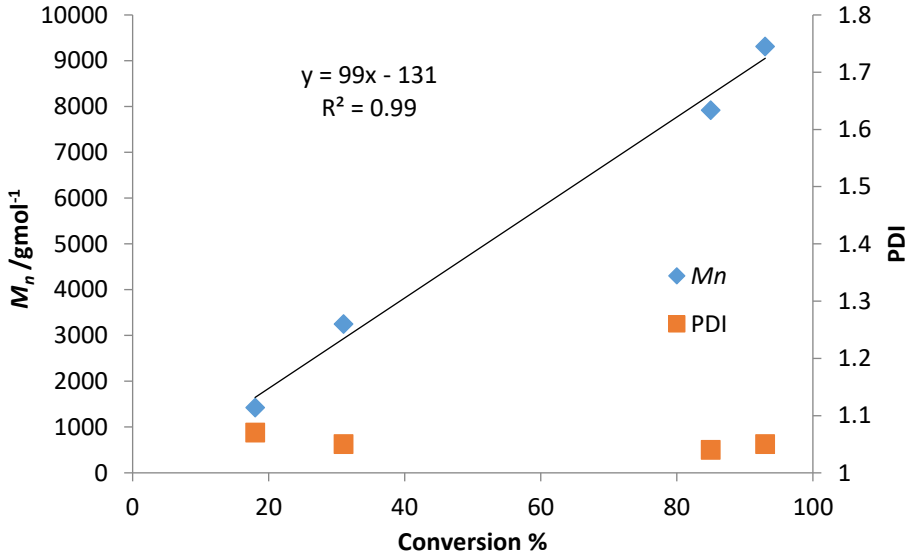

Figure 4.32: M_n and M_w/M_n against conversion for solution polymerisation of Zr(**14**)$_2$.

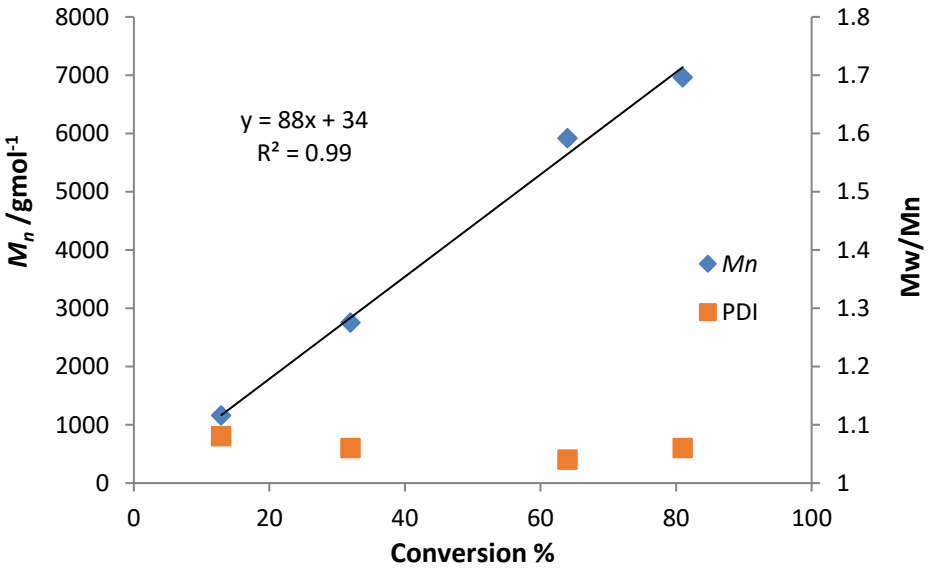

Figure 4.33: M_n and M_w/M_n against conversion for solution polymerisation of Zr(**15**)$_2$.

MALDI-ToF analysis was carried out for polymer derived from M(**14/16**)$_2$. For each sample, the anticipated chain ends of BnO- and H- are demonstrated {Table 4.21, for Zr(**14**)$_2$, Figure 4.34}. There is one main series with ~72 g/mol spacing indicating the presence of transesterification reactions. The molecular weights observed *via* MALDI are similar to that recorded by GPC. For Zr(**16**)$_2$, there is also a minor series related to ^{i}PrO- end groups, indicating the presence of either isopropanol or Zr(**16**)(O^{i}Pr)$_2$ within the initiator. The presence of these impurities could account for the relative broadening of molecular weight distribution for this initiator.

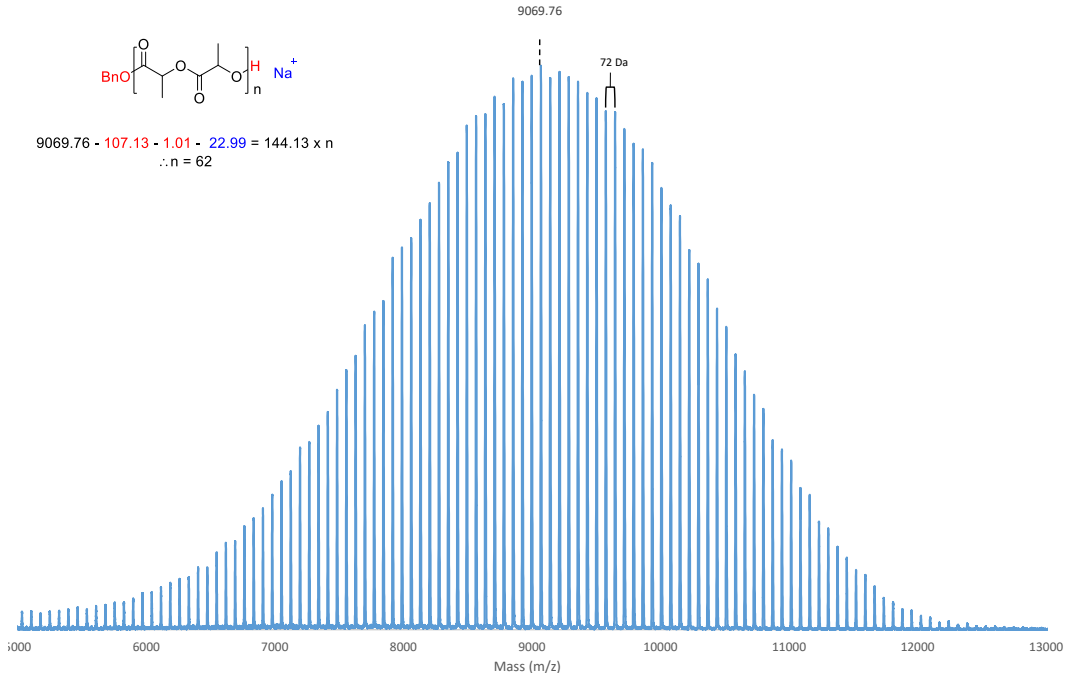

Figure 4.34: MALDI-ToF of PLA from solution polymerisation with Zr(**14**)$_2$.

Table 4.21: Summary of MALDI-ToF analysis of PLA from M(**14**/**16**)$_2$ complexes.

Initiator	Series	M_p /Da	End groups	n
Zr(14)$_2$	1_{Main}	9069.76	BnO-, H-, Na^+	62
	2_{Trans}	9142.09	BnO-, H-, Na	62.5
Zr(16)$_2$	1_{Main}	8203.89	BnO-, H-, Na^+	56
	2_{Trans}	8275.71	BnO-, H-, Na^+	56.5
	$3_{Impurity}$	8011.45	^{i}PrO-, H-, Na^+	55
Hf(14)$_2$	1_{Main}	7338.58	BnO-, H-, Na^+	50
	2_{Trans}	7265.89	BnO-, H-, Na^+	49.5

Conditions: [LA]:[I]:[BnOH] = 100:1:1, 80 °C, toluene, *rac*-LA.

Mechanistically, a coordination-insertion mechanism is not anticipated for M(**14-16**)$_2$ due to the coordinatively saturated complexes. Instead, it is proposed that an activated monomer mechanism is in operation. Such a mechanism has been postulated In the literature for ROP if *rac*-LA with metal initiators, for example alkali metals and In(III).[7, 31, 32] In this pathway, the LA carbonyl oxygen is still involved in coordination to the Lewis acidic metal but the attack of the co-initiator proceeds from outside the metal coordination sphere (Figure 4.35). This would mean that the polymer is not necessarily bound to the metal centre as would be observed for the coordination-insertion mechanism. Due to this, one may anticipate an increased rate of transesterification with unbound chains being activated by the carbonyl group in the same manner. Evidence for an activated monomer mechanism include the observed transesterifcation (MALDI-ToF) and the strong dependence on a co-initiator. ^{1}H NMR spectroscopic analysis of a polymerisation mixture ($CDCl_3$, 45 °C, 20:1:1) shows the production of PLA without any changes in the resonances attributed to Zr(**14**)$_2$, suggesting the metal structure is maintained throughout the reaction (Figure 4.36).

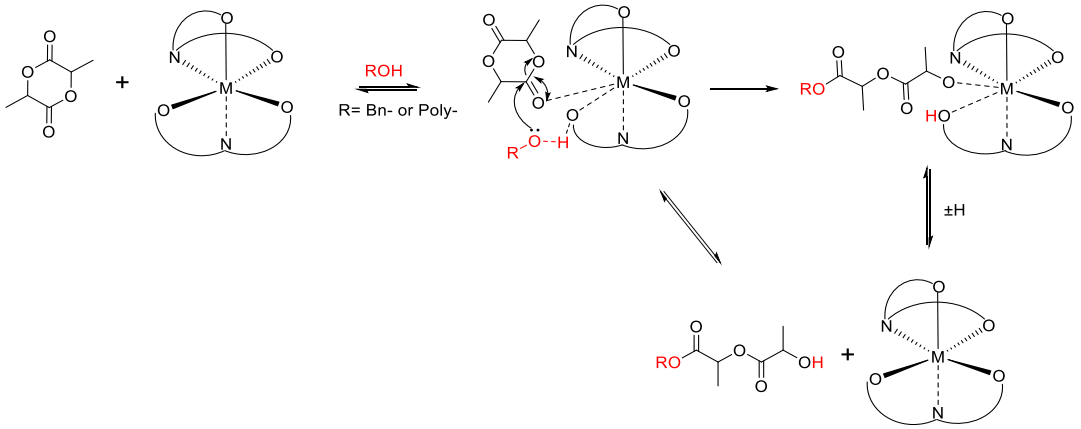

Figure 4.35: Schematic to illustrate the potential mechanism for the ROP with the bis-ligated complexes.

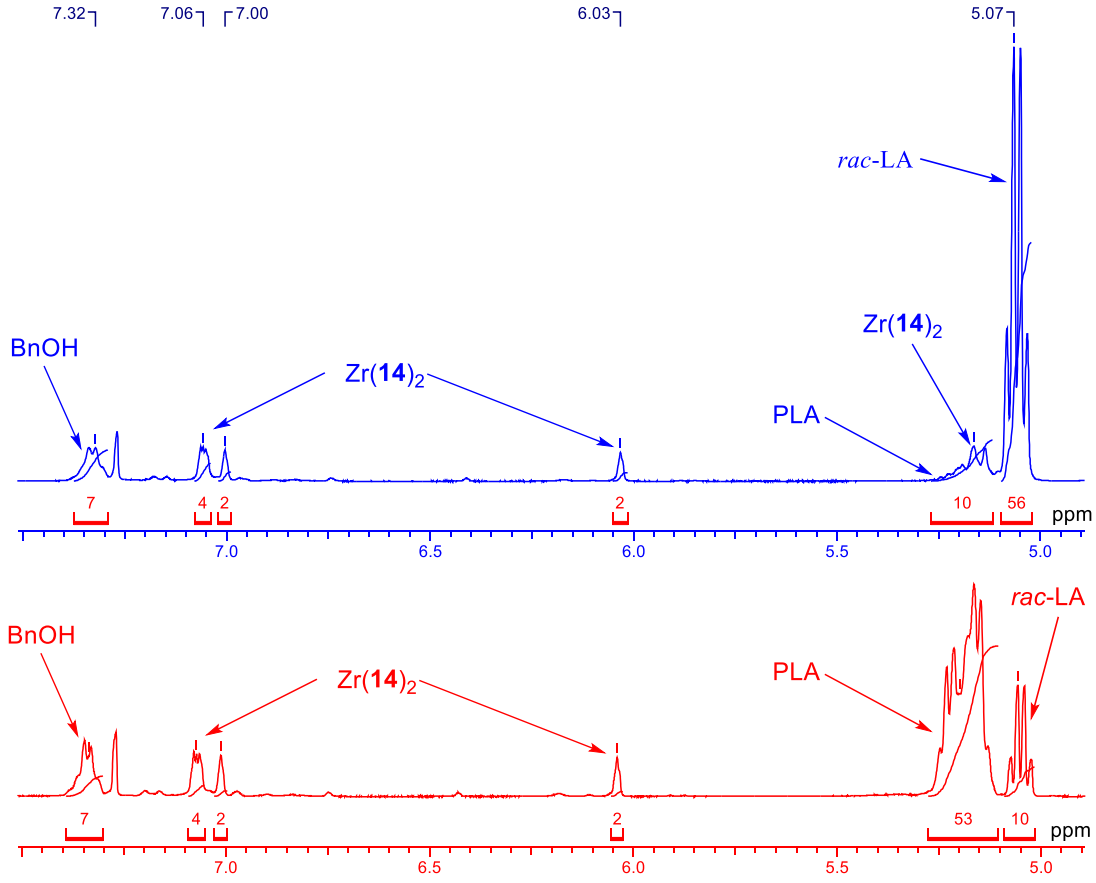

Figure 4.36: ^{1}H NMR spectra of Zr(**14**)$_2$ + BnOH + *rac*-LA (top) and Zr(**14**)$_2$ + BnOH + PLA + *rac*-LA (bottom).

The hafnium analogues of the bicyclic initiators, Hf(**14-16**)$_2$, were also tested for their activity towards the ROP of *rac*-lactide. An immediate disparity is seen compared to the Zr(IV) initiators, with a lower conversions being achieved for the Hf(IV) initiators in the same time frame. Zr(**14**)$_2$ reaches 93% after 24 hours while Hf(**14**)$_2$ only achieves 55%. A similar trend is also observed for Hf(**15/16**)$_2$. The difference between the two systems is thought to be related to the relative sensitivity of the initiators. The polymerisations were repeated for Zr(**14**)$_2$ and Hf(**14**)$_2$ with increased purity of monomer, *i.e.* doubly sublimed *rac*-LA. For the zirconium system, there was very little difference in the result with a similar conversion and stereocontrol being observed after 24 hours. Polymerisation of sublimed *rac*-LA with Hf(**14**)$_2$ gave a slight improvement in conversion with a 17% increase. It is suggested, therefore, that the hafnium based initiators are more susceptible to impurities in the LA, which inhibit the polymerisation.

Despite the difference in stability, the observed stereocontrol of Hf(**14-16**)$_2$ mirrors that of the zirconium analogues {for Hf(**14**)$_2$, P_r = 0.76}. Reasonable control is also observed over the polymer molecular weight with narrow distribution being achieved (Đ = 1.04 - 1.05). Reasonable correlation is observed between conversion and molecular weights. MALDI-ToF analysis was carried on PLA derived from the polymerisation of *rac*-LA with Hf(**14**)$_2$. As for the Zr(IV) analogues, this techniques confirms the presence of BnO- and H- end groups.

Batch kinetics were carried out for Hf(**14**)$_2$ with recrystallised *rac*-LA to allow for comparison with the Zr(IV) systems (Figure 4.31, Table 4.18). The apparent rate constant for this initiator was found to be almost four times smaller than that of the direct zirconium analogue, Zr(**14**)$_2$ {k_{app} = (0.031 ± 0.002) hr^{-1}}. The plot of molecular weight against conversion shows a marked deviation from linearity (R^2 = 0.92) and this may be related to the action of monomer impurities.

Polymerisation with the heteroleptic group IV complexes generally demonstrated increased activity, reaching higher conversion in a shorter timeframe (Table 4.22). Both solution and solvent free conditions were applied for the ROP of *rac*-LA with these initiators.

Table 4.22: Polymerisation data for *rac*-lactide with Zr(IV) alkoxide initiators, Zr(**1**)$_2$(O^{i}Pr)$_2$, Zr(**14**/**22**)(O^{t}Bu)$_2$ and Zr(**26**)(O^{t}Bu)$_2$. Zr(**H**)$_2$(O^{i}Pr)$_2$ data from the literature.

Initiator	Time /h	Conv. %[d]	P_r[e]	$M_{n,theo}$[f]	M_n[g]	Đ[g]
Zr(**1**)$_2$(O^{i}Pr)$_2$[a]	2	62	0.53	4500	2950	1.12
Zr(**1**)$_2$(O^{i}Pr)$_2$[b]	0.8	80	0.60	17350	6950	1.17
Zr(**14**)(O^{t}Bu)$_2$[a]	1	54	0.73	3950	5220	1.09
Zr(**14**)(O^{t}Bu)$_2$[b]	0.05	78	0.74	16900	20800	1.12
Zr(**22**)(O^{t}Bu)$_2$[a]	4	77	0.60	5600	6500	1.10
Zr(**22**)(O^{t}Bu)$_2$[b]	0.25	75	0.60	16300	15600	1.19
Zr(**26**)(O^{t}Bu)$_2$[a]	4	72	0.53	5250	16350	1.34
Zr(**26**)(O^{t}Bu)$_2$[c]	3	71	0.56	5200	5900	1.21
Zr(**26**)(O^{t}Bu)$_2$[b]	0.4	69	0.52	15000	13400	1.42

Conditions: [a] [LA]:[I]=100:1, 80 °C, toluene, [c] [LA]:[I]=300:1, 130 °C, solvent free, [c] [LA]:[I]:[BnOH]:=100:1:1, 80 °C, toluene [d] Determined *via* ^{1}H NMR spectroscopy. [e] P_r is the probability of heterotactic enchainment, determined *via* homonuclear decoupled ^{1}H NMR spectroscopy, [f] Theoretical molecular weight calculated from conversion {[LA]/[I] × (Conv. × 144.13)/2 + M_n(End Group)} (rounded to the nearest 50), [g] Determined from GPC (in THF) referenced against polystyrene standards with a correction factor of 0.58 applied.

The bis-ligated species, Zr(**1**)$_2$(O^{i}Pr)$_2$ was shown to be faster than the related Ti(IV) complex, Ti(**1**)$_2$(O^{i}Pr)$_2$. In solution (toluene, 80 °C), reasonable conversion was achieved after 2 hours and under solvent free conditions, less than 1 hour was required. However, similar to the Ti(IV) complex, only lower molecular weight was achievable with this initiator. The measured molecular weights were lower than the predicted value for two chains per metal centre and this is more pronounced for the solvent free reaction. The literature comparison Zr(**H**)$_2$(O^{i}Pr)$_2$ is shown to have comparable activity to Zr(**1**)$_2$(O^{i}Pr)$_2$.[24] However, in this system, stereocontrol is realised in both solution and under melt conditions (P_r = 0.68 - 0.74). Interestingly, the use of unsublimed LA with Zr(**H**)$_2$(O^{i}Pr)$_2$ for the solvent free reactions was observed to yield a more controlled polymerisation albeit with a reduction in molecular weight.

For Zr(**14**)(O^tBu)$_2$, a marked increase in activity is observed relative to both Ti(**14**)(O^iPr)$_2$ and Zr(**14**)$_2$. Under solution conditions, moderate conversion is realised after 1 hour and for the solvent-free ROP, 3 minutes is sufficient to afford high molecular weight. In both cases, the observed molecular weight is higher than the predicted value and this is likely related to initiator impurities. As Zr(**14**)(O^tBu)$_2$ was isolated with a small amount of Zr(**14**)$_2$, there is a reduction of active catalysts meaning less chains are likely to be initiated. The stereochemistry afforded by this alkoxide complex is slightly less that that achievable with Zr(**14**)$_2$ {for Zr(**14**)(O^tBu)$_2$, P_r = 0.73, for Zr(**14**)$_2$, P_r = 0.76}. Zr(**22**)(O^tBu)$_2$ is relatively more hindered than Zr(**14**)(O^tBu)$_2$ having two ^{t}Bu instead of Cl aryl substituents. As a consequence, the activity of this initiator is observed to be comparatively reduced. There is, however, an improvement on activity compared with the Ti(IV) analogue. Being isolated as a pure species, there is better agreement with measured and predicted molecular weight values. However, the stereocontrol is reduced compared to that afforded by Zr(**14**)(O^tBu)$_2$ {for Zr(**22**)(O^tBu)$_2$, P_r = 0.60}. Closer examination of the homonuclear decoupled ^{1}H spectrum for PLA derived from Zr(**22**)(O^tBu)$_2$ shows an unusual enhancement of the *isi* resonance (Figure 4.37). This is due to stereorandom transesterifcation giving rise to polymer linkages not typically seen on application of *rac*-LA.[30, 33, 34] These linkages are determined to be related to *iss*, *sss*, and *ssi* tetrads from analysis of the methine region in the $^{13}C\{^1H\}$ NMR spectrum (Figure 4.38) and should not be present for the ROP of *rac*-LA.[35] These tetrads coincide with the *isi* resonance in the ^{1}H NMR spectrum, hence the overall dominance of this resonance.

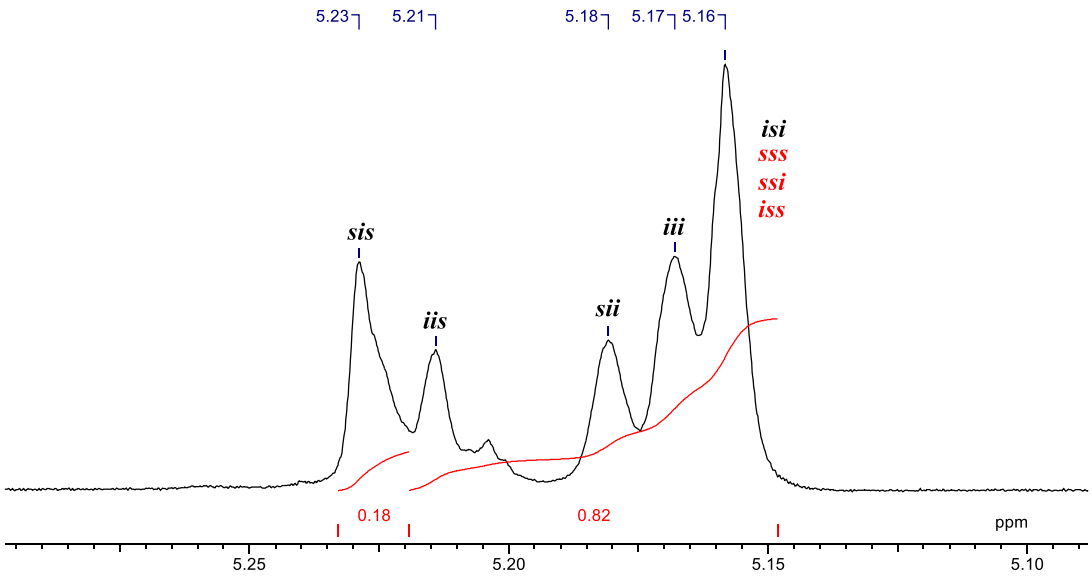

Figure 4.37: ^{1}H NMR ($CDCl_3$, 400MHz) homonuclear decoupled spectrum of PLA synthesised from solution polymerisation with Zr(**22**)(O^tBu)$_2$ (toluene, 80 °C).

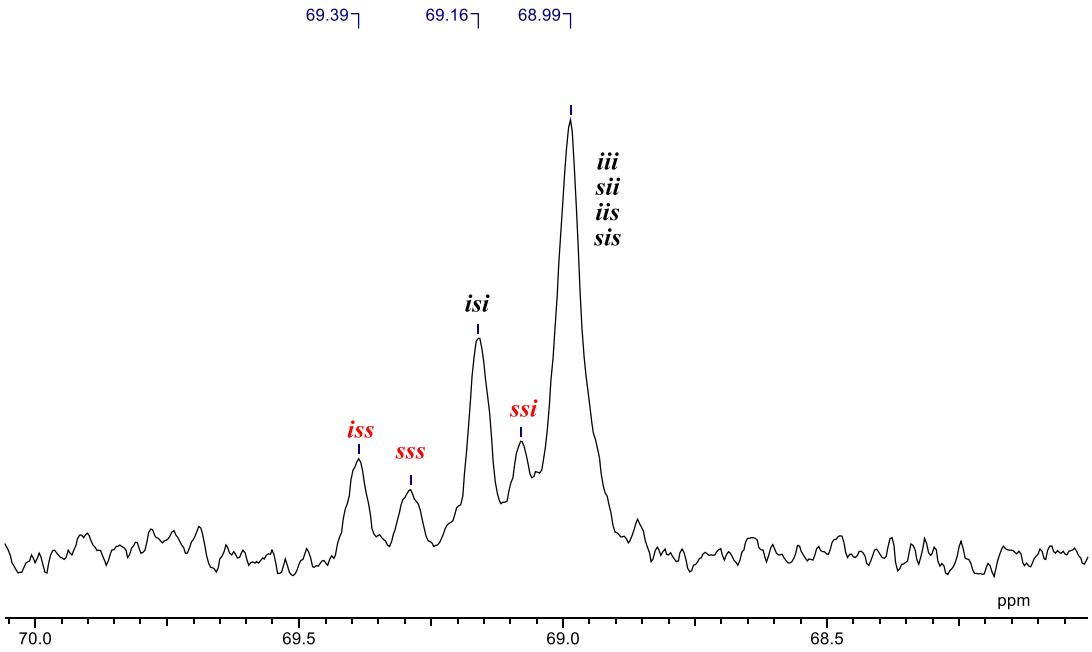

Figure 4.38: ^{13}C{^{1}H} NMR spectrum of PLA synthesised from solution polymerisation with Zr(**22**)(O^tBu)$_2$ (toluene, 80 °C).

The Zr(IV) salalen complex was also assessed for activity in the ROP of *rac*-LA. Initial polymerisations with Zr(**26**)(O^tBu)$_2$ suggested similar activity to the structural isomer, Zr(**22**)(O^tBu)$_2$ (72%, 4 hrs). However, there is a large difference between observed and theoretical molecular weight values for the solution polymerisation, with

a relatively broad distribution of chain lengths (Đ =1.34). Both of these facts may indicate a slow initiation process, due to the disfavoured insertion of ^{t}BuO- into the monomer.[36] To test this, polymerisation was carried out in the presence of one equivalence of BnOH. Under these conditions, the both molecular weight and weight distribution are reduced (Đ = 1.21) indicating an increase in control. The polymerisation is also observed to be more rapid (71%, 3 hrs). The solvent-free polymerisation achieves reasonable conversion within 30 minutes, however, a broad molecular weight distribution is observed under these conditions (Đ = 1.42). Under solution or melt conditions no stereocontrol is achieved by Zr(**26**)(O^{t}Bu)$_2$. The results for Zr(**26**)(O^{t}Bu)$_2$ are comparable to literature group IV salalen, Zr(**J**)(O^{i}Pr)$_2$.[28] Unusually, attempts to polymerise *rac*-LA with the related Zr(IV) salan, Zr(**31**)(O^{t}Bu)$_2$, were unsuccessful in solution and for solvent-free reactions.

MALDI-ToF analysis was carried analysis was carried out on the polymer derived from Zr(IV) alkoxides (Table 4.23). For Zr(**1**)$_2$(O^{i}Pr)$_2$, in solution, the observed molecular weight series is higher than GPC and more consistent with the theoretical value ($M_{n,MALDI}$ = 4200 g mol^{-1}). There is one major series with 72 g mol^{-1} spacing indicating undesirable transesterification reactions are occurring under these conditions, with ^{i}PrO- and H- end-groups present. There is also evidence of cyclic PLA oligomers from application the of Zr(**1**)$_2$(O^{i}Pr)$_2$ as well as TFA capped polymer (the TFA is the counterion for the Na(I) source in MALDI). In another instance, a series related to methoxy capped PLA was observable due to washing with MeOH. The polymer derived from the solvent-free polymerisation was also amenable to MALDI-ToF analysis. Similar observations are made as for the solution polymerisation, with ^{i}PrO- H- and TFA- end-groups present as well as cyclic structures. For the solvent-free MALDI-ToF spectrum, the distribution is not symmetrical with a substantial tail to low molecular weight.

For the bicyclic complex, Zr(**22**)(O^{t}Bu)$_2$, there are no peaks associated with the expected ^{t}BuO- end group *via* MALDI-ToF analysis. Instead, the main series, which has a spacing of 72 g mol^{-1}, correlates well with methoxy end groups. Evidently, counterproductive transesterifcation or cyclic oligomer ring opening occurs during polymer work-up. A minor series is present which is shown to possess no end-groups.

For the salalen complex, Zr(**26**)(O^tBu)$_2$, the polymer prepared in the absence of co-initiator is too large to be analysed by MALDI-ToF. However, the addition of BnOH afforded lower molecular weights amenable to characterisation. The spectrum is dominated by polymer containing the expected BnO- end group, with a symmetrical distribution and a 72 g mol^{-1} peak spacing. Trace amounts of ^{t}BuO- capped polymer is observed at lower molecular weight.

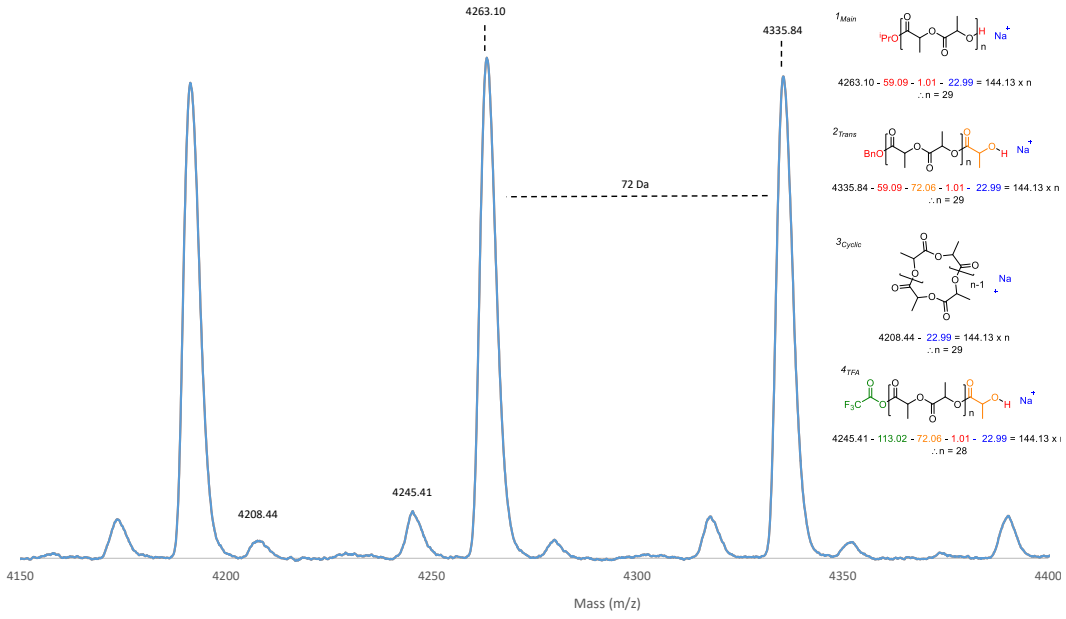

Figure 4.39: MALDI-ToF of PLA from solution polymerisation with Zr(**1**)$_2$(O^iPr)$_2$.

Table 4.23: Summary of MALDI-ToF analysis of PLA from Zr(IV) alkoxide complexes.

Initiator	Series	M_p /Da	End groups	n
Zr(1)$_2$(O^{i}Pr)$_2$[a]	1_{Main}	4263.10	^{i}PrO-, H-, Na^+	29
	2_{Trans}	4335.84	^{i}PrO-, H-, Na^+	29.5
	3_{Cyclic}	4208.44	Na^+	29
	4_{TFA}	4245.41	TFA-, H-, Na^+	28.5
Zr(1)$_2$(O^{i}Pr)$_2$[b]	1_{Main}	8734.81	^{i}PrO-, H-, Na^+	60
	2_{Trans}	8806.94	^{i}PrO-, H-, Na	60.5
	3_{TFA}	8789.37	TFA-, H-, Na^+	60.5
	4_{Cyclic}	8673.88	Na^+	60
Zr(22)(O^{t}Bu)$_2$[a]	1_{Main}	8556.58	MeO-, H-, Na^+	59
	2_{Trans}	8629.44	MeO-, H-, Na^+	59.5
	3_{Cyclic}	8530.53	Na^+	59
Zr(26)(O^{t}Bu)$_2$[c]	1_{Main}	8056.14	BnO-, H-, Na^+	50
	2_{Trans}	8125.16	BnO-, H-, Na^+	49.5
	3_{tBu}	5575.50	^{t}BuO-, H-, Na^+	38

Conditions: [a][LA]:[I] = 100:1, 80 °C, toluene.
[b][LA]:[I] = 300:1, 130 °C, solvent-free.
[c][LA]:[I]:[BnOH] = 100:1:1, 80 °C, toluene.

To ensure the activity of the bis-ligated complexes is not due to dissociated free ligand, a brief study was carried out to determine the ability of **14**H_2 to polymerise *rac*-lactide. It is noted that the bicyclic structural motif is not too dissimilar to DBU which is known to be active as an organocatalyst for ROP.[37] Under melt conditions (130°C, 24 hours, [LA]:[**14**H_2]:[BnOH] =100:1:1), PLA was produced by **14**H_2 affording a dark brown product. Reasonable conversion was achieved in the time (~75%) and there was a very slight isotactic bias (P_r = 0.40). GPC analysis indicates a molecular weight of 4900 $gmol^{-1}$ with a relatively broad distribution of 1.33. The broad molecular weight distribution could be a consequence of a slower rate of initiation compared to propagation as well as transesterification. Interestingly, MALDI-ToF analysis reveals two low molecular weight series (~3300 $gmol^{-1}$) with the dominant distribution having a spacing of 144 g mol^{-1} and the minor series, ~77 g mol^{-1}. The end groups are shown

to be BnO- and H-. Critically, application of **14**H_2 to the solution ROP at 80°C revealed no activity. It is postulated that exposure to high temperatures for an extended period of time causes a degradation of the ligand and the products of this can take part in ROP in some manner. The lack of activity in solution for **14**H_2 indicates that it is in fact the Zr/Hf complexes that are facilitating the ROP. Even for the melt polymerisation of Zr(**14**)$_2$, increased activity, level of control and polymer colouration would suggest the initiator remains intact and is enabling the polymerisation.

4.5 Conclusions

A range of different initiators based on a variety of metals and ligand classes have been applied to the ring opening polymerisation of lactide. For the imino monophenolate series, Al(**1**-**6**)Me_2, two different time scales were observed depending on the nature of the *ortho* aryl position. For bulkier groups, a longer polymerisation time was required (>16 hours) while reducing the steric loading at this position allowed for a fast polymerisation (< 4 hours). Depending on substituents both heterotactic and isotactic biases were observed. The monophenolate bicyclic Al(III) complexes, Al(**8**-**12**)Me_2 were also active for the ROP of *rac*-LA with the most selective initiator being Al(**11**)Me_2 (P_r = 0.28).

The bis-ligated Mg(II) and Zn(II) initiators were trialled for the ROP of *rac*-LA under both solution and melt conditions. In general, high activity was observed under both conditions with reaction times being less than one hour. Zn(**1**)$_2$ was observed to be more active that Mg(**1**)$_2$ and Mg(**A**)$_2$ under equal conditions. For the Mg(**A**/**1**)$_2$, the solvent-free polymerisations were hampered by insolubility of the initiators. Polymerisation was found to be possible in the absence of co-initiator, with monomer impurities or ligand groups assumed to carry out the initiation. An activated monomer is anticipated for these initiators.

For the bicyclic Al(III) initiators, Al(**14**-**22**)Me, reasonable conversions were achievable after 24 hours in each case. However, no stereocontrol was realised and there was no clear effect of varying aryl *ortho* substituents. MALDI-ToF analysis suggests larger aryl groups cause increased transesterification.

For the Al(III) salalens, Al(**26-30**)Me, activity was observed to be low with several days being required in solution to afford high conversions. Activity was increased slightly through inclusion of electron withdrawing groups {Cl or NO_2, Al(**29-30**)Me}. Slight isotactic {Al(**26**)Me, P_r = 0.37} and heterotactic {Al(**28**)Me, P_r = 0.68} bias were displayed by these initiators.

Compared to the salalen complexes, application of the Al(III) salan initiators, Al(**31-33**)O^{i}Pr afforded a dramatic increase in activity, requiring hours to attain high conversions in solution. The increased activity is thought to be related to the change in structure for these complexes. A strong isotactic bias was realised on application of Al(**31**)O^{i}Pr (P_m = 0.83, T_m = 177 °C, CH_2Cl_2, 25 °C). Kinetic analysis of Al(**31**)O^{i}Pr suggested a 1.56 rate order with respect to initiator concentration. The isotactic tendency was maintained under solvent free conditions and this series of initiators was found to be active under challenging industrial conditions. In comparison, the methylated salan, Al(**35**)Me, afforded activities comparable to that of the Al(III) salalen, Al(**26**)Me, both of which have identical geometries.

The triaryl Al(III) complexes, Al(**36**)O^{i}Pr and Al(**37**) were also trialled for the ROP of *rac*-LA. The alkoxide complex demonstrated reasonable activity and control under both solvent and melt conditions, however, Al(**36**)O^{i}Pr afforded no stereocontrol. In contrast, Al(**37**) was found to be inactive towards the ROP of *rac*-LA.

The Ti(IV) initiators were assessed for their polymerisation activity under melt conditions. Reaction times were found to range from 0.5 hours to 1 day. For the majority of initiators, the measured molecular weight was found to be consistent with two chains growing per metal centre.

The bis-ligated group (IV) initiators, M(**14-16**)$_2$ were trialled for the solution polymerisation of *rac*-LA. For M(**14-16**)$_2$, a heterotactic bias was realised (P_r ~ 0.76) and high conversion was achieved within 24 hours in solution. Kinetic analysis revealed the Zr(**14**)$_2$ (R = Cl) to be faster than Zr(**15**)$_2$ (R = Br). The resultant molecular weight of the polymer was found to be strongly dependent on the concentration of co-initiator. For the related Hf(IV) initiators, there was evidence that these species were more susceptible to monomer impurities, with a lower conversion being achievable

with unsublimed LA. An active monomer mechanism is postulated for this initiator series.

For the Zr(IV) alkoxide initiators, high activity was demonstrated. For Zr(**1**)$_2$(O^{i}Pr)$_2$ rapid polymerisation was observed but the resultant PLA moecular weight was found to be lower than expected. MALDI-ToF analysis indicated the presence of side reactions and cyclic PLA chains. For Zr(**14**)(O^{t}Bu)$_2$, increased activity is observed relative to the analogous bis-ligated species, Zr(**14**)$_2$. A similar stereochemical tendency is also realised (P_r = 0.73). The bulkier Zr(**22**)(O^{t}Bu)$_2$ initiator yielded less hetereotactic PLA and analysis by ^{1}H homonuclear decoupled NMR indicated the operation of stereorandom transesterifcation reactions. The Zr(IV) salalen, Zr(**26**)(O^{t}Bu)$_2$, demonstrated reasonable activity towards the polymerisation of *rac*-LA. However, the control of molecular weight was poor with a higher than expected value being measured. This was related to slow initiation with signs of improvement through addition of a co-initiator.

4.6 Future work

The ligands described in this thesis are all based upon the use of racemic 2-AMP, hence yielding racemic ligands. As a consequence of point chirality, this often led to the isolation of diastereomeric complexes. Therefore, the resolution of 2-AMP would allow for the preparation of enantiomerically pure complexes, which allows for a better understanding of subsequent catalysis. A possible route has been demonstrated in a patent (Figure 4.40).[38] This pathway begins at 2-pyridylacetic acid with tartaric acid subsequently used to separate *R*/*S* forms of 2-piperidineacetic acid *via* recrystallisation. It may also be viable to co-crystallise enantiomerically pure 2-(aminomethyl)piperidine directly from a reaction with tartaric acid.

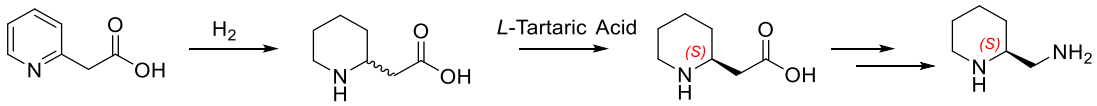

Figure 4.40: Literature preparation of enantiopure 2-AMP.[38]

The range of iminophenolate complexes from **1**-**6**H was limited by the equilibrium process. However, the complexes that were formed exhibited a degree of selectivity {Al(**1**-**6**)Me_2} or facilitated rapid polymerisation {Mg/Zn(**1**)$_2$}. Future work could expand on these results by carrying out further polymerisations with Al(**1**-**6**)Me_2 to understand both the origin of selectivity and the nature of the active species. For the Mg(II)/Zn(II) complexes, the series could be expanded {M(**2**-**6**)$_2$} to see if either activity or selectivity can be improved upon. These initiators could also be tested under immortal polymerisation conditions. Further to this, Ca(II) could provide an interesting comparison to these complexes. Calcium has a high natural abundance as well as a being abundant in the body, making it highly biocompatible. Ca(II) complexes have been widely reported for the ROP of lactide and typically show good activity and in some instances selectivity.[9, 39-43]

For the bicyclic bisphenolate ligands, a wide range of ligands/complexes have been reported. Best polymerisation results have been achieved with group (IV) metal centres and it is anticipated that further Zr(IV)/2-AMP complexes may yield active/selective initiators. A key challenge for this is to prepare a heteroleptic complex which could also allow for the preparation of mixed ligand species Zr(**L**^{1})(**L**^{2}).

The prepared salen complexes {Al(**26**-**30**)Me / Ti/Zr(**26**)(O^iPr)$_2$} generally afforded low activity and minor selectivity for ROP. Most promising results were achieved with the group (IV) complexes and the preparation of complexes with reduced ligand bulk is recommended.

The preparation of Al(III) salan based complexes was highly successful for the polymerisation of *rac*-LA. A further investigation into variation of the aryl substituents could prove fruitful for improving the system further. Some combinations of substituents are amenable to preparation using protocols discussed in this thesis (R^1 = R^2 = Me, R^3 = R^4 = Cl; R^1 = R^2 = Me, R^3 = H R^4 = NO_2; R^1 =Ad, R^2 = Me, R^3 = R^4 = Cl; R^1 =Ad, R^2 = Me, R^3 = H, R^4 = NO_2). Greater diversity may be achieved using protection chemistry (Figure 4.41).[44, 45] DFT modelling could be applied to help understand both the motivation for ligand arrangement {relative to Al(III) salalen} and the enhancements observed for ROP. Further insight could be achieved through preparation of a lactate model complex[4, 7, 23, 46] and *in situ* monitoring of melt polymerisations *via* FT-IR.[47]

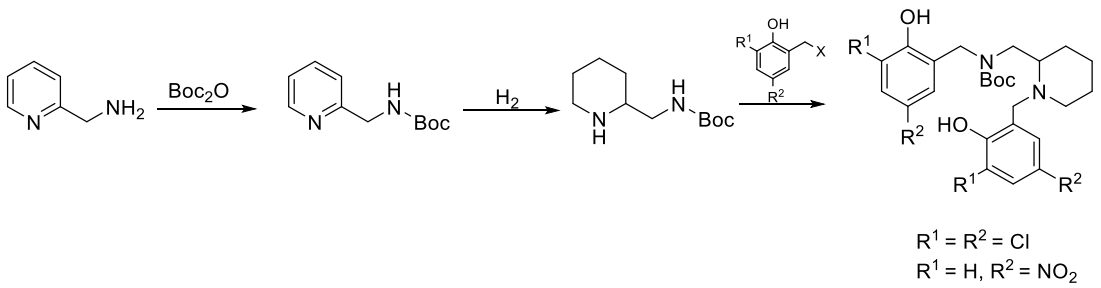

Figure 4.41: Literature procedure for Boc protection of 2-AMP,[44] and further reaction to a salan.

For triaryl phenol ligands, **36**H_2/**37**H_3, the range of aryl substituents could be expanded on. Complexation with other metals, such as Zr(IV), could also be of interest for these ligands. Initial work began on a further triaryl bisphenol, the structure of which was demonstrated by X-ray crystallography (Figure 4.42). This ligand features two separated phenol groups and could form interesting binuclear structures.

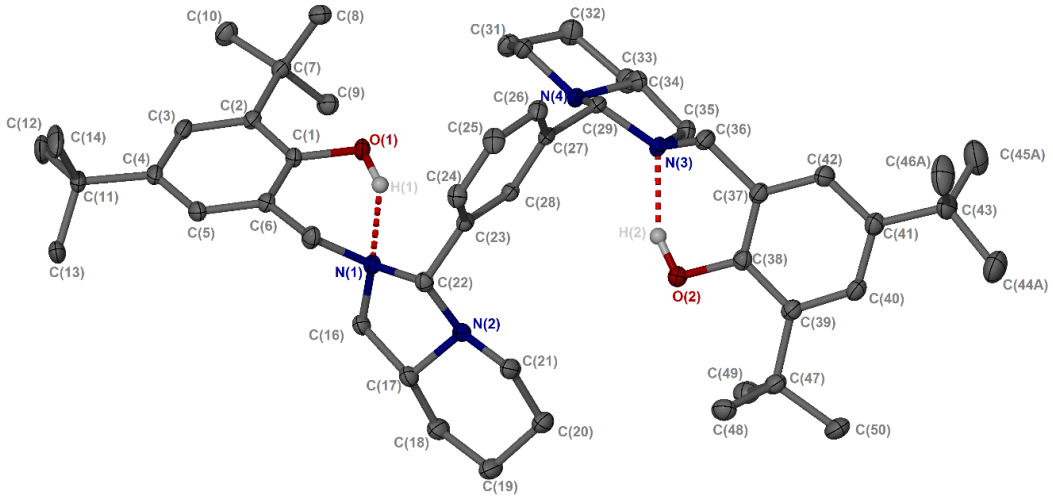

Figure 4.42: Solid state structure of **F**H_2. Ellipsoids are shown at the 30% probability level and all hydrogen atoms, except those involved in hydrogen bonding, have been removed for clarity.

In this thesis, the only monomer considered was lactide to assess whether stereocontrol is imparted by the prepared initiators. The field of ROP of cyclic esters is vast and there other monomers to choose from. In this way, the versatility of the initiators reported herein could be tested, with monomer ring size, functionality and bulk being varied. Seven membered ring caprolactone,[9, 48-52] and 4/5 membered butyrolactones[53-

[56] are commonly assessed in the literature, as well as the unsubstituted six membered glycolide.[57] An extension to this would be an investigation into the copolymerisation of monomers, which is important for tuning polymer properties.

4.7 References

1. S. Bian, S. Abbina, Z. Lu, E. Kolodka and G. Du, *Organometallics*, 2014, **33**, 2489-2495.
2. E. D. Cross, L. E. N. Allan, A. Decken and M. P. Shaver, *J. Polym. Sci., Part A: Polym. Chem.*, 2013, **51**, 1137-1146.
3. P. Hormnirun, E. L. Marshall, V. C. Gibson, R. I. Pugh and A. J. P. White, *Proc. Natl. Acad. Sci. U. S. A.*, 2006, **103**, 15343-15348.
4. N. Nomura, R. Ishii, Y. Yamamoto and T. Kondo, *Chem. Eur. J.*, 2007, **13**, 4433-4451.
5. E. L. Whitelaw, G. Loraine, M. F. Mahon and M. D. Jones, *Dalton Trans.*, 2011, **40**, 11469-11473.
6. P. A. Cameron, V. C. Gibson, C. Redshaw, J. A. Segal, A. J. P. White and D. J. Williams, *J. Chem. Soc., Dalton Trans.*, 2002, 415-422.
7. M. Normand, V. Dorcet, E. Kirillov and J.-F. Carpentier, *Organometallics*, 2013, **32**, 1694-1709.
8. L. Cuesta-Aluja, A. Campos-Carrasco, J. Castilla, M. Reguero, A. M. Masdeu-Bultó and A. Aghmiz, *J. CO_2 Util.*, 2016, **14**, 10-22.
9. J. B. L. Gallaway, J. R. K. McRae, A. Decken and M. P. Shaver, *Can. J. Chem.*, 2012, **90**, 419-426.
10. A. Pilone, K. Press, I. Goldberg, M. Kol, M. Mazzeo and M. Lamberti, *J. Am. Chem. Soc.*, 2014, **136**, 2940-2943.
11. M. D. Jones, L. Brady, P. McKeown, A. Buchard, P. M. Schafer, L. H. Thomas, M. F. Mahon, T. J. Woodman and J. P. Lowe, *Chem. Sci.*, 2015, **6**, 5034-5039.
12. H. Du, A. H. Velders, P. J. Dijkstra, J. Sun, Z. Zhong, X. Chen and J. Feijen, *Chem. Eur. J.*, 2009, **15**, 9836-9845.
13. T. M. Ovitt and G. W. Coates, *J. Polym. Sci., Part A: Polym. Chem.*, 2000, **38**, 4686-4692.
14. B. M. Chamberlain, M. Cheng, D. R. Moore, T. M. Ovitt, E. B. Lobkovsky and G. W. Coates, *J. Am. Chem. Soc.*, 2001, **123**, 3229-3238.
15. C. K. Williams, L. E. Breyfogle, S. K. Choi, W. Nam, V. G. Young, M. A. Hillmyer and W. B. Tolman, *J. Am. Chem. Soc.*, 2003, **125**, 11350-11359.
16. T. Ouhadi, A. Hamitou, R. Jerome and P. Teyssie, *Macromolecules*, 1976, **9**, 927-931.
17. Y. Yang, H. Wang and H. Ma, *Inorg. Chem.*, 2015, **54**, 5839-5854.
18. J. Börner, I. dos Santos Vieira, A. Pawlis, A. Döring, D. Kuckling and S. Herres-Pawlis, *Chem. Eur. J.*, 2011, **17**, 4507-4512.
19. K. B. Aubrecht, M. A. Hillmyer and W. B. Tolman, *Macromolecules*, 2002, **35**, 644-650.
20. A. F. Douglas, B. O. Patrick and P. Mehrkhodavandi, *Angew. Chem. Int. Ed.*, 2008, **120**, 2322-2325.

21. S. Abbina and G. Du, *ACS Macro Lett.*, 2014, **3**, 689-692.
22. I. Peckermann, A. Kapelski, T. P. Spaniol and J. Okuda, *Inorg. Chem.*, 2009, **48**, 5526-5534.
23. K. Phomphrai, P. Chumsaeng, P. Sangtrirutnugul, P. Kongsaeree and M. Pohmakotr, *Dalton Trans.*, 2010, **39**, 1865-1871.
24. A. J. Chmura, D. M. Cousins, M. G. Davidson, M. D. Jones, M. D. Lunn and M. F. Mahon, *Dalton Trans.*, 2008, 1437-1443.
25. A. J. Chmura, M. G. Davidson, M. D. Jones, M. D. Lunn and M. F. Mahon, *Dalton Trans.*, 2006, 887-889.
26. S. Gendler, S. Segal, I. Goldberg, Z. Goldschmidt and M. Kol, *Inorg. Chem.*, 2006, **45**, 4783-4790.
27. M. Kol, M. Shamis, I. Goldberg, Z. Goldschmidt, S. Alfi and E. Hayut-Salant, *Inorg. Chem. Commun.*, 2001, **4**, 177-179.
28. E. L. Whitelaw, M. D. Jones and M. F. Mahon, *Inorg. Chem.*, 2010, **49**, 7176-7181.
29. A. L. Zelikoff, J. Kopilov, I. Goldberg, G. W. Coates and M. Kol, *Chem. Commun.*, 2009, 6804-6806.
30. A. J. Chmura, M. G. Davidson, M. D. Jones, M. D. Lunn, M. F. Mahon, A. F. Johnson, P. Khunkamchoo, S. L. Roberts and S. S. F. Wong, *Macromolecules*, 2006, **39**, 7250-7257.
31. N. Maudoux, T. Roisnel, V. Dorcet, J.-F. Carpentier and Y. Sarazin, *Chem. Eur. J.*, 2014, **20**, 6131-6147.
32. S.-C. Rosca, D.-A. Rosca, V. Dorcet, C. M. Kozak, F. M. Kerton, J.-F. Carpentier and Y. Sarazin, *Dalton Trans.*, 2013, **42**, 9361-9375.
33. M. Bero, J. Kasperczyk and Z. J. Jedlinski, *Die Makromolekulare Chemie*, 1990, **191**, 2287-2296.
34. B. Calvo, M. G. Davidson and D. García-Vivó, *Inorg. Chem.*, 2011, **50**, 3589-3595.
35. M. T. Zell, B. E. Padden, A. J. Paterick, K. A. M. Thakur, R. T. Kean, M. A. Hillmyer and E. J. Munson, *Macromolecules*, 2002, **35**, 7700-7707.
36. C. Bakewell, T.-P.-A. Cao, N. Long, X. F. Le Goff, A. Auffrant and C. K. Williams, *J. Am. Chem. Soc.*, 2012, **134**, 20577-20580.
37. B. G. G. Lohmeijer, R. C. Pratt, F. Leibfarth, J. W. Logan, D. A. Long, A. P. Dove, F. Nederberg, J. Choi, C. Wade, R. M. Waymouth and J. L. Hedrick, *Macromolecules*, 2006, **39**, 8574-8583.
38. US Pat., 4 760 065, 1988.
39. H.-Y. Chen, H.-Y. Tang and C.-C. Lin, *Polymer*, 2007, **48**, 2257-2262.
40. M. H. Chisholm, J. Gallucci and K. Phomphrai, *Chem. Commun.*, 2003, 48-49.
41. M. H. Chisholm, J. C. Gallucci and K. Phomphrai, *Inorg. Chem.*, 2004, **43**, 6717-6725.
42. M.-W. Hsiao, G.-S. Wu, B.-H. Huang and C.-C. Lin, *Inorg. Chem. Commun.*, 2013, **36**, 90-95.
43. V. Poirier, T. Roisnel, J.-F. Carpentier and Y. Sarazin, *Dalton Trans.*, 2009, 9820-9827.
44. B. G. Shearer, J. P. Sullivan, J. P. Carter, R. M. Mathew, P. Waid, J. R. Connor, R. J. Patch and R. M. Burch, *J. Med. Chem.*, 1991, **34**, 2928-2931.
45. J. Perumattam, B. G. Shearer, W. L. Confer and R. M. Mathew, *Tetrahedron Lett.*, 1991, **32**, 7183-7186.

46. J. S. Klitzke, T. Roisnel, E. Kirillov, O. d. L. Casagrande and J.-F. Carpentier, *Organometallics*, 2014, **33**, 5693-5707.
47. C. J. Chuck, M. G. Davidson, G. Gobius du Sart, P. K. Ivanova-Mitseva, G. I. Kociok-Köhn and L. B. Manton, *Inorg. Chem.*, 2013, **52**, 10804-10811.
48. K. Bakthavachalam, A. Rajagopal and N. Dastagiri Reddy, *Dalton Trans.*, 2014, **43**, 14816-14823.
49. C.-T. Chen, C.-A. Huang and B.-H. Huang, *Dalton Trans.*, 2003, 3799-3803.
50. L. Chen, W. Li, D. Yuan, Y. Zhang, Q. Shen and Y. Yao, *Inorg. Chem.*, 2015, **54**, 4699-4708.
51. C. Egevardt, S. O. K. Giese, A. D. da C. Santos, A. Barison, E. L. de Sá, A. Z. Filho, T. A. da Silva, S. F. Zawadzki, J. F. Soares and G. G. Nunes, *J. Polym. Sci., Part A: Polym. Chem.*, 2014, **52**, 2509-2517.
52. M. A. Woodruff and D. W. Hutmacher, *Prog. Polym. Sci.*, 2010, **35**, 1217-1256.
53. J.-F. Carpentier, *Macromol. Rapid Commun.*, 2010, **31**, 1696-1705.
54. A. Amgoune, C. M. Thomas, S. Ilinca, T. Roisnel and J.-F. Carpentier, *Angew. Chem. Int. Ed.*, 2006, **45**, 2782-2784.
55. M. Hong and E. Y. X. Chen, *Nat Chem*, 2016, **8**, 42-49.
56. C. Xu, I. Yu and P. Mehrkhodavandi, *Chem. Commun.*, 2012, **48**, 6806-6808.
57. O. Dechy-Cabaret, B. Martin-Vaca and D. Bourissou, *Chem. Rev.*, 2004, **104**, 6147-6176.

Chapter 5

Experimental

Chapter 5: Experimental

5.1 General experimental methods

The preparation and characterisation of all metal complexes was carried out under inert argon atmosphere using standard Schlenk or glovebox techniques. All chemicals used were purchased from Aldrich and used as received except for *rac*- and *L*-LA which was recrystallised from dry toluene and $Ti(O^iPr)_4$ which was vacuum distilled prior to use. 3,5-di-*tert*-butyl-2-hydroxybenzylbromide,[1] 3,5-di-chloro-2-hydroxybenzylchloride,[2] 3,5-dimethylsalicylaldehyde,[3] 3-trityl-5-methylsalicylaldehyde,[4] 3-(1-adamantyl)-5-methylsalicylaldehyde,[5] were prepared according to literature methods. Dry solvents used in handling metal complexes were obtained *via* SPS (solvent purification system). ^1H and $^{13}C\{^1H\}$ NMR spectra were recorded on a Bruker 400 or 500 MHz instrument and referenced to residual solvent resonances. $CDCl_3$ was dried over CaH_2 prior to use with metal complexes. C_6D_6 and d_8-toluene were degassed and stored over molecular sieves for use with metal complexes Coupling constants are given in Hertz. Exchange spectroscopy (EXSY) data was acquired by Dr. John Lowe. Diffusional ordered spectroscopy (DOSY) NMR data was acquired by Dr. Tim Woodman. For DOSY NMR analysis, the standard Bruker pulse sequence ledgp2s[6] was used, with d1 of 5 seconds, 64k data points and 16 scans per gradient level. Typically the gradient pulse was 1700 μs, with a diffusion time of 0.1 s. Ten gradient strengths were used between 2 and 95 %. Data were processed using DOSY methods.[7] All ligands were characterised by electron-spray ionisation-mass spectrometry (ESI-MS) in positive mode. CHN microanalysis was performed by Mr. Stephen Boyer of London Metropolitan University.

All crystallographic data was collected on a SuperNova, EOS detector diffractometer using radiation CuKα (λ= 1.54184 Å) or Mo-Kα (λ= 0.71073 Å) or a Nonius kappa diffractometer using Mo-Kα (λ= 0.71073 Å) all recorded at 150(2) K. Data was collected by Dr. Matthew Jones with assistance from Dr. Mary Mahon and Dr. Gabriele Kociok-Köhn on more advanced crystallographic systems. All structures were solved by direct methods and refined on all F^2 data using the SHELXL-2014

suite of programs. All hydrogen atoms were included in idealized positions and refined using the riding model.

DFT calculations were carried out using Gaussian09 suite of codes (revision A.02).[8] The chosen functional (rωb97xD) has been developed to model dispersions forces as well accurately reproduce thermodynamic and kinetic experimental data.[9, 10] This protocol has also been successfully applied to metal complexes and their catalysis.[11, 12] Initial energy minimisations were carried out at a B3LYP level of theory with a 6-311+g(d,p) basis set. Further calculations were carried out rωb97xD/6-311+G(d) with temperature (298.15 K) and solvent (cpcm, toluene) included. Attainment of energy minima was confirmed by the absence of an imaginary frequency.

5.2 General polymerisation methods

Polymerisations were carried out in a Youngs ampoule under inert argon conditions. For a typical solution based polymerisation, *rac*-lactide (1.0 g, 0.69 mmol) was dissolved in dry toluene (10 ml) with the required amount of initiator ([LA]:[I] = 100:1). When required, a benzyl alcohol co-initiator (typically [I]:[BnOH] = 1:1, 7.2 µl) was added. The ampoule was then placed in a preheated oil bath (80 °C) and stirred for the set time. After polymerisation, a few drops of MeOH were added to quench the reaction. For immortal polymerisation initiators, this step was avoided to prevent chain transfer and instead the polymerisation quenched in air. Following quenching, the solvent was removed *in vacuo* and a crude ^{1}H NMR recorded. The polymer was then purified by washing with methanol to remove initiator and unreacted monomer. For solvent free polymerisations, a higher initiator ratio was employed (300:1) and the reaction performed at 130 °C or above. The polymerisation vessel was placed in a pre-heated oil bath and polymerisation start time commenced on the melting of the monomer. After polymerisation, the product was dissolved in CH_2Cl_2 (~10 ml) and a few drops of MeOH were added followed by solvent removal *in vacuo* and acquisition of a crude ^{1}H NMR. The polymer was then purified in the same fashion as for solution polymerisations. Under immortal polymerisation conditions ([LA]:[I]:[BnOH] = 3000:1:10), the reaction scale is doubled (*rac*-LA = 2.0 g). NMR kinetics were carried out in a J-Youngs tube in d_8-toluene (0.60 ml). The NMR tube was then placed into

the pre-heated NMR machine with data acquistition interval decided based on rapidity of the initiator under investigation.

All purified polymers were characterised by a combination of gel permeation chromatography (GPC) and homonuclear decoupled ^{1}H NMR spectroscopy. GPC was carried out at 1 ml min^{-1} at 35 °C with a THF eluent using a PLgel 5 µm MIXED-D 300 × 7.5 mm column. The system was referenced against 11 narrow molecular weight standards polystyrene standards with detection *via* refractive index response. A correction factor of 0.58 was applied to measured values.[13] Polymer tacticity was determined *via* ^{1}H NMR spectroscopy ($CDCl_3$) analysis of the homonuclear decoupled methine region utilizing the relationships demonstrated by Coates *et al*.[14]

MALDI-ToF mass spectra were determined on a Bruker Autoflex speed instrument using DCTB (trans-2-[3-(4-tert-Butylphenyl)-2-methyl-2-propenylidene]malononitrile) as the matrix and ionized using NaTFA. DSC analysis was recorded on a TA Instruments DSC Q20. The sample was held at 40 ºC for 1 minute, heated to 250 ºC at 5 ºC min^{-1} held at this temperature for 1 minute, cooled to 40 ºC at 5 ºC min^{-1} held at this temperature for 1 minute and finally heated to 250 ºC at 5 ºC min^{-1} - the T_m values are quoted for the second heating cycle.

5.3 Ligand synthesis and characterisation (Chapter 2)

5.3.1 Preliminary investigations

The assessment the of aryl substituent effect on product distribution of **A**H and **B**H was carried out on a small scale. Aldehyde (0.412 mmol) was dissolved in MeOH (2 ml) followed by addition of 2-(aminomethyl)piperidine (0.05ml, 0.41 mmol) dropwise, typically accompanied by yellow colouration of the solution. After 1 hr of stirring at room temperature, solvent was removed *in vacuo* and the crude product dissolved in $CDCl_3$ for NMR analysis.

5.3.2 Monophenolate ligand synthesis

Synthesis of imino monophenolates (1-6H): 2-(Aminomethyl)piperidine (1.0 ml, 8.24 mmol) was added dropwise to a solution of substituted salicylaldehyde (8.24 mmol) in methanol (50 ml). After stirring for 1 hour, solvent was removed yielding the final product in good purity. Two products (imino and cyclic) were observed with a ratio dependent on aryl substituents. Reaction of 3-(1-adamantyl)-5-methyl-2-salicylaldehyde was performed on 2.7 mmol scale.

1H: Isolated as an orange oil (>99% conversion, 9:1 imine:cyclic product).
Major product (Imine): ^{1}H NMR ($CDCl_3$, 400 MHz) δ = 13.63 (s, 1H; ArOH), 8.36 (s, 1H; ArCHN), 7.37 (d, *J* = 2.4 Hz, 1H; ArH), 7.07 (d, *J* = 2.5 Hz, 1H; ArH), 3.68 (ddd, *J* = 12.0, 4.5, 1.5 Hz, 1H; CH_2), 3.39 (dd, *J* = 12.0, 8.0 Hz, 1H; CH_2), 3.09 (m, 1H; CH_2), 2.84 (m, 1H; CH), 2.65 (m, 1H; CH_2), 1.83 (m, 1H; CH_2), 1.74 (m, 1H; CH_2) 1.63 (m, 1H; CH_2), 1.44 (s, 9H; $C(CH_3)_3$), 1.34 (m, 2H; CH_2), 1.29 (s, 9H; $C(CH_3)_3$), 1.23 (m, 1H; CH_2). $^{13}C\{^{1}H\}$ NMR ($CDCl_3$, 100 MHz) δ = 167.3 (ArCHN), 157.9, 140.1, 136.6, 126.9, 125.9, 117.7 (Ar), 66.2 (CH_2), 56.6 (CH), 46.8 (CH_2), 35.0, 34.0 ($C(CH_3)_3$), 31.4 ($C(CH_3)_3$), 30.7 (CH_2), 29.4 ($C(CH_3)_3$), 26.2, 24.5 (CH_2).
Minor product (Cyclic): ^{1}H NMR ($CDCl_3$, 400 MHz) δ = 11.60 (s, 1H; ArOH), 7.24 (d, *J* = 2.5 Hz, 1H; ArH), 6.93 (d, *J* = 2.5 Hz, 1H; ArH), 4.16 (s, 1H; $ArCHN_2$), 3.21(dd, *J* = 9.5, 7.0 Hz, 1H; CH_2), 2.96 (m, 2H; CH_2), 2.84 (m, 1H; CH_2), 2.43 (m, 1H; CH), 2.06 (m, 2H; CH_2), 1.95 (m, 2H; CH_2), 1.87 (m, 1H; CH_2), 1.40 (s, 9H; $C(CH_3)_3$), 1.26 (s, 9H; $C(CH_3)_3$). $^{13}C\{^{1}H\}$ NMR ($CDCl_3$, 100 MHz) δ= 153.9, 140.3, 136.1, 124.9, 124.0, 120.5 (Ar), 84.0 ($ArCHN_2$), 63.5 (CH), 50.5, 48.4 (CH_2), 35.0, 34.0 ($C(CH_3)_3$), 31.6, 29.5 ($C(CH_3)_3$), 29.0, 24.8, 23.8 (CH_2).
ESI-MS(MeOH): Calcd *m/z* $[C_{21}H_{34}N_2ONa]^+$ = 353.2569, found *m/z* = 353.2551

2H: Isolated as a yellow powder (0.92 g, 2.5 mmol, 93 %, 9:1 imine:cyclic product).
Major product (Imine): ^{1}H NMR ($CDCl_3$, 400 MHz) δ = 13.60 (s, 1H; ArOH), 8.33 (s, 1H; ArCHN), 7.08 (d, *J* = 2.0 Hz, 1H; ArH), 6.90 (d, *J* = 1.5 Hz, 1H; ArH), 3.70 (dd, *J* = 12.0, 4.5 Hz, 1H; CH_2), 3.42 (m, 1H; CH_2), 3.08 (br d, *J* = 11.5 Hz, 1H; CH_2), 2.90 (m, 1H; CH), 2.67 (td, *J* = 12.0, 3.0 Hz, 1H; CH_2), 2.28 (s, 3H; CH_3), 2.24 (t, *J* = 3.4 Hz, 1H; CH_2), 2.18 (br s, 6H; $CH_{2\ Ad}$), 2.09 (br s, 4H; $CH_2/CH_{\ ad}$), 1.83 (m, 1H;

CH_2), 1.78 (br s, 8H; CH_2/$CH_{2\ ad}$), 1.68 (m, 1H; CH_2). $^{13}C\{^1H\}$ NMR ($CDCl_3$, 100 MHz) δ = 167.3 (Ar*C*HN), 158.3, 137.4, 130.6, 129.5, 126.8, 118.3 (Ar), 66.0 (CH_2), 56.6 (CH), 46.7 (CH_2), 40.3, 37.1 ($CH_{2\ Ad}$), 36.9 ($C_{\ ad}$), 30.5 (CH_2), 29.1 ($CH_{\ ad}$), 25.9, 24.4 (CH_2), 20.7 (CH_3).
ESI-MS (MeOH): Calcd *m/z* $[C_{24}H_{34}N_2O_1Na]^+$= 389.2569, found *m/z* = 389.2572.

3H: Isolated as an orange oil (98 % conversion, 5:2 imine:cyclic product).
Major product (Imine): ^1H NMR ($CDCl_3$, 400 MHz) δ = 13.09 (s, 1H; ArOH), 8.28 (s, 1H; ArCHN) 7.20 (m, 15H; ArH), 7.11 (d, *J* = 1.9 Hz, 1H; ArH), 7.01 (d, *J* = 1.8 Hz, 1H; ArH), 3.56 (ddd, *J* = 12.1, 4.1, 1.3 Hz, 1H; CH_2), 3.28 (dd, *J* = 12.3, 8.3 Hz, 1H; CH_2), 3.00 (br d, *J* = 11.8 Hz, 1H; CH), 2.76 (m, 1H; CH_2), 2.56 (t d, *J* = 11.5, 2.6 Hz, 1H; CH_2), 2.23 (s, 3H; CH_3), 1.78 (m, 1H; CH_2), 1.56 (m, 2H; CH_2), 1.37 (m, 2H; CH_2), 1.11 (m, 1H; CH_2). $^{13}C\{^1H\}$ NMR ($CDCl_3$, 100 MHz) δ = 166.3 (Ar*C*HN), 157.8, 146.1, 145.6, 134.5, 134.4, 131.0, 127.1, 125.5, 118.6 (Ar), 66.2 (CH_2), 63.1 (CPh_3), 56.2 (CH), 46.7, 30.6, 26.1, 24.4 (CH_2), 20.7 (CH_3).
Minor product (Cyclic): ^1H NMR ($CDCl_3$, 400 MHz) δ = 10.94 (s, 1H; ArOH), 7.20 (m, 15H; ArH), 6.92 (d, *J* = 1.8 Hz, 1H; ArH), 6.88 (d, *J* = 1.7 Hz, 1H; ArH), 4.02 (s, 1H; $ArCHN_2$), 3.10 (m, 1H; CH_2), 2.80 (m, 1H; CH_2), 2.45 (br d, *J* = 11.8 Hz, 1H; CH_2), 2.28 (m, 1H; CH), 2.17 (s, 3H; CH_3), 1.87 (m, 1H; CH_2), 1.78 (m, 1H; CH_2), 1.70 (m, 1H; CH_2), 1.50 (m, 1H; CH_2), 1.21 (m, 2H; CH_2), 1.08 (m, 1H; CH_2). $^{13}C\{^1H\}$ NMR ($CDCl_3$, 100 MHz) δ = 153.7, 145.6. 134.9, 131.9, 130.9, 130.1, 127.0, 125.4, 121.4 (Ar), 83.3 ($ArCHN_2$), 63.3 (CH), 63.0 (CPh_3), 50.3, 47.9, 28.5, 24.4, 23.6 (CH_2), 20.8 (CH_3).
ESI-MS (MeOH): Calcd *m/z* $[C_{33}H_{34}N_2ONa]^+$ = 497.2569, found *m/z* = 497.2545.

4H: Isolated as an orange oil (97 % conversion, 3:1 imine:cyclic product).
Major product (Imine): ^1H NMR ($CDCl_3$, 400 MHz) δ = 13.26 (s, 1H; ArOH), 8.24 (s, 1H; ArCHN) 6.97 (s, 1H; ArH), 6.83 (s, 1H; ArH), 3.61 (ddd, *J* = 12.0, 4.5, 1.5 Hz, 1H; CH_2), 3.36 (ddd, *J* = 12.0, 8.0, 1.0 Hz, 1H; CH_2), 3.01 (br d, *J* = 12.0 Hz, 1H; CH), 2.79 (m, H; CH), 2.59 (d t, *J* = 12.0, 3.0 Hz, 1H; CH_2), 2.22 (s, 6H; 2×CH_3), 1.79 (m, 1H; CH_2), 1.68 (m, 1H; CH_2), 1.58 (m, 1H; CH_2), 1.37 (m, 2H; CH_2), 1.19 (m, 1H; CH_2).

$^{13}C\{^{1}H\}$ NMR ($CDCl_3$, 100 MHz) δ= 166.4 (Ar*C*HN), 157.0, 134.4, 129.0, 127.2, 125.6, 117.6 (Ar), 66.1 (CH_2), 56.7 (CH), 46.8, 30.7, 26.2, 24.5 (CH_2), 20.3, 15.4 (CH_3)

Minor product (Cyclic): ^{1}H NMR ($CDCl_3$, 400 MHz) δ = 11.44 (s, 1H; ArOH), 6.85 (s, 1H; ArH), 6.68 (s, 1H; ArH), 4.09 (s, 1H; $ArCHN_2$), 3.14 (dd, *J* = 9.0, 6.5 Hz, 1H; CH_2), 2.88 (m, 2H; CH_2), 2.18 (s, 3H; CH_3), 2.16 (s, 3H; CH_3), 2.00 (dd, *J* = 12.0, 3.0 Hz, 1H; CH_2), 1.90 (m, 2H; CH/CH_2), 1.79 (m, 1H; CH_2), 1.68 (m, 1H; CH_2), 1.58 (m, 1H; CH_2), 1.37 (m, 2H; CH_2). $^{13}C\{^{1}H\}$ NMR ($CDCl_3$, 100 MHz) δ = 131.7, 128.1 (Ar), 83.1 ($ArCHN_2$), 63.6 (CH), 50.4, 48.5, 29.1, 25.0, 23.8 (CH_2), 20.3, 15.6 (CH_3).

ESI-MS (MeOH): Calcd *m/z* $[C_{15}H_{23}N_2O_2]^+$ = 247.1810, found *m/z* = 247.1807.

5H: Isolated as a yellow oil (96 % conversion, 2:1 imine:cyclic product).

Major product (Imine): ^{1}H NMR ($CDCl_3$, 400 MHz) δ = 13.72 (s, 1H; ArOH), 8.32 (s, 1H; ArCHN) 6.89 (m, 1H; ArH), 6.84 (m, 1H; ArH), 6.78 (m, 1H; ArH), 3.88 (s, 3H; OCH_3), 3.65 (dd, *J* = 12.1, 4.3 Hz, 1H; CH_2), 3.43 (m, 1H; CH_2), 3.08 (br d, *J* = 11.8 Hz, 1H; CH_2), 2.81 (m, 1H; CH), 2.59 (m, 1H; CH_2), 1.79 (m, 1H; CH_2), 1.69 (m, 1H; CH_2), 1.58 (m, 1H; CH_2), 1.36 (m, 2H; CH_2), 1.21 (m, 1H; CH_2). $^{13}C\{^{1}H\}$ NMR ($CDCl_3$, 100 MHz) δ = 166.1 (ArCHN), 151.9, 148.4, 122.9, 117.9, 114.0, 111.9 (Ar), 65.4 (CH), 56.6 (OCH_3), 56.0, 46.7, 30.5, 26.1, 24.4 (CH_2).

Minor product (Cyclic): ^{1}H NMR ($CDCl_3$, 400 MHz) δ = 6.81 (m, 1H; ArH), 6.71 (m, 1H; ArH), 6.68 (m, 1H; ArH), 4.22 (s, 1H; $ArCHN_2$), 3.84 (s, 3H; OCH_3), 3.12 (dd, *J* = 9.3, 6.4 Hz, 1H; CH_2). 2.95 (m, 2H; CH_2), 2.42 (m, 1H; CH), 2.06 (t d, *J* = 11.3, 3.1 Hz, 1H; CH_2), 1.93 (m, 1H; CH_2), 1.84 (m, 1H; CH_2), 1.68 (m, 1H; CH_2), 1.58 (m, 1H; CH_2), 1.32 (m, 2H; CH_2).

$^{13}C\{^{1}H\}$ NMR ($CDCl_3$, 100 MHz) δ = 148.2, 146.9, 122.0, 121.8, 118.5, 118.4 (Ar), 82.6 ($ArCHN_2$), 63.4 (CH), 55.8 (OCH_3), 50.5, 48.5, 29.1, 24.8, 23.7 (CH_2).

ESI-MS (MeOH): Calcd *m/z* $[C_{14}H_{20}N_2O_2Na]^+$ = 271.1423, found *m/z* = 271.1390.

6H: Isolated as an orange oil (96 % conversion, 1:1 imine:cyclic product).

Product 1 (Imine): ^{1}H NMR ($CDCl_3$, 400 MHz) δ = 8.28 (s, 1H; ArCHN), 7.36 (m, 1H; ArH), 7.28 (dd, *J* = 8.7, 2.5 Hz, 1H; ArH), 6.85 (d, *J* = 8.7 Hz, 1H; ArH), 3.67 (ddd, *J* = 12.1, 4.4, 1.3 Hz, 1H; CH_2), 3.44 (dd, *J* = 12.1, 7.9 Hz, 1H; CH_2), 2.42 (m, 1H; CH),. 1.84 (m, 2H; CH_2), 1.72 (m, 2H; CH_2), 1.32 (m, 3H; CH_2), 1.21 (m, 1H;

CH_2). $^{13}C\{^1H\}$ NMR ($CDCl_3$, 100 MHz) δ = 164.5 (ArCHN), 160.2, 156.8, 133.4, 132.5, 119.0, 110.0 (Ar), 65.9 (CH_2), 63.4 (CH), 30.6, 24.7 24.3, 23.5 (CH_2).
Product 2 (Cyclic): ^1H NMR ($CDCl_3$, 400 MHz) δ = 7.36 (m, 1H; ArH), 7.16 (d, *J* = 2.5 Hz, 1H; ArH), 6.70 (d, *J* = 8.7 Hz, 1H; ArH), 4.16 (s, 1H; $ArCHN_2$), 3.20 (dd, *J* = 9.3, 6.5 Hz, 1H; CH_2), 2.91 (m, 2H; CH_2) 2.84 (m, 1H; CH), 2.07 (t d, *J* = 11.5, 2.9 Hz, 1H; CH_2), 1.96 (m, 1H; CH_2), 1.61 (m, 2H; CH_2), 1.41 (m, 2H; CH_2). 1.35 (m, 1H; CH_2) $^{13}C\{^1H\}$ NMR ($CDCl_3$, 100 MHz) δ = 134.9, 132.5, 123.8, 120.0 118.8, 110.4 (Ar), 82.2 ($ArCHN_2$), 56.4 (CH), 50.2, 48.3, 46.6, 28.8, 26.0 (CH_2).
ESI-MS (MeOH): Calcd *m/z* $[C_{13}H_{18}N_2OBr]^+$ = 297.0603, found *m/z* = 297.0608.

Synthesis of capped imino monophenolate, 7H: To a THF solution (50 ml) of **1**H (16.48 mmol) was added benzyl bromide (1.7 ml, 16.48 mmol) followed by Et_3N (2 eq, 4.6 ml, 33 mmol). The solution was heated to reflux for three hours after which the reaction was cooled and the precipitate was filtered. The filtrate was reduced *in vacuo* and the product isolated through MeOH or hexane recrystallisation. The product was isolated as yellow crystals (2.43g, 5.8 mmol, 35%).

^1H NMR ($CDCl_3$, 400 MHz) δ = 13.89 (s, 1H; ArOH), 8.34 (s, 1H; ArCHN), 7.40 (m, 3H; ArH), 7.33 (t, *J* = 7.7 Hz, 2H; ArH), 7.25 (m, 1H; ArH), 7.09 (d, *J* = 2.4 Hz, 1H; ArH), 4.11 (d, *J* = 13.6 Hz, 1H; $ArCH_2$), 3.98 (dd, *J* = 12.4, 4.0 Hz, 1H; CH_2), 3.68 (dd, *J* = 12.4, 7.3 Hz, 1H; CH_2), 3.43 (d, *J* = 13.6 Hz, 1H; $ArCH_2$), 2.81 (dt, *J* = 11.8, 4.6 Hz, 1H; CH_2), 2.71 (sept, *J* = 3.6 Hz, 1H; CH), 2.19 (m, 1H; CH_2), 1.81 (m, 1H; CH_2), 1.72 (m, 1H; CH_2), 1.56 (m, 3H; CH_2), 1.49 (s, 9H; $C(CH_3)_3$), 1.40 (m, 1H; CH_2), 1.34 (s, 9H; $C(CH_3)_3$). $^{13}C\{^1H\}$ NMR ($CDCl_3$, 100 MHz) δ = 166.6 (ArCHN), 158.3, 140.0, 139.8, 136.70, 128.9, 128.3, 126.9, 126.9, 125.9, 118.0 (Ar), 61.4, 61.2 (CH_2), 58.8 (CH), 51.9 (CH_2), 35.2, 34.3 ($C(CH_3)_3$), 31.7 ($C(CH_3)_3$), 29.7 (CH_2), 29.6 ($C(CH_3)_3$), 25.5, 23.2 (CH_2).
ESI-MS (MeOH): Calcd *m/z* $[C_{28}H_{40}N_2ONa]^+$ = 443.3038, found *m/z* = 443.3031.

Synthesis of bicyclic monophenolates 8-13H: Three routes were employed to prepare bicyclic monophenolate ligands.

I. Preparation of Imine condensation product and S_N2 reaction

The required salicylaldehyde was first reacted with 2-AMP as described for **1**-**6**H. For **8**H (3,5-dimethylsalicylaldehyde) reaction was carried out on 16.48 mmol scale. For **9**-**10**H (salicylaldehyde and 3,5-dichlorosalicylaldehyde), reaction was carried out at 8.24 mmol scale. The product of this condensation was dissolved in THF (50 ml) to which benzyl bromide (1 eq) and Et_3N (2 eq) were added. The solution was heated to reflux for three hours after which the reaction cooled and the precipitate was filtered. The filtrate was reduced *in vacuo* and the product isolated through MeOH recrystallisation.

8H: Isolated as a pale yellow powder (0.85g, 1.65 mmol, 15%).
^{1}H NMR ($CDCl_3$, 400 MHz) δ = 11.38 (s, 1H; ArOH),7.28 (m, 4H; ArH), 7.22 (m, 1H; ArH), 7.33 (t, *J* = 7.7 Hz, 2H; ArH), 6.92 (m, 1H; ArH), 6.63 (m, 1H; ArH), 3.93 (d, *J* = 13.3 Hz, 1H; $ArCH_2$), 3.82 (s, 1H; $ArCHN_2$), 3.47 (d, *J* = 13.3 Hz, 1H; $ArCH_2$), 2.84 (m, 2H;CH_2), 2.76 (dd, *J* = 9.7, 7.4 Hz, 1H; CH_2), 2.35 (m, 1H; CH), 2.25 (s, 3H; CH_3), 2.23 (s, 3H; CH_3), 1.99 (dt, *J* = 11.3, 3.4 Hz, 1H; CH_2), 1.77 (m, 2H; CH_2), 1.57 (m, 2H; CH_2), 1.32 (m, 2H; CH_2).^{13}C{^{1}H} NMR ($CDCl_3$, 100 MHz) δ = 154.2, 138.7, 131.8, 129.0, 128.8, 128.5, 127.2, 126.7, 125.2, 119.9, (Ar) 89.6 ($ArCHN_2$), 62.3 (CH), 56.9, 55.2, 49.2, 29.1, 24.9, 24.2 (CH_2), 20.6, 15.9 (CH_3).
ESI-MS (MeOH): Calcd *m/z* $[C_{22}H_{28}N_2ONa]^+$ = 359.2099, found *m/z* = 359.2116.

9H: Isolated as a pale yellow powder (0.55g, 1.79 mmol, 22%).
^{1}H NMR ($CDCl_3$, 400 MHz) δ = 11.55 (s, 1H; ArOH),7.26 (m, 3H; ArH), 7.22 (m, 3H; ArH), 6.99 (dd, *J* = 7.5, 1.6 Hz, 1H; ArH), 6.89 (dd, *J* = 6.8, 1.1 Hz, 1H; ArH), 6.78 (dd, 7.4, 1.1 Hz, 1H; ArH), 3.94 (d, *J* = 13.3 Hz, 1H; $ArCH_2$), 3.88 (s, 1H; $ArCHN_2$), 3.49 (d, *J* = 13.3 Hz, 1H; $ArCH_2$), 2.84 (m, 3H;CH_2), 2.38 (m, 1H; CH), 2.02 (dt, *J* = 11.7, 3.2 Hz, 1H; CH_2), 1.78 (m, 2H; CH_2), 1.57 (m, 2H; CH_2), 1.32 (m, 2H; CH_2).

$^{13}C\{^{1}H\}$ NMR ($CDCl_3$, 100 MHz) δ = 158.6, 138.5, 130.9, 129.9, 128.8, 128.5, 127.2, 121.1, 118.4, 116.9 (Ar), 89.4 ($ArCHN_2$), 62.21 (CH), 56.9, 55.1, 49.0, 29.1, 25.0, 24.1 (CH_2).
ESI-MS (MeOH): Calcd *m/z* $[C_{20}H_{24}N_2ONa]^+$ =331.1786, found *m/z* = 331.1775.

10H: Isolated as a pale yellow powder (2.11 g, 5.59 mmol, 68%).
^{1}H NMR ($CDCl_3$, 400 MHz) δ = 12.76 (s, 1H; ArOH),7.29 (m, 3H; ArH), 7.24 (m, 3H; ArH), 6.83 (d, *J* = 2.5 Hz, 1H; ArH), 3.89 (d, *J* = 13.2 Hz, 1H; $ArCH_2$), 3.86 (s, 1H; $ArCHN_2$), 3.54 (d, *J* = 13.3 Hz, 1H; $ArCH_2$), 2.84 (m, 2H;CH_2), 2.40 (m, 1H; CH), 2.02 (dt, *J* = 11.4, 2.9 Hz, 1H; CH_2), 1.79 (m, 2H; CH_2), 1.65 (m, 2H; CH_2), 1.53 (m, 1H; CH_2), 1.30 (m, 2H; CH_2).$^{13}C\{^{1}H\}$ NMR ($CDCl_3$, 100 MHz) δ = 153.4, 137.6, 129.7, 128.8, 128.7, 128.6, 127.6, 123.6, 122.6, 122.0 (Ar), 88.5 ($ArCHN_2$), 62.0 (CH), 56.9, 55.1, 48.9, 28.9, 24.8, 23.9 (CH_2).
ESI-MS (MeOH): Calcd *m/z* $[C_{20}H_{22}Cl_2N_2ONa]^+$ =399.1007, found *m/z* = 399.0977.

II. Preparation of diamine and cyclisation with 3,5-di-*tert*-butylsalicylaldehyde

11H: Benzaldehyde (0.84 ml, 8.24 mmol) was reacted with 2-AMP (1 ml, 8.24 mmol) in MeOH (50 ml). After 1 hour of stirring, $NaBH_4$ (2 eq, 0.63 g, 16.48 mmol) was added portionwise. Reaction was continued until decolouration on which H_2O (15 ml) was added to quench the reduction. Solvent was reduced *in vacuo* and the product was isolated as a clear oil *via* extraction with CH_2Cl_2. The resultant diamine (1.66 g, 8.13 mmol) was dissolved in hexane (50 ml) and 3,5-di-*tert*-butylsalicylaldehyde. (1.90, 8.13 mmol) was added. The reaction mixture was then stirred for 16 hours at reflux. After this period, the solution was left to stand allowing for the precipitation of product which was washed with cold hexane and isolated as white crystals (1.20g, 2.85 mmol, 35%).

^{1}H NMR ($CDCl_3$, 400 MHz) δ = 11.46 (s, 1H; ArOH), 7.25 (m, 5H; ArH), 7.19 (m, 1H; ArH), 6.79 (d, *J* = 2.5 Hz, 1H; ArH), 3.89 (d, *J* = 13.6 Hz, 2H; $ArCHN_2$/$ArCH_2$), 3.44 (d, *J* = 13.2 Hz, 1H; $ArCH_2$), 2.84 (m, 2H; CH_2), 2.75 (dd, *J* = 9.5, 7.5 Hz, 1H; CH_2), 2.36 (m, 1H; CH), 1.99 (td, *J* = 11.0, 3.0 Hz, 1H; CH_2), 1.76 (m, 2H; CH_2), 1.55 (m, 2H; CH_2), 1.45 (s, 9H; $C(CH_3)_3$), 1.28 (m, 2H; CH_2), 1.27 (s, 9H; $(CH_3)_3$).

$^{13}C\{^{1}H\}$ NMR ($CDCl_3$, 100 MHz) δ = 154.4, 140.1, 138.9, 135.4, 129.1, 128.9, 128.5, 123.1, 122.8, 121.5 (Ar), 90.0 ($ArCHN_2$), 61.9 (CH), 57.4, 56.3, 48.9 (CH_2), 34.9, 34.2 ($C(CH_3)_3$), 31.9, 29.7 ($C(CH_3)_3$), 28.9, 25.1, 24.2 (CH_2).
ESI-MS (MeOH): Calcd *m/z* $[C_{28}H_{40}N_2ONa]^+$ = 443.3038, found *m/z* = 443.3075.

III. Preparation of diamine and cyclisation with benzaldehyde or 2-pyridinecarboxaldehyde

12H: 3,5-di-*tert*-butylsalicylaldehyde (5.78 g, 24.72 mmol)was reacted with 2-AMP (3 ml, 24.72 mmol) in MeOH (100 ml).After 1 hour of stirring, $NaBH_4$ (3 eq, 2.85 g, 75 mmol) was added portionwise. Reaction was continued until decolouration on which H_2O (5 ml) was added to quench the reduction. Solvent was reduced *in vacuo* and the product was washed with H_2O (3 × 50 ml) and MeOH (1 × 25 ml) and dried to an off white powder (8.74 g, 20.3 mmol, 82%). The resultant diamine (0.67 g, 2 mmol) was dissolved in hexane (50 ml) and benzaldehyde (0.2 ml, 2 mmol) was added. The reaction mixture was then stirred for 16 hours at reflux. The solvent was then removed *in vacuo* and the residue redissolved in MeOH (25 ml). Addition of H_2O precipitated the product as a white powder (0.34 g, 0.81 mmol, 40%).

^{1}H NMR ($CDCl_3$, 400 MHz) δ = 9.13 (s, 1H; ArOH), 7.41 (m, 2H; ArH), 7.29 (m, 3H; ArH), 7.11 (m, 1H; ArH), 6.75 (d, *J* = 2.1 Hz, 1H; ArH), 3.93 (d, *J* = 13.3 Hz, 1H; $ArCH_2$), 3.62 (s, 1H; $ArCHN_2$), 3.47 (d, *J* = 13.3 Hz, 1H; $ArCH_2$), 2.83 (m, 2H; CH_2), 2.60 (br d, *J* = 10.4 Hz, 1H; CH_2), 2.41 (m, 1H; CH), 1.90 (t, *J* = 10.8 Hz, 1H; CH_2), 1.75 (m, 2H; CH), 1.53 (m, 1H; CH_2), 1.45 (m, 2H; CH_2), 1.35 (s, 9H; $(CH_3)_3$), 1.28 (m, 1H; CH_2) 1.24 (s, 9H; $(CH_3)_3$). $^{13}C\{^{1}H\}$ NMR ($CDCl_3$, 100 MHz) δ = 154.4, 140.1, 138.9, 135.4, 129.1, 128.9, 128.5, 123.1, 122.8, 121.5 (Ar), 90.0 ($ArCHN_2$), 61.9 (CH), 57.4, 56.3, 48.9 (CH_2), 34.9, 34.2 ($C(CH_3)_3$), 31.9, 29.7 ($C(CH_3)_3$), 28.9, 25.1, 24.2 (CH_2).
ESI-MS (MeOH): Calcd *m/z* $[C_{28}H_{41}N_2O]^+$ = 421.3219, found *m/z* = 421.3328.

13H: The 3,5-di-*tert*-butylsalicylaldehyde diamine (2.74 g, 8.24 mmol) was dissolved in hexane (50 ml) and 2-pyridinecarboxaldehyde (0.78 ml, 8.24 mmol) was added. The reaction mixture was then stirred for 16 hours at reflux. The solvent was then

removed *in vacuo* and the residue redissolved in MeOH (25 ml) and the product isolated by recrystallisation at -20 °C after 2 weeks (1.54 g, 3.75 mmol, 44%).

^{1}H NMR ($CDCl_3$, 400 MHz) δ = 10.44 (s, 1H; ArOH), 8.53 (d, *J* = 4.6 Hz, 1H; ArH), 7.72 (m, 2H; ArH), 7.23 (m, 1H; ArH), 7.14 (d, *J* = 2.1 Hz, 1H; ArH), 6.80 (d, *J* = 2.1 Hz, 1H; ArH), 4.08 (d, *J* = 13.6 Hz, 1H; $ArCH_2$), 3.88 (s, 1H; $ArCHN_2$), 3.47 (d, *J* = 13.6 Hz, 1H; $ArCH_2$), 2.94 (t, *J* = 9.9 Hz, 1H; CH_2), 2.85 (dd, *J* = 9.9, 7.1 Hz, 1H; CH_2), 2.67 (br d, *J* =10.8 Hz, 1H; CH), 2.51 (m, 1H; CH_2), 2.08 (m, 1H; CH_2), 1.80 (m, 2H; CH_2), 1.61 (m, 1H; CH_2), 1.50 (m, 1H; CH_2), 1.40 (m, 1H; CH_2), 1.35 (s, 9H; $(CH_3)_3$), 1.29 (m, 1H; CH_2) 1.26 (s, 9H; $(CH_3)_3$). $^{13}C\{^{1}H\}$ NMR ($CDCl_3$, 100 MHz) δ = 159.4, 154.3, 148.9, 140.3, 137.2, 135.4, 123.7, 123.3, 122.9, 122.9, 121.6 (Ar), 90.57 ($ArCHN_2$), 62.0 (CH), 57.5, 56.3, 49.1 (CH_2), 34.9, 34.2 ($C(CH_3)_3$), 31.8, 29.7 ($C(CH_3)_3$), 28.8, 25.1, 24.1 (CH_2).
ESI-MS (MeOH): Calcd *m/z* $[C_{27}H_{39}N_3ONa]^+$ =444.2990, found *m/z* = 444.2963.

5.3.3 Bisphenolate ligand synthesis

Synthesis of bicyclic bisphenolates (14-25H_2): Two routes were employed to prepare bicyclic bisphenolates:

I. Preparation of Imine condensation product and S_N2 reaction

Imine condensation reaction was carried out as for **1-6**H, with electron withdrawing substituted salicylaldehydes. Without further purification, the condensation product (5.23 mmol) was dissolved in THF (50 ml) and 3,5-di-*tert*-butyl-2-hydroxybenzylbromide (1.55 g, 5.23 mmol) was added. Triethylamine (2eq, 1 ml, 10.4 mmol) was added dropwise and the solution heated to reflux (70 °C) and stirred for 3 hours. The suspension was removed *via* filtration and the resultant supernatant reduced *in vacuo* to afford an orange oil from which a coloured solid was precipitated from methanol. This method was used for the production of **14-16**H_2.

***14*H_2:** Isolated as a pale yellow powder (2.23 g, 4.41 mmol, 84 %).
^{1}H NMR ($CDCl_3$, 400 MHz) δ = 11.83 (s, 1H; ArOH), 9.40 (s, 1H; ArOH), 7.22 (d, *J* = 2.5 Hz, 1H; ArH), 7.18 (d, *J* = 2.5 Hz, 1H; ArH), 6.78 (d, *J* = 2.5 Hz, 1H; ArH), 6.45 (d, *J* = 2.5 Hz, 1H; ArH), 4.00 (s, 1H; $ArCHN_2$), 3.93 (d, *J* = 13.0 Hz, 1H; $ArCH_2$), 3.87 (d, *J* = 13.0 Hz, 1H; $ArCH_2$), 3.08 (dd, *J* = 10.5, 6.5 Hz, 1H; CH_2), 3.00 (t, *J* = 10.0 Hz, 1H; CH_2), 2.89 (br d, *J* = 11.0 Hz, 1H; CH_2), 2.61 (m, 1H; CH), 2.15 (dt, *J* = 11.5, 3.0 Hz, 1H; CH_2), 1.93 (m, 2H; CH_2), 1.76 (m, 1H; CH_2), 1.64 (m, 1H; CH_2), 1.37 (m, 2H CH_2), 1.44 (s, 9H; $C(CH_3)_3$), 1.29 (s, 9H; $C(CH_3)_3$). $^{13}C\{^1H\}$ NMR ($CDCl_3$, 100 MHz) δ = 153.7, 152.4, 140.7, 135.7, 130.2, 129.0, 123.4, 123.1, 122.7, 122.7,121.7, 120.7, (Ar), 87.9 ($ArCHN_2$), 61.2 (CH), 58.5, 57.2, 48.7 (CH_2), 34.7, 34.1 ($C(CH_3)_3$), 31.6, 29.5 ($C(CH_3)_3$), 28.6, 24.7, 23.3 (CH_2).
ESI-MS (MeOH): Calcd *m/z* $[C_{28}H_{39}N_2O_2Cl_2]^+$=505.2366, found *m/z* = 505.2389.

***15*H_2**: Isolated as a yellow powder (2.02 g, 3.39 mmol, 65 %).
^{1}H NMR ($CDCl_3$, 400 MHz) δ = 12.00 (s, 1H; ArOH), 9.40 (s, 1H; ArOH), 7.49 (d, *J* = 2.5 Hz, 1H; ArH), 7.18 (d, *J* = 2.5 Hz, 1H; ArH), 6.75 (d, *J* = 2.5 Hz, 1H; ArH), 6.58 (d, *J* = 2.5 Hz, 1H; ArH), 3.97 (s, 1H; $ArCHN_2$), 3.91 (d, *J* = 13.5 Hz, 1H; $ArCH_2$), 3.86 (d, *J* = 13.5 Hz, 1H; $ArCH_2$), 3.08 (dd, *J* = 10.5 Hz, 6.5 Hz, 1H; CH_2), 2.99 (t, *J* = 10.5 Hz, 1H; CH_2), 2.88 (br d, *J* = 10.5 Hz, 1H; CH_2), 2.61 (m, 1H; CH), 2.15 (dt, *J* = 12.0, 3.0 Hz, 1H; CH_2), 1.92 (m, 2H; CH_2), 1.76 (m, 1H; CH_2), 1.63 (m, 1H; CH_2), 1.37 (m, 2H; CH_2), 1.29 (s, 9H; $C(CH_3)_3$), 1.28 (s, 9H; $C(CH_3)_3$).
^{13}C NMR ($CDCl_3$, 100 MHz) δ = 153.8, 153.7, 140.7, 135.7, 135.6, 132.5, 123.6, 123.1, 122.7, 120.7, 111.3, 110.4 (Ar), 87.8 ($ArCHN_2$), 61.2 (CH), 58.6, 57.3, 48.7 (CH_2), 34.8, 34.1 ($C(CH_3)_3$), 31.7, 28.6 ($C(CH_3)_3$), 28.6, 24.7, 23.4 (CH_2).
ESI-MS (MeOH): Calcd *m/z*$[C_{28}H_{39}N_2O_2Br_2]^+$ = 593.1378, found *m/z* = 593.1391.

***16*H_2**: Isolated as a yellow powder (2.56 g, 3.71 mmol, 71%).
^{1}H NMR ($CDCl_3$, 400MHz) δ = 12.17 (s, 1H; ArOH), 9.45 (s, 1H; ArOH), 7.85 (d, *J* = 2.0 Hz, 1H; ArH), 7.19 (d, *J* = 2.5 Hz, 1H; ArH), 6.75 (d, *J* = 2.0 Hz, 1H; ArH), 6.73 (d, *J* = 2.5 Hz, 1H; ArH), 3.90 (s, 1H; Ar*C*HN_2), 3.89 (d, *J* = 13.0 Hz, 1H; $ArCH_2$), 3.85 (d, *J* = 13.0 Hz, 1H; $ArCH_2$), 3.08 (dd, *J* = 10.0, 7.0 Hz, 1H; CH_2), 2.99 (t, *J* = 10.5 Hz, 1H; CH_2), 2.88 (br d, *J* = 11.0 Hz, 1H; CH_2), 2.61 (m, 1H; CH), 2.14 (dt, *J* = 3.0, 12.0 Hz, 1H; CH_2), 1.92 (m, 2H; CH_2), 1.76 (m, 1H; CH_2), 1.63 (m, 1H; CH_2), 1.37 (m, 2H CH_2), 1.29 (s, 9H; $C(CH_3)_3$), 1.28 (s, 9H; $C(CH_3)_3$).

$^{13}C\{^{1}H\}$ NMR ($CDCl_3$, 100 MHz) δ = 156.9, 153.7, 146.7, 140.6, 139.4, 135.6, 123.6, 122.8, 122.7, 120.7, 86.4, 80.7 (Ar), 87.6 ($ArCHN_2$), 61.1 (CH), 58.6, 57.3, 48.7 (CH_2), 34.8, 34.1 ($C(CH_3)_3$), 31.7, 29.5 ($C(CH_3)_3$), 28.6, 24.7, 23.4 (CH_2).
ESI-MS(MeOH): Calcd *m/z* $[C_{28}H_{39}N_2O_2I_2]^+$ = 689.1101, found *m/z* = 689.1082.

II. Preparation of Diamine and cyclisation with substituted salicylaldehyde

3,5-Di-*tert*-butylsalicylaldehyde (5.78 g, 24.72 mmol)was reacted with 2-AMP (3 ml, 24.72 mmol) in MeOH (100 ml).After 1 hour of stirring, $NaBH_4$ (3 eq, 2.85 g, 75 mmol) was added portionwise. Reaction was continued until decolouration on which H_2O (5 ml) was added to quench the reduction. Solvent was reduced *in vacuo* and the product was washed with H_2O (3 × 50 ml) and MeOH (1 × 25 ml) and dried to an off white powder (8.74 g, 20.3 mmol, 82%). The resultant diamine (1 eq) was dissolved in hexane (50 ml) and the required salicylaldehyde (1 eq) was added. The reaction mixture was then stirred for 16 hours at reflux. After this period, the product was isolated *via* recrystallisation. This method was used to prepare **17**-**22**H_2.

17*H_2*: Cyclisation with 5-bromosalicylaldehyde (3 mmol). Isolated as a pale yellow powder after MeOH wash (1.00 g, mmol, 1.94 mmol, 65%).
^{1}H NMR ($CDCl_3$, 400 MHz) δ = 10.83 (s, 1H; ArOH), 9.65 (br s, 1H; ArOH), 7.25 (dd, *J* = 8.7, 2.5 Hz, 1H; ArH), 7.19 (d, *J* = 2.4 Hz, 1H; ArH), 6.81 (d, *J* = 2.4 Hz, 1H; ArH), 6.77 (m, 2H; ArH), 3.99 (d, *J* = 13.2 Hz, 1H; $ArCH_2$), 3.92 (s, 1H; $ArCHN_2$), 3.76 (d, *J* = 13.2 Hz, 1H; $ArCH_2$), 3.02 (m, 1H; CH_2), 2.93 (m, 2H; CH_2), 2.57 (m, 1H; CH), 2.13 (dt, *J* = 11.8, 2.8 Hz, 1H; CH_2), 1.90 (m, 2H; CH_2), 1.76 (m, 1H; CH_2), 1.59 (m, 1H; CH_2), 1.38 (m, 2H; CH_2), 1.33 (s, 9H; $C(CH_3)_3$), 1.29 (s, 9H; $C(CH_3)_3$).
$^{13}C\{^{1}H\}$ NMR ($CDCl_3$, 100 MHz) δ = 157.0, 153.9, 140.6, 135.8, 133.4, 133.2, 123.4, 123.0, 122.4, 120.9, 118.8, 110.7 (Ar), 88.05 ($ArCHN_2$), 61.5 (CH), 57.9, 56.8, 48.9 (CH_2), 34.9, 34.3 ($C(CH_3)_3$), 31.8, 29.7 ($C(CH_3)_3$), 29.0, 25.0, 23.7 (CH_2).
ESI-MS (MeOH): Calcd *m/z* $(C_{28}H_{39}N_2O_2BrNa)^+$ = 537.2093 found *m/z* = 537.2084.

18H_2: Cyclisation with 5-nitrosalicylaldehyde (5 mmol). Recrystallised from MeOH as a yellow powder (1.29 g, 2.67 mmol, 53 %).

^{1}H NMR ($CDCl_3$, 400 MHz) δ = 12.10 (br s, 1H; ArOH), 9.38 (s, 1H; ArOH), 8.03 (dd, *J* = 8.9, 2.8 Hz, 1H; ArH), 7.58 (d, *J* = 2.8 Hz, 1H; ArH), 7.12 (d, *J* = 2.4 Hz, 1H; ArH), 6.90 (d, *J* = 8.9 Hz, 1H; ArH), 6.76 (d, *J* = 2.3 Hz, 1H; ArH), 4.08 (s, 1H; $ArCHN_2$), 4.01 (d, *J* = 13.3 Hz, 1H; $ArCH_2$), 3.84 (d, *J* = 13.2 Hz, 1H; $ArCH_2$), 3.04 (m, 2H; CH_2), 2.89 (br d, *J* = 10.4 Hz, 1H; CH_2), 2.64 (m, 1H; CH), 2.20 (dt, *J* = 11.7, 2.8 Hz, 1H; CH_2), 1.95 (m, 2H; CH_2), 1.79 (m, 1H; CH_2), 1.60 (m, 1H; CH_2), 1.42 (m, 2H; CH_2), 1.26 (s, 18H; $C(CH_3)_3$).

$^{13}C\{^1H\}$ NMR ($CDCl_3$, 100 MHz) δ= 164.2, 153.7, 141.1, 140.0, 135.8, 127.2, 126.7, 123.6, 122.9, 120.8, 120.6, 117.5 (Ar), 88.0 ($ArCHN_2$), 61.5 (CH), 58.4, 57.1, 48.8 (CH_2), 34.9, 34.2 ($C(CH_3)_3$), 31.7, 29.7 ($C(CH_3)_3$), 28.9, 24.9, 23.6 (CH_2).

ESI-MS (MeOH): Calcd *m/z* $[C_{28}H_{39}N_3O_4Na]^+$ = 504.2838 found *m/z* = 504.2847.

19H_2*:* Cyclisation with salicylaldehyde (2 mmol). Recrystallised from MeOH to yield a white powder (0.57 g, 1.31 mmol, 65 %).

^{1}H NMR ($CDCl_3$, 400 MHz) δ = 10.76 (s, 1H; OH), 9.91 (s, 1H; OH), 7.22 (dt, *J* = 8.0, 1.6 Hz 1H; ArH), 7.15 (d, *J* = 2.4 Hz, 1H; ArH), 6.90 (dd, *J* = 7.2, 1.3 Hz, 2H; ArH), 6.72 (m, 2H; ArH), 3.99 (d, *J* = 14.7 Hz, 2H; CH_2/$ArCH_2$), 3.62 (d, *J* = 13.3 Hz, 1H; $ArCH_2$), 2.98 (m, 2H; CH_2), 2.86 (t, *J* = 9.9 Hz, 1H; CH_2), 2.55 (td, *J* = 9.9, 4.9 Hz, 1H; CH), 2.12 (td, *J* = 11.8, 2.9 Hz, 1H; CH_2), 1.89 (d, *J* = 9.4 Hz, 2H; CH_2), 1.74 (d, *J* = 13.6 Hz, 1H; CH_2), 1.61 (m, 1H; CH_2), 1.43 (m, 2H; CH_2), 1.35 (s, 9H; $(CH_3)_3$), 1.26 (s, 9H; $(CH_3)_3$). $^{13}C\{^1H\}$ NMR ($CDCl_3$, 100 MHz) δ = 157.9, 154.0, 140.4, 135.6, 131.1, 130.5, 123.2, 123.0, 121.14, 120.1, 119.1, 117.0 (Ar), 88.3, 61.8 (CH), 56.9, 56.3, 48.9 (CH_2), 35.0, 34.2 ($C(CH_3)_3$) 31.8, 29.7 ($C(CH_3)_3$), 29.1, 25.1, 23.9 (CH_2).

ESI-MS (MeOH): Calcd *m/z* $(C_{28}H_{40}N_2O_2Na)^+$ = 459.2988 found *m/z* = 459.2965.

20H_2*:* Cyclisation with 3,5-dimethylsalicylaldehyde (2 mmol). Isolated as a white powder from MeOH (0.55 g, 1.18 mmol, 59 %).

^{1}H NMR ($CDCl_3$, 400 MHz) δ = 10.66 (s, 1H; OH), 10.05 (s, 1H; OH), 7.13 (d, *J* = 2.4 Hz, 1H; ArH), 6.87 (s, 1H; ArH), 6.72 (d, *J* = 2.4 Hz, 1H; ArH), 6.48 (s, 1H; ArH), 3.96 (s, 1H; $ArCH_2$), 3.93 (d, *J* = 13.3 Hz, 1H; $ArCH_2$), 3.66 (d, *J* = 13.4 Hz, 1H; $ArCH_2$), 2.99 (dd, *J* = 9.8, 7.0 Hz, 1H; CH_2), 2.94 (br d, *J* = 10.7 Hz, 1H; CH_2), 2.86

(t, *J* = 9.9 Hz, 1H; CH_2), 2.53 (m, 1H; CH), 2.23 (s, 3H; CH_3), 2.11 (s, 3H; CH_3), 2.08 (m, 1H; CH_2), 1.88 (br d, *J* = 9.3 Hz, 2H; CH_2), 1.73 (m, 1H; CH_2), 1.64 (m, 1H; CH_2), 1.40 (m, 2H; CH_2), 1.33 (s, 9H; $(CH_3)_3$), 1.25 (s, 9H; $(CH_3)_3$). $^{13}C\{^1H\}$ NMR ($CDCl_3$, 100 MHz) δ = 154.1, 153.6, 140.3, 135.6, 132.4, 129.2, 127.4, 125.3, 123.02, 122.9, 121.3, 118.9 (Ar), 88.43 ($ArCHN_2$), 61.8 (CH), 57.3, 56.7, 49.0 (CH_2), 35.0, 34.2 ($C(CH_3)_3$), 31.8, 29.7 ($C(CH_3)_3$), 29.1, 25.1, 23.9 (CH_2), 20.5, 15.8 (CH_3).
ESI-MS (MeOH): Calcd *m/z* ($C_{30}H_{44}N_2O_2Na$) = 487.3301 found *m/z* = 487.3272.

***21**H_2:* Cyclisation with 3-adamantyl-5-methylsalicylaldehyde (2 mmol). Isolated from reaction mixture as a white powder (0.32g, 0.55 mmol, 27 %).
^1H NMR ($CDCl_3$, 400 MHz) δ = 10.63 (s, 1H; OH), 10.17 (s, 1H; OH), 7.12 (d, *J* = 2.4 Hz, 1H; ArH), 6.94 (d, *J* = 1.8 Hz, 1H; ArH), 6.68 (d, *J* = 2.3 Hz, 1H; ArH), 6.52 (d, *J* = 1.8 Hz, 1H; ArH), 3.98 (d, *J* = 13.3 Hz, 1H; $ArCH_2$), 3.88 (s, 1H; $ArCH_2$), 3.55 (d, *J* = 13.6 Hz, 1H; $ArCH_2$), 2.93 (m, 3H; CH_2), 2.53 (m, 1H; CH), 2.19 (br s, 6H; $CH_{2\ Ad}$), 2.15 (s, 3H; CH_3), 2.08 (br s, 4H; CH_2/$CH_{\ ad}$), 1.87(m, 2H; CH_2), 1.79 (m, 6H; $CH_{2\ Ad}$), 1.71 (m, 1H; CH_2), 1.62 (m, 1H; CH_2), 1.49 (m, 1H; CH_2), 1.34 (s, 10H; CH_2/$(CH_3)_3$), 1.24 (s, 9H; $(CH_3)_3$). $^{13}C\{^1H\}$ NMR ($CDCl_3$, 100 MHz) δ = 154.9, 154.3, 140.0, 137.3, 135.6, 129.4, 128.4, 126.9, 122.8, 122.8, 121.1, 119.6 (Ar), 88.8 ($ArCHN_2$), 61.9 (CH), 56.6, 56.2, 48.7 (CH_2), 40.5, 37.5 ($CH_{2\ ad}$), 37.0 (C_{ad}), 35.0, 34.2 ($C(CH_3)_3$), 31.8, 29.7 ($C(CH_3)_3$), 29.4 ($CH_{\ ad}$), 29.1, 25.1, 24.0 (CH_2), 20.8 (CH_3).
ESI-MS (MeOH): Calcd *m/z* $[C_{39}H_{57}N_2O_2]^+$ = 585.4420 found *m/z* = 585.4424.

***22**H_2:* Cyclisation with 3,5-di-*tert*-butylsalicylaldehyde (6 mmol). Recrystallised from hexane as a white powder (2.72 g, 4.95 mmol, 83 %).
^1H NMR ($CDCl_3$, 400 MHz) δ = 10.63 (s, 1H; ArOH), 10.17 (br s, 1H; ArOH), 7.25 (d, *J* = 2.5 Hz, 1H; ArH), 7.14 (d, *J* = 2.3 Hz, 1H; ArH), 6.80 (d, *J* = 2.4 Hz, 1H; ArH), 6.75 (d, *J* = 2.4 Hz, 1H; ArH), 3.98 (d, *J* = 13.4 Hz, 1H; $ArCH_2$), 3.88 (s, 1H; $ArCHN_2$), 3.52 (d, *J* = 13.4 Hz, 1H; $ArCH_2$), 3.00 (br d, 1H; CH_2), 2.90 (m, 2H; CH_2), 2.53 (m, 1H; CH), 2.10 (dt, *J* = 11.8, 2.8 Hz, 1H; CH_2), 1.87 (m, 2H; CH_2), 1.72 (m, 1H; CH_2), 1.56 (m, 3H; CH_2), 1.44 (s, 9H; $C(CH_3)_3$), 1.33 (s, 9H; $C(CH_3)_3$) 1.25 (s, 9H; $C(CH_3)_3$), 1.24 (s, 9H; $C(CH_3)_3$).

$^{13}C\{^{1}H\}$ NMR ($CDCl_3$, 100 MHz) δ = 154.2, 154.1, 140.3, 139.9, 136.3, 135.5, 125.4, 124.5, 122.8, 122.8, 120.8, 119.1 (Ar), 89.1 61.8 (CH), 56.2, 55.7, 48.6 (CH_2), 34.9, 34.8, 34.1 ($C(CH_3)_3$), 31.7, 29.5, 29.5 ($C(CH_3)_3$), 29.1, 24.9, 23.9 (CH_2).
ESI-MS (MeOH): Calcd *m/z* ($C_{36}H_{56}N_2O_2Na$) = 571.4240 found *m/z* = 571.4225.

***23**H₂*: Salicylaldehyde (0.88 ml, 8.24 mmol) was reacted with 2-AMP (1 ml, 8.24 mmol) in MeOH (25 ml). After 1 hour of stirring, $NaBH_4$ (2 eq, 0.95 g, 16.48 mmol) was added portionwise. Reaction was continued until decolouration on which H_2O (5 ml) was added to quench the reduction. Solvent was reduced *in vacuo* to yield a yellow oil (1.03 g, 4.55 mmol, 55%). The resultant diamine was dissolved in hexane (50 ml) and salicylaldehyde (0.5 ml, 4.6 mmol) was added. The reaction mixture was then stirred for 16 hours at reflux. After this period, solvent was removed *in vacuo* and the product recrystallised from MeOH. Isolated as a white powder (1.33 g, 4.10 mmol, 89%).
^{1}H NMR ($CDCl_3$, 400 MHz) δ = 10.53 (s, 1H; OH), 10.05 (s, 1H; OH), 7.27 (td, *J* = 7.8, 1.8 Hz 1H; ArH), 7.11 (td, *J* = 7.7, 1.6 Hz 1H; ArH), 7.01 (dd, *J* = 7.4, 1.8 Hz, 1H; ArH), 6.94 (m, 2H; ArH), 6.80 (td, *J* = 7.4, 1.1 Hz 1H; ArH), 6.72 (m, 2H; ArH), 4.09 (d, *J* = 13.4 Hz, 1H; $ArCH_2$), 3.92 (s, 1H; $ArCHN_2$), 3.55 (d, *J* = 13.4 Hz, 1H; $ArCH_2$), 2.94 (m, 3H; CH_2), 2.55 (m, 1H; CH), 2.13 (td, *J* = 11.1, 2.9 Hz, 1H; CH_2), 1.88 (m, 2H; CH_2), 1.74 (m, 1H; CH_2), 1.61 (m, 1H; CH_2), 1.40 (m, 2H; CH_2). $^{13}C\{^{1}H\}$ NMR ($CDCl_3$, 100 MHz) δ = 157.8, 157.6, 130.9, 130.8, 129.0, 128.3, 121.8, 120.2, 119.3, 119.1, 117.3, 116.4 (Ar), 88.2 ($ArCHN_2$), 61.9 (CH), 55.9, 55.6, 48.8, 29.3, 25.0, 23.9 (CH_2).
ESI-MS (MeOH): Calcd *m/z* $[C_{20}H_{24}N_2O_2Na]^+$ = 347.1736 found *m/z* = 347.1747.

***24-25**H₂*: 3,5-Dichlorosalicylaldehyde (3.15 g, 16.48 mmol) was reacted with 2-AMP (2 ml, 16.48 mmol) in MeOH (25 ml). After 1 hour of stirring, $NaBH_4$ (3 eq, 1.71 g, 46 mmol) was added portionwise. Reaction was continued until decolouration on which H_2O (5 ml) was added to quench the reduction. Solvent was reduced *in vacuo* to yield a white solid (2.26 g, 7.81 mmol, 47%). The resultant diamine (1 eq) was dissolved in hexane (50 ml) and substituted salicylaldehyde (1 eq) was added. The reaction mixture was then stirred for 16 hours at reflux. After this period, solvent was removed *in vacuo* and the product precipitated from MeOH.

***24*H_2**: Cyclisation with 3,5-dichlorosalicylaldehyde (3 mmol). Isolated as a yellow solid (0.72 g, 1.56 mmol, 52%).

^{1}H NMR ($CDCl_3$, 400 MHz) δ = 10.85 (s, 2H; ArOH), 7.34 (d, *J* = 2.5 Hz, 1H; ArH), 7.22 (d, *J* = 2.4 Hz, 1H; ArH), 6.79 (d, *J* = 2.5 Hz, 1H; ArH), 6.77 (d, *J* = 2.5 Hz, 1H; ArH), 3.97 (m, 2H; $ArCH_2$/$ArCHN_2$), 3.65 (d, *J* = 13.8 Hz, 1H; $ArCH_2$), 2.96 (m, 3H; CH_2), 2.60 (m, 1H; CH), 2.15 (dt, *J* = 11.6, 3.0 Hz, 1H; CH_2), 1.92 (m, 2H; CH_2), 1.77 (m, 1H; CH_2), 1.62 (m, 1H; CH_2), 1.38 (m, 2H CH_2).

$^{13}C\{^1H\}$ NMR ($CDCl_3$, 100 MHz) δ = 152.6, 152.0, 130.9, 129.2, 128.9, 126.5, 123.83, 123.78, 122.7, 122.0, 121.9 (Ar), 87.4 ($ArCHN_2$), 61.6 (CH), 56.4, 55.8, 48.9, 28.9, 24.8, 23.5 (CH_2).

ESI-MS (MeOH): Calcd *m/z* $[C_{20}H_{20}N_2O_2Cl_4]^+$=461.0357, found *m/z* = 461.0352.

***25*H_2:** Cyclisation with 3,5-di-*tert*-butylsalicylaldehyde (2 mmol). Isolated as a white powder (0.54 g, 1.07 mmol, 53%).

^{1}H NMR ($CDCl_3$, 400 MHz) δ = 10.75 (s, 2H; OH), 7.28 (d, *J* = 2.5 Hz, 1H; ArH), 7.15 (d, *J* = 2.5 Hz, 1H; ArH), 6.70 (d, *J* = 2.4 Hz, 1H; ArH), 6.67 (d, *J* = 2.5 Hz, 1H; ArH), 4.01 (s, 1H; $ArCH_2$), 3.93 (d, *J* = 14.1 Hz, 1H; $ArCH_2$), 3.60 (d, *J* = 14.1 Hz, 1H; $ArCH_2$), 2.95 (m, 3H; CH_2), 2.54 (m, 1H; CH), 2.10 (td, *J* = 11.7, 2.8 Hz, 1H; CH_2), 1.90 (br d, *J* = 10.7 Hz, 2H; CH_2), 1.74 (m, 1H; CH_2), 1.60 (m, 1H; CH_2), 1.46 (s, 9H; $(CH_3)_3$), 1.39 (m, 2H; CH_2), 1.22 (s, 9H; $(CH_3)_3$). $^{13}C\{^1H\}$ NMR ($CDCl_3$, 100 MHz) δ = 154.2, 152.5, 140.9, 136.8, 128.6, 126.2, 125.5, 125.3, 124.7, 123.2, 121.5, 118.0 (Ar), 88.7 ($ArCHN_2$), 61.8 (CH), 56.6, 55.5, 48.8 (CH_2), 35.1, 34.1 ($C(CH_3)_3$), 31.7, 29.7 ($C(CH_3)_3$), 29.1, 25.0, 23.9 (CH_2).

ESI-MS (MeOH): Calcd *m/z* $[C_{28}H_{39}Cl_2N_2O_2]^+$ = 505.2389 found *m/z* = 505.2400.

Synthesis of salalens (26-30*H_2*): Without purification, the isolated imino monophenolate (**1**/**2**/**4**H, 8.24 mmol) was dissolved in THF (50 ml) and 3,5-di-*tert*-butyl-2-hydroxybenzylbromide (2.45 g, 8.24 mmol) was added. Triethylamine (2eq, 2.3 ml, 16.4 mmol) was added dropwise and the solution heated to reflux (70 °C) and stirred for 3 hours. The suspension was filtered and the resultant supernatant reduced *in vacuo* to afford an orange oil from which the product was isolated *via* recrystallisation from methanol. Note: Reaction of 3-(1-adamantyl)-5-methyl-2-salicyladehyde adduct was carried out on 2 mmol scale.

***26*H_2**: Further reaction of **1**H. Isolated as a yellow powder (2.85 g, 5.18 mmol, 63%). ^{1}H NMR ($CDCl_3$, 400 MHz) δ = 13.51 (s, 1H; ArOH), 11.10 (s, 1H; ArOH), 8.29 (s, 1H; ArCHN), 7.39 (d, *J* = 2.5 Hz, 1H; ArH), 7.20 (d, *J* = 2.5 Hz, 1H; ArH), 7.04 (d, *J* = 2.5 Hz, 1H; ArH), 6.86 (d, *J* = 2.5 Hz, 1H; ArH), 4.27 (br s, 1H; CH_2), 3.97 (dd, *J* = 12.5, 3.5 Hz, 1H; CH_2), 3.74 (dd, *J* = 12.5, 7.0 Hz, 1H; CH_2), 3.56 (m, 1H; CH_2), 2.87 (m, 1H; CH), 2.78 (m, 1H; CH_2), 2.33 (br s, 1H; CH_2), 1.72 (br m, 6H; CH_2), 1.46 (s, 9H; $C(CH_3)_3$), 1.37 (s, 9H; $C(CH_3)_3$), 1.31 (s, 9H; $C(CH_3)_3$), 1.29 (s, 9H; $C(CH_3)_3$). $^{13}C\{^1H\}$ NMR ($CDCl_3$, 100 MHz) δ = 167.3 (ArCHN), 157.9, 154.4, 140.3, 140.0, 136.6, 135.5, 127.0, 126.0, 123.1, 122.6, 121.1, 117.8 (Ar), 58.5 (CH_2), 56.7 (CH), 35.0, 34.8, 34.11, 34.09 ($C(CH_3)_3$), 31.7, 31.5, 29.5, 29.4 ($C(CH_3)_3$), 20.0 (CH_2).
ESI-MS (MeOH): Calcd *m/z* $[C_{36}H_{56}N_2O_2\,Na]^+$ = 571.4240, found *m/z* = 571.4230.

***27*H_2:** Further reaction of **4**H. Isolated as a yellow powder (2.62 g, 5.67 mmol, 69%). ^{1}H NMR ($CDCl_3$, 400 MHz) δ = 13.19 (s, 1H; ArOH), 11.07 (br s, 1H; ArOH), 8.23 (s, 1H; ArCHN), 7.19 (d, *J* = 2.5 Hz, 1H; ArH), 7.01 (s, 1H; ArH), 6.86 (d, *J* = 2.5 Hz, 1H; ArH), 6.84 (d, *J* = 2.5 Hz, 1H; ArH), 4.26 (br s, 1H; CH_2), 3.99 (dd, *J* = 12.5, 4.0 Hz, 1H; $ArCH_2$), 3.71 (dd, *J* = 12.2, 7.2 Hz, 1H; $ArCH_2$), 3.56 (br s, 1H; CH_2), 2.86 (m, 2H; CH/CH_2), 2.25 (s, 6H; $2\times CH_3$), 2.22 (m, 1H; CH_2), 1.84 (m, 1H; CH_2), 1.62 (m, 5H; CH_2), 1.37 (s, 9H; $C(CH_3)_3$), 1.28 (s, 9H; $C(CH_3)_3$). $^{13}C\{^1H\}$ NMR ($CDCl_3$, 100 MHz) δ = 166.4 (ArCHN), 156.9, 154.4, 140.4, 135.5, 134.3, 129.0, 127.1, 125.6, 123.1, 122.7, 121.1, 117.7 (Ar), 58.5 (CH_2), 56.7 (CH), 34.8, 34.1 ($C(CH_3)_3$), 31.7, 29.5 ($C(CH_3)_3$), 25.0 (CH_2), 20.3, 15.4 (CH_3).
ESI-MS (MeOH): Calcd *m/z* $[C_{30}H_{44}N_2O_2\,Na]^+$ = 487.3301, found *m/z* = 487.3332.

***28*H_2:** Further reaction of **2**H. Isolated as a yellow powder (1.02 g, 1.74 mmol, 87 %). ^{1}H NMR ($CDCl_3$, 400 MHz) δ = 13.45 (s, 1H; ArOH), 11.15 (br s, 1H; ArOH), 8.24 (s, 1H; ArCHN), 7.20 (d, *J* = 2.2 Hz, 1H; ArH), 7.07 (d, *J* = 2.0 Hz, 1H; ArH), 6.86 (d, *J* = 1.5 Hz, 1H; ArH), 6.84 (d, *J* = 2.5 Hz, 1H; ArH), 4.26 (br s, 1H; CH_2), 3.98 (br d, *J* = 13.0 Hz, 1H; $ArCH_2$), 3.69 (dd, *J* = 13.0, 7.5 Hz, 1H; $ArCH_2$), 2.93 (m, 2H; CH/CH_2), 2.28 (s, 3H; CH_3), 2.18 (br s, 7H; $CH_{2\,Ad}$), 2.08 (br s, 4H; $CH_2/CH_{\,ad}$), 1.80 (m, 10H; $CH_2/CH_{2\,\,ad}$), 1.64 (m, 2H; CH_2), 1.39 (s, 9H; $C(CH_3)_3$), 1.29 (s, 9H; $C(CH_3)_3$).

$^{13}C\{^{1}H\}$ NMR ($CDCl_3$, 100 MHz) δ = 167.1 (ArCHN), 158.2, 154.4, 140.3, 137.4, 135.5, 130.5, 129.5, 126.7, 123.2, 122.6, 121.1, 118.3 (Ar), 58.5 (CH_2), 56.7 (CH), 40.2, 37.1 ($CH_{2\ ad}$), 36.9 ($CH_{\ ad}$) 34.8, 34.1 ($C(CH_3)_3$), 31.7 ($CH_{\ ad}$), 29.5, 29.1 ($C(CH_3)_3$), 25.0 (CH_2), 20.6 (CH_3).
ESI-MS (MeOH): Calcd *m/z* $[C_{30}H_{45}N_2O_2]^+$ = 585.4420, found *m/z* = 585.4562.

The above method was modified using 3,5-dichloro-2-hydroxybenzyl chloride or 2-hydroxy-5-nitrobenzyl bromide, with **1**H, rather than 3,5-di-*tert*-butylbenzyl bromide. The same procedure was used, preparing ***29-30***H_2.

29H_2*:* Reaction with 3,5-dichloro-2-hydroxybenzyl chloride (16.48 mmol). Isolated as a yellow powder (2.74 g, 5.42 mmol, 33 %).
^{1}H NMR ($CDCl_3$, 400 MHz) δ = 8.28 (s, 1H; ArCHN), 7.39 (d, *J* = 2.5 Hz, 1H; ArH), 7.23 (d, *J* = 2.5 Hz, 1H; ArH), 7.04 (d, *J* = 2.5 Hz, 1H; ArH), 6.85 (d, *J* = 2.5 Hz, 1H; ArH), 4.24 (d, *J* = 14.8 Hz, 1H; $ArCH_2$), 4.00 (dd, *J* = 12.8, 3.5 Hz, 1H; CH_2), 3.62 (m, 2H; CH_2), 2.93 (m, 2H; CH/CH_2), 2.41 (m, 1H; CH_2), 1.87 (m, 1H; CH_2), 1.65 (m, 4H; CH_2), 1.44 (m, 10H; $CH_2/C(CH_3)_3$), 1.30 (s, 9H; $C(CH_3)_3$). $^{13}C\{^{1}H\}$ NMR ($CDCl_3$, 100 MHz) δ = 167.5 (ArCHN), 157.7, 152.9, 140.3, 136.7, 128.3, 127.2, 126.2, 126.0, 123.9, 123.2, 121.5, 117.6 (Ar), 57.9 (CH), 56.5, 53.8, 47.7 (CH_2), 35.0, 34.1 ($C(CH_3)_3$), 31.4, 29.4 ($C(CH_3)_3$), 24.5, 20.9, 17.8 (CH_2).
ESI-MS (MeOH): Calcd *m/z* $[C_{28}H_{38}Cl_2N_2O_2]^+$ = 505.2389, found *m/z* = 505.2385.

30H_2*:* Reaction with 2-hydroxy-5-nitrobenzyl bromide (16.48 mmol). Isolated as a yellow powder (2.53 g, 5.25 mmol, 32 %).
^{1}H NMR ($CDCl_3$, 400 MHz) δ = 8.32 (s, 1H; ArCHN), 8.07 (dd, *J* = 9.0, 2.8 Hz, 1H; ArH), 7.94 (d, *J* = 2.8 Hz, 1H; ArH), 7.41 (d, *J* = 2.5 Hz, 1H; ArH), 7.05 (d, *J* = 2.5 Hz, 1H; ArH), 6.81 (d, *J* = 9.0 Hz, 1H; ArH), 4.36 (m, 1H; CH_2), 3.95 (m, 1H; CH_2), 3.73 (m, 2H; CH_2), 2.93 (m, 2H; CH_2), 2.44 (m, 1H; CH), 1.89 (m, 1H; CH_2), 1.71 (m, 4H; CH_2), 1.52 (m, 1H; CH_2), 1.46 (s, 9H; $(CH_3)_3$), 1.31 (s, 9H; $(CH_3)_3$). $^{13}C\{^{1}H\}$ NMR ($CDCl_3$, 100 MHz) δ = 167.7 (ArCHN), 164.8, 157.7, 140.3, 139.9, 136.7, 127.3, 126.0, 125.0, 124.3, 121.6, 117.6, 116.6 (Ar), 57.4 (CH_2), 35.0, 34.1 ($C(CH_3)_3$), 31.4, 29.3 ($C(CH_3)_3$), 24.7 (CH_2).
ESI-MS (MeOH): Calcd *m/z* $[C_{28}H_{39}N_3O_4Na]^+$ = 504.2838, found *m/z* = 504.2849.

***Synthesis of secondary amine based salans, 31-34**H_2*: Salalen **26-27**H_2 or **29-30**H_2 (1 eq) was dissolved in methanol/THF (1:1) and $NaBH_4$ (3 eq) was added portionwise. The solution was then stirred until decolouration. At this point, H_2O (15 ml) was added to quench the reduction. The solution was reduced *in vacuo* and the resultant precipitate was collected by filtration and washed further with H_2O.

***31**H_2*: Reduction of **26**H_2 (10 mmol). Isolated as a white powder (4.80 g, 8.71 mmol, 87%).

^{1}H NMR ($CDCl_3$, 400 MHz) δ = 11.01 (br s, 2H; ArOH), 7.22 (d, *J* = 2.4 Hz, 1H; ArH), 7.20 (d, *J* = 2.4 Hz, 1H; ArH), 6.85 (d, *J* = 2.4 Hz, 1H; ArH), 6.73 (d, *J* = 2.4 Hz, 1H; ArH), 4.05 (d, *J* = 14.1 Hz, 1H; $ArCH_2$), 3.77 (d, *J* = 13.3 Hz, 1H; $ArCH_2$), 3.59 (br d, *J* = 13.2 Hz, 2H; $ArCH_2$), 2.99 (br s, 1H; CH_2), 2.88 (dd, *J* = 12.6, 5.4 Hz, 1H; CH_2), 2.78 (br dd, *J* = 12.6, 3.6 Hz, 1H; CH_2), 2.55 (m, 1H; CH), 2.31 (m, 1H; CH_2), 1.73 (br m, 3H; CH_2), 1.59 (br m, 3H; CH_2), 1.40 (s, 9H; $C(CH_3)_3$), 1.37 (s, 9H; $C(CH_3)_3$), 1.31 (s, 9H; $C(CH_3)_3$), 1.28 (s, 9H; $C(CH_3)_3$).

$^{13}C\{^1H\}$ NMR ($CDCl_3$, 100 MHz) δ = 154.4, 154.2, 140.8, 140.4, 135.84, 135.8, 123.1, 122.9, 122.87, 122.7, 121.6, 121.4. (Ar), 61.7 (CH) 58.9, 53.7, 49.4 (CH_2), 34.8, 34.2, 34.1 ($C(CH_3)_3$), 31.70, 31.67, 29.6, 29.5 ($C(CH_3)_3$) 29.9, 25.0 22.6 (CH_2). Note: CH/CH_2 resonances were weak in $^{13}C\{^1H\}$ NMR, 2D-HSQC was used to aid unambiguous identification/assignment.

ESI-MS (MeOH): Calcd m/z $[C_{36}H_{58}N_2O_2Na]^+$ = 573.4389, found m/z = 573.4395.

***32**H_2:* Reduction of **27**H_2 (10 mmol). Isolated as a white powder (3.87 g, 8.30 mmol, 83%).

^{1}H NMR ($CDCl_3$, 400 MHz) δ = 10.91 (s, 2H; ArOH), 7.22 (d, *J* = 2.4 Hz, 1H; ArH), 6.86 (d, *J* = 2.4 Hz, 1H; ArH), 6.84 (s, 1H; ArH), 6.51 (s, 1H; ArH), 4.02 (d, *J* = 14.1 Hz, 1H; $ArCH_2$), 3.68 (d, *J* = 13.6 Hz, 1H; $ArCH_2$), 3.63 (d, *J* = 14.1 Hz, 1H; $ArCH_2$), 3.53 (br d, *J* = 13.6 Hz, 1H; $ArCH_2$), 3.00 (m, 1H; CH_2), 2.83 (m, 2H; CH_2), 2.57 (br s, 1H; CH), 2.34 (m, 1H; CH_2), 2.20 (s, 3H; CH_3), 2.18 (s, 3H; CH_3), 1.72 (m, 3H; CH_2), 1.59 (m, 2H; CH_2), 1.40 (m, 1H; CH_2), 1.37 (s, 9H; $C(CH_3)_3$), 1.31 (s, 9H; $C(CH_3)_3$). $^{13}C\{^1H\}$ NMR (CDCl3, 100 MHz) δ = 154.1, 153.7, 140.8, 135.9, 130.5, 127.4, 126.4, 124.8, 122.81, 122.80, 121.5, 121.3 (Ar), 61.1 (CH), 58.6, 52.9, 52.5, 49.5 (CH_2), 34.8, 34.2 ($C(CH_3)_3$), 31.7, 29.5 ($C(CH_3)_3$), 28.7, 24.8, 23.0 (CH_2), 20.4, 15.5 (CH_3).

ESI-MS (MeOH): Calcd m/z $[C_{30}H_{46}N_2O_2Na]^+$ = 489.3457, found m/z = 489.3496.

***33*H_2:** Reduction of **29**H_2 (2.6 mmol). Isolated as a white powder (1.29 g, 2.54 mmol, 96%). ~5% of bicylic impurity, **25**H_2.
^{1}H NMR ($CDCl_3$, 400 MHz) δ = 7.25 (d, *J* = 2.5 Hz, 1H; ArH), 7.22 (d, *J* = 2.4 Hz, 1H; ArH), 6.84 (m, 2H; ArH), 4.14 (d, *J* = 14.6 Hz, 1H; $ArCH_2$), 3.92 (2xd, *J* = 13.4 Hz, 2H; $ArCH_2$), 3.50 (d, *J* = 14.4 Hz, 1H; $ArCH_2$), 2.89 (m, 3H; CH_2), 2.61 (m, 1H; CH), 2.30 (m, 1H; CH_2), 1.80 (m, 1H; CH_2), 1.73 (m, 1H; CH_2), 1.63 (m, 3H; CH_2), 1.42 (m, 1H; CH_2), 1.39 (s, 9H; $C(CH_3)_3$), 1.29 (s, 9H; $C(CH_3)_3$). $^{13}C\{^1H\}$ NMR (CDCl3, 100 MHz) δ = 154.0, 152.7, 140.7, 136.0, 128.4, 126.3, 123.8, 123.3, 123.3, 123.1, 121.5, 121.4 (Ar), 60.6 (CH), 56.8, 53.7, 51.5, 49.1 (CH_2), 34.8, 34.1 ($C(CH_3)_3$), 31.6, 29.5 ($C(CH_3)_3$), 28.9, 24.4, 22.4 (CH_2). Note: CH/CH_2 resonances were weak in $^{13}C\{^1H\}$ NMR, 2D-HSQC was used to aid unambiguous identification/assignment.
ESI-MS (MeOH): Calcd m/z $[C_{28}H_{40}Cl_2N_2O_2Na]^+$ = 529.2365, found m/z = 529.2349.

***34*H_2:** Reduction of **30**H_2 (4.2 mmol). Isolated as an orange powder (1.49g, 3.08 mmol, 73%).
^{1}H NMR ($CDCl_3$, 400 MHz) δ = 8.09 (dd, *J* = 9.0, 2.9 Hz, 1H; ArH), 7.91 (d, *J* = 2.8 Hz, 1H; ArH), 7.22 (d, *J* = 2.5 Hz, 1H; ArH), 6.83 (m, 2H; ArH), 4.25 (br d, *J* = 14.4 Hz, 1H; $ArCH_2$), 3.94 (2xd, *J* = 13.9 Hz, 2H; $ArCH_2$), 3.60 (br d, *J* = 14.3 Hz, 1H; $ArCH_2$), 2.92 (m, 3H; CH_2), 2.66 (m, 1H; CH), 2.34 (m, 1H; CH_2), 1.79 (m, 2H; CH_2), 1.62 (m, 3H; CH_2), 1.48 (m, 1H; CH_2), 1.37 (s, 9H; $C(CH_3)_3$), 1.29 (s, 9H; $C(CH_3)_3$). $^{13}C\{^1H\}$ NMR (CDCl3, 100 MHz) δ = 165.0, 154.2, 141.0, 140.2, 136.3, 125.4, 124.7, 123.6, 123.4, 121.7, 121.6, 116.8 (Ar), 60.7 (CH), 56.6, 54.0, 51.7, 49.3 (CH_2), 35.0, 34.3 ($C(CH_3)_3$), 31.8, 29.7 ($C(CH_3)_3$), 28.9, 24.4, 22.5 (CH_2). Note: CH/CH_2 resonances were weak in $^{13}C\{^1H\}$ NMR, 2D-HSQC was used to aid unambiguous identification/assignment.
ESI-MS (MeOH): Calcd m/z $[C_{28}H_{42}N_3O_4]^+$ = 484.3176, found m/z = 484.3149.

***Synthesis of tertiary amine based salan, 35*H_2:** Secondary amine, **31**H_2, (1.20 g, 2.2 mmol) was dissolved in warm methanol (50ml) and an aqueous solution of formaldehyde (37 wt%, 0.41 ml, 5 mmol) was added dropwise. After 2 hours of stirring, solvent was removed and the residue redissolved in a methanol/THF mixture. $NaBH_4$ (5 eq, 0.42 g, 11 mmol) was then added portionwise and the solution was a

stirred for a further 3 hours before being quenched with H_2O (15 ml). The solvent was reduced *in vacuo* and the white precipitate was washed with H_2O (3 × 50 ml) and MeOH (50 ml). Isolated as a white powder (0.65 g, 1.15 mmol, 53%).

^{1}H NMR ($CDCl_3$, 400 MHz) δ = 11.16 (br s, 1H; ArOH), 10.36 (br s, 1H; ArOH), 7.22 (d, *J* = 2.4 Hz, 1H; ArH), 7.20 (d, *J* = 2.4 Hz, 1H; ArH), 6.83 (d, *J* = 1.8 Hz, 2H; ArH), 4.08 (br m, 1H; $ArCH_2$), 3.70 (d, *J* = 13.3 Hz, 1H; $ArCH_2$), 3.58 (br d, *J* = 13.3 Hz, 2H; $ArCH_2$), 2.74 (br m, 4H; CH_2), 2.37 (m, 1H; CH), 2.25 (s, 3H; NCH_3), 1.84 (br s, 1H; CH_2), 1.57 (br m, 2H; CH_2), 1.49 (br m, 1H; CH_2), 1.42 (s, 9H; $C(CH_3)_3$), 1.41 (s, 10H; $C(CH_3)_3/CH_2$), 1.29(s, 9H; $C(CH_3)_3$), 1.28 (s, 10H; $C(CH_3)_3/CH_2$). $^{13}C\{^1H\}$ NMR ($CDCl_3$, 100 MHz) δ= 154.5, 153.9, 140.7, 140.4, 135.6, 135.4, 123.4, 123.3, 123.0, 122.6, 121.3, 120.9 (Ar), 63.4 58.3 (CH_2), 42.4 (NCH_3), 34.8, 34.2, 34.1 ($C(CH_3)_3$), 31.7, 29.6 ($C(CH_3)_3$), 24.3 (CH_2). Note: CH_2 resonances were weak in $^{13}C\{^1H\}$ NMR, 2D-HSQC was used to aid unambiguous identification/assignment.

ESI-MS (MeOH): Calcd m/z $[C_{37}H_{60}N_2O_2Na]^+$ = 587.4552, found m/z = 587.4518.

5.3.4 Triaryl phenolate ligand synthesis

Synthesis of triaryl bisphenolate, 36H_2: **7**H (1.93 g, 4.58 mmol) was dissolved in MeOH (50 ml) and $NaBH_4$ (5 eq, 0.87g) was added portionwise. The solution was stirred until observed to become colourless. After this period, H_2O (20 ml) was added and solution was reduced *in vacuo*. The resultant white precipitate was collected by filtration and washed with H_2O (25 ml) and MeOH (5 ml). Reduction of the imino moiety was confirmed *via* ^{1}H NMR spectroscopy. The reduction product (1.93 g, 4.56 mmol) was redissolved in THF (50 ml) followed by the addition of 3,5-di-*tert*-butyl-2-hydroxybenzylbromide (1.35 g, 4.56 mmol) and Et_3N (2 eq, 1.3 ml, 9.31 mmol).The solution was then heated at reflux for 3 hours after which the solution cooled and the precipitate removed *via* filtration. The supernatant was then reduced *in vacuo* and the resultant oil recrystallised from MeOH. Isolated as a white powder (2.08 g, 3.25 mmol, 71%).

^{1}H NMR ($CDCl_3$, 400 MHz) δ = 9.13 (s, 2H; ArOH), 7.46 (m, 2H; ArH), 7.24 (m, 3H; ArH), 7.20 (d, *J* = 2.5 Hz, 1H; ArH), 6.86 (d, *J* = 2.4 Hz, 1H; ArH), 4.04 (d, *J* = 12.4 Hz, 1H; $ArCH_2$), 3.95 (d, *J* = 13.2 Hz, 2H; $ArCH_2$), 3.73 (d, *J* = 12.7 Hz, 1H; $ArCH_2$), 3.01 (m, 5H; CH_2), 2.55 (m, 1H; CH_2), 2.21 (m 1H; CH), 1.71 (m, 1H; CH_2), 1.60 (m, 2H; CH_2), 1.45 (m, 3H; CH_2), 1.39 (s, 18H; $C(CH_3)_3$), 1.28 (s, 18H; $C(CH_3)_3$).

$^{13}C\{^{1}H\}$ NMR ($CDCl_3$, 100 MHz) δ = 152.8, 140.6, 136.3, 130.4, 128.4, 127.4, 125.1, 123.4, 122.1 (Ar), 57.4, 55.7 (CH_2), 53.7 (CH), 47.6 (CH_2), 35.1, 34.2 ($C(CH_3)_3$), 31.9, 29.8 ($C(CH_3)_3$), 22.7, 21.5, 19.7 (CH_2).
ESI-MS (MeOH): Calcd m/z $[C_{43}H_{64}N_2O_2\ Na]^+$ = 663.4866, found m/z = 663.4823.

Synthesis of trisphenolate, 37H_2: **31**H_2 (2.75 g, 5 mmol) was dissolved in THF (50 ml) and 3,5-di-*tert*-butyl-2-hydroxybenzylbromide (1.49 g, 5 mmol) and Et_3N (2 eq, 1.4 ml, 10 mmol) were added. The solution was then heated at reflux for 16 hours. After which, the precipitate was removed by filtration and the solution reduced *in vacuo*. The resultant solid was recrystallised from hexane or MeOH as a white powder (2.19 g, 2.85 mmol, 57 %).
^{1}H NMR ($CDCl_3$, 400 MHz) δ = 8.70 (br s, 2H; ArOH), 7.25 (d, *J* = 2.4 Hz, 2H; ArH), 7.18 (d, *J* = 2.4 Hz, 1H; ArH), 6.96 (d, *J* = 2.4 Hz, 1H; ArH), 6.80 (d, *J* = 2.4 Hz, 1H; ArH), 3.93 (br d, *J* = 12.1 Hz, 1H; $ArCH_2$), 3.84 (d, *J* = 13.3 Hz, 2H; $ArCH_2$), 3.58 (d, *J* = 11.8 Hz, 1H; $ArCH_2$), 3.46 (d, *J* = 13.2 Hz, 2H; $ArCH_2$), 2.85 (m, 2H; CH_2), 2.73 (m, 1H; CH or CH_2), 2.53 (m 1H; CH or CH_2), 2.35 (m, 1H; CH orCH_2), 1.77 (m, 1H; CH_2), 1.42 (s, 18H; $C(CH_3)_3$), 1.41 (s, 9H; $C(CH_3)_3$), 1.35 (m, 4H; CH_2), 1.30 (s, 18H; $C(CH_3)_3$) 1.28 (s, 9H; $C(CH_3)_3$), 1.02 (m, 1H; CH_2). $^{13}C\{^{1}H\}$ NMR ($CDCl_3$, 100 MHz) δ = 154.5, 152.2, 142.0, 140.4, 136.2, 135.6, 125.6, 123.8, 123.5, 122.83, 121.8, 120.9 (Ar), 58.7 (CH_2), 35.0, 34.3, 34.2 ($C(CH_3)_3$), 31.8, 31.8, 29.9, 29.7 ($C(CH_3)_3$), 28.3, 24.4 (CH_2).
ESI-MS (MeOH): Calcd m/z $[C_{51}H_{80}N_2O_3Na]^+$ = 791.6067, found m/z = 791.6064.

5.4 Complex synthesis and characterisation (Chapter 3)

5.4.1 Monophenolate complex synthesis

Synthesis of imino monophenolate aluminum complexes, Al(1-6)Me_2: The initial imine condensation was carried out in a Schlenk tube on a 2 mmol scale and was used directly after drying *in vacuo*. $AlMe_3$ (2M, 1 ml, 2 mmol) was added to a solution of **1**-**6**H (2 mmol) in toluene (10 ml). After complete addition, the solution was stirred for 1 hour before purification *via* filtration or recrystallisation.

Al(1)Me$_2$: Product precipitated from solution during complexation and collected by filtration as a yellow solid (0.56 g, 1.44 mmol, 72%). Crystals isolable from a hot toluene/hexane mixture.

^{1}H NMR (d$_8$-tol, 400 MHz) δ = 7.64 (d, *J* = 2.5 Hz, 1H; ArH), 7.41 (s, 1H;ArCHN), 6.81 (d, *J* = 2.5 Hz, 1H; ArH), 2.78 (br d, *J* = 13.5 Hz, 1H; CH$_2$), 2.48 (m, 2H; CH$_2$), 2.25 (m, 2H; CH/CH$_2$), 1.68 (s, 9H; C(CH$_3$)$_3$), 1.39 (m, 1H; CH$_2$),1.37 (s, 9H; C(CH$_3$)$_3$), 1.21 (br d, *J* = 13.0 Hz, 1H; CH$_2$), 1.11 (br dd, *J* = 13.5, 3.0 Hz, 1H; CH$_2$), 0.98 (t q, *J* = 13.0, 4.0 Hz, 1H; CH$_2$), 0.77 (q t, *J* = 13.0, 4.0 Hz, 1H; CH$_2$), 0.55 (t d, *J* = 12.0, 3.0 Hz, 1H; NH), 0.34 (q d, *J* = 13.0, 4.0 Hz, 1H; CH$_2$), -0.37 (s, 3H; AlMe), -0.50 (s, 3H; AlMe). ^{13}C{^{1}H} NMR (d$_8$-tol, 100 MHz) δ = 172.0 (ArCHN), 165.8, 141.0, 136.1, 131.1, 127.7 117.6 (Ar), 62.7 (CH$_2$), 54.4 (CH), 44.6 (CH$_2$), 35.6, 34.1 (*C*(CH$_3$)$_3$), 31.6, 29.7 (C(*C*H$_3$)$_3$), 26.5, 23.4 (CH$_2$), -6.8, -9.4 (AlMe). Note: ArH ^{13}C{^{1}H} resonance obscured by d$_8$-toluene.

Elemental analysis ($C_{23}H_{39}AlN_2O$) Calcd in %: C, 71.46; H, 10.17; N, 7.25. Found: C, 71.35; H, 10.29; N, 7.24.

Al(2)Me$_2$: Recrystallised from hot toluene to yield yellow crystals (0.32 g, 0.74 mmol, 37 %).

^{1}H NMR (d$_8$-tol, 400 MHz) δ = 7.40 (s, 1H; ArCHN), 7.19 (d, *J* = 2.5 Hz, 1H; ArH), 6.54 (d, *J* = 2.0 Hz, 1H; ArH), 2.80 (br d, *J* = 14.0 Hz, 1H; CH$_2$), 2.45 (m, 8H; CH$_2$ /CH$_{2\ ad}$), 2.27 (s, 3H; CH$_3$), 2.21 (m, 2H; CH$_2$/CH), 2.17 (m, 3H; CH $_{ad}$), 1.97 (br d, *J* = 11.5 Hz, 3H; CH$_{2\ ad}$), 1.83 (br d, *J* = 12.0 Hz, 3H; CH$_{2\ ad}$), 1.37 (br d, *J* = 13.5 Hz, 1H; CH$_2$), 1.20 (br d, *J* = 13.5 Hz, 1H; CH$_2$), 1.09 (br d, *J* = 12.5 Hz, 1H; CH$_2$), 0.97 (q t, *J* = 13.0, 3.5 Hz, 1H; CH$_2$), 0.76 (q t, *J* = 13.0, 3.5 Hz, 1H CH$_2$), 0.56 (d t, *J* = 12.0, 2.5 Hz, 1H; NH), 0.32 (q d, *J* = 12.5, 3.5, 1H; CH$_2$), -0.37 (s, 3H; AlMe), -0.54 (s, 3H; AlMe). ^{13}C{^{1}H} NMR (d$_8$-tol, 100 MHz) δ = 171.5 (ArCHN), 166.0, 141.6, 134.8, 131.2, 122.8, 118.3 (Ar), 62.6 (CH$_2$), 54.5 (CH), 44.6 (CH$_2$), 40.61, 37.9 (CH$_2$ $_{Ad}$), 37.5 (C $_{ad}$), 29.9 (CH $_{ad}$), 29.8, 26.5, 23.4 (CH$_2$), 20.9 (CH$_3$), -6.2, -9.0 (AlMe).

Elemental analysis ($C_{26}H_{39}AlN_2O$) Calcd in %: C, 73.90; H, 9.30; N, 6.63. Found: C, 73.73; H, 9.40; N, 6.54.

Al(3)Me$_2$: Product precipitated from reaction mixture and collected by filtration. Isolated as orange powder (0.81 g, 1.53 mmol, 76 %). Crystals isolable from a hot toluene/hexane mixture.

^{1}H NMR (C_6D_6, 400 MHz) δ = 7.64 (d, *J* = 2.5 Hz, 1H; ArH), 7.61 (d, *J* = 7.4 Hz, 6H; ArH), 7.41 (s, 1H;ArCHN), 7.04 – 7.04 (m, 9H; ArH), 6.81 (d, *J* = 2.5 Hz, 1H; ArH), 2.65 (br d, *J* = 13.6 Hz, 1H; CH_2), 2.47 (dd, *J* = 13.3, 4.3 Hz, 1H; CH_2), 2.36 (t, *J* = 11.6 Hz, 1H; CH_2), 2.19 (m, 2H; CH/CH_2), 2.10 (s, 3H; CH_3), 1.29 (br d, *J* = 13.1 Hz, 1H; CH_2), 1.10 (br d, *J* = 13.1 Hz, 1H; CH_2), 0.99 (dd, *J* = 12.7, 2.4 Hz, 1H; CH_2), 0.87 (qt, *J* = 12.7, 3.6 Hz, 1H; CH_2), 0.72 (q t, *J* = 12.8, 3.9 Hz, 1H; CH_2), 0.50 (t d, *J* = 10.4, 2.6 Hz, 1H; NH), 0.34 (q d, *J* = 12.4, 3.6 Hz, 1H; CH_2), -0.80 (s, 3H; AlMe), -0.91 (s, 3H; AlMe). ^{13}C{^{1}H} NMR (C_6D_6, 100 MHz) δ = 171.1 (ArCHN), 164.7, 146.7, 139.33, 139.27, 133.1, 131.9, 128.2, 127.9, 127.6, 125.6, 122.9, 118.9 (Ar), 64.1 (Ph_3C), 63.3 (CH_2), 54.2 (CH), 44.8 , 29.9, 26.4, 23.5 (CH_2), 20.74 (CH_3), -6.9, -9.4 (AlMe). Recrystallised with one molecule of toluene in the unit cell.
Elemental analysis consistently low on carbon, presumably due to the high moisture sensitivity of the samples and trace sample impurities.

Al(4)Me$_2$: Recrystallised from a toluene/hexane mixture to yield yellow crystals (0.177 g, 0.59 mmol, 29%).
^{1}H NMR (d_8-tol, 400 MHz) δ = 7.41 (s, 1H; ArCHN), 6.94 (s, 1H; ArH), 6.50 (s, 1H; ArH), 2.78 (br d, *J* = 13.5 Hz, 1H; CH_2), 2.63 (dd, *J* = 13.5, 4.5 Hz, 1H; CH_2), 2.54 (t, *J* = 12.0, 1H; CH_2), 2.31 (s, 3H; CH_3), 2.27 (m, 1H; CH), 2.27 (m, 1H; CH_2), 2.15 (s, 3H; CH_3), 1.42 (br d, *J* = 13.0 Hz, 1H; CH_2), 1.23 (br d, *J* = 13.0 Hz, 1H; CH_2), 1.14 (br dd, *J* = 13.0, 3.0 Hz, 1H; CH_2), 1.0 (q t, *J* = 13.0, 4.0 Hz, 1H; CH_2), 0.85 (q t, *J* = 13.0, 4.0 Hz, 1H; CH_2), 0.61 (br d t, *J* = 10.5, 2.0 Hz, 1H; NH), 0.42 (q d, *J* = 12.5 Hz, 4.0 Hz, 1H; CH_2), -0.39 (s, 3H; AlMe), -0.51 (s, 3H; AlMe). ^{13}C{^{1}H} NMR (d_8-tol, 100 MHz) δ = 171.3 (ArCHN), 164.9, 138.3, 130.8, 130.6, 123.1, 116.9 (Ar), 63.0 (CH_2), 54.5 (CH), 44.9, 30.0, 26.6, 23.6 (CH_2), 20.3, 16.5 (CH_3), -6.3, -8.6 (AlMe). Note: One Ar-CH_3 ^{13}C{^{1}H} resonance obscured by d_8-toluene.
Elemental analysis ($C_{17}H_{27}AlN_2O$) Calcd in %: C, 67.52; H, 9.00; N, 9.26. Found: C, 67.48; H, 9.13; N, 9.18.

Al(5)Me$_2$: Precipitated from reaction mixture. Redissolved with heat to yield yellow crystals (0.23 g, 0.77 mmol, 38%).
^{1}H NMR (C_6D_6, 400 MHz) δ = 7.46 (s, 1H; ArCHN), 6.80 (dd, *J* = 7.5, 1.7 Hz, 1H; ArH), 6.63 (dd, *J* = 8.0, 1.7 Hz; ArH), 6.53 (t, *J* = 7.7 Hz, 1H; ArH), 3.60 (s, 3H; OMe), 2.74 (d, *J* = 13.6 Hz, 1H; CH_2), 2.39 (m, 2H; CH_2), 2.17 (m, 2H; CH/CH_2),

1.30 (br d, *J* = 13.2 Hz, 1H; CH_2), 1.13 (d, *J* = 13.3 Hz, 1H; CH_2), 1.02 (dd, *J* = 13.0, 3.0 Hz, 1H; CH_2), 0.89 (qt, *J* = 12.9, 3.8 Hz, 1H; CH_2), 0.68 (qt, *J* = 12.9, 4.0 Hz, 1H; CH_2), 0.56 (td, *J* = 11.8, 2.6 Hz, 1H; NH), 0.26 (m, 1H; CH_2), -0.25 (s, 3H; AlMe), -0.40 (s, 3H; AlMe). $^{13}C\{^1H\}$ NMR (C_6D_6, 100 MHz) δ = 171.4 (ArCHN), 160.5, 152.8, 126.0, 118.8, 118.5, 114.4 (Ar), 62.6 (CH_2), 56.6 (OCH_3), 54.3 (CH), 44.6, 29.6, 26.4, 23.3 (CH_2), -5.9, -8.6 (AlMe).
Elemental analysis ($C_{16}H_{25}AlN_2O_2$) Calcd in %: C, 63.14; H, 8.28; N, 9.20. Found: C, 60.20; H, 8.27; N, 8.97.

Al(6)Me₂ : Recrystallised from toluene as orange crystals (0.16 g, 0.45 mmol, 23%).
^1H NMR (C_6D_6, 400 MHz) δ = 7.14 (dd, *J* = 9.0, 2.7 Hz, 1H; ArH), 7.11 (s, 1H; ArCHN), 6.96 (d, *J* = 2.5 Hz, 1H; ArH), 6.78 (d, *J* = 9.0 Hz; ArH), 2.75 (d, *J* = 13.9 Hz, 1H; CH_2), 2.35 (m, 2H; CH_2), 2.17 (m, 2H; CH/CH_2), 1.31 (d, *J* = 13.8 Hz, 1H; CH_2), 1.15 (d, *J* = 13.5 Hz, 1H; CH_2), 1.02 (dd, *J* = 13.1, 2.6 Hz, 1H; CH_2), 0.90 (qt, *J* = 12.9, 3.6 Hz, 1H; CH_2), 0.70 (qt, *J* = 13.1, 3.8 Hz, 1H; CH_2), 0.57 (t, *J* = 11.9 Hz, 1H; NH), 0.26 (qd, *J* = 12.7, 3.8 Hz 1H; CH_2), -0.31 (s, 3H; AlMe), -0.47 (s, 3H; AlMe). $^{13}C\{^1H\}$ NMR (C_6D_6, 100 MHz) δ = 170.4 (ArCHN), 167.7, 139.5, 138.8, 125.2, 120.0, 105.6 (Ar), 62.9 (CH_2), 54.5 (OCH_3), 54.3 (CH), 44.8, 29.9, 26.7, 23.5 (CH_2), -6.7, -8.2 (AlMe).
Elemental analysis ($C_{15}H_{22}AlN_2OBr$) Calcd in %: C, 51.00; H, 6.28; N, 7.93. Found: C, 50.84; H, 6.19; N, 8.00.

Al(7)Me₂: To a solution of **7**H (0.418g, 1 mmol) in toluene (10 ml), $AlMe_3$ (2M, 0.5 ml, 1 mmol) was added dropwise. After three hours, the removal of solvent yielded a yellow powder. (0.31g, 0.65 mmol, 65 %).
^1H NMR (C_6D_6, 400 MHz,) δ = 7.14 (s, 1H; ArH), 7.41 (s, 1H; ArCHN), 7.26 (m, 2H; ArH), 7.19 (m, 2H; ArH), 7.11 (m, 1H; ArH), 6.84 (m, 1H; ArH), 3.64 (m, 2H; CH_2), 3.29 (d, *J* = 13.9 Hz, 1H; $ArCH_2$), 2.89 (m, 1H; CH_2), 2.76 (m, 1H; CH), 2.55 (m, 1H; CH_2), 2.09 (m, 1H; CH_2), 1.61 (s, 9H; $C(CH_3)_3$), 1.49 (m, 1H; CH_2), 1.31 (s, 9H; $C(CH_3)_3$), 1.27 (m, 2H; CH_2), 1.16 (m, 2H; CH_2), 1.01 (m, 1H; CH_2), -0.28 (s, 6H; AlMe). $^{13}C\{^1H\}$ NMR (C_6D_6, 100 MHz) δ = 173.2 (ArCHN), 162.3, 141.3, 140.5, 139.3, 132.0, 129.3, 129.0, 127.6, 119.5 (Ar), 59.6 (CH), 59.0, 58.5, 51.0 (CH_2), 36.0, 34.5 ($C(CH_3)_3$), 31.9, 30.0 ($C(CH_3)_3$), 27.8, 24.6, 22.7 (CH_2), -8.9 (AlMe).

Elemental analysis ($C_{30}H_{45}AlN_2O$) Calcd in %: C, 75.59; H, 9.52; N, 5.88. Found: C, 73.03; H, 9.64; N, 5.75.

Synthesis of imino monophenolate magnesium and zinc complexes, Mg(1)$_2$/Zn(1)$_2$: The initial imine condensation was carried out in a Schlenk tube on a 2 mmol scale and was used directly after drying *in vacuo.* Mg(^{n}Bu)$_2$ or Zn(Et)$_2$ (1M, 1 ml, 1 mmol) was added to a solution of **1**H (2 mmol) in toluene (10 ml). After complete addition, the solution was stirred for 1 hour before solvent removal. Both complexes were isolated *via* hexane recrystallisation.

Mg(1)$_2$: Isolated as pale yellow crystals (0.42 g, 0.62 mmol, 62%).
^{1}H NMR (C_6D_6, 400 MHz) δ = 8.05 – 7.99 (m, 2H; ArCHN), 7.62 – 7.55 (m, 2H; ArH), 7.11 – 7.05 (m, 2H; ArH), 3.69 – 3.34 (2x t, *J* = 13.1 Hz, *J* = 12.9 Hz, 1H; CH_2), 3.27 – 2.90 (m, 3H; CH_2/CH), 2.86 – 2.62 (m, 2H; CH_2/CH), 2.59 – 2.29 (m, 2H; CH/CH_2), 2.18 – 2.02 (m, 1H; CH_2), 1.88 – 1.72 (m, 1H; CH_2), 1.56 – 1.45 (m, 2H; CH_2), 1.68 – 1.57 (m, 18H; C(CH_3)$_3$), 1.42 – 1.38 (m, 18H; C(CH_3)$_3$), 1.37 – 1.26 (m, 2H; CH_3), 1.18 – 0.94 (m, 4H; CH_2) 0.82 – 0.44 (m, 4H; CH_2). ^{13}C{^{1}H} NMR (C_6D_6, 100 MHz) δ = 169.8, 169.7 (Ar), 169.6, 169.5 (ArCHN), 169.3 (Ar), 169.2, 169.0 (ArCHN), 169.0, 140.8, 140.6, 140.5, 132.4, 132.2, 131.8, 131.7, 129.3, 129.1, 129.0, 128.9, 128.5, 128.32, 128.3, 128.2, 128.0, 127.9, 127.8, 119.90, 119.8 (Ar), 64.2, 64.0, 64.0 (CH_2), 57.8, 57.7, 56.8, 56.4 (CH), 46.7, 46.1, 46.0, 45.4 (CH_2), 35.8, 35.73, 35.71, 34.02, 33.99 (*C*(CH_3)$_3$), 32.1, 32.0 (C(*C*H_3)$_3$), 31.6, 31.4 (CH_2), 30.3, 30.3, 30.2, 30.1 (C(*C*H_3)$_3$), 27.6, 27.5, 27.3, 27.2, 24.3, 24.1, 24.0 (CH_2).
Elemental analysis ($C_{42}H_{66}MgN_4O_2$) Calcd in %: C, 73.83; H, 9.74; N, 8.20. Found: C, 73.78; H, 9.77; N, 8.15.

Zn(1)$_2$: Isolated as yellow crystals (0.38 g, 0.53 mmol, 53%).
^{1}H NMR (C_6D_6, 400 MHz) δ = 7.98 (m, 2H; ArCHN), 7.62 – 7.52 (m, 2H; ArH), 7.00 (m, 2H; ArH), 3.58 – 3.34 (m, 1H; CH_2), 3.12 – 2.67 (m, 5H; CH_2/CH), 2.55 – 1.74 (m, 4H; CH_2), 1.69 – 1.59 (m, 18H; C(CH_3)$_3$), 1.56 – 1.45 (m, 2H; CH_2), 1.44 – 1.36 (m, 18H; C(CH_3)$_3$), 1.35 – 1.00 (m, 6H; CH_2), 0.93 – 0.56 (m, 4H; CH_2). ^{13}C{^{1}H} NMR (C_6D_6, 100 MHz) δ = 171.1, 170.7, 169.9 (Ar), 169.7, 169.3, 141.5, 141.4 (Ar*C*HN), 141.28, 141.26, 132.7, 132.5, 132.3, 132.2, 129.44, 129.35, 129.3, 129.1, 128.4, 128.35, 128.3, 128.2, 128.1, 118.6, 118.2 (Ar), 64.4, 64.0, 63.8, 63.7 (CH_2),

57.2, 57.1, 56.9, 56.7 (CH), 46.8, 46.2, 46.0, 45.6 (CH_2), 35.9, 35.8, 34.0 ($C(CH_3)_3$), 32.0, 31.9 ($C(CH_3)_3$), 31.7, 31.4, 31.1 (CH_2), 30.2, 30.1, 30.1 ($C(CH_3)_3$), 27.6, 27.5, 27.3, 27.2, 24.4, 24.3, 24.2 (CH_2).
Elemental analysis ($C_{42}H_{66}ZnN_4O_2$) Calcd in %: C, 69.64; H, 9.18; N, 7.73. Found: C, 69.67; H, 9.04; N, 7.66.

***Mg(A)$_2$*:** As above using **A**H (0.65 g, 2 mmol). Washed with hexane yielding a yellow powder (0.53 g, 0.79 mmol, 79 %).
^{1}H NMR ($CDCl_3$, 400 MHz) δ = 8.47 (s, 2H; ArCHN), 7.80 (d, *J* = 4.9 Hz, 2H; ArH), 7.54 (td, *J* = 7.7, 1.5 Hz, 2H; ArH), 7.23 (m, 2H; ArH), 7.16 (m, 2H; ArH), 6.92 (d, *J* = 2.6 Hz, 2H; ArH), 6.88 (t, *J* = 6.5 Hz, 2H; ArH), 5.35 (d, *J* = 19.0 Hz, 2H; PyrCH_2), 4.84 (d, *J* = 19.0 Hz, 2H; PyrCH_2), 1.26 (s, 9H; $C(CH_3)_3$), 1.11 (s, 9H; $C(CH_3)_3$). $^{13}C\{^1H\}$ NMR ($CDCl_3$, 100 MHz) δ = 169.7 (ArCHN), 169.0, 158.1, 147.7, 140.5, 137.2, 131.2, 128.4, 127.8, 122.3, 121.4, 119.1 (ArH), 61.5 (CH_2), 35.2, 33.8 ($C(CH_3)_3$), 31.8, 29.4 ($C(CH_3)_3$).
Elemental analysis ($C_{42}H_{54}MgN_4O_2$) Calcd in %: C, 75.16; H, 8.11; N, 8.35. Found: C, 75.05; H, 8.25; N, 8.26.

Synthesis of monophenolate bicyclic aluminium complexes, Al(11-13)Me$_2$: To a solution of monophenolate bicyclic ligand, **11-13**H (1 eq), in toluene (10 ml) was added $AlMe_3$ (1 eq, 2M) dropwise. The solution was stirred for three hours before solvent was removed *in vacuo* to yield the desired complex for Al(**11-12**)Me_2.

Al(11)Me$_2$: Reaction of **11**H (0.42 g, 1 mmol). Isolated a white powder with trace impurities (0.31 g, 0.65 mmol, 65 %).
^{1}H NMR (C_6D_6, 400MHz), δ = 7.68 (s, 1H; ArH), 7.08 (m, 3H; ArH), 6.96 (m, 2H; ArH), 6.82 (s, 1H; ArH), 3.80 (d, *J* = 14.1 Hz, 1H; ArCH_2), 3.67 (d, *J* = 14.4 Hz, 1H; ArCH_2), 3.64 (s, 1H; ArCHN_2), 2.87 (t, *J* = 9.0 Hz, 1H; CH_2), 2.72 (t, *J* = 9.0 Hz, 1H; CH_2), 2.56 (d, *J* = 7.3 Hz, 1H; CH_2), 1.94 (s, 9H; $C(CH_3)_3$), 1.54 (m, 2H; CH/CH_2), 1.42 (s, 9H; $C(CH_3)_3$), 1.35 (m, 3H; CH_2), 1.15 (m, 1H; CH_2), 1.00 (m, 1H; CH_2), 0.73 (m, 1H; CH_2), -0.14 (s, 3H; AlMe), -0.27 (s, 3H; AlMe). $^{13}C\{^1H\}$ NMR (C_6D_6, 100MHz) δ = 157.8, 139.7, 138.0, 133.0, 132.2, 128.7, 128.5, 127.5, 125.9, 116.6 (Ar), 89.2 (ArCHN_2), 63.3 (CH), 54.9, 51.1, 49.3 (CH_2), 35.8, 34.3 ($C(CH_3)_3$), 32.2, 32.1 ($C(CH_3)_3$), 30.2, 27.2, 24.2 (CH_2), -5.8, -8.3 (AlMe).

Elemental analysis ($C_{30}H_{45}N_2O_1Al_1$) Calcd in %: C, 75.59; H, 9.52; N, 5.88. Found: C, 75.46; H, 9.60 ; N, 5.77.

Al(12)Me$_2$: Reaction of **12**H (0.27 g, 0.65 mmol). Isolated a white powder with trace impurities (0.21 g, 0.44 mmol, 68 %).
^{1}H NMR (C_6D_6, 400MHz) δ = 7.56 (d, *J* = 7.5 Hz, 1H; ArH), 7.53 (s, 1H; ArH), 7.56 (d, *J* = 5.6 Hz, 1H; ArH), 7.11 (t, *J* = 7.0 Hz, 1H; ArH), 7.04 (m, 2H; ArH), 6.72 (s, 1H; ArH), 4.59 (s, 1H; $ArCHN_2$), 3.63 (d, *J* = 11.1 Hz, 1H; $ArCH_2$), 3.38 (d, *J* = 14.4 Hz, 1H; $ArCH_2$), 3.31 (dd, *J* = 10.0, 4.6 Hz, 1H; CH_2), 2.30 (m, 3H; CH/CH_2), 1.74 (s, 9H; $C(CH_3)_3$), 1.51 (m, 1H; CH_2), 1.39 (m, 1H; CH_2), 1.31 (s, 9H; $C(CH_3)_3$), 1.18 (m, 3H; CH_2), 0.82 (m, 2H; CH_2), -0.18 (s, 3H; AlMe), -0.25 (s, 3H; AlMe). $^{13}C\{^1H\}$ NMR (C_6D_6,100MHz) δ = 156.9, 138.6, 138.4, 133.2, 132.8, 130.1, 128.3, 127.9, 124.8, 124.5, 121.0 (Ar), 86.2 (ArCHN), 60.6 (CH), 59.7, 59.6, 48.8 (CH_2), 35.6, 34.2 ($C(CH_3)_3$), 32.1 30.1 ($C(CH_3)_3$), 28.3, 25.0, 23.6 (CH_2), -7.4, -9.7 (AlMe). Elemental analysis consistently low on carbon, presumably due to the high moisture sensitivity of the samples and trace sample impurities.

Al(13)Me$_2$: Reaction of **13**H (0.42 g, 1 mmol). Recrystallised from hexane:toluene mixture yielding light brown crystals (0.21 g, 0.440 mmol, 44 %).
^{1}H NMR (C_6D_6, 400MHz), δ = 8.34 (d, *J* = 4.4 Hz, 1H; ArH), 7.60 (s, 1H; ArH), 6.91 (m, 3H; ArH), 6.55 (m, 1H; ArH), 4.25 (br s, 1H; $ArCH_2$), 3.91 (s, 1H; $ArCHN_2$), 3.62 (d, *J* = 13.7 Hz, 1H; $ArCH_2$), 3.26 (dd, *J* = 11.1, 6.0 Hz, 1H; CH_2), 3.13 (br s, 1H; CH_2), 2.45 (br d, *J* = 10.0 Hz, 1H; CH_2), 2.02 (br s, 1H; CH), 1.82 (s, 9H; $C(CH_3)_3$), 1.61 (m, 1H; CH_2), 1.42 (s, 9H; $C(CH_3)_3$), 1.34 (m, 1H; CH_2), 1.16 (m, 3H; CH_2), 0.87 (m, 2H; CH_2), -0.03 (s, 3H; AlMe), -0.63 (s, 3H; AlMe). $^{13}C\{^1H\}$ NMR (C_6D_6, 100MHz) δ = 157.9, 153.1, 148.9, 139.1, 137.2, 136.8, 128.4, 124.6, 124.0, 123.7, 120.2 (Ar), 90.1 ($ArCHN_2$), 60.7 (CH), 60.7, 56.6, 49.0 (CH_2), 35.7, 34.3 ($C(CH_3)_3$), 32.2, 30.1 ($C(CH_3)_3$), 28.0, 24.8, 25.5 (CH_2), -12.4 (AlMe).
Elemental analysis ($C_{29}H_{44}N_3O_2Al_1$) Calcd in %: C, 72.92; H, 9.29; N, 8.80. Found: C, 72.77; H, 9.24; N, 8.83.

5.4.2 Bisphenolate aluminium complex synthesis

Synthesis of bicyclic bisphenolate aluminum complexes, Al(14-22)Me: $AlMe_3$ (2M, 0.5 ml, 1 mmol) was added dropwise to a solution of **14**-**22**H_2 (1 mmol) in toluene (10 ml) at 40 °C. After complete addition, the solution was then heated to 80 °C and complexation allowed for 3 hours. Solvent was then removed *in vacuo* to yield the crude product which was typically purified by recrystallisation.

Al(14)Me: Recrystallised to yield colourless crystals (0.160 g, 0.29 mmol, 29 %).
^{1}H NMR (d_8-tol, 400MHz), δ = 7.48 (d, *J* = 2.5 Hz, 1H; ArH), 7.31 (d, *J* = 2.5 Hz, 1H; ArH), 6.73 (d, *J* = 2.5 Hz, 1H; ArH), 6.58 (d, *J* = 2.5 Hz, 1H; ArH), 3.40 (d, *J* = 12.5 Hz, 1H; $ArCH_2$), 2.97 (s, 1H; $ArCHN_2$), 2.71 (d, *J* = 12.5 Hz, 1H; $ArCH_2$), 2.55 (dd, *J* = 11.0, 8.0 Hz, 1H; CH_2), 2.19 (br d, *J* = 10.5 Hz, 1H; C*H*), 2.05 (dd, *J* = 11.0, 9.5 Hz, 1H; CH_2), 1.60 (s, 9H; $C(CH_3)_3$), 1.41 (s, 9H; $C(CH_3)_3$), 1.29 (m, 3H; CH_2), 1.04 (m, 5H; CH_2), -0.39 (s, 3H; AlMe). $^{13}C\{^1H\}$ NMR (d_8-tol, 100MHz) δ = 155.9, 154.2, 139.7, 138.8, 131.7, 129.8, 126.8, 125.1, 123.9, 121.5, 121.0, 120.6, (Ar), 90.8 ($ArCHN_2$), 61.3 (CH), 57.1, 55.4, 48.3 (CH_2) 35.4, 34.3 ($C(CH_3)_3$), 32.0, 30.1 ($C(CH_3)_3$), 28.0, 24.4, 24.1 (CH_2), -12.4 (AlMe). Note: One ArH $^{13}C\{^1H\}$ resonance obscured by d_8-toluene.
Elemental analysis ($C_{29}H_{39}Cl_2N_2O_2Al_1$) Cald in %: C, 63.85; H, 7.21; N, 5.14. Found: C, 63.77; H, 7.31; N, 5.07.

Al(15)Me: Recrystallised to yield colourless crystals (0.362 g, 0.57 mmol, 57%).
^{1}H NMR (d_8-tol, 400 MHz), δ = 7.66 (d, *J* = 2.5 Hz, 1H; ArH), 7.48 (d, *J* = 2.5 Hz, 1H; ArH), 6.76 (d, *J* = 2.5 Hz, 1H; ArH), 6.73 (d, *J* = 2.5 Hz, 1H; ArH), 3.38 (d, *J* = 12.5 Hz, 1H; $ArCH_2$), 2.94 (s, 1H; $ArCHN_2$), 2.67 (d, *J* = 12.5 Hz, 1H; $ArCH_2$), 2.55 (dd, *J* = 11.0, 8.0 Hz, 1H; CH_2), 2.18 (br d, *J* = 10.0 Hz, 1H; CH_2), 2.04 (dd, *J* = 11.0, 9.5 Hz, 1H; CH_2), 1.60 (s, 9H; $C(CH_3)_3$), 1.42 (s, 9H; $C(CH_3)_3$), 1.28 (m, 3H; CH_2), 1.04 (m, 4H; CH_2), 0.81 (m, 1H; CH_2), -0.38 (s, 3H; AlMe). $^{13}C\{^1H\}$ NMR (d_8-tol, 100 MHz) δ = 156.0, 155.5, 139.7, 138.8, 137.3, 133.4, 125.1, 123.9, 120.99, 120.95, 117.3, 108.6, (Ar), 90.8 ($ArCHN_2$), 61.3 (CH), 57.1, 55.4, 48.3 (CH_2), 35.4, 34.3 ($C(CH_3)_3$), 32.1, 30.1 ($C(CH_3)_3$), 28.0, 24.4, 24.1 (CH_2), -12.4 (AlMe). Note: One ArH $^{13}C\{^1H\}$ resonance obscured by d_8-toluene.

Elemental analysis ($C_{29}H_{39}Br_2N_2O_2Al_1$) Cald in %: C, 54.90; H, 6.20; N, 4.42. Found: C, 54.78; H, 6.33; N, 4.33.

Al(16)Me: Recrystallised to yield colourless crystals (0.52 g, 0.71 mmol, 71%).
^{1}H NMR (d_8-tol, 400 MHz) δ = 8.11 (d, *J* = 2.0 Hz, 1H; ArH), 7.50 (d, *J* = 2.2 Hz, 1H; ArH), 6.97 (d, *J* = 2.0 Hz, 1H; ArH), 6.73 (d, *J* = 2.5 Hz, 1H; ArH), 3.34 (d, *J* = 12.5 Hz, 1H; $ArCH_2$), 2.87 (s, 1H; $ArCHN_2$), 2.59 (d, *J* = 13.0 Hz, 1H; $ArCH_2$), 2.51 (dd, *J* = 11.0, 8.0 Hz, 1H; CH_2), 2.16 (br d, *J* = 10.5 Hz, 1H; CH_2), 2.02 (dd, *J* = 11.0, 9.5 Hz, 1H; CH_2), 1.61 (s, 9H; $C(CH_3)_3$), 1.42 (s, 9H; $C(CH_3)_3$), 1.25 (m, 3H; CH_2), 1.05 (m, 4H; CH_2), 0.78 (m, 1H; CH_2), -0.38 (s, 3H; AlMe). $^{13}C\{^1H\}$ NMR (d_8-tol, 100 MHz) δ = 158.2, 155.9, 148.5, 140.4, 139.6, 138.7, 125.1, 123.9, 121.0, 120.3, 94.3 (Ar) 90.6 ($ArCHN_2$), 78.3 (Ar), 61.2 (CH), 56.9, 55.2, 48.3 (CH_2), 28.0, 24.3, 24.1 (CH_2), 35.4, 34.3 ($C(CH_3)_3$), 32.1, 30.1 ($C(CH_3)_3$), -13.1 (AlMe). Note: One ArH $^{13}C/^1H$ resonance obscured by d_8-toluene.
Elemental analysis ($C_{29}H_{39}I_2N_2O_2Al_1$) Calcd in %: C, 47.82; H, 5.40; N, 3.85. Found: C, 47.96; H, 5.37; N, 3.67.

Al(17)Me: Recrystallised to yield colourless crystals (0.32 g, 0.56 mmol, 56%).
^{1}H NMR (C_6D_6, 400 MHz), δ = 7.56 (d, *J* = 2.1 Hz, 1H; ArH), 7.20 (dd, *J* = 8.7, 2.4 Hz, 1H; ArH), 6.94 (d, *J* = 2.4 Hz, 1H; ArH), 6.78 (m 2H; ArH), 3.66 (d, *J* = 12.7 Hz, 1H; $ArCH_2$), 3.03 (s, 1H; $ArCHN_2$), 2.65 (d, *J* = 12.7 Hz, 1H; $ArCH_2$), 2.51 (dd, *J* = 10.9, 8.0 Hz, 1H; CH_2), 2.16 (br d, *J* = 10.3 Hz, 1H; CH_2), 2.01 (t, *J* = 10.3 Hz, 1H; CH_2), 1.67 (s, 9H; $C(CH_3)_3$), 1.62 (m, 1H; CH), 1.43 (s, 9H; $C(CH_3)_3$), 1.34 (m, 2H; CH_2), 1.06 (m, 4H; CH_2), 0.78 (m, 1H; CH_2), -0.31 (s, 3H; AlMe). $^{13}C\{^1H\}$ NMR (C_6D_6, 100 MHz) δ = 158.9, 156.1, 139.7, 138.8, 134.9, 134.3, 125.0, 124.2, 123.6, 121.3, 120.2, 108.9 (Ar), 91.0 ($ArCHN_2$), 61.4 (CH), 57.1, 55.3, 48.4 (CH_2), 35.5, 34.4 ($C(CH_3)_3$), 32.1, 30.2 ($C(CH_3)_3$), 28.1, 24.4, 24.2 (CH_2), -12.1 (AlMe).
Elemental analysis ($C_{29}H_{40}Br_1N_2O_2Al_1$) Calcd in %: C, 62.70; H, 7.26; N, 5.04. Found: C, 62.41; H, 7.47; N, 4.88.

Al(18)Me: Recrystallised to yield yellow crystals (0.45 g, 0.86 mmol, 86 %).
^{1}H NMR (C_6D_6, 400 MHz), δ = 7.76 (d, *J* = 8.8 Hz, 1H; ArH), 7.85 (s, 1H; ArH), 7.53 (s, 1H; ArH), 6.78 (s, 1H; ArH), 7.65 (d, *J* = 8.8 Hz, 1H; ArH), 3.51 (d, *J* = 12.6 Hz, 1H; $ArCH_2$), 3.12 (s, 1H; $ArCHN_2$), 2.77 (d, *J* = 12.6 Hz, 1H; $ArCH_2$), 2.50 (t, *J* = 9.5

Hz, 1H; CH_2), 2.16 (m, 1H; CH_2), 2.05 (t, *J* = 9.9 Hz, 1H; CH_2), 1.72 (m, 1H; CH), 1.65 (s, 9H; $C(CH_3)_3$), 1.45 (m, 1H; CH_2) 1.39 (s, 9H; $C(CH_3)_3$), 1.34 (m, 2H; CH_2), 1.06 (m, 3H; CH_2), 0.82 (m, 1H; CH_2), -0.31 (s, 3H; AlMe). $^{13}C\{^1H\}$ NMR (C_6D_6, 100 MHz) δ = 165.6, 155.8, 140.2, 139.3, 138.8, 128.4, 128.2, 125.2, 124.2, 121.63, 121.1, 118.5 (Ar), 90.4 ($ArCHN_2$), 61.3 (CH), 57.0, 55.4, 48.1 (CH_2), 35.4, 34.4 ($C(CH_3)_3$), 32.0, 30.1 ($C(CH_3)_3$), 28.1, 24.4, 24.1 (CH_2), -12.3 (AlMe).
Elemental analysis ($C_{29}H_{40}N_3O_4Al_1$) Calcd in %: C, 66.77; H, 7.73; N, 8.06. Found: C, 66.73; H, 7.85; N, 7.93.

Al(19)Me: Recrystallised from hexane:toluene mixture to yield colourless crystals (0.22 g, 0.47 mmol, 47 %).
^1H NMR (C_6D_6, 400 MHz), δ = 7.57 (d, *J* = 2.3 Hz, 1H; ArH), 7.19 (m, 1H; ArH), 7.14 (m, 1H; ArH), 6.74 (m, 3H; ArH), 3.85 (d, *J* = 12.7 Hz, 1H; $ArCH_2$), 3.25 (s, 1H; $ArCHN_2$), 2.64 (d, *J* = 12.7 Hz, 1H; $ArCH_2$), 2.55 (dd, *J* = 10.8, 8.3 Hz, 1H; CH_2), 2.47 (br d, *J* = 10.5 Hz, 1H; CH_2), 2.06 (t, *J* = 10.7 Hz, 1H; CH_2), 1.74 (m, 1H; CH), 1.69 (s, 9H; $C(CH_3)_3$), 1.48 (m, 1H; CH_2) 1.42 (s, 9H; $C(CH_3)_3$), 1.38 (m, 1H; CH_2), 1.09 (m, 4H; CH_2), 0.82 (m, 1H; CH_2), -0.26 (s, 3H; AlMe). $^{13}C\{^1H\}$ NMR (C_6D_6, 100 MHz) δ = 159.8, 156.2, 139.4, 138.7, 132.3, 132.1, 124.9, 124.1, 121.8, 121.5, 117.9, 117.5 (Ar), 91.85 ($ArCHN_2$), 61.6 (CH), 57.0, 55.2, 48.6 (CH_2), 35.5, 34.4 ($C(CH_3)_3$), 32.1, 30.2 ($C(CH_3)_3$), 28.2, 24.5, 24.3 (CH_2), -11.93 (AlMe).
Elemental analysis ($C_{29}H_{41}N_2O_2Al_1$) Calcd in %: C, 73.08; H, 8.67; N, 5.88. Found: C, 73.25; H, 8.81; N, 5.84.

Al(20)Me: Recrystallised to yield colourless crystals (0.072 g, 0.143 mmol, 14 %).
^1H NMR (C_6D_6, 400 MHz), δ = 7.57 (s, 1H; ArH), 7.00 (s, 1H; ArH), 6.76 (s, 1H; ArH), 6.51 (m, 1H; ArH), 3.89 (d, *J* = 12.7 Hz, 1H; $ArCH_2$), 3.28 (s, 1H; $ArCHN_2$), 2.71 (d, *J* = 12.8 Hz, 1H; $ArCH_2$), 2.56 (m, 2H; CH_2), 2.40 (s, 3H; CH_3), 2.25 (s, 3H; CH_3), 2.08 (t, *J* = 10.7 Hz, 1H; CH_2), 1.76 (m, 1H; CH), 1.70 (s, 9H; $C(CH_3)_3$), 1.51 (td, *J* = 10.4, 4.2 Hz. 1H; CH_2), 1.42 (s, 9H; $C(CH_3)_3$), 1.37 (m, 1H; CH_2), 1.13 (m, 4H; CH_2), 0.84 (m, 1H; CH_2), -0.29 (s, 3H; AlMe). $^{13}C\{^1H\}$ NMR (C_6D_6, 100 MHz) δ = 156.3, 155.6, 139.4, 138.7, 134.0, 130.1, 129.6, 125.7, 124.9, 124.1, 121.6, 116.6 (Ar), 92.3 ($ArCHN_2$), 61.7 (CH), 57.1, 55.3, 48.8 (CH_2), 35.5, 34.4 ($C(CH_3)_3$), 32.1, 30.2 ($C(CH_3)_3$), 28.2, 24.5, 24.4 (CH_2), 20.6, 17.0 (CH_3), -11.5 (AlMe).

Elemental analysis consistently low on carbon, presumably due to the high moisture sensitivity of the samples.

Al(21)Me: Reaction of **21**H_2 (0.05 mmol). Recrystallisation unsuccessful, solvent removed to yield a white powder (0.21 g, 0.34 mmol, 68%).
^{1}H NMR (C_6D_6, 400 MHz), δ = 7.58 (s, 1H; ArH), 7.29 (s, 1H; ArH), 6.74 (s, 1H; ArH), 6.58 (s, 1H; ArH), 3.89 (d, *J* = 12.7 Hz, 1H; $ArCH_2$), 3.28 (s, 1H; $ArCHN_2$), 2.11 (m, 9H; CH_2 / $CH_{2\ ad}$), 2.38 (s, 3H; CH_3), 2.16 (s, 3H; CH_{ad}), 2.04 (t, *J* = 10.3 Hz, 1H; CH_2), 1.92 (br d, *J* = 11.8 Hz, 3H; $CH_{2\ ad}$), 1.81 (br d, *J* = 11.8 Hz, 3H; $CH_{2\ ad}$), 1.75 (m, 1H; CH), 1.71 (s, 9H; $C(CH_3)_3$), 1.52 (t, *J* = 10.3 Hz,. 1H; CH_2) 1.44 (s, 9H; $C(CH_3)_3$), 1.38 (m, 1H; CH_2), 1.14 (m, 4H; CH_2), 0.84 (m, 1H; CH_2), -0.24 (s, 3H; AlMe). $^{13}C\{^1H\}$ NMR (C_6D_6, 100 MHz) δ = 156.7, 156.3, 140.6, 139.3, 138.7, 130.7, 130.4, 125.8, 124.8, 124.0, 121.6, 117.9 (Ar), 92.8 ($ArCHN_2$), 61.8 (CH), 56.9, 55.2, 48.8 (CH_2), 41.1, 37.9 ($CH_{2\ ad}$), 37.8 (C_{ad}), 35.5, 34.4 ($C(CH_3)_3$), 32.2, 30.1 ($C(CH_3)_3$), 29.9 (CH_{ad}), 28.3, 24.6, 24.4 (CH_2), 21.1 (CH_3), -11.79 (AlMe)
Elemental analysis consistently low on carbon, presumably due to the high moisture sensitivity of the samples and trace sample impurities.

Al(22)Me: Recrystallisation unsuccessful, solvent removed to yield a white powder (0.46 g, 0.781 mmol, 78%).
^{1}H NMR (C_6D_6, 400 MHz), δ = 7.69 (s, 1H; ArH), 7.58 (s, 1H; ArH), 6.87 (s, 1H; ArH), 6.70 (s, 1H; ArH), 3.90 (d, *J* = 12.8 Hz, 1H; $ArCH_2$), 3.37 (s, 1H; $ArCHN_2$), 2.56 (m, 3H; CH_2), 2.08 (t, *J* = 10.7 Hz, 1H; CH_2), 1.79 (m, 1H; CH), 1.72 (s, 9H; $C(CH_3)_3$), 1.71 (s, 9H; $C(CH_3)_3$), 1.56 (m, 1H; CH_2), 1.45 (s, 9H; $C(CH_3)_3$), 1.44 (s, 9H; $C(CH_3)_3$),1.39 (s, 9H; $C(CH_3)_3$), 1.56 (m, 1H; CH_2), 1.14 (m, 4H; CH_2), 0.85 (m, 1H; CH_2), -0.24 (s, 3H; AlMe). $^{13}C\{^1H\}$ NMR (C_6D_6, 100 MHz) δ = 156.4, 156.2, 139.9, 139.3, 139.2, 138.7, 126.9, 126.5, 124.8, 124.1, 121.6, 117.4 (Ar), 93.1 ($ArCHN_2$), 61.8 (CH), 56.9, 55.2, 48.7 (CH_2), 35.8, 35.5, 34.4, 34.3 ($C(CH_3)_3$), 32.2, 32.1, 30.2, 30.1 ($C(CH_3)_3$), 28.3, 24.6, 24.4 (CH_2), -11.75 (AlMe).
Elemental analysis ($C_{29}H_{41}N_2O_2Al_1$) Calcd in %: C, 75.47; H, 9.76; N, 4.76. Found: C, 75.30; H, 9.83; N, 4.62.

Synthesis of dinuclear aluminum bicyclic complexes: To a solution of **14**/**16**H_2 (1 mmol), in toluene (10ml), $AlMe_3$ (2M, 1ml, 2 mmol) was added. After one hour of stirring, solvent was removed and the product purified *via* recrystallisation from a toluene:hexane mixture.

Al_2(14)Me_4: Isolated as colourless crystals with ~5% of Al(**14**)Me (0.12 g, 0.194 mmol, 19 %).

^{1}H NMR (d_8-tol, 400MHz), δ = 7.51 (d, *J* = 2.4 Hz, 1H; ArH), 7.43 (d, *J* = 3.1 Hz, 1H; ArH), 7.35 (d, *J* = 2.6 Hz, 1H; ArH), 6.68 (d, *J* = 2.5 Hz, 1H; ArH), 5.23 (s, 1H; $ArCHN_2$), 4.17 (d, *J* = 13.4 Hz, 1H; $ArCH_2$), 3.44 (d, *J* = 5.1 Hz, 1H; CH_2), 2.59 (d, *J* = 13.6 Hz, 1H; CH_2), 2.53 (br d, *J* = 10.9 Hz, 1H; CH), 2.07 (m, 2H; CH_2), 1.50 (s, 10H; $C(CH_3)_3$), 1.43 (m, 1H; CH_2), 1.28 (m, 1H; CH_2), 1.21 (s, 11H; $C(CH_3)_3$), 0.85 (m, 2H; CH_2), 0.12 (s, 3H; AlMe), 0.06 (s, 3H; AlMe), -0.82 (s, 3H; AlMe), -1.07 (s, 3H; AlMe). $^{13}C\{^1H\}$ NMR (d_8-tol, 100MHz) δ = 156.0, 150.7, 147.3, 141.0, 137.2, 130.9, 127.0, 126.7, 126.6, 126.4, 126.3, 123.2 (Ar), 83.2 ($ArCHN_2$), 62.7 (CH), 61.7, 60.5, 50.7 (CH_2), 35.7, 34.6 ($C(CH_3)_3$), 31.6, 31.5 ($C(CH_3)_3$), 27.6, 24.7, 23.5 (CH_2), -6.2, -12.4 (AlMe).

Elemental analysis ($C_{32}H_{48}Cl_2N_2O_2Al_2$) Cald in %: C, 62.23; H, 7.83; N, 4.54. Found: C, 62.15; H, 7.69; N, 4.31.

Al_2(16)Me_4: Isolated as colourless crystals (0.50 g, 0.625 mmol, 63 %).

^{1}H NMR (d_8-tol, 400 MHz), δ = 7.76 (s, 1H; ArH), 7.38 (d, *J* = 2.5 Hz, 1H; ArH), 6.63 (s 1H; ArH), 6.42 (s 1H; ArH), 4.26 (br s, 1H; CH_2), 3.42 (br s, 1H; CH_2), 3.02 (d, *J* = 13.1 Hz, 1H; CH_2), 2.85 (s 1H; $ArCHN_2$), 2.32 (br t, *J* = 10.2 Hz, 1H; CH_2), 1.90 (d, *J* = 11.8 Hz, 1H; CH_2), 1.75 (s, 10H; CH/$C(CH_3)_3$), 1.36 (m, 1H; CH_2), 1.19 (m, 11H; CH_2/ $C(CH_3)_3$), 1.11 (m,1H; CH_2), 0.84 (m, 3H; CH_2), -0.06 (s, 3H; AlMe), -0.36 (s, 9H; AlMe). $^{13}C\{^1H\}$ NMR (d_8-tol, 100 MHz) δ = 157.9, 148.2, 138.8, 127.6, 124.8 121.2 (Ar), 91.5 ($ArCHN_2$), 60.8 (CH), 58.2, 57.7, 47.4 (CH_2), 36.1, 34.4 ($C(CH_3)_3$), 32.0, 31.6 ($C(CH_3)_3$), 28.3, 24.2, 23.9 (CH_2), -4.2, -11.7 (AlMe).

Elemental analysis ($C_{32}H_{48}I_2N_2O_2Al_2$) Calcd in %: C, 48.01; H, 6.04; N, 3.50. Found: C, 47.90; H, 5.92; N, 3.50.

Synthesis of Aluminum salalen complexes, Al(26-30)Me: $AlMe_3$ (2M, 0.5 ml, 1 mmol) was added dropwise to a solution of **26**-**30**H_2 (1 mmol) in toluene (10 ml) at 40 °C. After complete addition, the solution was then heated to 80 °C and complexation allowed for 3 hours. Solvent was then removed *in vacuo* and the product recrystallised from a hexane:toluene mixture.

Al(26)Me: Isolated as yellow crystals (0.326 g, 0.55 mmol, 55%). Two main series at a ratio of 3:2.

Major product: ^{1}H NMR (C_6D_6, 400 MHz,) δ = 7.76 (m, 1H; ArH), 7.57 (d, *J* = 2.5 Hz, 1H; ArH), 7.49 (s, 1H; ArCHN), 6.99 (d, *J* = 2.5 Hz, 1H; ArH), 6.88 (m, 1H; ArH), 3.83 (d, *J* = 12.5 Hz, 1H; $ArCH_2$), 3.66 (d, *J* = 13.0 Hz, 1H; $ArCH_2$), 3.13 (t, *J* = 13.0 Hz, 1H; CH_2), 2.66 (m, 2H; CH/CH_2), 2.28 (m, 2H; CH_2), 2.21 (dd, *J* = 14.0, 5.0 Hz; 1H; CH_2), 1.83 (s, 9H $C(CH_3)_3$), 1.65 (s, 9H $C(CH_3)_3$), 1.45 (s, 9H $C(CH_3)_3$), 1.36 (s/m, 10H $C(CH_3)_3/CH_2$), 0.91 (m, 2H; CH_2), 0.69 (br t, *J* = 13.0 Hz, 1H; CH_2), 0.58 (br d, *J* = 13.3 Hz, 1H; CH_2), -0.23 (s, 3H; AlMe); $^{13}C\{^1H\}$ NMR (C_6D_6, 100 MHz) δ = 173.0 (Ar*C*HN), 166.0, 157.3, 141.4, 138.6, 138.3, 137.0, 131.7, 127.3, 124.3, 124.1, 121.7, 117.8 (Ar), 55.7, 55.2 (CH_2), 51.5 (N*C*H$(CH_2)_2$), 46.2 (CH_2), 35.8, 35.6, 34.3, 34.2 (*C*$(CH_3)_3$), 32.3, 31.6, 30.3, 30.1 (C(*C*$H_3)_3$), 23.6, 20.6, 17.5 (CH_2), -8.6 (AlMe).

Minor product: ^{1}H NMR (C_6D_6, 400 MHz,) δ = 7.76 (m, 1H; ArH), 7.63 (d, *J* = 2.5 Hz, 1H; ArH), 7.44 (s, 1H;ArCHN), 7.03 (d, *J* = 2.5 Hz, 1H; ArH), 6.88 (m, 1H; ArH), 3.52 (d, *J* = 12.0 Hz, 1H; $ArCH_2$), 3.24 (d, *J* = 12.0 Hz, 1H; $ArCH_2$), 2.87 (t, *J* = 13.0 Hz, 1H; CH_2), 2.75 (m, *J* = 13.5 Hz, 1H; CH), 2.28 (m, 1H; CH_2), 1.87 (s, 9H $C(CH_3)_3$), 1.83 (s, 9H $C(CH_3)_3$), 1.47 (s, 9H $C(CH_3)_3$), 1.39 (s, 9H $C(CH_3)_3$), 1.36 (m, 2H; CH_2), 1.09 (m, 3H; CH_2), 0.91 (m, 2H; CH_2), 0.69 (br t, *J* = 13.0 Hz, 1H; CH_2) -0.42 (s, 3H; AlMe). $^{13}C\{^1H\}$ NMR (C_6D_6, 100 MHz) δ = 173.8 (ArCHN), 166.3, 157.5, 141.5, 138.5, 138.2, 137.0, 131.9, 127.3, 123.94, 123.90, 121.7, 117.9 (Ar), 57.7 (CH), 56.7, 48.9, 44.8 (CH_2), 35.9, 35.8, 34.4 (*C*$(CH_3)_3$), 32.3, 31.7, 30.5, 30.3 (C(*C*$H_3)_3$), 20.5, 18.7, 18.4 (CH_2), -11.0 (AlMe).

Elemental analysis ($C_{37}H_{57}AlN_2O_2$) Calcd in %: C, 75.47; H, 9.76; N, 4.76. Found: C, 75.33; H, 9.85; N, 4.88.

Al(27)Me: Isolated as yellow crystals (0.241g, 0.477 mmol, 48%). Two series with a ratio approximately 1:1.

Series 1: ^{1}H NMR (C_6D_6, 400 MHz,) δ = 7.55 (s, 1H; ArH), 7.50 (s, 1H; ArCHN), 7.05 (s, 1H; ArH), 6.98 (s, 1H; ArH), 6.62 (s, 1H; ArH), 3.83 (d, *J* = 13.0 Hz, 1H; $ArCH_2$), 3.63 (d, *J* = 13.0 Hz, 1H; $ArCH_2$), 3.20 (m, 1H; CH_2), 2.57 (m, 1H; CH), 2.56 (s, 3H; CH_3), 2.54 (s, 3H; CH_3), 2.38 (m, 2H; CH_2), 2.04 (dd, *J* = 14.1, 4.0 Hz, 1H; CH_2), 1.84 (s, 9H $C(CH_3)_3$), 1.61 (s, 9H $C(CH_3)_3$), 1.39 (m, 2H; CH_2), 1.08 (m, 1H; CH_2), 0.89 (m, 1H; CH_2), 0.69 (m, 1H; CH_2), 0.53 (br d, *J* = 14.4 Hz, 1H; CH_2), -0.19 (s, 3H; AlMe); $^{13}C\{^{1}H\}$ NMR (C_6D_6, 100 MHz) δ = 172.0 (Ar*C*HN), 165.7, 157.3, 139.0, 138.5, 138.2, 131.0, 130.1, 124.1, 123.8, 123.5, 121.6, 116.7 (Ar), 56.4, 55.3 (CH_2), 51.9 (CH), 46.2 (CH_2), 35.6, 35.3 ($C(CH_3)_3$), 30.1, 30.0 ($C(CH_3)_3$), 23.6, 20.4, 18.7 (CH_2), 16.6, 16.4 (CH_3), -8.1 (AlMe).

Series 2: ^{1}H NMR (C_6D_6, 400 MHz,) δ = 7.59 (s, 1H; ArH), 7.50 (s, 1H;ArCHN), 7.07 (s, 1H; ArH), 6.98 (s, 1H; ArH), 6.62 (s, 1H; ArH), 3.27 (d, *J* = 12.0 Hz, 1H; $ArCH_2$), 3.18 (d, *J* = 12.0 Hz, 1H; $ArCH_2$), 2.84 (m, 1H; CH), 2.75 (br d, 1H; CH_2) 2.66 (br t, *J* = 13.5 Hz, 1H; CH_2), 2.38 (m, 2H; CH_2), 2.17 (s, 6H; CH_3), 1.46 (s, 9H $C(CH_3)_3$), 1.44 (s, 9H $C(CH_3)_3$), 1.39 (m, 2H; CH_2), 1.08 (m, 1H; CH_2), 0.89 (m, 2H; CH_2), 0.69 (br t, *J* = 13.2 Hz, 1H; CH_2), -0.31 (s, 3H; AlMe). $^{13}C\{^{1}H\}$ NMR (C_6D_6, 100 MHz) δ= 172.9 (ArCHN), 165.8, 157.6, 138.7, 138.3, 137.9, 130.9, 130.3, 124.1, 123.7, 123.5, 121.3, 116.9 (Ar), 56.9 (CH), 55.5, 48.6, 45.0 (CH_2), 34.36, 34.34 ($C(CH_3)_3$), 32.31, 31.27 ($C(CH_3)_3$), 20.7 (CH_2), 20.51, 20.47 (CH_3), 18.41 17.4 (CH_2), -10.5 (AlMe). Notes: Form 1 resonance at 3.20 ppm obscured by Form 2. CH resonance at 2.57 ppm obscured by CH_3 resonance.

Elemental analysis ($C_{31}H_{45}AlN_2O_2$) Calcd in %: C, 73.78; H, 8.99; N, 5.55. Found: C, 73.64; H, 9.08; N, 5.45.

Al(28)Me: Isolated as yellow crystals (0.265 g, 0.424 mmol, 42 %). Two series with a ratio of 3:2.

Major product: ^{1}H NMR (C_6D_6, 400 MHz) δ = 7.55 (d, *J* = 2.5 Hz, 1H; ArH), 7.50 (s, 1H; ArCHN), 7.32 (m, 1H; ArH), 6.99 (m, 1H; ArH), 6.62 (m, 1H; ArH), 3.96 (d, *J* = 13.0 Hz, 1H; $ArCH_2$), 3.57 (d, *J* = 13.0 Hz, 1H; $ArCH_2$), 3.15 (m, 1H; CH_2), 2.71 (m, 1H; CH), 2.66 (m, 1H; CH_2), 2.60 (m, 6H; $CH_{2\ Ad}$), 2.32 (m, 4H; CH_2/CH_{Ad}), 2.26 (s, 3H; CH_3), 2.06 (m, 3H; $CH_{2\ Ad}$), 1.97 (dd, *J* = 14.1, 5.3 Hz; 1H; CH_2), 1.90 (m, 3H; $CH_{2\ Ad}$), 1.61 (s, 9H $C(CH_3)_3$), 1.44 (s, 9H $C(CH_3)_3$), 1.43 (m, 1H; CH_2), 1.37 (m, 1H;

CH_2), 1.07 (m, 1H; CH_2), 0.83 (m, 1H; CH_2), 0.68 (br t, *J* = 14.4 Hz, 1H; CH_2), 0.48 (br d, *J* = 13.9 Hz, 1H; CH_2), -0.23 (s, 3H; AlMe). $^{13}C\{^1H\}$ NMR (C_6D_6, 100 MHz) δ = 173.0 (ArCHN), 166.1, 157.3, 141.8, 138.5, 138.3, 135.5, 130.8, 123.9, 123.8, 123.6, 121.9, 118.4 (Ar), 55.4, 54.6 (CH_2), 50.4 (CH), 48.7 (CH_2), 41.0, 37.9 ($CH_{2\ ad}$), 37.7 ($C_{\ ad}$), 35.5, 34.3 ($C(CH_3)_3$), 32.2, 29.8 ($C(CH_3)_3$) 29.8 ($CH_{\ ad}$), 20.9 (CH_3), 20.8, 19.7, 17.5 (CH_2), -7.7 (AlMe).

Minor product: ^1H NMR (C_6D_6, 400 MHz,) δ = 7.60 (d, *J* = 2.5 Hz, 1H; ArH), 7.48 (s, 1H; ArCHN), 7.32 (m, 1H; ArH), 6.99 (m, 1H; ArH), 6.62 (m, 1H; ArH), 3.32 (d, *J* = 12.0 Hz, 1H; $ArCH_2$), 3.15 (m, 1H; $ArCH_2$), 2.79 (m, 1H; CH), 2.66 (m, 1H; CH_2), 2.60 (m, 6H; $CH_{2\ Ad}$), 2.32 (m, 5H; $CH_2/CH_{\ Ad}$), 2.28 (s, 3H; CH_3), 2.06 (m, 3H; $CH_{2\ Ad}$), 1.90 (m, 3H; $CH_{2\ Ad}$), 1.83 (s, 9H $C(CH_3)_3$), 1.47 (s, 9H $C(CH_3)_3$), 1.37 (m, 3H; CH_2), 1.07 (m, 1H; CH_2), 0.90 (m, 1H; CH_2), 0.84 (m, 2H; CH_2), -0.42 (s, 3H; AlMe). $^{13}C\{^1H\}$ NMR (C_6D_6, 100 MHz) δ = 173.8 (ArCHN), 166.6, 157.6, 141.8 138.5, 138.2, 136.0, 131.2, 127.3, 123.94, 123.90, 121.7, 117.9 (Ar), 56.5 (CH), 55.5, 45.5, 45.0 (CH_2) 41.0, 37.7 ($CH_{2\ ad}$), 35.7 ($C_{\ ad}$), 35.5, 34.4 ($C(CH_3)_3$), 35.7 ($C(CH_3)_3$), 30.1 (CH_3), 30.0 ($CH_{\ ad}$), 23.6, 18.2, 18.0 (CH_2), -9.7 (AlMe). Notes: $ArCH_2$ and CH_2 resonances of minor and major series overlap at 3.15 ppm.

Elemental analysis ($C_{37}H_{57}AlN_2O_2$) Calcd in %: C, 75.47; H, 9.76; N, 4.76. Found: C, 75.33; H, 9.85; N, 4.88.

Al(29)Me: Recrystallisation unsuccessful, resultant precipitate isolated as yellow powder (0.37 g, 0.678 mmol, 68 %). Two series with a ratio approximately 2:1.

Treated as one species: ^1H NMR (C_6D_6, 400 MHz,) δ = 7.76 (m, 1H; ArH), 7.48 – 7.30 (4 × s, 2H; ArH/ArCHN), 6.87 – 6.71 (4 × s, 2H; ArH), 3.52 – 3.24 (2 × d, *J* = 13.2, 12.2 Hz, 1H; CH_2), 3.18 – 2.71 (m, 3H, CH_2), 2.55 – 2.14 (m, 4H; CH/CH_2), 1.83 (m, 9H $C(CH_3)_3$), 1.38 (s, 9H $C(CH_3)_3$), 1.29 (m, 1H; CH_2), 0.93 – 0.74 (m, 2H; CH_2), 0.65 – 0.47 (m, 2H; CH_2), -0.29 – -0.35 (2 × s, 3H; AlMe). $^{13}C\{^1H\}$ NMR (C_6D_6, 100 MHz) δ = 174.0, 173.4 (ArCHN), 166.1, 165.8, 156.1, 155.6, 142.0, 137.5, 132.3, 132.0, 130.0, 127.2, 127.1, 125.6, 124.2, 120.4, 117.6 (Ar), 56.8 (CH_2), 55.5 (CH), 55.0 (CH_2), 52.0 (CH), 48.6, 45.8, 43.9 (CH_2), 35.82, 35.80 34.2 ($C(CH_3)_3$), 31.6 29.93, 23.90 ($C(CH_3)_3$), 23.4, 20.6, 19.8, 18.3, 18.0, 17.1 (CH_2). Note: Complex had low solubility in common NMR solvents.

Elemental analysis ($C_{29}H_{39}AlCl_2N_2O_2$) Calcd in %: C, 63.85; H, 7.21; N, 5.14. Found: C, 63.40; H, 7.37; N, 5.01.

Al(30)Me: Recrystallisation unsuccessful, resultant precipitate isolated as yellow powder (0.38 g, 0.73 mmol, 73 %). Two series with a ratio approximately 5:2.
Major product: ^{1}H NMR (C_6D_6, 400 MHz) δ = 8.12 (dd, *J* = 9.0, 2.9 Hz, 1H; ArH), 7.99 (m, 2H; ArH), 7.76 (m, 1H; ArH), 7.43 (s, 1H; ArCHN), 6.86 (d, *J* = 2.5 Hz, 1H; ArH), 6.77 (d, *J* = 9.0 Hz, 1H; ArH), 2.94 (m, 2H; CH_2), 2.78 (m, 1H; CH), 2.51 (m, 1H; CH_2), 2.40 (m, 2H; CH_2), 2.30 (m, 1H; CH_2), 1.78 (s, 9H $C(CH_3)_3$), 1.39 (s, 9H $C(CH_3)_3$), 1.32 (m, 2H; CH_2), 1.03 (m, 1H; CH_2), 0.89 (m, 1H; CH_2), 0.62 (br d, *J* = 13.6 Hz, 1H; CH_2), 0.55 (br d, *J* = 14.1 Hz, 1H; CH_2), -0.36 (s, 3H; AlMe); $^{13}C\{^{1}H\}$ NMR (C_6D_6, 100 MHz) δ = 174.2 (ArCHN), 168.0, 165.8, 141.6, 138.5, 132.4, 128.4, 127.4, 126.9, 125.5, 121.6, 120.0, 117.7 (Ar), 56.8 (CH), 54.8, 48.5, 43.6 (CH_2), 35.8, 34.2 ($C(CH_3)_3$), 31.6, 29.7 ($C(CH_3)_3$), 23.3, 21.4, 17.0 (CH_2), -9.9 (AlMe).
Minor product: ^{1}H NMR (C_6D_6, 400 MHz) δ = 8.06 (dd, *J* = 9.0, 2.9 Hz, 1H; ArH), 7.99 (m, 1H; ArH), 7.76 (m, 1H; ArH), 7.35 (s, 1H;ArCHN), 6.84 (d, *J* = 2.5 Hz, 1H; ArH), 6.64 (d, *J* = 9.0 Hz, 1H; ArH), 6.62 (s, 1H; ArH), 3.52 (d, *J* = 13.4 Hz, 1H; $ArCH_2$), 3.34 (d, *J* = 13.6 Hz, 1H; CH_2), 3.14 (m, 1H; CH_2), 2.31 (m, 1H; CH), 2.25 (m, 1H; CH_2), 2.18 (br s, 1H; CH_2), 2.04 (dd, *J* = 14.1, 5.1 Hz, 1H; CH_2), 1.78 (s, 9H $C(CH_3)_3$), 1.39 (s, 9H $C(CH_3)_3$), 1.20 (m, 1H; CH_2), 1.02 (m, 1H; CH_2), 0.80 (m, 2H; CH_2), 0.44 (m, 2H; CH_2), -0.30 (s, 3H; AlMe). $^{13}C\{^{1}H\}$ NMR (C_6D_6, 100 MHz) δ = 173.4 (ArCHN), 167.5, 165.6, 141.4, 138.8, 137.9, 137.6, 132.1, 126.8, 126.0, 121.9, 120.5, 117.5 (Ar), 55.2 (CH_2), 53.1 (CH), 51.6, 45.8 (CH_2), 35.7, 34.2 ($C(CH_3)_3$), 31.6, 29.8 ($C(CH_3)_3$), 19.4, 18.1, 17.7 (CH_2). -8.1 (AlMe).
Elemental analysis consistently low on carbon, presumably due to the high moisture sensitivity of the samples and trace sample impurities.

***Synthesis of aluminium salalen alkoxide complex, Al(26)OBn*. 26**H_2, (0.55 g, 1 mmol) was dissolved in toluene (10ml) and heated to 50 °C. $AlMe_3$ (2M, 0.5 ml, 1 mmol) was added dropwise and after complete addition, the solution was heated to 80 °C and stirred for 2 hours. The temperature was then reduced to 50 °C and BnOH (0.10ml, 1eq, 1 mmol) was added dropwise. Temperature was then adjusted to 80 °C for one hour after which the solvent was removed *in vacuo* and the product recrystallised from hexane/toluene mixture. Isolated as yellow crystals (0.195 g, 0.286 mmol, 29 %).

^{1}H NMR ($CDCl_3$, 400MHz) δ = 8.36 (s, 1H; ArCHN),7.59 (d, *J* = 2.5 Hz 1H; ArH), 7.29 (d, *J* = 2.5 Hz, 1H; ArH), 7.23 (m, 4H; ArH), 7.12 (m, 1H; ArH), 6.92 (d, *J* = 2.5 Hz, 1H; ArH), 6.93 (d, *J* = 2.5 Hz, 1H; ArH), 4.92 (d, *J* = 13.6 Hz, 1H; $ArCH_2$), 4.79 (d, *J* = 13.6 Hz, 1H; $ArCH_2$), 3.92 (d, *J* = 12.2 Hz, 1H; $ArCH_2$), 3.82 (t, *J* = 13.4 Hz, 1H; CH_2), 3.72 (d, *J* = 12.2 Hz, 1H; $ArCH_2$), 3.48 (m, 2H; CH/CH_2), 3.26 (dt, *J* = 13.8, 2.6 Hz, 1H; CH_2), 2.77 (br d, *J* = 14.5 Hz, 1H; CH_2), 1.91 (m, 1H; CH_2), 1.80 (m, 1H; CH_2), 1.71 (m, 1H; CH_2), 1.57 (s, 9H $C(CH_3)_3$), 1.51 (s, 9H $C(CH_3)_3$), 1.48 (m, 2H; CH_2), 1.34 (s, 9H $C(CH_3)_3$), 1.32 (s, 9H $C(CH_3)_3$), 1.23 (m, 1H; CH_2). ^{13}C NMR ($CDCl_3$,100 MHz) δ = 173.7 (ArCHN) 165.8, 156.7, 146.6, 140.8, 138.2, 137.7, 137.3, 132.1, 127.5, 127.3, 127.1, 126.3, 125.4, 123.5, 123.4, 120.8, 117.5 (Ar), 65.4 (CH_2), 57.9 (CH), 56.4, 48.9, 44.7 (CH_2), 35.4, 35.2, 34.0, 33.9 ($C(CH_3)_3$), 31.8, 31.3, 30.1, 29.8 ($C(CH_3)_3$), 23.5, 20.8, 17.5 (CH_2).
Elemental analysis ($C_{43}H_{61}AlN_2O_3$) calcd in %: C, 75.85; H 9.03; N, 4.11. Found: C, 75.44; H 9.04; N, 4.12.

Synthesis of aluminium salan complexes, Al(31-34)O^{i}Pr. Ligand, **31-34**H_2, (1 mmol) was dissolved in toluene (10ml) and heated to 50 °C. $AlMe_3$ (2M, 0.5 ml, 1 mmol) was added dropwise and after complete addition, the solution was heated to 80 °C and stirred for 2 hours. The temperature was then reduced to 50 °C and ^{i}PrOH (0.15ml, 2eq, 2 mmol) was added dropwise. Temperature was then adjusted to 80 °C for one hour after which the solvent was removed *in vacuo* and the product recrystallised from hexane/toluene mixture.

***Al(31)O^{i}Pr*:** Isolated as colourless crystals (0.31 g, 0.49 mmol, 49%).
^{1}H ($CDCl_3$, 400MHz) δ = 7.30 (d, *J*= 2.4 Hz, 1H; ArH), 7.27 (1H; ArH), 6.86 (d, *J*= 2.3 Hz, 1H; ArH), 6.81 (d, *J*= 2.2 Hz, 1H; ArH), 4.61 (dd, *J*= 13.1, 3.1 Hz, 1H; $ArCH_2$), 4.28 (d, *J*= 13.2 Hz, 1H; $ArCH_2$), 4.19 (sept, *J*= 5.9 Hz, 1H; O*CH*$(CH_3)_2$) 4.10 (d, *J*= 13.2 Hz, 1H; $ArCH_2$), 3.64 (dd, *J*= 13.1, 2.1 Hz, 1H; $ArCH_2$), 3.34 (br d, *J*= 13.8 Hz, 1H; NH), 3.05 (m, 1H; CH), 2.93 (m, 2H; CH_2), 2.59 (dt, *J*= 12.0, 4.3 Hz, 1H; CH_2), 2.46 (br t, *J*= 13.5 Hz, 1H; CH_2), 2.21 (m, 1H; CH_2), 1.59 (m, 1H; CH_2), 1.55 (s, 9H; $C(CH_3)_3$), 1.52 (m, 1H; CH_2), 1.48 (m, 1H; CH_2), 1.42 (s, 9H; $C(CH_3)_3$), 1.32 (m, 19H; $C(CH_3)_3$/CH_2), 1.21 (m, 1H; CH_2), 1.08 (d, *J*= 5.7 Hz, 3H; OCH(CH_3)$_2$), 0.94 (d, *J*= 5.7 Hz, 3H; OCH(CH_3)$_2$).

$^{13}C\{^{1}H\}$ NMR ($CDCl_3$, 100 MHz) δ= 158.1, 156.9, 138.5, 138.1, 137.5, 136.3, 124.1, 123.8, 123.7, 123.2, 120.7, 118.3 (Ar), 62.1 (O*C*H(CH_3)$_2$), 58.8 (CH), 57.0, 51.2, 44.3, 41.3 (CH_2), 35.3, 35.2, 34.0, 33.9 (*C*(CH_3)$_3$), 31.9, 31.8, 30.6, 29.9 (C(*C*H_3)$_3$), 28.4, 27.9 (OCH(*C*H_3)$_2$), 20.5, 18.8, 18.2 (CH_2). Note: ArH resonance at 7.27 coincides with residual solvent resonance ($CDCl_3$), doublet splitting assumed. CH_3 resonance of isopropoxide coincides with residual solvent resonance (Hexane).
Elemental analysis ($C_{39}H_{63}AlN_2O_3$) calcd in %: C, 73.78; H 10.00; N, 4.41. Found: C, 71.20; H 10.50; N, 4.41.

Al(32)O^{i}Pr: Isolated as colourless crystals (0.31 g, 0.61 mmol, 61%).
^{1}H NMR ($CDCl_3$, 400MHz) δ = 7.29 (d, *J* = 2.4 Hz, 1H; ArH), 6.85 (s, 1H; ArH), 6.83 (d, *J* = 2.3 Hz, 1H; ArH), 6.64 (s, 1H; ArH), 4.47 (dd, *J* = 12.9, 3.1 Hz, 1H; ArCH_2), 4.24 (sept, *J* = 5.9 Hz, 1H; OC*H*(CH_3)$_2$), 4.18 (d, *J* = 12.8 Hz, 1H; ArCH_2), 4.05 (d, *J* = 12.8 Hz, 1H; ArCH_2), 3.54 (dd, *J* = 13.9, 2.4 Hz, 1H; ArCH_2), 3.45 (m, 1H; NH), 3.09 (m, 1H; CH), 2.83 (q, *J* = 12.8 Hz 1H; CH_2), 2.68 (br d, *J* = 14.7 Hz, 1H; CH_2), 2.61 (dt, *J* = 12.4, 5.0 Hz, 1H; CH_2), 2.20 (s, 3H; CH_3), 2.16 (m, 2H; CH_2), 2.07 (s, 3H; CH_3), 1.58 (m, 1H; CH_2), 1.55 (s, 9H; C(CH_3)$_3$), 1.50 (m, 1H; CH_2), 1.40 (m, 1H; CH_2), 1.30 (s, 9H; C(CH_3)$_3$), 1.25 (m, 1H; CH_2), 1.10 (m, 4H; CH_2/OCH(C*H*$_3$)$_2$), 0.97 (d, *J* = 5.1 Hz, 3H; OCH(C*H*$_3$)$_2$). $^{13}C\{^{1}H\}$ NMR ($CDCl_3$, 100 MHz) δ = 158.1, 156.2, 137.3, 136.3, 131.3, 128.5, 127.1, 125.2, 124.0, 123.3, 120.2, 118.5 (Ar), 62.4 (O*C*H(CH_3)$_2$), 57.8 (CH), 56.0, 50.4, 44.2, 39.3 (CH_2), 35.1, 34.0, (*C*(CH_3)$_3$), 31.9, 29.8 (C(*C*H_3)$_3$), 28.4, 27.9 (OCH(*C*H_3)$_2$), 20.4 (CH_3), 20.0, 18.5, 17.7 (CH_2), 17.2 (CH_3).
Elemental analysis ($C_{33}H_{51}AlN_2O_3$) calcd in %: C, 71.97; H 9.33; N, 5.09. Found: C, 69.78; H 9.12; N, 4.93.

Al(33)O^{i}Pr: Isolated as colourless crystals (0.28 g, 0.47 mmol, 47%).
^{1}H NMR ($CDCl_3$, 400MHz) δ = 7.33 (d, *J* = 2.4 Hz, 1H; ArH), 7.26 (1H; ArH), 6.85 (m, 2H; ArH), 4.52 (dd, *J* = 13.3, 3.5 Hz, 1H; ArCH_2), 4.21 (d, *J* = 13.4 Hz, 1H; ArCH_2), 4.08 (m, 2H; ArCH_2/OC*H*(CH_3)$_2$) 4.10 (d, *J* = 13.2 Hz, 1H; ArCH_2), 3.59 (d, *J* = 13.3 Hz, 1H; ArCH_2), 3.44 (m, 1H; NH), 3.12 (m, 1H; CH), 2.99 (q, *J* = 12.8 Hz 1H; CH_2), 2.67 (m, 2H; CH_2), 2.34 (m, 1H; CH_2), 2.13 (m, 1H; CH_2), 1.55 (m, 2H; CH_2), 1.41 (s, 9H; C(CH_3)$_3$), 1.30 (s, 9H; C(CH_3)$_3$), 1.26 (m, 2H; CH_2), 1.12 (d, *J* = 5.7 Hz, 3H; OCH(C*H*$_3$)$_2$), 0.99 (d, *J* = 5.7 Hz, 3H; OCH(C*H*$_3$)$_2$).

$^{13}C\{^{1}H\}$ NMR ($CDCl_3$, 100 MHz) δ = 156.8, 156.3, 138.9, 138.5, 129.9, 126.7, 124.4, 124.2, 123.8, 121.0, 120.1, 118.5 (Ar), 63.3 (O*C*H(CH_3)$_2$), 58.5 (CH), 54.8, 51.3, 44.6, 41.1 (CH_2), 35.2, 34.1 (*C*(CH_3)$_3$), 31.9, 29.8 (C(*C*H_3)$_3$), 28.1, 27.8 (OCH(*C*H_3)$_2$), 20.3, 18.5, 17.9 (CH_2).
Elemental analysis ($C_{31}H_{45}AlCl_2N_2O_3$) calcd in %: C, 62.94; H 7.67; N, 4.74. Found: C, 60.82; H 7.15; N, 5.10.

***Al(33)O^{i}Pr*:** Complexation observed to become brown and the isolated solid was found to be insoluble in common NMR solvents (0.42 g, 0.74 mmol, 74%).
Elemental analysis ($C_{31}H_{46}AlN_3O_5$) calcd in %: C, 65.59; H 8.17; N, 7.40. Found: C, 62.22; H 8.48; N, 7.39.

***[Al(31)OH]$_2$*:** Al(**31**)O^{i}Pr in a $CDCl_3$ solution was exposed to air for several days, after which clear crystals were isolated. A minor series was observable in the spectrum.
^{1}H NMR ($CDCl_3$, 400MHz) δ = 7.27 (m, 2H; ArH), 7.11 (d, *J* = 2.4 Hz, 2H; ArH), 6.77 (d, *J* = 2.5 Hz, 2H; ArH), 6.63 (d, *J* = 2.4 Hz, 2H; ArH), 5.22 (m, 2H; NH), 4.22 (d, *J* = 13.8, 2.6 Hz, 2H; CH_2), 3.99 (d, *J* = 12.8 Hz, 2H; ArCH_2), 3.87 (d, *J* = 12.4 Hz, 2H; ArCH_2), 3.26 (m, 2H; CH), 3.18 (d, *J* = 13.8 Hz, 2H; CH_2), 3.03 (q, *J* = 12.3 Hz, 2H; CH_2), 2.72 (m, 2H; CH_2), 2.56 (d, *J* = 14.1 Hz, 2H; CH_2), 2.09 (m, 4H; CH_2), 1.60 (s, 18H; C(CH_3)$_3$), 1.58 (m, 4H; CH_2), 1.49 (m, 2H; CH_2), 1.26 (s, 18H; C(CH_3)$_3$), 1.23 (s, 18H; C(CH_3)$_3$), 1.18 (s, 18H; C(CH_3)$_3$), 1.12 (m, 2H; CH_2), 0.96 (m, 2H; CH_2).
$^{13}C\{^{1}H\}$ NMR ($CDCl_3$, 100 MHz) δ = 154.5, 154.3, 140.9, 140.5, 136.0, 135.9, 123.3, 123.1, 123.0, 122.9, 121.7, (Ar), 53.85 (CH_2), 35.0, 34.3, 32.0, 31.9 (*C*(CH_3)$_3$), 31.8, 30.4, 29.8, 29.6 (C(*C*H_3)$_3$).

***Synthesis of aluminium salan complexes Al(31/35)Me*:** Ligand, **31**/**35**H_2 (1 mmol) was dissolved in toluene (10ml) and heated to 50 °C. $AlMe_3$ (2M, 0.5 ml, 1 mmol) was added dropwise and after complete addition, the solution was heated to 80 °C and stirred for 3 hours. After this time, solvent was removed and the crude product purified.

Al(31)Me: Crude residue washed with hexane and isolated as a white powder (0.24 g, 0.41 mmol, 41%). Four species observed in solution.

Treated as one species: ^{1}H NMR (C_6D_6, 400MHz) δ = 7.68-7.60 (m 2H; ArH), 7.00-6.90 (m 2H; ArH), 3.93-3.66 (m, 2H; CH_2), 3.54-3.26 (m, 1H; CH_2), 3.18-2.76 (m, 2H; CH/CH_2), 2.72-2.03 (m, 3H; CH/CH_2), 1.96-1.80 (m, 18H; ($C(CH_3)_3$), 1.74-1.61 (m, 3H; CH_2), 1.53-1.43 (m, 20H; (CH_2/$C(CH_3)_3$), 1.08-0.93 (m, 1H; CH_2), 0.70-0.41 (m, 2H; CH_2), -0.52- -0.63 (m, 3H; $AlCH_3$). ^{13}C{^{1}H} NMR (C_6D_6,100 MHz) δ = 158.7, 158.0, 157.8, 157.0, 139.3, 139.5, 139.0, 138.8, 138.6, 138.4, 138.2, 138.2, 137.8, 137.4, 136.8, 136.6, 129.3, 128.6, 128.3, 124.6, 124.4, 124.3, 124.3, 124.0, 123.8, 123.8, 123.70, 123.6, 123.1, 123.00, 122.9, 122.6, 122.0, 121.5, 121.1, 120.5, 118.2 (Ar), 58.2, 57.9 (CH), 57.2 57.0 (CH_2), 54.4 (CH), 53.6, 51.8, 49.7, 49.0, 48.4, 43.5, 41.3 (CH_2), 36.0, 35.9, 35.9, 35.8, 35.7, 35.6, 34.4, 34.34, 34.33, 34.31, 34.29 (*C*(CH_3)$_3$), 32.4, 32.3, 32.28, 32.25, 32.2, 30.8, 30.7, 30.6, 30.6, 30.5, 30.3 (C(*C*H_3)$_3$), 23.9, 20.3, 19.9, 18.9, 18.4, 18.2, 18.0, 17.5 (CH_2), -5.5, 7.6, -11.0 (AlMe).

Elemental analysis consistently low on carbon, presumably due to the high moisture sensitivity of the samples.

Al(35)Me: Recrystallised from cold toluene/hexane(0.21 g, 0.35 mmol, 35%). For species in solution

Treated as one species: ^{1}H NMR (C_6D_6, 400MHz) δ = 7.67-7.60 (m 2H; ArH), 7.02-6.81 (m 2H; ArH), 4.32-391 (m, 1H; CH_2), 3.90-3.64 (m, 1H; CH_2), 3.54-3.11 (m, 1H; CH_2), 2.84-2.45 (m, 3H; CH/CH_2), 2.33-2.09 (m, 2H; CH_2), 1.94-1.85 (m, 12H; NCH_3/($C(CH_3)_3$), 1.83-1.70 (m, 9H; (CH_3)$_3$), 1.49-1.43 (m, 19H; (CH_2/$C(CH_3)_3$), 1.42-1.23 (m, 3H; CH_2), 1.15-0.96 (m, 1H; CH_2),0.73-0.50 (m, 2H; CH_2), -0.43- -0.63 (m, 3H; $AlCH_3$). ^{13}C NMR (100 MHz, C_6D_6) δ = 158.5, 158.1, 157.5, 156.9, 139.4, 138.9, 138.6, 138.5, 138.4, 137.6, 137.0, 125.1, 124.8, 124.4, 124.3, 124.1, 124.0, 123.8, 123.8, 121.5, 120.3, 119.9 (Ar), 65.1, 62.2, 61.0, 59.6, 56.8 (CH_2), 56.6 (CH), 49.7 (CH_2), 46.1 (CH_3), 45.7 (CH_2), 44.1 (CH_3), 43.2 (CH_2), 36.1, 36.0, 36.96, 35.88, 34.68, 34.65, 34.6 (*C*(CH_3)$_3$), 32.7, 32.6, 31.0, 30.9, 30.8, 30.7 (C(*C*H_3)$_3$), 24.1, 20.6, 18.7, 18.5, 17.7 (CH_2), -10.2, -12.4 (AlMe).

Elemental analysis consistently low on carbon, presumably due to the high moisture sensitivity of the samples.

Synthesis of triaryl bisphenolate aluminium complex, Al(36)O^{i}Pr: Ligand, **36**H_2, (0.641 g, 1 mmol) was dissolved in toluene and heated to 50 °C. At this temperature, $AlMe_3$ (2M, 0.5 ml, 1 mmol) was added dropwise. After this period, the solution was heated to 80 °C for 3 hours. After this period, the solvent was removed and the residue washed with hexane. Isolated as a pale yellow powder (0.20 g, 0.47 mmol, 47 %).

^{1}H NMR ($CDCl_3$, 400MHz) δ = 7.77 (d, *J* = 7.0 Hz, 2H; ArH), 7.29 (m, 2H; ArH), 7.23 (m, 3H; ArH), 6.70 (d, *J* = 2.4 Hz, 1H; ArH), 6.59 (d, *J* = 2.4 Hz, 1H; ArH), 4.80 (d, *J* = 11.8 Hz, 1H; $ArCH_2$), 4.66 (sept, *J* = 5.9 Hz, 1H; $OCH(CH_3)_2$) 3.97 (d, *J* = 11.9 Hz, 1H; $ArCH_2$), 3.87 (d, *J* = 13.4 Hz, 1H; $ArCH_2$), 3.63 (d, *J* = 12.4 Hz, 1H; $ArCH_2$), 3.46 (t, *J* = 12.8 Hz, 1H; CH_2), 3.32 (m, 2H; CH_2/CH), 3.02 (m, 2H; CH_2), 2.78 (d, *J* = 13.4 Hz, 1H; $ArCH_2$), 2.05 (m, 2H; CH_2), 1.86 (m, 1H; CH_2), 1.60 (m, 1H; CH_2), 1.50 (s, 9H; $C(CH_3)_3$), 1.43 (s, 9H; $C(CH_3)_3$), 1.33 (m, 5H; CH_2/$OCH(CH_3)_2$), 1.42 (m, 12H; $C(CH_3)_3$/$OCH(CH_3)_2$), 1.25 (s, 9H; $C(CH_3)_3$), 1.22 (m, 1H; CH_2). ^{13}C{^{1}H} NMR ($CDCl_3$, 100 MHz) δ = 155.7, 155.4, 138.7, 138.6, 138.0, 137.8, 136.6, 131.1, 128.7, 128.4, 124.1, 123.9, 123.9, 123.6, 121.1, 121.1 (Ar), 63.2 ($OCH(CH_3)_2$), 59.1, 57.0, 55.8, 53.0, 48.1 (CH_2), 47.6 (CH), 35.2, 35.1, 34.2 ($C(CH_3)_3$), 31.94, 31.89, 29.9, 29.8 ($C(CH_3)_3$), 28.5, 28.1 ($OCH(CH_3)_2$), 21.7, 19.5, 19.2 (CH_2).
Elemental analysis consistently low on carbon, presumably due to the high moisture sensitivity of the samples and trace sample impurities.

Synthesis of trisphenolate aluminium complex, Al(37): Ligand, **37**H_2, (0.384 g, 0.5 mmol) was dissolved in toluene and heated to 50 °C. At this temperature, $AlMe_3$ (2M, 0.5 ml, 1 mmol) was added dropwise. After this period, the solution was heated to 80 °C for 3 hours. The solution was then cooled and the solvent removed *in vacuo*. The residue was then washed with hexane to yield a pale yellow solid (0.20 g, 0.25 mmol, 51%)

^{1}H NMR (C_6D_6, 400MHz) δ = 7.70 (d, *J* = 2.5 Hz, 1H; ArH), 7.67 (d, *J* = 2.4 Hz, 1H; ArH), 7.49 (d, *J* = 2.4 Hz, 1H; ArH), 7.03 (d, *J* = 2.4 Hz, 1H; ArH), 6.91 (d, *J* = 2.4 Hz, 1H; ArH), 6.65 (d, *J*= 2.3 Hz, 1H; ArH), 4.10 (m, 2H; CH_2),), 3.94 (d, *J*= 13.3 Hz, 1H; $ArCH_2$), 3.62 (d, *J* = 13.3 Hz, 1H; $ArCH_2$), 3.13 (t, *J* = 13.3 Hz, 1H; CH_2), 2.93 (br d, *J* = 14.3 Hz, 1H; CH_2), 2.68 (m, 1H; CH), 2.61 (d, *J* = 13.4 Hz, 1H; $ArCH_2$), 2.53 (d, *J* = 12.4 Hz, 1H; $ArCH_2$), 2.23 (t, *J* = 13.7 Hz, 1H; CH_2), 2.00 (s, 9H; $C(CH_3)_3$), 1.82 (s, 9H; $C(CH_3)_3$), 1.60 (s, 9H; $C(CH_3)_3$), 1.49 (s, 9H; $C(CH_3)_3$), 1.43

(s, 10H; $CH_2/C(CH_3)_3$), 1.32 (s, 10H; $CH_2/C(CH_3)_3$), 1.05 (m, 1H; CH_2), 0.75 (br d, *J* = 13.4 Hz, 1H; CH_2), 0.53 (br d, *J* = 14.4 Hz, 1H; CH_2), 0.41 (br d, *J* = 14.3 Hz, 1H; CH_2), 0.30 (m, 1H; CH_2). $^{13}C\{^1H\}$ NMR (C_6DC_6, 100 MHz) δ = 158.4, 156.2, 156.1, 139.4, 139.4, 139.3, 139.0, 138.3, 137.4, 125.0, 124.6, 124.5, 124.4, 123.3, 123.28, 121.9, 121.7, 118.9 (Ar), 61.4, 59.6, 58.0 (CH_2), 54.4 (CH), 54.2, 42.2 (CH_2), 36.0, 35.9, 35.7, 34.5, 34.28, 34.27 ($C(CH_3)_3$), 32.3, 32.2, 32.1, 31.8, 30.4, 30.3 ($C(CH_3)_3$), 20.2, 18.2 (CH_2).

Elemental analysis ($C_{51}H_{77}AlN_2O_3$) calcd in %: C, 77.23; H 9.79; N, 3.53. Found: C, 77.14; H 9.81; N, 3.42.

5.4.3 Group IV complexes

Synthesis of imino monophenolate titanium complex, Ti(1)(O^{i}Pr)$_2$: $Ti(O^iPr)_4$ (0.30 ml, 1 mmol) was added dropwise to ligand, **1**H_2 (0.504 g, 2 mmol) in CH_2Cl_2 (10ml). After 1 hour, solvent was removed *in vacuo* and complex recrystallised from hexane to yield yellow crystals (0.18 g, 0.218 mmol, 22%). Multiple species in solution.

Treated as one species: ^1H NMR ($CDCl_3$, 400 MHz), δ = 8.09 – 8.00 (m, 2H; ArCHN), 7.50 – 7.42 (m, 2H; ArH), 7.10 – 7.04 (m, 2H; ArH), 4.82 – 4.53 (m, 2H; $OCH(CH_3)_2$), 4.06 – 3.89 (m, 1H; CH_2), 3.73 – 3.15 (m, 2H; CH_2), 3.10 – 2.83 (m, 5H; CH/CH_2), 2.57 – 2.17 (m, 3H; CH/CH_2), 1.72 – 1.59 (m, 1H; CH_2), 1.56 – 1.52 (m, 19H; $CH_2/C(CH_3)_3$), 1.47 – 1.37 (m, 4H; CH_2), 1.32 – 1.28 (m, 19H; $CH_2/C(CH_3)_3$), 1.24 – 1.10 (m, 4H; CH_2), 1.06 – 0.93 (m, 12H; $C(CH_3)_2$) 0.85 – 0.70 (m, 2H; NH). $^{13}C\{^1H\}$ NMR ($CDCl_3$, 100 MHz) δ = 168.2, 168.0, 167.7, 167.0 (ArCHN), 161.7, 138.69, 138.67, 138.60, 138.58, 137.6, 137.5, 137.45, 129.5, 129.3, 129.3, 129.1, 128.3, 128.3, 128.1, 121.9, 121.5 (Ar), 78.1, 78.0, 77.83, 77.80 ($OCH(CH_3)_2$), 69.2, 68.7, 68.5 (CH_2), 55.1, 54.8, 54.7, 54.7 (CH), 47.0, 47.0, 46.9, 46.8 (CH_2), 35.4, 35.37, 34.22, 34.2 ($C(CH_3)_3$), 31.6, 30.5, 30.4, 30.2, 30.1, 30.4, 30.2, 30.1 ($C(CH_3)_3$), 26.2, 26.1 (CH_2), 26.05, 25.99, 25.90, 25.86, 25.8 ($HC(CH_3)_2$), 24.62, 24.5, 24.4 (CH_2). Elemental analysis ($C_{48}H_{80}TiN_4O_4$) calcd in %: C, 69.88; H 9.77; N, 6.79. Found: C, 68.15; H 10.35; N, 6.76.

Synthesis of bicyclic bisphenolate titanium complexes, Ti(14/22)(O^iPr)$_2$: $Ti(O^iPr)_4$ (0.30 ml, 1 mmol) was added dropwise to ligand, **14**/**22**H_2 (1 mmol) in CH_2Cl_2 (10ml). After 1 hour, solvent was removed *in vacuo* and the complexes recrystallised from hexane.

Ti(14)(O^iPr)$_2$: Isolated as yellow crystals (0.35g, 0.52 mmol, 53%).
^{1}H NMR ($CDCl_3$, 400 MHz), δ = 7.31 (d, *J* = 2.4 Hz, 1H; ArH), 7.21 (d, *J* = 2.4 Hz, 1H; ArH), 7.17 (d, *J* = 2.4 Hz, 1H; ArH), 6.85 (d, *J* = 2.3 Hz, 1H; ArH), 5.09 (2×sept, *J* = 6.1 Hz, 2H; OC*H*$(CH_3)_2$), 4.66 (s, 1H; ArCHN_2), 3.43 (dd, *J* = 10.1 Hz, 7.0 Hz, 1H; CH_2), 3.37 (br d, *J* = 10.4, 1H; CH_2), 3.26 (d, *J* = 12.7 Hz, 1H; ArCH_2), 3.14 (d, *J* = 12.7 Hz, 1H; ArCH_2), 2.39 (t, *J* = 10.6 Hz, 1H; CH_2), 2.30 (br q, *J* = 9.8 Hz, 1H; CH_2), 1.91 (m, 2H; CH_2), 1.78 (m, 3H; CH_2), 1.47 (s, 9H; C$(CH_3)_3$), 1.45 (d, *J*= 4.6 Hz, 3H; OCH(C*H*$_3)_2$), 1.44 (d, *J* = 4.8 Hz, 3H; OCH(C*H*$_3)_2$), 1.37 (m, 2H; CH_2), 1.25 (m 15H; C$(CH_3)_3$/OCH(C*H*$_3)_2$). ^{13}C{^{1}H} NMR ($CDCl_3$, 100 MHz,) δ = 158.8, 158.5, 141.7, 135.4, 128.9, 126.7, 125.0, 124.6, 124.5, 123.1, 123.0, 121.8 (Ar), 81.8, 80.8, 79.7 (CH), 65.3 (CH_2) 57.2 (CH), 55.5, 51.5 (CH_2), 34.9, 34.2 (*C*$(CH_3)_3$), 31.6, 29.7 (C(*C*$H_3)_3$), 29.2 (CH_2), 26.3, 26.1, 25.94, 25.91 (CH_3), 24.7, 24.4 (CH_2).
Elemental analysis ($C_{34}H_{50}Cl_2N_2O_4Ti_1$) Calcd in %: C, 60.99; H, 7.53; N, 4.18. Found: C, 60.88; H, 7.68; N, 4.26.

Ti(22)(O^iPr)$_2$: Isolated as a pale yellow powder (0.20 g, 0.281 mmol, 28 %)
^{1}H NMR ($CDCl_3$, 400 MHz), δ = 7.26 (d, *J* = 2.4 Hz, 1H; ArH), 7.20 (d, *J* = 2.5 Hz, 2H; ArH), 6.88 (d, *J* = 2.4 Hz, 1H; ArH), 5.08 (m, 2H; OC*H*$(CH_3)_2$), 4.74 (s, 1H; ArCHN_2), 3.48 (m, 1H; CH_2), 3.36 (m, 2H; CH_2), 3.28 (d, *J* = 12.7 Hz, 1H; ArCH_2), 3.08 (d, *J* = 12.7 Hz, 1H; ArCH_2), 2.35 (m, 2H; CH/CH), 1.86 (m, 5H; CH_2), 1.47 (s, 9H; C$(CH_3)_3$), 1.44 (m, 16H; CH(C*H*$_3)_2$/CH_2/C$(CH_3)_3$), 1.35 (s, 9H; C$(CH_3)_3$). 1.26 (m, 12H; OCH(C*H*$_3)_2$/C$(CH_3)_3$). 1.19 (d, *J* = 6.2 Hz, 3H; OCH(C*H*$_3)_2$). ^{13}C{^{1}H} NMR ($CDCl_3$, 100 MHz) δ = 160.2, 158.2, 139.9, 139.9, 134.2, 134.1, 124.3, 124.0, 122.6, 121.8, 121.6, 119.6. (Ar), 81.9 (ArCHN_2), 78.6, 77.2 (O*C*H$(CH_3)_2$), 64.2 (CH), 56.0, 54.2, 51.0 (CH_2), 33.94, 33.90, 34.4, 33.2 (*C*$(CH_3)_3$), 30.8, 30.7, 28.6, 28.5 (C(*C*$H_3)_3$), 28.2 (CH_2), 25.7, 25.6, 25.5, 25.4 (OCH(*C*$H_3)_2$), 23.9, 23.5 (CH_2).
Elemental analysis ($C_{42}H_{68}N_2O_4Ti_1$) Calcd in %: C, 70.76; H, 9.62; N, 3.93. Found: C, 67.84; H, 9.85; N, 3.87.

Synthesis of salalen/salan titanium complexes, Ti(26/31)(O^iPr)$_2$: $Ti(O^iPr)_4$ (0.30 ml, 1 mmol) was added dropwise to ligand, **26/31**H_2 (1 mmol) in CH_2Cl_2 (10ml). After 1 hour, solvent was removed *in vacuo* and the complexes recrystallised from hexane

Ti(26)(O^iPr)$_2$: Isolated as yellow crystals (0.15 g, 0.22 mmol, 22 %) Two species in a ratio of 5:1.

Major series: ^{1}H NMR ($CDCl_3$, 400 MHz) δ = 7.94 (d, *J* = 1.5 Hz, 1H; ArCHN), 7.48 (d, *J* = 2.6 Hz, 1H; ArH), 7.16 (d, *J* = 2.5 Hz, 1H; ArH), 6.98 (d, *J* = 2.5 Hz, 1H; ArH), 6.91 (d, *J* = 2.1 Hz, 1H; ArH), 5.15 (sept, *J* = 6.1 Hz, 1H; OC*H*$(CH_3)_2$), 4.59 (m, 2H; OC*H*$(CH_3)_2$/CH_2), 4.51 (t, *J* = 13.9 Hz, 1H; CH_2), 4.15 (m, 2H; CH_2), 3.21 (br d, *J* = 14.8 Hz, 1H; CH_2), 3.08 (m, 2H; CH/CH_2), 2.09 (m, 1H; CH_2), 1.74 (m, 2H; CH_2), 1.57 (m, 2H; CH_2),1.51 (s, 9H; C$(CH_3)_3$), 1.37 (m, 1H; CH_2), 1.32 (s, 9H; C$(CH_3)_3$), 1.29 (s, 9H; C$(CH_3)_3$), 1.24 (d, *J* = 6.0 Hz, 3H; OCH(C*H*$_3)_2$), 1.22 (d, *J* = 6.2 Hz, 3H; OCH(C*H*$_3)_2$), 1.12 (d, *J* = 6.2 Hz, 3H; OCH(C*H*$_3)_2$), 1.09 (d, *J* = 6.2 Hz, 3H; OCH(C*H*$_3)_2$), 1.03 (s, 9H; (C$(CH_3)_3$). ^{13}C{^{1}H} NMR ($CDCl_3$, 100 MHz) δ = 161.1 (ArCHN), 160.1, 158.4, 137.8, 136.1, 136.0, 134.7, 128.0, 126.6, 123.0, 122.1, 121.04, 121.02 (Ar), 76.2, 73.9, (O*C*H$(CH_3)_2$), 60.4 (CH), 57.4, 53.6, 50.5 (CH_2), 34.3, 33.6, 33.0 (*C*$(CH_3)_3$), 30.8, 30.4, 28.9, 28.5 (C(*C*$H_3)_3$), 25.54, 25.51, 25.4, 25.2 (OCH(*C*$H_3)_2$), 20.0, 18.7, 18.4 (CH_2).

Minor series: ^{1}H NMR ($CDCl_3$, 400 MHz), δ = 7.91 (s, 1H; ArCHN), 7.43 (d, *J* = 2.6 Hz, 1H; ArH), 7.16 (d, *J* = 2.5 Hz, 1H; ArH), 6.97 (m, 1H; ArH), 6.93 (d, *J* = 2.5 Hz, 1H; ArH), 5.30 (sept, *J* = 6.2 Hz, 1H; OC*H*$(CH_3)_2$), 4.33 (sept, *J* = 6.0 Hz, 1H; OC*H*$(CH_3)_2$), 4.27 (d, *J* = 12.9 Hz, 1H; ArCH_2), 3.98 (m, 2H; CH_2), 3.52 (m, 3H; CH/CH_2), 2.99 (m, 1H; CH_2), 2.29 (m, 1H; CH_2), 2.09 (m, 1H; CH_2), 1.98 (m, 1H; CH_2), 1.60 (m, 1H; CH_2), 1.59 (m, 1H; CH_2) 1.54 (s, 9H; C$(CH_3)_3$), 1.48 (m, 1H; CH_2), 1.31 (d, *J* = 6.2 Hz, 3H; OCH(C*H*$_3)_2$), 1.30 (s, 9H; C$(CH_3)_3$), 1.28 (s, 9H; C$(CH_3)_3$), 1.16 (s, 9H; (C$(CH_3)_3$), 1.09 (d, *J* = 6.2 Hz, 3H; OCH (C*H*$_3)_2$), 1.00 (d, *J* = 6.0 Hz, 3H; OCH(C*H*$_3)_2$), 0.90 (d, *J* = 6.0 Hz, 3H; OCH(C*H*$_3)_2$). ^{13}C{^{1}H} NMR ($CDCl_3$, 100 MHz) δ = 162.3 (ArCHN), 161.5, 159.7, 137.7, 136.5, 135.6, 135.0, 127.9, 126.7, 123.0, 122.5, 122.3, 120.7 (Ar), 75.7, 73.6 (O*C*H$(CH_3)_2$), 62.9 (CH), 62.7 56.9, 51.2 (CH_2), 34.3, 33.7, 33.0, 32.9 (*C*$(CH_3)_3$), 30.9, 30.4, 28.7, 28.6 (C(*C*$H_3)_3$), 25.3, 25.02, 25.01, 24.9 (OCH(*C*$H_3)_2$), 23.5, 19.5, 17.6 (CH_2). Note: $(CH_3)_2$*C*H resonance overlapped with residual solvent resonance in ^{13}C{^{13}H} spectrum.

Elemental analysis ($C_{42}H_{68}N_2O_4Ti_1$) Calcd in %: C, 70.76; H, 9.62; N, 3.93. Found: C, 70.62; H, 9.71; N, 3.92.

Ti(31)(O^{i}Pr$_2$): Isolated as yellow crystals (0.35 g, 0.49 mmol, 49 %) ~5% impurity, presumed diastereomer.

^{1}H NMR ($CDCl_3$, 400 MHz), δ = 7.25 (s, 1H; ArH), 7.21 (s, 1H; ArH), 6.91 (s, 1H; ArH), 6.77 (s, 1H; ArH), 4.81 (sept, *J* = 6.0 Hz, 1H; OC*H*(CH_3)$_2$), 4.70 (m, 2H; OC*H*(CH_3)$_2$/CH_2), 4.38 (d, *J* = 13.1 Hz, 1H; ArCH_2), 3.96 (d, *J* = 13.2 Hz, 1H; ArCH_2), 3.69 (m, 2H; CH_2), 3.30 (q, *J* = 12.7 Hz, 1H; CH_2), 3.01 (d, *J* = 14.7 Hz, 1H; CH_2), 2.93 (br d, *J* = 13.3 Hz, 1H; CH), 2.65 (br d, *J* = 12.3 Hz, 1H; NH), 2.30 (br d, *J* = 11.9 Hz, 1H; CH_2), 1.90 (q, *J* = 13.7 Hz, 1H; CH_2), 1.69 (m, 1H; CH_2), 1.53 (s. 9H; (C(CH_3)$_3$), 1.50 (m, 1H; CH_2), 1.33 (s. 9H; (C(CH_3)$_3$), 1.31 (br s. 11H; CH_2/(C(CH_3)$_3$), 1.24 (d, *J* = 6.0 Hz, 3H; OCH(C*H*$_3$)$_2$), 1.19 (d, *J* = 6.2 Hz, 3H; OCH(C*H*$_3$)$_2$), 1.15 (m, 1H; CH_2) 1.13 (d, *J* = 6.2 Hz, 3H; OCH(C*H*$_3$)$_2$), 0.95 (d, *J* = 6.0 Hz, 3H;OCH(C*H*$_3$)$_2$). ^{13}C{^{1}H} NMR ($CDCl_3$, 100 MHz) δ = 159.3, 158.9, 138.5, 138.1, 136.0, 135.8, 124.5, 123.6, 123.5, 123.0, 122.5, 121.6 (Ar), 77.3, 77.0 (O*C*H(CH_3)$_2$), 56.8, 54.0 (CH_2), 53.2 (CH), 49.6, 49.0 (CH_2), 35.4, 35.3, 34.3, 34.2 (*C*(CH_3)$_3$), 32.0, 32.0, 31.8, 30.5, 29.8 (C(*C*H$_3$)$_3$), 26.8, 26.8, 26.6, 26.3 (OCH(*C*H$_3$)$_2$), 21.0, 19.7, 19.0 (CH_2). Note: O*C*H(CH_3)$_2$ resonance overlapped with residual solvent resonance in ^{13}C{^{13}H} spectrum.

Elemental analysis ($C_{42}H_{70}N_2O_4Ti_1$) Calcd in %: C, 70.56; H, 9.87; N, 3.92. Found: C, 70.45; H, 9.94; N, 3.92.

Synthesis of imino monophenolate zirconium complex, Zr(1)(O^{i}Pr)$_2$: A solution of Zr(O^{i}Pr)$_4$·HO^{i}Pr (0.387 g, 1 mmol, 10 ml CH_2Cl_2) was added dropwise to ligand, **1**H_2 (0.504 g, 2 mmol) in CH_2Cl_2 (10ml). After 1 hour, solvent was removed *in vacuo* and complex recrystallised from hexane to yield pale yellow crystals (0.24 g, 0.27 mmol, 27%). Multiple species in solution.

Treated as one species*:* ^{1}H NMR ($CDCl_3$, 400 MHz), δ = 8.13 – 8.01 (m, 2H; ArCHN), 7.49 (s, 2H; ArH), 7.12 – 7.03 (m, 2H; ArH), 4.39 – 4.21 (m, 2H; OC*H*(CH_3)$_2$), 3.71 – 3.55 (m, 2H; CH_2), 3.19 – 2.79 (m, 6H; CH/CH_2), 2.55 – 2.14 (m, 3H; CH/CH_2), 1.71 – 1.61 (m, 2H; CH_2), 1.58 – 1.48 (m, 19H; CH_2/C(CH_3)$_3$), 1.47 – 1.33 (m, 4H; CH_2), 1.32 – 1.28 (m, 20H; CH_2/C(CH_3)$_3$), 1.24 – 1.18 (m, 2H; CH_2), 1.17 – 1.11 (m, 6H; OCH(C*H*$_3$)$_2$), 1.08 – 0.97 (m, 6H; OCH(C*H*$_3$)$_2$) 0.96 – 0.81 (m, 2H; NH).

$^{13}C\{^{1}H\}$ NMR ($CDCl_3$, 100 MHz) δ = 170.1, 169.9 (ArCHN), 169.3, 160.7, 160.4, 138.9, 138.8, 138.4, 129.9, 129.8, 128.9, 128.9, 121.9, 121.7, 121.5, 121.3 (Ar), 71.5, 71.4 (O*C*H(CH_3)$_2$), 69.0 (CH_2), 54.5, 54.32 (CH), 46.8, 46.6 (CH_2), 35.5, 34.2 (*C*(CH_3)$_3$), 31.62, 31.60, 30.2, 30.1, 30.0, 29.9 (C(*C*H_3)$_3$), 27.4, 27.3, 27.1 (OCH(*C*H_3)$_3$), 26.1, 24.3, 24.3 (CH_2).

Elemental analysis ($C_{48}H_{80}ZrN_4O_4$) calcd in %: C, 66.39; H 9.29; N, 6.45. Found: C, 66.28; H 9.16; N, 6.46.

Synthesis of bis-ligated zirconium complexes, Zr(trans-14-16)$_2$.: Zr(O^iPr)$_4$.HO^iPr (0.388 g, 1 mmol) was dissolved in hexane (10 ml) and ligand **14**-**16**H_2 (2 mmol) was added. The solution was heated to reflux (70 °C) for 24 hours before purification by filtration or crystallisation.

Zr(14)$_2$: Product precipitated from solution during complexation and collected *via* filtration as a white powder (0.86 g, 0.78 mmol, 78 %). Crystals isolable from hexane/CH_2Cl_2 mixture.

^{1}H NMR ($CDCl_3$, 400 MHz), δ = 7.11 (d, *J* = 2.5 Hz, 2H; ArH), 7.08 (d, *J* = 2.5 Hz, 2H; ArH), 7.04 (d, *J* = 2.5 Hz, 2H; ArH), 6.06 (d, *J* = 2.5 Hz, 2H; ArH), 5.19 (d, *J* = 12.0 Hz, 2H; ArCH_2), 3.83 (t, *J* = 11.5 Hz, 2H; CH_2), 3.60(d, *J* = 12.0 Hz, 2H; ArCH_2), 3.56 (s, 2H; ArCHN_2) 3.12 (dd, *J* = 12.0 ,5.0 Hz, 2H; CH_2), 2.48 (br d, *J* = 10.5 Hz, 2H; CH), 2.37 (m, 2H; CH_2), 1.82 (m, 4H; CH_2), 1.74 (m, 2H; CH_2), 1.62 (m, 2H; CH_2), 1.53 (m, 3H; CH_2), 1.35 (s, 18H; C(CH_3)$_3$), 1.29 (m, 3H; CH_2), 1.18 (s, 18H; C(CH_3)$_3$). $^{13}C\{^{1}H\}$ NMR ($CDCl_3$, 100 MHz) δ = 157.0, 153.1, 141.6, 136.0, 129.1, 128.4, 125.6, 124.6, 124.6, 124.2, 124.2, 121.5 (Ar), 92.3 (ArCHN_2), 62.9, 61.9 (CH_2), 60.1 (CH), 49.5 (CH_2), 34.9, 34.2 (*C*(CH_3)$_3$), 31.8, 30.1 (C(*C*H_3)$_3$), 27.3, 24.5, 23.4 (CH_2).

Elemental analysis ($C_{56}H_{72}Cl_4N_4O_4Zr_1$) Calcd in %: C, 61.24; H, 6.61; N, 5.10. Found: C, 61.16; H, 6.70; N, 5.13.

Zr(15)$_2$: Product precipitated from solution during complexation and collected *via* filtration as a white powder (1.06 g, 0.82 mmol, 82 %). Crystals isolable from hexane.

^{1}H NMR ($CDCl_3$, 400 MHz), δ = 7.39 (d, *J* = 2.5 Hz, 2H; ArH), 7.09 (d, *J* = 2.5 Hz, 2H; ArH), 7.03 (d, *J* = 2.5 Hz, 2H; ArH), 6.22 (d, *J* = 2.5 Hz, 1H; ArH), 5.27 (d, *J* = 12.0 Hz, 2H; ArCH_2), 3.80 (t, *J* = 11.5 Hz, 2H; CH_2), 3.60 (d, *J* = 12.0 Hz, 2H; ArCH_2N), 3.54 (s, 2H; ArCHN_2) 3.11 (dd, *J* = 12.0, 5.0 Hz, 2H; CH_2), 2.46 (br d, *J* =

10.5 Hz, 2H; CH), 2.36 (m, 2H; CH_2), 1.81 (m, 4H; CH_2), 1.72 (m, 2H; CH_2), 1.62 (m, 2H; CH_2), 1.51 (m, 3H; CH_2), 1.36 (s, 18H; $C(CH_3)_3$), 1.30 (m, 3H; CH_2), 1.17 (s, 18H; $C(CH_3)_3$). $^{13}C\{^1H\}$ NMR ($CDCl_3$, 100 MHz) δ = 157.0, 154.4, 141.6, 136.0, 134.5, 131.9, 126.0, 124.6, 124.3, 124.1, 115.4, 108.7 (Ar), 93.2 ($ArCHN_2$), 63.0, 62.0 (CH_2), 60.9 (CH), 49.5 (CH_2), 34.9, 34.2 ($C(CH_3)_3$), 31.9, 30.3 ($C(CH_3)_3$), 27.3, 24.5, 23.4 (CH_2).

Elemental analysis ($C_{56}H_{72}Br_4N_4O_4Zr_1$) Calcd in %: C, 52.71; H, 5.69; N, 4.39. Found: C, 52.64; H, 5.56; N, 4.51.

Zr(trans-16)$_2$: Product precipitated from solution during complexation and collected *via* filtration as a white powder (0.96 g, 0.66 mmol, 66%).

^1H NMR ($CDCl_3$, 400 MHz), δ = 7.75 (d, *J* = 2.0 Hz, 2H; ArH), 7.10 (d, *J* = 2.5 Hz, 2H; ArH), 7.02 (d, *J* = 2.5 Hz, 2H; ArH), 6.39 (d, *J* = 2.0 Hz, 2H; ArH), 5.47 (d, *J* = 12.0 Hz, 2H; $ArCH_2$), 3.75 (t, *J* = 12.0 Hz, 2H; CH_2), 3.57 (d, *J* = 12.0 Hz, 2H; $ArCH_2$), 3.47 (s, 2H; $ArCHN_2$), 3.08 (dd, *J* = 12.0, 5.0 Hz; 2H; CH_2), 2.40 (br d, *J* = 10.5, 2H; CH), 2.34 (m, 2H; CH_2), 1.80 (m, 4H; CH_2), 1.69 (m, 3H; CH_2), 1.58 (m, 3H; CH_2), 1.51 (m, 4H; CH_2), 1.37 (s, 18H; $C(CH_3)_3$), 1.18 (s, 18H; $C(CH_3)_3$). $^{13}C\{^1H\}$ NMR ($CDCl_3$, 100 MHz) δ = 157.5, 157.0, 145.6, 141.5, 138.9, 136.0, 125.6, 124.7, 124.3, 124.0, 93.1 (Ar), 92.4 ($ArCHN_2$), 78.6 (Ar), 63.4, 62.0 (CH_2), 60.9 (CH), 49.5 (CH_2), 35.0, 34.3 ($C(CH_3)_3$), 32.0, 30.5 ($C(CH_3)_3$), 27.2, 24.5, 23.4 (CH_2).

Elemental analysis ($C_{56}H_{72}I_4N_4O_4Zr_1$) Calcd in %: C, 45.94; H, 4.96; N, 3.83. Found: C, 45.99; H, 5.07; N, 3.71.

Synthesis of bis-ligated zirconium complexes, Zr(cis-16)$_2$: $Zr(O^iPr)_4OH^iPr$ (0.388 g, 1 mmol) was dissolved in CH_2Cl_2 (10 ml) and ligand **16**H_2 (1.38 g, 2 mmol) was added. After 3 hours, solvent was removed *in* vacuo and product recrystallised from hot hexane mixture as colorless crystals (0.14 g, 0.10 mmol, 10 %).

^1H NMR ($CDCl_3$, 400 MHz) δ = 7.74 (d, *J* = 2.0 Hz, 1H; ArH), 7.66 (d, *J* = 2.0 Hz, 1H; ArH), 7.60 (d, *J* = 2.0 Hz, 1H; ArH), 7.14 (d, *J* = 2.0 Hz, 1H; ArH), 7.06 (d, *J* = 2.0 Hz, 1H; ArH), 6.98 (d, *J* = 2.0 Hz, 1H; ArH), 6.54 (d, *J* = 2.0 Hz, 1H; ArH), 6.15 (d, *J* = 2.0 Hz, 1H; ArH), 5.47 (s, 1H; $ArCHN_2$), 5.21 (d, *J* = 12.0 Hz, 1H; $ArCH_2$), 4.90 (dd, *J* = 9.5, 8.0 Hz, 1H; CH_2), 4.02 (d, *J* = 14.0 Hz, 1H; $ArCH_2$), 3.78 (t, *J* = 11.5 Hz, 1H; CH_2), 3.65 (dd, *J* = 12.0, 6.0 Hz, 2H; CH_2), 3.59 (s, 1H; $ArCHN_2$), 3.33 (br d, *J* = 10.5 Hz, 1H; CH_2), 3.15 (dd, *J* = 12.0, 6.0 Hz, 1H; CH_2), 2.70 (br q, *J* = 8.0

Hz, 1H; CH), 2.41 (m, 3H; CH_2), 2.27 (m, 1H; CH_2), 1.85 (m, 8H; CH_2), 1.63 (m, 1H; CH_2), 1.46 (s, 9H; $C(CH_3)_3$), 1.37 (s, 9H; $C(CH_3)_3$), 1.31 (m, 4H; CH_2), 1.23 (s, 9H; $C(CH_3)_3$), 1.21 (s, 9H; $C(CH_3)_3$). $^{13}C\{^1H\}$ NMR ($CDCl_3$, 100 MHz) δ = 161.2, 158.0, 156.0, 155.9, 146.2, 145.8, 141.8, 140.2, 138.9, 136.3, 135.4, 135.0, 125.7, 125.3, 124.7, 124.1, 124.0, 123.8, 123.7, 122.8, 92.7 (Ar), 92.6 ($ArCHN_2$), 87.8 (Ar), 82.1 ($ArCHN_2$), 80.8, 78.3 (Ar), 63.9 (CH), 63.3, 63.2, 63.1, 61.2 (CH_2), 60.7 (CH), 50.5, 48.7 (CH_2), 34.8, 34.7, 34.3, 34.0 ($C(CH_3)_3$), 32.0, 31.6, 30.3, 30.2 ($C(CH_3)_3$), 29.7, 28.0, 25.0, 24.7, 24.2, 23.5 (CH_2).

Elemental analysis ($C_{56}H_{72}I_4N_4O_4Zr_1$) Calcd in %: C, 45.94; H, 4.96; N, 3.83. Found: C, 45.85; H, 5.01; N, 3.84.

Synthesis of bicyclic bisphenolate zirconium complexes, Zr(14/22)(O^{t}Bu)$_2$: $Zr(O^tBu)_4$ (0.34 ml, 1 mmol) was added dropwise to ligand, **14/22**H_2 (1 mmol) in CH_2Cl_2 (10ml). The solution was stirred at room temperature for 16 hours before solvent removal and recrystallisation from hexane.

Zr(14)(O^{t}Bu)$_2$: Isolated as colourless crystals (0.24 g, 0.32 mmol, 32%). Sample contained <10% of Zr(**14**)$_2$.

^1H NMR ($CDCl_3$, 400 MHz), δ = 7.34 (d, *J* = 2.5 Hz, 1H; ArH), 7.24 (d, *J* = 2.4 Hz, 1H; ArH), 7.19 (d, *J* = 2.5 Hz, 1H; ArH), 6.83 (d, *J* = 2.4 Hz, 1H; ArH), 4.51 (s, 1H; $ArCHN_2$), 3.43 (m, 2H; CH_2), 3.21 (d, *J* = 12.7 Hz, 1H; $ArCH_2$), 3.15 (d, *J* = 12.9 Hz, 1H; $ArCH_2$), 2.43 (m, 2H; CH/CH_2), 1.91 (m, 2H; CH_2), 1.79 (m, 3H; CH_2), 1.47 (s, 9H; $C(CH_3)_3$), 1.44 (s, 9H; $C(CH_3)_3$), 1.38 (m, 2H; CH_2), 1.33 (s, 9H; $C(CH_3)_3$). 1.25 (s, 9H; $C(CH_3)_3$). $^{13}C\{^1H\}$ NMR ($CDCl_3$, 100 MHz) δ = 157.1, 157.0, 141.1, 136.5, 129.4, 126.0, 125.7, 125.3, 124.2, 123.7, 123.3, 123.0 (Ar), 81.9 (ArCHN), 65.0 (CH), 56.1, 56.0, 51.6 (CH_2), 35.2, 34.4 ($C(CH_3)_3$), 32.8, 32.7, 31.8, 29.9 ($C(CH_3)_3$, 29.3, 24.9, 24.6 (CH_2). Note $OC(CH_3)_3$ resonance not visible in $^{13}C\{^1H\}$ spectra, assumed hidden by $CDCl_3$ resonance.

Elemental analysis ($C_{38}H_{55.8}N_{2.2}O_4Zr_1$) Calcd in %: C, 58.65; H, 7.28; N, 3.91. Found: C, 58.57; H, 7.16; N, 3.89.

Zr(22)(O^{t}Bu)$_2$: Isolated as colourless crystals (0.24 g, 0.306 mmol, 31 %).
^{1}H NMR ($CDCl_3$, 400 MHz), δ = 7.30 (d, *J* = 2.5 Hz, 1H; ArH), 7.24 (d, *J* = 2.5 Hz, 1H; ArH), 7.22 (d, *J* = 2.3 Hz, 1H; ArH), 6.87 (d, *J* = 2.4 Hz, 1H; ArH), 4.58 (s, 1H; $ArCHN_2$), 3.45 (m, 1H; CH_2), 3.25 (m, 2H; CH_2/$ArCH_2$), 3.12 (d, *J* = 12.0 Hz, 1H; $ArCH_2$), 2.45 (m, 2H; CH/CH_2), 1.86 (m, 5H; CH_2), 1.48 (2 x s, 19H; CH_2/$C(CH_3)_3$), 1.44 (s, 10H; CH_2/$C(CH_3)_3$), 1.36 (s, 9H; $C(CH_3)_3$). 1.34 (s, 9H; $C(CH_3)_3$). 1.27 (s, 9H; $C(CH_3)_3$). ^{13}C{^{1}H} NMR ($CDCl_3$, 100 MHz) δ = 159.1, 157.5, 140.4, 140.3, 136.3, 136.2, 125.8, 124.9, 123.4, 123.3, 122.8, 121.5 (Ar), 82.8 ($ArCHN_2$), 76.7 ($OC(CH_3)_3$), 64.8 (CH), 55.6, 55.5, 52.2 (CH_2), 35.2, 34.6, 34.4 ($C(CH_3)_3$), 33.12, 30.10, 32.0, 31.9, 29.9 ($C(CH_3)_3$), 29.2, 25.0, 24.7 (CH_2).
Elemental analysis ($C_{44}H_{72}N_2O_4Zr_1$) Calcd in %: C, 67.37; H, 9.25; N, 3.57. Found: C, 67.45; H, 9.26; N, 3.63.

Synthesis of salalen/salan zirconium complexes, Zr(26/31)(O^{t}Bu)$_2$: $Zr(O^tBu)_4$ (0.34 ml, 1 mmol) was added dropwise to ligand, **26/31**H_2 (1 mmol) in CH_2Cl_2 (10ml). The solution was stirred at room temperature for 16 hours before solvent removal and recrystallisation from hexane

Zr(26)(O^{t}Bu)$_2$: Isolated as colourless crystals (0.64 g, 0.81 mmol, 81%) Two species in a ratio of 5:1.
Major series: ^{1}H NMR ($CDCl_3$, 400 MHz), δ = 7.89 (d, *J* = 1.6 Hz, 1H; ArCHN), 7.48 (d, *J* = 2.5 Hz, 1H; ArH), 7.15 (d, *J* = 2.6 Hz, 1H; ArH), 6.92 (d, *J* = 2.5 Hz, 1H; ArH), 6.90 (d, *J* = 2.4 Hz, 1H; ArH), 4.63 (td, *J* = 13.1, 1.6 Hz, 1H; CH_2), 4.39 (d, *J* = 12.9 Hz, 1H; $ArCH_2$), 4.34 (m, 1H; CH_2), 4.07 (d, *J* = 13.2 Hz, 1H; $ArCH_2$), 3.05 (m, 2H; CH_2), 2.94 (m, 1H; CH), 2.09 (m, 1H; CH_2), 1.73 (m, 2H; CH_2), 1.58 (m, 2H; CH_2), 1.55 (s, 9H; $C(CH_3)_3$), 1.32 (m, 1H; CH_2), 1.30 (s, 9H; $C(CH_3)_3$), 1.29 (s, 9H; $C(CH_3)_3$), 1.28 (s, 9H; $C(CH_3)_3$), 1.20 (s, 9H; ($C(CH_3)_3$), 1.07 (s, 9H; ($C(CH_3)_3$). ^{13}C{^{1}H} NMR ($CDCl_3$, 100 MHz) δ = 164.6 (ArCHN), 160.0, 159.5, 138.5, 136.5, 136.4, 129.3, 128.3, 124.2, 123.6, 122.0, 121.5 (Ar), 74.9, 74.5 ($OC(CH_3)_3$), 61.7, 57.4 (CH_2), 54.2 (CH), 50.3 (CH_2), 35.5, 34.9, 34.2, 34.1 ($C(CH_3)_3$), 33.2, 33.1, 33.08, 32.9, 32.1, 31.7, 30.0, 29.4 ($C(CH_3)_3$), 21.5, 19.6, 19.2 (CH_2).

Minor series: ^{1}H NMR ($CDCl_3$, 400 MHz), δ = 7.84 (s, 1H; ArCHN), 7.43 (d, *J* = 2.6 Hz, 1H; ArH), 7.15 (d, *J* = 2.5 Hz, 1H; ArH), 6.96 (d, *J* = 2.6 Hz, 1H; ArH), 6.92 (m, 1H; ArH), 4.30 (m, 1H; $ArCH_2$), 4.00 (m, 2H; CH_2), 3.87 (m, 1H; CH), 3.50 (t d, *J* = 13.9, 2.0 Hz, 1H; CH_2), 3.39 (br dd, *J* = 13.4, 3.6 Hz, 1H; CH_2), 2.95 (m, 1H; CH_2), 2.32 (m, 1H; CH_2), 2.09 (m, 1H; CH_2), 1.96 (m, 1H; CH_2), 1.64 (m, 1H; CH_2), 1.59 (m, 1H; CH_2), 1.54 (s, 9H; $C(CH_3)_3$), 1.44 (m, 1H; CH_2), 1.33 (s, 9H; $(C(CH_3)_3)$, 1.30 (s, 9H; $(C(CH_3)_3)$, 1.28 (s, 9H; $(C(CH_3)_3)$, 1.15 (s, 9H; $(C(CH_3)_3)$, 1.08 (s, 9H; $(C(CH_3)_3)$. $^{13}C\{^{1}H\}$ NMR ($CDCl_3$, 100 MHz) δ = 166.0 (ArCHN), 161.4, 159.8, 138.4, 138.1, 136.9, 136.7, 129.2, 128.5, 124.0, 123.7, 123.5, 122.2 (Ar), 75.2, 74.6 ($OC(CH_3)_3$), 63.6 (CH_2), 63.4 (CH), 56.2, 52.7 (CH_2), 35.5, 34.9, 34.2, 34.1 ($C(CH_3)_3$), 33.10, 33.08, 32.1, 31.7, 29.9, 29.7 ($C(CH_3)_3$), 24.7, 20.6, 18.1 (CH_2). Elemental analysis ($C_{44}H_{72}N_2O_4Zr_1$) Calcd in %: C, 67.38; H, 9.25; N, 3.57. Found: C, 67.21; H, 9.31; N, 3.50.

Zr(31)(O^{t}Bu)$_2$: Isolated a colourless crystals (0.11 g, 0.140 mmol, 14 %).
^{1}H NMR ($CDCl_3$, 400 MHz), δ = 7.26 (s, 1H; ArH), 7.21 (s, 1H; ArH), 6.92 (s, 1H; ArH), 6.75 (s, 1H; ArH), 4.80 (d, *J* = 13.6 Hz, 1H; $ArCH_2$), 4.56 (d, *J* = 12.9 Hz, 1H; $ArCH_2$), 3.91 (d, *J* = 12.9 Hz, 1H; $ArCH_2$), 3.64 (d, *J* = 13.3 Hz, 1H; $ArCH_2$), 3.46 (t, *J* = 13.8 Hz, 1H; CH_2), 3.24 (q, *J* = 12.9 Hz, 1H; CH_2), 3.03 (d, *J* = 13.9 Hz, 1H; CH_2), 2.83 (br d, *J* = 11.2 Hz, 1H; CH), 2.29 (t, *J* = 11.2 Hz, 2H; CH_2/NH), 1.93 (q, *J* = 13.7 Hz, 1H; CH_2), 1.65 (m, 1H; CH_2), 1.53 (s, 9H; $C(CH_3)_3$), 1.52 (s. 9H; $C(CH_3)_3$), 1.46 (m, 1H; CH_2), 1.32 (s. 18H; $C(CH_3)_3$), 1.30 (s. 9H; $C(CH_3)_3$), 1.27 (m, 2H; CH_2), 1.22 (s. 9H; $C(CH_3)_3$), 1.08 (m, 1H; CH_2). $^{13}C\{^{1}H\}$ NMR ($CDCl_3$, 100 MHz) δ = 158.4, 157.7, 138.0, 137.9, 136.7, 136.3, 124.7, 124.2, 123.4, 123.4, 123.1, 121.5 (Ar), 75.9, 75.5 ($OC(CH_3)_3$), 56.1, 53.9 (CH_2), 52.6 (CH), 48.2, 47.2 (CH_2), 35.4, 35.3, 34.3, 34.2 ($C(CH_3)_3$), 33.4, 33.3, 32.1 32.0, 30.3, 29.8 ($C(CH_3)_3$), 21.0, 19.3, 18.4 (CH_2). Elemental analysis ($C_{44}H_{74}N_2O_4Zr_1$) Calcd in %: C, 67.21; H, 9.49; N, 3.56. Found: C, 66.93; H, 9.42; N, 3.47.

Synthesis of bis-ligated hafnium complexes Hf(14-16)$_2$: Hf(O^{i}Pr)$_4$·HO^{i}Pr (0.415 g, 1 mmol) was dissolved in hexane (10 ml) and ligand **14**-**16**H_2 (2 mmol) was added. The solution was heated to reflux (70 °C) for 24 hours before purification by recrystallisation.

Hf(13)$_2$: Recrystallised from hexane/CH_2Cl_2/toluene mixture as colorless crystals. (0.875 g, 0.738 mmol, 74 %).

^{1}H NMR ($CDCl_3$, 400 MHz), δ = 7.12 (d, *J* = 2.5 Hz, 2H; ArH), 7.11 (d, *J* = 2.5 Hz, 2H; ArH), 7.02 (d, *J* = 2.5 Hz, 2H; ArH), 6.05 (d, *J* = 2.5 Hz, 2H; ArH), 5.26 (d, *J* = 12.0 Hz, 2H; $ArCH_2$), 3.84 (t, *J* = 12.0 Hz, 2H; CH_2), 3.64 (s, 2H; $ArCHN_2$), 3.59 (d, *J* = 12.0 Hz, 2H; $ArCH_2$), 3.13 (dd, *J* = 12.5, 5.0 Hz, 2H; CH_2), 2.49 (br d, *J* = 10.5 Hz, 2H; CH), 2.37 (m, 2H; CH_2), 1.83 (m, 4H; CH_2), 1.74 (m, 2H; CH_2), 1.63 (m, 2H; CH_2), 1.54 (m, 3H; CH_2), 1.35(s, 18H; $C(CH_3)_3$), 1.31 (m, 3H; CH_2), 1.19 (s, 18H; $C(CH_3)_3$). $^{13}C\{^1H\}$ NMR ($CDCl_3$, 100 MHz) δ = 157.2, 153.2, 141.3, 136.6, 129.0, 128.2, 125.5, 125.2, 124.5, 124.2, 123.9, 121.5 (Ar), 92.4 ($ArCHN_2$), 63.1, 62.1 (CH_2) 60.9 (CH), 49.5 (CH_2), 34.8, 34.1 ($C(CH_3)_3$), 31.8, 30.1 ($C(CH_3)_3$), 27.2, 24.5, 23.3 (CH_2). Note: CH_2Cl_2 present in the crystal unit cell and ^{1}H NMR spectra.

Elemental analysis ($C_{56}H_{72}Cl_4N_4O_4Hf_1$) Calcd in %: C, 56.74; H, 6.12; N, 4.73. Found: C, 56.59; H, 6.27; N, 4.62.

Hf(15)$_2$: Recrystallised from hexane/CH_2Cl_2 mixture as colorless crystals (0.481 g, 0.353 mmol, 35 %).

^{1}H NMR ($CDCl_3$, 400 MHz), δ = 7.42 (d, *J* = 2.5 Hz, 2H; ArH), 7.12 (d, *J* = 2.5 Hz, 2H; ArH), 7.03 (d, *J* = 2.5 Hz, 2H; ArH), 6.22 (d, *J* = 2.5 Hz, 2H; ArH), 5.34 (d, *J* = 12.0 Hz, 2H; $ArCH_2$), 3.82 (t, *J* = 11.5 Hz, 2H; CH_2), 3.62 (s, 2H; $ArCHN_2$), 3.58 (d, *J* = 12.0 Hz, 2H; $ArCH_2$), 3.13 (dd, *J* = 12.0, 4.5 Hz; 2H; CH_2), 2.46 (br d, *J* = 10.0 Hz, 2H; CH), 2.37 (m, 2H; CH_2), 1.83 (m, 4H; CH_2), 1.72 (m, 2H; CH_2), 1.63 (m, 2H; CH_2), 1.54 (m, 3H; CH_2), 1.36(s, 18H; $C(CH_3)_3$), 1.31 (m, 3H; CH_2), 1.19 (s, 18H; $C(CH_3)_3$). $^{13}C\{^1H\}$ NMR ($CDCl_3$, 100 MHz) δ = 157.3, 154.6, 141.3, 136.7, 134.5, 131.8, 125.9, 124.5, 124.2, 124.0, 116.0, 108.7 (Ar), 92.4 ($ArCHN_2$), 63.2, 62.1 (CH_2), 60.9 (CH), 49.5 (CH_2), 34.9, 34.2 ($C(CH_3)_3$), 31.9, 30.2 ($C(CH_3)_3$), 27.2, 24.5, 23.4 (CH_2). Note: CH_2Cl_2 present in the crystal unit cell and ^{1}H NMR spectra.

Elemental analysis ($C_{56}H_{72}Br_4N_4O_4Hf_1$) Calcd in %: C, 49.34; H, 5.32; N, 4.11. Found: C, 49.59; H, 5.49; N, 4.09.

Hf(trans-16)$_2$: Second recrystallisation from hexane/CH_2Cl_2 mixture yield isomer as colorless crystals (0.293g, 0.189 mmol, 19 %).

^{1}H NMR ($CDCl_3$, 400 MHz), δ = 7.77 (d, *J* = 2.0 Hz, 2H; ArH), 7.11 (d, *J* = 2.5 Hz, 2H; ArH), 7.02 (d, *J*=2.5 Hz, 2H; ArH), 6.39 (d, *J* = 2.0 Hz, 2H; ArH), 5.53 (d, *J* = 12.0 Hz, 2H; $ArCH_2$), 3.78 (t, *J* = 11.5 Hz, 2H; CH_2), 3.58 (m, 4H; $ArCHN_2$/$ArCH_2$), 3.10 (dd, *J* = 12.5, 5.0 Hz; 2H; CH_2), 2.46 (br d, *J* = 10.5 Hz, 2H; CH), 2.34 (m, 3H; CH_2), 1.81 (m, 5H; CH_2), 1.70 (m, 2H; CH_2), 1.61 (m, 2H; CH_2), 1.52 (m, 2H; CH_2), 1.37 (s, 18H; $C(CH_3)_3$), 1.31 (m, 2H; CH_2), 1.18 (s, 18H; $C(CH_3)_3$). $^{13}C\{^{1}H\}$ NMR ($CDCl_3$, 100 MHz) δ = 157.6, 157.2, 145.6, 141.2, 138.8, 136.6, 125.5, 124.5, 124.1, 124.0, 93.6, 78.6 (Ar), 92.5 ($ArCHN_2$), 63.5, 62.2 (CH_2), 60.8 (CH), 49.5 (CH_2), 34.9, 34.2 ($C(CH_3)_3$), 32.2, 30.4 ($C(CH_3)_3$), 27.1, 24.5, 23.3 (CH_2).
Elemental analysis ($C_{56}H_{72}I_4N_4O_4Hf_1$) Calcd in %: C, 43.36; H, 4.68; N, 3.61. Found: C, 43.24; H, 4.74; N, 3.55.

Hf(cis-16)$_2$: Isolated from second recrystallisation from hexane/CH_2Cl_2 mixture as colorless crystals (0.429 g, 0.277 mmol, 28 %).
^{1}H NMR ($CDCl_3$, 400 MHz) δ = 7.75 (d, *J* = 2.0 Hz, 1H; ArH), 7.66 (d, *J* = 2.0 Hz, 1H; ArH), 7.58 (d, *J* = 2.0 Hz, 1H; ArH), 7.15 (d, *J* = 2.5 Hz, 1H; ArH), 7.07 (d, *J* = 2.5 Hz, 1H; ArH), 6.97 (d, *J* = 2.5 Hz, 1H; ArH), 6.53 (d, *J* = 2.0 Hz, 1H; ArH), 6.15 (d, *J* = 2.5 Hz, 1H; ArH), 5.50 (s, 1H; $ArCHN_2$), 5.28 (d, *J* = 12.0 Hz, 1H; $ArCH_2$), 4.96 (dd, *J* = 10.0, 8.0 Hz, 1H; CH_2), 4.07 (d, *J* = 14.0 Hz, 1H; $ArCH_2$), 3.76 (m, 2H; CH_2), 3.67 (s, 1H; $ArCHN_2$), 3.64 (d, *J* = 12.5 Hz, 1H; CH_2), 3.34 (br d, *J* = 11.0 Hz, 1H; CH_2), 3.16 (dd, *J* = 12.0, 6.0 Hz, 1H; CH_2), 2.70 (br q, *J* = 8.0 Hz, 1H; CH), 2.40 (m, 3H; CH/CH_2), 2.28 (m, 1H; CH_2), 1.92 (br d, *J* = 12.0 Hz, 1H; CH_2), 1.82 (m, 7H; CH_2), 1.63 (m, 2H; CH_2), 1.45 (s, 9H; $C(CH_3)_3$), 1.37 (s, 9H; $C(CH_3)_3$), 1.22 (s, 9H; $C(CH_3)_3$), 1.21 (s, 9H; $C(CH_3)_3$), 1.19 (m, 3H; CH_2). $^{13}C\{^{1}H\}$ NMR ($CDCl_3$, 100 MHz) δ = 161.7, 158.1, 156.4, 155.9, 146.2, 145.8, 141.4, 140.1, 138.8, 136.8, 136.1, 134.9, 125.5, 125.3, 124.7, 124.1, 124.0, 123.7, 123.4, 122.6, 93.2 (Ar), 92.7 ($ArCHN_2$), 88.5 (Ar), 82.0 ($ArCHN_2$), 80.6, 78.4 (Ar), 63.9 (CH), 63.5, 63.4, 63.3, 61.4 (CH_2), 60.6 (CH), 50.6, 48.7 (CH_2), 34.8, 34.7, 34.2, 33.9 ($C(CH_3)_3$), 32.1, 31.6, 30.2, 30.18 ($C(CH_3)_3$). 29.7, 28.0, 25.0, 24.7, 24.2, 23.5 (CH_2).
Elemental analysis ($C_{56}H_{72}I_4N_4O_4Hf_1$) Calcd in %: C, 43.36; H, 4.68; N, 3.61. Found: C, 43.24; H, 4.75; N, 3.62.

5.5 References

1. A. Sokolowski, J. Müller, T. Weyhermüller, R. Schnepf, P. Hildebrandt, K. Hildenbrand, E. Bothe and K. Wieghardt, *J. Am. Chem. Soc.*, 1997, **119**, 8889-8900.
2. D. Basu, M. M. Allard, F. R. Xavier, M. J. Heeg, H. B. Schlegel and C. N. Verani, *Dalton Trans.*, 2015, **44**, 3454-3466.
3. P. D. Knight, P. N. O'Shaughnessy, I. J. Munslow, B. S. Kimberley and P. Scott, *J. Organomet. Chem.*, 2003, **683**, 103-113.
4. A. I. Kochnev, I. I. Oleynik, I. V. Oleynik, S. S. Ivanchev and G. A. Tolstikov, *Russ. Chem. Bull.*, 2007, **56**, 1125-1129.
5. A. Sattler, J. A. Labinger and J. E. Bercaw, *Organometallics*, 2013, **32**, 6899-6902.
6. A. S. Altieri, D. P. Hinton and R. A. Byrd, *J. Am. Chem. Soc.*, 1995, **117**, 7566-7567.
7. R. Evans, Z. Deng, A. K. Rogerson, A. S. McLachlan, J. J. Richards, M. Nilsson and G. A. Morris, *Angew. Chem. Int. Ed.*, 2013, **52**, 3199-3202.
8. Gaussian 09, Revision A.02, M. J. Frisch, G. W. Trucks, H. B. Schlegel, G. E. Scuseria, M. A. Robb, J. R. Cheeseman, G. Scalmani, V. Barone, B. Mennucci, G. A. Petersson, H. Nakatsuji, M. Caricato, X. Li, H. P. Hratchian, A. F. Izmaylov, J. Bloino, G. Zheng, J. L. Sonnenberg, M. Hada, M. Ehara, K. Toyota, R. Fukuda, J. Hasegawa, M. Ishida, T. Nakajima, Y. Honda, O. Kitao, H. Nakai, T. Vreven, J. A. Montgomery, Jr., J. E. Peralta, F. Ogliaro, M. Bearpark, J. J. Heyd, E. Brothers, K. N. Kudin, V. N. Staroverov, R. Kobayashi, J. Normand, K. Raghavachari, A. Rendell, J. C. Burant, S. S. Iyengar, J. Tomasi, M. Cossi, N. Rega, J. M. Millam, M. Klene, J. E. Knox, J. B. Cross, V. Bakken, C. Adamo, J. Jaramillo, R. Gomperts, R. E. Stratmann, O. Yazyev, A. J. Austin, R. Cammi, C. Pomelli, J. W. Ochterski, R. L. Martin, K. Morokuma, V. G. Zakrzewski, G. A. Voth, P. Salvador, J. J. Dannenberg, S. Dapprich, A. D. Daniels, O. Farkas, J. B. Foresman, J. V. Ortiz, J. Cioslowski, and D. J. Fox, Gaussian, Inc., Wallingford CT, 2009.
9. J.-D. Chai and M. Head-Gordon, *PCCP*, 2008, **10**, 6615-6620.
10. J.-D. Chai and M. Head-Gordon, *J. Chem. Phys.*, 2008, **128**, 084106.
11. M. D. Jones, L. Brady, P. McKeown, A. Buchard, P. M. Schafer, L. H. Thomas, M. F. Mahon, T. J. Woodman and J. P. Lowe, *Chem. Sci.*, 2015, **6**, 5034-5039.
12. A. Buchard, F. Jutz, M. R. Kember, A. J. P. White, H. S. Rzepa and C. K. Williams, *Macromolecules*, 2012, **45**, 6781-6795.
13. J. Baran, A. Duda, A. Kowalski, R. Szymanski and S. Penczek, *Macromol. Rapid Commun.*, 1997, **18**, 325-333.
14. B. M. Chamberlain, M. Cheng, D. R. Moore, T. M. Ovitt, E. B. Lobkovsky and G. W. Coates, *J. Am. Chem. Soc.*, 2001, **123**, 3229-3238.

Chapter 6

Appendix

6.1 Ligand X-ray diffraction data (Chapter 2)

10H

Empirical formula	$C_{20}H_{22}Cl_2N_2O$
Formula weight	377.30
Temperature	150(2) K
Wavelength	1.54184 Å
Crystal system, space group	Monoclinic, *P2₁*
Unit cell dimensions	a = 8.65350(10) Å α = 90° b = 10.23770(10) Å β = 90.742(1)° c = 10.26090(10) Å γ = 90°
Volume	908.957(16) $Å^3$
Z, Calculated density	2, 1.379 Mg/m^3
Absorption coefficient	3.288 mm^{-1}
F(000)	396
Crystal size	0.30 x 0.20 x 0.05 mm^3
Theta range for data collection	4.31 to 71.92°
Limiting indices	$-10\leq h\leq 10$, $-12\leq k\leq 12$, $-12\leq l\leq 12$
Reflections collected / unique	15722 / 3508 [R(int) = 0.0389]
Completeness to theta = 71.92°	99.9 %
Max. and min. transmission	0.8529 and 0.4387
Refinement method	Full-matrix least-squares on F^2
Data / restraints / parameters	3508 / 1 / 227
Goodness-of-fit on F^2	1.042
Final R indices [$I>2\sigma(I)$]	R_1 = 0.0256, wR_2 = 0.0684
R indices (all data)	R_1 = 0.0257, wR_2 = 0.0685
Absolute structure parameter	0.001(8)
Largest diff. peak and hole	0.209 and -0.209 $e.Å^{-3}$

14H_2

Empirical formula	$C_{28}H_{38}Cl_2N_2O_2$
Formula weight	505.50
Temperature	150(2) K
Wavelength	0.71073 Å
Crystal system, space group	Triclinic, *P*-1
Unit cell dimensions	a = 10.7434(9) Å α = 85.543(8)° b = 11.2767(11) Å β = 87.130(7)° c = 11.9090(11) Å γ = 70.262(8)°
Volume	1353.5(2) $Å^3$
Z, Calculated density	2, 1.240 Mg/m^3
Absorption coefficient	0.267 mm^{-1}
F(000)	540
Crystal size	0.30 x 0.20 x 0.20 mm^3
Theta range for data collection	3.61 to 27.48°
Limiting indices	$-13\leq h\leq 13$, $-14\leq k\leq 14$, $-15\leq l\leq 15$
Reflections collected / unique	12476 / 6195 [R(int) = 0.0212]
Completeness to theta = 27.48°	99.7 %
Max. and min. transmission	0.9486 and 0.9242
Refinement method	Full-matrix least-squares on F^2
Data / restraints / parameters	6195 / 0 / 321
Goodness-of-fit on F^2	1.013
Final R indices [$I>2\sigma(I)$]	R_1 = 0.0398, wR_2 = 0.0942
R indices (all data)	R_1 = 0.0503, wR_2 = 0.1001
Largest diff. peak and hole	0.337 and -0.238 $e.Å^{-3}$

37H_3

Empirical formula	$C_{51}H_{80}N_2O_3$
Formula weight	769.17
Temperature	150(2) K
Wavelength	0.71073 Å
Crystal system, space group	Triclinic, *P*-1
Unit cell dimensions	a = 10.2950(3) Å α = 99.3840(10)° b = 13.5730(5) Å β = 94.6830(10)° c = 18.0460(7) Å γ = 98.938(2)°
Volume	2442.84(15) $Å^3$
Z, Calculated density	2, 1.046 Mg/m^3
Absorption coefficient	0.063 mm^{-1}
F(000)	848
Crystal size	0.30 x 0.20 x 0.20 mm^3
Theta range for data collection	3.52 to 25.04°
Limiting indices	$-12\leq h\leq 12$, $-16\leq k\leq 15$, $-21\leq l\leq 21$
Reflections collected / unique	24866 / 8565 [R(int) = 0.0826]
Completeness to theta = 25.04°	99.0 %
Max. and min. transmission	0.9875 and 0.9813
Refinement method	Full-matrix least-squares on F^2
Data / restraints / parameters	8565 / 36 / 566
Goodness-of-fit on F^2	1.011
Final R indices [$I>2\sigma(I)$]	R_1 = 0.0578, wR_2 = 0.1337
R indices (all data)	R_1 = 0.1168, wR_2 = 0.1619
Largest diff. peak and hole	0.469 and -0.214 e.$Å^{-3}$

EH_2

Empirical formula	$C_{56}H_{88}N_4O_2$
Formula weight	849.30
Temperature	150(2) K
Wavelength	0.71073 Å
Crystal system, space group	Triclinic, *P*-1
Unit cell dimensions	a = 11.7962(7) Å α = 86.171(5)° b = 14.0793(9) Å β = 75.621(5)° c = 17.0072(10) Å γ = 74.485(6)°
Volume	2636.4(3) $Å^3$
Z, Calculated density	2, 1.070 Mg/m^3
Absorption coefficient	0.485 mm^{-1}
F(000)	936
Crystal size	0.20 x 0.10 x 0.05 mm^3
Theta range for data collection	3.258 to 68.568°
Limiting indices	$-14\leq h\leq 10$, $-16\leq k\leq 16$, $-20\leq l\leq 20$
Reflections collected / unique	14380 / 9517 [R(int) = 0.0258]
Completeness to theta = 67.68°	99.1 %
Max. and min. transmission	1.0000 and 0.9864
Refinement method	Full-matrix least-squares on F^2
Data / restraints / parameters	9517 / 92 / 700
Goodness-of-fit on F^2	1.026
Final R indices [$I>2\sigma(I)$]	R_1 = 0.0546, wR_2 = 0.1326
R indices (all data)	R_1 = 0.0783, wR_2 = 0.1504
Largest diff. peak and hole	0.334 and -0.250 $e.Å^{-3}$

6.2 Complex X-ray diffraction data (Chapter 3)

Al(**1**)Me_2

Empirical formula	$C_{23}H_{39}AlN_2O$
Formula weight	386.54
Temperature	150(2) K
Wavelength	1.54184 Å
Crystal system, space group	Monoclinic, *P2₁/c*
Unit cell dimensions	a = 15.1677(3) Å α = 90° b = 11.97470(10) Å β = 115.389(2)° c = 14.1461(2) Å γ = 90°
Volume	2321.18(6) $Å^3$
Z, Calculated density	4, 1.106 Mg/m^3
Absorption coefficient	0.855 mm^{-1}
F(000)	848
Crystal size	0.20 × 0.20 × 0.05 mm^3
Theta range for data collection	4.90 to 72.02°
Limiting indices	-18≤h≤18, -13≤k≤14, -17≤l≤13
Reflections collected / unique	27269 / 4551 [R(int) = 0.0381]
Completeness to theta = 72.02°	99.8 %
Max. and min. transmission	0.9585 and 0.8476
Refinement method	Full-matrix least-squares on F^2
Data / restraints / parameters	4551 / 0 / 252
Goodness-of-fit on F^2	1.047
Final R indices [I>2σ(I)]	R_1 = 0.0506, wR_2 = 0.1350
R indices (all data)	R_1 = 0.0565, wR_2 = 0.1393
Largest diff. peak and hole	1.036 and -0.392 e.$Å^{-3}$

Al(**2**)Me_2

Empirical formula	$C_{26}H_{39}AlN_2O$
Formula weight	422.57
Temperature	150(2) K
Wavelength	1.54184 Å
Crystal system, space group	Monoclinic, $P2_1/c$
Unit cell dimensions	a = 7.4788(3) Å α = 90° b = 14.4657(6) Å β = 97.752(4)° c = 21.7312(11) Å γ = 90°
Volume	2329.53(18) $Å^3$
Z, Calculated density	4, 1.205 Mg/m^3
Absorption coefficient	0.899 mm^{-1}
F(000)	920
Crystal size	0.20 × 0.10 × 0.05 mm^3
Theta range for data collection	6.46 to 66.58°
Limiting indices	$-8\leq h\leq 8$, $-17\leq k\leq 17$, $-3\leq l\leq 25$
Reflections collected / unique	4094 / 4094 [R(int) = 0.0000]
Completeness to theta = 66.58°	99.5 %
Max. and min. transmission	0.9564 and 0.8407
Refinement method	Full-matrix least-squares on F^2
Data / restraints / parameters	4094 / 0 / 275
Goodness-of-fit on F^2	1.137
Final R indices [I>2σ(I)]	R_1 = 0.0979, wR_2 = 0.2207
R indices (all data)	R_1 = 0.1124, wR_2 = 0.2319
Largest diff. peak and hole	0.908 and -0.595 $e.Å^{-3}$

Al(**3**)Me_2

Empirical formula	$C_{42}H_{47}AlN_2O$
Formula weight	622.79
Temperature	150(2) K
Wavelength	1.54184 Å
Crystal system, space group	Triclinic, *P-1*
Unit cell dimensions	a = 9.4609(2) Å α = 68.692(3)° b = 13.1087(4) Å β = 89.789(2)° c = 15.3077(6) Å γ = 78.354(2)°
Volume	1727.22(10) $Å^3$
Z, Calculated density	2, 1.198 Mg/m^3
Absorption coefficient	0.773 mm^{-1}
F(000)	668
Crystal size	0.25 × 0.14 × 0.07 mm^3
Theta range for data collection	3.108 to 73.428°
Limiting indices	$-8\leq h\leq 11$, $-16\leq k\leq 16$, $-19\leq l\leq 18$
Reflections collected / unique	19980 / 6838 [R(int) = 0.0232]
Completeness to theta = 67.684°	100.0 %
Max. and min. transmission	1.00000 and 0.82159
Refinement method	Full-matrix least-squares on F^2
Data / restraints / parameters	6838 / 134 / 585
Goodness-of-fit on F^2	1.064
Final R indices [$I>2\sigma(I)$]	R_1 = 0.0412, wR_2 = 0.1049
R indices (all data)	R_1 = 0.0457, wR_2 = 0.1083
Largest diff. peak and hole	0.323 and -0.239 $e.Å^{-3}$

Al(**4**)Me_2

Empirical formula	$C_{34}H_{52}Al_2N_2O$
Formula weight	602.76
Temperature	150(2) K
Wavelength	1.54184 Å
Crystal system, space group	Monoclinic, $P2_1/n$
Unit cell dimensions	a = 20.035(2) Å α = 90° b = 8.6659(13) Å β = 107.052(13)° c = 20.646(3) Å γ = 90°
Volume	3426.9(8) $Å^3$
Z, Calculated density	4, 1.168 Mg/m^3
Absorption coefficient	1.031 mm^{-1}
F(000)	1304
Crystal size	0.10 × 0.10 × 0.05 mm^3
Theta range for data collection	4.62 to 66.60°
Limiting indices	$-18\leq h\leq 23$, $-10\leq k\leq 10$, $-24\leq l\leq 15$
Reflections collected / unique	14397 / 6028 [R(int) = 0.0565]
Completeness to theta = 66.60°	99.4 %
Max. and min. transmission	0.9503 and 0.9039
Refinement method	Full-matrix least-squares on F^2
Data / restraints / parameters	6028 / 0 / 387
Goodness-of-fit on F^2	1.050
Final R indices [$I>2\sigma(I)$]	R_1 = 0.1110, wR_2 = 0.2705
R indices (all data)	R_1 = 0.1495, wR_2 = 0.3003
Largest diff. peak and hole	1.900 and -0.440 $e.Å^{-3}$

Al(**5**)Me_2

Empirical formula	$C_{16}H_{25}Al_2N_2O$
Formula weight	304.36
Temperature	150(2) K
Wavelength	1.54184 Å
Crystal system, space group	Monoclinic, *P2₁/c*
Unit cell dimensions	a = 16.3562(6) Å α = 90° b = 7.7839(2) Å β = 106.198(4)° c = 13.4058(5) Å γ = 90°
Volume	1639.01(10) $Å^3$
Z, Calculated density	4, 1.233 Mg/m^3
Absorption coefficient	1.130 mm^{-1}
F(000)	656
Crystal size	0.20 × 0.20 × 0.10 mm^3
Theta range for data collection	5.63 to 71.95°
Limiting indices	$-20\leq h\leq 18$, $-8\leq k\leq 9$, $-15\leq l\leq 16$
Reflections collected / unique	16985 / 3206 [R(int) = 0.0237]
Completeness to theta = 71.95°	99.3 %
Max. and min. transmission	0.8954 and 0.8056
Refinement method	Full-matrix least-squares on F^2
Data / restraints / parameters	3206 / 0 / 193
Goodness-of-fit on F^2	1.084
Final R indices [I>2σ(I)]	R_1 = 0.0670, wR_2 = 0.1848
R indices (all data)	R_1 = 0.0699, wR_2 = 0.1873
Largest diff. peak and hole	0.846 and -0.411 $e.Å^{-3}$

Mg(**1**)$_2$

Empirical formula	$C_{56}H_{82}MgN_4O_2$
Formula weight	867.56
Temperature	150(2) K
Wavelength	1.54184 Å
Crystal system, space group	Monoclinic, *P2$_1$/n*
Unit cell dimensions	a = 10.6847(9) Å α = 90° b = 26.0458(7) Å β = 100.316(7)° c = 19.3381(11) Å γ = 90°
Volume	5294.6(6) Å^3
Z, Calculated density	4, 1.088 Mg/m^3
Absorption coefficient	0.604 mm^{-1}
F(000)	1896
Crystal size	0.20 × 0.15 × 0.15 mm^3
Theta range for data collection	2.876 to 72.004°
Limiting indices	-13≤h≤11, -26≤k≤32, -23≤l≤23
Reflections collected / unique	42079 / 10345 [R(int) = 0.0252]
Completeness to theta = 67.984°	99.9 %
Refinement method	Full-matrix least-squares on F^2
Data / restraints / parameters	10345 / 110 / 800
Goodness-of-fit on F^2	1.088
Final R indices [I>2σ(I)]	R_1 = 0.0685, wR_2 = 0.1784
R indices (all data)	R_1 = 0.0742, wR_2 = 0.1828
Largest diff. peak and hole	0.793 and -0.416 e.Å^{-3}

Zn(**1**)$_2$

Empirical formula	$C_{21}H_{33}Zn_{0.5}N_2O$
Formula weight	362.18
Temperature	150(2) K
Wavelength	1.54184 Å
Crystal system, space group	Tetragonal, *I-42d*
Unit cell dimensions	a = 24.0450(2) Å α = 90° b = 24.0450(2) Å β = 90° c = 14.5399(2) Å γ = 90°
Volume	8406.42(15) Å^3
Z, Calculated density	16, 1.145 Mg/m^3
Absorption coefficient	1.086 mm^{-1}
F(000)	3136
Crystal size	0.05 × 0.05 × 0.05 mm^3
Theta range for data collection	3.55 to 72.41°
Limiting indices	-29≤h≤29, -29≤k≤19, -17≤l≤17
Reflections collected / unique	28432 / 4148 [R(int) = 0.0298]
Completeness to theta = 72.41°	99.8 %
Max. and min. transmission	0.9477 and 0.9477
Refinement method	Full-matrix least-squares on F^2
Data / restraints / parameters	4148 / 0 / 292
Goodness-of-fit on F^2	1.027
Final R indices [I>2σ(I)]	R_1 = 0.0259, wR_2 = 0.0668
R indices (all data)	R_1 = 0.0283, wR_2 = 0.0682
Absolute structure parameter	-0.40(19)
Largest diff. peak and hole	0.119 and -0.328 e.Å^{-3}

Al(**13**)Me_2

Empirical formula	$C_{58}H_{88}Al_2N_6O_2$
Formula weight	955.30
Temperature	150(2) K
Wavelength	0.71093 Å
Crystal system, space group	Monoclinic, *P2₁*
Unit cell dimensions	a = 13.1890(7) Å α = 90° b = 9.9959(7) Å β = 101.140(6)° c = 22.0325(13) Å γ = 90°
Volume	2849.9(3) $Å^3$
Z, Calculated density	2, 1.113 Mg/m^3
Absorption coefficient	0.096 mm^{-1}
F(000)	1040
Crystal size	0.30 × 0.10 × 0.10 mm^3
Theta range for data collection	3.34 to 25.70°
Limiting indices	-16≤h≤16, -12≤k≤12, -26≤l≤26
Reflections collected / unique	27949 / 10675 [R(int) = 0.0583]
Completeness to theta = 25.70°	99.3 %
Max. and min. transmission	0.9905 and 0.9719
Refinement method	Full-matrix least-squares on F^2
Data / restraints / parameters	10675 / 1 / 629
Goodness-of-fit on F^2	1.050
Final R indices [I>2σ(I)]	R_1 = 0.0668, wR_2 = 0.1256
R indices (all data)	R_1 = 0.0942, wR_2 = 0.1376
Absolute structure parameter	0.22(17)
Largest diff. peak and hole	0.378 and -0.212 e.$Å^{-3}$

Al(**14**)Me

Empirical formula	$C_{32}H_{46}AlCl_2N_2O_2$
Formula weight	588.59
Temperature	150(2) K
Wavelength	0.71073 Å
Crystal system, space group	Triclinic, *P-1*
Unit cell dimensions	a = 8.7940(8) Å α = 74.378(3)° b = 12.2980(8) Å β = 87.933(5)° c = 15.3990(8) Å γ = 79.786(3)°
Volume	1578.32(19) $Å^3$
Z, Calculated density	2, 1.238 Mg/m^3
Absorption coefficient	0.264 mm^{-1}
F(000)	630
Crystal size	0.20 × 0.20 × 0.10 mm^3
Theta range for data collection	3.63 to 27.51°
Limiting indices	$-11\leq h\leq 11$, $-15\leq k\leq 15$, $-19\leq l\leq 19$
Reflections collected / unique	33911 / 7169 [R(int) = 0.0452]
Completeness to theta = 27.51°	99.0 %
Max. and min. transmission	0.9740 and 0.9490
Refinement method	Full-matrix least-squares on F^2
Data / restraints / parameters	7169 / 0 / 360
Goodness-of-fit on F^2	1.026
Final R indices [$I>2\sigma(I)$]	R_1 = 0.0384, wR_2 = 0.1052
R indices (all data)	R_1 = 0.0481, wR_2 = 0.1134
Largest diff. peak and hole	0.424 and -0.434 $e.Å^{-3}$

Al(**15**)Me

Empirical formula	$C_{35}H_{46}AlBr_2N_2O_2$
Formula weight	713.54
Temperature	150(2) K
Wavelength	0.71073 Å
Crystal system, space group	Monoclinic, *P21/n*
Unit cell dimensions	a = 17.4539(4) Å α = 90° b = 8.5772(2) Å β = 107.060(3)° c = 23.1237(6) Å γ = 90°
Volume	3309.42(15) $Å^3$
Z, Calculated density	4, 1.432 Mg/m^3
Absorption coefficient	2.510 mm^{-1}
F(000)	1476
Crystal size	0.30 × 0.20 × 0.20 mm^3
Theta range for data collection	3.334 to 30.082°
Limiting indices	$-23\leq h\leq 23$, $-11\leq k\leq 12$, $-31\leq l\leq 32$
Reflections collected / unique	28073 / 8618 [R(int) = 0.0352]
Completeness to theta = 25.242°	99.8 %
Max. and min. transmission	1.00000 and 0.73702
Refinement method	Full-matrix least-squares on F^2
Data / restraints / parameters	8618 / 0 / 332
Goodness-of-fit on F^2	1.022
Final R indices [$I>2\sigma(I)$]	R_1 = 0.0402, wR_2 = 0.0841
R indices (all data)	R_1 = 0.0633, wR_2 = 0.0926
Largest diff. peak and hole	1.610 and -1.215 e.$Å^{-3}$

Al(**19**)Me

Empirical formula	$C_{29}H_{41}AlN_2O_2$
Formula weight	476.62
Temperature	150(2) K
Wavelength	1.54184 Å
Crystal system, space group	Monoclinic, *Ia*
Unit cell dimensions	a = 10.9940(2) Å α = 90° b = 24.1594(2) Å β = 116.697(2)° c = 11.16620(10) Å γ = 90°
Volume	2649.66(6) $Å^3$
Z, Calculated density	4, 1.195 Mg/m^3
Absorption coefficient	0.877 mm^{-1}
F(000)	1032
Crystal size	0.25 × 0.20 × 0.20 mm^3
Theta range for data collection	3.66 to 67.10°
Limiting indices	$-13\leq h\leq 11$, $-28\leq k\leq 28$, $-13\leq l\leq 13$
Reflections collected / unique	17594 / 4295 [R(int) = 0.0253]
Completeness to theta = 67.10°	100.0 %
Max. and min. transmission	0.8442 and 0.8106
Refinement method	Full-matrix least-squares on F^2
Data / restraints / parameters	4295 / 2 / 314
Goodness-of-fit on F^2	1.079
Final R indices [$I>2\sigma(I)$]	R_1 = 0.0302, wR_2 = 0.0881
R indices (all data)	R_1 = 0.0303, wR_2 = 0.0883
Absolute structure parameter	-0.03(3)
Largest diff. peak and hole	0.388 and -0.194 e.$Å^{-3}$

Al_2(**14**)Me_4

Empirical formula	$C_{32}H_{48}Al_2Cl_2N_2O_2$
Formula weight	617.58
Temperature	150(2) K
Wavelength	1.54184 Å
Crystal system, space group	Triclinic, *P-1*
Unit cell dimensions	a = 9.83480(10) Å α = 105.702(2)° b = 10.8816(2) Å β = 104.2760(10)° c = 16.7190(3) Å γ = 90.2940(10)°
Volume	1664.32(5) $Å^3$
Z, Calculated density	2, 1.232 Mg/m^3
Absorption coefficient	2.497 mm^{-1}
F(000)	660
Crystal size	0.10 × 0.05 × 0.05 mm^3
Theta range for data collection	4.23 to 72.04°
Limiting indices	$-11\leq h\leq 11$, $-13\leq k\leq 13$, $-20\leq l\leq 20$
Reflections collected / unique	32164 / 6512 [R(int) = 0.0421]
Completeness to theta = 72.04°	99.5 %
Max. and min. transmission	0.8853 and 0.7883
Refinement method	Full-matrix least-squares on F^2
Data / restraints / parameters	6512 / 0 / 371
Goodness-of-fit on F^2	1.018
Final R indices [$I>2\sigma(I)$]	R_1 = 0.0409, wR_2 = 0.1060
R indices (all data)	R_1 = 0.0422, wR_2 = 0.1074
Largest diff. peak and hole	0.685 and -0.428 $e.Å^{-3}$

Al_2(**16**)Me_4

Empirical formula	$C_{32}H_{47}Al_2I_2N_2O_2$
Formula weight	799.48
Temperature	150(2) K
Wavelength	1.54184 Å
Crystal system, space group	Triclinic, *P-1*
Unit cell dimensions	a = 9.6640(2) Å α = 100.820(3)° b = 13.3516(5) Å β = 94.405(2)° c = 14.0522(5) Å γ = 100.520(2)°
Volume	1739.36(10) $Å^3$
Z, Calculated density	2, 1.526 Mg/m^3
Absorption coefficient	14.914 mm^{-1}
F(000)	802
Crystal size	0.20 × 0.10 × 0.10 mm^3
Theta range for data collection	4.69 to 70.07°
Limiting indices	$-11 \leq h \leq 9$, $-16 \leq k \leq 15$, $-17 \leq l \leq 17$
Reflections collected / unique	18015 / 6603 [R(int) = 0.0354]
Completeness to theta = 70.07°	99.9 %
Max. and min. transmission	0.3170 and 0.1544
Refinement method	Full-matrix least-squares on F^2
Data / restraints / parameters	6603 / 0 / 371
Goodness-of-fit on F^2	1.048
Final R indices [$I>2\sigma(I)$]	R_1 = 0.0502, wR_2 = 0.1285
R indices (all data)	R_1 = 0.0510, wR_2 = 0.1292
Largest diff. peak and hole	2.292 and -2.359 $e.Å^{-3}$

Al(**26**)Me

Empirical formula	$C_{37}H_{57}AlN_2O_2$
Formula weight	588.83
Temperature	150(2) K
Wavelength	0.71073 Å
Crystal system, space group	Monoclinic, *P21/n*
Unit cell dimensions	a = 17.6460(7) Å α = 90° b = 10.2930(5) Å β = 93.839(3)° c = 19.4100(8) Å γ = 90°
Volume	3517.5(3) $Å^3$
Z, Calculated density	4, 1.112 Mg/m^3
Absorption coefficient	0.090 mm^{-1}
F(000)	1288
Crystal size	0.20 × 0.10 × 0.10 mm^3
Theta range for data collection	3.02 to 25.00°
Limiting indices	-20≤h≤20, -12≤k≤12, -22≤l≤23
Reflections collected / unique	30292 / 6148 [R(int) = 0.0846]
Completeness to theta = 25.00°	99.1 %
Max. and min. transmission	0.9910 and 0.9822
Refinement method	Full-matrix least-squares on F^2
Data / restraints / parameters	6148 / 0 / 393
Goodness-of-fit on F^2	1.078
Final R indices [I>2σ(I)]	R_1 = 0.1174, wR_2 = 0.3031
R indices (all data)	R_1 = 0.1664, wR_2 = 0.3544
Largest diff. peak and hole	0.944 and -0.577 e.$Å^{-3}$

Al(**26**)OBn

Empirical formula	$C_{43}H_{58}AlN_2O_3$
Formula weight	677.89
Temperature	150(2) K
Wavelength	1.54184 Å
Crystal system, space group	Triclinic, *P-1*
Unit cell dimensions	a = 10.9794(3)Å α = 115.692(3)° b = 14.2923(4) Å β = 100.605(3)° c = 15.1168(5) Å γ = 102.864(2)°
Volume	1974.85(10) $Å^3$
Z, Calculated density	2, 1.140 Mg/m^3
Absorption coefficient	0.748 mm^{-1}
F(000)	734
Crystal size	0.15 × 0.15 × 0.15 mm^3
Theta range for data collection	3.42 to 73.47°
Limiting indices	$-13\leq h\leq 9$, $-17\leq k\leq 17$, $-18\leq l\leq 18$
Reflections collected / unique	22257 / 7904 [R(int) = 0.0206]
Completeness to theta = 73.47°	99.6 %
Max. and min. transmission	0.8961 and 0.8961
Refinement method	Full-matrix least-squares on F^2
Data / restraints / parameters	7904 / 0 / 453
Goodness-of-fit on F^2	1.042
Final R indices [I>2σ(I)]	R_1 = 0.0427, wR_2 = 0.1162
R indices (all data)	R_1 = 0.0459, wR_2 = 0.1191
Largest diff. peak and hole	0.624 and -0.273 e.$Å^{-3}$

Al(**27**)Me

Empirical formula	$C_{31}H_{42}AlN_2O_2$
Formula weight	501.65
Temperature	150(2) K
Wavelength	1.54184 Å
Crystal system, space group	Triclinic, *P-1*
Unit cell dimensions	a = 8.3422(8) Å α = 100.197(7)° b = 9.3504(7) Å β = 101.412(8)° c = 19.2341(18) Å γ = 94.028(7)°
Volume	1438.8(2) $Å^3$
Z, Calculated density	2, 1.158 Mg/m^3
Absorption coefficient	0.832 mm^{-1}
F(000)	542
Crystal size	0.20 × 0.05 × 0.05 mm^3
Theta range for data collection	7.68 to 65.09°
Limiting indices	$-9\leq h\leq 9$, $-10\leq k\leq 10$, $-22\leq l\leq 22$
Reflections collected / unique	8570 / 8570 [R(int) = 0.0000]
Completeness to theta = 65.09°	99.6 %
Max. and min. transmission	0.9596 and 0.8512
Refinement method	Full-matrix least-squares on F^2
Data / restraints / parameters	8570 / 1 / 350
Goodness-of-fit on F^2	1.076
Final R indices [I>2σ(I)]	R_1 = 0.0977, wR_2 = 0.2461
R indices (all data)	R_1 = 0.1271, wR_2 = 0.2724
Largest diff. peak and hole	0.489 and -0.434 $e.Å^{-3}$

Al(**31**)O^{i}Pr

Empirical formula	$C_{167}H_{278}Al_4N_8O_{12}$
Formula weight	2697.88
Temperature	150(2) K
Wavelength	1.54184 Å
Crystal system, space group	Monoclinic, *I2/a*
Unit cell dimensions	a = 29.9091(5) Å α = 90° b = 11.0908(2) Å β = 108.075(2)° c = 25.9834(4) Å γ = 90°
Volume	8193.8(3) Å^3
Z, Calculated density	2, 1.093 Mg/m^3
Absorption coefficient	0.710 mm^{-1}
F(000)	2968
Crystal size	0.20 × 0.15 × 0.04 mm^3
Theta range for data collection	3.108 to 73.331°
Limiting indices	-34≤h≤37, -9≤k≤13, -32≤l≤29
Reflections collected / unique	24017 / 8123 [R(int) = 0.0186]
Completeness to theta = 67.684°	99.9 %
Max. and min. transmission	1.00000 and 0.80973
Refinement method	Full-matrix least-squares on F^2
Data / restraints / parameters	8123 / 75 / 549
Goodness-of-fit on F^2	1.021
Final R indices [I>2σ(I)]	R_1 = 0.0368, wR_2 = 0.0989
R indices (all data)	R_1 = 0.0399, wR_2 = 0.1017
Largest diff. peak and hole	0.323 and -0.288 e.Å^{-3}

Al(**32**)O^{i}Pr

Empirical formula	$C_{33}H_{51}AlN_2O_3$
Formula weight	550.74
Temperature	150(2) K
Wavelength	1.54184 Å
Crystal system, space group	Monoclinic, *P2$_1$/c*
Unit cell dimensions	a = 12.1388(3) Å α = 90° b = 19.0837(2) Å β = 102.663(2)° c = 14.1406(2) Å γ = 90°
Volume	3196.04(10) Å^3
Z, Calculated density	4, 1.145 Mg/m^3
Absorption coefficient	0.811 mm^{-1}
F(000)	1200
Crystal size	0.05 × 0.05 × 0.03 mm^3
Theta range for data collection	3.73 to 70.04°
Limiting indices	-14≤h≤14, -23≤k≤23, -17≤l≤17
Reflections collected / unique	48822 / 6068 [R(int) = 0.0266]
Completeness to theta = 70.04°	100.0 %
Max. and min. transmission	0.9800 and 0.9606
Refinement method	Full-matrix least-squares on F^2
Data / restraints / parameters	6068 / 0 / 366
Goodness-of-fit on F^2	1.073
Final R indices [I>2σ(I)]	R_1 = 0.0333, wR_2 = 0.0863
R indices (all data)	R_1 = 0.0362, wR_2 = 0.0881
Largest diff. peak and hole	0.232 and -0.256 e.Å^{-3}

Al(**33**)O^{i}Pr

Empirical formula	$C_{83}H_{114}Al_2Cl_4N_4O_6$
Formula weight	1459.54
Temperature	150(2) K
Wavelength	1.54184 Å
Crystal system, space group	Triclinic, *P-1*
Unit cell dimensions	a = 10.7101(8) Å α = 104.467(4)° b = 13.2504(5) Å β = 103.670(6)° c = 15.5183(9) Å γ = 101.247(5)°
Volume	1995.0(2) Å^3
Z, Calculated density	1, 1.215 Mg/m^3
Absorption coefficient	1.978 mm^{-1}
F(000)	782
Crystal size	0.2 × 0.2 × 0.2 mm^3
Theta range for data collection	3.578 to 73.111°
Limiting indices	-13≤h≤10, -16≤k≤16, -18≤l≤19
Reflections collected / unique	23019 / 7960 [R(int) = 0.0282]
Completeness to theta = 67.684°	100.0 %
Max. and min. transmission	1.00000 and 0.76005
Refinement method	Full-matrix least-squares on F^2
Data / restraints / parameters	7960 / 42 / 521
Goodness-of-fit on F^2	1.032
Final R indices [I>2σ(I)]	R_1 = 0.0376, wR_2 = 0.1009
R indices (all data)	R_1 = 0.0416, wR_2 = 0.1040
Largest diff. peak and hole	0.405 and -0.350 e.Å^{-3}

Al(**35**)Me

Empirical formula	$C_{38}H_{61}AlN_2O_2$
Formula weight	604.87
Temperature	150(2) K
Wavelength	1.54184 Å
Crystal system, space group	Monoclinic, *P21/c*
Unit cell dimensions	a = 13.8780(1) Å α = 90° b = 13.0013(1) Å β = 98.232(1)° c = 20.8565(2) Å γ = 90°
Volume	3724.41(5) $Å^3$
Z, Calculated density	4, 1.079 Mg/m^3
Absorption coefficient	0.712 mm^{-1}
F(000)	1328
Crystal size	0.10 × 0.05 × 0.05 mm^3
Theta range for data collection	3.22 to 73.08°
Limiting indices	$-17\leq h\leq 17$, $-16\leq k\leq 16$, $-25\leq l\leq 21$
Reflections collected / unique	27494 / 7423 [R(int) = 0.0230]
Completeness to theta = 73.08°	99.7 %
Max. and min. transmission	0.9653 and 0.9322
Refinement method	Full-matrix least-squares on F^2
Data / restraints / parameters	7423 / 0 / 403
Goodness-of-fit on F^2	1.077
Final R indices [$I>2\sigma(I)$]	R_1 = 0.0472, wR_2 = 0.1193
R indices (all data)	R_1 = 0.0512, wR_2 = 0.1228
Largest diff. peak and hole	0.557 and -0.304 $e.Å^{-3}$

Al(**35**)O^{i}Pr

Empirical formula	$C_{40}H_{65}AlN_2O_3$
Formula weight	648.92
Temperature	150(2) K
Wavelength	0.71073 Å
Crystal system, space group	Triclinic, *P-1*
Unit cell dimensions	a = 11.1545(14) Å α = 116.216(14)° b = 13.7919(18) Å β = 100.559(11)° c = 15.328(2) Å γ = 99.030(10)°
Volume	2002.6(5) Å^3
Z, Calculated density	2, 1.076 Mg/m^3
Absorption coefficient	0.087 mm^{-1}
F(000)	712
Crystal size	2.00 × 0.10 × 0.10 mm^3
Theta range for data collection	3.29 to 27.48°
Limiting indices	-14≤h≤12, -17≤k≤17, -17≤l≤19
Reflections collected / unique	18669 / 9175 [R(int) = 0.0251]
Completeness to theta = 27.48°	99.8 %
Max. and min. transmission	0.9914 and 0.8460
Refinement method	Full-matrix least-squares on F^2
Data / restraints / parameters	9175 / 0 / 430
Goodness-of-fit on F^2	1.035
Final R indices [I>2σ(I)]	R_1 = 0.0626, wR_2 = 0.1538
R indices (all data)	R_1 = 0.0892, wR_2 = 0.1730
Largest diff. peak and hole	1.026 and -0.522 e.Å^{-3}

[Al(**31**)OH]$_2$

Empirical formula	$C_{76}H_{118}Al_2Cl_2N_4O_6$
Formula weight	1663.10
Temperature	150(2) K
Wavelength	0.71073 Å
Crystal system, space group	Triclinic, *P-1*
Unit cell dimensions	a = 11.7478(11) Å α = 85.242(13)° b = 12.5068(19) Å β = 81.311(10)° c = 15.084(3) Å γ = 80.121(10)°
Volume	2154.6(5) Å^3
Z, Calculated density	1, 1.282 Mg/m^3
Absorption coefficient	0.456 mm^{-1}
F(000)	880
Crystal size	0.20 × 0.17 × 0.15 mm^3
Theta range for data collection	3.313 to 28.180°
Limiting indices	-15≤h≤10, -15≤k≤16, -17≤l≤18
Reflections collected / unique	16953 / 8665 [R(int) = 0.0296]
Completeness to theta = 25.242°	99.3 %
Max. and min. transmission	1.00000 and 0.97671
Refinement method	Full-matrix least-squares on F^2
Data / restraints / parameters	8665 / 53 / 540
Goodness-of-fit on F^2	1.026
Final R indices [I>2σ(I)]	R_1 = 0.0630, wR_2 = 0.1368
R indices (all data)	R_1 = 0.0986, wR_2 = 0.1569
Largest diff. peak and hole	0.876 and -0.501 e.Å^{-3}

[Al(**32**)OH]$_2$

Empirical formula	$C_{31}H_{46}AlCl_3N_2O_3$
Formula weight	628.03
Temperature	150(2) K
Wavelength	1.54184 Å
Crystal system, space group	Triclinic, *P-1*
Unit cell dimensions	a = 10.110(2) Å α = 98.680(12)° b = 12.1812(18) Å β = 97.700(14)° c = 14.768(2) Å γ = 112.387(16)°
Volume	1625.5(5) Å^3
Z, Calculated density	2, 1.283 Mg/m^3
Absorption coefficient	3.078 mm^{-1}
F(000)	668
Crystal size	0.20 × 0.10 × 0.10 mm^3
Theta range for data collection	3.10 to 73.48°
Limiting indices	-12≤h≤8, -15≤k≤14, -18≤l≤18
Reflections collected / unique	16744 / 6492 [R(int) = 0.0306]
Completeness to theta = 73.48°	99.3 %
Max. and min. transmission	0.7483 and 0.5781
Refinement method	Full-matrix least-squares on F^2
Data / restraints / parameters	6492 / 0 / 377
Goodness-of-fit on F^2	1.054
Final R indices [I>2σ(I)]	R_1 = 0.0419, wR_2 = 0.1142
R indices (all data)	R_1 = 0.0451, wR_2 = 0.1179
Largest diff. peak and hole	0.729 and -0.527 e.Å^{-3}

Al(**36**)O^{i}Pr

Empirical formula	$C_{46}H_{69}AlN_2O_3$
Formula weight	725.01
Temperature	150(2) K
Wavelength	1.54184 Å
Crystal system, space group	Monoclinic, *P2$_1$/n*
Unit cell dimensions	a = 11.4506(3) Å α = 90° b = 25.7201(6) Å β = 90.096(3)° c = 14.6888(5) Å γ = 90°
Volume	4326.0(2) Å^3
Z, Calculated density	4, 1.113 Mg/m^3
Absorption coefficient	0.708 mm^{-1}
F(000)	1584
Crystal size	0.05 × 0.05 × 0.02 mm^3
Theta range for data collection	3.44 to 66.60°
Limiting indices	-13≤h≤13, -30≤k≤30, -17≤l≤15
Reflections collected / unique	60070 / 7658 [R(int) = 0.1042]
Completeness to theta = 66.60°	100.0 %
Max. and min. transmission	0.9860 and 0.9655
Refinement method	Full-matrix least-squares on F^2
Data / restraints / parameters	7658 / 39 / 514
Goodness-of-fit on F^2	1.055
Final R indices [I>2σ(I)]	R_1 = 0.0672, wR_2 = 0.1723
R indices (all data)	R_1 = 0.0865, wR_2 = 0.1864
Largest diff. peak and hole	0.412 and -0.594 e.Å^{-3}

Ti(**1**)(O^iPr)$_2$

Empirical formula	$C_{48}H_{80}N_4O_4Ti$
Formula weight	825.06
Temperature	150(2) K
Wavelength	1.54184 Å
Crystal system, space group	Triclinic, *P-1*
Unit cell dimensions	a = 9.7501(3) Å α = 76.731(3)° b = 14.1972(4) Å β = 80.759(3)° c = 19.0565(7) Å γ = 71.707(3)°
Volume	2426.49(15) $Å^3$
Z, Calculated density	2, 1.129 Mg/m^3
Absorption coefficient	1.828 mm^{-1}
F(000)	900
Crystal size	0.15 × 0.10 × 0.05 mm^3
Theta range for data collection	3.340 to 72.125°
Limiting indices	$-12\leq h\leq 9$, $-17\leq k\leq 17$, $-22\leq l\leq 23$
Reflections collected / unique	21882 / 9545 [R(int) = 0.0213]
Completeness to theta = 67.684°	100.0 %
Refinement method	Full-matrix least-squares on F^2
Data / restraints / parameters	9545 / 2 / 568
Goodness-of-fit on F^2	1.034
Final R indices [$I>2\sigma(I)$]	R_1 = 0.0398, wR_2 = 0.1068
R indices (all data)	R_1 = 0.0429, wR_2 = 0.1091
Largest diff. peak and hole	0.727 and -0.326 e.$Å^{-3}$

Ti(**14**)(O^iPr)$_2$

Empirical formula	$C_{34}H_{49}Cl_2N_2O_4Ti$
Formula weight	668.55
Temperature	150(2) K
Wavelength	1.54184 Å
Crystal system, space group	Triclinic, *P-1*
Unit cell dimensions	a = 10.6236(5) Å α = 101.894(6)° b = 11.1469(8) Å β = 102.235(4)° c = 16.0773(9) Å γ = 102.233(5)°
Volume	1754.47(18) Å^3
Z, Calculated density	2, 1.266 Mg/m^3
Absorption coefficient	3.765 mm^{-1}
F(000)	710
Crystal size	0.20 × 0.10 × 0.10 mm^3
Theta range for data collection	4.42 to 66.60°
Limiting indices	-9≤h≤12, -11≤k≤13, -19≤l≤15
Reflections collected / unique	11316 / 6174 [R(int) = 0.0481]
Completeness to theta = 66.60°	99.7 %
Max. and min. transmission	0.7046 and 0.5197
Refinement method	Full-matrix least-squares on F^2
Data / restraints / parameters	6174 / 0 / 427
Goodness-of-fit on F^2	1.036
Final R indices [I>2σ(I)]	R_1 = 0.0748, wR_2 = 0.2018
R indices (all data)	R_1 = 0.0797, wR_2 = 0.2088
Largest diff. peak and hole	1.299 and -0.779 e.Å^{-3}

Ti(**26**)(O^iPr)$_2$

Empirical formula	$C_{42}H_{68}N_2O_4Ti$
Formula weight	712.88
Temperature	150(2) K
Wavelength	1.54184 Å
Crystal system, space group	Monoclinic, *I2/a*
Unit cell dimensions	a = 23.0224(3) Å α = 90° b = 14.3012(1) Å β = 113.744(2)° c = 28.4630(4) Å γ = 90°
Volume	8578.13(18) Å^3
Z, Calculated density	8, 1.104 Mg/m^3
Absorption coefficient	1.985 mm^{-1}
F(000)	3104
Crystal size	0.20 × 0.20 × 0.15 mm^3
Theta range for data collection	4.44 to 72.06°
Limiting indices	-24≤h≤28, -12≤k≤17, -34≤l≤35
Reflections collected / unique	34998 / 8360 [R(int) = 0.0351]
Completeness to theta = 72.06°	98.9 %
Max. and min. transmission	0.7550 and 0.6923
Refinement method	Full-matrix least-squares on F^2
Data / restraints / parameters	8360 / 4 / 473
Goodness-of-fit on F^2	1.057
Final R indices [I>2σ(I)]	R_1 = 0.0412, wR_2 = 0.1100
R indices (all data)	R_1 = 0.0458, wR_2 = 0.1137
Largest diff. peak and hole	0.695 and -0.481 e.Å^{-3}

Ti(**31**)(O^iPr)$_2$

Empirical formula	$C_{42}H_{70}N_2O_4Ti$
Formula weight	714.90
Temperature	150(2) K
Wavelength	1.54184 Å
Crystal system, space group	Triclinic, *P-1*
Unit cell dimensions	a = 11.6663(4) Å α = 100.146(3)° b = 13.5176(5) Å β = 92.922(2)° c = 14.0421(4) Å γ = 107.314(3)°
Volume	2068.41(13) $Å^3$
Z, Calculated density	2, 1.148 Mg/m^3
Absorption coefficient	2.058 mm^{-1}
F(000)	780
Crystal size	0.15 × 0.10 × 0.05 mm^3
Theta range for data collection	3.217 to 73.488°
Limiting indices	$-14\leq h\leq 14$, $-16\leq k\leq 16$, $-17\leq l\leq 11$
Reflections collected / unique	25143 / 8285 [R(int) = 0.0381]
Completeness to theta = 67.684°	100.0 %
Refinement method	Full-matrix least-squares on F^2
Data / restraints / parameters	8285 / 0 / 462
Goodness-of-fit on F^2	1.017
Final R indices [I>2σ(I)]	R_1 = 0.0395, wR_2 = 0.1062
R indices (all data)	R_1 = 0.0437, wR_2 = 0.1093
Largest diff. peak and hole	0.351 and -0.360 $e.Å^{-3}$

Zr(**1**)(O^iPr)$_2$

Empirical formula	$C_{48}H_{80}N_4O_4Zr$
Formula weight	868.38
Temperature	150(2) K
Wavelength	1.54184 Å
Crystal system, space group	Triclinic, *P-1*
Unit cell dimensions	a = 9.7777(2) Å α = 76.662(2)° b = 14.3460(3) Å β = 81.066(2)° c = 19.2145(6) Å γ = 71.741(2)°
Volume	2480.42(11) $Å^3$
Z, Calculated density	2, 1.163 Mg/m^3
Absorption coefficient	2.143 mm^{-1}
F(000)	936
Crystal size	0.15 × 0.10 × 0.10 mm^3
Theta range for data collection	3.307 to 73.592°
Limiting indices	$-12\leq h\leq 9$, $-17\leq k\leq 17$, $-23\leq l\leq 23$
Reflections collected / unique	31337 / 9948 [R(int) = 0.0325]
Completeness to theta = 67.684°	99.9%
Max. and min. transmission	1.00000 and 0.27970
Refinement method	Full-matrix least-squares on F^2
Data / restraints / parameters	9948 / 14 / 586
Goodness-of-fit on F^2	1.056
Final R indices [$I>2\sigma(I)$]	R_1 = 0.0292, wR_2 = 0.0734
R indices (all data)	R_1 = 0.0326, wR_2 = 0.0752
Largest diff. peak and hole	0.423 and -0.481 e.$Å^{-3}$

Zr(**14**)$_2$

Empirical formula	$C_{61}H_{84}Cl_4N_4O_4Zr$
Formula weight	1170.34
Temperature	150(2) K
Wavelength	0.71073 Å
Crystal system, space group	Triclinic, *P-1*
Unit cell dimensions	a = 13.9740(8) Å α = 74.900(3)° b = 14.3110(7) Å β = 87.307(3)° c = 17.2770(6) Å γ = 73.892(2)°
Volume	3203.6(3) Å^3
Z, Calculated density	2, 1.213 Mg/m^3
Absorption coefficient	0.384 mm^{-1}
F(000)	1236
Crystal size	0.10 × 0.10 × 0.10 mm^3
Theta range for data collection	3.53 to 25.17°
Limiting indices	-16≤h≤16, -17≤k≤17, -20≤l≤20
Reflections collected / unique	31292 / 31292 [R(int) = 0.0000]
Completeness to theta = 25.17°	97.5%
Max. and min. transmission	0.9626 and 0.9626
Refinement method	Full-matrix least-squares on F^2
Data / restraints / parameters	31292 / 39 / 682
Goodness-of-fit on F^2	0.994
Final R indices [I>2σ(I)]	R_1 = 0.1055, wR_2 = 0.2676
R indices (all data)	R_1 = 0.1781, wR_2 = 0.3078
Largest diff. peak and hole	2.027 and -1.330 e.Å^{-3}

$Zr(\mathbf{15})_2$

Empirical formula	$C_{61}H_{84}Br_4N_4O_4Zr$
Formula weight	1348.18
Temperature	150(2) K
Wavelength	0.71073 Å
Crystal system, space group	Triclinic, *P-1*
Unit cell dimensions	a = 13.8853(9) Å α = 74.488(4)° b = 14.3894(6) Å β = 86.590(5)° c = 17.4919(8) Å γ = 74.048(5)°
Volume	3237.5(3) $Å^3$
Z, Calculated density	2, 1.383 Mg/m^3
Absorption coefficient	2.683 mm^{-1}
F(000)	1380
Crystal size	0.30 × 0.10 × 0.10 mm^3
Theta range for data collection	3.53 to 27.48°
Limiting indices	$-17\leq h\leq 18$, $-17\leq k\leq 18$, $-22\leq l\leq 22$
Reflections collected / unique	14806 / 14806 [R(int) = 0.0000]
Completeness to theta = 27.48°	99.8%
Max. and min. transmission	0.7752 and 0.4999
Refinement method	Full-matrix least-squares on F^2
Data / restraints / parameters	14806 / 78 / 726
Goodness-of-fit on F^2	1.025
Final R indices [$I>2\sigma(I)$]	R_1 = 0.0641, wR_2 = 0.1444
R indices (all data)	R_1 = 0.1055, wR_2 = 0.1668
Largest diff. peak and hole	2.216 and -1.166 $e.Å^{-3}$

Zr(*cis*-**16**)$_2$

Empirical formula	$C_{62}H_{86}I_4N_4O_4Zr$
Formula weight	1550.17
Temperature	150(2) K
Wavelength	1.54184 Å
Crystal system, space group	Monoclinic, *P21/c*
Unit cell dimensions	a = 19.5802(5) Å α = 90° b = 18.0805(3) Å β = 108.576(3)° c = 19.3122(5) Å γ = 90°
Volume	6480.7(3) Å^3
Z, Calculated density	4, 1.589 Mg/m^3
Absorption coefficient	16.704 mm^{-1}
F(000)	3080
Crystal size	0.10 × 0.05 × 0.05 mm^3
Theta range for data collection	4.60 to 72.35°
Limiting indices	-24≤h≤23, -22≤k≤15, -23≤l≤23
Reflections collected / unique	62482 / 12706 [R(int) = 0.0838]
Completeness to theta = 72.35°	99.3%
Max. and min. transmission	0.4889 and 0.2859
Refinement method	Full-matrix least-squares on F^2
Data / restraints / parameters	12706 / 0 / 690
Goodness-of-fit on F^2	1.013
Final R indices [I>2σ(I)]	R_1 = 0.0531, wR_2 = 0.1337
R indices (all data)	R_1 = 0.0640, wR_2 = 0.1436
Largest diff. peak and hole	1.507 and -1.207 e.Å^{-3}

Hf(**14**)$_2$

Empirical formula	$C_{30.25}H_{39}Cl_3Hf_{0.5}N_2O_2$
Formula weight	658.23
Temperature	150(2) K
Wavelength	1.54184 Å
Crystal system, space group	Triclinic, *P-1*
Unit cell dimensions	a = 10.3949(2) Å α = 91.0520(10)° b = 13.7142(3) Å β = 96.1700(10)° c = 22.8673(3) Å γ = 109.546(2)°
Volume	3049.12(10) Å^3
Z, Calculated density	4, 1.434 Mg/m^3
Absorption coefficient	5.958 mm^{-1}
F(000)	1350
Crystal size	0.30 × 0.20 × 0.20 mm^3
Theta range for data collection	4.55 to 71.99°
Limiting indices	-12≤h≤12, -16≤k≤16, -26≤l≤28
Reflections collected / unique	22743 / 11724 [R(int) = 0.0241]
Completeness to theta = 71.99°	97.8%
Max. and min. transmission	0.3820 and 0.2680
Refinement method	Full-matrix least-squares on F^2
Data / restraints / parameters	11724 / 0 / 714
Goodness-of-fit on F^2	1.038
Final R indices [I>2σ(I)]	R_1 = 0.0330, wR_2 = 0.0868
R indices (all data)	R_1 = 0.0334, wR_2 = 0.0871
Largest diff. peak and hole	1.025 and -1.025 e.Å^{-3}

Hf(**15**)$_2$

Empirical formula	$C_{57.50}H_{75}Br_4Cl_3HfN_4O_4$
Formula weight	1490.69
Temperature	150(2) K
Wavelength	0.71073 Å
Crystal system, space group	Triclinic, *P-1*
Unit cell dimensions	a = 10.3957(5) Å α = 89.912(3)° b = 13.6050(5) Å β = 84.053(4)° c = 22.9024(11) Å γ = 69.887(4)°
Volume	3023.2(2) Å^3
Z, Calculated density	2, 1.638 Mg/m^3
Absorption coefficient	4.548 mm^{-1}
F(000)	1486
Crystal size	0.20 × 0.18 × 0.10 mm^3
Theta range for data collection	3.249 to 26.372°
Limiting indices	-11≤h≤12, -11≤k≤16, -28≤l≤28
Reflections collected / unique	18821 / 12294 [R(int) = 0.0295]
Completeness to theta = 25.242°	99.7%
Max. and min. transmission	1.00000 and 0.71587
Refinement method	Full-matrix least-squares on F^2
Data / restraints / parameters	12294 / 1 / 695
Goodness-of-fit on F^2	1.065
Final R indices [I>2σ(I)]	R_1 = 0.0401, wR_2 = 0.0945
R indices (all data)	R_1 = 0.0530, wR_2 = 0.1015
Largest diff. peak and hole	1.962 and -1.158 e.Å^{-3}

Hf(*cis*-**16**)$_2$

Empirical formula	$C_{68}H_{100}HfI_4N_4O_4$
Formula weight	1723.60
Temperature	150(2) K
Wavelength	0.71073 Å
Crystal system, space group	Orthorhombic, *Fdd2*
Unit cell dimensions	a = 54.9146(5) Å α = 90° b = 35.8227(3) Å β = 90° c = 13.38270(10) Å γ = 90°
Volume	26326.3(4) Å^3
Z, Calculated density	16, 1.739 Mg/m^3
Absorption coefficient	3.511 mm^{-1}
F(000)	13632
Crystal size	0.30 × 0.2 × 0.2 mm^3
Theta range for data collection	3.183 to 27.483°
Limiting indices	-70≤h≤64, -46≤k≤46, -17≤l≤17
Reflections collected / unique	51826 / 14439 [R(int) = 0.0337]
Completeness to theta = 25.242°	99.7%
Max. and min. transmission	1.00000 and 0.80243
Refinement method	Full-matrix least-squares on F^2
Data / restraints / parameters	14439 / 1 / 634
Goodness-of-fit on F^2	0.990
Final R indices [I>2σ(I)]	R_1 = 0.0186, wR_2 = 0.0374
R indices (all data)	R_1 = 0.0216, wR_2 = 0.0377
Absolute structure parameter	-0.007(2)
Largest diff. peak and hole	0.520 and -0.452 e.Å^{-3}

Zr(**14**)(O^tBu)$_2$·HO^tBu

Empirical formula	$C_{40}H_{64}Cl_2N_2O_5Zr$
Formula weight	815.05
Temperature	150(2) K
Wavelength	1.54184 Å
Crystal system, space group	Monoclinic, *P2$_1$/c*
Unit cell dimensions	a = 9.7895(1) Å α = 90° b = 16.8042(1) Å β = 100.021(1)° c = 26.7416(1) Å γ = 90°
Volume	4332.01(6) Å^3
Z, Calculated density	4, 1.250 Mg/m^3
Absorption coefficient	3.535 mm^{-1}
F(000)	1728
Crystal size	0.20 × 0.20 × 0.15 mm^3
Theta range for data collection	3.120 to 73.508°
Limiting indices	-12≤h≤10, -20≤k≤20, -33≤l≤33
Reflections collected / unique	156312 / 8709 [R(int) = 0.0422]
Completeness to theta = 67.684°	100.0%
Refinement method	Full-matrix least-squares on F^2
Data / restraints / parameters	8709 / 0 / 471
Goodness-of-fit on F^2	1.035
Final R indices [I>2σ(I)]	R_1 = 0.0264, wR_2 = 0.0672
R indices (all data)	R_1 = 0.0274, wR_2 = 0.0680
Largest diff. peak and hole	0.493 and -0.751 e.Å^{-3}

Zr(**22**)(O^tBu)$_2$

Empirical formula	$C_{88}H_{144}N_4O_8Zr_2$
Formula weight	1568.50
Temperature	150(2) K
Wavelength	1.54184 Å
Crystal system, space group	Triclinic, *P-1*
Unit cell dimensions	a = 11.3200(4) Å α = 78.072(3)° b = 11.4648(5) Å β = 72.528(3)° c = 18.7325(7) Å γ = 76.808(3)°
Volume	2232.65(16) Å^3
Z, Calculated density	1, 1.167 Mg/m^3
Absorption coefficient	2.317 mm^{-1}
F(000)	844
Crystal size	0.15 × 0.10 × 0.05 mm^3
Theta range for data collection	4.005 to 72.415°
Limiting indices	-13≤h≤13, -14≤k≤14, -23≤l≤23
Reflections collected / unique	16035 / 16035 [R(int) = 0.0000]
Completeness to theta = 67.684°	100.0%
Refinement method	Full-matrix least-squares on F^2
Data / restraints / parameters	16035 / 0 / 479
Goodness-of-fit on F^2	1.011
Final R indices [I>2σ(I)]	R_1 = 0.0357, wR_2 = 0.0974
R indices (all data)	R_1 = 0.0408, wR_2 = 0.0987
Largest diff. peak and hole	0.592 and -0.741 e.Å^{-3}

Zr(**26**)(O^tBu)$_2$

Empirical formula	$C_{47}H_{79}N_2O_4Zr$
Formula weight	827.34
Temperature	150(2) K
Wavelength	0.71073 Å
Crystal system, space group	Monoclinic, *C2/c*
Unit cell dimensions	a = 24.0620(6) Å α = 90° b = 15.1035(3) Å β = 117.531(3)° c = 30.6787(8) Å γ = 90°
Volume	9886.7(5) Å^3
Z, Calculated density	8, 1.112 Mg/m^3
Absorption coefficient	0.261 mm^{-1}
F(000)	3576
Crystal size	0.20 × 0.15 × 0.15 mm^3
Theta range for data collection	3.326 to 29.558°
Limiting indices	-31≤h≤30, -20≤k≤16, -40≤l≤41
Reflections collected / unique	41135 / 12003 [R(int) = 0.0283]
Completeness to theta = 25.242°	99.7%
Refinement method	Full-matrix least-squares on F^2
Data / restraints / parameters	16035 / 0 / 479
Goodness-of-fit on F^2	1.057
Final R indices [I>2σ(I)]	R_1 = 0.0391, wR_2 = 0.0913
R indices (all data)	R_1 = 0.0552, wR_2 = 0.1015
Largest diff. peak and hole	0.688 and -0.405 e.Å^{-3}

[Zr(**14***)(O^iPr)]O_2

Empirical formula	$C_{69.50}H_{103.50}Cl_4N_4O_7Zr$
Formula weight	1431.30
Temperature	150(2) K
Wavelength	0.71073 Å
Crystal system, space group	Triclinic, *P-1*
Unit cell dimensions	a = 14.8910(10) Å α = 110.900(3)° b = 15.0540(9) Å β = 94.443(3)° c = 19.5020(15) Å γ = 110.191(4)°
Volume	3731.5(4) $Å^3$
Z, Calculated density	2, 1.274 Mg/m^3
Absorption coefficient	0.473 mm^{-1}
F(000)	1505
Crystal size	0.20 × 0.10 × 0.05 mm^3
Theta range for data collection	3.55 to 25.10°
Limiting indices	$-17\leq h\leq 17$, $-17\leq k\leq 16$, $-23\leq l\leq 23$
Reflections collected / unique	23285 / 11993 [R(int) = 0.0939]
Completeness to theta = 25.10°	90.3%
Max. and min. transmission	0.9767 and 0.9114
Refinement method	Full-matrix least-squares on F^2
Data / restraints / parameters	11993 / 120 / 891
Goodness-of-fit on F^2	1.082
Final R indices [$I>2\sigma(I)$]	R_1 = 0.0973, wR_2 = 0.2350
R indices (all data)	R_1 = 0.1328, wR_2 = 0.2606
Largest diff. peak and hole	1.334 and -1.003 $e.Å^{-3}$

6.3 Optimised DFT geometries and calculated Gibbs free energies

Al(**7***)Me_2

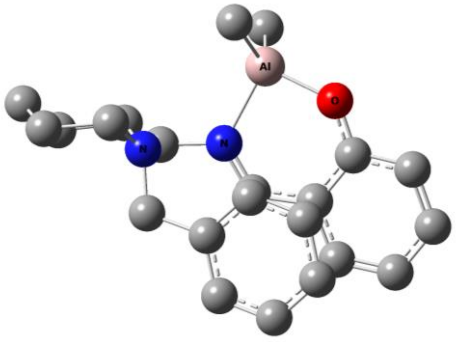

0 1			
Al	-2.20150802	-1.12755872	0.43859364
N	1.61736394	-1.54984164	0.37549087
C	-3.63108538	-2.03426827	-0.57578916
H	-3.30275258	-2.99765683	-0.98900777
H	-3.98640098	-1.43476613	-1.42345773
H	-4.50989386	-2.25410805	0.04331694
O	-2.56029948	0.61474569	0.77514116
N	-0.81368862	-0.72123501	-0.93186666
C	1.21295683	1.13180333	1.24109127
C	0.89602943	2.43480641	1.61387893
C	1.42150617	3.51206136	0.91210923
H	1.15819819	4.52707573	1.19083554
C	2.27232766	3.27940554	-0.16481741
C	2.58643830	1.97771104	-0.53372942
H	3.24451586	1.80255137	-1.38220224
C	2.05600879	0.89043534	0.16220806
C	2.39907279	-0.52074017	-0.28885036
H	2.27125550	-0.57563844	-1.37437338
H	3.47486981	-0.68137103	-0.13585892
C	2.34868810	-2.26008454	1.41927003
H	1.61488603	-2.75370013	2.06855460
H	2.87099613	-1.52522214	2.03877902
C	3.32174331	-3.30656945	0.86487866
H	4.12821409	-2.80618515	0.31466310
H	3.79620158	-3.84689633	1.69030730
C	2.59335422	-4.27885856	-0.06532073
H	1.90243224	-4.89388452	0.52611166
H	3.30236914	-4.96840711	-0.53312312
C	1.79390004	-3.52732395	-1.13301433
H	2.47771410	-3.01978515	-1.82664574
H	1.19983641	-4.22866913	-1.72920673
C	0.88183017	-2.48895437	-0.46647077

H	0.22128042	-3.03145743	0.22207189
C	-0.01141627	-1.80078457	-1.50182590
H	0.58001349	-1.42016898	-2.34172851
H	-0.69026264	-2.55454468	-1.91266478
C	-0.64531012	0.46849727	-1.39690962
H	0.08728247	0.60307679	-2.19688575
C	-1.31080961	1.67129481	-0.96893474
C	-2.22550646	1.69437602	0.11573891
C	-2.77150444	2.93546210	0.49333208
C	-2.43066602	4.09298781	-0.17627763
H	-2.86846082	5.03543344	0.13883583
C	-1.53006961	4.07272788	-1.24895210
C	-0.97813335	2.86891986	-1.62698795
H	-0.26061648	2.83368448	-2.44192149
H	2.68144154	4.11422397	-0.72545134
H	0.21936326	2.60581082	2.44492437
H	0.77488772	0.28713423	1.76073212
C	-1.48219244	-1.99297063	2.05380675
H	-1.42542976	-3.08553374	1.97091239
H	-0.47877864	-1.63674326	2.30952466
H	-2.12423659	-1.78486892	2.91963154
H	-1.26336680	4.98867111	-1.76333811
H	-3.46634874	2.95198464	1.32587681

Sum of electronic and thermal Free Energies= -1282.562467
Frequencies -- 17.6630 33.1212 43.7391

Al(**10**)Me_2 – N(1) Coordination

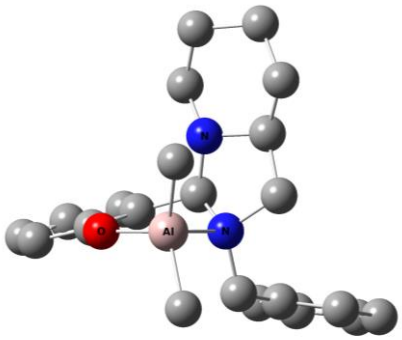

0 1

H	-3.04401553	-3.56471562	1.11298031
O	-1.36560658	-1.65329566	1.39802502
N	0.35856667	-0.00362382	-0.22760739
C	-2.02496667	-1.88178288	0.27529055
H	-4.02155809	-2.67808354	-2.98349907
N	-1.47250671	1.30006369	-0.24322732
C	-2.92396958	-2.95993807	0.22023518
C	-3.63507555	-3.24151672	-0.93316579
H	-4.32346094	-4.08106126	-0.94476462
C	-3.46884392	-2.46082933	-2.07638416
C	-2.57867512	-1.39935654	-2.03229249
H	-2.43869267	-0.77967850	-2.91486724
C	-1.85663429	-1.09003832	-0.87813934
C	-0.96953266	0.12307557	-0.91586080
H	-0.77003101	0.35431767	-1.97788766
C	-2.76008627	1.81862513	-0.66017710
H	-3.51698013	1.04394452	-0.52029498
H	-2.75107095	2.08402999	-1.73522999
C	-3.08450372	3.05108435	0.18105464
H	-4.03647310	3.47723761	-0.14860836
H	-3.21376554	2.73462482	1.22163758
C	-1.97264863	4.10081876	0.09724278
H	-2.19186942	4.93898452	0.76460078
H	-1.93856683	4.51070705	-0.92045620
C	-0.60782833	3.49411540	0.43861880
H	0.19246364	4.21968424	0.26161870
H	-0.57085601	3.21019069	1.49384962
C	-0.39180041	2.26289276	-0.42219100
H	-0.37282687	2.58627198	-1.48194922
C	0.85871682	1.40940213	-0.16920519
H	1.61035129	1.58586307	-0.93739227
H	1.31177293	1.60154596	0.80564797
C	1.28738330	-0.96319490	-0.89256215
H	0.82471103	-1.94931401	-0.81061278
H	2.19420039	-0.98675826	-0.28834102
C	1.63945313	-0.67369913	-2.33234001
C	2.78015139	0.06599063	-2.64548105
H	3.42569164	0.42347753	-1.84810583
C	3.11602421	0.33373972	-3.96790310
H	4.00805261	0.90907365	-4.19243026
C	2.31631008	-0.14680783	-4.99838094

H	2.57913023	0.05548782	-6.03140655
C	1.18859175	-0.90515532	-4.69980883
H	0.57064386	-1.30042352	-5.49921896
C	0.85612802	-1.16870678	-3.37642136
H	-0.01628051	-1.77480750	-3.15054737
Al	0.03916101	-0.60511193	1.74886343
C	1.65999477	-1.63594727	2.21466260
H	2.57885527	-1.03598426	2.16507028
H	1.58760374	-1.98261156	3.25379750
H	1.82968535	-2.52844671	1.60153207
C	-0.40357490	0.86382631	2.98210930
H	-1.33292209	1.37456128	2.71346725
H	-0.54183990	0.45231800	3.99123201
H	0.37573475	1.62981300	3.07756722

Sum of electronic and thermal Free Energies= -1282.557528

Frequencies -- 24.0520 33.1326 47.6277

Al(**10**)Me_2 – N(2) Coordination

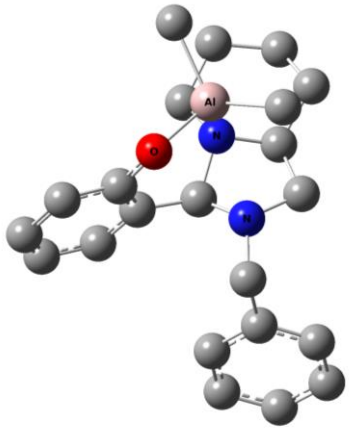

0 1

H	-2.92322818	-3.32016617	1.27423121
O	-1.65411284	-1.07422871	1.45042237
N	0.30758684	0.23693050	-0.48310469
C	-2.07404699	-1.60395330	0.31629212
H	-3.46225515	-3.13393625	-2.99196930
N	-1.54178684	1.43794054	-0.14982759
C	-2.76673797	-2.82490306	0.32168780
C	-3.25129474	-3.37083476	-0.85552610
H	-3.78837967	-4.31401104	-0.82360854
C	-3.06931980	-2.71464538	-2.07245538
C	-2.37142611	-1.51590353	-2.08661721
H	-2.21577906	-0.99459094	-3.02778985
C	-1.85168730	-0.96205771	-0.91739733
C	-1.05148523	0.30483008	-0.99787143
H	-1.08558826	0.65285427	-2.04689230
C	-2.85478452	1.98023586	-0.56199034
H	-3.62686569	1.24865762	-0.31620736
H	-2.84863376	2.10283217	-1.65377391
C	-3.13535618	3.31891192	0.12239745
H	-4.05521836	3.72916085	-0.30347997
H	-3.33446857	3.14365767	1.18022015
C	-1.99126479	4.32767694	-0.01707931
H	-2.19613935	5.20389063	0.60350096
H	-1.93343278	4.68242493	-1.05332302
C	-0.64516195	3.70123116	0.36249503
H	0.17808156	4.38784669	0.14560795
H	-0.60366666	3.47875707	1.43328521
C	-0.47695330	2.43888270	-0.45597984
H	-0.63035756	2.72040829	-1.50843387
C	0.80813647	1.60877002	-0.39360706
H	1.45671699	1.88632292	-1.23301858
H	1.36658809	1.74818347	0.53548092
C	1.21156906	-0.78712884	-0.97633577
H	0.72328641	-1.75435205	-0.83281821
H	2.08989800	-0.77529823	-0.32361359
C	1.64054159	-0.62987982	-2.42275667
C	2.75846872	0.13383289	-2.76228143
H	3.36694299	0.57410358	-1.97688295

C	3.11573188	0.32332088	-4.09340385
H	3.98899222	0.91907937	-4.33900113
C	2.35984922	-0.25670126	-5.10669028
H	2.63906056	-0.11295169	-6.14542259
C	1.25452063	-1.03585381	-4.78035637
H	0.66990537	-1.50733483	-5.56389850
C	0.90155279	-1.22052752	-3.44823205
H	0.04885507	-1.84386766	-3.19785579
Al	-1.45092572	0.66920060	1.83980649
C	0.23973424	1.00888674	2.79392767
H	0.56172027	2.05505507	2.84491258
H	0.11589056	0.68378134	3.83597583
H	1.07470131	0.43102918	2.38304128
C	-3.08655421	1.25148526	2.78479344
H	-4.01412258	1.18891075	2.20325840
H	-3.22217419	0.57712347	3.64172167
H	-3.03319526	2.26348221	3.20444582

Sum of electronic and thermal Free Energies= -1282.552934
Frequencies -- 26.3595 35.3116 49.0124

6.4 Selection of GPC traces (Chapter 4)

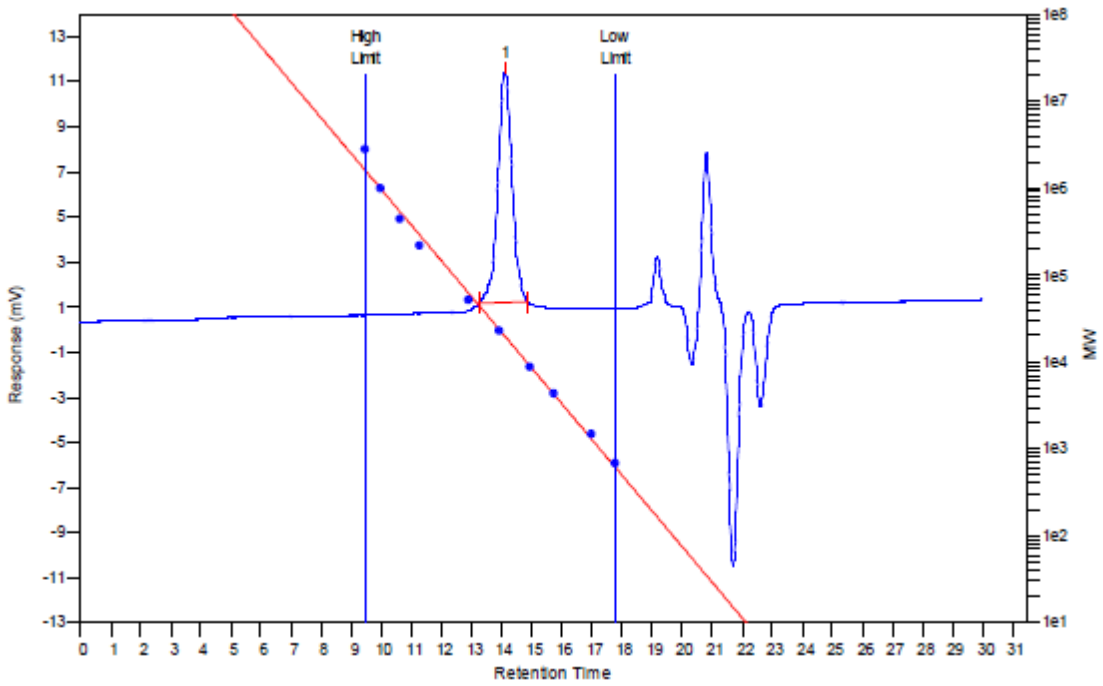

Figure 6.1 GPC trace of PLA prepared by solution polymerisation with Al(**28**)Me.

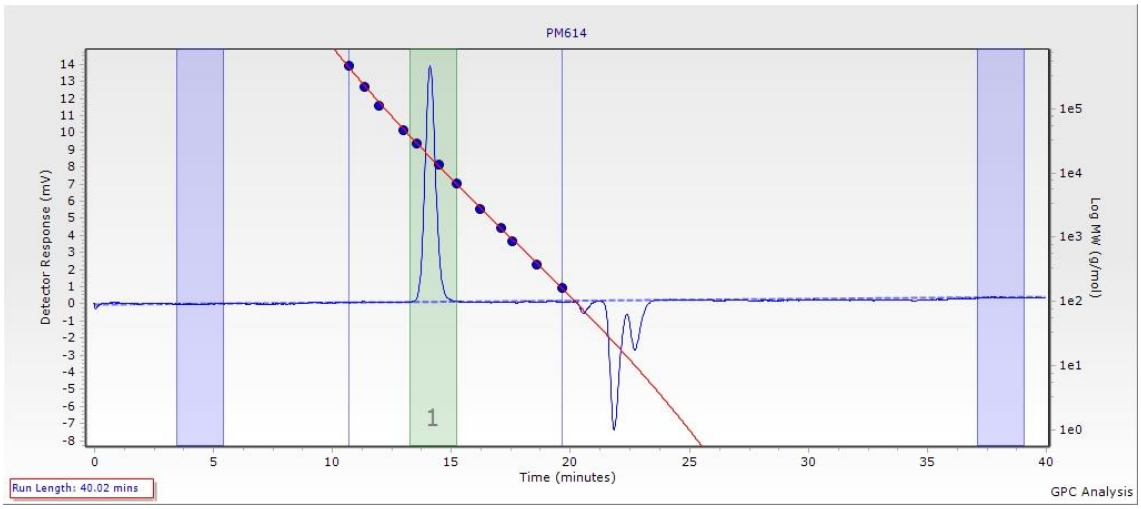

Figure 6.2: GPC trace of PLA prepared by solution polymerisation with Al(**31**)O^{i}Pr.

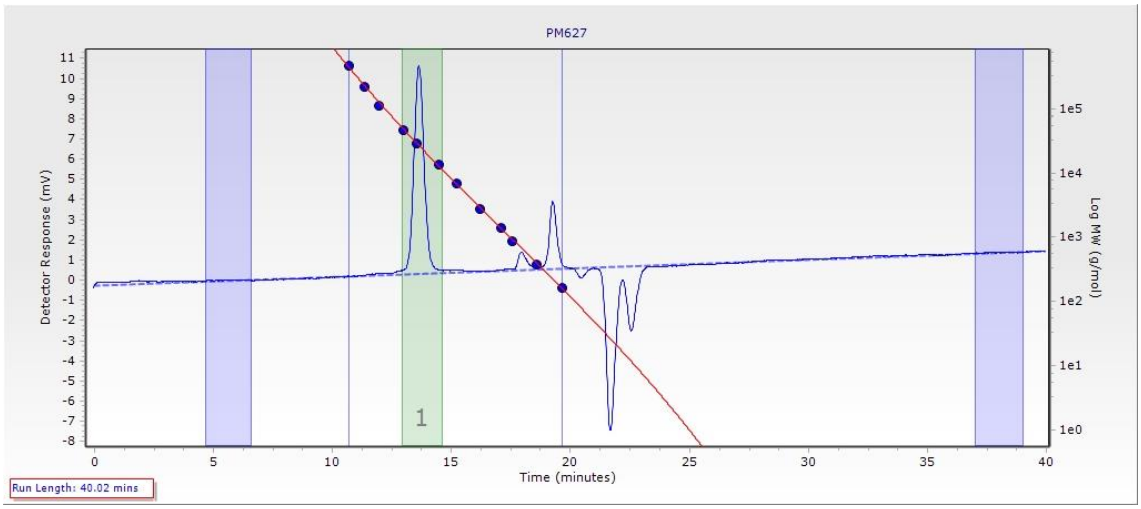

Figure 6.3: GPC trace of PLLA prepared by solution polymerisation with Al(**31**)O^{i}Pr.

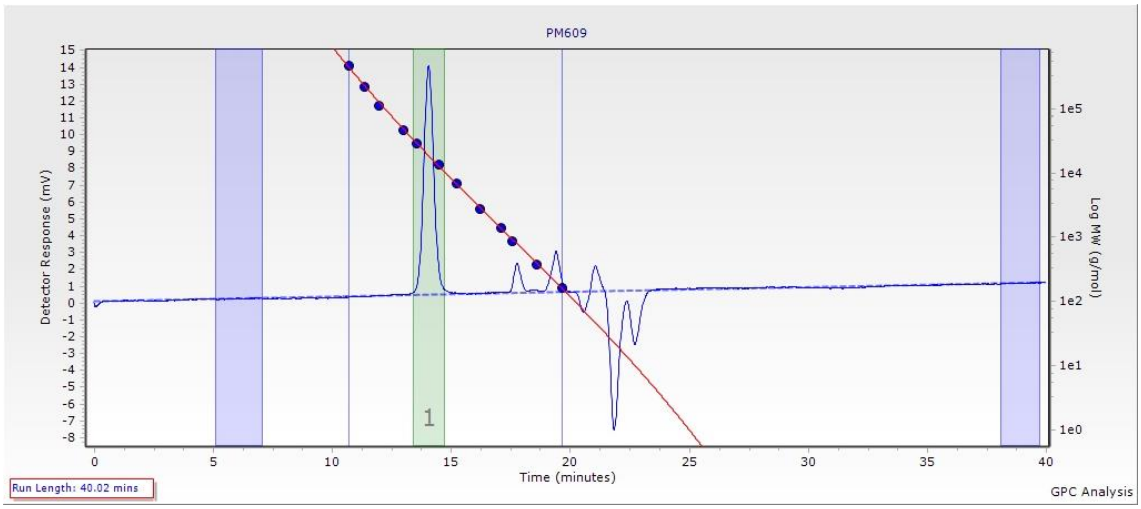

Figure 6.4: GPC trace of PLA prepared by solution polymerisation with Al(**32**)O^{i}Pr.

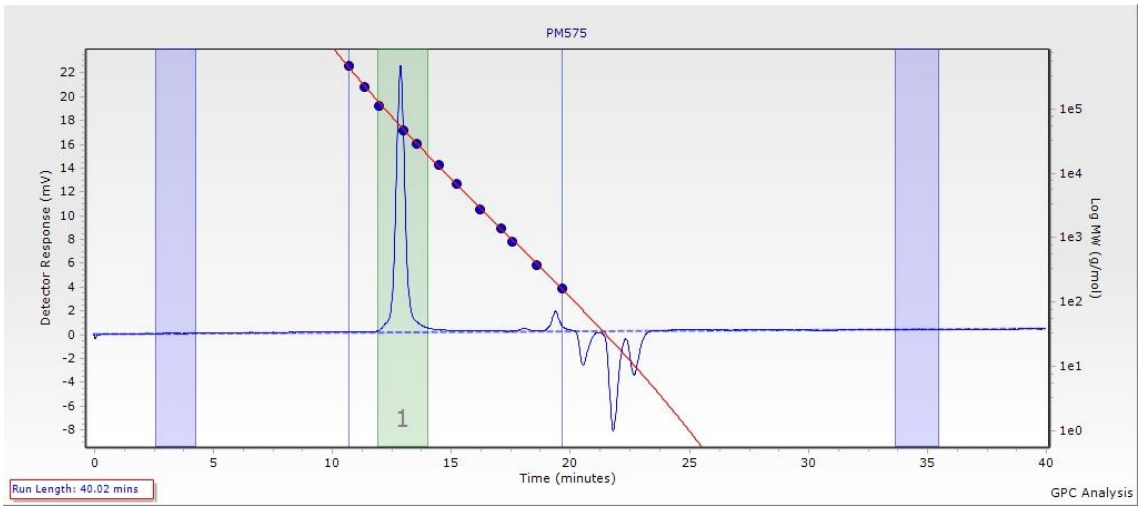

Figure 6.5: GPC trace of PLA prepared by solvent free polymerisation with Al(**31**)O^{i}Pr.

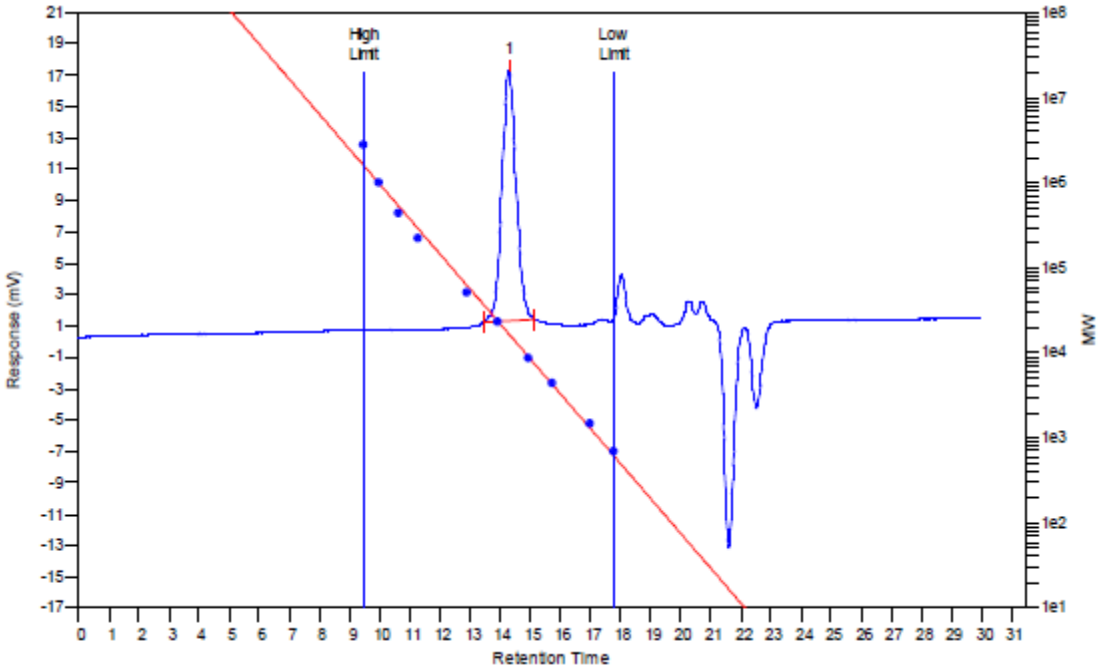

Figure 6.6: GPC trace of PLA prepared in solution with Zr(**14**)$_2$.

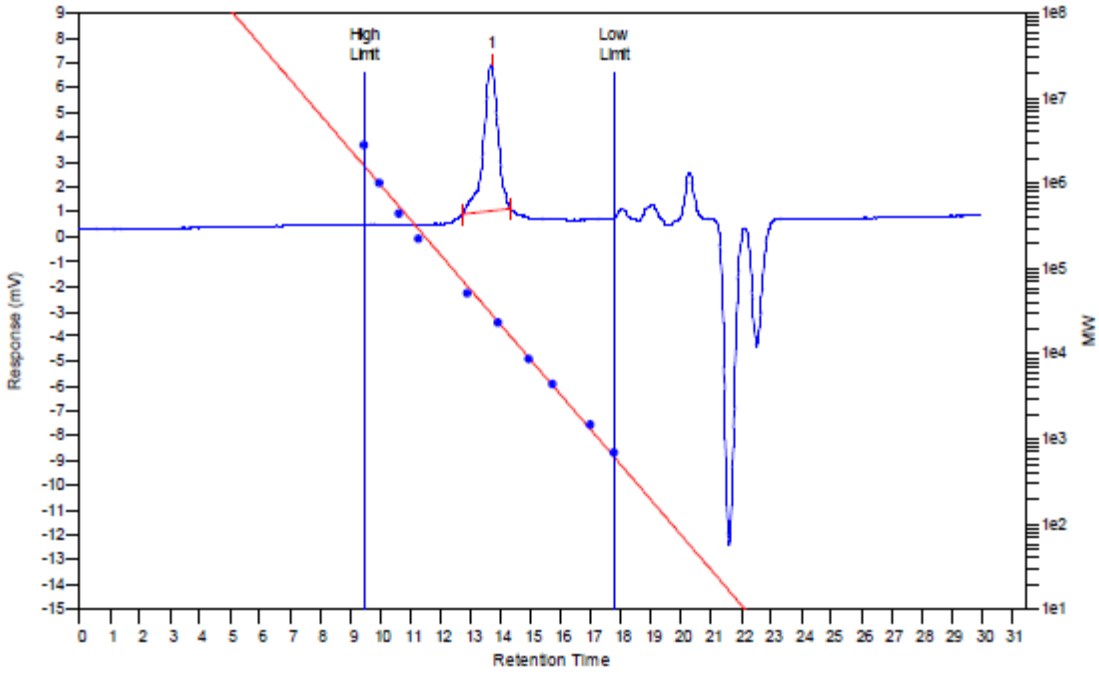

Figure 6.7: GPC trace of PLA prepared by bulk polymerisation with Zr(**14**)$_2$.

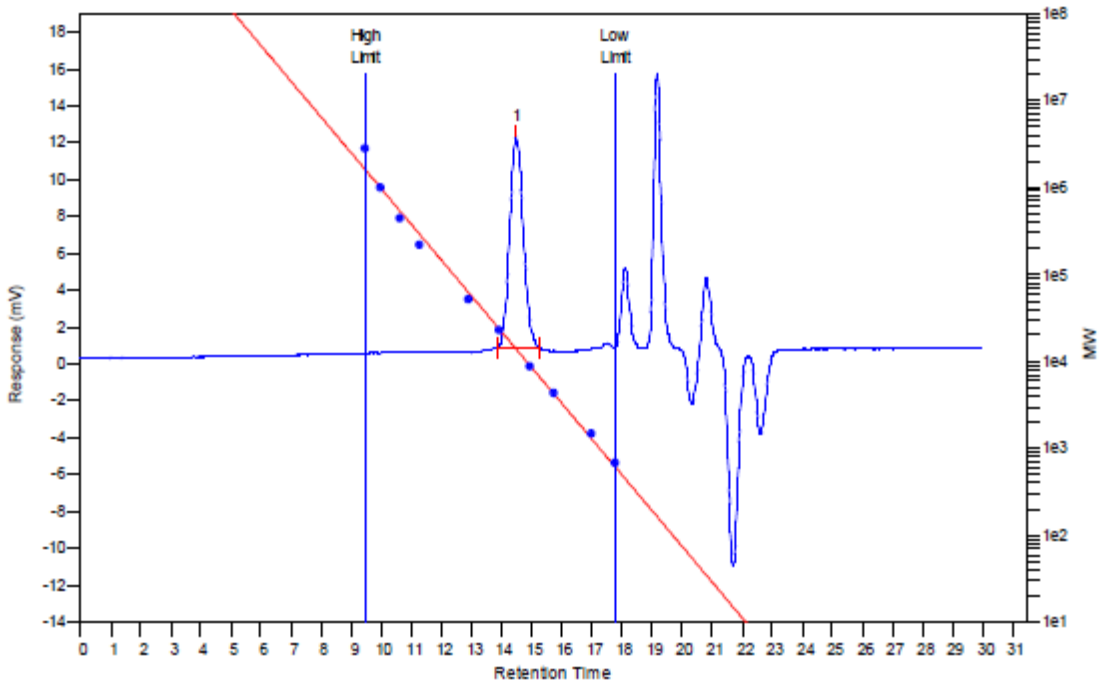

Figure 6.8: GPC trace of PLA prepared by solution polymerisation with Hf(**14**)$_2$.